TE WHARE WĀNANGA O TE ŪPOKO O TE IKA A MĀUI

VICTORIA
UNIVERSITY OF WELLINGTON

Breath exosomes: Proteomics and functional enrichment analysis in the development of methodology for future diagnostic devices

BY

Déanna Fleur Shea

A thesis
submitted to the Victoria University of Wellington
in fulfilment of the requirements for the degree of
Doctor of Philosophy
in ***Chemistry***

Victoria University of Wellington
2021

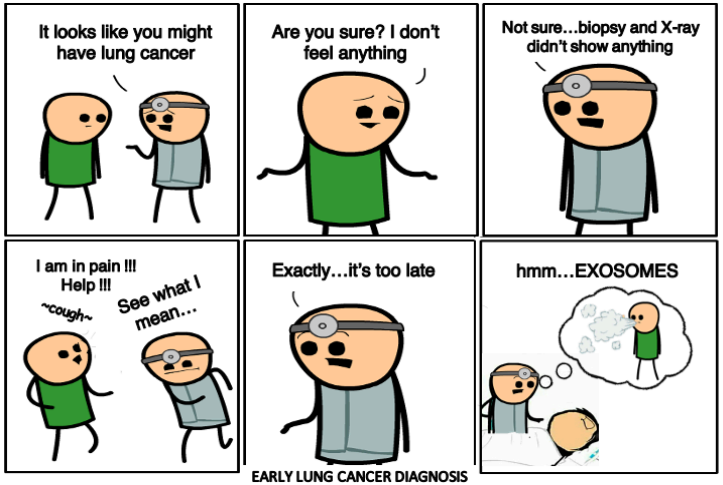

ACKNOWLEDGEMENTS

Vouloir c'est pouvoir.
-Monique Selim, Pouvoirs et Marché au Vietam:Les Morts et l'État, 2003

I wish to express my sincere appreciation to my primary supervisor, Paul Teesdale-Spittle, for his continuous support, constructive criticism, invaluable advice, and ingenious suggestions. More importantly, Paul has helped me to realize the power of critical reasoning. Paul, with his immense knowledge in many disciplines as well as plentiful experience had encouraged me in all the time during my academic research and demonstrated what a hard-working scientist can accomplish. His patience cannot be underestimated! I want to believe that our relationship was built on mutual respect and trust, equal to equal. While being completely different in scientific approaches, way of thinking, and even personality, we were an excellent team! I loved our meetings for little scientific battles we had. There were few times when he let me win. Paul has been a good listener and mediator. I recall a few moments when I was galloping into his office because I could not wait to report my results and had no idea what to do with my excitement.

I would also like to extend my deepest gratitude to my secondary supervisor, Nathaniel Davis, for willing to go the extra mile to help me successfully complete my research project. I'm extremely grateful to Nate for his effort to dive into understanding biochemistry and biology and connect those disciplines with his expertise in photon physics.

I'm extremely grateful to Professor John Spencer. It was such an honor to be able to teach undergraduate students together. I have always considered John as my mentor. His wisdom and expertise guided me through my personal and professional development. I loved our meaningful coffee chats where we talked about literally everything. He always made himself available when I asked for advice.

I would like to pay my special regards to David Flynn. David with his excellent sense of humor largely contributed to the success of my research work. There were many good and memorable moments when we shared a good laugh. I don't recall seeing David grumpy. David always seemed to bring the best in me whenever we talked. He always asked good questions and he never made it about himself. We laughed together talking about Netflix shows, baking, and sharing life stories.

I'd like to acknowledge Thomas Nann, my primary former supervisor on my first year of PhD, who made me an offer to start PhD and move across the ocean to the beautiful country, New Zealand, or how I call it "Sheep Land". I would like to recognize the help and effort of my other former supervisor, Renee Goreham, for securing the funds for the PhD project and introducing me to the world of extracellular vesicles. It happened that they both moved to Australia where they are continuing their research. I would like to thank proteomic wizards, Bio21 center located in Melbourne, Australia and Lifeng Peng for assisting me with the important part of my project.

Surely this project was not be possible without the financial help that I had received from MacDiarmid Institute, Wellington medical foundation research for life, Curtis-Gordon scholarship, and Postgraduate Student Association at VUW that have supported me with scholarship and gave me an opportunity to present my research on conferences worldwide.

My success, the completion of my dissertation, would not have been possible without the support and nurturing of my friend, my partner, and my dear future husband, Michael Shea, who lent moral and emotional support in this very intensive PhD journey. Thank you for putting up with me being sat in the office for hours on end every weekend and staying up late working in the lab.

I would like to say a special thank you to my parents, Zarema and Fleur, and my partner's parents, Susan and Bill, whose guidance, support, and encouragement has been invaluable throughout this study despite the distance between us. It was their love that raised me up to more than I can be.

I would like to extend my sincere thanks to Rory Besaans, who was the first person whom I met in School of Biological Sciences. Sadly, I cannot remember our first encounter. I am deeply indebted to Rory, who was there for me when I almost lost my path. I must also thank Sven Sondhauss, a MALDI geek, and Anna Tribe, my friend and my lab bench mate with whom we worked at the same lab for the past two years. I was lucky to have friends like them, who never wavered in their support.

I am indebted to Susan Wu and Mark Roden who were always so helpful in numerous ways. I also had a great please of working with members of Nate Davis' group: Damon De Clerk, Sanutep Chen, Calum Gordon, and Jake Hardy, who also were my partners in crime in teaching several undergrad courses.

And finally, I would like to thank all volunteers who participated in my breath study generously donating their exhaled breath condensate and contributed to the characterization of breath-derived exosomal proteome that has been done for the first time!

TABLE OF CONTENTS

LIST OF ABBREVIATIONS

ACN: acetonitrile

APS: ammonium persulfate

AuNP: gold nanoparticles

BAL: bronchoalveolar lavage

BEP: breath exosomal proteome

BSA: bovine serum albumin

CCM: conditioned cell culture media

CRC: colorectal cancer

CT: computer tomography

ctDNA: circulating tumor deoxyribonucleic acid

Cryo-SEM: cryogenic-scanning electron microscopy

DLS: dynamic light scattering

DNA: deoxyribonucleic acid

DTT: dithiothreitol

EBC: exhaled breath condensate

EBUS: endobronchial ultrasounds

EBUS-TBNA: endobronchial ultrasounds-transbronchial needle aspiration

ESCRT: endosomal sorting complex required for transport

EV: extracellular vesicles

FA: formic acid

FBS: fetal bovine serum

FLIM: fluorescent lifetime imaging microscopy

FRET: Förster resonance energy transfer

GO: gene ontology

IAA: iodoacetamide

IRF: instrument response function

ISEV: international society of extracellular vesicles

iTRAQ: isobaric tags for relative and absolute quantification

KEGG: Kyoto encyclopedia of genes and genomes

LC-MS/MS: liquid chromatography-tandem mass spectrometry

LDCT: low dose computer tomography

MALDI-TOF-MS: matrix-assisted laser desorption ionization-time of flight mass spectroscopy

MISEV: minimal information for studies of extracellular vesicles

MRI: magnetic resonance imaging

NHS-Ester: *N*-hydroxysuccinimidyl ester

NSCLC: non-small cell lung cancer

NTA: nanoparticle tracking analysis

PBS: phosphate buffered saline

PEG: polyethylene glycol

PEP: posterior error probability

PET: positron emission tomography

PROSPR: protein organic solvent precipitation

RNA: ribonucleic acid

SDS: sodium dodecyl sulfate

SEC: size exclusion chromatography

SERC: surface enhanced Raman spectroscopy

sEVs: small extracellular vesicles

SNAREs: soluble *N*-ethylmaleimide-sensitive factor attachment protein receptors

SCLC: small cell lung cancer

SILAC: stable isotope labeling by/with amino acids in cell culture

STEM-EDS: scanning transmission electron microscopy - energy dispersive spectroscopy

TEM: transmission electron microscopy

TEMED: tetramethylethylenediamine

TFA: trifluoroacetic acid

TMT: tandem mass tag

UC: differential ultracentrifugation

LIST OF FIGURES

LIST OF TABLES

ABSTRACT

Exosomes are a type of extracellular vesicle that carry cargo, including proteins and nucleic acids, that reports on the conditions of their cell of origin. Exosomes can be isolated from a range of biological fluids, including blood and urine, and their use in clinical diagnostic applications has been extensively researched. Breath is an excellent source of biomarkers. Exosomes collected from exhaled breath concentrate offer untapped potential in the field. For example, exosomes secreted from the cells of the lung carry biomarkers of lung health and so report selectively on lung health. However, whilst several publications report the presence of breath exosomes, and some discuss potential applications, there is no published work on developing standardized procedures for isolating high purity exosomes for biomarker identification, nor have breath exosomes been extensively characterized. Studying exosomes can potentially increase the specificity of diagnosis with an ultimate goal to translate early diagnosis into early treatment.

In this study we report results of optimized methodology for isolation of exosomes from human breath and undertaken phenotyping of breath exosomes by comparing them to cell-derived exosomes. Determining the benchmark proteome of breath exosomes became the major achievement of this study. The proteome profile of breath-derived exosomes was identified for the first time from exosomes obtained from the breath of 55 healthy volunteers indicating that the protein cargo of cell- and breath-derived exosomes are somewhat similar. The results of this study suggest that the exosomal breath proteome may be used in future studies identifying new biomarkers of lung dysfunction, including lung cancer. The possibility of identifying putative lung cancer biomarkers was shown using exosomes isolated from the lung cancer cell model (A549), from which four candidates were selected and examined. Promising results from time-resolved studies concluded that a FRET-based assay can be considered as a new way to prove the presence of exosomes and with an ability to differentiate between cancer and normal cells. We foresee the use of exosomes in non-invasive breath-based clinical applications for medical diagnostics for lung cancer as an important future application.

CHAPTER 1. INTRODUCTION

1.1 EXOSOMES

1.1.1 General characteristics of exosomes

Over 54 years ago, when Wolf first discovered exosomes while observing platelets in human plasma, he referred them as “platelet dust”[1]. Exosomes were simply considered as “trash compartments”[2]. The term “exosomes” was proposed later in 1987 by Johnstone et al[2] to clarify that they are a specific subtype of vesicles. They are small single-membraned vesicles formed by an endosomal route (i.e., through multivesicular bodies) and sized between 40 and 100 nm, although some sources consider them as ranging in size from 30 to 150 nm. Exosomes are enriched with proteins, nucleic acids, and lipids and originated from inward budding of the cellular membrane[3,4] (Fig. 1).

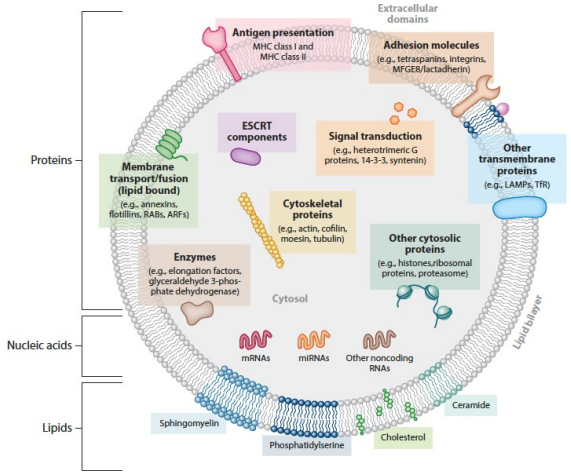

Figure 1. Overall composition of extracellular vesicles. *Adapted from Colombo et al [5].*

Exosomes are generated by all type of cells and can be found in all biological fluids including tissue samples. In recent decades, exosomes have been isolated and characterized from various types of biological fluids, such as blood and plasma[6,7], serum[8], urine[9–11] , breast milk[12–14], saliva[15–19], tears[20], and cerebral spinal fluid[21]. Several studies show that some exosomes remain associated with the original cell, whilst others are more widely distributed continuing sending signals to other surrounding cells[22–25]. More recently, their role has proven

to be more important than previously thought. For example, it is now believed that exosomes enable intercellular communication[22,26] by trafficking contents (nucleic acids, proteins and lipids) that provide information about the cell of origin and play vital roles in many cell mechanisms, including altering immune cell responses[27], enhancing angiogenesis[28], and inducing apoptosis[29,30]. Cellular components of exosomes can be "reassembled" into new vesicles and passed to other cells keeping intercellular communication active[31]. In addition, proteins found within exosomes have been shown to reflect the cell of origin[5,22].

Besides exosomes, other subtypes of mammalian-derived extracellular vesicles (EVs) are known. They are larger in size than exosomes and known as microvesicles (or ectosomes) and apoptotic bodies[22,31,32]. The difference between exosomes and other EVs is in their biogenesis and will be explained below in 1.1.2. Briefly, microvesicles can reach up to 1 µm in diameter and are formed by outward budding, which is the opposite process of exosome formation. The composition of microvesicles will depend on the composition of the parental cell, the microenvironment, and on the triggers that resulted in their release[22,33,34]. Apoptotic bodies can range in size anywhere from 50 nm to 5000 nm. Unlike exosomes and microvesicles, they are highly enriched with proteins associated with the Golgi apparatus, nucleus, and mitochondria due to their release by dying cells[35,36].

Although the protein content of EVs depends on their route of formation[33,36,37], there are no specific single markers to distinguish exosomes from other subtypes of EVs. Instead, a combination of markers can be used to characterize each type of EV[38]. For example, the transmembrane protein CD81 is commonly found in exosomes, while another transmembrane protein, CD63, can be found in many EVs including exosomes[38,39] and microvesicles. A combination of CD81 and CD63 is generally considered an exosome-specific combination[40]. In a similar manner, several markers should be detected to verify the subtype of many types of EVs [40,41].

1.1.2 Biogenesis and secretion of exosomes

The discovery of the molecular content of EVs opened a new page, allowing researchers to learn more about the biogenesis of exosomes. Exosomes are formed within endosomal membranes after going through several steps: formation and maturation of early endosomes; the inward budding of the early endosome membrane results in formation of intraluminal vesicles and so forming multivesicular bodies; transport of multivesicular bodies to the plasma

membrane; fusion of multivesicular bodies with plasma membrane; and release of the vesicular content as exosomes[26,32] (Fig. 2).

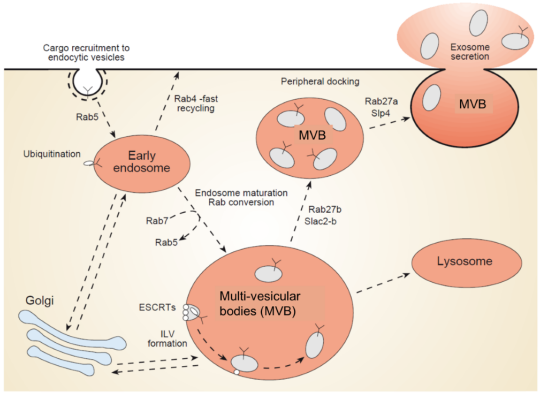

***Figure 2. Formation and secretion of exosomes**. Adapted from Henrix and Hume [42].*

The formation and maturation of early endosomes begin with the endocytic pathway. The endosomal network is a very dynamic system where each compartment represents a unique identity. Each compartment can be easily altered by communication between cargo that gets transferred between membrane-bound compartments. This is the place where the initial cargo sorting "decision" occurs, and the fates of future exosomes are decided. There are several mechanisms associated with membrane trafficking. The two most important mechanisms that not only actively participate in trafficking but also control the membrane identity and function are an alteration in phosphatidylinositol phospholipids and activation of Rab family GTPases. Phosphatidylinositol phospholipids are responsible for directional flow of membrane cargoes and have a close relationship with RabGTPases[43]. Although the process of exosome biogenesis is not fully understood, studies have shown that several molecules of the Rab family (Rab GTPases) are directly involved in the process by allowing the formation of early endosomes: Rab5 in transporting early endosomes, Rab4 and Rab11 in sorting and recycling endosomes, and Rab7 in lysosomes and targeted degradation of endosome cargo proteins.

The maturation process of early endosomes and their conversion to multivesicular bodies is also known as the Rab cascade[44–46]. Briefly, Rab5 recruits guanine-nucleotide exchange factors that then recruit Rab7, which follow recruitment of GTPase-activated proteins. During this process, the membrane's identity changes from a Rab5 to a Rab7 domain, which allows formation of more complex domains such as intraluminal vesicles and later multivesicular

bodies. Rab5 and Rab7 continue to actively participate in the endosome maturation process allowing further membrane fusion and creating a platform for protein localization that can be recognized by a zinc finger phosphoinositide-binding domain named after the four proteins – Fab1p, YOTB, Vac1p, and EEA1[47,48]. Further, ubiquitination, which depends on the RabGTPases mentioned above[49], also plays an important role. Ubiquitin is a small protein that triggers degradation when fusion of multivesicular bodies and the lysosome occurs sending a signal to release the content from plasma membrane via intraluminal. However, not all proteins that get sorted to intraluminal vesicles are destined for degradation. Some proteins, like tetraspanins, tend to accumulate on the plasma membrane creating tetraspanin-enriched microdomains that assist with selection of exosomal cargo (proteins and miRNA) and participate in binding and uptake exosomes by cells. Those intraluminal vesicles that are not targeted to the lysosome are progenitors for exosomes, and the tetraspanins they bear will be defined cargo of exosomes[50]. The process of initial clustering of ubiquitinated cargo is a beginning step in a process of exosomal formation in which endosomal sorting complex required for transport (ESCRT) machinery directly participates. This complex involved in this step is widely described in the literature as ESCRT-0. Some of the clustered cargo will be incorporated into intraluminal vesicles and will become an important part of future exosomes[2,3].

The process of exchange of compartments within an endosomal network is known as endosomal maturation and this is the first step of the ESCRT machinery (Fig. 3).

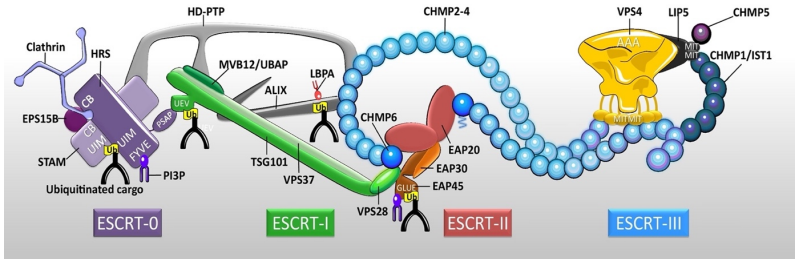

Figure 3. Model of ESCRT Machinery*. The diagram shows interactions between different subunits of machinery: ESCRT-0 components in purple, ESCRT-I in green, ESCRT-II in red, and ESCRT-III associated in blue. Relevant domains are identified. Ubiquitinated (Ub) cargo, phosphatidylinositol 3-phosphate (PI3P), lyso(bis)phosphatidic acid (LBPA), and clathrin associated with ESCRT-0 included as a model targeting factor. Lipids shown as yellow flags indicate PI3P binding cites. Deubiquitinating enzymes such as AMSH and UBPY, ubiquitin ligases, and the kinases Aurora B and ULK3 are known to interact with several ESCRT subunits. Abbreviations: CB, clathrin-box motif; FYVE, Fab1p/YOTB/Vac1p/EEA1 domain; GLUE, GRAM-like ubiquitin in EAP45 domain; MIT, microtubule interacting and transport domain; Ub, ubiquitin; UEV, ubiquitin-conjugated enzyme E2 variant; UIM, ubiquitin-interacting motif. Adapted from Christ et al [51].*

This process reflects that proteins including phosphatidylinositol kinases like PIKfyve get recruited at this stage, causing a shift from phosphatidylinositol-3-phosphate to phosphatidylinositol-3,5-bisphosphate. This conversion of the phosphatidylinositol is an important maturation step and is linked to recruitment of parts of the ESCRT machinery.

The inward budding of the early endosome membrane results in formation of intraluminal vesicles, thereby creating multivesicular bodies, and marks the next step of endosome maturation assisted by the ESCRT machinery[26]. The ESCRT-I and ESCRT-II complexes play a critical role in formation of future exosomes as they are responsible for clustering of ubiquitinated proteins into intraluminal vesicles, initiated by ESCRT-0 (the step described above)[52]. The role of ESCRT-I is to communicate with ESCRT-0 and ESCRT-II. The ESCRT-I complex consists of several proteins, Tsg 101, Vps28, Vps37, and hMvb12 (Fig. 3)[52]. Attention has been given to tumor susceptibility gene 101 (Tsg101)[53]. A recent study by Villarroya-Beltri et al[54] has shown that Tsg101 is directly involved in the lysosomal degradation process of multivesicular bodies proteins. A posttranslational ubiquitin-like modification that is known as ISGylation can regulate multivesicular bodies[54]. Once Tsg 101 is ISGylated, then secretion of exosomes is suppressed and fusion of multivesicular bodies with lysosome is promoted. ESCRT-II has a Y-shaped heterotetrametric structure and contains several Vps units that interact with arriving cargo and other proteins. The main role of the ESCRT-II complex is to initiate the assembly of ESCRT-III, which will drive vesicle budding to generate intraluminal vesicles. Mature multivesicular bodies can then either fuse with the plasma membrane and result in exosome secretion or fuse with lysosomes or autophagosomes, thereby degrading their cargo[22,55]. Protein degradation is instigated following fusion of multivesicular bodies with autophagic vacuoles by a calcium-dependent mechanism. The single multivesicular body then has a choice to go down two different pathways. If a vesicle chooses to go down by lysosome degradation pathway, it cannot go on to become an exosome[22,55]. In the cancer microenvironment, the balance between fusion with the plasma membrane and fusion with lysosomes is shifted, resulting in the increased release of exosomes compared to the healthy cellular environment[56].

Intraluminal vesicles formation is a lipid-driven process that requires the presence of specific lipids such as lysobisphosphatidic acid and ceramides obtained from late endosomes and their membrane constituents. Those lipids create a lipid platform to which ESCRT-0 binds and sorts ubiquitinated membrane proteins. The intraluminal vesicles formation goes through two important steps: enrichment with tetraspanins and recruiting ESCRT complexes to the site where formation of intraluminal vesicles occurs. Previous studies suggested that ESCRT-I and

II begin the process of intraluminal membrane budding that ESCRT-II had activated. Briefly, the presence of specific liquids assists in recruiting ESCRT-I and II complexes. Later in the process, ESCRT-III is recruited by the ESCRT 0-II complexes through one of two proteins-programmed cell death 6 interacting protein (PCD6IP), which is also known as Alix, and Tsg101 that is associated with PCD6IP. Alix, being directly involved in budding and scission processes, in fact plays the role of a communication bridge, connecting ESCRT-I and ESCRT-III and keeping interactions with all ESCRT units through a highly charged assembly of multimers[57]. Deubiquitinating enzymes (Fig. 3) actively contribute to the recycling of ubiquitin before degradation occurs and controlling proteins stability. $AMSH_3$ (Associated Molecule with the SH_3 domain of signal transduction adaptor molecule) is one such DUB. Through the $AMSH_3$-ESCRT-III interaction, cargo is deubiquitinated[58]. Once the ubiquitin tag gets removed from the cargo protein, the cargo is released into the intraluminal vesicles[59].

Cleavage of the budded membrane by fission and the process of splitting ILVs are the last steps involving the ESCRT machinery[5,33,60]. From previous stages, after membrane invagination (ESCRT-II) and maturing into a vesicle (ESCRT-III assembly), the future exosome is still attached to the membrane by a neck region (Fig. 2). Sequestration of cargo and membrane scission promote narrowing down the neck of the vesicle. Sorting of cargo is finalized during this step. It becomes packed into a vesicle by recruiting deubiquitination machinery with assistance of the ESCRT-III assembly (Fig. 3)[2]. Through these processes, the ESCRT machinery operates by following a "sort-pack-transport" principle.

Secretion of exosomes occurs when vesicles with packaged cargo are released to the extracellular space. This is the last step in exosomal biogenesis. Once the formation of multivesicular bodies is completed, they can either fuse with lysosome followed by degradation of their cargo or fuse with the plasma membrane followed by secretion of exosomes. How the fate of multivesicular bodies is determined is not well-known. During the transport of multivesicular bodies to the plasma membrane, other molecules and interactions are actively involved, for example the interaction between the "molecular switches" (small GTPases) from the Rab family and other molecules. As has been previously mentioned, Rab family proteins regulate vesicular trafficking. Further, Rab27 is required for peripheral docking of multivesicular bodies to the plasma membrane. Specifically, Rab27a, along with its effectors synaptotagmin-like 4 (Slp4) and exophilin 5 (Slac2b)[33,61] appears to be involved in future exosome secretion with general tetraspanin EV markers (Alix, Tsg101, and CD63). After multivesicular bodies docking with the plasma membrane, the final release of exosomes is facilitated by the soluble *N*-ethylmaleimide-sensitive factor attachment protein receptors

(SNAREs). SNAREs are a small tail-anchored protein family that mediate the fusion of multivesicular bodies with the target membrane and so finally lead to vesicle release.

Alongside ESCRT dependent processes, the role of other pathways, such as ceramide biosynthesis pathways, should be mentioned. Complex lipids such as ceramide can be associated with the biogenesis of exosomes contributing to inward budding to form intraluminal vesicles[62]. Several studies have shown that an enzyme that produces ceramide from sphingomyelin acts as inhibitor that can reduce the number of exosomes released by cell[63,64]. However, this is not always the case as in some cells the exosomal release was not affected by the synthesis of ceramide[65,66]. In a review on exosomes biogenesis and release, it has been mentioned that there is a possibility that both the ESCRT-dependent mechanism and ceramide biosynthesis pathways can contribute to exosome biogenesis resulting in formation of different subpopulations of exosomes[26].

The biogenesis pathways of other EVs are different from that of exosomes. For example, microvesicles are a subtype of EVs of a similar size to exosomes (100 nm). Due to their similar size, exosomes and microvesicles are described in the literature as a "mixed population"[67]. They were originally referred to as microparticles and were discovered in human plasma derived from platelets in 1967[1]. Microvesicles can be distinguished from exosomes as they bud directly from the plasma membrane followed by pinching off from the membrane. Some of the steps are in common with those of exosome formation[22], as proteins associated with Golgi complex and endoplasmic reticulum can be trafficked to multiple subtypes of EVs[33]. Microvesicles and exosomes can be distinguished as they have particular proteins that correspond to different EVs subtypes[39].

1.1.3 Exosomal cargo

As previously mentioned in 1.1.1, exosomes are loaded with different proteins, RNAs (non-coding, messenger RNA, and micro-RNA), DNA, lipids, and other cellular components. These exosomal components are conveniently cataloged in the ExoCarta database[68]. Exosomal cargo may vary and depends on the physiological and pathological conditions of the organism. Cargo is packed during exosome biogenesis as has been previously described in 1.1.2. It is known that the exosomal cargo includes molecules that convey important information about the cell of origin[22,69] (Fig. 1), including whether the cell of origin is diseased or not[22,70]. For example, viral infections, neurodegeneration (prions[71],

Alzheimer's[72], Huntington's[71]), and cancer all lead to different cargo profiles compared to the progenitor healthy cells and tissues[73,74].

Protein profiles of exosomes have been extensively studied and reported from lymphoid tumors[75], sarcoma[76,77], ovarian cancer[78], breast cancer [79] including various sources of biological fluids, such as umbilical cord[80], placenta[81], serum/plasma[82,83], saliva[84,85], cerebrospinal fluid[86,87], and sweat[88]. According to a recent review paper overviewing the characterization of exosomes by Lin et al[89], the past five years have shown a continuous growth in interest in the exosomes field, as supported by over a thousand published studies. Various research groups for the past few years have recognized the high potential of exosomes to provide novel non-invasive biomarkers for clinical diagnosis based on their unique biogenesis, great stability and diversity[90–101]. Most importantly, several studies recognized exosomes as minimally-invasive cancer biomarker[92] and specifically exosome proteins[102]. Thus, exosomes can offer prognostic information based on their cargo and can therefore be considered as biomarkers and nanocarriers[103]. However, their limitation in clinical settings is explained by the difficulty of isolation, purification and general analysis due to the lack of standardized methods[36].

The protein cargo of an exosome arises from the processes of exosome biogenesis explained above in 1.1.2 and as suggested in recent studies[22,57]. The physical interaction between membrane proteins and proteins that have been considered as general exosome markers, such as the tetraspanins, has been widely studied in the exosome research community[22,24,104,105].

Tetraspanins are a family of proteins with four transmembrane domains that can be found in all cell types[106]. Those transmembrane domains have a unique signature that allows them to be differentiated from other membrane proteins. This signature is a large accumulation of cysteines that are present in the large extracellular loop that connects domains 3 and 4 and extends 3-5 nm from the plasma membrane[107]. Tetraspanins actively interact with intracellular and other membrane proteins through a variety of specific molecular interactions[108] and participate in the major steps of vesicle formation and transportation[105].

It has been confirmed that tetraspanins, specifically CD9, CD63, CD81, CD151, and Tspan8, are highly enriched in exosomes. These tetraspanins are therefore frequently used as general markers to define exosomes from other subtypes of EVs[109]. The pathway through which tetraspanins become recruited to exosomes has not yet been fully understood. However, it has been proposed that the recruitment of tetraspanins to exosomes is directly associated with the origin of exosomes. An initial attempt to explain the interaction of tetraspanins with exosomes was made through sorting motifs[107,110], which was later replaced by interaction with

adaptor protein complexes, as some tetraspanins (CD9 and Tspan 8) do not rely on the sorting motif to integrate into exosomes.

In addition, it is believed that small transmembrane proteins such as tetraspanins can function as building blocks of larger protein assemblies and participate in trafficking of transmembrane proteins[109]. The impact of tetraspanins on the composition of exosomes is huge as they play a direct role on selective enrichment of specific protein-biomarkers that can be used for non-invasive diagnosis. Tetraspanins form a network with exosomal proteins and other proteins in the cellular microenvironment regulating signaling pathways.

Tetraspanins are actively engaged in many biological functions of the membrane. According to Bari et al[111], one of the important functions of tetraspanins is to regulate morphogenesis of membrane protrusions by altering the membrane curvature, possibly associated with rearranging the actin cytoskeleton.

As has been mentioned previously, exosomes are not the only type of vesicles present in the extracellular space. It has been proposed that no subtype of EVs can be identified by a single protein marker[34]. A combination of protein markers and biophysical techniques is required for characterisation of any specific EV subtype.

The difference in proteomic profiling between exosomes, EVs, and other types of vesicles, such as apoptotic blebs therefore supports their route of formation as some vesicles (e.g., microvesicles) form outside of the membrane[36,37,112]. Their cargo will be differentiated by their biogenesis, functions and other criteria[36,113]. Besides proteins, exosome cargo also consist of lipids[114–117] and nucleic acids[103,118,119].

The RNA cargo in exosomes was confirmed by two independent studies that demonstrated transport of functional miRNA and changes in cellular behavior due to exosomal uptake *in vitro* experiments[120,121]. In a similar experiment, but *in vivo*, EVs exchange between tumor cells was visualized in living mice by using the Cre-LoxP system[122]. Interestingly, subtypes of RNAs such as small non-coding RNAs including micro RNAs, can also be transported as a part of an EVs' cargo. Particularly in cancer development[67,123], attention has fallen on the role of exosomal micro RNA[124–126]. It has been reported that tumor-derived exosomes can modify the tumor microenvironment (TME) by transferring non-coding RNAs and micro RNA (particularly micro RNA-21 and -29) to target cells[127].

The transfer of micro RNA was initially demonstrated by Pegtel et al[128] who confirmed delivery of viral micro RNAs via exosomes from Epstein-Barr virus infected cells into neighboring healthy cells that, as result, showed repression of virus-targeted genes. This

illustrates the general case that exosomes from a donor cell can alter the intracellular environment of a recipient cell[129,130].

Exosome-mediated micro RNA transfer was also examined for parasite-derived exosomes *in vivo.* In one study, the parasitic genome was used to determine whether any of the micro RNA sequences that they found in the serum of infected mice came from the parasite[131]. Briefly, to determine whether parasite-derived exosomes can transfer micro RNA to mammalian cells, mouse small intestinal epithelial cells were incubated with *Heligmosomoides polygyrus* exosomes, and as a result changes in gene expression were noted. Specifically, two genes *Dusp1* and *Il33r* were strongly downregulated. Interestingly, exosomes derived from mouse cells did not alter those genes but showed the same uptake level as parasite-derived exosomes. That confirmed that exosomes and associated micro RNA can regulate genes that are responsible for immunity by suppression of pathogenic responses and acting as immunomodulators.

Although the transfer of exosomes during cell-cell interactions has been described, it is still difficult to define the mechanisms regulating transfer of a specific micro RNA to a recipient cell, including whether the transfer occurred specifically via an exosome[132]. As described in 1.1.2, packaging of RNA into EVs occurs during their biogenesis. Several studies have reported that the molecular profile of micro RNAs in EVs does not necessarily repeat the profile of the parental cell[133,134]. However, each micro RNA profile still represents the nature of the cell from which it was derived, leading to a distinct set of micro RNA from different cell sources[135]. In addition, tetraspanins, which have been mentioned previously, were addressed as “scaffolds of membrane microdomains” that directly participate in loading future exosomes with messenger RNA and micro RNA[104].

Genomic DNA is also loaded into exosomes[136,137], but this is less studied than RNA. There are not that many descriptions of how DNA gets incorporated in EVs. Interestingly, genomic DNA has been detected more commonly in cancer cell-derived exosomes than those from healthy cells[138]. This raises the possibility that the DNA found in exosomes may provide opportunities for highly sensitive cancer detection, and reveal information about tumor-specific mutations that could be valuable in therapy[139]. Although both single and double stranded DNA are found within exosomes [140], several studies propose that the majority of DNA that is associated with tumor-derived exosomes is double-stranded[137,141,142].

There is a long-established interest in the lipid profiles of exosomes[143]. Lipids, as well as proteins, play specific roles in formation and functions of exosome biogenesis[144]. In general, exosomes are enriched in sphingomyelin, phosphatidylserine, cholesterol, and

lysophosphatidylcholine accounting for about 10% of all phospholipids and glycosphingolipids[145,146]. Lipids in exosomes are related to the lipids in their parental cells; however, their sorting ratio does not show equality. In one example, exosomes from two different cell types (mast and dendritic cells) were observed and compared. The ratio of lipids such as phosphatidylcholine, phosphatidylethanolamine, phosphatidylserine, phosphatidylinositol, and sphingomyelin were compared. According to the results, the composition of lipids in the exosomes from dendritic cells was 26:26:19:20 respectively while the combination in dendritic cells itself was 43:23:12:9. The same study showed that cholesterol at similar levels in the exosomes as in their parent dendritic cells. Vesicles isolated from the placenta showed elevated levels of cholesterol and sphingomyelin, while the level of phosphatidylglycerol was half that in vesicles derived from dendritic cells[147,148].

1.2 THE VALUE OF EXOSOMES

1.2.1 The importance of exosomes

What makes exosomes so important in the human body is their ability to facilitate intercommunication among cells causing specific cellular responses[31] such as transferring, signaling, and activating receptors of cells [22,149]. The binding of exosomes to their target cells is probably determined by specific interactions of proteins enriched in the membrane of EVs, including tumor-derived exosomes, and proteins on the target cell[150]. In addition, they can help to adapt to microenvironmental stresses[151,152] or alter the cell itself causing pathological changes[153,154]. According to Masaoutis et al[125] the growing interest in exosomes is explained by their ability to modulate gene expression post-transcriptionally[155]. For example, released EVs interfere with the immune system[155], forcing various immune cells, such as macrophages, natural killer (NK) cells, along with B and T cells, to suppress or promote tumor progression. Lung tumor-derived exosomes containing micro RNA-21 and -29 can activate TLR 8 in immune cells, which can lead to tumor growth followed by metastasis[156–158] and can activate TLR 8 in immune cells[106]. Several studies have shown that exosomes are responsible for delivering immunogenic molecules causing the initiation, growth and progression of cancer[17,104,105], malignancy and drug resistance of tumors[133,159–161]. As described above, EVs contribute to various pathological conditions.

Another area of interest in exosome-related research is the search for biomarkers that can be interrogated by diagnostics that are less invasive and more rapid than current processes[123]. Thus, from the early description of being cellular waste as described in 1.1.1, exosomes have

become recognized as important in the chain of cellular intercommunication[4,33,162] including pathogenic processes[153,154].

1.2.2 Review of current leading biomarkers for cancer found in exosomes

Exosomes carry multiple cargos, which report information of the health status of the cells from which they were released, which is communicated to neighbouring cells[22,163–165] . Moreover, cancer cells tend to release larger quantities of EVs compared to healthy cells[166–168], which can promote communication between tumor, tumor microenvironment, and metastatic sites[165]. Cells constantly communicate with each other by releasing vesicles in the environment in which they grow. The crosstalk between healthy and tumor cells happens through the same vesicle release mechanism. According to Alipoor et al[3], these multi-signal messengers (i.e., EVs) have an ability to educate the tumor's microenvironment and so favor optimal conditions for the tumor, making effective therapeutic strategies difficult. Therefore, unique proteins that arise from the tumor microenvironment offer a potential avenue for diagnosis.

The clinical significance of exosome cargo as potential biomarkers in cancer has been discussed in 1233 manuscripts up to September 2018[169]. The importance of detection of tumors at an early stage has been recognized in many studies. Early detection is associated with a greatly improved prognosis. This underlines the value of exploring new biomarkers that can be detected at the earliest stages of cancer onset. Exosomes have great potential to contribute to our understanding of tumors development based on their molecular cargo. The variety of potential cancer protein biomarkers determined through proteomic approaches found on exosomes isolated from different biological fluids is shown in the Table 1.

Table 1. Potential cancer biomarkers found in exosomes secreted in different body fluids[170].

Cancer type	Potential Cancer Biomarkers	Source
Bladder Cancer	TACSTD2, EDIL-3, Mucin4, EPS8L2, α6-integrin, MUC-1, Basigin	Urine
Breast cancer	Survivin, Survivin-2B, CEA, Tumor antigen15-3	Blood
Colorectal cancer	CEA	Blood
Lung cancer	EpCAM, EGFR, CEA, LRG-1	Blood
Lung cancer	NY-ESO-1	Serum
Lung cancer	LRG1	Urine
Lung cancer	CD171, EGFR	Plasma
Melanoma	CD63, Caveolin1, TYRP2, VLA-4, HSP70	Blood
Nasopharyngeal cancer	LMP1, Galectin-9, BARF-1	Blood, Saliva
Ovarian cancer	Claudin-4, L1CAM, CD24, ADAM10, EMMPRIN, TGFβ1, MAGE3/6	Blood
Pancreatic cancer	GPC1, MIF	Blood
Prostate cancer	Transmembrane, protease, Serine2-ETS, β-catenin, PCA3, PSA, PSMA, ITGA3, ITGB1, survivin, PTEN	Urine
Renal cell carcinoma	MMP-9, EMMPRIN, Carbonic anhydrase	Urine
Spongioblastoma	EGFR-VIII, EGFR, PDPN, IDH1	Blood
Stomach cancer	HER-2/neu, CCR6	Blood

Meanwhile, several protein biomarkers that are present in lung cancer compared with normal lung tissue have been identified. For example, NY-ESO-1 protein has been found in serum exosomes[171,172], LRG1 protein in urinary exosomes[173], and CD171[174] and EGFR[175] in plasma exosomes. There is no doubt that the protein profile of exosomes provides potential biomarkers with high sensitivity and selectivity for cancer. However, the small number of proteins isolated, often found in very low abundance, creates a substantial challenge for biomarker identification[176]. Not all exosome proteins are membrane-associated proteins. However, some of them are directly associated with NSCLC growth and cancer invasion, including upregulation of EGFR protein[177–179]. For example, the prognostic value of EGFR protein expression alone, which plays a critical role in the cell signaling pathways, is not as high. Although the role of EGFR protein and other tumor associated proteins (claudins, KRAS, and other RAB-family proteins)[172] in cell cancer in well studied, there is not much evidence of EGFR protein transferred by exosomes[172]. Despite uncertainties of exosomes' EGFR protein, Huang et al[180] concluded that EGFR protein is present in "80 % of exosomes purified from lung cancer biopsies" while Zhang et al[181] showed co-dependence between exosome-regulated EGFR protein and metastasis in liver cancer. Proteomic analysis of exosomes will define the protein cargo associated with exosomes and allow evaluation of potential biomarkers of the

lung cancer tissue origin. On the other hand, it is a useful marker when combined with other specific proteins[182,183].

In addition to exosome protein biomarkers, nucleic acid biomarkers offer an avenue for earlier disease detection. Indeed, nucleic acids can be used in–ultrasensitive molecular diagnostics, but this is not without its limitations. As with protein biomarkers, the same micro RNA can be present in different types of tumors which results in poor outcome in diagnosis of a particular type of cancer. For example, an extensive investigation reported the presence of micro RNA-21 in several types of cancer (breast, liver, endometrial, esophageal) including lung cancer[184]. In particular, micro RNA exosomal biomarkers directly related to lung cancer have been highlighted in several studies[170,185,186] detecting 12 specific overexpressed miRNA[90]. Exosome-associated RNA has been proposed to have value as a diagnostic biomarker, including micro RNA-193a for CLC[187] and micro RNA-222-3p as for NSCLC[188].

The information that exosome can provide may have a tremendous impact in future biomedical applications and particularly diagnostic techniques for cancer. To avoid the risk of developing diagnostics for non-selective biomarkers, a database with a set of defined biomarkers characterizing exosome content must be developed.

1.2.3 Existing exosome-based diagnostics

The increases in understanding of the origins, roles, and composition of exosomes described above have laid the framework for their use in diagnostics. Although exosomes and their molecular cargo have not been fully characterized, there are several approaches that exploit the use of exosomes in early cancer detection. Application of exosomes in early tumor diagnosis has been mentioned in several clinical trials for tumors. For example, micro RNA profile of exosome has been used as a complimentary tool in the diagnosis of breast cancer[189], cholangiocarcinoma and gallbladder cancer[190], and prostate cancer[191]. In lung cancer a diagnostic approach that combines exosomal RNA/DNA and cfDNA provides a sensitivity of 89%[192]. This is especially important as detection of the early stages of tumors has been an ongoing challenge in oncology in various types of cancer, whilst treatments applied at these early stages of tumor development prove the highest chances of therapeutic success. The applications of exosomes to cancer diagnosis have been previously mentioned in 1.2.1 -1.2.2. These advantages can be extended by the concept of liquid biopsies. Application of exosomes as liquid biopsy in clinical diagnosis of cancer[192] holds a promise to detect potential targets

with minimum invasive treatment. Liquid biopsy points to the sampling and analysis of the biological fluids that contain nucleic acids, circulating tumor cells and exosomes. That makes them excellent candidates for development of new diagnostic tests. There are several studies that report the potential of exosomes in early tumor diagnosis. These include use of a KRAS mutation in circulating exosome DNA (exoDNA) for diagnosis of colorectal cancer (CRC) and pancreatic ductal carcinoma and EGFR T790M protein with a combination of exoRNA/DNA and cfDNA in NSCLC[193]. Another interesting study was conducted to investigate the clinical value of plasma exosomes in NSCLC. This study analyzed patients samples from early and advanced stages of NSCLC including healthy population cohort investigating the correlation between Tim-3 and Galectin-9 exosome indicators[194].

Deep learning-based surface enhanced Raman spectroscopy (SERS) has been proposed as a tool for cancer diagnostics. This technique analyses specific signals produced by cancer-derived exosomes[194]. Although results of this study resulted in 95% accuracy of diagnosis for cancer patients at stage I and II, this technique is still considered relatively new[195,196] and needs further investigation considering the heterogeneity of exosomes[197].

1.3 LUNG CANCER

1.3.1 Lung cancer

Cancer is ranked in the top four causes of death in 135 countries, with an estimated 19.3 million new cases worldwide in 2020 and approximately 10 million cancer-associated deaths[198]. According to the World Health organization, cancer is the second most common leading cause of death before the age of 70 years worldwide. Globally, about 1 in 6 deaths is due to cancer. Although lung cancer is only the second most common cancer in both men and women, it is the leading cause of cancer death with an estimated 1.8 million deaths due to lung cancer in 2020[199]. There are two major types of lung cancer: non-small cell lung cancer (NSCLC) and small cell lung cancer (SCLC). NSCLC is more common and a leading cause of cancer-related mortality in worldwide with an overall 5-year survival rate of 19.3%. The 5 -year survival rate for SCLC is 10%[200]. NSCLC has four stages, along with two substages for stages I-III. Statistics show that the frequency of diagnosis of early stages, when curative treatment is possible, is very low compared to the more advanced stages (Table 2). This is because early stages are asymptomatic and current diagnostic methods, such as biopsy and radiography, are unable to detect the smallest tumors. Therefore, the main way lung cancer is diagnosed is when it causes symptoms such as a cough or pain. By that time lung cancer has

already progressed to advanced stages. Once advanced stage has been reached, the rate of survival drastically drops. It is important to differentiate between cancer staging. While clinical staging is generally based on the results received after tests, for example, radiography or biopsy, pathological staging is based on the results after surgical procedure and therefore provides a better assessment on tumor development[201].

Table 2. 5-year survival rate for non-small cell lung cancer (NSCLC) and small cell lung cancer (SCLC) by pathological stage.

Stage	IA	IB	IIA	IIB	IIIA	IIIB	IV
NSCLC [200]	50%	43%	36%	25%	19%	7%	2%
SCLC [202,203]	38%	21%	38%	18%	13%	9%	1%

Another study reported that the 5-year survival rate varies between clinical and pathological stages, in which case the percentage for stage IV NSCLC survivors, for example, can be from 2% by clinical stage to 13% by pathological stage[202]. NSCLC includes several subtypes of primary cancer, of which adenocarcinoma is the most common invasive lesion (50%). Squamous and large cell carcinoma account for 25% and 10 % respectively of all lung cancers and NSCLC tumors[204]. SCLC account for the remaining 15% of lung cancer cases and is considered an aggressive cancer associated with smoking[205]. This type of cancer tends to grow very quickly and is characterized by an early metastatic spread. SCLC is a potentially curable type of cancer with a survival rate up to 25% and consists of two stages: limited and extensive[206,207].

1.3.2 Lung cancer and current diagnostics

As indicated above, lung cancer develops through 4 different stages. At stage I the cancer is located only in one small area. Stage II means that cancer has grown but has not spread yet. If lung cancer is diagnosed at stage I or II, patients have more chances for survival as it has not spread to nearby tissues and organs. Stage III is when cancer largely develops and progresses to nearby tissues and lymph nodes. At stage IV, the cancer has spread to other organs of the body. Stage III is still an operable one; however, chances for survival decrease to almost half of the previous stage (Table 2). Early detection in lung cancer is especially challenging[208,209], and consequently lung cancer and resultant metastatic disease are frequently fatal[210].

Diagnostic imaging is widely used for staging, following up, and assessing lung cancer treatment. Chest radiography, computed tomography (CT) scans, magnetic resonance imaging

(MRI), and positron emission tomography (PET) scans are the most common[211]. Around 80% of patients who present with cough, breathlessness, and chest pain receive chest radiography as their first routine procedure[211,212]. CT and MRI scans can image the thoracic cavity more effectively than chest radiography, identifying specific features and therefore can be effectively employed in detection. Combining PET and CT scans can improve diagnostic imaging by reducing false-positive interpretation from an individual imaging technique[213].

Additional tests for lung cancer include examination of the lungs lining by direct invasive techniques, such as bronchoscopy, resection biopsy, and transthoracic needle aspiration[214,215] can provide an accurate diagnosis of the tumor. Other types of tissue diagnosis are sputum cytology and pleural fluid cytology (thoracentesis). Both are non-invasive methods and are often used in clinical staging but require a follow-up test if results have been negative in response to cancer markers.

An overview of current diagnostics methods reviewing their potential advantages and disadvantages are presented in the Table 3.

Table 3. Advantages and disadvantages of current diagnostics methods. *Most common diagnostic methods for lung cancer are marked by asterisk **

Test	What does it show	Advantages	Disadvantages
Chest X-ray*	Images of the lungs and surrounding tissues	Commonly available; 75.4% sensitivity at 1 year (study was based on individuals >50 years old[216]; unexpensive[209]	The nodule size detection is limited to 1 to 2 cm; low visibility due to other spiculated masses from previous complications; false-positive rate 9-15%[217]; requires follow-up imaging[218]
low-dose spiral CT (LDCT)*	3-D views of the lungs	Resolution capabilities under less than 1 cm; better contrast resolution (compared to chest X-ray); evaluation of the entire [219]	High false-positive rates 20-50%; limited detection of cancer on early stages over detection of already existing tumor in later stages III-IV[218]
Lab tests (ctDNA, NGS)	Mutations that occur in a cancer cells' genome	87% sensitivity and 81% specificity on the stages II-III; non-invasive[220,221]	Low sensitivity in stage I (15%); limited by cost[222,223]
PET/CT*	Detailed soft tissues presented in cross-sectional images	Greater resolution of nodules and tumor pathology (compared to chest X-ray and CT); more accurate than CT in the detection or exclusion of mediastinal nodal metastases[218]	High false-positive rate (up to 50%); at least 20% are over diagnosed; inability to locate the tumor due to the blurry images[221]; cost-effective
EBUS	Cell abnormalities	Direct visualization of nodes; high sensitivity (85%); real-time sampling (less risk of major vessel puncture); guided sampling[215,224]	Less core tissue for sampling; low negative predictive value; cannot, image or sample subaortic and paraoesophageal lymph nodes; repeated invasive sampling in early stages of cancer[225]
Biopsy	Cell abnormalities	Rapid, minimally invasive, and economical test, liquid biopsy presents oncologists with real-time information about a tumor[214]	Lack of standardization around procedures; difficulty in comparing different technology platforms; lower sensitivity (stage I)[214]

Bronchoscopy	Cell abnormalities	Abilities in investigate area out of reach (smaller bronchi; Higher sensitivity of 85–87% when lesions were >20 mm and an overall sensitivity of 69.7%; accuracy 89%[205,215]	Bleeding (0.12%), hypoxia, loss of airway, pneumothorax (0.1–0.16%), or mortality (0–0.02%)[226]; sensitivity depends on the size and position; repeated invasive sampling in early stages of cancer of the tumor (34-88%)[205]
MRI*	Detailed images of soft tissues in the body	Better soft tissue contrast, multiplanar imaging capability (over CT)[227,228]; can quickly recognize nodule between 1-2 cm with 82% specificity[229,230]	Slower and more expensive with poorer spatial resolution (compared to CT)[218]; inability to recognize nodules less than 0.4 cm[229,230]
Sputum cytology	Cell abnormalities	Combining with quantitative image cytometry can lead to a specificity of 90% and sensitivity of 80%[231]	Squamous cell lung cancer only

1.3.3 Failure of current diagnostics in detection of lung cancer

Improved detection leads to better knowledge of lung cancer progression. Despite current cancer treatment therapies (e.g. chemotherapy, radiotherapy, surgery)[125,126,209] and good diagnostic tools (e.g. sputum cytology, chest radiography (and later on low-dose spiral computer tomography (CT), and tissue sample (biopsy))[209] lung cancer still remains the leading cause of cancer-related deaths around the world[3,205,232]. The reason for this is inability to detect lung cancer early enough so that the correct treatment can be chosen. Most available diagnostics described above lack sensitivity and have other limitations.

Diagnostic imaging has been described in many comparative studies concluding that the tumor evaluation and treatment depends on a type of lung cancer. For example, CT and MRI have poorer outcomes in identifying tumors, while PET scans are able to confirm NSCLC in 83% of the cases[218]. Although PET scans have proven their clinical values in some cases, the application of PET itself in identifying primary malignancies remains controversial due to false-positive findings and resolution[233,234]. PET scans as a molecular imaging technique that observe malignant cells and measure the cellular glucose uptake. The glycolytic rate is visualized by using ^{18}F-fluorodeoxyglucose. One of the important limitations of PET scans is difficulty and sometimes their inability to precisely localize the tumor due to the blurry images of anatomical structures or indirect inflammation[235]. Besides that, PET is a very expensive diagnostic method, which is a major drawback that needs further improvement[236].

A comparative study has been conducted on almost 12,000 healthy individuals to find out the performance of MRI in the detection of lung cancer and its ability to define asymptomatic patients[237]. Results of the study showed that 4.8% had suspicious nodules, and ultimately only 0.4% of the cohort had lung cancer confirmed. MRI was evaluated in another

study that discussed relevance of the size for malignant tumors. All nodules less than 4 mm and smaller showed inconclusive results, while nodules between 10 and 20 mm were recognizable as the malignancy of masses showing 28% to 82% respectively[229,230]. MRI imaging can be compromised by respiratory movements by forming masses that can be mistakenly assumed as tumor masses[238]. Nonetheless, MRI has advantages over CT scans delivering results in multiplanar format and having the ability to very quickly determine existing tumors[227,228].

Another approach is the Saccomanno technique, which involves collection of sputum samples. It has been widely used and showed positive results[231]. However, when this method was compared to fresh smears from lung cancer patients, the Saccomanno method was not able to identify small cell carcinoma while the second method (fresh smears) did[239]. Sputum cytology is still a useful diagnostic test and in some countries is used more often than biopsy[240–242].

Surgical lung cancer diagnosis is undertaken in early stages of cancer to reduce morbidity. The most common procedure is a standard resection that is often combined with chemo/radiotherapy[243]. However, several studies have reported that tumor masses often confirmed as benign tumors and do not always associate with lung cancer[244]. That raises the question about unnecessary surgical procedures that could potentially result in medical complications to a patient needing months of long recovery. The paradox of preoperative and no preoperative tissue diagnosis was explained in Sihoe's et al. study[244]. In this study, the surgery was performed in 443 patients with an early confirmed or suspected lung cancer mass. Another 206 (46.5%) patients did not have preoperatively confirmed diagnosis. Among patients without preoperative diagnosis only 8 % were found to have a benign tumor. In addition, 52.9% of the cases suspected to be tumors on the basis of preoperative diagnosis were not confirmed as lung cancer. The study concluded that proceeding with surgery without preoperative diagnosis is safe, but only in the case of patients who have a suspicious lung mass already identified. Therefore, new methods for earlier lung cancer detection are essential[205,245,246].

1.3.4 New diagnostic methods under development

One recently developed method of diagnosis looks at the distinctive appearance of gene expression from bronchial epithelial cells that shows differences between the gene expression profile in healthy and cancer cells. The study proposed a gene expression classifier consisting

of a combination of 17 cancer genes (from an initially identified group of 232 genes). The gene classifier panel was then used alongside the bronchoscopy procedure to increase sensitivity[247]. Another novel concept that increases sensitivity of lung cancer detection is radiomics. Radiomics combines data from several diagnostics (CT, PET, MRI) allowing verification of diagnosis and choosing treatments more effectively[248]. The idea behind this method is to detect the tumor and define the correct tumor phenotype, which further can improve clinical decision making[249].

Detection of an abnormal tumor antigen can be another way of diagnosing a tumor, even in early stages. This method is based on producing a signal by autoantibodies in response of detection tumor masses. This method seems to be applicable on all stages of lung cancer based on identified panel of autoantibodies. The initial clinical study to test the sensitivity and specificity of this method was conducted in 2011 showing high sensitivity up to 93%[250]. However, the sensitivity was later reported being around 37-40% which is very low and needs to be improved for the overall test accuracy[251].

Characterization of the complement cascade and specifically analyzing the level of plasma circulating complement component (C4d) could be an alternative way of detecting lung cancer[252]. However, in patients who appear to have emphysema and COPD this test didn't show significant elevation and therefore cannot be used in people who are at risk of lung cancer. Results of this test also showed great specificity (89%), but just as a previous test with AAbs it resulted in low sensitivity in a very close values of 44%[253].

Evidence suggested that tumor suppressor genes can be detected through abnormally methylated DNA circulating in the serum of lung cancer patients in all tumor stages[254]. Several studies have specifically tested this method on patients in stages I and II. Results from investigations into differences in DNA methylation of a range of markers between lung cancer patients and non-cancer controls were somewhat similar and were compared by reported percentage of the sensitivity and specificity in plasma and sputum. The final numbers for sensitivity and specificity in plasma were 62% to 76% and 74% to 84% respectively, and 63% to 86% and 72% to 92% in sputum, respectively[255–257].

Real-time endobronchial ultrasounds (EBUS) has been developed to guide the established technique of transbronchial needle aspiration (TBNA) that offers a higher sensitivity using a larger scanning range[215]. The accuracy and performance of EBUS-TBNA has been studied by several research groups. A study proposed by Navani et al[224] recruited patients that had already undergone initial diagnosis by CT scans and were suspected to have lung cancer (stages I to IIIA). Following the primary goal of defining the time-to-treatment

decision, this randomized trial concluded that detection of tumor was faster by EBUS-TBNA (14 days) compared to CT scans and staging diagnosis (29 days). For this reason, they propose that EBUS-TBNA should be considered as the initial method of lung cancer investigation. A year later, another study concluded that EBUS-TBNA reduces the time for diagnosis if it chosen as the initial test[258]. Analyzes of cytological samples collected by EBUS-TBNA also showed reassuring results, declaring the sensitivity and specificity reached 94.52% and 95.12%, respectively[259]. Minor concerns to sensitivity mentioned in this study were associated with a lymph node size threshold[260]. In addition, EBUS-TBNA is less invasive than surgery and recommended for patients who need an initial staging[261].

Circulating tumor DNA (ctDNA) and next-generation sequencing (NGS) of ctDNA have been recognized as sensitive and non-invasive tools for detection of early stages of cancer[262–264]. The role of ctDNA as a biomarker of advanced stages of lung cancer has been already proven[220]. However, the evidence of its application in early stages needs more proof due to a low sensitivity that is 15% at stage I compared to 100% at stages II-III[222,223]. A newly proposed way of defining biomarkers, NGS, is based on genomic alteration in the tumor. Interestingly, a study that included over 400 patients, where half of them were patients were without known cancer, has been reported with the same output as in the previous mentioned ctDNA studies. Further, the data indicated that the proportion of cancer patients with ctDNA was rather large with different cancer types than in patients without known cancer[265]. Although the presence of ctDNA in early stages of cancer has been reported[265,266], tumor detection has to be achieved against a background of non-tumor derived ctDNA. The low level of ctDNA results in a lot of unnecessary data for analysis, such as signal to noise ratio, and becomes computationally challenging making it incredibly difficult to apply this method for routine screening and especially for early stages[221,267]. As a result, this method seems to be more appropriate for more advanced stages. Cohen et al[265] proposed combining this method with protein biomarkers (protein) for a stronger sensitivity in detection.

Raman spectroscopy combined with principal component analysis (PCA) has been further investigated[268] after it attracted interest in medical diagnoses of nasopharyngeal cancer[269], head and neck[270], and lung cancer[271]. Several studies that have applied Raman spectroscopic analysis for *in vivo* early lung cancer detection reported that sensitivity and specificity in detection of precancerous lesions were acceptable and could differentiate between malignant, benign, and normal lung tissue[272].

Apart from nucleic acid sequencing and Raman spectroscopy, mass-based proteomic analysis, tandem-mass-tag (TMT)[176] and triple stable isotope labeling by/with amino acids in

cell culture (SILAC) quantitative proteomics approach are becoming more applicable in diagnostics[273]. Those will be described in Chapter 3 (subchapter 3.1.2)

In summary, there are no current or developing methods that could reliably give an early diagnosis. Existing diagnostics are invasive and noneffective. On the other hand, the concept of studying breath exosomes can open a new non-invasive and more effective avenue for diagnosis. Breath exosomes collected from exhaled breath condensate (EBC) could be a better option for biomarkers as they are largely free of contaminants that whole EBC struggles with. Despite the promise of new techniques, challenges in diagnosis of early-stage tumors remain high. Therefore, new methods of non-invasive diagnostics for early stages are highly desirable.

1.4 BREATH-DERIVED EXOSOMES

1.4.1 How breath-derived exosomes are characterized

In general, exosomes have been divided into two groups: cell-derived exosomes and exosomes "derived from body fluids (plasma, urine, spinal fluid, saliva, and etc)" [126]. However, another important source of exosomes – breath – has been largely ignored. Although the potential of exosomes obtained from EBC has been considered[114,274–276], their application has not been extensively explored. Whilst there are several studies that have reported biomarkers in EBC, in general these have used either crude EBC[172-174] or exosome-enriched fractions[114,274,275]. In the study by Youssef at al[275], exosome-enriched fractions from airways obtained from bronchoalveolar lavage fluid collected from 43 asthmatic patients and 42 healthy individuals were analyzed. The study confirmed no significant differences between groups in the proportion of extracellular vesicles that contained the general tetraspanin marker CD63. However, the expression levels of other markers (i.e., CD54 and HLA-DR) were significantly higher in the diseased group. In addition, the analysis of lipid signatures of asthmatic patients showed significant differences ($\rho < 0.05$) in the level of phosphoglycerolipids and sphingolipids compared to healthy group[114] supporting the sphingomyelinase inhibitors that can reduce the number of exosomes release by cell. In the Sinha et al[275] study 20 EBC samples collected from 10 asthmatic and 10 healthy individuals were compared with the goal of finding disease signature in micro RNA. As a result, 11 micro RNA markers were noticed as differently expressed in the diseased group compared to healthy individuals. Amongst these 11, 3 (hsa-miR-574-5p, hsa-miR-516a-5p, and hsa-miR-421)[277] had been previously reported in association with asthma. Interestingly, they showed that the majority of the identified exosomal micro RNA is similar to that identified in EBC suggesting

that exosomes obtained from EBC contain microRNAs that can act as biomarkers. However it was not a focus of their work to characterize or confirm the purity of the exosomes that they obtained through immunoaffinity isolation.

It is expected that exosomes isolated from EBC will be particularly rich in those originating from lung tissue and, through biomarker analysis, reveal the status of lung health. For example, these breath-derived exosomes may carry distinctive molecular biomarkers of lung cancer, a disease where early detection is particularly challenging but urgently required to enhance overall survival for lung cancer patients[205,245,246,278–280].

1.4.2 Biomarkers in exhaled breath condensate

Exhaled breath condensate (EBC) is a promising source of biomarkers for monitoring the lung and respiratory system. Collection of EBC is non-invasive and requires tidal breathing into a cooled condenser or a collection vessel. In comparison, collection of bronchoalveolar lavage for biomarker analysis is substantially more invasive and the level of biomarkers found in EBC can be much higher than in bronchoalveolar lavage[281]. There has been significant growth in EBC research in recent years to identify biomarkers for diseases including chronic obstructive pulmonary disease (COPD)[282–285] and asthma[286–288].

Investigations related to genomic DNA mutations in EBC (specifically in the p53, EGFR, p16, and KRAS genes) were reported by several groups[289–291]. Since then more investigations have been done and detection of small amounts of DNA in EBC samples has been reported[292–294]. Cancer-associated mutations in DNA were extensively researched by Youssef's group using next-generation sequencing[295]. In their first study, the researchers studied mutations of 22 cancer genes in a healthy population. This study suggests that EBC could be adopted for lung cancer detection in its earlystage[295]. In their second study, following the same methodology, EBC collected from patients diagnosed with various types of lung cancer and group of healthy population was compared. As anticipated, some differences in the level of DNA mutations between groups were noticeable. In order to analyze whether there are differences in cancer-associated mutations in DNA before and after treatment (chemotherapy), EBC of 8 lung cancer diagnosed patients was collected before and after treatment. Unfortunately, after conducting statistical analysis the difference was not statistically significant (ρ=0.83), although the number of mutations in the treated group was lower compared to the non-treated patients[296].

EBC as a source of biomarkers has been extensively researched for its clinical usefulness especially for early stage lung cancer detection[297–304]. Examples of previously identified breath-based biomarkers for lung cancer can be found in Table 4.

Table 4. Breath-based biomarkers for lung cancer detection.

Cytokines	DNA, protein, peptides	Oxidative stress	Others
Interleukin-2[305]	S100A11, ANXA1, ENO1, FABP5[302]	Hydrogen peroxide[306,307]	Lipid peroxidation[308,309]
Interleukin-6[310]	Let-7[304]	Nitric oxide[307]	
Tumor necrosis factor-α[305]	KRT1, KRT6A, KRT6B, KRT6C, KRT9, KRT10[302]	8-isoprostane[311]	
	3p microsatellite alterations[292,312]		
	p53 mutations[289]		
	Endothelin-1[313]		
	Leptin[305]		

A recent study used a proteomic approach in exploring lung cancer biomarkers in EBC from 20 individuals (n=10 diseased and n=10 healthy). They reported identification of a total 1151 proteins from which four (S100A11, ANXA1, ENO1, FABP5) (Table 4) were identified as novel biomarkers for lungcancer[302].

Although it seems that EBC could potentially offer biomarkers for several diseases, diagnostic accuracy of its use in needs to be improved. For example, detection of COPD based on previously identified EBC inflammatory markers remains challenging and health history or concurrent diseases need to be considered[283]. Another study in which EBC biomarkers were compared to bronchoalveolar lavage biomarkers showed no significant correlation[281].

Some limitations in defining biomarkers from EBC include concentration of sample, low limit of sensitivity (due to being highly diluted), and contaminants, such as saliva and volatile organic compounds. On another hand, exosomes derived from EBC could be a better option for biomarkers than whole EBC, as exosomes can be purified away from the contaminants that can be present in whole EBC.

1.5 AIMS AND OBJECTIVES OF THE PROJECT

Aim of the project:

The aims of this project were to characterize exosomes collected from exhaled breath condensate using physicochemical and proteomic methods, to use cell culture models to identify putative biomarkers of lung cancer found on exosomes, and to develop a proof-of-principle test for these biomarkers.

Objectives:

1. Optimize methodology to isolate exosomes from cell models of normal lung tissue (WI-38 cells) and lung cancer (A549 cells) to identify the proteins found in these exosomes and to propose biomarkers of lung cancer using proteomic methodology.

2. Isolate exosomes from human breath and identify the proteins found in these exosomes using proteomic methodology.

3. Define the proteome of exosomes from cell models of normal lung tissue (WI-38 cells) and lung cancer (A549 cells) to demonstrate that it is possible to identify potential biomarkers of lung cancer and evaluate whether those may be revealed on exosomes to develop a proof-of-principle test using cell culture model. Secondly, determine the benchmark proteome from breath-derived exosomes and use those exosomes as a negative control to test the proposed putative biomarkers of lung disease.

4. Develop a sensitive FRET-based assay to detect interaction between exosomes and proposed putative lung cancer biomarkers with a final goal to distinguish biomarkers between cancer and non-tumorigenic exosomes.

CHAPTER 2. ISOLATION AND QUANTIFICATION OF CELL- AND BREATH-DERIVED EXOSOMES

Aim :

The aim of this chapter was to describe the isolation of cell- and breath-derived exosomes and their characterization using physicochemical methods.

Objectives:

1. Optimize methodology to isolate exosomes from cell models of normal lung tissue (WI-38 cells) and lung cancer (A549 cells) that are sufficiently high quality from cell-based sources.
2. Apply optimized methodology to isolate exosomes from human breath and undertake phenotyping of breath exosomes by comparing them to cell-derived exosomes.

2.1 INTRODUCTION

2.1.1 Importance of purity and quality of exosomes

Since their first discovery, exosomes have attracted the attention of many researchers, increasing the size of researchers in the EVs field. The origin of exosomes and some of their uses were described in Chapter 1. There are extensive further applications that are beyond the scope of this thesis. However, these additional uses have been extensively reviewed[314–319].

The previous chapters explained that EVs, including exosomes, can be found in many biological fluids and tissue samples. In order to claim the presence of EVs, the isolate must be an extracellular fluid, which in this case can be either a biological fluid or conditioned cell culture medium. It is important that collection of EVs, including exosomes, should be "optimal" - designed to avoid any mechanical disruption. Despite the potential of exosomes, there are many obstacles that limit their application. Although methods of exosome isolation are generally easy, current techniques are costly and only obtain low yields and purity[320,321]. Today, several techniques have been offered for isolation, characterization, and analysis of the functional properties of exosomes that will be described later in this chapter.

Application of exosomes requires an ability to differentiate them from other subtypes of EVs. A motivation for developing guidelines for studies involving exosomes was based on ensuring reproducibility. Therefore a list of minimal information for studies of extracellular vesicles (MISEV) was published in 2014 and was based on expertise of International Society

of Extracellular Vesicles (ISEV) board members actively involved in exosome research [322]. This document provided basic, yet critical, information, such as methods of isolation and characterization. With rapidly growing interest in this research area, many uncertainties and issues seem to appear quickly and require further clarification, especially with respect to exosomes. After a few years, an updated document – MISEV 2018, was produced by the EV community (>380 authors)[38]. The updated minimal requirement summarized, updated, and clarified the most important points from MISEV2014.

Further, the requirements based on mammalian EVs were corrected and clarified on pre-analytical phase. That included specification on detailed culture and harvesting condition (e.g., passage number, density, and culture volume), medium preparation (e.g., exosomes-depleted serum), storage, separation and concentration, quantification including total proteins, lipids, and RNA. The conclusion of the minimal requirements updates recommended use of the preferred generic term "extracellular vesicles" unless the vesicles are defined by biochemical characteristics matching a particular subtype. According to MISEV 2018[38] , an EV will be called an exosome only after showing "at least three positive markers of EVs, including at least one cytosolic protein and transmembrane/lipid-bound protein; at least one negative marker; and characterized by two different but complimentary techniques (for example, transmission electron microscopy (TEM) and dynamic light scattering (DLS))". In addition, isolated EVs have to be evaluated for their purity as non-EV structures (e.g., lipoproteins[323]) can be present potentially interfering with characterization. For example, to be characterized as exosomes, proteins associated with Golgi apparatus, endoplasmic reticulum, mitochondria, autophagosomes or nuclear components must not be expected as they are present in larger EVs[38].

Methodological approaches for isolation and quantification of exosomes, their proteomic analysis and finally detection are critical for choosing a biomarker for diagnostic purposes and will be discussed in the next subchapters.

2.2 LITERATURE REVIEW OF EXOSOME ISOLATION METHODS

2.2.1 Differential ultracentrifugation (UC)

The most common method of exosomes isolation is differential ultracentrifugation (UC). UC has been used for decades and still remains as a standard method of isolation[324–326]. This widely employed technique[327–329] has the advantage of minimal sample manipulation. The

collected source of biological fluid can be simply transferred to an appropriate centrifugation tube shortly after collection and proceed following a chain of sequential steps with increasing centrifugation force as well as duration. This method is applicable for large sample volumes, such as conditioned cell culture medium, as small samples will result in a luck of purity[330,331].

However, the efficiency of the method is lacking the purity of vesicles, not even mentioning being time-consuming and labor-intensive. Livshits et al[330] present a very interesting theoretical analysis of exosomes isolation by differential centrifugation. They base his conception on the type of rotor that is used in common isolation protocol and the importance of "cut-off" sizes for vesicles. His analytical explanation is based on the theory that smaller particles, which presence are fewer compared to larger particles, may finish their migration together with larger particles. The issue with that is that the acceleration force (which governs migration rate) is dependent on particle size, with larger vesicles being subject to greater forces, and so is offset by larger vesicles being retarded more by the ultracentrifugation medium. Another obstacle is co-precipitated aggregates, lipoproteins, and contaminants[332]. Other research groups reported that even with a prolonged UC cycle including overnight[333], impurities were still observed in exosome samples[334]. Théry et al[324] suggested to dilute the sample with an equal volume of the buffer (1×PBS) if the original sample has a high viscosity.

2.2.2 Size exclusion chromatography (SEC)

Size exclusion chromatography (SEC) is equally often used, and preferable to UC as it allows separation of exosomes while keeping their original shape[335]. This method allows rapid and gentle isolation of EVs based on their size by using prepacked columns with porous bead resins[335]. The order of exosome elution from the column depends on their hydrodynamic radius. This method has several advantages, such as being less time consuming and needing less sample volume than in UC method. Vesicles isolated by SEC also experience minimal damage and deformation and do not require specialized equipment and space to conduct the process[336]. Further, SEC is applicable for isolation of exosomes from a variety of biological fluids. Unfortunately, SEC leaves the purified exosomes in a diluted state, necessitating further manipulation for some applications[327]. For example, while it always works for cell culture conditioned medium, it seems that the presence of lipoproteins in EVs samples remains challenging for samples from human plasma[337]. Several attempts optimizing the SEC method for human plasma included plasma dilution to reduce the viscosity and prolonged cycles of UC[338], optimization the CCM by adapting it to a reduced FBS or FBS-free medium[54], and

finally switching to exosomes-depleted FBS[339,340]. In addition, Guerreiro et al[341] proposed that using ultrafiltration prior to SEC allows to separate exosomes from many of the smaller proteins in the sample. A study by Davis et al[342] also confirms that using SEC method helps to avoid unnecessary impurities and best suited of all commonly applied isolation techniques.

2.2.3 Density gradient centrifugation

Density gradient centrifugation is mostly used after a crude EV population had been isolated[343], but is also applicable for viruses and lipoproteins. Previously, it has been mentioned that UC causes deformation and even breakage of vesicles and accumulation of other aggregates during the process. Density gradient centrifugation is highly effective in separation of vesicles without deformation, even though the gradient undergoes ultracentrifugation for a longer duration 16 h[344] or 24 h[345] and at higher centrifugal force (210,000×*g*) than UC.

The medium for density gradient isolation frequently includes a sucrose or iodixanol (OptiPrep) gradient. According to Chen et al[346], sucrose gradients achieves high level of purity that other methods are not able to provide. This method follows the same steps as standard ultracentrifugation, but with an addition of the sucrose cushion in the last step. That being said, there are several disadvantages. For example, this method is not suitable for low sample volumes as it requires several steps of centrifugation and can occasionally cause breakage of vesicles[327,347]; moreover, it is a time-consuming method as the last step includes 24 h of ultracentrifugation[331] that can prolong isolation for 2 days. Another disadvantage is a high cost[327,348] that prevents many research group even to consider it. In addition, it is not suitable for downstream applications (protein and RNA profiling[349]) and requires a verification of the absence of co-isolated materials[350].

The outcome of using density gradient separation over other methods often prevailed in plasma-derived exosomes based on their size similar to lipoproteins[351]. However, it has been shown that combining density gradient centrifugation with other purification methods leads to greater degrees of exosome purification[345].

2.2.4. Immunoaffinity capture

This method uses magnetic microbeads (streptavidin-modified are most common) with which exosomes get incubated with. Briefly, after incubation with magnetic beads, they recover by rinsing a column or magnetically separating exosomes microbead complex, washing

them in 1×PBS solution, centrifuging at the similar force as final step for UC method, eluting with a special buffer or even lysing with buffer for electrophoresis and further analysis[352].

Challenges in this method show the importance of establishing the correct ratio between antibodies, exosomes, and beads in characterization of melanoma cell–derived exosome[353]. However, as it shown in this study, it is possible to isolate specific exosomes based on a defined target, leaving unwanted vesicles aside. Other studies also confirm the immunoaffinity capture method allows to isolate subpopulation of EVs without contamination and with "retained biological activities"[354,355]. The same studies proposed that the immunoaffinity method coupled with other techniques involving physical separation or other isolation procedures gives a high purity of the final exosome elution. At the end, application of this method allows to eliminate large aggregates including unwanted proteins and even lipids[356].

2.2.5 Filtration-based techniques

Filtration techniques usually play an additional role to the other methods described in this section and is not used as a main method of isolation. Filtration is based on separation of vesicles based on their size or molecular weight, eliminating particles that are not included in the size-range of the vesicles of interest. Filtration can be used at any stage of isolation. For example, in the beginning of the process using media enriched in vesicles to remove larger vesicles and cell debris, and at the final step to ensure the presence of a particular size of vesicle in the solution[357]. Most often, filtration accompanies UC (plasma[358], uterine aspirates[359], urine[360], and other different biological fluids[361]) and SEC (CCM[336,362–364] and plasma[341]).

Membranes with pore diameters of 0.8, 0.45, 0.22, and 0.1 μm are most common in the isolation process[335]. Application of filtration method for exosomes isolation alone is still remaining challenging. Very often, vesicles get stuck to the membrane filter which results in their loss[360] causing filter plugging and deformation of filters[335,357,360]. Some proteins also adhere to the membrane, which results in loosing potential proteomic information[365].

Functional studies by Benedikter et al[336] have introduced a 0.22 μm filtration step aiming to concentrate and purify small EVs (sEVs). The same study also concluded that using 10 kDa filters show completely recovery of vesicles at a much higher concentration that when using 100 kDa filters, where recovery was only 40%[363,364]. On the other hand, several studies reported challenges where isolation of exosomes using a filtration method was not efficient. For example, the cryo-SEM microscopy analysis conducted by Heath et al[366] showed lipid droplets and other large contaminants combined with cell-derived EVs samples isolated by tangential

flow filtration. In contrast, another research group confirmed highly purified exosomes could be isolated by sequential filtration, which generated exosomes free from protein aggregates[333]. A notable advantage of tangential flow filtration is that it works well for large volume samples as has been reported by Buscatto et al[367].

2.2.6 Precipitation-based techniques

Precipitation methods have been designed for their simplicity. They usually include adding a solution that contains an organic solvent such as polyethylene glycol (PEG) or acetone, then quick centrifugation at low speed (3,000-5,000×*g*), and a wash with 70% ethanol. Garcia-Romero et al[368] found exosome isolation by PEG is a quick and low cost technique that provides high yield of EVs suitable for future biomarker discovery. A two-step PEG-precipitation was found to more successfully purify exosomes than other methods[369]. Rider et al[370] suggested that a higher PEG concentration than is conventionally used can increase precipitation of smaller vesicles and is therefore useful for isolation of exosomes. Further, the experiment was done on different biological fluids including plasma, saliva, urine, and CSF showing not only a high yield with retention of biological activities.

Interestingly, another research group[371] suggested that precipitation methods by PEG and PROSPR (Protein Organic Solvent PRecipitation) are ideal for biomarker discovery and specifically for therapeutic uses as they are both capable of removing abundant proteins from the sample. However, the same study reported that they were unable to image exosomes isolated by the PEG method. An attempt to isolate exosomes by PEG followed by washing and pelleting by UC was performed by Ludwig et al[369] on both small and large scales. The goal of their research work was to test the efficacy of the PEG method in concentrating sEVs. In order to prove the efficiency of this method, further investigation in detection of residual PEG particles in the final samples was performed by barium-iodide staining techniques. As a result, it had been confirmed that all PEG residues were washed out making this technique suitable for sEVs enrichment. Despite retaining their functional activities after PEG precipitation, those sEVs are not recommended for molecular analysis due to their low purity. In addition, the same study concluded that PEG precipitation is unable to separate different type of sEVs within the sample. It has been previously reported that molecular weight of PEG can affect the precipitation process[372].

A recent report by Gallart-Palau et al[373] presented an experimental workflow for isolating enriched EVs from the CNS using PROSPR method. According to their results, the percentage

of isolated EVs revealed that somewhere around 80% of observed vesicles were exosomes and 75% of identified proteins reported to be associated directly with exosomes. Their results confirm that PROSPR method is applicable to exosome isolation and can be easily and inexpensively performed and offers potential in clinical settings. On the other hand, there are a few limitations. Using organic solvents may interfere with the functional properties of EVs causing their fusion[371] and won't be suitable for a large sample volume. Although several studies have proven that PROSPR can be successfully used in exosome isolation and specifically with an increased concentration of exosome proteins. However, identifying tumor-specific proteins still remains challenging and application of PROSPR to this end needs further validation[335].

Charge-based precipitation coupled with PEG confirmed successful recovery of vesicles from small volume samples when tested on different biological fluids including saliva and human liver stem cells[374]. This study used various doses of protamine to induce exosomes isolation and evaluate the ability of EVs to retain their biological activities after isolation. Another research group led by Klymiuk et al[375] that applied the same method, but on an equine mesenchymal stem cell line reported vesicles aggregation, which didn't seem to be an issue in a previous study.

A novel "salting-out" technique proposed by Brownlee et al[376] works by mixing the sample with 0.1 M acetate buffer at pH 7.4 allows to rapid isolation fast without specialized equipment. Their study confirmed that salted-out EVs are indistinguishable from those obtained by well-known and preferable method ultracentrifugation. The efficiency of this method was confirmed by Kotmakçi et al[377] and Sáenz-Cuesta et al[378]. However, vesicle aggregation, contamination with non-EV proteins, the presence of polymers, and the need for an extra purification step are limitations of this method[356,377].

The one-step precipitation method from different biological fluids is also used in several commercial EV isolation kits, such as ExoQuick (System Biosciences), Exo-Spin (Cell Guidance Systems), Total Exosome Isolation (Invitrogen), and ExoPrep (HansaBioMed).

2.2.7 Microfluidic technologies

Microfluidic methods are relatively fast and efficient, but costly and require special equipment[379]. These methods operate on a micrometre scale and use combined strategies that allow efficient isolation. Currently, there are several devices that can be coupled

with as electrophoresis (blood and plasma samples)[380], magnetism[381,382], applied acoustics[383] (whole blood), and immunoaffinity[384].

A microfluidic system with an integrated acoustic-fluidic device is able to separate exosomes from other vesicles based on their size, as confirmed by nanoparticle tracking analysis (NTA)[383]. It requires as little as 50 μL of the sample[36]. In addition, the same study was able to demonstrate the removal of unwanted blood components, such as red and white blood cells. Another study that used an acoustic nanofilters was based on "in-flow size fractionation". It reported 80% exosome recovery rate from CCM and red blood cells[385]. Successful coupling of immunoaffinity capture and electrophoresis was shown by Vaidyanathan et al[386] who were searching for non-invasive biomarkers in cancer. Cho et al[387] discussed the concept of electro-mitigation; however this attempt was not partially successful for exosome isolation, but resulted in 65% recovery of EVs. The use of microfluidic devices for liquid biopsies, including the isolation of exosomes, and their role in capturing and detecting biomarkers has been recently reviewed[388].

"Lab-on-a-chip" methods use small sample volumes and can typically be carried using less hands-on time. This approach has proven successful in working with blood plasma samples, naming high viscosity and contamination with non-specific proteins as downside effects[389].

2.2.8 Commercial isolation kits

A large proportion of exosomes are lost in the process of purification, especially during separation from other subtypes of EVs, proteins, and cell debris. To combat this problem, commercial exosome isolation kits that take less time and provide high purity samples can be used.

There are several kits available on the market, including ExoEasy Maxi Kit (Qiagen), Pure Exo exosomes isolation kit (101Bio), and Exosomes Purification kit (Norgen Biotek). Most of them are very easy to work with and do not require specific equipment. The basic principle of commercials kits is sedimentation by using a polymeric agent. Depending on the kit, isolation can usually be done in a short time (within an hour) and following simple procedures[357]. The formation of pellets containing exosomes is achieved by mixing the sample with a provided solution and then centrifuging on low speed (700-1500×g). Current challenges for most kits are their cost, low protein yield, sample volume dependency, and inability to differentiate sub-classes of EVs[379,390]. The major drawback for commercial kits is that the

polymeric reagent[349] that can affect characterization of exosomes and their biological activities due to contamination with residual matrix[391], non-vesicular molecules[390], and other impurities associated with commercial kits[379].

2.3 LITERATURE REVIEW ON EXOSOME CHARACTERIZATION

2.3.1 Dynamic light scattering (DLS), nanoparticle tracking analysis (NTA), and Tunable Resistive Pulse Sensing (TRPS).

Three common methods for characterizing exosomes (such as counting and sizing) are DLS, NTA, and TRPS. As DLS was used extensively in this thesis, an overview of this technique included below. A brief description of other two techniques (NTA and TRPS) is also included for comparative purposes.

DLS can be used to determining the size distribution of exosomes and microvesicles in a fluid (Fig. 4). The sample is illuminated at a fixed angle and changes in the subsequent scattering pattern are monitored. Particles move randomly through the solution following Brownian motion. The movement velocity depends on the hydrodynamic diameter of the particle, the temperature and viscosity.

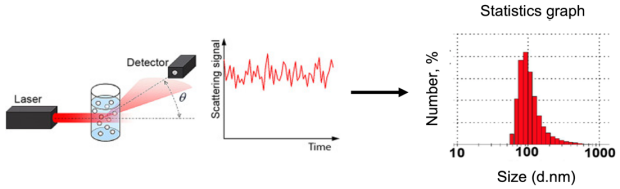

Figure 4. Dynamic light scattering (DLS) with example of analysis of EVs [392,393].

This Brownian motion causes changes in light scattering when a laser passes through the solution, proportional to the hydrodynamic size of the solutes. A diffusion coefficient of particles (D τ) can be used to determine from the data, and from this the hydrodynamic radius of the particles can be determined using the Stokes-Einstein's equation (eq 1):

$$D_\tau = k_B T / 6\pi\eta R \qquad \text{(eq 1)}$$

where k_B is the Boltzmann coefficient, T is the temperature, η is the viscosity, and r is the radius of the vesicle[394]. One of the biggest advantages of DLS is that it can measure particles

ranging in size from 500 nm to 6 µm, but it is predominantly useful for determining particle size when the samples contains monodisperse particles[395]. DLS struggles to calculate accurate particles sizes in polydispersed systems[396], due to the larger particles leading to a greater degree of scattering, making detection of small particles very problematic[397,398].

Several studies use DLS to characterize EVs from cell culture and plasma[4], ovarian cancer cells[399], and pre- and post-filtration frozen plasma[400]. Overall, DLS is useful in providing the diameter range of EVs. However, no other information such as morphology, subtype or other biochemical information cannot be determined by this method. Unlike DLS, NTA is an image-based method although it follows the same Brownian principles (Fig. 5).

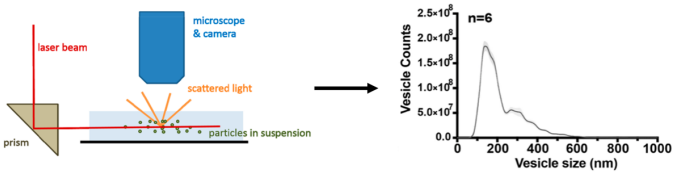

Figure 5. Nanoparticle tracking analysis (NTA) with example of analysis of EVs [393,396].

NTA allows characterization of vesicles on a single-particle level, which is critically important as EVs are known to be heterogeneous in size[401]. The sample preparation is as easy as for DLS and samples can be recovered after measurements. When preparing the sample, it is important to follow the protocol and bring the sample to correct concentration, viscosity, and dilutions. The recommended working concentration of EVs should be in the range of 2×10^8 - 20×10^8/mL[402,403]. In addition, refractive index (RI) should be considered[404,405] as it can influence detection limits along with pre-analytical conditions (preparation and storage)[402]. Gardiner et al[404] has identified RI for the variety of EVs in including urinary (fresh and lyophilized), neuroblastoma, blood, activated platelets, and placental (small and large) concluding that the values become much smaller as diameter of vesicles decreases. Other challenges might include air bubbles, temperature changes, and laser alignment[406,407].

The tunable resistive pulse sensing (TRPS) method (Fig. 6) is considered as one of the major techniques for EV characterization, including counting and sizing[350,408,409].

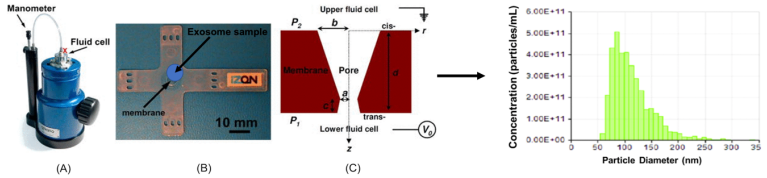

Figure 6. TRPS (qNano, Izon) system. *(A) The Izon qNano unit, (B) cross-shaped nanopore including the elastic membrane in the center of which exosomes will be applied (the size of pore can vary depends on the vesicles size), and (C) the cross-section of a pore with example of analysis of EVs*[410,411].

Before measurements, samples of EVs are diluted in a conductive electrolyte buffer and then applied in the middle of a membrane pore that is located on the top of fluid cell. EVs are measured as a result of a change in the electrical resistance when they move across the pore of the membrane. Each vesicle produces a resistive pulse that is used to measure the size of an individual vesicle. The vesicle concentration is proportional to the count of resistive pulses per minute. An advantage of TRPS is its ability to characterize a polydisperse sample, providing distinct peaks for each different size group. A disadvantage of this techniques is that larger EVs can cause blockage of membrane pores[408].

2.3.2 Microscopy-based characterization

Transmission electron microscopy (TEM) is commonly used for the imaging of EVs and can give an idea of the structure and morphology[395,412]. This technique has been extensively used in this thesis to validate morphology of exosomes and used in combination with immunoblotting that will be described later. Electron microscopy uses electrons that pass through the sample to form an image (Fig. 7). The image forms when the transmitted or the unscattered electrons hit a fluorescent screen that produces an image based on the density of the material. This image is then photographed by a camera. TEM needs to be done in vacuum as the electrons can be easily deflected. Additionally, the sample cannot be aqueous and needs to be dehydrated as imaging performed under vacuum conditions. This can affect structure and morphology[396]. To prevent that, the sample can be fixed with 4% paraformaldehyde (PFA) solution to preserve the original rounded shape[33]. Since EVs are composed of low electron dense atoms (for example, carbon), TEM of exosomes has decreased contrast of exosomes when compared to metal nanoparticles. For this reason usually a negative staining method (2% uranyl acetate solution) is used[396,413]. Immunolabeling techniques using gold nanoparticles (AuNP) conjugated with specific antibodies can be used to classify specific membrane proteins

expression on EVs surface[414,415]. The first study where the size distribution of the vesicles were reported at the single EV level was successfully conducted by Brisson et al[414]. Disadvantages of this method might include imaging under a non-native environment, some artefacts related to staining and sample storage, and vesicles deformation due to their dehydration[416]. Another point of disadvantages are long imaging hours, requirements of highly trained personnel, and sample preparation.

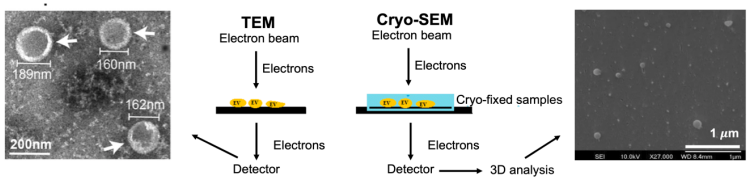

Figure 7. Transmission electron microscopy (TEM) and cryo-scanning electron microscopy (cryo-SEM) principle with example of analysis of EVs [393,396,417].

Cryo-scanning electron microscopy (cryo-SEM) allows imaging samples in their own environment as sample is being flash frozen and viewed below -100˚C (Fig. 7). This method, similarly to TEM, was used in this thesis to characterize morphology of exosomes, and was especially useful in assessing the purity of exosomes. This method is considered as one of the supplemental sources in confirming size and morphology of EVs. Unlike TEM, cryo-SEM does not have special procedures for sample preparation such as embedding and dehydrating. The sample simply gets immobilized by cooling it in liquid nitrogen. Cryo-SEM microscopy allows for superior quality images that confirms the rounded shape of vesicles, as has been reported by several research groups[418–421]. There has been a notable increase in use of cryo-microscopy, and it has even become a preferred method for examining morphology of vesicles as it is free of the dehydration-derived artefacts that can be found with TEM[420]. In addition, a few groups reported that different subcategories of EVs[422] and multilayered vesicles[419,423] can be also identified and detected. The diameter of vesicles analyzed by cryo-SEM can be slightly larger than TEM reported[424]. This can be explained samples remain hydrated during the imaging process and not desiccated as in TEM sample preparation, leading to liquid expansion when being cooled by liquid nitrogen. Challenges will included presence of frozen artefacts, low signal-to-noise ratio due to the sample thickness, sample preparation and operating skills on TEM[416,425]. Like TEM, cryo-SEM can be combined with immunoblotting with AuNP,

which has been successfully done by using EVs from different sources: embryo-endometrial[426], plasma[373,427], and platelets[414].

Atomic force microscopy is a well-known method for analysis at the nano scale that works by recording interactions between the probing tip and the surface of the sample (Fig. 8). It can be used in EV imaging and has been successfully reported in several studies[428,429].

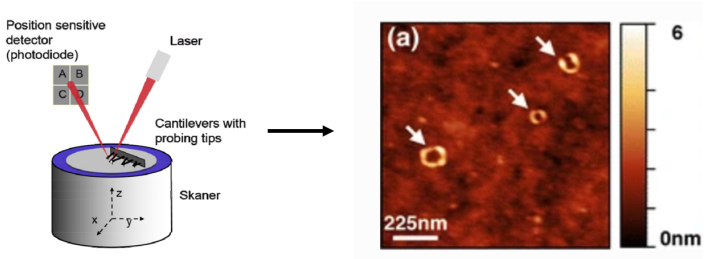

Figure 8. Atomic force microscopy principle with example of analysis of EVs [396,429].

Confocal immunofluorescent microscopy is a broadly used technique that is used to provide a high-resolution three-dimensional image with an ability to focus on a thin layer in the sample of interest. Frequently samples are labeled (via direct [430–432] and indirect [433,434] approaches) with a specific antibody conjugated to a fluorescent dye as shown in Figure 9. Briefly, a laser is focused on an objective lens after being reflected by a dichroic mirror. Once light excites the fluorophore dye it emits at a different wavelength and travels back through the objective lens and mirror creating an image (Fig. 9).

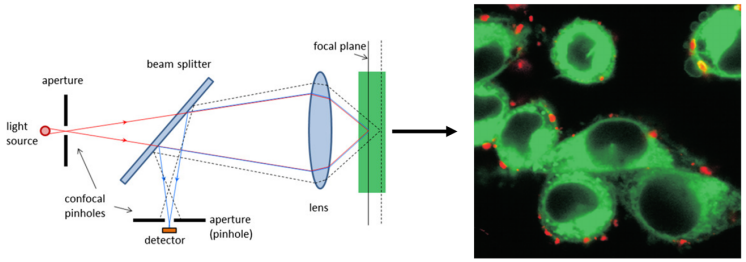

Figure 9. Confocal microscopy principle with example of analysis of exosomes stained with Cy5 (red). *Cell membrane is stained with PTK-7 (green)[435,436].*

Labeling of EVs does not always require use of antibodies. For example, a research study of the cellular uptake of prostate cancer-derived EVs led by Roberts-Dalton et al[433] reported that a novel thiol-based indirect labeling method allows imaging EVs over 6 h without compromising EVs' integrity and fully retaining their biological function in inducing differentiation of fibroblasts. Another successful example of indirect fluorescent labeling was described by Gangadaran et al[437] by using *Renilla* luciferase (Rluc) dye in EVs derived from thyroid cancer cells in mice. Visualization by fluorescence microscopy can be very useful in preparation for flow cytometry experiments, as will be briefly described below.

2.3.3 Flow cytometry

The principle of flow cytometry based on identifying particles in suspension passing through a laser beam collecting fluorescence from specific labels as well as forward and side scattered light. The data from the latter can be translated into particle size[438,439] (Fig. 10).

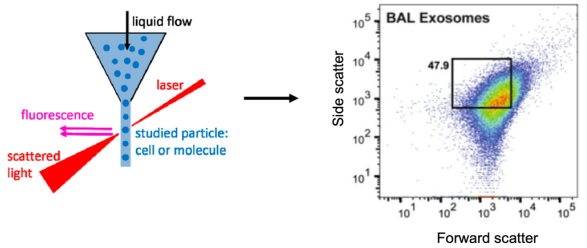

Figure 10. Flow cytometry principle[114,396]. *BAL- bronchoalveolar lavage*

Currently, flow cytometry is widely used in analyzing EVs (300-500 nm in size[396,440–442]) and their components[443] allowing collection of information about particles' phenotype, such as their number and size[396]. However, several studies reported detection of EVs in a size of 200 nm[444], 280 nm[445,446], and 160-200 nm[447,448]. Historically it has been notoriously difficult when applied to EVs due to their size, heterogeneity, and previous lack of markers that could distinguish a specific population of interest[449]. Conjugation of EVs with microspheres (polystyrene-organosilicate composites[450], streptavidin-coated particles[451], fluorescent multiplex beads[448,452], latex beads[453,454], and silica microspheres[406]) seems to be able resolve this issue. Application of conjugated EVs has been shown in characterization of serum exosomes of patients with pancreatic cancer[136] and EVs isolated from normal and pre-

eclampsia conditions in pregnant women[443]. A new algorithm based on Coulter principle[455] has been proposed for distinguishing between EVs and cells, cell debris, and other aggregates[447].

2.3.4 Western blot

Western blotting is one of the most widely applied bulk analysis techniques for EVs analysis (Fig. 11)[5,456]. WB techniques are routinely used to detect a specific protein of interest extracted from cells or other sources, including exosomes[38].

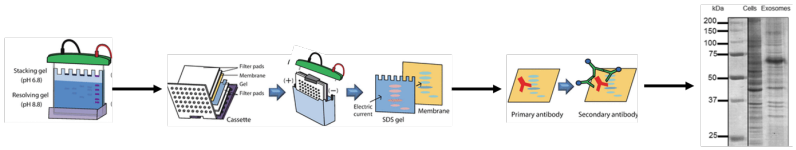

Figure 11. Western blotting technique [410,457].

Besides detecting and visualizing protein on a gel, it can also give a relative quantification of a protein in the sample. The process of blotting takes a few days as it includes several steps (protein separation by gel electrophoresis, their transfer to a membrane, and detection by antibodies). Each step is equally important. It is a very meticulous technique that combines the resolution of polyacrylamide gel electrophoresis with the specificity of immunoassays.

2.3.5 Liquid chromatography-tandem mass spectrometry (LC-MS/MS)

Liquid chromatography-tandem mass spectrometry (LS-MS/MS) has been frequently used in clinical studies allowing collection of data from protein analysis to identify biomarkers for various diseases[458]. This technique is very useful in applications if the sample is complex. Therefore, it can be a great asset for characterization of EVs. Separating analytes based on their physicochemical properties allows identification of their unique mass spectra (Fig. 12).

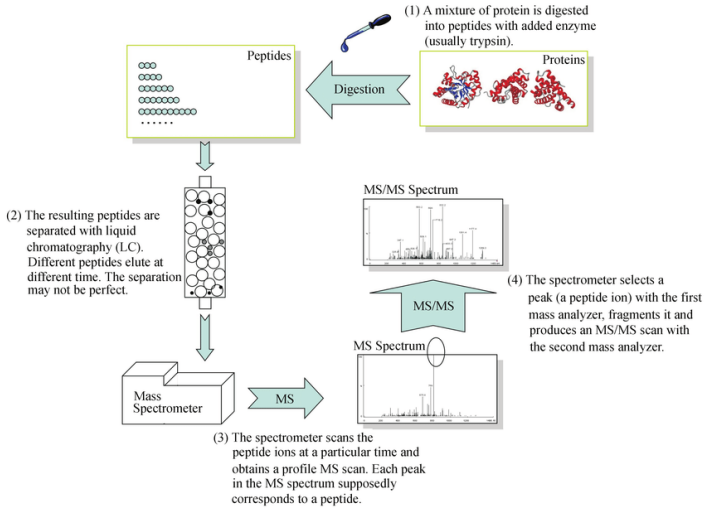

Figure 12. Principle of LC-MS/MS [459].

A sample for LC-MS/MS needs to be free from contamination with components that interfere with either the chromatographic separation or the mass spectrometry. This method of characterization will be described in Chapter 3.

2.4 METHODS

2.4.1 Cell culture

A549 cells (ATCC®), derived from lung carcinoma tissue, were cultured in Dulbecco's modified Eagle's medium with 10% heat inactivated fetal bovine serum (FBS) (Sigma, St. Louis, MO, USA) and 1% Penicillin (Gibco™, USA). After reaching 80% confluency, cells were washed with phosphate buffered saline (PBS) with a final concentration of 0.01 M (composition NaCl-137 mM, KCL-2.7 mM, Na_2HPO_4-10 mM) (later referred as 1×PBS), trypsinized, and collected by centrifugation (300×*g* for 5 min). Subcultures were made at a ratio of 1:3 in a 5% CO_2 humidified atmosphere at 37 °C for 2 days. After this time, the medium was replaced with fresh medium (washing, subculturing, and centrifugation steps were omitted) with a final concentration of 5% heat inactivated FBS for 24 h, and then bathed in

medium containing 2% exosome depleted FBS (Gibco™, USA) for 12 h to eliminate the risks associated with FBS background. The exosome-rich conditioned cell culture medium (CCM) was then collected to proceed with exosome isolation.

WI-38 cells (ATCC®), derived from normal embryonic (3 months gestation) lung tissue, were cultured in Eagle's minimum essential medium with 10% heat inactivated FBS (Sigma, St. Louis, MO, USA) and 1% Penicillin (Gibco™, USA). Subculturing and further steps were carried out as described above, except using medium and subculturing was undertaken using a ratio of 1:4.

2.4.2 Collection of breath-derived exosomes

To standardize EBC, no food was taken for 3 h prior to collection. Samples were collected from a single individual for three days. EBC was collected using a chilled tube assembly consisting of a mouthpiece through which breath was exhaled and a 15 mL , collection vessel. The subject exhaled for approximately 60 min, with condensate collected in a tube directly maintained at 0 °C. After the third collection, samples were pooled together. Collected EBC was filtered through 0.22 µm MF-Millipore MCE membrane (Millex-GS, Merck Millipore Ltd., UK). The collected EBC was kept in low protein-binding tubes and used within 3 days of preparation. The ethical application was not required as the leading researcher used its own breath. Three biological replicates were collected from the same individual. Each biological replicate was collected within three days. Each of these biological replicates was run in two technical replicates for proteomic analysis (Ch. 3) and in two technical replicates in western blotting. The total volume of each biological replicate was 36 mL.

2.4.3 Exosomes isolation by differential ultracentrifugation (UC)

To obtain CCM, cells were seeded at initial density 1.9×10^6 cells/mL reaching confluency 8.3×10^6 cells per T-75. Exosomes were isolated as described[327] with an additional step after the first centrifugation. Briefly, CCM from 3.7×10^7 cells first were centrifuged for 5 min at 300×*g* to pellet dead cells. Then for 20 min at 700×*g*, followed by 10 min centrifugation at 2,000×*g* to pellet cellular debris, 10 min centrifugation at 10,000×*g* and run through the 0.45 µm filter (Millipore, Millex-GP, gamma sterilized). Then CCM was concentrated by using ultrafiltration centrifugal concentrators with a molecular weight cut off 10 kDa (Pierce, protein concentrators, PES, 10 K MWCO). Recovered supernatant was collected from each step and

transferred to a new tube before taking the next centrifugation step. Then supernatant was centrifuged at 10,000×*g* for 30 minutes and recovered exosomes-rich supernatant was transferred to a clean polycarbonate bottle with cap assembly, 10.4 mL, 16×76 mm (Beckman Coulter, cat. 355603) and undergone 90 min spin at 100,000×*g* (Beckman Coulter Optima L-100 XP Ultracentrifuge) using type 70.1 Ti rotor, fixed angle, titanium, 12×13.5 mL rotor (Beckman Coulter Life Sciences). Then supernatant was decanted and exosomes were re-suspended in cold fresh Phosphate Buffered Saline (PBS) with a final concentration of 0.01 M ((composition NaCl -137 mM, KCl- 2.7 mM, Na_2HPO_4- 10 mM) (later labeled as 1×PBS), pH 7.4 (Thermo Fisher)). Then exosomes were centrifuged again for another 60 min at 100,000×*g*. This step was included as a washing step from any medium debris that could stick to exosomes. After the final step, supernatant was poured off and pellets (exosomes) were re-suspended in 100 µL of cold 1×PBS, pH 7.4 and stored at 4 °C for future experiments. Protein concentration in the breath exosomes sample was measured by using a micro-BCA assay (BCA Rapid Gold BCA assay kit).

2.4.4 Exosomes isolation by size exclusion chromatography (SEC)

Exosomes were isolated following standard methodology[329] modified as followed. First, CCM[328,460] underwent 5 min centrifugation at 300×*g*, then 20 min at 700×*g*, and finally at 10,000×*g* for 10 min. The collected supernatant was filtered through a 0.45 µm syringe filter (Millipore, Millex-GP, gamma sterilized) in order to separate microvesicles and remove unnecessary proteins and other biological materials. Then the volume of CCM was reduced to 0.5 mL using a centrifugal filter device protein concentrator with a molecular-weight cut-off of 10 kDa (ThermoFisher, Pierce Protein Concentrators PES, 10 K MWCO, 0.5 mL). A qEVoriginal column (Izon Science) was equilibrated with 1×PBS, pH 7.4 (phosphate buffered saline) buffer that was freshly filtered through a 0.22 µm (Millipore, Millex-GP, gamma sterilized). The first 5 fractions were voided (0.5 mL for each fraction) and fractions 6-10 were collected individually. Fresh isolated exosomes were dispersed in the same equilibration buffer. According to Izon Science, the peak of exosomes elution should be in fraction 8. That was confirmed later by TEM, DLS, and western blotting. Following use, the column was washed with 40-60 mL of the filtered buffer and stored vertically at 4 °C.

2.4.5 Preparation biological samples for transmission electron microscopy (TEM)

The exosome sample (4 µL) was mixed with 8% paraformaldehyde in equal parts (1:1 ratio, v/v) and dropped on a formvar/heavy carbon coated (300 mesh) grid (GSCU300CH-50, ProSciTech) that was previously plasma cleaned for 10 min. The sample was left for 10-15 min to dry, followed by 2 washing cycles with Milli-Q water. After, the sample was stained with 4% uranyl acetate for 15 min in the dark. The grid was washed again with Milli-Q water and air dried. Before imaging the sample, the grid was plasma cleaned for 10 min. Images were analyzed on Jeol 2100F using Gatan Microscopy Suite Software 3.0.

2.4.6 Synthesis of gold nanoparticles (AuNP)

AuNPs were synthesized according to the protocol described by Liu and Lu[461]. First fresh aqua regia was made by mixing HCl and HNO_3 in a 3:1 ratio and then used to soak two-neck 200-mL flasks, stopper, condenser, and magnetic stir bar for 25 min. Then all parts were rinsed several times in sterile deionized water. Secondly, Milli-Q water (98 mL) and 50 mM $HAuCl_4$ (2 mL) were added to a two-neck flask bringing the final concentration to 1 mM. The flask was then placed on a hot plate. When the solution began to reflux, the stopper was removed, and 38.8 mM sodium citrate (10 mL) was added resulting in color change from yellow to deep red. The solution was left to reflux for another 20 min under stirring. Once the solution was cooled down at RT, the diameter of nanoparticles was around 15 nm as measured by DLS. The size of AuNPs was further confirmed by TEM with defined size range of 18-20 nm. The magnitude of charge repulsion "ζ potential" was then measured by using DLS with a result of -35 mV.

2.4.7 Immunolabeling exosomes for TEM

Immunolabeling of exosomes was performed as described by Jung and Mun[415] with a few differences. A sample (4 µL) of freshly isolated EVs were dropped on a formvar/heavy carbon coated (300 mesh) grid (GSCU300CH-50, ProSciTech) that was previously plasma cleaned for 10 min and left to dry for about 20-25 min at room temperature (RT). An aliquot (5 µL) of primary antibody cocktail (anti-CD63 (mouse monoclonal (TS63), ab59479, Abcam) and anti-CD81 (mouse monoclonal (M38), ab79559, Abcam) tetraspanin general markers with a dilution ratio of 1:100 in 1×PBS containing 1% Bovine Serum Albumin (BSA), pH 7.4 was placed onto the exosomes. Sample were left overnight in a plastic container with a closed lid

secured with parafilm. Next day, the sample was washed in blocking buffer (1×PBS containing 1% BSA, pH 7.4) three times for 5 min each. Gold nanoparticles (AuNPs) were synthesized according to the method of Liu and Lu[461] described above in 2.4.6 and conjugated to the secondary antibody (m-IgGκ BP-HRP, sc-516102, Santa Cruz Biotechnology, INC) as previously described[415]. The grid was incubated with AuNP-conjugated secondary antibody (5 µL) diluted to a ratio of 1:500 in 1×PBS containing 1% BSA, pH 7.4 for 1 hour at RT in a sealed container and secured with parafilm to prevent evaporation. The grid then was washed 5 times with Milli-Q water, air dried, and stained with 4% uranyl acetate in the dark as described above. Before imaging, the sample was plasma cleaned for 10 min. Images were analyzed on Jeol 2100F using Gatan Microscopy Suite Software 3.0.

2.4.8 Cryo-scanning electron microscopy (Cryo-EM)

Samples were prepared by using the freeze-fracturing technique. The exosome sample (5 µL) was manually dropped on top of the sample stage and then rapidly cooled and frozen in liquid nitrogen. Then the frozen sample was transferred under vacuum to a cold preparation chamber (Alto 2500, Gatan) where the sample was mounted on the stage maintained at -140 °C and fractured to expose interior structural details of the sample. The sample was coated with platinum (5-10 nm) and imaged on a cryogenic scanning electron microscope (JSM6500F, JEOL) equipped with a 97 µA emission gun. All samples were imaged at a working distance of 8.4 mm using low acceleration voltage (10 kV).

2.4.9 Exosomes purification and characterization by western blot

Samples from breath (total volume of EBC 36 mL) and CCM from 3.74×10^7 cells (both cell lines) were assayed using western blotting to confirm that the isolation procedure produced purified exosomes. Isolation of exosomes was performed as previously described in 2.4.4, with blotting undertaken on samples from pooled fractions 7, 8, and 9 of SEC isolation as well as probing individual fractions isolated by use of the same qEV original columns (Izon Science) and from ultracentrifugation. Sterile medium free of exosomes and with no FBS added was used as negative controls. These negative controls were assayed to ensure that there were no contaminating proteins from media or supplements. Samples were suspended in lysis buffer (50 mM Tris-HCl pH 8.0, 150 mM NaCl, 1% NP-40) and subjected to two rounds of vigorous vortexing (10 s) and cooling on ice (20-30 min). Samples were finally centrifuged at 10,000×g

for 10 min. The pellet was discarded, and the protein concentration of the supernatant was determined using a micro-BCA assay (Pierce Rapid Gold BCA Protein Assay Kit) according to the manufacturer's instructions. Samples were mixed with 4× sodium dodecyl sulfate (SDS) sample buffer (0.2 M Tris-HCL, 0.4 M dithiothreitol (DTT), 8% SDS (w/v), 6 mM Bromophenol blue, 4.3 M glycerol) and heated for 5 min at 95 °C. Samples containing approximately 20 µg of protein were loaded on a 10% acrylamide gel, and proteins separated by electrophoresis. The western blot was performed according to the protocol described by Lim[462] with minor amendments: 5% BSA was used as a blocking agent; the membrane was probed with anti-CD63 at 1:800 dilution (TS63; Invitrogen, ref. 10628D), anti-CD81 at 1:800 dilution (M38; Invitrogen, ref.10630D) and secondary mouse monoclonal (goat anti-mouse) secondary antibody conjugated to Horseradish Peroxidase at 1:5000 dilution (Santa Cruz, sc-2031). Total loaded protein lysate ~ 20 µg/lane for all samples including negative controls. Blotting was performed using 2µg/mL of anti-CD63 and anti-CD81. The goat anti-mouse secondary antibody was used at a concentration of 0.08 µg/mL. The membrane was visualized on the ChemiDoc Amersham Imager 600 (General Electric).

2.4.10 Dynamic light scattering (DLS)

The hydrodynamic diameter of freshly isolated exosomes were measured using the Zetasizer ZS90 (Malvern Instruments, UK) as previously described[463]. All measurements were conducted at RT. Polydispersity index values varied in the range of 0.178-0.232. The size distribution profile of vesicles was obtained from three biological replicates, with each measured in triplicate. Each measurement was obtained from 12 runs following 30 s equilibration.

2.4.11 Statistical analysis

Analyses were performed using Prism GraphPad scientific 2D graphing and statistical software, version 9.1.1 (223) for macOS, April 16, 2021, San Diego, California. Data analysis for DLS measurements was completed using Malvern Zetasizer Software 7.12 (Malvern Instruments, Malvern, UK).

2.5 RESULTS

To characterize exosomes from EBC it was first necessary to optimize methods for isolation of pure, intact, and high-quality exosomes. To this end, exosomes obtained from conditioned medium from cultured A549 cells were isolated by two methods: ultracentrifugation (UC) and size-exclusion chromatography (SEC). A549 cells are derived from a human lung carcinoma and were chosen as a straightforward cell model of lung cancer. The WI-38 fibroblast cell line is derived from the lung tissue of a three-month gestational fetus and was chosen as a cell model of healthy lung tissue. Both cell lines were used at early passages (A549 passage 2 and WI-38 passage 3) and periodically monitored for any abnormalities in their morphology[464]. Initially, exosomes were isolated by ultracentrifugation. This method was chosen for its simplicity and compatibility with large volume samples. Figure 13 shows cryo-SEM images of the isolated exosomes.

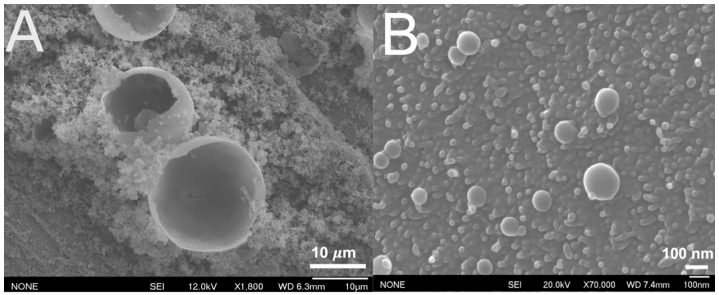

Figure 13. Characterization of UC-based isolated cell (A549)-derived exosomes by cryo-SEM. *On the figure: (A) other EVs and protein aggregates and (B) exosomes isolated from A549 cell culture model. Images are representative of two independent experiments. Scale bar 10 µm and 100 nm.*

Some of the disadvantages of this method previously described in 2.2.1 can be seeing on Figure 13 A, including possible mechanical damage of vesicles and co-isolated protein aggregates. However, much more pure samples (Fig. 13 B) were obtained following the optimization of UC. This included filtering exosome-enriched cell culture medium through a 0.45 µm filter after the 10,000×*g* centrifugation step, and pellet removal and re-centrifuging the isolated exosome at 100,000×*g* for a second time for another 60 min allowing them to wash in 1×PBS and then pelleted again by centrifugation, bringing the total centrifugation time to 2.5 h.

The second method of isolation, SEC, was tested in this study on the cell-derived exosomes from the same cell culture model (A549) with the goal of obtaining exosomes that

would be higher in purity comparing to UC method and intact after isolation. Figure 14 shows cryo-SEM images of the SEC-based isolated exosomes.

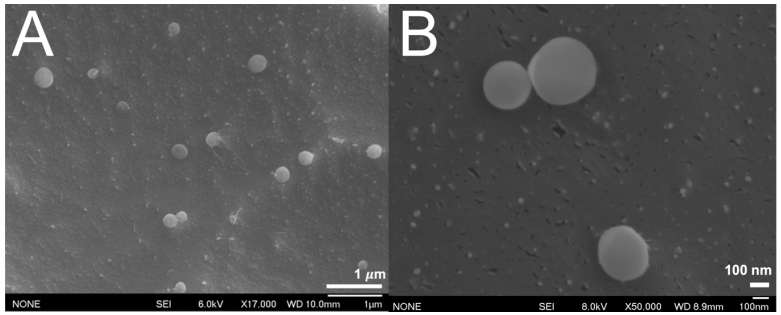

Figure 14. Characterization of SEC-based isolated cell (A549)-derived exosomes by cryo-SEM. *(A) Exosomes from pooled fractions 7-9 and (B) exosomes from pooled fractions 7 and 8 only. Images are representative of two independent experiments. Scale bar 1 μm and 100 nm.*

As expected[337], SEC-based isolation (undertaken using Izon Science qEV original columns) is highly effective at isolation of pure exosomes, preserving them in their intact shape (Fig. 14 A and B) and largely free of the membrane-like plaques or protein aggregates associated with the initial UC conditions[119,352] (Fig. 13 A). As anticipated[329], A549 cell-derived exosomes eluted from SEC after the column void volume which is represented by the first six 0.5 mL fractions. Although exosomes can be obtained from subsequent combined size exclusion fractions (fractions 7-9)[337] (Fig. 14 A), we found that the two fractions (7 and 8) (Fig. 14 B) immediately following the void volume gave the highest purity exosomes, showing a size range (45-100 nm) that is consistent with exosomes by cryo-SEM microscopy (Fig.15) and DLS (Fig. 16).

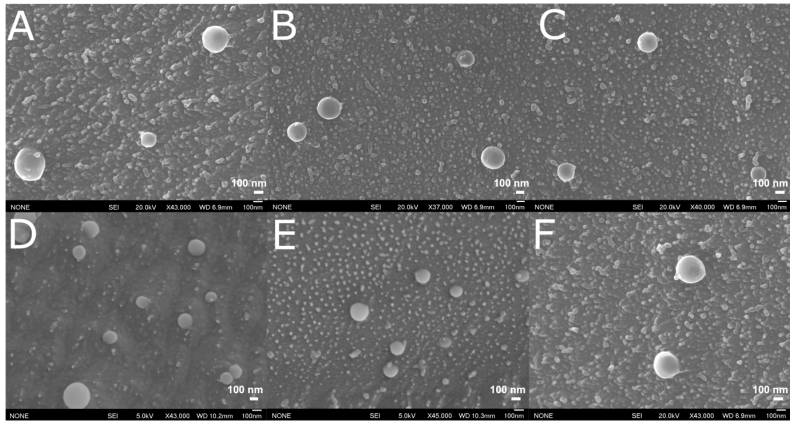

Figure 15. Cryo-SEM images of SEC-based isolated cell (A549 and WI-38)-derived exosomes. *Images are representative of individual fractions (A) 7, (B) 8, and (C) for A549 and (D-E) WI-38 cell-derived exosome for the same fractions respectively. Scale bar 100 nm.*

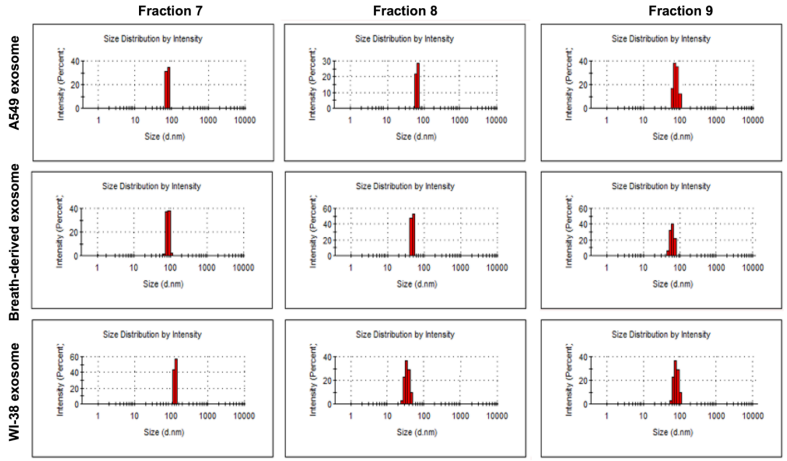

Figure 16. DLS analysis of cell- and breath-derived exosomes. *Size distributions of exosomes for fractions 7-9 isolated from A549, EBC, and WI-38. The polydispersity index (PDI) varied in the range of 0.178-0.232. The Y-axis shows intensity in percentage, and X-axis corresponds to the size of the vesicles (d. nm). The plots show the mean from all three biological replicates performed in three technical replicates and repeated three times. The error bar are not visible due to insufficient variability in the data.*

Although the DLS data suggest that vesicles in fraction 9 are similar in size to those from the earlier fractions, TEM analysis of individual fractions demonstrated that this fraction

contains smaller vesicles in some replicates (Fig. 17) and as a precaution against contamination, such later fractions should not be used where high purity exosomes are required.

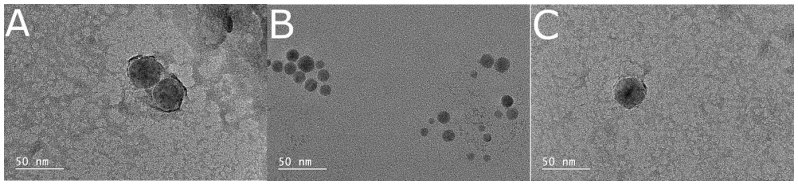

Figure 17. TEM images of smaller EVs of cellular and breath origin. *Images are representative of smaller EVs found in fraction 9 from (A) A549 cells, (B) EBC, and (C)WI -38 cells. Scale bar 50 nm.*

The optimized conditions were then applied to isolation of exosomes from WI-38 healthy lung tissue cell model and EBC. As can be seen in Figures 15 and 16, the vesicle sizes for each isolated fraction are consistent across the cell lines and EBC and are in the 45-100 nm range expected for exosomes in fractions 7 and 8 (Fig. 18).

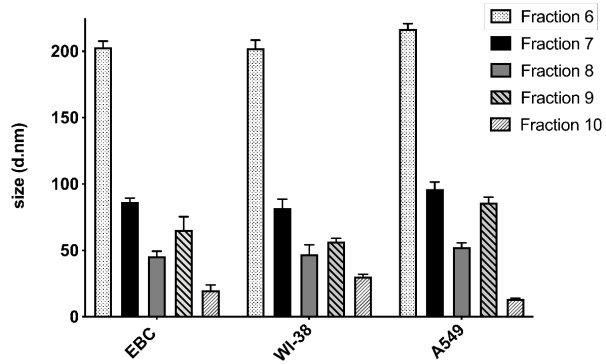

Figure 18. Size distribution of cell- and breath-derived exosomes. *The distribution of vesicle diameters (d.nm) as determined by DLS for SEC fractions isolated vesicles from EBC, WI-38, and A549 cells. The Y-axis corresponds to the size of the vesicles (d.nm). Data represents the average of three biological replicates, each evaluated through three technical replicates. Error bars represent the standard deviation of the biological replicates. The figure was generated by using Prism GraphPad Software (version 9.1.1) for macOS, San Diego, California.*

This was further confirmed through microscopy on breath-derived exosomes (Fig. 19). Again, vesicles from fractions 7 and 8 were consistent across replicates and of morphology

consistent with exosomes (Fig. 16). This confirmed that these fractions are suitable for use in the development of exosome-based diagnostics.

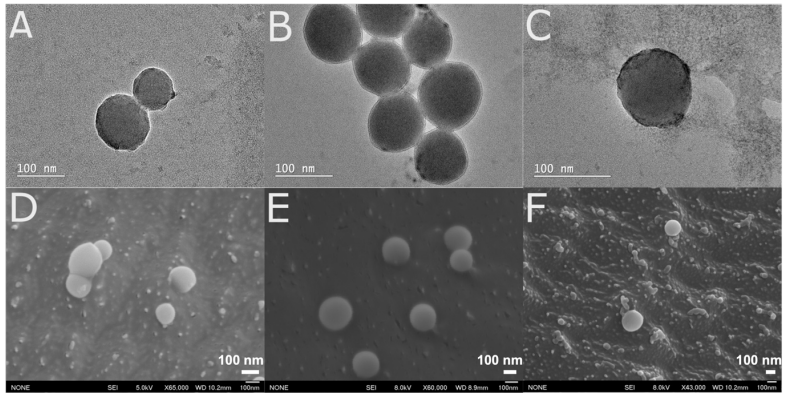

Figure 19. Characterization of SEC-based isolated breath-derived exosomes by TEM and cryo-SEM. *Images are representative of breath-derived exosomes isolated from EBC showing fractions (A) 7, (B) 8, and (C) 9 and cryo-SEM images of fractions (D) 7, (E) 8, and (F) 9. Scale bar 100 nm.*

The scanning transmission electron microscopy-energy dispersive spectroscopy (STEM-EDS) chemical mapping technique was used to distinguish exosomes from contaminants that might be present in the sample. This powerful analytical technique enabled analyzing the elemental identity of exosomes and was performed on exosomes isolated from EBC (Fig. 20).

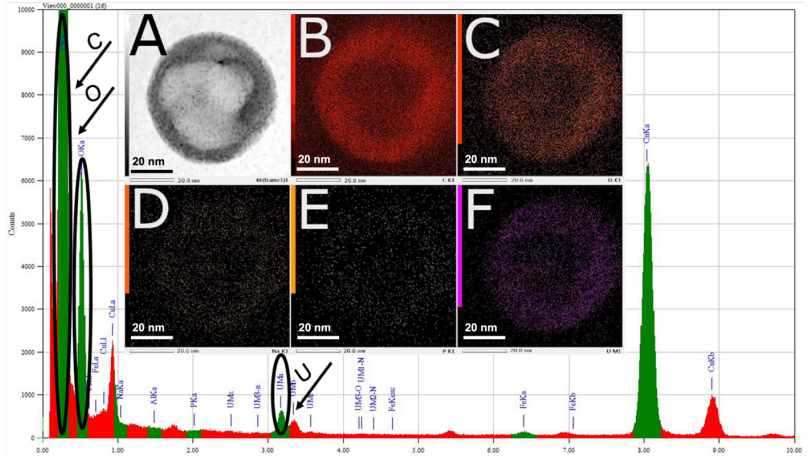

***Figure 20. STEM-EDS map and full EDS spectrum of a single breath-derived exosome**. Images are representative of a SEC-based isolated (fraction 8) single breath-derived exosome. EDS elemental analysis spectrum shows well-defined peaks of carbon, oxygen, and uranium labeled with an arrow. The elemental mapping includes (A) bright field image and elements identified in the vesicle: (B) carbon, (C) oxygen, (D) sodium, (E) silica, and (F) uranium. The Y-axis represents the number of counts per channel and the X-axis represents X-ray energy (keV). Scale bar 20 nm.*

The sample was placed on a copper grid and stained with uranyl acetate, explaining the presence of these otherwise unexpected elements in the EDS spectrum. The presence of abundant carbon and oxygen that maps as co-located with the exosome is consistent with it being of organic origin. This validation is important, as nanosphere impurities within the same size range as exosomes under certain circumstances were observed. These might arise from etching of lab glassware during buffer storage or autoclaving, as water etching of glass has been reported[465]. Silica nanoparticles of this size range are known[466] and this would be consistent with their STEM-EDS map and EDS spectrum (Fig. 21).

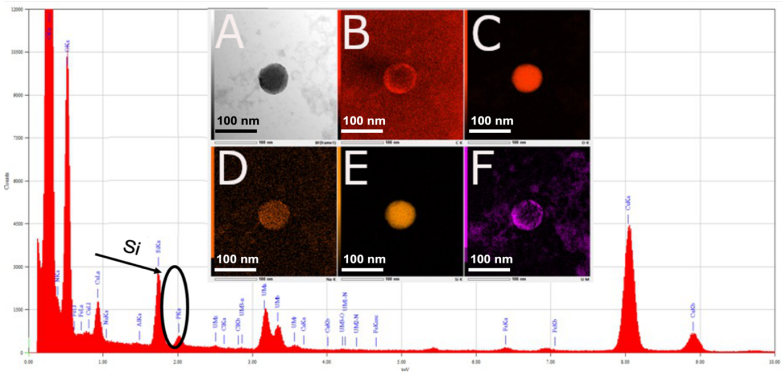

***Figure 21. STEM-EDS map and full EDS spectrum of a silica (silicon dioxide) ball**. Images are representative of a silicon dioxide ball that mimics morphology of exosomes. EDS elemental analysis spectrum shows a well-defined silica peak labeled with an arrow. The elemental mapping includes (A) a bright field image, (B) carbon, (C) oxygen, (D) sodium, (E) silica, and (F) uranium. The Y-axis represents the number of counts per channel and the X-axis represents X-ray energy (keV). Scale bar 100 nm.*

To confirm further that the isolated vesicles were exosomes, immunoblotting was performed using a cocktail of primary antibodies against CD63 and CD81, which are known general tetraspanin EV markers[467] (Fig. 22 A and B) that are embedded in the surface of exosomes. The immunoblotting was visualized using TEM through gold nanoparticles (AuNP) (Fig. 23), conjugated to a secondary antibody (m-IgGκ BP-HRP) that interacts with both primary antibodies. A negative control, when the sample was blotted only with the secondary

antibody, was performed to show that there was no non-specific binding (Fig. 22 C). This confirms that individual putative exosomes contain a relevant marker.

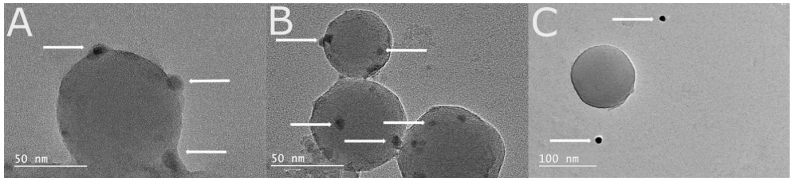

***Figure 22. Grid-immunoblotting-based exosome detection**. TEM images of exosomes from (A) WI-38 cells and (B) EBC treated first with a cocktail of anti-CD63 and anti-CD81 then with a secondary antibody conjugated to AuNP. (C) EBC exosomes were also treated only with the secondary antibody, indicating that association of the AuNP with the exosome is dependent on the presence of the primary antibody. White arrows on images point to selected AuNPs.*

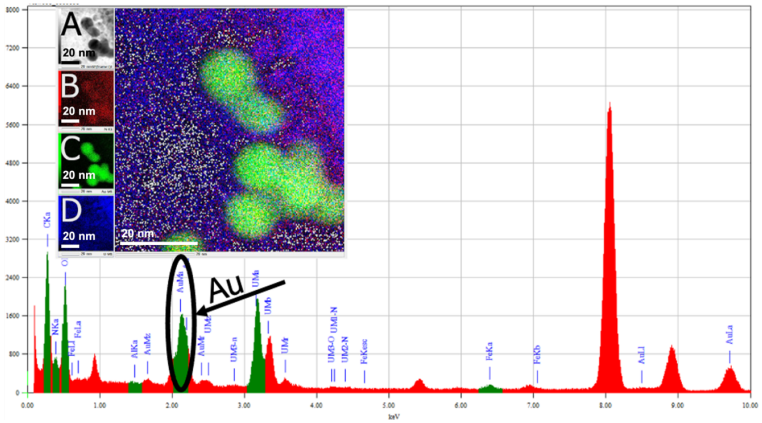

***Figure 23. STEM-EDS map and full EDS spectrum of AuNP used in grid-immunoblotting**. The images are representative of AuNP conjugated to the secondary antibodies used for immunoblotting. EDS elemental analysis spectrum shows a well-defined gold peak labeled with an arrow. The elemental mapping includes (A) a bright field image, (B) nitrogen, (C) gold, and (D) uranium including overlay of all elements. The Y-axis represents the number of counts per channel and the X-axis represents X-ray energy (keV). Scale bar 20 nm.*

In contrast, conventional western blotting approaches only report the average presence of markers within the sample for non-tumorigenic exosomes including cell- and breath-derived exosomes (Fig. 24 A) as well as their presence in the whole proteome of both cell lines (Fig. 24 B).

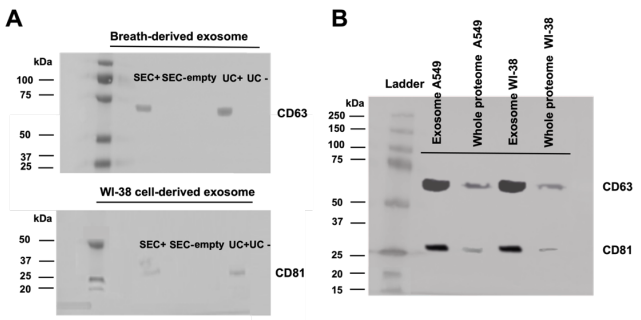

Figure 24. Validation of cell- and breath-derived exosomes by western blot analysis*. Western blot analysis using general tetraspanin EV markers CD63 and CD81 on cell (WI-38)- and breath-derived exosomes. (A) Samples that contain exosomes isolated by two different methods SEC (combined fractions 7-9) and UC are labeled SEC+ and UC+, respectively. Exosome-free negative samples (matching total protein content to exosome samples) are also shown and isolated by the same methods are labeled SEC- and UC-, respectively. The selected markers demonstrate that the methodology of breath exosome isolation is equivalent to the established isolation methods from cell culture medium. (B) Validation of the same markers is also shown on cell-derived exosome isolated by UC from A549 and WI-38 cells and their whole proteome.*

2.6 DISCUSSION

It is well known that cell culture media can contain several types of membrane vesicles, including apoptotic blebs and microvesicles in addition to exosomes [22,31, 38,39]. Because of this, the purification steps used to isolate exosomes are critical to yield and purity. Although, UC is a simple and low-cost method of extraction that is amenable to large sample sizes, vesicles isolated through UC were found to be fragmented and impure (Fig. 13 A). This is consistent with previous observations[468,469] and can be explained as the consequence of shearing force that can potentially change the original morphology of the vesicle deforming it[325,470].

Previous studies have also found that vesicles isolated by UC do not demonstrate the purity associated with other forms of isolation[337,352], which makes results from use of the samples uncertain. Although immunoaffinity capture gives high quality exosomes[352], we chose to use SEC as it is not biased towards exosomes bearing the particular markers chosen for immunoaffinity capture, but generates similarly pure exosomes[337,352]. A feature of SEC is the ability to optimize towards yield or purity. As our envisaged use for breath-derived exosomes is for development of diagnostics, we optimized for purity, rejecting fractions from the size exclusion column that are likely to contain contaminating vesicles or protein aggregates. However, in the later stages of this study, the UC method was re-considered and applied with

several modifications leading to isolation of exosomes with much higher purity than originally isolated via UC. The rationale behind this decision is explained in Chapter 3 (3.3.1).

Whilst our isolation protocol delivered samples with a relatively homogeneous range of sizes that are consistent with exosomes, further phenotyping[471,472] was required to confirm that these breath-derived vesicles are genuine exosomes. This phenotyping provides characterization of breath-derived exosomes that is missing from current literature. Exosomes derived from breath are consistent with those from other sources.

Our experience is that breath exosome samples stored for more than a day begin to lose their well-defined morphology and artifacts begin to appear in samples analyzed through microscopy (Fig. 21). Whilst we have used both TEM and cryo-SEM in this phenotyping work, we found that cryo-SEM provides better definition of morphology of the vesicles, as noted by Wu et al[91]. The composition of the isolated vesicles is fully consistent with exosomes, being comprised of organic matter (STEM-EDS) and having a protein content consistent with conventional cell-derived exosomes.

The use of STEM-EDS is a valuable method of distinguishing exosomes from silica nanospheres, which can be readily mistaken for exosomes based on microscopy alone as they are morphologically similar. Early in our method optimization, silica contamination was found when running STEM-EDS elemental analysis. It seemed likely that these contaminants came from the glass used in reagent storage. Analysis of PBS stored in glass confirmed that it is a potential source of silica contamination (Fig. 21). Our methodology delivered breath-derived exosomes that were free of silica nanosphere impurity through use of a 1×PBS buffer that was prepared on the day it was to be used and immediately transferred to high grade plasticware following filtration (0.22 µm MF-Millipore MCE membrane (Millex-GS, Merck Millipore Ltd., UK)).

The average of size of the particles was roughly similar across the major exosome-containing fractions as would be expected following size exclusion chromatography. The vesicles are in the range of 45-100 nm as seen by DLS, cryo-SEM and TEM. STEM-EDS demonstrates that they are of organic origin, and the isolated EVs are confirmed to contain protein. Evidence from microscopy, DLS, and protein composition points to the need to undertake careful method development for demanding applications, such as diagnostics. Based on the results of this study, only a narrow range of size exclusion fractions are found to contain clean exosomes. Fractions eluting after these are contaminated with smaller structures (Fig. 17) and high protein content. In general, protein concentration is indicative of exosome concentration[38]. However, this will not be true where vesicles are contaminated with protein

aggregates. Normalising the protein concentration to DLS intensity, acting as a useful proxy of exosome concentration, powerfully illustrates this with the last collected sample fraction containing up to approximately 10 times more protein per unit of isolated exosomes than the pure exosome fractions. Given their potential use in protein-based diagnostics, it is particularly important to avoid such protein contamination in purified exosome fractions.

The immunoblotting-grid technique was used to validate the presence of the general tetraspanin EV markers CD63 and CD81 which are embedded in the surface of exosomes. These were first described by Brlansky and Derrick[473] in detection of plant viruses, but have since been used extensively as exosome markers[415,416]. Whilst technically demanding, this technique provided a high standard of proof that the exosome-specific markers are located on the purified exosomes.

2.7 CONCLUSION

The aim of this chapter was to describe the isolation of cell- and breath-derived exosomes and characterize them using physicochemical methods. We aimed firstly to optimize the methodology to isolate exosomes that are sufficiently high quality from cell-based sources and, secondly, to apply the optimized methodology to isolate exosomes from human breath. Following this, phenotyping of breath exosomes was carried out by comparing them to cell-derived exosomes. This study provides detailed characterization and comparison of two methods of isolation: ultracentrifugation and size-exclusion chromatography.

Through careful characterization, this study confirms that exosomes can be isolated in a highly purified form from breath. Using size exclusion chromatography, these exosomes can be isolated in sufficient purity to be used for diagnostic purposes, such as proposed for early-stage detection of lung cancer. These demanding applications require highly purified exosomes. Isolation based on size exclusion chromatography should be linked to different tests to determine which fractions contain exosomes of sufficient purity. We found that a subset of chromatographic fractions is reproducibly of high standard, passing metrics on morphology, size, exosome-located markers, and protein contamination. The application of ultracentrifugation gave samples that were pure as those obtained from size-exclusion chromatography, whilst having the advantage that isolation from large sample is possible with several modifications.

Phenotyped exosomes from EBC are equivalent to exosomes isolated from more conventional sources, such as cell culture media. The findings from this chapter will allow us to characterize breath-derived exosomes with a goal to determine whether exosomes obtained from WI-38 cells provide a valid proxy for breath-derived exosomes using bioinformatics techniques based on the identified proteomes (i.e., compare WI-38 cell proteome to human breath proteome). In addition, proteomic analysis of exosomes from cell models of normal lung tissue (WI-38 cells) and lung cancer (A549 cells) will be used to propose biomarkers. Western blotting technique will be used to test whether proposed biomarkers of lung cancer from the cell studies are absent from the exosomes of breath of healthy human volunteers.

CHAPTER 3. PROTEOMIC PROFILING CELL- AND BREATH-DERIVED EXOSOMES AND PROPOSED BIOMARKERS

Aim:

The aims of this chapter were to 1) define the proteome of exosomes from cell models of normal lung tissue (WI-38 cells) and lung cancer (A549 cells) to demonstrate that it is possible to identify potential biomarkers of lung cancer and evaluate whether those may be revealed on exosomes to develop a proof-of-principle test using cell culture model and 2) determine the benchmark proteome from breath-derived exosomes and use those exosomes as a negative control to test the proposed putative biomarkers of lung disease.

Objectives:

1. Identify the proteins found in cell- and breath-derived exosomes using proteomic methodology.
2. Use proteomic analysis of exosomes from cell models of normal lung tissue (WI-38 cells) and lung cancer (A549 cells) to propose biomarkers of lung cancer.
3. Determine whether exosomes obtained from WI-38 cells provide a valid proxy for breath-derived exosomes using bioinformatics techniques based on the identified proteomes. Use western blotting to test whether proposed biomarkers of lung cancer from the cell studies are absent from the exosomes derived from the breath of healthy human volunteers.

3.1 INTRODUCTION

3.1.1 Overview of proteomics

One of the first steps towards modern-day proteomics was the introduction of two-dimensional gel (2D-gel) by O'Farrell in 1975[474], who developed the protein separation technique while studying *Escherichia coli*. This technique was able to resolve 1100 different components with a maximum of 5000 proteins. Although electrophoresis allowed for separation of proteins, there was difficulty in separating hydrophobic and extremely acidic or basic proteins[475] and had low reproducibility[476]. At that time, Edman degradation was the main technique for protein identification through sequencing and was of low sensitivity[477]. The major improvement in proteomics was associated with creating the first database of proteins based on 2D gels analysis. The prototype of this database was the result of 3 years' work of

electroblotting and isoelectric focusing done by Aebersold et al[478–480] who realized the great potential of internal sequencing analysis.

The word "proteome" was created by Mark Wilkins while doing his PhD studies at Macquarie University in Australia and represent two worlds "PROTEin" and "genOME" combined together. The term "proteomic" appeared in 1995 and was defined as a large-scale characterization of the entire set of proteins that plays a critical role of all living organisms, tissues and cells[481]. Mass spectrometry was used in proteomic studies as it could provide molecular fingerprinting to identify proteins.

With its further development, proteomics split in several branches relating to slightly different experimental goals. For example, protein expression (comparing proteomes between samples), structural proteomics (determination of atomic resolution three-dimensional protein structures on a genome-wide scale in order to better understand the relationship between protein sequence, structure, and function)[482], functional proteomics (characterization of enzyme activities as well as protein-protein interactions), proteome mining (drug discovery target), and finally post-translational modification analysis including phosphorylation, glycosylation, methylation, acetylation, amidation, and many other types[483,484].

Since the introduction of 2D gels, proteomics has become more established, and new technologies related to sample preparation and analysis have emerged. Nowadays, the three pillars of human proteomics include protein fractionation techniques (complex protein or peptide mixtures), mass spectrometry technology to acquire the data for individual protein identification, and bioinformatic analysis (those steps will be described later in this chapter)[485]. Before proceeding with sample preparation, the methodological approach of the experiment has to be chosen. There are two main methodological approaches: bottom-up and top-down proteomics. The choice of the most suitable approach depends on the type of study being undertaken, such as proposing biomarkers or developing a protein-based drug.

3.1.2 Proteomic approaches and techniques in identification of proteins and reliable biomarkers

There are two common approaches for protein characterization: bottom-up and top-down approaches. Each of them has their own advantages and disadvantages. The bottom-up approach with label-free quantification for identification of proteins is based on spectral counting of identified matched peptides after MS/MS analysis. This was a primary method used in this study and is explained in detail below. Two other strategies, labeling and chemical

tagging, are also considered bottom-up approaches. For comparative purposes, the top-down approach is also briefly introduced.

Bottom-up proteomics is often used in large-scale studies of proteins. This method is based on digestion of proteins (in-solution or in-gel) before they can be identified through liquid-chromatography-tandem mass spectroscopy (LC-MS/MS). Once the sample is in the instrument, peptides are separated by LC, ionized, volatilized, and passed into the first mass spectrometer (MS-1), which then separates those ions based on their mass-to-charge ratio (m/z). Peptide ions are fragmented into daughter ions in a collision chamber and passed through to the second spectrometer (MS-2), which separates and detects the fragment ions, also based on their m/z values. Substantial informatics analysis allows determination of the sequence of peptides detected in MS-1 based on the MS-2 daughter fragment ions. These sequences are used to predict the proteins present in the original sample[486]. Various schemes of quantification are available, which are based on the signal intensities at either MS-1 or MS-2. MS-2-based quantification is most common if the original sample is a complex mixture.

Bottom-up proteomics is a widely used method of protein identification with an absolute quantitation of protein expression. There are several strategies that have been developed to assist with better quantification. The most employed are metabolic labeling, chemical tagging, and label-free quantification.

The metabolic labeling approach uses stable isotopes to label amino acids in cell culture (SILAC) during cell growth and division. Since first introduced in 2002, this method uses signal quantification from MS-1 spectra and was described by several groups[487–489]. The method was developed to allow accurate quantification of the differences between different cell populations, such as a treatment and control in an experiment. One cell population is cultured in standard culture media, while another cell population is incubated with media containing isotopically labeled amino acids, typically including arginine or lysine containing six ^{13}C labels. The treatment population can be combined with the control, yet still be distinguished by mass spectrometry as one is “heavy” (containing the isotopically labeled amino acids) and the other is “light” (containing non-labeled amino acids). Mixing populations allows greater sensitivity in the experiment and higher reproducibility as treatment and control are quantified simultaneously in the same LC-MS/MS run. Simultaneous quantification is achieved in the mass spectrometry spectra as each peptide will appear as a doublet that has distinct mass differences, the heavy or light version. Based on the relative mass spectrometry signal intensities from the mixed population, the differential protein abundances between two

samples can be calculated by comparing the intensity differences of the pair of isotope labeling peaks in mass spectrometry[490].

Two common methods of quantification use chemical tagging: isobaric tags for relative and absolute quantification (iTRAQ) and tandem mass tags (TMT)[491]. Both approaches are based on defining intensity of reporters ions of different masses that are released from isobarically labeled peptides[492,493]. Because of the isobaric nature of these tags, they have identical physicochemical properties, more specifically identical masses. Tagged samples, for example from treatment and control cell populations, can be mixed, and peptides from each population appear in MS-1 as a single composite peak reporting the same mass value and resulting from the same retention time. Following fragmentation of the labeled peptides, MS-2 based quantification generates reports of ion peaks from different tag fragment masses and so allows quantification of the different cell populations under study. Both iTRAQ and TMT tags have the same general components: reporter and balance groups and label amino termini of peptides and the side chains of lysine. However, the structure of the isobaric tags differs between the approaches. iTRAQ uses 4-plex and 8-plex isobaric tags[494], while TMT uses 2, 4, 6, 10, 16-plex[495] and even 27-plex[496]. Based on their molecular differences, iTRAQ and TMT use different isobaric tags to simultaneously identify and quantify proteins.

Whilst labeling methods, such as SILAC, iTRAQ and TMT can be multiplexed, label-free quantification is usually chosen if several separate samples need to be compared as it allows comparison of a sample with any other samples, whereas in labeled experiments, samples directly compared with those samples that were physically mixed and measured together with a control in one run. There are currently two fundamentally different approaches: quantification of ion intensity (changes in either peptide peak areas or peak heights) and quantification of spectra (spectral counting of identified matched peptides after MS/MS analysis). The second of these was used in this study.

The principle of chemical tagging for both techniques is generally the same. The iTRAQ and TMT markers are used for labeling proteins inside living cells. Both techniques can label proteins from multiple sets of data (treatments and controls). For example, changes in protein abundances can be compared between cancer and non-tumorigenic samples[497]. Although the principle of labeling peptides is the same, their molecular structure and labeling specification are different.

In one approach to quantification of ion intensity, the area for the m/z peak of each peptide is determined, as this has a linear relationship to peptide concentration. This approach has some challenges with reproducibility and can result in different peak intensities depending

on the machine settings and sample preparation. Unlike quantification of ion intensity, spectral counting, which was used in this study, compares numbers of identified MS/MS spectra from the same protein present in the same sample in each of multiple LC-MS/MS datasets[493]. While this approach does not require complex data analysis compared to the quantification of ion intensity approach, normalization is required. This approach had been usefully demonstrated in studies that directly relate to this project: biomarker identification[498] and the ability to distinguish between cancerous and non-tumorigenic cells[499].

Top-down proteomics is based on analysis of intact proteins without use of enzymatic digestion. Unlike the bottom-up approach, top-down proteomics retains more information about the parent proteins in the sample, and so is most likely to identify PTMs that cannot be detected through the bottom-up approach.

3.1.3 Proteomics studies of exosomes

Although isolation and purification of exosomes is challenging[357,500,501], several studies have presented comparative proteomic analyzes of exosomes and circulating EVs from different biological fluids[174,502,503].

Recently, numerous studies have reported that the composition and content of exosomes can be used for cancer diagnosis (Tables 1 and 4). Proteomic studies demonstrate that exosomes carry a complement of proteins that indicates the nature of their cell of origin.

This will include proteins that can be used as biomarkers of disease, facilitating use of exosomes in a cancer diagnostic device. Using exosomes for diagnostics based on proteomic analysis requires high purity exosomes, free of contamination from other EVs or protein aggregates. This requires careful attention to the isolation methodology (as demonstrated in Chapter 2), which may need to be matched to the source of exosomes, as obtaining high quality exosomes from some biological materials can be especially challenging.

In the past 20 years, mass spectrometry studies have been investigating the composition of exosomes in order to facilitate biomarker discovery. The specific protein cargo of exosomes arises from the combination of the parental cell type and its environmental conditions as previously described in 1.1.3. Both bottom-up and top-down proteomic approaches have been applied to the study of the protein profile of exosomes. Early proteomic analysis of vesicles mainly concentrated on characterization of highly abundant proteins that were separated using 2D gels and then characterized by matrix-assisted laser desorption ionization-time of flight mass spectroscopy (MALDI-TOF-MS), through which important exosome markers

(tetraspanins, annexin, and heat-shock proteins) were identified. At that stage only a small number of proteins could be identified. Later, with an improvement of EV isolation techniques[504], protein separation, and mass spectroscopy, thousands of proteins from various types of biological samples have been identified and the integrated web-accessible database (Vesiclepedia) has been created[505].

A comprehensive study of the exosome proteome was undertaken by Choi et al[506]. This study acknowledged that mass spectrometry analysis can identify “thousands of vesicular proteins” and so proceed with their cataloging and other interrelationships. This study explored protein-protein interaction of mammalian vesicles underlining the topology of exosome proteins. By using integrated proteomic data, they were able to generate a platform that identifies protein-candidates related to EVs. Extensive studies over the past 10 years have attempted to characterize the exosome proteome and especially the cancer exosomal proteome. This interest in the proteome of various sources of exosomes arises from a desire to develop clinical diagnostic tools for early detection or monitoring of disease. For example, comparative proteomic evaluation has been reported on exosomes isolated from different biological fluids, such as urinary exosomes[507], circulating serum exosomes[508], and seminal plasma exosomes[509] as well as proteome of specific cancer related exosomes such as bladder cancer exosome[510] and ovarian cancer exosomes[78].

3.2 METHODS

3.2.1 Protein precipitation for cell- and breath-derived exosomes

Exosomes were purified as described in 2.4.1. Collected exosomes were lyzed with 8 M urea solution following flash-frozen (-80°C)/thawed cycle (hot running tap water) repeated 3 times. The lysate was vortexed for about 10 s between each cycle. Then samples were centrifuged at 13,000×*g* for 5 min and protein rich supernatant was collected and transferred into clean Eppendorf LoBind tubes. Then proteins were precipitated by addition of 400 µL of acetone per 100 µL of supernatant followed by chilling at -20 °C. After 1 hour, vials were vortexed and centrifuged at 13,000×*g* for 10 min. Acetone was carefully pipetted and residual acetone was removed by air-drying, providing a dry protein pellet for analysis. The pellet of proteins was collected from the bottom of the Eppendorf tube, resuspended in 10 µL of 8 M urea, and kept for further analysis.

3.2.2 Whole proteome precipitation

Cells (A549 and WI-38, 2.1×10^7cells/each cell line) were detached with trypsin, transferred to a 50 mL centrifuge tube (Falcon®), and centrifuged at 300×*g* for 5 minutes. Medium was decanted and pellets were washed twice with 5 ml of ice-cold 1×PBS. Pellets then were recentrifuged at 300×*g* for 5 min. PBS was decanted and pellets were subjected to lysis with 8 M urea following flash-frozen (-80°C)/thawed cycle (hot running tap water) repeated 3 times. The lysate was vortexed for about 10 s between each cycle while the sample was in liquid phase. Samples were centrifuged at 13,000×*g* for 5 min, and protein-rich supernatant was collected and transferred into a clean Eppendorf tube. Proteins were precipitated by addition of 400 µL acetone per 100 µL of supernatant, followed by cooling to -20 °C. After 1 hour, vials were vortexed and centrifuged at 13,000×*g* for 10 min. Acetone was carefully aspirated, and residual acetone was removed by air-drying. The pellet of proteins was collected from the bottom of the Eppendorf tube, resuspended in 10 µL of 8 M urea, and kept for further analysis.

3.2.3 Protein quantification assay

A Pierce BCA Rapid Gold protein assay kit (Thermo Fisher) was used to quantify the amount of protein in the sample following manufacturer's instructions. First, two-fold serial dilutions of an albumin standard (BSA) were performed, covering protein concentration in a working range of 20-2000 µg/mL. A 20 µL aliquot of each of the standard dilutions was added to a 96-well microtiter plate in triplicate. Then, 10 µL of a cell- or exosome-derived protein sample was added to each well (in triplicate) in the same 96-well plate and brought up to 20 µL final volume (2-fold dilution). The working reagent was made by following the ratio 50:1 (reagent A: B, v/v). Then 200 µL of the working reagent was added. The plate was wrapped in aluminum foil and left on the bench for 10 min. The absorbance of the samples was determined at excitation wavelength (λ_{ex}) of 480 nm and emission measured at a wavelength (λ_{em}) of 525 nm using an EnSpire 2300 multilabel plate reader (Perkin Elmer). The blank absorbance (buffer + working reagent) value was measured and subtracted from the absorbance value of the standards and all samples. The protein concentration of each sample was determined through application of the BSA standard curve, which was constructed using Prism GraphPad software (version 9.1.1 (223)) for macOS, April 16, 2021), San Diego, California.

3.2.4 Protein digestion (in-solution)

Protein pellets from acetone precipitation were treated with dithiothreitol (DTT) to a final concentration of 10 mM. Samples were wrapped in foil, vortexed and heated at 56 °C for 15 min followed by another 15 min incubation step with agitation (shaking) at RT. Samples were alkylated with 10 mM iodoacetamide (IAA) at RT in the dark for 30 min and diluted with high-grade LC-MS water so that the residual urea concentration was no more than 2 M. The protein concentration was determined as described in section 3.2.3, and sufficient quantity of trypsin was added so that it was present in a 1:50 ratio (trypsin: protein, w/w). The solution was carefully mixed and incubated overnight at 37 °C. The resultant peptides were purified using 100 µL OMIX C18 tips by using different stock solutions: washing solution (0.1% trifluoroacetic acid (TFA)), conditioning solution (50% acetonitrile (ACN)/water, v/v), and elution solution (50% ACN/water, v/v/0.1% formic acid (FA)) as follows: 100 µL of conditioning solution was aspirated and solvent was discarded. This step was repeated 10 times. From this point, no air was drawn into the tip. The same cycle was repeated but with 100 µL of washing solution finishing the equilibration step and moving on to the sample binding step. The sample was loaded into tip and then dispensed. This aspirate-dispense cycle was repeated 5 times for maximum efficiency. After aspirating 100 µL of washing solution, the solvent was discarded. The washing step was repeated 4 times. For the final, elution step, 100 µL of elution solution was aspirated and the peptides in the total volume of 100 µL were eluted into a new vial. Eluted peptides were transferred into a SpeedVac vacuum concentrator (Labconco CentriVap Concentrator, 78100-00) attached to the CentriVap Ultra-low cold Trap (Labconco, model 7811021; with specification -50 °C and 99.3% sample recovery). After drying samples for 40 min, completely dried peptides were resuspended in 20 µL of 0.1% FA and then transferred to a glass sample vial for LC-MS/MS analysis.

3.2.5 Protein digestion (gel-tube method)

Protein pellets precipitated from exosomes as described in 3.2.1 were resuspended in 20 µL of 8 M urea solution. The purification began with making gel plugs. To a 20 µL sample of resuspended protein, 2% SDS (20 µL of 10% SDS stock), water (30-35 µL), 7.5% acrylamide/bis-acrylamide (25 µL), 0.25% tetramethylethylenediamine (TEMED) (0.25 µL) were added making a final volume of 100 µL. The sample was vortexed and centrifuged until all bubbles disappeared. To that, 0.25% ammonium persulfate (APS) (5 µL) was added to

initiate polymerization. The tube was briefly vortexed and rapidly centrifuged. After polymerization, the formed gel plug was fixed in 2% phosphoric acid, 30% ethanol for 1 hour. Briefly, the fixative solution was added on top of gel plug, the gel plug was lifted with clean plastic tip, and tube was placed upside-down on a rocking table. After an hour, the fixing solution was replaced with fresh 2% phosphoric acid and 30% ethanol solution and fixed for another hour. Then solution from the tube was aspirated and gel plugs were left in 30% ethanol for 1 hour to shrink (at this point, gel plugs can be stored at -20 °C if the experiment needs to be split into several days). After, the 30% ethanol solution was discarded, and gel plugs were cut into 2 mm sections and each section into approximately 2 mm^3 pieces. Gel pieces were placed into a clean 2 mL Eppendorf tube, washed four times with 400 µL 75% ACN, 25% NH_4HCO_3 at 25 mM, and then dehydrated with 400 µL ACN. The ACN was removed. Reduction of disulfide bonds was initiated by adding DTT to a final concentration of 10 mM to cover all gel pieces. Samples were wrapped in foil, vortexed, and heated at 60°C for 30 min followed by alkylation with 55 mM IAA at RT in the dark for 20 min. After the alkylation, the solution was aspirated, and gel pieces were washed 3 times in 200 µL 25 mM NH_4HCO_3 and 200 µL ACN and dehydrated twice with 200 µL ACN. Trypsin was added at a 1:100 (trypsin: protein, w/w) ratio in a volume sufficient to cover all gel pieces and incubated overnight at 37 °C. To extract peptides, 200 µL 60% ACN in 0.1% FA solution was added for 1 hour under agitation. The solution containing digested peptides was aspirated and transferred to a clean vial. To further extract peptides, 160 µL 100% ACN was added for 30 min under agitation. The solution after the second extraction was aspirated and pooled together with the first collected extract, bringing the final volume to 360 µL. Gel pieces then were discarded. The peptide solutions were dried in a CentriVap and resuspended in 0.1% FA as described in 3.2.4.

3.2.6 Peptide quantification

The peptide mixture (resuspended in 10 µL of 0.1% FA) obtained following method (peptide digestion) was quantified using a Pierce Quantitative Fluorometric Peptide assay kit (Thermo Fisher) following manufacturer's instructions. The fluorescently labeled peptides were detected using a fluorescence plate reader (EnSpire 2300 multilabel plate reader, Perkin Elmer) with excitation wavelength (λ_{ex}) of 390 nm and emission measured at a wavelength (λ_{em}) of 475 nm. For the measurements, 10 µL of the peptide digest assay standard (1 mg/mL), 1.5 mL, tryptic digest of a protein standard, in 50 mM ammonium bicarbonate and 0.05%

sodium azide provided with the kit and processed purified protein samples were transferred in a fluorescent-compatible black 96-well microplate (ThermoFisher). Peptide digest assay standard was prepared in 1:2 fold dilutions. Then, 70 µL of Fluorometric Peptide Assay Buffer was added to each well followed by 20 µL of Fluorometric Peptide Assay Reagent added to each well. After 5 min of incubation time measurements were taken. The standard curve was used to determine the peptide concentration of each unknown sample.

3.2.7 Matrix-assisted laser desorption ionization-time of flight mass spectroscopy (MALDI-TOF-MS)

For mass spectrometry analysis, 1 µL of protein-containing eluate was purified using 100 µL OMIX C18 tips and mixed in a 1:1 ratio (v/v) with α-cyano-4-hydroxycinnamic acid matrix. The matrix was prepared fresh on the day of the experiment. To 10 mg of the previously mentioned matrix (ThermoFisher) 50:50 water/ACN (v/v) with 0.1% TFA final concentration was added. The mixture was first vigorously vortexed for 1 min to dissolve (some undissolved matrix will remain), then centrifuged for 20 sec at 2,000×*g*, and transferred to a new tube. In duplicate, 1 µL of the final solution was deposited onto reusable target AB SCIEX Opti-Tof™ Cal Mix 5 plate with 384 sample positions and allowed to air dry. The AB SCIEX TOF/TOF™ 5800 matrix-assisted laser desorption/ionization time-of-flight tandem mass spectrometer (MALDI-TOF-MS) was calibrated using 700-4000 m/z calibration mix. Tandem mass spectrometry was performed on the 20 most intense peaks in each sample, generated by applying 8,000 laser power per spot. To assign identities to the sample, the ProteinPilot™ (SCIEX) software (v.5.0)[511] was used.

3.2.8 LC-MS/MS analysis (cell-derived exosomes and whole proteome)

The peptide mixture (resuspended in 20 µL of 0.1% FA) obtained following method 3.2.4 was quantified using a Pierce Quantitative Fluorometric Peptide assay kit (Thermo Fisher) following manufacturer's instructions. The fluorescently labeled peptides were detected using a fluorescence plate reader (EnSpire 2300 multilabel plate reader, Perkin Elmer) with excitation wavelength (λ_{ex}) of 390 nm and emission measured at a wavelength (λ_{em}) of 475 nm. For the measurements, 10 µL of the peptide digest assay standard (1 mg/mL), 1.5 mL, tryptic digest of a protein standard, in 50mM ammonium bicarbonate and 0.05% sodium azide provided with the kit and processed purified protein samples were transferred in a fluorescent-

compatible black 96-well microplate (Thermo Fisher). Peptide digest assay standard was prepared in 2-fold dilutions. Then, 70 µL of Fluorometric Peptide Assay Buffer was added to each well followed by 20 µL of Fluorometric Peptide Assay Reagent added to each well. After 5 min of incubation time measurements were taken. The standard curve was used to determine the peptide concentration of each unknown sample. After quantifying the peptide abundance, each sample was checked using MALDI-TOF/TOF by using α-cyano-4-hydroxycinnamic acid matrix for the presence of contaminants. Then 10 µL of peptide samples described in 3.2.4 - 3.2.5 were placed in mass spectrometry vials with inserts and subjected to LC-MS/MS on a QExactive plus Orbitrap mass spectrometer (Thermo Fisher) with a nanoESI interface in conjunction with an Ultimate 3000 RSLC nanoHPLC (Dionex Ultimate 3000). The LC system was equipped with an Acclaim Pepmap nano-trap column (Dinoex-C18, 100 Å, 75 µm x 2 cm) and an Acclaim Pepmap RSLC analytical column (Dinoex-C18, 100 Å, 75 µm x 50 cm). The tryptic peptides were injected to the enrichment column at a flow of 5 µL/min of 2% ACN (v/v) containing 0.1% FA (v/v) for 5 min before the enrichment column was switched in-line with the analytical column. The eluents were 5% DMSO in 0.1% formic acid (v/v) (solvent A) and 5% DMSO in 100% ACN (v/v) and 0.1% FA (v/v) (solvent B). The flow gradient was (i) 0-6 min at 3% B, (ii) 6-95 min, 3-22% B (iii) 95-105 min 22-40% B (iv) 105-110 min, 40-80% B (v) 110-115 min, 80-80% B (vi) 115-117 min, 80-3% and equilibrated at 3% B for 10 minutes before the next sample injection. The QExactive plus mass spectrometer was operated in the data-dependent mode, whereby full MS1 spectra were acquired in positive ion mode, 70 000 resolution, automatic gain control target of $3e^6$ and maximum injection time of 50 ms. Fifteen of the most intense peptide ions with charge states ≥2 and intensity threshold of $1.7e^4$ were isolated for MS/MS. The isolation window was set at 1.2 m/z and precursors fragmented using normalized collision energy of 30, 17 500 resolution, autonomic gain control target of $1e^5$ and maximum IT time of 100 ms. Dynamic exclusion was set to be 30 s. Raw files were processed using Proteome Discoverer software v2.4 (Thermo Fisher) against the entire SwissProt human proteome database (TAXID-9606, v2019).

3.2.9 LC-MS/MS analysis (breath-derived exosomes and whole breath)

Samples were injected using the auto-sampler on an UltiMate 3000 liquid chromatography system (Thermo Fisher) connected inline to the Orbitrap Fusion™ Lumos™ Tribrid Mass Spectrometer (Thermo Fisher) fitted with the Nanospray Flex NG ion source. Xcalibur 4.2 software (Thermo Fisher) was used for method set up (Orbitrap HCD-Low Load

with peptide concentration less than 500 ng), control of the LC-MS/MS runs and data acquisition. Peptides were separated using a flow rate of 0.3 µL/min and fractionated with a C18 column (Dionex, LC Packings, Netherland). A 85-min buffer gradient was constructed from 0.1% buffer A (60% ACN, 40% high performance liquid chromatography-grade water (v/v), and 0.1% FA 10mM ammonium formate) and buffer B (0.1% FA in 80% ACN, v/v). This consisted of a linear gradient of 96% Buffer A to 4% Buffer B to 100% Buffer B over 60 min. 100% Buffer B was maintained for 5 min, before dropping back to 4% Buffer B in 96% Buffer A over 5 minutes. The eluted peptides were ionized for detection by the Orbitrap Fusion™ Lumos™ Tribrid Mass Spectrometer (Lumos) by electron spray ionization with a silica tip emitter and the instrument's conditions set to 2.5 kV voltage and transfer tube temperature of 275 °C. Ions with m/z range between 200 - 2000 m/z were analyzed during the 85-min acquisition time using Fourier transform mass spectrometry (FTMS) in the Orbitrap, with data-dependent MS/MS on the top 6 intensity ions dynamically selected for collision-induced dissociation (CID) fragmentation and detection in the LTQ. The dynamic exclusion settings used were as follows: repeat count 2, repeat duration 30 s; exclusion list size 500; exclusion duration 90 s. A full scan (50 ms maximum injection time) in the FTMS at a resolution of 30,000 identified the 6 highest abundance ions and selected them for CID (1.5 isolation width, normalized collision energy 35%, activation Q 0.25, activation time 30 ms) in the LTQ after accumulation of 500,000 ions with 10 ms maximum injection time was used as MS2 isolation option. Between sample runs was a wash of a gradient from 2% Buffer B to 98% Buffer B across 30 min. Mass spectra were analyzed with both Sequest HT and Mascot search methods using Proteome Discoverer software v2.4 (ThermoFisher) against the entire SwissProt human proteome database (TAXID-9606, v2019). Parameters were set to a maximum of 2 missed cleavages with peptide lengths ranging from 5 to 144 amino acids selected. A precursor mass tolerance of 10 ppm and fragment mass tolerance of 0.8 Da with fixed cysteine carbamidomethylation modification.

3.2.10 Lipid contamination removal (ethyl acetate wash)

The wash followed the protocol that was used for period detergent removal from processed peptides samples[512]. First, water-saturated ethyl acetate was prepared by mixing 10 mL of Milli-Q (Millipore) water and 80 mL of ethyl acetate in a 125-mL glass bottle. The bottle was capped with its glass stopper and vigorously shaken for 1 min at RT breaking the water

into small droplets. The bottle was then set to rest for 5 min. The shake-rest cycle was repeated 3 times. The solution containing peptides were transferred to a glass vial. All following procedures were performed using a glass vial to avoid PEG contamination while using organic solvents. Then, 1 mL of water-saturated ethyl acetate mixture was added to the peptide solution, the cap was closed, and the contents vortexed vigorously on a shaker for 1 min at RT. The sample then was centrifuged for 15 sec at 12,000×*g* to separate the ethyl acetate phase from the aqueous phase. After organic phase separation, the upper level of ethyl acetate was carefully aspirated by using a glass Pasteur pipette. A small quantity of organic phase was left to prevent the loss from the aqueous peptide-containing phase. This cycle was repeated 3 times. After the final round of the cycle, the remaining small amount of organic phase was removed by placing the sample in a SpeedVac (Labconco CentriVap Concentrator, 78100-00) attached to the CentriVap Ultra-low cold Trap (Labconco, model 7811021; with specification -50 °C and 99.3% sample recovery) for 5 min at RT.

3.2.11 Exosomes characterization by western blotting

Cell- and breath-derived exosomes were assayed using western blotting to validate proposed biomarkers established after mass spectrometry analysis. Isolation of exosomes was performed as previously described in 2.4.3. Negative control samples free of exosomes were also assayed. Samples were suspended in lysis buffer (50 mM Tris-HCl pH 8.0, 150 mM NaCl, 1% NP-40) and subjected to two rounds of vigorous vortexing (10 s) and cooling on ice (20-30 min). Samples were finally centrifuged at 15,000×*g* for 10 min. The pellets were discarded, and the protein concentration of the supernatant was determined using a micro-BCA assay (Pierce BCA Protein Assay Kit) according to the manufacturer's instructions. Samples containing approximately 20 µg of protein were loaded on a 10% acrylamide gel, and proteins separated by electrophoresis. The western blot was performed according to the protocol described by Lim[462] with minor amendments: 5% BSA was used as a blocking agent and samples were heated for 15 min at 65 °C; the membrane was probed with several primary (monoclonal and polyclonal) antibodies as follows: primary monoclonal – Alix (1A12; Santa Cruz, ref. sc-53540) at 1:800; anti-CD63 (TS63; Invitrogen, ref. 10628D) at 1:1000 dilution; anti-CD81 (M38; Invitrogen, ref. 10630D) at 1:1000 dilution, and secondary mouse IgG kappa binding protein (m-IgGk BPP) conjugated to Horseradish Peroxidase (HRP) (Santa Cruz, ref. sc-516102) at 1:3000 dilution. Primary polyclonal unconjugated antibodies (all rabbit/IgG), all from Invitrogen: RhoC (ref. PA5-77866) at 1:300 dilution; MYOF (ref. PA5-53134) at

1:300 dilution; SLC2A8 (ref. AP5-42463) at 1:1000 dilution; CD151 (ref. PA5-78960) at 1:1000 dilution, and secondary goat anti-rabbit IgG conjugated to HRP (Santa Cruz, ref. sc-2004) at 1:3000 dilution. All exosome (cell- and breath-derived) and whole breath samples were loaded on a 10% acrylamide gel as pure purified proteins at concentration 100 ng in total volume of 10 µL, while whole proteome samples were loaded as lysate at 20 µg in a total of 20 µL. The membrane was visualized on a ChemiDoc Amersham Imager 600 (General Electric).

3.2.12 Breath samples collection from volunteers

Collection of breath samples was conducted through a study that has been approved by VUW human ethics committee (application #28700: Determining disease biomarkers in breath-derived exosomes for new diagnostic tools; approved September 9, 2020). The national Health and Disability Ethics Committee defined the project as being out of scope for their review. Both documents can be found in Appendix.

Fifty-five participants (30 males and 25 females), who were non-smokers and free from known lung disorders or severe breathing disorders, participated in the study. Each participant was breathing into a tube for a maximum of 30 minutes, producing on average 1.5-2 mL of EBC. A total of 60 samples was collected, as five participants (four males and one female) donated breath twice and contributed to two samples. These 60 individual samples were divided into three equal groups, with samples pooled (V_{total} typically 34 mL) three days after collection. The third sample was collected from volunteers that did not participate in either of samples one or two.

Given the situation related to COVID-19 at the time, we ensured that participants were not at-risk during sample collection. Before collecting the sample, the consent form was given to familiarize participants with procedure and steps. A standard operating procedure description was kept in the lab where principal investigator conducted the research. Each participant was given a sterile tube assembly (see attached picture showing the assembly), which was wrapped with an ice pack to keep it cool (Fig. 25).

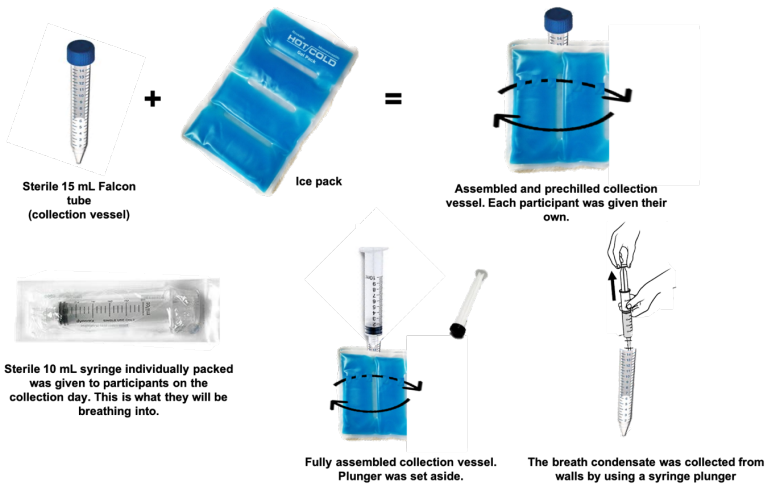

Figure 25. Collection vessel assembly for exhaled breath condensate.

Sample collection required each participant to blow into a tube used to collect the condensate through a cooled collection vessel. The diameter of the tube allowed participants to breathe normally, although there is a small risk of developing dizziness. The list of participants was kept separately. The time, date, volume, and a label 'Exhaled Breath Condensate' of collected sample was written on the same collection vessel that a participant used during the study. Once a sample had been collected, it was stored at 4 °C and pooled with other samples approximately every 3 days. Combined samples were transferred into a new tube and re-labeled with the new date and volume only. This procedure continued until a minimum of 20 samples had been collected. After combining samples, the original tubes were discarded.

3.2.13 Statistical analysis

Analyses were performed using Prism GraphPad scientific 2D graphing and statistical software, version 9.1.1 (223) for macOS, April 16, 2021, San Diego, California. Regression analysis was used to fit a straight-line model for the Rapid Gold BCA protein assay standard curve.

Area-proportional Venn diagrams were generated using BioVenn[513] for the comparison and visualization of identified proteins in all samples used in this study.

STRING (v11.5)[514] was used to visualize major protein complexes identified in the core of the breath exosome proteome. The network of identified proteins was constructed with minimum required interaction score with a high confidence threshold (STRING confidence score >0.7). The confidence score is the approximate probability computed by combining probabilities from the different evidence channels and corrected for the probability of randomly observing an interaction that a predicted link exists between two enzymes in the same metabolic map in the KEGG database. Disconnected nodes from the network were removed.

GO enrichment analysis was performed using Shiny GO v0.61[515] and g:Profiler (version e104_eg51_p15_3922dba)[516]. Shiny GO v0.61 is based on a large annotation database derived from Ensembl and STRING that allows graphical visualization of enrichment analysis and gene characteristics along with an ability to retrieve information of protein network and KEGG pathways. g:Profiler was used to perform gene ontology enrichment analysis based on statistical significance (p-value <0.05).

3.3 RESULTS

3.3.1 Optimization of analytical methods

Developing standardized procedures for isolating high-quality and purity of intact breath exosomes was essential for identification of biomarkers. Previous research methods were adapted and optimized for this study. Remaining issues and limitations of the research were noted.

The methodology was developed using cell-derived exosomes, providing reproducible access to a ready supply of exosomes for method optimisation. The most difficult part in this project was collecting sufficient exosome protein for proteomic characterization. It was important to maximize the yield of exosomes so that a sufficient amount of protein can be extracted for mass spectrometry analysis. Due to the low abundance of protein in exosomes in sample sizes used in the earlier characterisation work described in Chapter 2, it was obvious that it was necessary to adapt the previous isolation approach to collect a larger amount of exosomes. This was achieved by combining several samples together and using concentrators to reduce the volume of the starting material (CCM or EBC) and simultaneously to pellet different possible non-exosome protein aggregates from the exosomes. Initially, samples for proteomic analysis were isolated by SEC. However, when mass spectra were collected from several runs, it was not possible to analyze samples, as the amount of protein was so low that

no well- define peaks were present on a chromatogram. SEC-isolated exosomes provided only half of the amount of protein obtained from UC-isolated exosomes. Based on results from Chapter 2 and the fact that optimization of UC method led to better purity, the UC isolation method was chosen as it most readily provided the required increase in the volume of the starting material (CCM and EBC). However, choosing an appropriate method for exosome isolation that results in higher yield was only the part of the problem. Protein loss was identified as the main challenge that needed to be overcome. It seemed that protein and peptide adsorption onto surfaces such as tubes and tips in the experiment occurred during the sample preparation leading to low recovery of proteins during sample preparation. Several solutions were evaluated that could prevent non-specific sample adsorption. For example, during the first step of protein extraction, several lysis buffers containing components such as 8 M urea, 6 M urea +2 M thiourea, and NP-40 were compared to determined highest product outcome after protein isolation, with the 8 M urea lysis buffer being the most effective. The concentrations of proteins in the samples were 0.868, 2.439, 0.535 mg/mL. During this step, it was found that the BCA assay is not practical for determination of protein concentration. Determination of protein concentration using the Lowry assay was also rejected due to lack of sensitivity for these low abundance samples. Finally, the Rapid Gold BCA assay was chosen as the most compatible with all chosen buffers, whilst offering the required sensitivity.

At the next step, protein precipitation and solubilization of proteins, several protein precipitating reagents were tried, such as methanol and chloroform, or acetone. The greater protein recovery was achieved with the acetone precipitation method, with a total peptide quantification 934 ng vs 498 ng for an equivalent sample using methanol and chloroform. To investigate whether the organic solvent plays a difference in adsorption, simultaneous testing of different vials (regular Eppendorf tubes vs LoBind tubes vs glass vials) was conducted. While the application of detergents/organic solvents is required for the extraction of hydrophobic proteins and necessary to maintain proteins solubility in solution after their precipitation, organic solvents in the peptide sample can suppress the ionization signal and so must be removed prior to LC-MS/MS analysis. In this study, water-saturated ethyl-acetate wash applied immediately after digestion of proteins to remove lipid contamination. As shown later in the results section, this washing step played a positive role by increasing peptide signal intensity. It has also resulted in the excellent reproducibility of signal intensities for all samples.

Although preference was given to traditional in-solution tryptic digestion, an attempt to try an alternative method of protein digestion was made. The decision was based on the hypothesis that low quantity of proteins might be caused by hydrophobic membrane proteins

that are difficult to re-dissolve after acetone precipitation. The gel-tube method described in 3.2.5 is a novel approach aimed to enhance analysis of complex membrane proteins, was proposed as an alternative approach. This method skipped the precipitation step and suggested higher quantity of proteins after elution.

To achieve reliable quantitative LC-MS/MS measurements, the injection volume for each sample was determined individually. The injection volume was selected based on the peptide concentration to prevent overloading the column, avoid broadening the peaks, and produce high-performance separation. To ensure that carryover was reduced during the mass spectrometry runs, different combinations of washing/flushing steps for the injection path were tested to remove residuals from previous samples and autosampler components.

3.3.2 Evaluation of peptide recovery after traditional in-solution digestion and gel-tube methods on cell-derived exosomes

To prepare a proteomic sample, the most common method, digestion in-solution was used. This method includes several steps of protein processing once they were harvested from an exosome sample: denaturation, reduction, alkylation, and digestion.

After collection of exosome samples and validation of their presence and morphology as previously described in Chapter 2, proteins were precipitated and quantified. Due to the low abundance of proteins in exosomes, a suitable assay with the high sensitivity for protein quantification was required. Several protein quantification assays were tested (BCA, Rapid Gold BCA, and Lowry assays). Protein quantification from each sample was completed by highly sensitive and selective colorimetric detection of the cuprous cation (Cu1+) by Rapid Gold bicinchoninic acid assay (Rapid Gold BCA) and Pierce Quantitative Fluorometric Peptide Assay (both ThermoFisher Scientific) quantification kit after the purification step to ensure that digestion was successful. The rapid Gold BCA assay was also optimized for protein quantification by conducting time-course experiments with 5-, 10-, 15-, and 30-minutes intervals, taking measurements after initial 5 minute. Standard curves for all data intervals were graphed and linear regression analysis was used. The smallest Sum of Squares (*SS*) equal to 1.282 was determined for the 10-min interval, while values for 5-, 15-, and 30-min intervals were larger (2.000, 1.942, and 1.366 respectively). A value closer to zero indicates the smaller random error component suggesting that this fit will be more suitable. The coefficient of determination (r^2) values of different time intervals were also examined to establish which time interval result in the data showing the closest fit to the regression line. The 10-min interval had

the highest r^2 value (0.997), while the 5-, 15-, and 30-min values were 0.987, 0.972, and 0.950 respectively. Based on these results, the 10-min interval was selected for measurement, and it was advantageous as it gave a useable amount of signal for a short experimental time (Fig. 26).

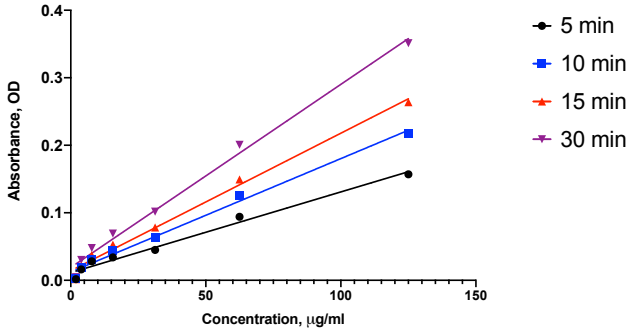

Figure 26. Optimization of standard curve for Rapid Gold BCA Protein assay kit. *The Y-axis shows the absorbance, and X-axis corresponds to the protein concentration (µg/mL). The figure was generated by using Prism GraphPad Software (version 9.1.1) for macOS, San Diego, California.*

The deciding factor for successful proteomic analysis was the quantity of proteins after peptide digestion. Before moving on to the experimental part with breath-derived exosomes, the attempt to increase the number of proteins recovery after their isolation and peptide digestion was first tested on cell-derived exosomes. First, fractionated exosomes were collected as described in 2.4.4, and the proteins were quantified. During protein precipitation, new challenges were discovered. Unexpected loss of over 50% of proteins between the initial protein quantification and final peptide quantification occurred. This most likely occurred at the final step after tryptic digestion and purification using C18 reverse phase tips of peptide mixture (Fig. 27 A).

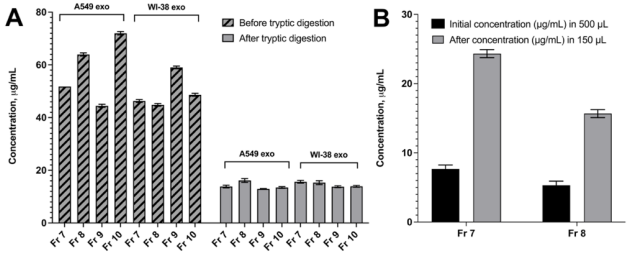

Figure 27. Protein quantification on purified proteins from SEC-based isolated cell-derived exosomes. *The graphs showing (A) protein quantification on purified proteins from cell (A549 and WI-38)-derived exosomes before and after tryptic digestion for individual fractions 7-10 and (B) difference in protein quantification before and after sample concentration showing on A549 cell-derived exosomes. The Y-axis corresponds to the protein concentration (µg/mL). The bar graph was constructed by plotting the mean of three biological replicates performed in three technical replicates and repeated three times. Error bars represent the standard deviation. The figure was generated by using Prism GraphPad Software (version 9.1.1) for macOS, San Diego, California.*

The peptide quantification after tryptic digestion varied from 13 to 15 µg/mL that is almost 3-4 times less that the initial concentration of purified proteins. Although combining several individual fractions and concentrating the volume of digested proteins after elution noticeably increased the final concentration of protein in the sample (Fig. 27 B) that still was not sufficient to perform a high-quality mass-spectrometry analysis to identify proteins. To provide further sample, the number of cells was increased toward the more concentrated CCM enriched in exosomes (Appendix, Table S 1) and proteins from the exosomes were combined. Based on protein quantification data it was determined that at least 3.4×10^7 cells were needed to obtain sufficient protein for mass spectrometric analysis, providing in excess of 100 mL of CCM. The increased volume of CCM from 34 mL to over 100 mL forced to a change of isolation method from SEC to UC, as UC is more convenient to operate with larger volumes. From this point, all exosomes were isolated by UC method as described in 2.4.3 (Fig. 28).

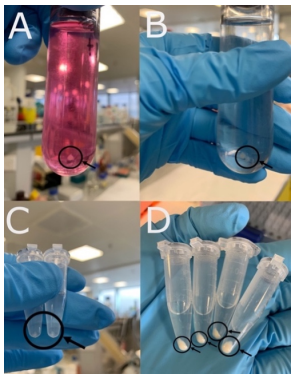

Figure 28. Cell (WI-38)-derived exosomes and their cellular content isolated by UC method. *On the figure: cell-derived exosome pellets after (A) 1st round of UC isolation and (B) 2nd round of UC; (C) lyzed cell-derived exosomes with 8 M urea; (D) acetone-precipitated exosome protein.*

After finalizing the preferred method for exosome isolations, the proteins extracted from exosomes isolated by UC were quantified. As discussed in 3.3.1, an alternative method of protein digestion, the gel-tube method described in 3.2.5, was applied. Unexpectedly, the peptide quantification after protein digestion by the gel-tube method suggested a higher quantity of proteins was present after elution than was introduced to the gel-tube (Fig. 29).

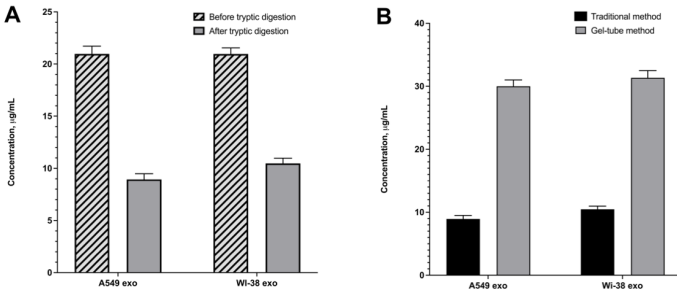

Figure 29. Protein quantification on purified proteins from UC-based isolated cell-derived exosomes. *The graphs are showing protein quantification on purified proteins from cell (A549 and WI-38)-derived exosomes isolated by UC before and after tryptic digestion by (A) traditional in-solution digestion and (B) difference in protein quantification after tryptic digestion and gel-tube digestion. The Y-axis corresponds to the protein concentration (µg/mL). The bar graphs was constructed by plotting the mean of three biological replicates performed in three technical replicates and repeated three times. Error bars represent the standard deviation. The figure was generated by using Prism GraphPad Software (version 9.1.1) for macOS, San Diego, California.*

Based on the results reported in Figure 29, the final quantity of proteins after digestion by the gel-tube method was three times higher than proteins digested by traditional method. Further investigation of both methods by MALDI confirmed that more peaks in a mass range corresponding to peptide masses were observed after the gel-tube digestion method than after traditional digestion in-solution method (Fig. 30).

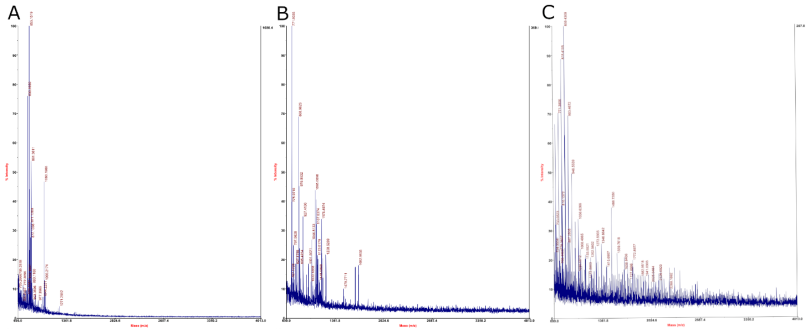

Figure 30. MALDI-TOF spectra of cell-derived exosomes. *The figure is a representative of results of protein masses after purification with traditional method (in-solution digestion) for (A) WI-38 cell-derived exosomes and gel-tube method for cell-derived exosomes (B) WI-38 and (C) A549. The Y-axis corresponds to the signal intensity and the X-axis corresponds to mass (m/z).*

Surprisingly, after conducting LC-MS/MS analysis, no proteins could be identified from the samples processed by the gel-tube method. This suggested that substantial work would be required to optimize gel-tube digestion, or that it is not applicable for this type of biological sample (Fig. 31).

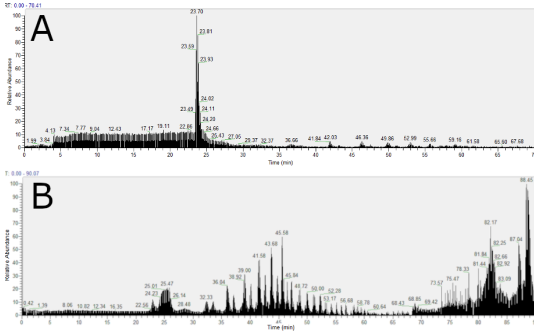

Figure 31. LC-MS/MS chromatogram of cell (A549)-derived exosomes digested by two different methods. *The figure is showing LC-MS/MS chromatogram of A549 cell-derived exosomes (A) digested by gel-tube and (B) digested in-solution, where Y-axis corresponds to relative abundance of the detected ions, and X-axis corresponds to time.*

Ultimately, it was decided to follow the standard, in-solution digestion, method with highly concentrated protein samples. Based on the reported protein quantity data from cell-derived exosomes, it was concluded that it is safe to apply the same approach on breath-derived exosomes. Peptide quantification was undertaken after digestion for all samples including exosomes and whole proteomes (Fig. 32).

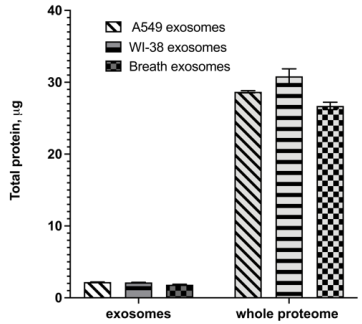

Figure 32. Total protein concentration in the sample after digestion. *Total protein (µg) after protein digestion for all exosome samples (cell- and breath-derived), whole proteome of A549 and WI-38 cell lines, and whole breath. The Y-axis shows the total protein (µg). The error bars represent the standard deviation of the biological replicates (n=3). The figure was generated by using Prism GraphPad Software (version 9.1.1) for macOS, San Diego, California.*

For the mass spectrometric analysis, three biological samples were prepared for each exosome and whole proteome sample. Each sample was run in 2 technical replicates and then analyzed by using Proteome Discoverer software v2.4 (ThermoFisher) where the data was searched against the entire SwissProt human protein database (TAXID=9606, v2019). The full list of proteins identified in each cell-derived exosome sample and whole proteome can be found in the Appendix (Tables S2-S5). The proteins identified as present from A549 and control WI-38 cell-derived exosomes were compared, as shown in Table 5 and Figure 33 generated by using BioVenn software[513].

Table 5. Statistical data of proteins identified in cell-derived exosomes. *The number of proteins identified in exosome samples from A549 and WI-38 cells showing total, unique, and overlapped proteins across two samples. Each group consisted of three biological replicate samples run in technical duplicates.*

Sample	Total proteins identified	Unique proteins	Total overlap proteins
A549	306	143 (30.82%)	163 (35.13%)
WI-38	321	158 (34.05)	

Figure 33. Area-proportional Venn diagram for proteins identified in cell-derived exosomes. *Comparison diagram of proteins identified in lung cancer (A549) and healthy lung tissue (WI-38) cell-derived exosomes. Each group consisted of three biological replicate samples run in duplicate. Generated by using BioVenn software.*

The number of identified proteins in each group was very similar, as might be expected given samples contained equivalent protein abundances, starting from the equivalent cell counts and amount of CCM, as well as peptide abundance loaded onto the mass spectrometer. More than half of the proteins in each sample were in common between exosomes isolated from the two different cell sources.

Gene ontology (GO) functional enrichment analysis was applied to proteins that were found in triplicate for exosome samples from each cell line (Table 6, Fig. 34). The bioinformatics analysis undertaken using ShinyGO v.0.61software[515].

Table 6. Enrichment analysis of proteins identified in cell-derived exosomes. *The table shows analysis of proteins identified in A549 and WI-38 cell-derived exosomes based on hypergeometric distribution followed by FDR correction showing top three cellular components, molecular functions, and biological process.*

Cellular components			
A549	**P_{adj}**	**WI-38**	**P_{adj}**
Extracellular exosome	4.50E-168	Extracellular exosome	7.71E-206
Extracellular vesicle	1.69E-165	Extracellular vesicle	5.30E-203
Extracellular organelle	2.10E-165	Extracellular organelle	7.13E-203
Molecular function			
Cell adhesion molecule binding	1.23E-44	Structural molecule activity	2.59E-42
Structural molecule activity	5.18E-39	Extracellular matrix structural constituent	1.01E-41
Protein-containing complex binding	3.70E-26	Cell adhesion molecule binding	1.37E-35
Biological process			
Establishment of localization	9.78E-30	Regulated exocytosis	1.04E-36
Transport	4.97E-29	Exocytosis	7.40E-35
Establishment of localization in cell	1.66E-27	Extracellular matrix organization	1.13E-32

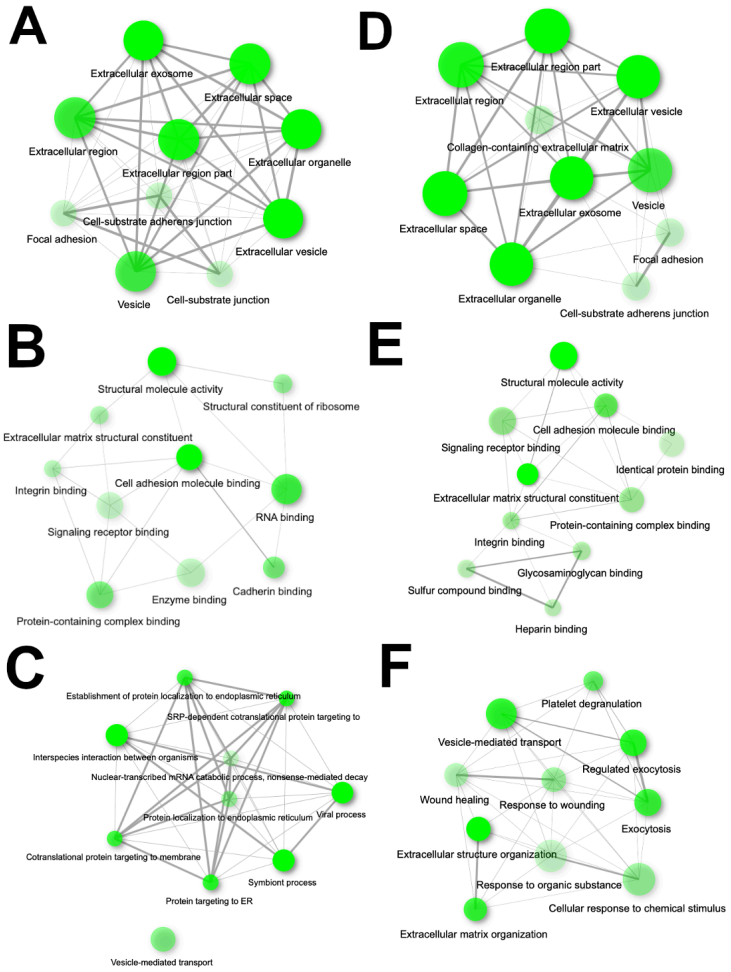

Figure 34. Enrichment analysis of proteins identified in cell-derived exosomes*. The figure is showing expression differences that are consistent across sets of genes identified in (A, B, and C) A549 and (C, D, and E) WI-38 cell-derived exosomes based on hypergeometric distribution followed by FDR correction showing (A, D) cellular components, (B, E) molecular functions (MF), and (C, F) biological process (BP); ρ -value cut-off (FDR, Benjamini and Hochberg [517]) =0.05. Two nodes are connected if they share as least 20% or more genes. Less transparent nodes are more significantly enriched gene sets. Bigger nodes represent larger gene sets. Thicker edges represent more overlapped genes.*

Notably, the three most significant terms in cellular components for both study groups are the same and following the same order: extracellular organelle, extracellular vesicles, and extracellular exosomes, which confirms that analysis was indeed conducted on exosomes and not any other subtypes of EVs. The molecular function ontologies associated with the two cell lines were similar in components but with different relative enrichments for structural molecule activity and cell adhesion molecule binding. As expected, the biological function ontologies were completely different, which can be explained by the nature of the two cell lines. While the vesicle-mediated transport BP ontology was strongly enriched with the lung cancer mimicking A549 cells, terms related to extracellular structure organization were most enriched for exosomes isolated from WI-38 cells, mimicking normal lung tissue. The full list of GO analysis for both cell-derived exosomes undertaken using g:Profiler software[516] can be found in Appendix, Tables S 6 and S 7.

3.3.3 Selection of lung cancer biomarkers

The search for potential biomarkers for lung cancer began with the 143 proteins that were unique to exosomes from A549 cells. Briefly, proteins that were found at least three times were selected as main candidates and proteins found at least twice were also selected. Then, selection of candidates was continuing based on the sum of Posterior Error Probability (PEP) score for each protein in each replicate. Based on PEP score, the raw list of proteins was narrowed down from 143 proteins to 22 proteins (Appendix, Table S 8) that were found twice and only 11 unique proteins that were found at least three times in A549 cell-derived exosomes but were not in any WI-38 cell-derived exosomes. After validation of exosomes through the functional GO enrichment analysis, the identified proteins from A549 cell-derived exosomes were checked to identify whether they had been previously identified as cancer markers in literature. The preliminary list of nine potential biomarkers was further refined based on the antibody availability and on the strength of literature evidence to support application as a prognostic marker, ideally in lung cancer, and likely abundance in exosome samples (Table 7). The availability of antibodies against the potential biomarker was also considered, as these will be required for the FRET-based assay design that is described in Chapter 4.

***Table 7. Preliminary list of biomarker candidates**. The list of biomarker candidates based on the number of replicates each were found in A549 cell-derived exosome (from a total of 3 experimental replicates), sum of PEP score, and types of cancer in which the protein has been previously identified.*

Protein accession number	Description	Gene code	# of replicates	Sum of PEP score	Cancers in which the protein has been previously identified.
Q9NZM1	Myoferlin	MYOF	3	38.13	Bladder, colorectal, ovarian, prostate
P11021	78 kDa glucose-regulated protein	HSPA5	3	39.4	Bladder, breast, colorectal, liver, ovarian, prostate
P02774	vitamin D-binding protein	GC	3	32.11	Colorectal, prostate
P01116	GTPase KRAS	KRAS	3	1.9	Colon, breast, liver, bladder, ***lung***
P48509	CD151 antigen	CD151	3	1.678	Prostate, breast, colon, ***NSLC***, pancreatic
P15151-1	Poliovirus receptor	PVR	3	1.97	Colorectal, breast, prostate, ***lung***, liver
P11166	Solute carrier family 2, facilitated glucose transporter member 1	SLC2A1/ GLUT	3	5.35	Colorectal, breast, prostate, ***lung***, liver
P08134	Rho-related GTP-binding protein RhoC	RHOC	3	5.5	Colorectal, breast, prostate, ***lung,*** liver
P60953	Cell division control protein 42 homolog	CDC42	3	5.864	Colorectal, breast, prostate, ***lung***, liver

From this, four candidate protein-biomarkers were prioritized: CD151 antigen (CD151), solute carrier family 2-facilitated glucose transporter member 1 (SLC2A1, also known as GLUT), myoferlin (MYOF), and Rho-related GTP-binding protein RhoC (RhoC) (Table 8).

Table 8. Literature review of selected biomarkers identified in A549 cells and their association with cancer origin.

Gene code	Cancer origin	Gene code	Cancer origin
CD151	Colorectal [518]	**MYOF**	Breast [519, 520]
	Liver [521, 522]		Colon [523]
	Lung [524]		Lung [525, 526]
	Melanoma [527]		Pancreatic [528]
	Ovarian [529]	**RhoC**	Bladder [530]
	Pancreatic [531]		Breast [532–536]
	Prostate [537]		Gastric [538, 539]
SLC2A1 (GLUT)	Breast [540]		Liver [541]
	Colon [542]		Lung [543, 544]
	Gastric [545,546]		Ovarian [547]
	Lung [548–552]		Pancreatic [553]
			Renal [554]

CD151 enhances the motility, invasion and metastasis of cancer cells[484]. GLUT is responsible for increased cellular glucose uptake and increased aerobic glycolysis in recipient tumor cells. MYOF plays a role in the plasmalemma repair mechanism of endothelial cells that permits rapid resealing of membranes disrupted by mechanical stress and is involved in endocytic recycling. Finally, RhoC regulates a signal transduction pathway linking plasma

membrane receptors to the assembly of focal adhesions and actin stress fibers and serves as a microtubule-dependent signal that is required for the myosin contractile ring formation during cell cycle cytokinesis.

Some proteins (CDC42, KRAS, and PVR) in Table 8 had a higher score than the chosen biomarker candidates but were not selected for the final round of candidates. All three proteins are generally considered for cancer therapy rather than diagnostics. For example, CDC42 is most often mutated in cancer and could be overexpressed via signalling through oncogenic receptor and so not considered as a diagnostic marker[555]. KRAS is also considered as mutated oncogene and rather highlights as high-priority therapeutic target[556,557]. Finally, although RVP is highly expressed in several types of cancer including lung cancer, but it is more common to find it in ovarian and colorectal cancer. In addition, PVR is gaining more scientific interest as therapeutic target[558]. That being said, these proteins can be considered as a back-up option to the selected biomarkers and could be considered alongside the four selected biomarkers in future clinical studies involving lung cancer patients.

These proposed biomarkers were validated through western blotting. The selectivity of each marker between exosomes from A549 and WI-38 cells was analyzed individually in triplicate (Appendix, Figs. S 1- S 10), as well as through a combined cocktail of markers (Fig. 35).

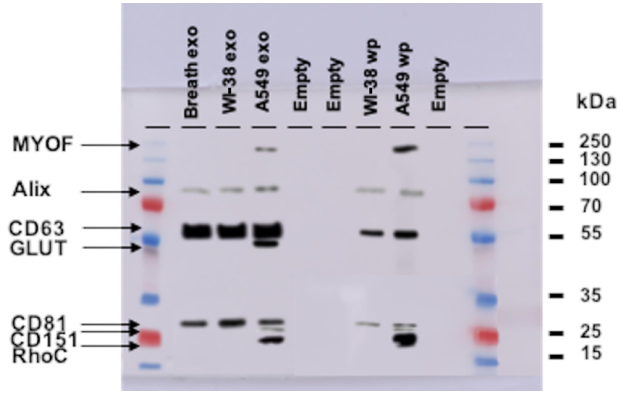

***Figure 35. Validation of proposed biomarkers CD151, GLUT, MYOF, and RhoC.** Western blot showing CD151, GLUT, MYOF, and RhoC blotting on A549 exosome lysate and cell (whole proteome) lysate. Note, that markers are only shown in cancer cell-derived exosomes and cancer cell model lysates and absent in WI-38 cell- and breath-derived exosomes. Western blotting of general tetraspanin EV markers (Alix, CD63, and CD81) are also shown.*

According to the western blot results, the proposed lung cancer protein biomarkers were only identified in A549 cell-derived exosomes and its whole proteome, which was expected. WI-38 cell-derived exosomes, WI-38 whole proteome, and breath-derived exosomes, playing the role of controls, did not show any of the proposed lung cancer markers, verifying that proposed biomarkers are able to distinguish between cancer and healthy lung exosomes. As exosomes are time consuming to isolate, it was useful to know whether markers on exosomes could be identified from within whole breath condensate. Therefore, exosome samples, including those derived from a sample of human breath, were compared to whole breath using general tetraspanin EV markers (Fig. 36).

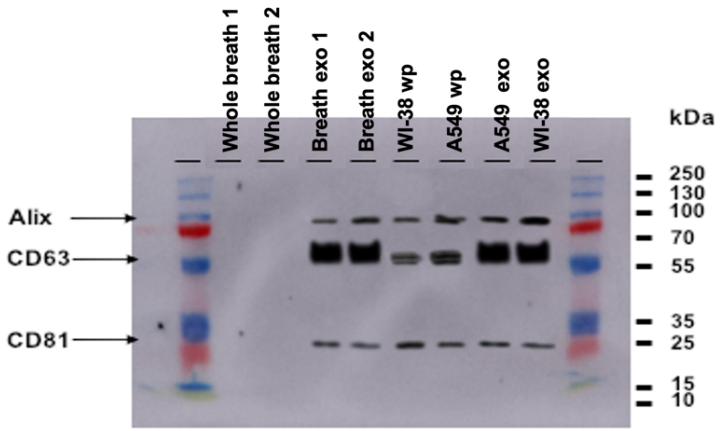

***Figure 36. Validation of exosomes by western blotting**. The cell (A549, WI-38)- and breath-derived exosomes were validated using general tetraspanin EV markers (Alix, CD63, and CD81) in comparison to whole breath and cellular (WI-38/A549) whole proteome.*

Disappointingly, the general tetraspanin EV markers (Alix, CD63, and CD81) could not be identified in whole breath, although they were apparent in all purified exosome samples. This may indicate that it will be necessary to go through at least a step of exosome enrichment as part of any future exosome biomarker-based diagnostic device.

3.3.4 Characterization of cellular whole proteome

The whole proteome from the A549 and WI-38 cells was also compared. The analysis reported that 646 proteins were identified as common proteins across case and control study. The unique proteins identified in WI-38 whole proteome will be later compared with proteins identified in whole breath of volunteers participated in the determination of benchmark breath proteome. The full list of proteins can be seen in Appendix, Tables S 4 and S 5.

3.3.5 Characterization of breath-derived exosomes (preliminary studies)

After collection of exhaled breath condensate, breath-derived exosomes were isolated as described in 2.4.3 (Fig. 37).

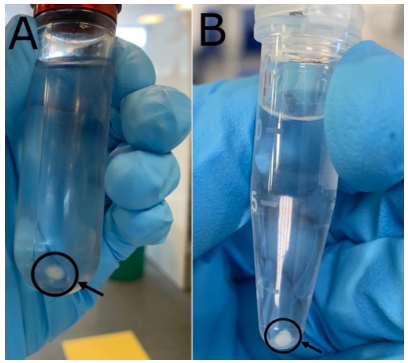

***Figure 37. Characterization of breath-derived exosomes**. On the figure: (A) washed pelleted breath-derived exosomes by UC method and (B) acetone precipitated proteins from the same sample.*

Based on the optimized protocol for increasing protein concentration after digestion, samples (×20) were pooled together in one. Three biological replicate samples were prepared to go through identification analysis. A 1 µl aliquot from each digested protein sample was combined with 1 µl of α-cyano-4-hydroxycinnamic acid matrix and air-dried prior to analysis by MALDI-TOF-MS described in 3.2.6. Then samples were subjected to MS analysis, after which it has been noted that the chromatogram from some samples had high signal intensity at longer retention times. It was presumed that this arose from lipid contamination. It seemed that the lipid: protein content ratio was higher than in cell-derived exosomes. Samples (Fig. 38)

then were washed with ethyl acetate as described in 3.2.9 and were re-probed again by using MALDI-TOF-MS as described above.

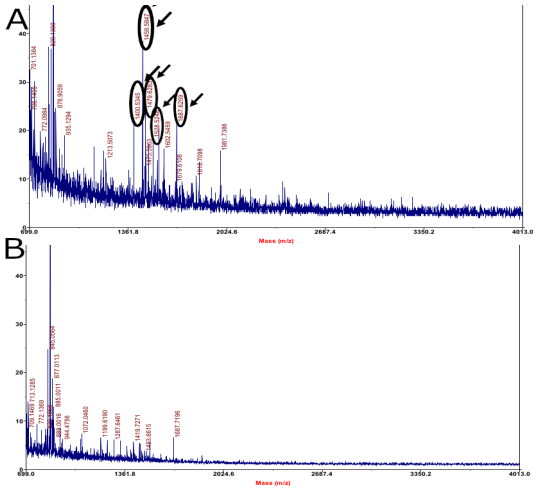

Figure 38. MALDI-TOF spectra of breath-derived exosomes. *The spectra are representative of sample (A) before and (B) after an ethyl acetate wash. Highlighted peaks circled before wash and disappeared after the wash. The Y-axis corresponds to the signal intensity and the X-axis corresponds to mass (m/z).*

Based on the spectrum, large peaks that were previously noticed around 1600 m/z have noticeably decreased. Comparing the results of MALDI spectrum before (Fig. 38 A) and after (Fig. 38 B) it was clear that the contamination is much reduced by the ethyl acetate wash.

Breath-derived exosome samples named as E1, E2, and E3 and were subjected to MS analysis. Samples were run in two technical duplicates to make sure that the injection volume is sufficient for protein identification. The injection volumes were adjusted to deliver consistent peptide amounts to the mass spectrometric analysis (Appendix, Table S 9). Statistical data collected after analyzing samples through PD software is shown on Table 9.

Table 9. Statistical data of proteins identified in breath-derived exosomes. *The number of proteins identified in exosome samples from the same individual showing total, unique, and overlapped proteins across three samples. Each group consisted of three biological replicate samples run in technical duplicates.*

Sample	Total proteins identified	Unique proteins	Shared proteins	Overlap proteins across 3 samples
E1	504	181(21.22%)	34 (3.99%) (E1+E2)	230 (26.96%)
E2	575	176 (20.63%)	135(15.83%) (E2+E3)	
E3	462	38(4.45%)	59 (6.92%) (E1+E3)	

The similarities and differences between samples is shown by a Venn diagram in Figure 39, generated by using BioVenn software[513].

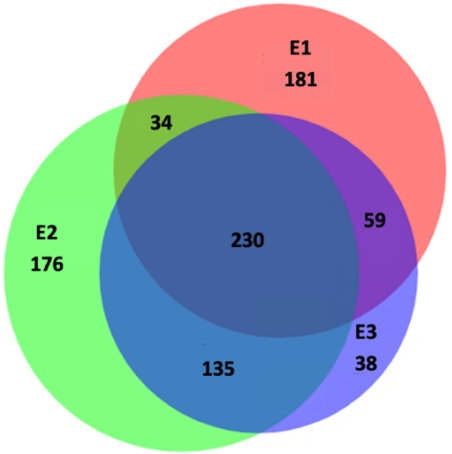

Figure 39. Area-proportional Venn diagram for proteins identified in breath-derived exosome samples from the same individual. *Comparison diagram of proteins identified in breath-derived exosomes from the same individual across 3 biological samples (E1, E2, and E3). Each biological replicate sample run in duplicate. Generated by using BioVenn software.*

To support the fact that the number of total proteins identified in each sample was slightly different, the chromatogram from each sample was analyzed (Fig. 40). These differences between the samples from the same individual may relate to the fact that they were collected at different times.

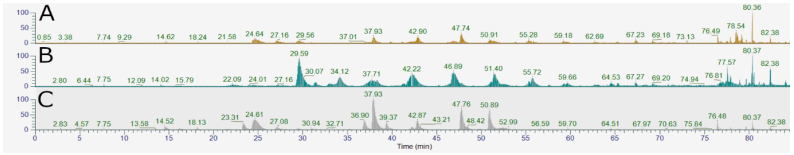

Figure 40.Chromatogram of breath-derived exosome samples*. The chromatogram represents three biological samples: (A) E1, (B) E2, and (C) E3.*

3.3.6 Characterization of whole breath (preliminary studies)

To define if there are any common proteins between EBC and breath exosomes, the whole breath proteome was also obtained as described in 3.2.2. The total number of proteins identified are summarized in Table 10 and Figure 41.

Table 10. Statistical data of proteins identified in whole breath. *The number of proteins identified in whole breath samples from the same individual showing total, unique, and overlapped proteins across three samples. Each group consisted of three biological replicate samples run in technical duplicates.*

Sample	Total proteins identified	Unique proteins	Shared proteins	Overlap proteins across 3 samples
WHB1	518	124 (17.46%)	107 (15.07%) (WHB1+WHB2)	256 (36.06%)
WHB2	461	80 (11.27%)	18 (2.54%) (WHB2+WHB3)	
WHB3	399	94 (13.24%)	31 (4.37%) (WHB1+WHB3)	

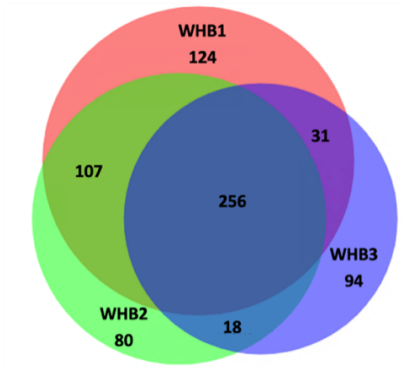

Figure 41. Area-proportional Venn diagram for proteins identified in whole breath samples from the same individual. *Comparison diagram of proteins identified in whole breath from the same individual across 3 biological samples (WHB1, WHB2, and WHB3). Each biological replicate sample run in duplicate. Generated by using BioVenn software.*

According to the data analysis, 709 proteins were identified at least once, and 410 proteins were identified at least twice.

Finally, a comparison was made between proteins found in breath exosomes and those found in the whole breath sample (Table 11, Fig. 42).

Table 11. Statistical data of proteins identified in combined samples of breath-derived exosomes and combined samples of whole breath from the same individual. *The number of proteins identified in combined individual samples of breath-derived exosomes and whole breath samples from the same individual showing total, unique, and overlapped proteins across two samples. Each group consisted of three biological replicate samples run in technical duplicates.*

Sample	Total proteins identified	Unique proteins	Total overlap proteins
E combined	786	503 (43.78%)	283 (24.63%)
WHB combined	646	363 (31.59%)	

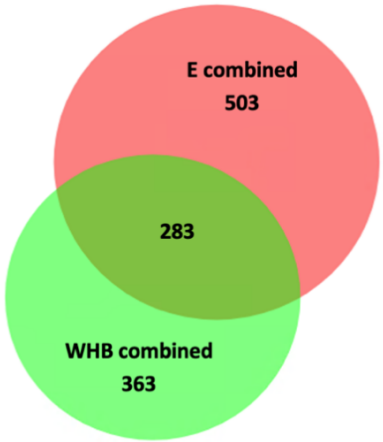

Figure 42. Area-proportional Venn diagram for proteins identified in combined individual samples of breath-derived exosomes and whole breath samples from the same individual. *Comparison diagram of proteins identified in all combined samples of breath-derived exosomes (E combined) and whole breath (WHB combined) from the same individual. Each biological replicate sample run in duplicate. Generated by using BioVenn software.*

This preliminary study of breath-derived exosomes and whole breath was conducted on samples collected from a single individual. It allowed methodology to be optimized ready for application on creating the benchmark proteome of breath exosomes from a healthy population. As the data represents only a single individual, a detailed analysis of the proteins identified was not undertaken. Results of the larger study on exosomes collected from the breath of healthy volunteers' study will be presented in next section.

3.3.7 Determination of the benchmark proteome of breath exosomes

Breath-derived exosomes from EBC were isolated by ultracentrifugation and assessed by western blotting with general tetraspanin EV markers (Fig. 43 A) and cryo- SEM (Fig. 43 B).

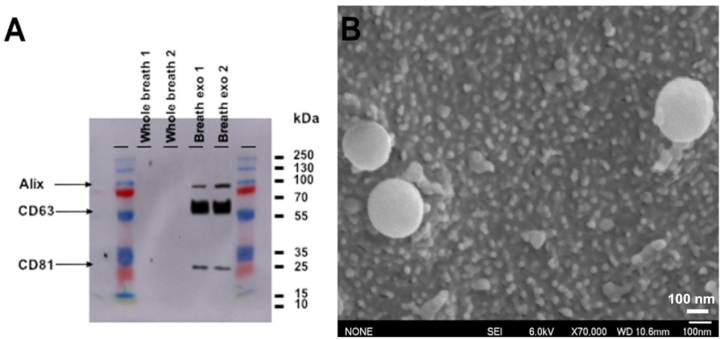

Figure 43. Characterization of breath-derived exosomes by western blot analysis and Cryo-SEM*. The validation of breath-derived exosomes was confirmed by (A) western blotting using general tetraspanin EV markers-Alix, CD63, and CD81. (B) The size and morphology of exosomes were validated by cryo-SEM imaging. Scale bar 100 nm .*

As described in sections 2.3.4 and 3.2.10, isolated exosomes were grouped into three samples that were individually subjected to proteomic analysis. A total of 730 unique proteins were identified (Appendix, Table S 10). As shown in Table 12, there was a large difference in the number of proteins identified between samples.

Table 12. Statistical data of proteins identified in breath-derived exosomes collected from volunteers. *The number of proteins identified in exosome samples from volunteers showing total, unique, and overlapped proteins across three samples. Each group consisted of three biological replicate samples run in technical duplicates.*

Sample	Total proteins identified	Unique proteins	Shared proteins	Overlap proteins across 3 samples
S1	233	62 (8.53%)	41 (5.64%) (S1+S2)	122 (16.78%)
S2	610	321 (44.15%)	126 (17.33%) (S2+S3)	
S3	303	47 (6.46%)	8 (1.1%) (S1+S3)	

This may arise as these are low abundance samples, with many peptide signals being around the limits of detection of the mass spectrometer.

From 730 unique proteins, 297 proteins were found in at least twice across three samples as shown in Figure 44 (Appendix, Table S 11). These 297 proteins were defined as the core of the breath exosome proteome (BEP).

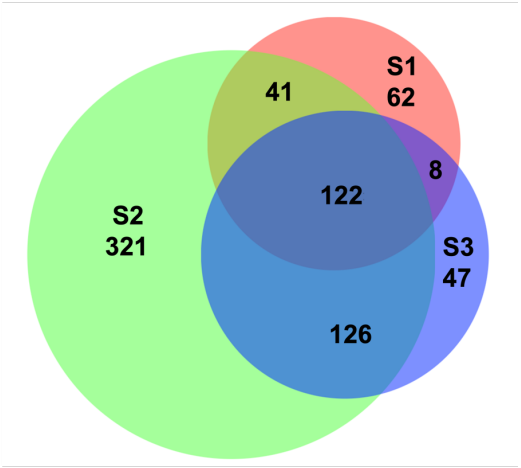

Figure 44. Area-proportional Venn diagram for proteins identified in breath-derived exosome samples from volunteers. *Comparison diagram of proteins identified in breath-derived exosomes from volunteers across 3 biological samples (S1, S2, and S3). Each biological replicate sample run in duplicate. Generated by using BioVenn software.*

The functional gene ontology (GO) enrichment analysis of the core BEP was performed using g:Profiler database[516] for functional interpretation of gene list. Although the core of the BEP was identified consisting of 297 proteins, 5 proteins (Immunoglobulin lambda constant 7 (A0M8Q6), Immunoglobulin kappa constant (P01834l), Immunoglobulin heavy constant gamma 3 (P01860), IgGFc-binding protein (Q9Y6R7), and Immunoglobulin heavy variable 3/OR16-9 (non-functional) (S4R460)) were not included in the analysis as they were absent from the g:Profiler database. The GO enrichment analysis revealed that of the 292 proteins, 235 have a GO cellular component annotation to the extracellular exosome, being the most strongly enriched term in this analysis (P_{adj} 3.43×10^{-166}). The top three GO biological process annotations are immune effector process (132 terms, P_{adj} 2.50×10^{-78}), leukocyte mediated immunity (120 terms, P_{adj} 1.56×10^{-77}), and regulated exocytosis (113 terms, P_{adj} 5.05×10^{-75}). GO molecular function and cellular components are shown on Figures 45 B and C respectively.

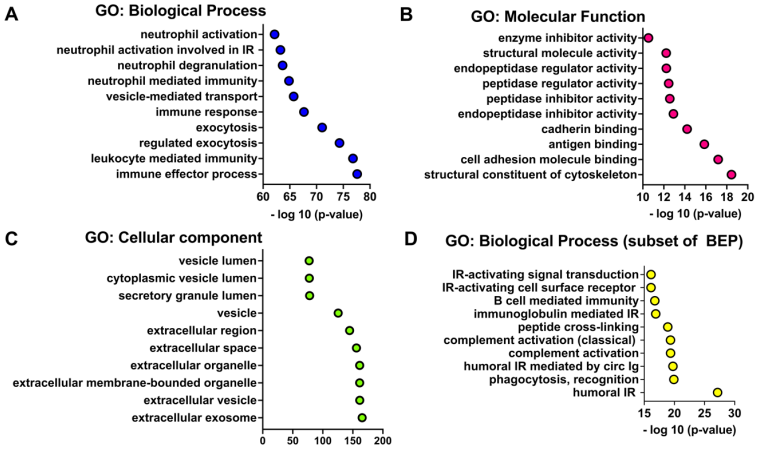

***Figure 45. The functional GO enrichment analysis of the core of the breath exosome proteome**. Results of functional enrichment analysis to examine the (A) biological process, (B) molecular function, and (C) cellular component of the core BEP proteins. The subset of the core BEP consisting of 184 proteins (GO: BP) is shown under D. The Y-axis represents term, and X-axis represents negative $\log_{10}$ of adjusted p-value. The figure was generated by using Prism GraphPad Software (version 9.1.1) for macOS, San Diego, California.*

Among these proteins, identified as the core of the breath exosome proteome, a few of them were associated with exocytosis. There were considerable overlaps between proteins annotated to many of the biological process ontologies. As exosomes are formed through a regulated exocytosis pathway, we were particularly concerned that some biological processes may have been reported as significantly enriched only because they shared proteins with the regulated exocytosis ontology. Removing the exocytosis-associated proteins removed those other apparent enrichments, revealing more relevant biological processes associated with the identified proteins. For that reason, the list of 297 proteins were narrowed down and a follow-up GO functional enrichment analysis was completed with the 184-protein subset (Appendix, Table S12) of the core BEP proteins, those not annotated to the regulated exocytosis term. Within this subset of proteins, the most enriched cellular component ontology is extracellular space (158 terms, P_{adj} 3.94×10^{-89}) with the most significant parental biological processes being humoral immune response (41 terms, P_{adj} 6.36×10^{-28}), humoral immune response mediated by circulating immunoglobulin (29 terms, P_{adj} 2.21×10^{-20}), and complement activation (26 terms, P_{adj} 5.11×10^{-20}). A full list of GO term enrichments undertaken using g:Profiler database[516] is in the Appendix, Tables S 13-14. Although the purification gave high quality exosomes free of protein contamination, there is a contribution from proteins associated with the salivary system.

Kyoto Encyclopedia of Genes and Genomes (KEGG) pathway analysis using KEGG database[559] for both the core BEP and the 184-protein subset revealed the contribution of the salivary system, with 12 proteins annotated to salivary secretion in the core BEP (Fig. 46, shown in red).

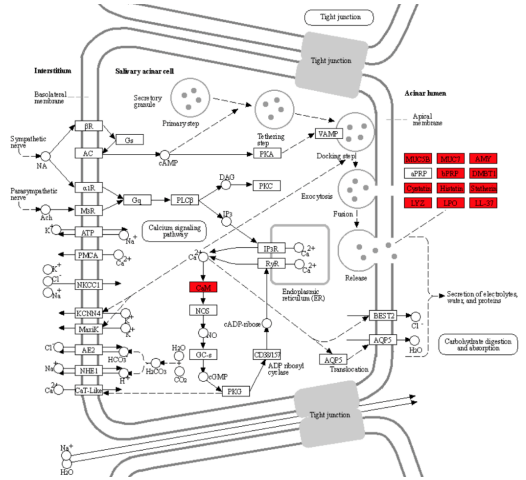

***Figure 46. KEGG pathway of proteins associated with salivary secretion**. The proteins activated in salivary secretion are highlighted in red boxes. The figure is generated by using ShinyGO v.0.61 software.*

Among those 12 proteins, 10 proteins were found in the 184-protein subset excluding alpha-amylase 1A (AMY) and cathelicidin (LL-37). However, this number may be higher as our pathway analysis only covered 179 of the core BEP proteins and 97 of the smaller subset. Among those salivary proteins, four major protein families (cystatins (CST1, CST2, CST4, CST5), histatin (HTN1, HTN3), mucin (MUC5B), and statherin (STATH)) were found. The proteins from the first two families can be found in saliva and have been produced by parotid and submandibular glands, which are the most important glands responsible for saliva production[560]. In addition, mucin is thought contribute to the lubricating and viscoelastic properties of whole saliva[561]. Statherin plays a role in stabilizing saliva supersaturated with calcium salts by inhibiting the precipitation of calcium phosphate salts[562].

To fully understand of the biological processes associated with the proteome of breath exosomes, the STRING database[514] was used to visualize the protein network, as well as functional associations (Fig. 47).

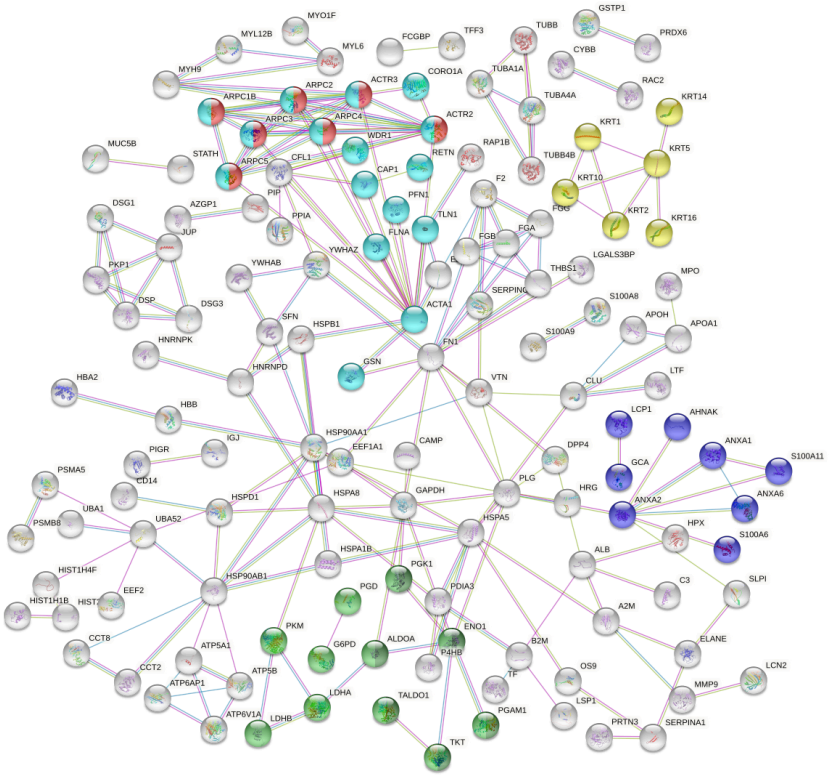

Figure 47. The network of identified proteins of the core BEP constructed by STRING. *The proteins in the network are represented with high confidence with major clusters highlighted in yellow (Keratin), red (Arp2/3 protein complex), purple (mixed cluster including Tetraspanin family and Annexin), green including dark green (Glycolysis), and teal (RhoGTPase proteins involved in activation of WASPs and WAVEs and actin binding). The connections indicate that these proteins are part of a physical complex, and the thickness indicates the strength of the connection within the complex showing their confidence. Disconnected nodes from the network were removed.*

The first largest cluster is the RhoGTPase cluster, proteins of which play an important role in exosome biogenesis by regulating protein transport and membrane recycling from endosomal compartments[563]. The second largest cluster consists of proteins associated with glycolysis and the pentose phosphate pathway. Both complexes are involved in the glucose metabolism[564]. Further, the pentose phosphate pathway protein complex is a major key in exosome-mediated intracellular communication[565]. It is also important to mention that simultaneous inhibition of the glycolysis and oxidative phosphorylation (not shown) triggers

increase of exosomes secretion[566]. Moreover, glycolytic enzymes are involved in ATP production that can be easily affected during cancer progression due to a decrease of ATPase activity[567]. The third largest cluster of proteins is associated with the tetraspanin family and annexin, proteins of which are concentrated on the plasma membrane of EVs and play a fundamental role in EV biogenesis[568]. The fourth protein cluster consists of the Arp2/3 protein complex, which is shared with the RhoGTPase cluster described above. The ARP2/3 complex is involved in the formation of actin branches. Interestingly, this complex has been previously reported as one of the key players in endocytosis[569,570] and EVs release[571]. The keratin complex has been also highlighted in the network of identified proteins as a major constituent of proteins found in the breath-derived exosomes.

Finding similarities and differences that exist among different types of exosomes piqued our interest, and comparison was made with literature data of the urinary exosome proteome, a source chosen because it is also collected by a non-invasive approach. Identification and proteomic profiling of exosomes in human urine has been studied for decades resulting in a database of 1160 proteins[507,572]. First, proteins identified in the core of the breath exosome proteome and urine-derived exosomes were compared to derive the profile similarities (Fig. 48).

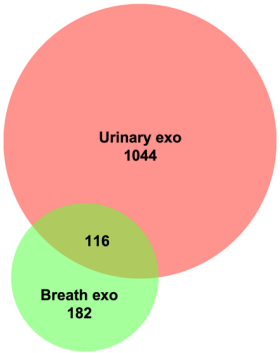

Figure 48. Area-proportional Venn diagram for proteins identified in breath-derived and urinary exosomes. *Comparison diagram of proteins identified in breath-derived exosomes from volunteers and urinary exosomes across two samples. The proteins identified in urinary exosomes used in this figure was taken from previous published database[507,572]. Generated by using BioVenn software.*

It appeared that almost 40% of proteins identified in breath exosomes are also present in urinary exosomes. Then, we decided to look at unique families of proteins identified in urine-

and breath-derived exosomes (Fig. 49). A significant similarity would suggest that the proteins are related.

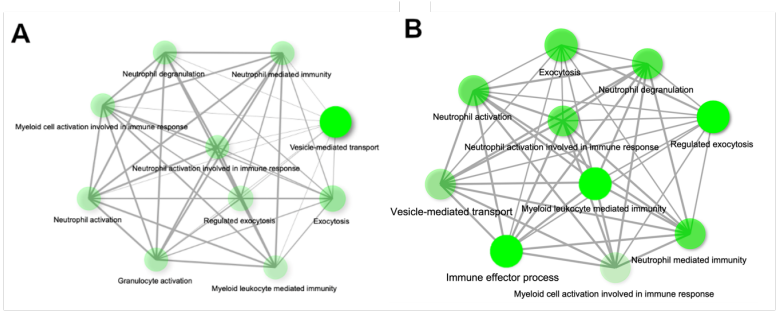

Figure 49. The functional GO enrichment analysis of urine and the core of the breath-derived exosome proteome*. The diagram is showing only BP component of unique proteins identified in (A) urine exosomes and (B) the core of the BEP. Two pathways (nodes) are connected if they share 20% or more genes. Less transparent nodes are more significantly enriched gene sets. Bigger nodes represent larger gene sets. Thicker edges represent more overlapping genes. The figure was generated by ShinyGo v0.61 software.*

The GO analysis of the biological component identified more similarities than expected, highlighting the same terms with slightly different enrichment values. The main difference identified among terms of the biological component was the leading term. For urine exosomes the most enriched biological component ontology was vesicle-mediated transport (276 terms, P_{adj} 6.57×10^{-56}), while for the core of breath exosomes it was immune effector process (132 terms, P_{adj} 2.50×10^{-78}). The analysis of shared proteins identified five members of the component of the chaperonin-containing T-complex that plays role in regulating transport vesicles to cilia and actin folding[573]. The analysis of molecular function identified two similarities: the groups of proteins associated with “cell adhesion molecule binding” and “cadherin binding”.

3.3.8 Other co-isolated vesicles

During TEM imaging of breath-derived exosomes, some larger vesicles were co-isolated with exosomes. Based on their size range (200-500nm) and shape, they potentially could be considered as microvesicles or larger extracellular vesicles (Fig. 50 A and B).

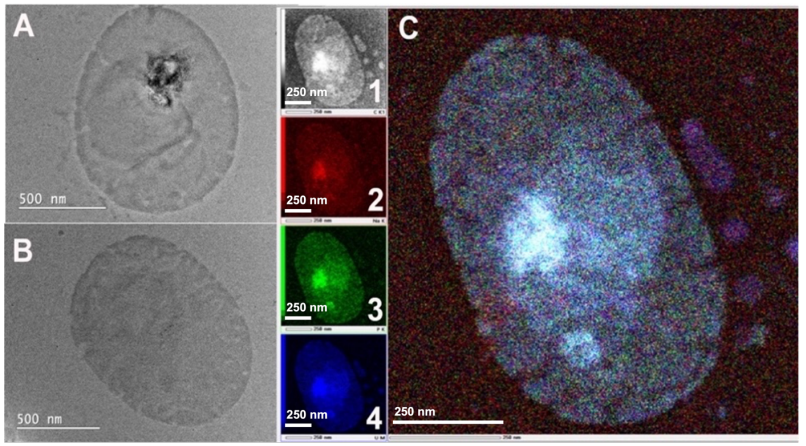

Figure 50. Characterization of larger EVs by TEM and STEM-EDS. *TEM images of larger EVs (A-B) eluted with exosomes fraction after ultracentrifugation ;scale bar 500 nm. (C) The STEM-EDS analysis of a single vesicle found in breath (1) carbon, (2) nitrogen, (3) phosphorus, and (4) uranium. Scale bar 250 nm.*

STEM-EDS was performed to distinguish their origin. The results are shown in Figure 50 C. The sample was placed on a copper grid and stained with uranyl acetate, explaining the presence of these otherwise unexpected elements in the EDS spectrum. The presence of abundant carbon and oxygen that maps as co-located with larger vesicles is consistent with it being of organic origin. At this point no further investigation was done as it was not the aim of this study. However, the findings were noted for further studies.

3.3.9 Comparison of cell- and breath-derived exosomes

To consider whether the exosomes derived from cells make a good model of breath exosomes, and to determine the nature of differences between them, the proteins identified from these two sources compared with each other (Fig. 51).

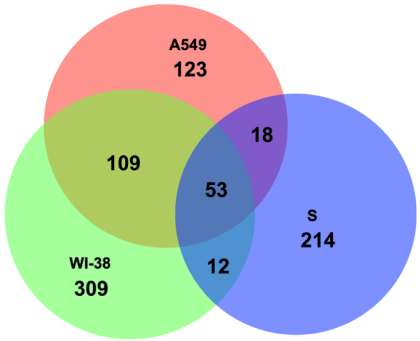

Figure 51. Area-proportional Venn diagram for proteins identified in cell- and the core of the breath-derived exosome proteome from volunteers. *Comparison diagram of proteins identified in cell (A549 and WI-38)-derived exosome and the core of the breath-derived exosome proteome from volunteers (S). Each biological replicate sample run in duplicate. Generated by using BioVenn software.*

Of the 297 proteins identified as the core of the breath exosomes proteome, relatively few are found in common with the exosomes identified from the cell models. It is likely that with larger samples and repeated proteome determination, the apparent disparity between cell and breath exosomes will decrease. However, the difference between the two sample types is also likely to reflect the range of cell and tissue types contributing to breath exosomes, which will be much wider than the lung cells represented by the A549 and WI-38 models.

3.5 DISCUSSION

Lung cancer is the leading cause of cancer death[205,574]. The frequency of diagnosis of early stages when curative treatment is possible is very low compared to the more advanced stages[205]. This is because early stages are asymptomatic and, additionally, the current diagnostic methods discussed in 1.3.2 are unable to detect the smallest tumors. To date, there are no biomarkers or biomarker-based screening assays that can accurately predict lung cancer development in early stages. Therefore, there is clearly a high need for the identification of biomarkers and the development of new analytical tools that can reduce the cancer burden through its early detection. For this reason, this study proposes the understanding of the breath exosomes collected from EBC through evaluation of their protein cargo.

Results from this chapter identified potential lung cancer biomarkers are only found in exosomes derived from A549 cells, used as a model of lung cancer. They were also in the

whole proteome of A549 cells and were absent in negative controls (the WI-38 cell model of normal lung and breath-derived exosomes from healthy volunteers).

It was first necessary to increase the amount of protein within analyzed samples. That includes detailed analysis of each step during protein extraction and troubleshooting for the optimization of the process. Among those, selection of an appropriate buffer solution for protein extraction, the volume of starting solution from which exosomes will be extracted, and the method of protein digestion were highlighted. The following issues were also identified in the literature review as discussed in 3.1.2. The selection of an appropriate buffer solution played an important role of separating proteins from other non-relative cellular components, such as lipids, by protect the integrity of proteins. It was important to find out which lysis buffer is most compatible with the exosome proteins. In previously reported studies the choice of lysis buffer varied, most commonly used lysis buffers are urea[575], a combination of urea and thiourea[576], RIPA buffer, NP-40[577], and guanidium chloride[578]. The choice of the buffer will always be dictated by the nature of the sample from which proteins will be extracted. Use of thiourea provides a potent denaturant that can improve the solvation efficiency and so gives a high yield of proteins. However, this buffer is more applicable to use in gel-digestion method rather than in solution[579]. Two comparative studies on the relative benefits of buffers such as NP-40, SDS, 8 M urea[580] (1st study) and RIPA, SDS, 8 M urea[581] (2nd study) have concluded that 8 M urea is the most generally reliable chaotropic agent in such lysis buffers. Based on these reports, the most common buffers (NP-40, 8 M urea, and combination of urea/thiourea) were also tested on exosome samples reporting 8 M urea buffer as a preferable choice.

The complication with the volume of starting solution from which exosomes were extracted was resolved through gradually increasing the cell count until the ideal number of total cells was found and through selection of the most suitable lysis buffer. However, that only partially solved the challenge. With breath-derived exosomes, it was not possible to apply the same methodological approach. At this stage, EBC was collected at different volumes and proteins were quantified each time until it reached the number close to the number of proteins identified from cell-derived exosomes. That being said, the volume of the starting solution containing exosomes was not the only factor responsible for the low protein recovery.

The discovery of the new putative biomarkers in this study was adopted and pursued through the analysis of protein cargo of the case (A549) and control (WI-38) cell-derived exosomes that then was compared to protein set of breath-derived exosomes. As a result of this comparison, the identified biomarkers were able evaluate the correlation between two protein sets contributed to distinguishing lung dysfunctionality from healthy lungs. Along with this,

the benchmark proteome of exosomes isolated from the breath of healthy volunteers was fully characterized for the first time. It must be noted that LC-MS/MS analysis has its own limitation in detection of low-abundance proteins that still remains challenging. The results of this study suggest that the reliability of the data obtained from a sample will depend on the quality of the sample preparation. We cannot forget the fact that exosomes are expected to be rich in lipid-associated proteins, which may be inherently difficult to resolubilize after acetone precipitation. Further, the peptides obtained from tryptic digestion may be similarly hydrophobic and readily lost through precipitation or retention on the C18 micropipettes.

An alternative method of protein digestion, the gel-tube method, was proposed and tested. The gel-tube system sets a sample in acrylamide followed by polymerization. The sample is washed in the gel, and so is never precipitated. Tryptic digestion was undertaken following methodology used for in-gel digestion. This method is reported to improve sample recovery with higher efficiency through in-gel protein trapping. A study described by Lu et al[582] compared gel-tube and SDS-polyacrylamide gel electrophoresis methods, reporting that gel-tube provides a better sequence coverage for peptides from membrane proteins extracted from prostate cancer cells. The efficiency of the gel-tube method for characterization of membrane proteins was further validated in comparison to in-solution digestion[583,584,585]. Despite the relative ease of implementation and reported positive outcome, this method was not successful for breath-derived exosomes as no proteins could be identified following this procedure. After numerous attempts to address the issues with protein recovery, it was decided to proceed with the standard method (digestion in-solution) but with an increase of the sample concentration to avoid insufficient number of proteins that can further compromise mass spectrometry analysis. This approach was first used on the preliminary study of breath-derived exosomes and was described in 3.3.5.

Whilst numerous protein biomarkers have been already discovered and reported from different sources of exosomes (Table 1), there is no information on breath exosome proteome that can shed light on new candidate biomarkers. Breath should be considered as an open avenue that offers a huge potential for a non-invasive identification of promising biomarkers. This study has revealed that the protein cargo of breath exosomes can be used to distinguish changes in protein sets between a lung cancer cell model and exosomes from healthy lung cell model suggesting that breath exosomes can be used to evaluate lung health becoming a serious competitor to plasma exosomes. To answer the question whether the proposed biomarkers can provide an accurate diagnosis of lung cancer, the proteome of clinical patients diagnosed with lung cancer, including different stages of this disease must be characterized. Results of this

future study can determine potential clinical usefulness for the early prediction of lung cancer and support breath as an assessable biological fluid for the discovery of biomarkers.

The present study highlights two other major findings: characterization of benchmark proteome from breath-derived exosomes and the importance of breath proteome as a negative control when investigating the specificity of proposed biomarkers. Although, the focus of the study was on evaluation of breath exosomes defining their potential application in diagnosis, the possibility of using whole breath was also considered. Since we could not provide evidence of the presence of even standard tetraspanin EV markers in whole breath samples by LC-MS/MS (3.3.6) or western blotting (3.3.7) or, there was no point in attempting our exosome-led diagnostics on whole breath.

Protein contamination of BEP described in 3.3.7 most likely occurred during EBC collection as contaminating proteins that originated from tissues and organs associated with respiratory tract and airways were noted. The most common contamination that has been previously described in several studies is associated with saliva proteins[586,587]. Further, it has been reported that 10% of the "respiratory droplets" present in EBC are associated with oral portion of the airway, which includes tongue and salivary glands[588]. Results of this study reported 12 proteins associated with salivary glands and 11 proteins associated with a group including salivary glands, lymphoid tissue[589,590], esophagus, and tongue. Lastly, the STRING analysis identified keratin protein complex amongst other largest protein complexes (Fig. 47). Fifteen proteins associated with keratin family were found in the core of BEP. Five out of 15 proteins were associated with skin, while other 10 proteins had esophagus and tongue origin. This is not surprising as exogenous proteins or environmentally-derived proteins, such as keratins, that are present in condensate from the room and dust could also contribute contaminants of highly abundant proteins[591,592].

The GO functional enrichment analysis and proteins' network revealed insights of the breath proteome by highlighting several processes that are directly associated with exosomes biogenesis. In detail, the functional GO enrichment analysis of the core BEP revealed that breath-derived exosomes are indeed formed by the exosomes pathway which was confirmed by enriched cellular component "extracellular exosomes" (P_{adj} 3.43×10^{-166}). As exosomes are constantly released by all types of cell (healthy and diseased), it was important to determine whether a common subset of proteins can be determined across all types of exosomes mentioned in this study. Another question that this study tried to answer was whether there are cell type-specific proteins that can be found in the proteome of cellular exosomes that are similar or different to breath-derived exosomes[592]. The presence of proteins associated with

cell adhesion molecule binding was shared between all types of exosomes. Interestingly, the cell-derived exosomes had integrin and RNA binding in their top 10, while breath-derived exosomes did not have either of them. Breath-derived exosomes were dominated by proteins associated with antigen binding. This is not surprising as exosome have been previously recognized as mediators of immune regulation[593]. Biological processes such as "vesicle-mediated transport", "transport", "regulated exocytosis" are common between the protein profiles of cell- and breath- derived exosomes and is consistent with previous studies[594,595]. While "leukocyte mediated immunity" was predominant for breath exosomes, "establishment of localization" was leading in A549 exosomes, and "extracellular matrix organization" in WI-38 exosomes. Further analysis of biological processes revealed numerous similarities between WI-38 cell- and breath-derived exosomes, suggesting that selected model can provide a valid proxy. However, breath- and A549 cell-derived exosomes shared more common proteins than breath- with WI-38 cell-derived exosomes. This may arise from incomplete sampling of the proteome of these various types of exosomes, as well as from the contribution of exosomes from the airways other than the lung.

In summary, the results of this study indicate that the protein cargo of cell- and breath-derived exosomes are somewhat similar. This level of similarity is not unusual. For example, two studies confirm that the protein profile of total blood exosomes resembles the protein profile of plasma exosomes[78,596]. A comparative analysis of the proteome of breath-derived exosomes from this study and the proteome of urine-derived exosomes from the literature was also undertaken and is presented in 3.3.7. This analysis showed that not only were over a third of the proteins found in exosomes obtained from breath shared in common with exosomes from urine, but also that most of the gene ontologies associated with the proteomes of exosomes from these two sources. That allows us to conclude that proteins identified in breath exosomes are somewhat similar to proteins identified in other types of exosomes isolated from different biological fluids as previously described in Chapter 2.

3.5.1 Limitations

The determination of the benchmark healthy lung exosome proteome was conducted using samples mainly from people in young adulthood (18 to 30 years). The median age for lung cancer is 70 years[597], therefore this benchmark proteome is not appropriately age-matched for a future proteomic study on exosomes isolated from lung cancer patients.

However, the benchmark proteome is a valuable resource, being the first reported from exosomes isolated from breath, and has been obtained from an appropriate population for comparison with many other lung dysfunctions. In this study it was not possible to distinguish whether there are important differences between the proteins identified from male or female participants, as samples were pooled. Gender differences and individual variations in comprehensive analysis of proteome samples have been previously reported[598,599]. This was done as the aim of the study was not to elucidate such differences, but rather to gain a broad overview of the proteins associated with exosomes isolated from breath, and any use of this data in developing diagnostic tests of lung function will ideally draw on proteins not associated with sex-associated differences.

A large sample volume of exhaled breath was needed to recover enough exosomes to identify their protein cargo. Additional work is required to minimize the volume required to conduct the comprehensive analysis of exosomes, as it would be best to avoid prolonged breath collection from people suffering with lung dysfunction in any future matched study looking for biomarkers of disease. Ideally, the breath collection should be simple and fast with max 10-15 minutes of breath donation. Any final diagnostic techniques will need to work well on much lower sample volumes, once biomarkers are established. In this study, only a single cell line was used to represent each of healthy lung and lung cancer. These cell models may not fully and accurately reflect the physiological condition they were chosen to represent. Validation of the proposed biomarkers will require different cell models.

This study, however, did not set out to determine definitive biomarkers. Instead, the experiments aimed to prove that it would be possible to detect potential biomarkers in exosomes, and to thereafter develop an analytical tool to determine the presence or absence of such biomarkers, and this aim was most readily established with a simple set of cell models. Whether this limitation is anticipated, this was not a major problem in this study. The findings were relevant and represented in-depth understanding of the research goal in this chapter.

Although all proteins found in exosomes in this study are well characterized, not all of them are recorded in every database used in the proteomic analysis. For example, whilst some proteins were excluded because they were annotated as commonly found in saliva in the Human Proteome Atlas (HPA)[600], other proteins may also be contaminants in the sample relating to saliva but retained in the analysis as HPA had no annotation for them. Similarly, some protein accessions were not found in the gene ontology or KEGG pathway analysis. Omission or inclusion of such proteins from the analysis will have impacted in a small way on the proteomic analysis. However, a sufficient number of proteins were identified that the

impact of this should be minimal, especially as our analysis focused on the most strongly enriched terms or consistently identified protein complexes. Challenges highlighted in this chapter need to be taken for consideration for the future research to improve the interpretation and clinical usefulness of exosome-based protein biomarkers. Combining results presenting in this study with a future characterization of breath proteome from lung cancer diagnosed patients can provide comprehensive understanding whether the putative biomarkers can be used in diagnosis and clinical staging of lung cancer disease.

3.6 CONCLUSION

The first aim of this chapter was to determine the proteome of exosomes from cell models of normal lung tissue (WI-38 cells) and lung cancer (A549 cells) and to demonstrate that it is possible to identify potential biomarkers of lung cancer. After conducting proteomic analysis of exosomes from cell models, four putative biomarkers (GLUT, MYOF, CD151, and RhoC) were proposed. These proposed biomarkers were found only in exosomes isolated from the A549 cell model of lung cancer and were absent in exosomes from WI-38 cells and from exosomes isolated from the breath of healthy human volunteers.

The second aim of this chapter was to determine the benchmark proteome from breath-derived exosomes and the use of those exosomes as a negative control to test the proposed putative biomarkers of lung cancer. The proteome profile of breath-derived exosomes was identified for the first time from exosomes obtained from the breath of 55 healthy volunteers. Through GO functional enrichment analysis we showed that exosomes isolated from healthy lung cells and breath are similarly “programmed” reporting roughly similar biological processes, which we had expected.

The study suggests that the proteome of breath-derived exosomes may be used in future studies identifying new biomarkers of lung dysfunction, with a final goal of proposing lung cancer biomarkers. Researchers have to be mindful that protein contamination of EBC specimens with salivary and other exogenous proteins could interfere with characterization of the exosomal proteome[601]. At the end of this study, it has been determined that exosomes obtained from WI-38 cells could provide a valid proxy for breath-derived exosomes using bioinformatics techniques based on the identified proteomes.

The next chapter will investigate whether exosome-based biomarkers can be detected using FRET methodology.

CHAPTER 4. DETECTION OF EXOSOMES - DIAGNOSTIC APPLICATION

Aim:

The aim of this chapter was to develop a sensitive test for the presence of the selected biomarkers of lung cancer found on exosomes from cell models.

Objectives:

1. Select antibodies corresponding to the proposed biomarkers, and label with fluorescent dyes to give suitable FRET pairs.

2. Determine the FRET efficiency of each proposed fluorescent labeled antibody pair by conjugating them with all sources of exosomes with the goal of selecting 1-2 pairs using a FRET-based assay using time-correlated single photon counting.

4.1 INTRODUCTION

4.1.1 Overview of sensor detection methods

The final component of this study was to look whether it is possible to develop a sensitive test for the presence of the selected biomarkers of lung cancer found on exosomes from cell models. This section will briefly give an overview of sensor devices and describe the requirements of sensors that are critical for diagnostic purposes.

Sensors are widely used not only in medicine, but also in other areas such as security, food safety, and drug discovery as they allow detection of specific processes (biological, chemical, or physical) or molecules, for example protein and micro RNA biomarkers[602] or gene mutation[603]. Novel sensors that can improve medical care, contribute insights into disease processes or assist with early detection are desirable. The pioneering work in developing sensors belongs to Clark who in 1956 developed an oxygen electrode for measuring oxygen levels in blood that was later named the “Clark electrode”. This remarkable electrode was initially used in the heart-lung machine that Leland C. Clark Jr. also pioneered. A few years later, in 1962, the first prototype of a biosensor, a glucose biosensor, was introduced by the same inventor [604]. What differentiates a biosensor from other sensors is that it uses a molecule

derived from a biological origin, often referred to as a bioreceptor, as an integral part of the sensor function.

Sensors measure biological or chemical reactions by generating signals proportional to the concentration of an analyte. Since Clark's glucose sensor, the field of biosensors started to rapidly develop, expanding both the number of devices and the scope of their application[605]. A urea-specific enzyme electrode was developed in 1969 by Guilbault and Montalvo Jr[606], a fiber-optic biosensor for carbon dioxide and oxygen detection in 1975 by Lubbers and Optiz[607], and several commercial biosensors have been developed[608–611]. The potential applications of biosensors have been extensively researched both *in vitro* and *in vivo*. Implantable biosensors, for example, allow continuous measurements in living organisms.

A medical sensing device must have components that allow it to achieve recognition, signalization, and quantification. Those components are a sensor, a transducer, and a system to display or record the outcome of the test[612]. High performance biosensors must have specific characteristics. The most important characteristic of any type of biosensor is selectivity, which enables detection of a specific analyte in a sample. Once detection occurs, the response needs to be converted to a signal. The ability of a sensor to provide consistent responses when a sample is measured several times is known as reproducibility. This is the second most important characteristic. An ideal sensor provides a stable signal over a range of ambient conditions. Whilst every useful sensor has to be selective, consistent and stable, another important factor is sensitivity, as this defines the limit of detection. However, in order to contribute to disease diagnostics, new analytical methods that are high in efficiency and can use small sample volumes need to be developed.

Depending on the method of signal transduction, biosensors can be grouped as optical, electrochemical, mechanical, acoustic, or magnetic (piezoelectric). Some biomolecules are difficult to detect so are studied via an attached label (antibody, fluorophore, or radioactive isotope) that does not affect the behavior of the labeled analyte. This was relevant to the study as two fluorophores (donor and acceptor) conjugated to antibodies were used in developing a FRET-based biosensor assay. While a variety of labels can be used, the labeling strategy must be carefully considered based on the intended application as some labels might block binding sites. Based on their method of detection, biosensors can be divided into two large groups: label-based and label-free[613]. Label-based biosensors have fluorescent, colorimetric, or luminescent signal labels that can provide specificity to the biosensors. This approach has been taken to detect interaction initially between a pair of general tetraspanin EV markers (CD63 and CD81) and then pairs of proposed biomarkers. In contrast, label-free biosensors

directly generate the signal by interaction with the analyte of interest[614]. Optical biosensors are the most common type of biosensor and have been developed in both label-based and label-free formats.

There are several fluorescence-based techniques that include a fluorescent reporter that is necessary to detect the target analyte. Fluorescence-based biosensors can take many formats, and can use technologies that include sandwich immunoassays, immuno-magnetic beads, and FRET[615]. Fluorescent labeling of proposed biomarkers with a pair of fluorophore dyes can be employed to examine interactions through FRET, as has been shown in this study.

4.1.2 Principles of FRET and its application in biosensors

Identification of biomarkers can contribute to diagnosis and thus improve potential for therapeutic intervention and so improve outcomes. Ideally, biomarkers would enable early detection of disease. For decades, researchers have been working on the discovery of biomarkers that recognize a specific disease, and through application in biosensors may have sufficient sensitivity and selectivity to detect low signal abundance in small volumes of samples of biological origin. For a long time, researchers were curious as to whether it was possible to interpret and visualize events happening in living organisms on a molecular level. FRET-based biosensors have been perceived as an excellent and powerful tool, recognizing and defining the concentration of a target molecule. For sensing purposes, FRET-based biosensors have been extensively used in many biomedical applications including bioimaging and drug screening[616]. My rationale behind choosing FRET-based biosensing methods was that they are relatively simple and provide rapid and sensitive diagnostics, even down to single-cell level, and work in heterogeneous samples, such as exosomes[617].

As has been previously mentioned, FRET-based biosensors require two fluorescent probes: a donor and an acceptor. FRET operates through a distance-dependent transfer of energy. Briefly, the FRET process begins with excitation of the donor containing a fluorophore dye that initially absorbs the energy that then transfers it to an acceptor containing another fluorophore dye located in close proximity (typically less than 10 nm away)[618] arising from spectral overlap of the donor's emission and the acceptor's absorption spectra. Due to this process, the fluorescence intensity of the donor decreases, while the acceptor's emission intensity increases. Another requirement for FRET to occur is that there has to be a dipole-dipole interaction between the acceptor and donor[619].

Although FRET is usually used to study intermolecular interactions or conformational changes within a molecule, it can be also applied to biological assays. The key advantage of using FRET-based assays over biochemical assays is to achieve better subcellular resolution in a living cell[620]. The efficiency of a FRET-based assay can be optimized by choosing ideal FRET pairs (donor and acceptor fluorophore dyes) that are essential for the high performance of the assay.

This study introduces a FRET-based assay that was developed to detect the interaction between the proposed putative lung cancer biomarkers on an exosome surface with an ultimate goal to detect cancer using markers on exosomes. The assay was made by using a pair of antibodies corresponding to the proposed biomarkers, one labeled with a donor fluorophore and another with an acceptor fluorophore. These labeled fluorophores are incubated with the exosomes in solution. FRET efficiency is a distance-dependent matter for this method of detection. Binding of fluorophore-labeled antibodies in close proximity will occur only when the selected biomarker pair is co-located on an exosome surface and is in sufficient abundance to bring a high number of biomarker pairs within the distance limits of FRET. Based on the separation distance, the FRET efficiency can either decrease or increase. Two main methods of measuring the FRET efficiency are spectral methods[621] and photoluminescence (PL) lifetime measurements[412,622,623]. In this study, PL lifetime measurement by time-correlated single photon counting (TCSPC) was chosen because neither the concentration of the fluorophore dyes nor light scattering in the sample affect measurements. The PL lifetime refers to the average time that a fluorophore spends in an excited state before returning to the ground state. By measuring the PL lifetime, changes in the fluorophore's surroundings that impact lifetime can be observed and quantified. The presence of an appropriate acceptor fluorophore allowing for FRET provides a new pathway for the donor fluorophore to return to the ground state, resulting in a reduced PL lifetime. The process of energy transfer is shown on a simplified Jablonski diagram below (Fig. 52).

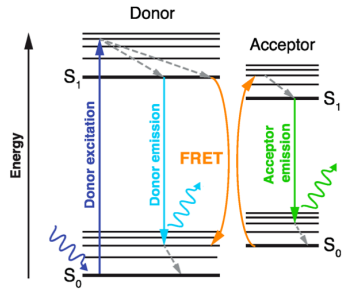

Figure 52. The Jablonski energy transfer diagram*. The simplified diagram is showing energy transition including excitation of the ground state (S_0) and mechanisms of decay of excited states (S_1) to return to the ground state[624].*

The energy transfer process from a molecule in the excited state begins when the molecule from the ground state (S_0) gets excited after absorbing energy from a photon. From the excited state, a molecule returns to the ground state in one of three forms: emission of a photon, non-radiative decay, or FRET[625]. During the process when electrons go from excited states to the ground state, a loss of vibrational energy occurs. As a result of that, the emission spectrum becomes shifted to longer wavelengths than the excitation spectrum. This process of energy difference between absorption and emission spectra of a molecule was investigated by Sir George Gabriel Stokes who studied the properties of fluorescence and first observed this phenomenon in 1852, which was later named after him as the Stokes shift[626]. During his observation, Stokes noticed that the wavelength of the exciting light was always lower than the wavelength of emitted fluorescent light. Later, the differentiated transition moments between absorption and emission were explained by Alexander Jablonski in an energy diagram that was then named after him as the "Jablonski energy diagram" (Fig. 52) and used to explain several processes including delayed fluorescence [627].

As previously mentioned, the close proximity of the pairs is the most critical element for FRET. In this study, we tested whether pairs of proteins that are abundant in exosomes would be within the separation threshold required to give FRET using a simple fluorophore-conjugated antibody system. That was initially validated for general tetraspanin EV markers CD63 and CD81. If these two proteins are abundantly co-located on an exosome, we should expect the donor and acceptors fluorophores to be in close proximity and as a result observe reduction in PL lifetime, the FRET effect. However, a few more conditions have to be met.

The absorption spectrum of the acceptor must overlap the fluorescence emission of the donor (Fig. 53 A). This degree is known as the spectral overlap integral (*J*).

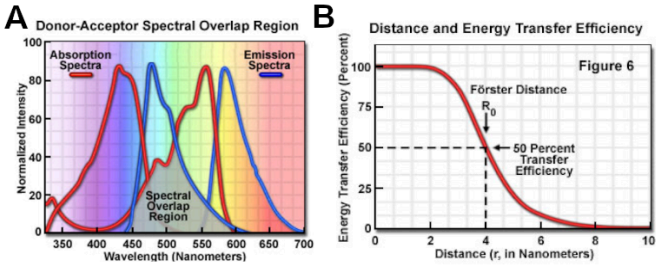

***Figure 53. Schematic representation of FRET**. The figure is showing (A) the spectral overlap integral and (B) fluorescence lifetime decay showing distance and energy transfer efficiency. Adapted from Olympus-lifescience.com*

Further, the dipole-dipole interaction between donor and acceptor resulting in energy transition expects dipoles to be aligned in parallel orientation. Finally, there are two key distances: the separation of the acceptor and donor fluorophores (*r*) and the Förster distance (R_0) of the donor fluorophore. The Förster distance is the distance at which energy transfer is 50% efficient (Fig. 53 B). That means that 50% of excited donor energy is deactivated by FRET. The rate at which the non-radiative transfer of energy between a donor and an acceptor fluorophore occurs is known as k_T and is defined in equation 2 (eq 2):

$$k_T = (1/\tau_D) *[(R_0/r)^6] \qquad \text{(eq 2)},$$

where τ_D is the fluorescence lifetime of the donor in the absence of the acceptor, R_0 is the Förster radius, and *r* is the distance between the donor and acceptor fluorophores. Assuming that a pair is compatible with the previously stated requirements, the efficiency (*E*) can be calculated using equation 3 (eq 3):

$$E= R_0^6/(r^6 + R_0^6) \qquad \text{(eq 3)}.$$

The magnitude of the Förster radius (R_0) is highly dependent on the spectral properties of the donor and acceptor fluorophores and their mutual orientation.

Förster demonstrated that the most useful distance between donor and acceptor is between 2 and 9 nm and with the R_0 values around 5 nm for organic fluorophores. In practice,

the distance can vary somewhere between 4-7 nm due to the background noise[628]. Besides the already mentioned factors, there are a number of other important features, such as the fluorescence quantum yield of the donor in the absence of an acceptor (Φ_d), the refractive index of the solution (*n*), the orientation factor of each molecule (k^2), and by the already mentioned spectral overlap integral (*J*). The relationship between these factors and the Förster distance (R_0) is shown below (eq 4):

$$R_0=9.78 \times 10^3(n^{-4} * \Phi_d * k^2 * J)^{1/6} \text{ Å} \qquad \text{(eq 4)}.$$

In practice, there are several limitations that can affect FRET measurements. The first limitation is associated with the different brightness level of fluorophores when imaged together, forcing one channel to become a dominant. This challenge can be avoided if the brightness level of selected dyes is relatively similar. The second limitation is a donor-acceptor stoichiometry that can interfere with detection if pairs lie outside of defined ratios 1:10 or 10:1. Excess concentration of one or the other will result in an absence of FRET even though the pair might meet prior requirements, such as the Förster distance. The next challenge that can be easily reduced by choosing a well-separated donor and acceptor is crossover or bleed-through between spectral overlap of selected pairs. An advantage of analyzing FRET using PL lifetime measurement of the donor is that it overcomes this problem. Finally, the inappropriate alignment of selected pairs, when the Förster radius between fluorophores is greater than 6 nm, can lead to a false negative or undetectable signal. That can often happen in protein-protein interactions if fluorophores are attached to the opposite sides of the protein-protein complex[629].

4.1.3. FRET, exosomes, and cancer diagnostics

The range of biological applications of FRET has exploded over the past few years leading to an improved understanding of dynamic interactions of proteins that have significant impacts on signaling pathways. Current techniques, such as fluorescence imaging or electronic microscopy, were unable to provide reliable measurements due to limitations in spatial resolution or lack of labeling techniques[630]. On the other hand, the application of intermolecular FRET had overcome those challenges. Generally, FRET application can be often seen in the characterization of membrane systems through protein-protein or lipid-protein interactions. It is a relatively simple and very powerful approach to study membrane biophysics[631]. As described in section 4.1.2, FRET can be determined by differences in photoluminescence,

intensity (steady state), or by detection of the fluorophore lifetime (time-resolved) that was used in this study. Time-resolved FRET measurements have one main advantage over steady state intensity measurements: the measurement is independent of the concentration of the fluorophore dyes. This is important in many biological applications, such as bioimaging. Although not used in this study, a brief description of microscopy imaging analysis is included for comparative purposes.

Fluorescence microscopy is considered a fundamental unit of biomedical imaging due to its high sensitivity to the molecular environment and the ability to recognize changes in molecular confirmations. As a powerful technique, Fluorescent Lifetime Imaging Microscopy (FLIM) can provide a high-resolution analysis of changes occurring in cells on the molecular level by introducing fluorophores into molecular environments. FLIM can be used to monitor disease progression and drug efficacy reflecting insights into various processes in cells and tissues. Similar to FRET, FLIM exploits the lifetime property of fluorescence. However, FLIM offers several advantages over FRET. For example, the ability to visualize changes of fluorophore behavior in molecular environments within the proximity of FRET pairs that cannot be achieved only based on intensity measurements[618,630]. Another advantage is being independent of fluorophore concentration and detected intensity considered as "a self-referenced measurement"[623]. That being said, there are several drawbacks that prevent FLIM taking a dominant approach over FRET. First, imaging is much more time consuming and requires more complicated high-cost equipment. Secondly, imaging in live cells can be challenging due to autofluorescence of cells and pH level[630].

Alternatively, in some cases the combination of FLIM-FRET could be a better option. A FLIM-FRET combination only uses the lifetime measurements of the donor. This use of only the lifetime donor mean that while some pairs are not effective in FRET experiments due to their spectral overlap issues, these can be used in FLIM-FRET[622].

FRET-based applications gain their popularity due to the implementation of FRET techniques into molecular diagnostics. This interest was based on the ability to monitor molecular dynamics of cell membranes and other molecular interactions[632]. Further, FRET-based biosensors and assays were utilized not only to study cellular dynamics but also applied on a single-cell level. Cancer biomarkers, such as proteins, DNA and micro RNA, can be used in ensemble with a FRET-based platform for monitor progression of diseases or their early diagnosis[633]. The advantage of FLIM was used by Wong's research group in identifying the status of dimerization of human epidermal growth factor receptors on circulating EVs in breast cancer[634]. Briefly, chosen receptors EFGR and HER3 were labeled with a fluorescently

conjugated primary antibodies pair of FRET fluorophores (Alexa 546 F4 (EGFR) and Cy5 2F12 (HER3)). Then the lifetime of the donor was measured, and FRET was calculated based on the donor's lifetime with and without the acceptor (eq 3). Then lifetime images before and after treatment were compared tracking the changes related to the separation of chosen receptors in residual tumors.

FRET was successfully applied to monitor protein synthesis in single live cancer cells as an aid to visualizing the production of proteins generated from fluorescently labeled tRNAs[635]. The selected cell line (multiple myeloma cells U266) was transfected with fluorescently labeled tRNAs that were used by ribosomes for protein translation. The study concluded that monitoring protein synthesis by FRET has a higher efficiency and sensitivity and can be mapped in real time compared to other previous successfully used methods, such as isotopic labeling of amino acids or non-radioactive surface sensing of translation assay based on flow cytometry principles. In another example a FRET-based immunoassay demonstrated the ability to distinguish between SCLC and NSCLC lung carcinoma[636]. Implementation of other types of cancer biomarkers, such us micro RNA, was proposed by using amplified time-gated FRET that can advance the possibilities of micro RNA-based cancer diagnostics and research[633,637].

As mentioned in 4.1.1, FRET-based sensors can be used in living organisms. An example of that is shown by Nobis's group that engineered a RhoA FRET biosensor mouse to monitor RhoA activity in normal tissue homeostasis and disease progression in-vivo[638]. In that study, the FRET biosensor was utilized to investigate the activity of the small GTPase molecule, RhoA, and access changes associated with different stages of mammary gestation. Further, monitoring changes in RhoA activity in the same mouse contributed to understanding the efficacy of drug-targeting in breast and pancreatic cancer. This study showed that FRET-based biosensors allow investigation of changes in the crosstalk between molecules of interest during disease progression. This offers potential to optimize drug targeting. Another example is developing a FRET-based molecular probe to monitor enzyme activity in breast cancer which allowed the researchers to detect tumors in vivo against a background of normal tissue[639].

Besides FRET/FLIM application in diagnostics, it has been also demonstrated as a preclinical tool to access drug delivery and efficacy in live tumors[640] and to experimentally validate a list of potential genes implicated in cancer, predicted by the gene prioritizing tool MaxLink[641]. In addition, FRET/FLIM was used for phenotyping analysis of EVs that could improve the efficacy of the general principle EV-based diagnosis[439]. There is also a published use of FRET/FLIM to determine the efficiency of engineering the lipid composition of exosomes[642]. FRET pairs (donor-acceptor), i.e., ORP3–TRITC/VAP-A–GFP, Rab7–

RFP/ORP3-FITC, and Rab7–RFP/VAP-A–GFP, were used to determine potential interactions between ORP3, VAP proteins, and Rab7 in the biogenesis and dynamics of NEI-associated late endosomes. A recent study that reported using FRET with exosomes described the invention of a FRET magnetic aptamer-sensor that allows rapid and efficient detection of epithelial cancer achieved by magnetic enrichment of exosomes with aptamer functionalized fluorescent superparamagnetic microparticles assembled with gold nanoparticles conjugated with complementary DNA. The strategy of exosome detection was based on the FRET pair effect between quantum dot functionalized aptamer particles and gold nanoparticles with complementary DNA[643].

Quantitative FRET imaging was applied to visualize the pro-tumorigenic and pro-metastatic membrane-type 1 invasiveness of live cancer cells that can aid screening of effective anti-cancer inhibitors[644]. Furthermore, FLIM has routinely been used in living cells for measuring of signaling events, such as protein-protein interactions[645,646].

In summary, FRET-based sensing has been widely used in biomedical applications including diagnostics. The FRET-based assay operates through a distance-dependent transfer of energy between a donor and acceptor. Implementation of FRET techniques into molecular diagnostics based on antibody-antigen interaction can be utilized for early detection of various disease including lung cancer. In addition, the efficiency of a FRET-based assay can be optimized by choosing ideal FRET pairs (donor and acceptor fluorophore dyes).

4.2 METHODS

4.2.1 Preparation of AlexaFluor 488 (AF488)/AlexaFluor 546 (AF546)-proposed biomarkers conjugates

The labeling of proposed biomarkers with fluorophore dye, either AF488 (λ_{ex}=488 nm; λ_{em}=520 nm) or AF546 (λ_{ex}=556 nm; λ_{em}=573 nm) *N*-hydroxysuccinimide ester (ThermoFisher), followed a previously published protocol[647]. Briefly, 1 mg of AF488 was diluted in 100 µL dimethyl sulfoxide (DMSO) and used immediately. Antibodies (CD151, GLUT, MYOF, RhoC) used in the conjugation (identical to those described in 3.2.10) were diluted in freshly made 0.1 M sodium bicarbonate buffer, pH 8.3 in ratio 1:10 at the final protein concentration of 5 mg/mL and of 20 µL volume. To this solution, 1 µL of the reactive dye solution (AF488-NHS ester) was added and incubated overnight in dark place at 4 °C under gentle shaking. After the incubation, unbound dye was removed by buffer exchange using protein desalting spin columns (ThermoFisher; 700 µL of resin in 10 mM Tris, pH 7.5

with 0.02% sodium azide). First, the packing buffer was removed by centrifuging the column for 1 min in a swinging bucket centrifuge at 1,000×*g*. Then, the column was equilibrated with 400 µL exchange buffer (1×PBS (phosphate buffered saline with a final concentration of 0.01 M (composition NaCl -137 mM, KCl- 2.7 mM, Na_2HPO_4- 10 mM)) pH7.4 with 0.9% sodium azide). After loading the sample, the column was centrifuged for 5 min at 1,000×*g* and the purified sample was collected and stored at 4 °C.

4.2.2 Determination of Degree of Labeling (DOL)

After the process of labeling antibodies was complete, the unbound dye was removed through gel filtration using buffer exchange columns. Once all excess of unbound dye was removed, the degree of labeling was determined following several steps. First, the absorbance of the purified antibody-dye conjugate from 4.2.1 or 4.2.2 was measured at 280 nm to estimate the protein concentration. The molar concentration of the antibody ($C_{IgG,\,M}$) in the sample was calculated using equation 5 (eq 5):

$$C_{IgG,\,M} = ((A_{280} - A_{dye}(\lambda_{dye})CF)/\varepsilon_{IgG}L)DF \qquad \text{(eq 5)},$$

where A_{280} is the measured absorbance of the sample, $A_{dye}(\lambda_{dye})$ is the measured absorbance of the sample at the identified wavelength of maximum absorbance of the labeling fluorophore, CF is the ratio for a solution of the fluorophore alone of $A_{dye}(280)/A_{dye}(\lambda_{dye})$, ε_{IgG} is the molar absorption coefficient of the antibody at 280 nm (equal to 203,000 $M^{-1}cm^{-1}$), L is the optical path length, and DF is the dilution factor applied to the labeled antibody in determining the absorbance values. Similarly, the molar concentration for the conjugated dye in the labeled sample ($C_{dye,\,M}$) was calculated by using equation 6 (eq 6):

$$C_{dye,\,M} = (A_{dye}(\lambda_{dye})/\varepsilon_{dye}L)DF \qquad \text{(eq 6)}.$$

The degree of labeling (DOL) was determined from equation 7 (eq 7):

$$DOL = C_{dye,\,M}/C_{IgG,M} \qquad \text{(eq 7)}.$$

In this study, extinction coefficients (ε) of 71000 $M^{-1}cm^{-1}$ with CF 0.11 for AF488 and 104000 $M^{-1}cm^{-1}$ with CF 0.12 for AF546 were used [648].

4.2.3 Exosome conjugation with labeled antibodies

The antibodies against CD81, CD151, GLUT, and RhoC were conjugated with the AF488 donor fluorophore and antibodies against CD63, CD151, GLUT, and MYOF were conjugated with the AF546 acceptor fluorophore. Four controls chosen: 1) both fluorophore-labeled antibodies (AF488/546) in the absence of exosomes; 2) exosomes conjugated with labeled a donor-labeled antibody with free AF546 dye; 3) exosomes in the presence of both free dyes AF488/546; and 4) exosomes conjugated with only the donor-labeled antibody. Exosomes conjugated with both labeled antibodies were considered as the 'FRET sample'. Cell- and breath-derived exosomes were isolated by ultracentrifugation as described above in 2.4.3 and re-suspended in 20 µL of fresh 1×PBS. Then 1 µL of each of AF488- and AF546-labeled antibodies were added to all required FRET controls and the sample established above and incubated for 2 h at RT in the dark under gentle shaking. Samples volumes were adjusted to 0.5 mL with 1×PBS and passed through a size exclusion column (qEVoriginal column, Izon Science) to remove unbound fluorophore conjugates as previously described in 2.4.4. Samples were stored in the dark at 4 °C until required. Free dye required for controls 2 and 3 was used at the same concentration as measured in the labeled antibody samples. Determination of dye concentration in the FRET sample was done through absorbance measurements for both dyes (AF488 and AF546) as described in 4.2.4 using a Cary 100 ultraviolet-visible spectrophotometer.

4.2.4 Determination of fluorescent dye concentration in the FRET sample

Measurements were taken at absorbance wavelength (λ_{ex}) of 494 nm and emission measured at a wavelength (λ_{em}) of 517 nm for AF488 and with absorbance wavelength (λ_{ex}) of 556 nm and emission measured at a wavelength (λ_{em}) of 573 nm for AF546at 488 nm using a Cary 100 ultraviolet-visible spectrophotometer. Then, the concentration was calculated using the Beer-Lambert Law equation.

4.2.5 Time-resolved studies and FRET measurements

A labeled exosome sample of total volume 22 µL was transferred into a UV-transparent cuvette (3.5 mL, light path 10 mm± 0.08 mm, wavelength range 190 nm-2.5 µm, ThorLabs) for PL measurements and diluted up to 2 mL with 1×PBS. The PL lifetimes of the sample and

controls were determined with a F980 Fluorescence Spectrometer (Edinburgh Photonics). PL decay scans were collected at a time scale of 500 ns over 1024 channels (0.4883 ns time/ch), 10,000 peak counts with the 1.5 ms (microseconds) pulse period, with excitation wavelength (λ_{ex}) of 380 nm and emission measured at a wavelength (λ_{em}) of 520 nm. The Förster distance value of 6.4 Å was taken from the literature[625]. The instrument response function (IRF) was measured using fresh milk to scatter excitation light. The raw data was collected and averaged from three biological samples and repeated twice for each condition. The ONE all-inclusive F980 software packaging was used to analyze the fluorescent lifetime data and to undertake decay fitting to approximate the IRF. Tail fitting was based on the Marquardt-Levenberg algorithm using a two exponential decay fit, which in almost all cases provided a higher quality fit to experimental data that a single exponential fit in these complex samples. The quality of fit was determined through chi-squared (χ^2) and residual plots. The average lifetime (τ_{avg}) of the donor in the FRET test sample and controls was obtained by TCSPC using equation 8 (eq 8):

$$\tau_{avg} = (\alpha_1\tau_1^2 + \alpha_2\tau_2^2)/ (\alpha_1\tau_1 + \alpha_2\tau_2) \quad \text{(eq 8)},$$

where τ is the lifetime and α is the pre-exponential factor for each of the two exponential functions. The efficiency of energy transfer for different acceptors and donors was calculated using the donor in the presence and absence of the acceptor using equation 9 (eq 9):

$$E_e = 1-\tau_{avgDA}/\tau_{avgD} \quad \text{(eq 9)},$$

where E is the FRET efficiency, $\tau_{avg\ DA}$ is the PL lifetime of a donor-labeled antibody that is co-conjugated onto an exosome sample with an acceptor-labeled antibody (i.e. from the "FRET sample"), and τ_{avgD} is the PL lifetime of an donor-labeled antibody conjugated onto an exosomes sample in the presence of acceptor free in solution (i.e., from control 2). In addition, the distance of separation between donor and acceptor (r) was quantified using Förster distance (R_0, 6.4 Å) in the equation 10 (eq 10):

$$r = \sqrt[6]{[(1/E) - 1] * R_0} \quad \text{(eq 10)}.$$

4.2.6 Statistical analysis

Analyses were performed using Prism GraphPad scientific 2D graphing and statistical software, version 9.1.1 (223) for macOS, April 16, 2021, San Diego, California. The six replicates' data from FRET samples and controls were tested for normality of distribution by constructing a Quantile-Quantile (Q-Q) graphical scatterplot using the Normality Tests diagnostic function. To confirm the statistical difference between FRET samples and controls, a two-tailed t-test was applied with a confidence level set to 95% and based on statistical significance (p-value <0.05).

4.3 RESULTS

This section describes the results from several steps. In order to collect accurate and sufficient data from the experiment, several steps were followed. First, the antibodies were labeled with fluorophore dyes to later take part in the FRET-based assay. Second, the degree of labeling was measured to ensure the quality of the assay. For that, the concentration of the dyes in the FRET samples was defined. Third, selected FRET pairs were tested first on A549 cell-derived exosomes to select the most efficient pair/pairs. Finally, the pair/pairs showing greatest percentage of efficiency were further tested on negative controls: WI-38 cell-derived exosomes and breath-derived exosomes. The results of each step are reported below.

4.3.1 Labeling antibodies and determination of degree of labeling

Antibodies were labeled as described in 4.2.1, and the degree of labeling was determined as described in 4.2.2. Because the presence of unlabeled or multiple-labeled antibodies can alter the FRET signal, determination of this parameter was critical for FRET experiments to ensure reproducibility and quality control of fluorescence intensity of fluorophore-labeled bioconjugates. The results of degree of labeling are shown in Table 11.

Table 13. Degree of labeling after labeling antibodies with selected fluorophore pairs AF488/AF546.

Donor (AF488) + proposed biomarker	Donor	Acceptor (AF546) + proposed biomarker	Acceptor
CD81	8.642	**CD63**	5.894
RHOC	8.21	**CD151**	5.43
GLUT	8.34	**MYOF**	5.75
CD151	7.98	**MYOF**	4.54
CD151	8.28	**GLUT**	5.97

In general, the ideal degree of labeling for both donor and acceptor labeled antibodies is considered within the acceptable range of 2 to 10 (dye molecules per protein)[649]. That suggests that results reported in Table 13 are within the acceptable levels of labeling.

For reproducibility of the experiment, it was necessary to measure the apparent dye concentration in the dye-labeled antibody solutions to get the dye concentrations in the controls and the sample to match. That was done to keep data consistency. The absorbance spectra for the dye component in cell-derived exosomes that was conjugated to antibodies is shown on Figure 54.

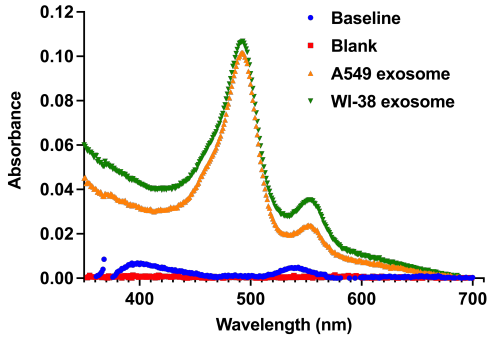

Figure 54.The absorbance spectra for the dye component in cell-derived exosomes conjugated to antibodies. *On the figure, A549 exosomes are represented by orange line and WI-38 exosomes are shown in green. The baseline is represented by the blue line, while blank is by the red line. The Y-axis represents absorbance values, and X-axis represents wavelength (nm). The figure was generated by using Prism GraphPad Software (version 9.1.1) for macOS, San Diego, California.*

The concentration of the dye components of the fluorescently labeled antibodies are shown in Table 14.

Table 14. Absorbance values of dyes and their concentration in the sample. *The concentration of dye component in exosomes conjugated with fluorescent labeled antibodies was calculated based on dyes' absorbance values and the extinction coefficients were taken from the literature[648].*

Sample	Dye	Absorbance values	Extinction coefficients (liter/mol-cm)	Concentration (μM)
A549	AF488	0.097137	71000	1.368
A549	AF546	0.022299	104000	0.214
WI-38	AF488	0.102822	71000	1.448
WI-38	AF546	0.032806	104000	0.31544

After antibodies were labeled and the degree of labeling was determined, the next step was testing FRET pairs on A549 cell-derived exosomes.

4.3.2 Determination of the FRET efficiency on general tetraspanin EV markers (preliminary study)

Although widely used in molecular diagnostics, FRET-based assays have not been previously applied to confirm the presence of exosomes by using protein biomarkers. In this study, two fluorophore dyes AF488 (donor) and AF546 (acceptor) were chosen as the donor and acceptor respectively, as these had been successfully used in FRET experiments[625]. First, the FRET assay was tested with labeled (the chosen dyes were attached to an antibody) antibodies corresponding general tetraspanin EV markers (CD63 and CD81) which are embedded in the surface of exosomes. The key, sample, and controls selected to assess the potential for non-specific interactions chosen for the experiment are presented on Figure 55.

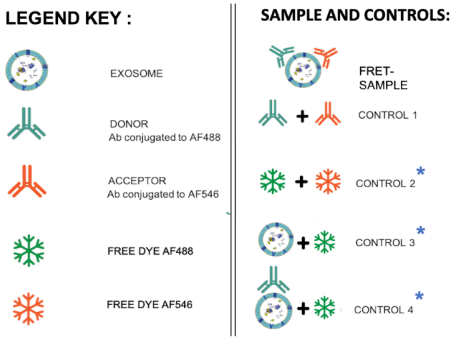

***Figure 55. Legend key for the initial FRET experiment**. Controls 2-4 marked by an asterisk were later modified.*

The results of the FRET experiment based on the data of six replicates for each sample are reported in Figure 56, where panel A represents all controls previously defined in Figure 55, and panels B-D show the FRET outcome for cell- and breath-derived exosomes compared to the controls.

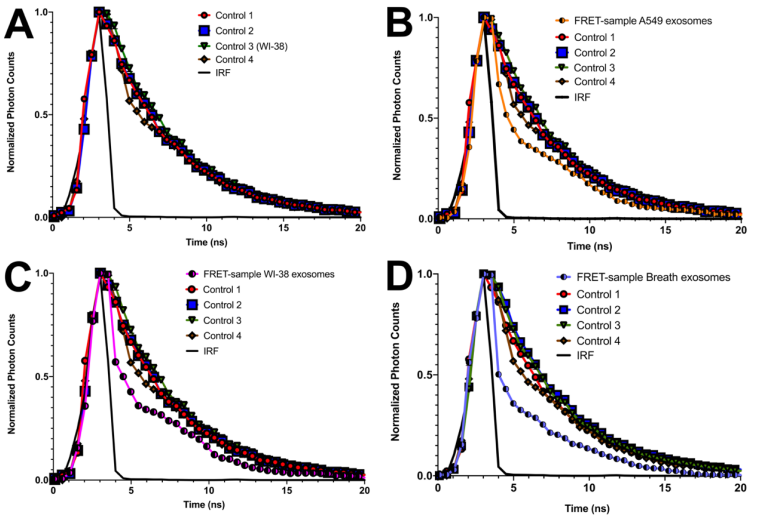

***Figure 56. PL lifetime analysis of cell- and breath-derived exosomes labeled with general tetraspanin antibodies.** PL lifetimes obtained by TCSPC with excitation wavelength (λ_{ex}) of 380 nm and emission measured at a wavelength (λ_{em}) of 520 nm of (A) controls and (B,C) cell (A549, WI-38 respectively)- and (D) breath-derived exosomes conjugated with fluorescently labeled antibodies corresponding to the general tetraspanin markers (CD63 and CD81) showing four selected controls and FRET (donor-acceptor) samples. Antibodies against the selected biomarkers for these measurements were labeled as follows: anti-CD63 AF488 - anti-CD81 AF546. Controls on panels B-D are identical to those shown on panel A. The Y-axis represents normalized photon counts, and X-axis represents decay time (ns). The instrument response (IRF) is shown on each panel in black. The experiment was performed on three biological samples and run in duplicate. The error bars represent standard deviation. Some error bars are not visible as the data in the duplicates were close to identical. The figure was generated by using Prism GraphPad Software (version 9.1.1) for macOS, San Diego, California.*

Based on experimental data, a significant decrease was observed in the PL lifetime of the donor when the dye-conjugates were attached to antibodies against the general tetraspanin EV markers CD63 and CD81 and incubated with any of A549 cell - (43.8% efficiency), WI-38 cell - (44.3% efficiency), or breath-derived exosomes (55.9% efficiency) (Table 15).

***Table 15. PL lifetime analysis of cell- and breath-derived exosomes labeled with fluorophore-conjugated general tetraspanin antibodies**. Emission decay analysis of a pair of antibodies corresponding to general tetraspanin markers (CD63 and CD81) on cell- and breath-derived exosomes. The data was collected from three biological samples run in duplicate.*

Source of exosome	τ_{avg} (ns)	τ_{avg} cntl (ns)	*E* (%)	*r* (nm)	p^a
A549	2.02±0.010	3.59±0.005	43.8	7.34	7.7×10^{-22}
WI-38	2.02±0.001	3.63±0.003	44.3	7.35	6.0×10^{-24}
Breath	1.59±0.003	3.60±0.004	55.9	7.13	1.4×10^{-23}

τ_{avg} – PL lifetime of FRET pairs, shown ± standard deviation; τ_{avg} cntl– PL lifetime of control, PL lifetime of the exosomes conjugated with a AF488 labeled antibody in the presence of free AF546 dye control, shown ± standard deviation; E (%) – FRET efficiency; r – distance between the donor and acceptor fluorophores

[a] p-values from unpaired, two-tailed t-test comparing PL lifetime of sample to control

As expected, given this experiment was using general tetraspanin EV markers, the lifetime decay for both cell-derived exosomes is almost identical, which resulted in a very similar FRET efficiency. Lifetime decay for breath exosomes was slightly faster than in cell-derived exosomes reporting higher efficiency. At that point a positive outcome observed in reduction in PL lifetimes was expected as these markers (CD63 and CD81) are both known to be abundant on exosomes. The ability of a FRET-based assay to distinguish between cancerous and non-tumorigenic exosomes was tested via the use of the proposed biomarkers (CD151, GLUT, MYOF and RhoC) and described in the next subchapter 4.3.3.

4.3.3 Determination of the FRET efficiency of proposed biomarkers

For this experiment, antibodies corresponding to proposed biomarkers were labeled with the donors (CD151, GLUT, and RHOC) and the acceptors (CD151, GLUT, and MYOF) creating four pairs: RHOC-CD151, GLUT-MYOF, CD151-MYOF, and CD151-GLUT (Fig. 57).

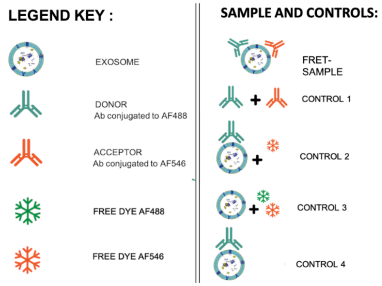

Figure 57. Various controls and FRET samples for the FRET-based detection assay.

Among these four pairs, separate donor-labeled and acceptor-labeled samples of CD151 and GLUT were prepared. This decision was determined by the choice to test two of the markers as both donor and acceptor and opted to use the strongest (GLUT) and weakest (CD151) bands on the blot in Figure 35 for this purpose. Controls were selected to assess the potential for non-specific interactions, as shown in Appendix, Figs. S 1-10.

First, PL lifetime measurements of dyes and conjugated dyes were collected. There were no change between the isolated donor dyes' photoluminescence (PL) and that of the conjugated complexes (Fig. S 11). Then, PL lifetime measurements were carried out with A549 cell-derived exosomes with pairs of donor- and acceptor-labeled antibodies (Fig. 58).

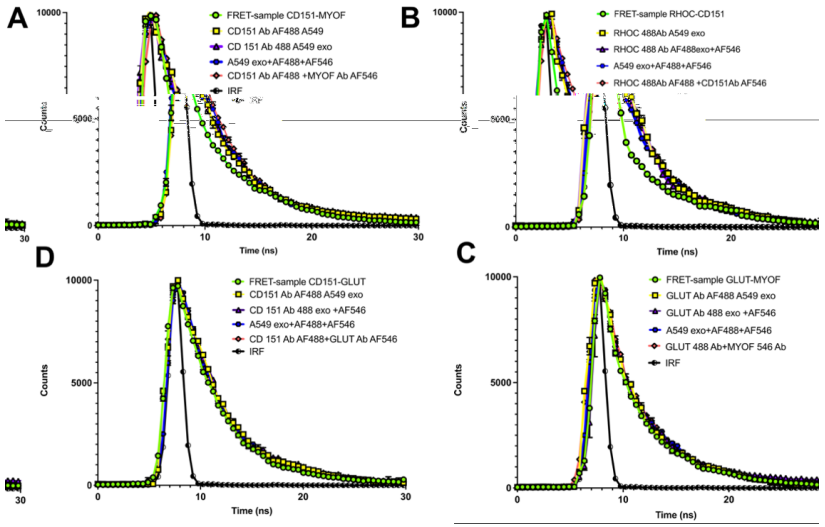

Figure 58. PL lifetime analysis of A549 cell-derived exosomes labeled with proposed biomarkers. *PL lifetimes obtained by time-correlated single photon counting (TCSPC) (λ_{ex}=380 nm; λ_{em}=520 nm) of A549 cell-derived exosomes conjugated with fluorescently labeled antibodies corresponding to the proposed biomarkers in combination of (A) CD151-MYOF, (B) RhoC-CD151, (C) GLUT-MYOF, and (D) CD151-GLUT respectively showing four selected controls and FRET (donor-acceptor) samples. Antibodies against the selected biomarkers for these measurements were labeled as follows: CD151 AF488-MYOF AF546, RhoC AF488-CD151 AF546, GLUT AF488-MYOF AF546, and CD151 AF488-GLUT AF546. The Y-axis represents normalized photon counts, and X-axis represents decay time (ns). The instrument response (IRF) is shown on each panel in black (dashed). The experiment was performed on three biological samples and run in duplicate. The error bars represent standard deviation. Some error bars are not visible as the data in the duplicates were close to identical. The figure was generated by using Prism GraphPad Software (version 9.1.1) for macOS, San Diego, California.*

The FRET efficiency was calculated for all proposed pairs. The derived data is in Table 16.

Table 16. PL lifetime analysis of A549 cell-derived exosomes labeled with fluorophore-conjugated antibodies corresponding proposed biomarkers. *Emission decay analysis of pairs of antibodies corresponding proposed biomarkers. The data was collected from three biological samples run in duplicate.*

FRET pairs	τ_{avg} (ns)	τ_{avg} cntl (ns)	*E* (%)	*r* (nm)	p^a
CD151-MYOF	3.94±0.010	4.25±0.075	7.30	9.77	$1.2x10^{-4}$
RhoC-CD151	3.40±0.027	4.29±0.027	20.8	8.00	$2.2x10^{-15}$
GLUT-MYOF	4.22±0.032	4.33±0.008	2.53	11.8	$9.5x10^{-6}$
CD151-GLUT[b]	4.29±0.043	4.02±0.039	NA	NA	$4.5x10^{-7}$

τ_{avg} – PL lifetime of FRET pairs, shown ± standard deviation; τ_{avg} cntl– PL lifetime of control, PL lifetime of the exosomes conjugated with a AF488 labeled antibody in the presence of free AF546 dye control, shown ± standard deviation; E (%) – FRET efficiency; r – distance between the donor and acceptor fluorophores

[a] *p-values from unpaired, two-tailed t-test comparing PL lifetime of sample to control*

[b] *The derived data for pair CD151-GLUT is not shown as the lifetime of the sample was longer than the controls.*

The data in Table 16 confirms that the highest FRET efficiency occurred in the CD151-MYOF and RhoC-CD151. Therefore, we decided to proceed only with these two pairs, CD151-MYOF and RhoC-CD151, that are significant and have the largest difference between the control and FRET-samples. No efficiency or spacing is calculated for the CD151-GLUT pair, given the increase lifetime in the FRET sample noted above.

Then, the six replicates' data were tested for normality of distribution by constructing a Quantile-Quantile (Q-Q plot) (Fig. 59). The data in the scatterplot lies along the diagonal, confirming that the data is normally distributed.

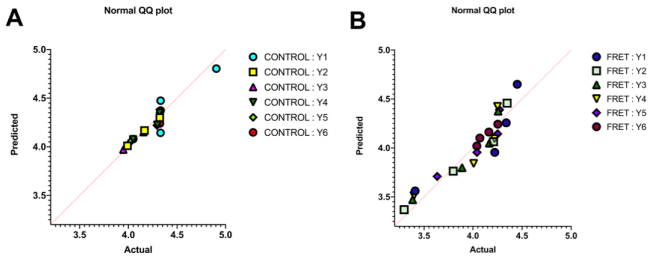

Figure 59. Normal Q-Q (Quantile-Quantile) scatterplots*. The Q-Q scatterplots are showing Control and FRET sets of quantiles to confirm the normal distribution. The Y-axis represents theoretical quantiles, and X-axis represents sample quantiles (n=6). The figure was generated by using Prism GraphPad Software (version 9.1.1) for macOS, San Diego, California.*

After verifying that data from these experiments was normally distributed, controls and FRET-sample pairs were compared using the t-test. T-test was performed to identify whether the fluorescence lifetimes in the samples were significantly different from the controls (Fig. 60).

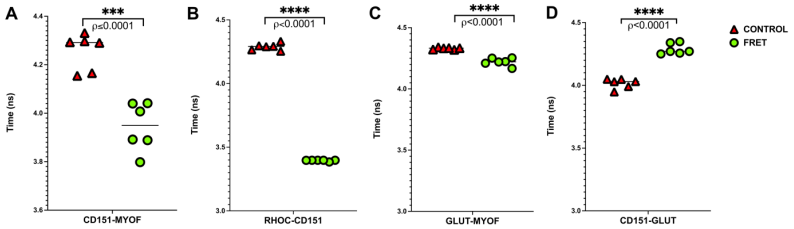

Figure 60. T-test statistical analysis of FRET pairs on A549 cell-derived exosomes. *Statistical representation of the two-tailed t-test for all proposed FRET pairs: (A) CD151-MYOF, (B) RHOC-CD151, (C) GLUT-MYOF, and (D) CD151-GLUT (n=6) when tested on exosome isolated from A549 cells. The p-value for all pairs was equal (A) or below 0.0001 showing very significant results. The Y-axis represents the decay time (ns). The figure was generated by using Prism GraphPad Software (version 9.1.1) for macOS, San Diego, California.*

From the results of the t-test, two pairs were excluded. Although pairs GLUT-MYOF (C) and CD151-GLUT (D) did show a statistically significant difference (ρ <0.0001), the absolute difference between samples and controls for the GLUT-MYOF pair was very small, which could hamper future application to a diagnostic assay. Unexpectedly, the data for the FRET sample with the CD151-GLUT pair showed a longer lifetime than the controls.

The confirmation of hypothesis by evidence allowed moving to the final step of the experimental study: to confirm that the proposed FRET-based assay was able to distinguish between exosomes derived from a model of lung cancer (A549 cells) and exosomes derived from other sources (WI-38 cells and EBC of healthy volunteers) (Fig. 61). The FRET-samples and controls were chosen following the same combinations annotated in Figure 57.

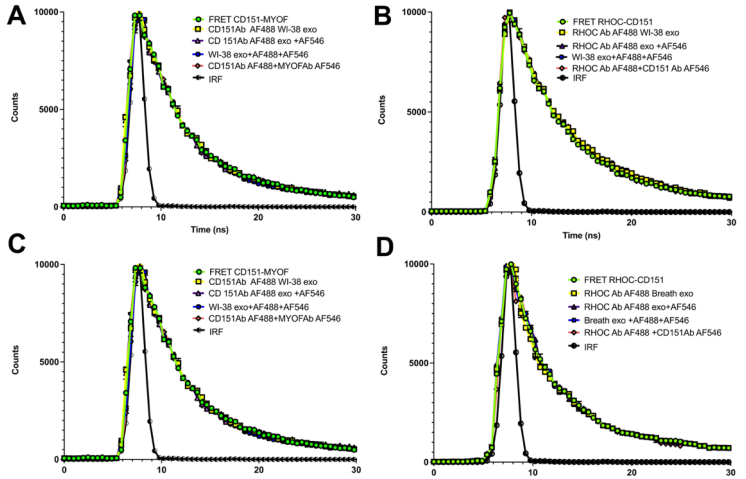

Figure 61. PL lifetime analysis of WI-38 cell- and breath-derived exosomes labeled with proposed biomarkers*. PL lifetimes obtained by time-correlated single photon counting (TCSPC) (λ_{ex}=380 nm; λ_{em}=520 nm) of (A,B) WI-38 cell- and (C,D) breath-derived exosomes conjugated with fluorescently labeled antibodies corresponding to the most efficient pairs of proposed biomarkers in combination of CD151-MYOF and RhoC-CD151 respectively showing four selected controls and FRET (donor-acceptor) samples. Antibodies against the selected biomarkers for these measurements were labeled as follows: (A,C) CD151 AF488-MYOF AF546 and (B, D) RhoC AF488-CD151 AF546. The Y-axis represents normalized photon counts, and X-axis represents decay time (ns). The instrument response (IRF) is shown on each panel in black (dashed). The experiment was performed on three biological samples and run in duplicate. The error bars represent standard deviation. Some error bars are not visible as the data in the duplicates were close to identical. The figure was generated by using Prism GraphPad Software (version 9.1.1) for macOS, San Diego, California.*

The decay lifetimes of the FRET samples and controls for WI-38 cell- and breath-derived exosomes were very similar. The derived lifetime data of these pairs is shown in Table 17.

Table 17. PL lifetime analysis of successful FRET pairs on negative control samples*. Emission decay analysis of the most efficient pairs of fluorophore-conjugated antibodies (RHOC-CD151 and CD151-MYOF) tested on negative controls (WI-38 cell (annotated as W)- and breath (annotated as B)-derived exosomes). The data was collected from three biological samples run in duplicate.*

FRET pairs	τ_{avg} (ns)	τ_{avg} cntl (ns)	*E* (%)[b]	*r* (nm)[b]	*p*[a]
CD151-MYOF (W)	6.59±0.010	6.35±0.017	NA	NA	$4.1x10^{-14}$
RhoC-CD151 (W)	6.92±0.025	6.81±0.008	NA	NA	$1.1x10^{-6}$
CD151-MYOF (B)	4.09±0.011	4.09±0.009	NA	NA	0.3
RhoC-CD151 (B)	3.86±0.024	3.63±0.007	NA	NA	$8.2x10^{-10}$

τ_{avg} – PL lifetime of FRET pairs, shown ± standard deviation; τ_{avg} cntl– PL lifetime of control, PL lifetime of the exosomes conjugated with a AF488 labeled antibody in the presence of free AF546 dye control, shown ± standard deviation; E (%) – FRET efficiency; r – distance between the donor and acceptor fluorophores

[a] *p-values from unpaired, two-tailed T tests comparing PL lifetime of sample to control*

[b] *The derived data for all pairs is not shown as the lifetime of the sample was longer/or equal than/to the controls.*

After verifying that data from these experiments was normally distributed, controls and FRET-sample pairs were compared using the t-test (Fig. 62).

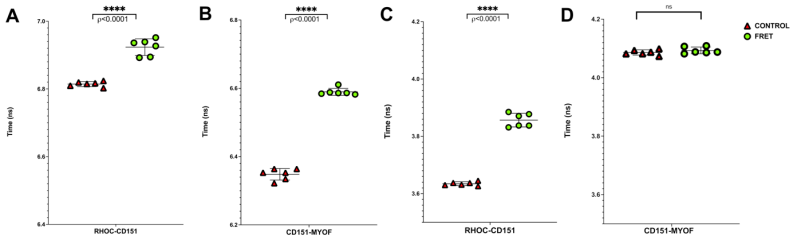

Figure 62. T-test statistical analysis of FRET pairs on WI-38 cell- and breath-derived exosomes. *Statistical representation of the two-tailed t-test (n=6) for two chosen FRET pairs, RHOC-CD151 and CD151-MYOF, tested on negative control samples (A,B) WI-38 cell- and (C,D) breath-derived exosomes. The ρ-value for all pairs, except CD151-MYOF for (D) breath-derived exosomes, was below 0.0001 showing extremely significant results. Pair CD151-MYOF has a non-significant ρ-value ($\rho = 0.2674$). The Y-axis represents the decay time (ns). The figure was generated by using Prism GraphPad Software (version 9.1.1) for macOS, San Diego, California.*

Whilst three of the four samples showed statistically significant differences between the FRET sample and the control ($\rho < 0.0001$), the magnitude of the differences for CD151-MYOF pair tested on breath-derived exosomes was relatively small ($\rho = 0.2674$), and with the slightly shorter lifetimes found in the controls – the opposite of what would be expected for FRET.

Put together, these results showed that two of our proposed pairs of biomarkers can distinguish exosomes derived from a cell model of lung cancer and from exosomes derived from a model of normal lung tissue or from the breath of healthy volunteers.

4.4 DISCUSSION

The research challenge in this chapter was associated with choosing suitable methods and techniques to test several pairs of biomarkers that were combinations of the putative biomarkers identified as a result of the proteomic analysis identified in Chapter 3.

The clinical relevance of FRET-based assays has been shown in oncology, protein-protein interaction, micro RNAs, diagnosis of infectious disease (bacterial infection and sepsis), prenatal screening, in point-of-care devices, and including their application to cancer diagnostic assays[633].

One of the challenges in this chapter was to develop a more straightforward FRET-based assay system to determine the co-location of a pair of biomarkers, which we reasoned would lead to higher diagnostic specificity than a single marker. As has been previously mentioned in 4.1.2., FRET depends on distance-dependent energy transfer between a donor and acceptor pair of fluorophores. Therefore, chosen marker pairs would need to both be present as abundant constituents of the same exosome, a characteristic we hoped would readily distinguish between exosomes from a model of lung cancer and from models of normal lung. The energy transfer associated with FRET can be determined by differences in PL, intensity, or by detection of the fluorescence lifetime. Time-resolved fluorescence lifetime measurements have the advantage that they are independent of the concentration of the fluorophores, and so were chosen as the basis for the assay system in this study. Quantitative FRET measurements were employed. Achieving this milestone required making of custom fluorescent-labeled antibodies corresponding to appropriate donor and acceptor pairs followed by conjugation of these custom labels with different sources of exosomes. The fluorophore pair AF488/AF546 was chosen as the ideal combination to attain this goal.

In order to obtain high-quality FRET data, several appropriate controls were selected. Selected antibodies corresponding to the proposed biomarkers identified in Chapter 3 were directly labeled with fluorophore dyes and exploited in the experimental study.

During the selection process six pairs of fluorophore candidates (AF488/546, AF 488/514, AF488/532, AF647/680, AF647/700, AND AF647/750) were taken for consideration, given they had appropriate levels of spectral overlap. The final choice was made after confirming the performance of the dyes based on the distance separating the donor and acceptor and the brightness and stability of the fluorophores. Based on a review of literature that reports data analysis results of FRET pairs tested on biological systems, one out of the six previously mentioned FRET pairs, AF488/546, was considered optimal. It appears, that the

same FRET pair had been used in several studies where AF488 played a role as a donor and AF546 was an acceptor[625,650,651]. In the first study, the pair was successfully used to support nano communication by playing roles as nano transmitters and receivers creating multi-input multi-output FRET communication channels. The results of this study showed that the AF488/546 pair was the most successful pair compared to AF405/488 and AF405/546[625]. A second paper utilized the same fluorophore dyes to study protein-protein interactions suggesting that their application to in solution FRET would have value in drug discovery and could potentially be developed into a drug screening platform[650]. A further study investigated bleed-through from excitation leading to cross talk in emission detection. The study pointed out that the concentration of the donor and acceptor should be in the same order of magnitude to result in accurate calculation of FRET efficiency[651]. After demonstrating meeting the needs of FRET requirements, the AF488/546 pair was selected for conjugation with proposed biomarkers.

The FRET experiment began with labeling antibodies and determination of the degree of labeling. First, the selection of donors and acceptors for proposed antibodies took place. Previously, in 4.1.2 it was said that the efficiency of FRET-based assay depends on the choice of FRET pairs (donor and acceptor fluorophore dyes) that are essential for the high performance of the assay. The choice of labeling antibodies with the donors or the acceptors and the pair placement was made based on the result from western blotting reported in Chapter 3 (Fig. 35, Appendix Figs. S 1-10), specifically, the width of the band. Because the method of FRET efficiency was chosen to be based on the detection of the donor fluorophore's lifetime, antibodies with strong distinct bands were labeled with the donors. The biomarkers that formed the most distinct bands in the western blot experiment were conjugated with the acceptor fluorophore. That resulted in forming four pairs (donor-acceptor): RHOC-CD151, GLUT-MYOF, CD151-MYOF, and CD151-GLUT.

Labeling antibodies was not the end point of this step. It was necessary to know the concentration of dye conjugated to antibodies as it was an essential point for selected controls ensuring a good quality of the assay. For that, the degree of protein labeling based on the antibodies and dye absorbances had to be determined. Although choosing the ideal FRET pair was essential, the optimization of labeled antibodies was equally important. To ensure that the FRET signal would be maximized, it was necessary to minimize any interference during the labeling process. Following that, the unbound dye was removed through the gel filtration process using buffer exchange columns. That was critical for the labeled antibodies to

recognize protein on the surface of exosomes. Use of appropriate controls and replicate experiments ensured that high quality data was obtained.

FRET assays have not been previously applied to confirm exosomes by using protein biomarkers. Given this lack of prior art, before proceeding to test its application with the proposed protein biomarkers, it was first attempted using general tetraspanin EV markers CD63 and CD81. This was undertaken to test the specificity and sensitivity of this FRET-based assay. The assay was developed following several steps. First, EBC was collected and followed by exosome isolation (ultracentrifugation). Exosomes were then stored at 4 °C until the next step. Second, antibodies corresponding to the proposed biomarkers were labeled with a selected donor and acceptor fluorophore pair. After removal of any excess dye, exosomes were incubated with the labeled antibodies. Exosomes were re-isolated by SEC to pellet unconjugated dyes and antibodies. Third, samples containing several controls and exosome samples conjugated with labeled donor and acceptor were prepared and followed by lifetime measurements. The expectations of the detection methods were as followed. If FRET occurs, the lifetime of the donor will be much shorter in the FRET system than in a control where the dyes are not brought into close proximity.

As described above, the first step was set up initially using the known tetraspanin EV markers, anti-CD63 and anti-CD81, and exosomes were conjugated with a pair of fluorescently labeled antibodies corresponding to these markers. At that point a positive outcome was expected as these markers are both known to be abundant on exosomes. The second step was to test the selective detection of exosome from the A549 lung cancer cell model via the use of the proposed biomarkers (CD151, GLUT, MYOF and RhoC). Several pairwise combinations of CD151, GLUT, MYOF, and RhoC were tested. At the outset of this study, it was uncertain whether the biomarkers proposed on the basis of the proteomic analysis in Chapter 3 would be present in sufficient abundance and suitably co-located in order to generate a distinct FRET signal. Although, the proposed biomarkers were previously validated by western blotting as has been shown on Figure 35, neither pairs containing GLUT provided a large reduction in fluorescence lifetime and failed to evidence energy transfer in our assay. However, pairs containing CD151 showed the highest FRET efficiencies (20.8%).

The fact that cancer cell growth is associated with increased glucose metabolism was reported a long time ago and is well-documented. In addition, many studies had reported the overexpression of GLUT protein, especially GLUT-1, in a variety of malignancies and so is associated with tumor growth[652–655]. One study based on the proteomic analysis reported GLUT-1 and other two exosome membrane proteins as potential breast cancer biomarkers[656].

The GLUT-1 was only detected in exosomes isolated from the breast cancer cell line and were absent in non-cancerous epithelial cell-derived exosomes.

In contrast, the CD151-MYOF and RhoC-CD151 pairs showed high enough FRET efficiency to conclude that energy transfer on A549 cell-derived exosomes was successful. The clinical significance of CD151 gene expression predicting the behavior of lung cancer has been reported in several studies. CD151 gene has been reported that one of the markers associated with an early stage of metastasis[657]. The same gene was shown to be associated with poor outcome in respiratory disease, such as asthma, influenza, and pulmonary fibrosis, including lung cancer, suggesting that CD151 should be considered as a biomarker that can be used in screening and also as a prognostic tool[658]. Furthermore, CD151 has been proposed to target exosomes to tissues including lung, lymph node, and stroma[659]. The clinical usefulness of CD151 as a cancer biomarker was illustrated with in a study that demonstrated that CD151 protein embedded on the surface of exosomes is as powerful a marker of squamous cell cancer and SCLC as multimarker models[171]. The overexpression of CD151 was also studied in lung tissue samples obtained from surgically resected NSLC also suggesting the importance value of CD151 as a biomarker[660]. In this study, we had presented results of application of CD151 as a putative protein biomarker for cancer diagnosis in the FRET assay in two different combinations, CD151-MYOF and RhoC-CD151, which were the only two combinations showing higher FRET efficiency and therefore successfully detected lung cancer exosomes.

Although myoferlin has been mostly associated with breast and pancreatic cancer, there is evidence that myoferlin can act as a novel target for detection of lung cancer[526], and is a potential candidate in clinical diagnosis[661]. In addition, a recent study identified its role in inhibition of the proliferation of cancer cells[662].

Whereas the overexpression of RhoC proteins in various types of cancer has been reported, the role of RhoC protein in cancer still needs to be elucidated[663]. A functional study of lung cancer metastasis suggested that RhoC contributes to metastasis by mediating cell motility but does not affect tumor growth[664]. The overexpression of RhoC proteins was also a subject of Lu's research group, who also confirmed the effect of the protein on cell motility, proposing it initiates the chain of changes in the epithelia-mesenchymal transitions process, which then causes rearrangement in the cytoskeleton contributing to tumor metastasis[543]. In addition, RhoC protein belongs to the superfamily of proteins that has been known to be involved in dysregulation of guanosine diphosphate (GDP)-hydrolyze guanosine triphosphate (GTP) cycle that plays a crucial role in cancer development[665,666].

To validate the hypothesis that proposed biomarkers can only be detected on cancer cell-derived exosomes, exosomes from WI-38 cells and human breath were tested. The proposed biomarkers were not evident in exosomes from these sources by western blotting or FRET (Figs. 35 and 62, respectively).

It is rare that a single biomarker can provide an accurate diagnosis. The goal of biomarker discovery is frequently to identify several biomarkers that can be developed together into an assay for tumor diagnosis. There are several examples utilizing FRET with protein cancer biomarkers to monitor disease repones in testicular[667], prostate[668], breast[669], and ovarian cancers[670].

4.1 Limitations

This study is based on potential biomarkers chosen for their presence in exosomes from a single cell model of lung cancer. It is not known if these are general markers of lung cancer or simply markers of the A549 cells and so this study includes some limitations. The success of this experimental design was directly related to specific methodological choices.

Firstly, one of the limitations is assay sensitivity and so the limit of detection needs to be established. This is required to determine the volume of EBC required in order to get detectable signal in a future clinical diagnostic assay. This is the most important limitation for taking future work into clinical trial. Briefly, in this study, the total volume of EBC collected for one sample was 34 mL. That required participation of 20 volunteers from which EBC was pooled. Given the fact that each volunteer contributed 2 mL on average into a pooled sample breathing for 30 min, this would add up to 10 hours of breathing if a sample were to be collected from a single individual. This seems almost impossible to expect from a lung cancer patient.

Secondly, it would be highly desirable not to have to do large amounts of sample preparation for a lung cancer bioassay. This study shows that some form of exosome enrichment is required as exosome markers cannot be detected in whole breath, however a range of exosome enrichment strategies has not been investigated in order to see which would be the easiest and quickest to do as part of a diagnostic test, whilst still giving a FRET signal from general tetraspanin EV markers. Further work with healthy volunteers is required.

Finally, the goal of this study was not to identify final biomarkers, but to assess whether there was any potential to discover and detect potential biomarkers on exosomes. There was no clinical validation to support the proposed biomarkers. It is certainly possible that the biomarkers presented in this study might be unable to distinguish between healthy individuals

and those with lung cancer. Recommendations that need to be taken into consideration to explore the full potential of breath exosomes are required using additional lung cancer models, and ultimately clinical studies to determine the ideal combination of exosome-based biomarkers.

4.5 CONCLUSION

The aim of the research presented in this chapter was to develop a sensitive test for the presence of the selected biomarkers of lung cancer found on exosomes from cell models identified in Chapter 3. The aim was achieved through two objectives: labeling the antibodies corresponding to the proposed biomarkers, and determination of the FRET efficiency of each proposed fluorescent labeled antibody pair by conjugating them with all sources of exosomes with the end goal of selecting one to two pairs using a FRET-based assay using time-correlated single photon counting.

This study has shown that the FRET-based assay was able to distinguish between lung cancer cell-derived exosomes and exosomes isolated from breath of healthy volunteers and a cell model of normal lung tissue based on identified potential biomarkers of lung cancer using a proteomic analysis. This study confirms that data from time-resolved studies can be used for a sensitive test to confirm the presence of cancer biomarkers.

Briefly, the concept of using a FRET-based test was first assessed with the general tetraspanin EV markers, anti-CD63 and anti-CD81. These findings suggested that this assay functioned satisfactorily enough to continue with proposed biomarkers. Further, this aspect of the study indicates that a FRET-based assay can be considered as a new way to prove the presence of exosomes. This step also confirmed the sensitivity of this assay.

In this study, four proposed combinations of labeled antibodies corresponding to proposed biomarkers were tested. Two of these combinations, RHOC-CD151 and CD151-MYOF labeled with fluorophore pairs AF488/546, were effective in distinguishing exosomes from a model of lung cancer from exosomes isolated from a healthy lung cell model and human breath collected from healthy volunteers. On the other hand, the pairs GLUT-MYOF and CD151-GLUT showed no significant difference resulting in absence of FRET signal suggesting that the proposed combinations do not have a strong specificity for lung cancer, although their signal was previously reported through western blotting.

The findings of this study suggest that the data from time-resolved studies can be applicable for a sensitive test to validate the presence of cancer biomarkers. The study

contributes to our understanding that exosome proteins can be used to distinguish between healthy and lung cancer exosomes. These results add to the rapidly expanding field of exosomes and their use for diagnostics, although further optimization is required as described in the next Chapter 5.

CHAPTER 5. FUTURE WORK

The research presented in this thesis opened new opportunities and highlighted several topics for further research.

In this study, the determination of a benchmark healthy lung exosome proteome was conducted using samples from patients in a variety of age groups, with a majority representing young adulthood (18 to 30 years). Future studies should draw on a range of groups as age diversity to ensure that the population is widely represented including geriatric patients. Additionally, including sex-gender variables in the research data has been recommended to evaluate the risk and benefits for each group[671]. In this study no distinction was made between proteins because samples were pooled, and it was not possible to differentiate samples. Gender differences and individual variations in comprehensive analysis of proteome samples have been previously reported[598,599]. Another suggestion that can be made is to increase the number of volunteers in order to create a larger data set and therefore provide a better insight into the breath proteome.

This study investigated the breath proteome only from healthy volunteers. It will be interesting to see how the proteome of exosomes from lung cancer patients differs. Unfortunately, due to time limitations, the characterization of human breath proteome from lung cancer patients was not possible in this thesis. Characterization of the human lung cancer proteome collected from exhaled breath will be critical to verify the utility of the biomarkers that were proposed during this research study and validate those markers by proposed method of detection, the FRET-based assay. Biomarkers can identify or recognize the disease and indicate its stage. Therefore, characterization of the proteome of exosomes from the breath of cancer patients ideally needs to be conducted in patients in different age groups and with different stages of lung cancer to obtain a full picture.

Several questions arising from this research should be addressed in future studies. First, it will be beneficial to find out if the proposed biomarkers are general for lung cancer or specific for A549 cells. For that, further cell models need to be tested. In this thesis, we have only used a healthy lung cell model (WI-38), which did behave as we expected. However, it would be useful to compare to other cell lines to determine the specificity of the proposed biomarkers. Cell models may not fully and accurately reflect the physiological condition they were chosen to represent. Validation of the proposed biomarkers will require different cell models. That will provide a linkage between the proposed biomarkers and a clinical end report evaluating its clinical usefulness.

Second, the breath collection technique is a difficult process and crucial for further advances in detecting biomarkers from breath. Ideally, the sample collection method should be adapted for personal physiology allowing collection to be simple and fast. With the current settings, described in this study, the collection will satisfy the goal of characterization of benchmark proteome from average of lung cancer patients, but will be difficult to apply on an individual as it will take several hours to collect the volume sufficient enough for analysis. To overcome these challenges, improving the performance of analytical methods that facilitates diagnosis on smaller sample volumes, whilst retaining a high degree of reproducibility, will be crucial. Third, before moving to clinical trials to test the proposed diagnostic tool on lung cancer patients, it is critical to establish the volume that would be necessary to perform the experiment on individual samples. Because in this study we collected and pooled samples, establishing the volume of the individual sample was not set as a goal, however it would be necessary to determine this for clinical use. Work with healthy volunteers is required to determine the limits of detection of the assay, to define the volume of EBC required for a clinical diagnostic assay. Once that is determined, clinical trial needs to take place. That will include collection of the breath from lung cancer patients following by exosome isolation. The putative markers first will need to be verified by western blotting before moving onto FRET detection.

Meanwhile, the proteome of lung cancer exosomes needs to be characterized. This has not been done yet, although EBC from cancer patients has been reported. For that, firstly, exhaled breath condensate from lung cancer patients needs to be collected and characterized to establish exosome-based biomarkers that are characteristic of lung cancer. Secondly, the same FRET detection method would be used to verify that the biomarkers can distinguish between cancer and healthy exosomes. A preliminary study conducted on a sample from one individual gave us a rough idea of the necessary volume to be sufficient for the analysis. One of the suggestions that we would like to make is to conduct studies on a series of samples of decreasing volumes, but the same concentration of the EBC collected from healthy individuals without pooling them together as it will give an excellent representation of volume and detection abilities for already established FRET-based assay.

Third, “multiplexed” detection involving three FRET pairs, or even multiple target detection using nano-assembled FRET-based systems can be used to improve sensitivity. For example, using exosomes in ensemble with lipids or DNA molecules. Ultimately, further development of a simple FRET-based diagnostic assay offers the possibility of a device that

can be used for a point-of-care testing. Application to early diagnosis of lung cancer based on exosomes isolated from breath is especially attractive.

Lastly, the characterization of breath exosomes can be expanded by investigating other molecular cargoes, such us RNA and lipids, in healthy and cancerous exosomes.

CHAPTER 6. GLOBAL CONCLUSION

This thesis discusses breath-derived exosomes and their potential use in breath-based clinical applications for medical diagnostics for lung dysfunction, including cancer.

Although exosomes isolated from various biological fluids have been heavily studied and reported, breath has been overlooked as another source of exosomes[601,672]. Breath is an excellent source of exosomes that can be collected non-invasively, which is an advantage over some other biological fluids. Although there are several publications acknowledging their presence, breath exosomes have been poorly characterized[275]. This study identified and set out to fill this knowledge gap. The project's aim was to characterize breath-derived exosomes and evaluate whether they can be used in clinical diagnostics. Exosomes contain parent cell-specific proteins, suggesting that breath exosomes could be a useful tool for distinguishing between healthy and cancerous lungs. This has been recently proven on plasma exosomes[673]. Therefore, this study focused on exploring the proteome of exosomes secreted from cell models of normal lung tissue (WI-38 cells) and lung cancer (A549 cells). It was hypothesized that differentially expressed proteins could be used as biomarkers to help to identify lung dysfunction, including early-stage cancer. A proof-of-principle test for these biomarkers was developed, with a final goal to distinguish between lung cancer and healthy lung exosomes.

This project was divided into several aims and objectives which were addressed in three chapters: isolation and quantification of exosomes, proteomic profiling of cell- and breath-derived exosomes and identification of proposed biomarkers, and detection of exosomes-diagnostic application. Together, these chapters show the characterization of breath exosomes and provide a proof-of-principle for their use as a diagnostic tool.

Chapter 2 described the optimization of the methodology for exosome isolation. Two methods of isolation were discussed: ultracentrifugation and size-exclusion chromatography. For exosomes to be used for biomarker identification, it is important to obtain high quality exosomes that are free of contaminating protein aggregates or other vesicles. Experimental findings from this chapter revealed three key points. First, the methodology for isolation of high purity exosomes from EBC was established. The isolated vesicles were confirmed as exosomes through immunostaining with gold nanoparticles and were characterized by transmission electron microscopy, cryo-scanning electron microscopy, dynamic light scattering, and protein quantification assays. Exosomes isolated through SEC fractionation can be sufficiently pure and applicable for diagnostic purposes. However, the volume of biological fluid is a limitation of this method. On the other hand, samples that are as pure as from size

exclusion chromatography can be obtained through a modified ultracentrifugation method in which a large volume of the initial biological fluid is used. Second, the results suggested that highly characterized breath-derived exosomes are phenotypically consistent with exosomes from other sources. This was determined by comparing breath-derived exosomes to cell-derived exosomes from a lung cancer cell line and a healthy lung cell line. Finally, it was noted that buffers used for exosome isolation are likely to become contaminated when stored in labware. To avoid possible contamination, it is preferable to use freshly prepared buffers.

The aim of Chapter 3 was to identify putative biomarkers of lung disease, evaluate whether those may be revealed in the proteome of exosomes, and to characterize the proteome of breath-derived exosomes. This was achieved through proteomic analysis of the proteome of cell- and breath- derived exosomes. Proteomics employs mass spectrometry to detect, identify, and characterize proteins[674] . Analysis of differential protein expression can be used to identify candidate biomarker proteins that are present in cancer tissues and absent in normal tissue. The identification of clinically useful biomarkers for lung cancer detection in early stages is a primary issue and a medical need[675].

Cell-derived exosomes were used initially to optimize the protocol. The fact that the cell count can be easily controlled allowed an estimation of the number of proteins that would be sufficient for proteomic analysis. Once the protocol was optimized, proteomic analysis of breath-derived exosomes was attempted, beginning with a sample collected from one individual only. The 2 mL starting volume of EBC collection did not provide enough proteins for detection, after accounting for peptide loss during the purified step using C18 tips. After increasing the volume collected and performing extensive optimization, visible protein peaks were finally seen. To determine the benchmark of a healthy breath-exosome proteome we conducted a study in which 55 healthy participants donated their EBC. Since our goal was to define the average of breath proteome, single samples were not analyzed but pooled together. Participants were divided into three groups of 20 and EBC samples were pooled and combined within the group within three days. Then, breath exosomes were isolated and confirmed biochemically and electron microscopy. The exosomes were then subjected to in-depth characterization by LC-MS/MS analysis.

The significant proteins shared across three breath proteome samples were then analyzed through gene ontology functional enrichment analysis to define the core of the breath exosome proteome. Characterization of the breath exosome proteome has never been previously reported. Bioinformatics techniques were used to compare the benchmark proteome of exosomes derived from human breath to the proteome of exosomes obtained from WI-38 cells

to show that these cells were a valid proxy for breath-derived exosomes. The benchmark of the breath exosome proteome from healthy volunteers allows for future comparison to exosomes obtained from conditions of lung dysfunction, including lung cancer. We foresee their use in non-invasive breath-based clinical applications for medical diagnostics for lung cancer as an important future application. Another significant finding included potential lung cancer biomarkers identified from cell-derived exosomes. We reported nine biomarkers, four of which were selected as most likely to be efficient in identifying early-stage lung cancer. Proposed biomarkers were validated through the western blotting, which confirmed the absence of cancer biomarkers on healthy lung cell-derived exosomes and breath-derived exosomes collected from volunteers.

Chapter 4 combined findings from the previous two chapters and applied them into development of a sensitive test that should recognize proposed cancer biomarkers on lung cancer exosomes. The FRET-based assay was developed to detect the interaction between exosomes and putative lung cancer biomarkers with a final goal to distinguish between lung cancer and healthy lung exosomes. The assay involved a pair of antibodies corresponding to proposed biomarkers, one of them labeled with a donor fluorophore and the other labeled with an acceptor fluorophore. These were incubated with the exosomes in solution. Based on our assumption that proposed biomarkers are present at a low abundance in the samples, we were looking for a sensitive detection method. As proof-of-principle, we tested the chosen fluorophore pair on known general tetraspanin EV markers CD63 and CD81 which are embedded on the surface of exosome before moving on to antibodies corresponding to proposed biomarkers. Calculation of the lifetime decays of the donor in the proposed FRET pairs compared to controls showed that the FRET-based assay can distinguish between cancerous and non-tumorigenic exosomes. In conclusion, the thesis has discussed the application of breath-derived exosomes for non-invasive diagnosis of lung health by using the developed FRET-based assay with the ultimate goal of early-stage diagnosis of lung cancer.

PUBLICATIONS

**There is no work presented in publications #2 and #3 is included in the thesis. Components of the publication #1 that were done by Déanna Shea (Ayupova) used in the section 2.2.3 (cryo-SEM image of breath-derived exosomes) and section 2.5 (Fig. 22 western blotting validation of breath-derived exosomes) of this thesis. Publication #4 has been used as citation in section 1.1.1.*

1. Dobhal, G., Datta, A., **Ayupova, D.**, Teesdale-Spittle, P., Goreham RV. Isolation, Characterisation and Detection of Breath-derived Extracellular Vesicles. *Scientific Reports.* **2020**; 10:1738. doi: 10.1038/s41598-020-73243-5[1]

2. **Ayupova D**, Dobhal G, Laufersky G, Nann T, Goreham RV. An In Vitro Investigation of Cytotoxic Effects of InP/Zns Quantum Dots with Different Surface Chemistries. *Nanomaterials (Basel).* **2019**; 9(2):135. doi: 10.3390/nano9020135. PMID: 30678192; PMCID: PMC6409980.

3. Dobhal G, **Ayupova D**, Laufersky G, Ayed Z, Nann T, Goreham RV. Cadmium-Free Quantum Dots as Fluorescent Labels for Exosomes. *Sensors*. **2018**; 18(10): 3308. doi: 10.3390/s18103308

4. Goreham, R.V., Ayed, Z., **Ayupova, D**., Dobhal, G. Extracellular Vesicles: Nature's Own Nanoparticles. Reference Module in Materials Science and Materials Engineering. Book-chapter 2018. doi: 10.1016/b978-0-12-803581-8.10412-6.

[1] G.D. conducted experiments including the isolation and characterization of extracellular vesicles, surface plasmon resonance; A.D. conducted EIS experiments; **D.A. conducted experiments of isolation of extracellular vesicles, cell culture and western blot experiment and analysis**. R.G. and P.T. conceptualized the project and supervised the experimental work.

[2] Conceptualization-**D.A.** and R.G.; methodology-**D.A.**, G.D., and G.L.; software-**D.A.;** validation-**D.A.** and G.D.; formal analysis-**D.A.**, and G.D.; investigation-**D.A**., G.D., R.G., and T.N.; resources, R.G. and T.N.; data curation-**D.A**., and R.G.; writing—original draft preparation, **D.A.** and R.G.; writing—review and editing, **D.A.**, G.D., and R.G.; visualization-**D.A.**, G.D., and R.G.; supervision, R.G. and T.N.; project administration, R.G. and T.N.; funding acquisition, R.G. and T.N.

[3] Conceptualization-G.D. and R.V.G. Methodology-G.D., **D.A.** ,and G.L.; software, G.D.; validation-G.D. and **D.A.**; formal analysis-G.D. and **D.A.**; investigation-G.D., **D.A.**, R.V.G., G.L.,T.N.; resources, R.V.G. and T.N.; data curation-G.D., **D.A.**, and R.V.G.; writing—original draft preparation, G.D. and R.V.G.; writing—review and editing, G.D., **D.A.**, G.L. and R.V.G.; visualization-G.D., **D.A.**, and R.V.G.; supervision-R.V.G. and T.N.; project administration-R.V.G. and T.N.; funding acquisition-R.V.G. and T.N.

[4] Conceptualization-R.V.G.; Methodology-R.V.G., Z.A. (bacterial -derived OMVs), **D.A. (cell-derived EVs and exosomes),** G.D.; investigation-R.V.G., Z.A., **D.A.**; resources-R.V.G. and T.N.; writing—original draft preparation-R.V.G., Z.A., **D.A.**; writing—review and editing, R.V.G, Z.A., **D.A.**, and G.D.; project administration-R.V.G. and T.N.; funding acquisition-R.V.G. and T.N.

REFERENCES

1. Wolf P. The Nature and Significance of Platelet Products in Human Plasma. Br J Haematol. 1967 May;13(3):269–88.

2. Johnstone RM, Adam M, Hammond JR, Orr L, Turbide C. Vesicle formation during reticulocyte maturation. Association of plasma membrane activities with released vesicles (exosomes). J Biol Chem. 1987 Jul 5;262(19):9412–20.

3. Alipoor SD, Mortaz E, Varahram M, Movassaghi M, Kraneveld AD, Garssen J, et al. The Potential Biomarkers and Immunological Effects of Tumor-Derived Exosomes in Lung Cancer. Front Immunol. 2018 Apr 18;9.

4. Goreham RV, Ayed Z, Ayupova D, Dobhal G. Extracellular Vesicles: Nature's Own Nanoparticles. In: Reference Module in Materials Science and Materials Engineering. Elsevier; 2018

5. Colombo M, Raposo G, Théry C. Biogenesis, secretion, and intercellular interactions of exosomes and other extracellular vesicles. Ann Rev Cell Dev Biol. 2014;30:255–89.

6. Tamkovich SN, Yunusova NV, Stakheeva MN, Somov AK, Frolova AE, Kiryushina NA, et al. Isolation and characterization of exosomes from blood plasma of breast cancer and colorectal cancer patients. Biochemistry (Moscow), Supplement Series B: Biomed Chem. 2017 Jul;11(3):291–5.

7. Nguyen DB, Thuy Ly TB, Wesseling MC, Hittinger M, Torge A, Devitt A, et al. Characterization of Microvesicles Released from Human Red Blood Cells. Cell Physiol Biochem. 2016;38(3):1085–99.

8. Manterola L, Guruceaga E, Pérez-Larraya JG, González-Huarriz M, Jauregui P, Tejada S, et al. A small noncoding RNA signature found in exosomes of GBM patient serum as a diagnostic tool. Neuro-Oncology. 2014 Apr;16(4):520–7.

9. Huebner AR, Somparn P, Benjachat T, Leelahavanichkul A, Avihingsanon Y, Fenton RA, et al. Exosomes in Urine Biomarker Discovery. In: Gao Y, editor. Urine Proteomics in Kidney Disease Biomarker Discovery. Dordrecht: Springer Netherlands; 2015. p. 43–58.

10. Street JM, Koritzinsky EH, Glispie DM, Star RA, Yuen PST. Urine Exosomes. In: Adv Clin Chem. Elsevier; 2017. p. 103–22.

11. Bryzgunova OE, Zaripov MM, Skvortsova TE, Lekchnov EA, Grigor'eva AE, Zaporozhchenko IA, et al. Comparative Study of Extracellular Vesicles from the Urine of Healthy Individuals and Prostate Cancer Patients. Carter DRF, editor. PLOS ONE. 2016 Jun 15;11(6):e0157566.

12. de la Torre Gomez C, Goreham RV, Bech Serra JJ, Nann T, Kussmann M. "Exosomics"—A Review of Biophysics, Biology and Biochemistry of Exosomes With a Focus on Human Breast Milk. Front Genet. 2018 Mar 27;9.

13. Hock A, Miyake H, Li B, Lee C, Ermini L, Koike Y, et al. Breast milk-derived exosomes promote intestinal epithelial cell growth. J Pediatr Surg. 2017 May;52(5):755–9.

14. Liao Y, Du X, Li J, Lönnerdal B. Human milk exosomes and their microRNAs survive digestion in vitro and are taken up by human intestinal cells. Mol Nutr Food Res. 2017 Nov;61(11):1700082.

15. Sharma S, Rasool HI, Palanisamy V, Mathisen C, Schmidt M, Wong DT, et al. Structural-mechanical characterization of nanoparticle exosomes in human saliva, using correlative AFM, FESEM, and force spectroscopy. ACS Nano. 2010 Apr 27;4(4):1921–6.

16. Sharma S, Gillespie BM, Palanisamy V, Gimzewski JK. Quantitative nanostructural and single-molecule force spectroscopy biomolecular analysis of human-saliva-derived exosomes. Langmuir. 2011 Dec 6;27(23):14394–400.

17. Ogawa Y, Kanai-Azuma M, Akimoto Y, Kawakami H, Yanoshita R. Exosome-like vesicles with dipeptidyl peptidase IV in human saliva. Biol Pharm Bull. 2008 Jun;31(6):1059–62.

18. Palanisamy V, Sharma S, Deshpande A, Zhou H, Gimzewski J, Wong DT. Nanostructural and Transcriptomic Analyses of Human Saliva Derived Exosomes. Hansen IA, editor. PLoS ONE. 2010 Jan 5;5(1):e8577.

19. Zlotogorski-Hurvitz A, Dayan D, Chaushu G, Korvala J, Salo T, Sormunen R, et al. Human saliva-derived exosomes: comparing methods of isolation. J Histochem Cytochem. 2015;63(3):181–9.

20. Grigor'eva AE, Tamkovich SN, Eremina AV, Tupikin AE, Kabilov MR, Chernykh VV, et al. Exosomes in tears of healthy individuals: Isolation, identification, and characterization. Biochemistry (Moscow) Supplement Series B: Biomed Chem. 2016 Apr;10(2):165–72.

21. Akers JC, Ramakrishnan V, Kim R, Skog J, Nakano I, Pingle S, et al. miR-21 in the Extracellular Vesicles (EVs) of Cerebrospinal Fluid (CSF): A Platform for Glioblastoma Biomarker Development. Chen M, editor. PLoS ONE. 2013 Oct 21;8(10):e78115.

22. Bebelman MP, Smit MJ, Pegtel DM, Baglio SR. Biogenesis and function of extracellular vesicles in cancer. Pharmacol Therapeut 2018 Aug;188:1–11.

23. Truong G, Guanzon D, Kinhal V, Elfeky O, Lai A, Longo S, et al. Oxygen tension regulates the miRNA profile and bioactivity of exosomes released from extravillous trophoblast cells – Liquid biopsies for monitoring complications of pregnancy. Bouma GJ, editor. PLOS ONE. 2017 Mar 28;12(3):e0174514.

24. Verweij FJ, Bebelman MP, Jimenez CR, Garcia-Vallejo JJ, Janssen H, Neefjes J, et al. Quantifying exosome secretion from single cells reveals a modulatory role for GPCR signaling. J Cell Biol. 2018 Mar 5;217(3):1129–42.

25. Möbius W, Ohno-Iwashita Y, Donselaar EG van, Oorschot VMJ, Shimada Y, Fujimoto T, et al. Immunoelectron Microscopic Localization of Cholesterol Using Biotinylated and Non-cytolytic Perfringolysin O. J Histochem Cytochem. 2002 Jan;50(1):43–55.

26. Hessvik NP, Llorente A. Current knowledge on exosome biogenesis and release. Cell Mol Life Sci. 2018 Jan;75(2):193–208.

27. Shenoda BB, Ajit SK. Modulation of Immune Responses by Exosomes Derived from Antigen-Presenting Cells. Clin Med Insights Pathol. 2016;9(Suppl 1):1–8.

28. Fan G-C. Hypoxic exosomes promote angiogenesis. Blood. 2014 Dec 11;124(25):3669–70.

29. Alzahrani FA, El-Magd MA, Abdelfattah-Hassan A, Saleh AA, Saadeldin IM, El-Shetry ES, et al. Potential Effect of Exosomes Derived from Cancer Stem Cells and MSCs on Progression of DEN-Induced HCC in Rats. Stem Cells International. 2018 Aug 27;2018:1–17.

30. Théry C, Boussac M, Véron P, Ricciardi-Castagnoli P, Raposo G, Garin J, et al. Proteomic analysis of dendritic cell-derived exosomes: a secreted subcellular compartment distinct from apoptotic vesicles. J Immunol. 2001 Jun 15;166(12):7309–18.

31. Meldolesi J. Exosomes and Ectosomes in Intercellular Communication. Curr Biol. 2018 Apr 23;28(8):R435–44.

32. Tamkovich SN, Tutanov OS, Laktionov PP. Exosomes: Generation, structure, transport, biological activity, and diagnostic application. Biochemistry (Moscow) Supplement Series A: Membr Cell Biol. 2016 Jul;10(3):163–73.

33. Raposo G, Stoorvogel W. Extracellular vesicles: Exosomes, microvesicles, and friends. J Cell Biol. 2013 Feb 18;200(4):373–83.

34. Yáñez-Mó M, Siljander PR-M, Andreu Z, Bedina Zavec A, Borràs FE, Buzas EI, et al. Biological properties of extracellular vesicles and their physiological functions. J Extracell Vesicles. 2015 Jan 1;4(1):27066.

35. Borges FT, Reis LA, Schor N. Extracellular vesicles: structure, function, and potential clinical uses in renal diseases. Braz J Med Biol Res. 2013 Oct;46(10):824–30.

36. Doyle L, Wang M. Overview of Extracellular Vesicles, Their Origin, Composition, Purpose, and Methods for Exosome Isolation and Analysis. Cells. 2019 Jul 15;8(7):727.

37. Jeppesen DK, Fenix AM, Franklin JL, Higginbotham JN, Zhang Q, Zimmerman LJ, et al. Reassessment of Exosome Composition. Cell. 2019 Apr;177(2):428-445.e18.

38. Théry C, Witwer KW, Aikawa E, Alcaraz MJ, Anderson JD, Andriantsitohaina R, et al. Minimal information for studies of extracellular vesicles 2018 (MISEV2018): a position statement of the International Society for Extracellular Vesicles and update of the MISEV2014 guidelines. J Extracell Vesicles. 2018 Dec;7(1):1535750.

39. Witwer KW, Soekmadji C, Hill AF, Wauben MH, Buzás EI, Di Vizio D, et al. Updating the MISEV minimal requirements for extracellular vesicle studies: building bridges to reproducibility. J Extracell Vesicles. 2017;6(1):1396823.

40. Tkach M, Kowal J, Théry C. Why the need and how to approach the functional diversity of extracellular vesicles. Philosophical Transactions of the Royal Society B: Biol Sci. 2018 Jan 5;373(1737):20160479.

41. Østergaard O, Nielsen CT, Iversen LV, Jacobsen S, Tanassi JT, Heegaard NHH. Quantitative proteome profiling of normal human circulating microparticles. J Proteome Res. 2012 Apr 6;11(4):2154–63.

42. Hendrix A, Hume AN. Exosome signaling in mammary gland development and cancer. Int J Dev Biol. 2011;55(7–9):879–87.

43. Elkin SR, Lakoduk AM, Schmid SL. Endocytic pathways and endosomal trafficking: a primer. Wiener Medizinische Wochenschrift. 2016 May;166(7–8):196–204.

44. Markgraf DF, Peplowska K, Ungermann C. Rab cascades and tethering factors in the endomembrane system. FEBS Letters. 2007 May 22;581(11):2125–30.

45. Bonifacino JS, Glick BS. The Mechanisms of Vesicle Budding and Fusion. Cell. 2004 Jan;116(2):153–66.

46. Pfeffer SR. Rab GTPases: specifying and deciphering organelle identity and function. Trends Cell Biol. 2001 Dec 1;11(12):487–91.

47. Hutagalung AH, Novick PJ. Role of Rab GTPases in Membrane Traffic and Cell Physiology. Physiol Rev. 2011 Jan;91(1):119–49.

48. Spang A, Shiba Y, Randazzo PA. Arf GAPs: gatekeepers of vesicle generation. FEBS Lett. 2010 Jun 18;584(12):2646–51.

49. Piper RC, Dikic I, Lukacs GL. Ubiquitin-Dependent Sorting in Endocytosis. Cold Spring Harbor Perspectives in Biology. 2014 Jan 1;6(1):a016808–a016808.

50. van Niel G, Porto-Carreiro I, Simoes S, Raposo G. Exosomes: A Common Pathway for a Specialized Function. J Biochem. 2006 Jul 1;140(1):13–21.

51. Christ L, Raiborg C, Wenzel EM, Campsteijn C, Stenmark H. Cellular Functions and Molecular Mechanisms of the ESCRT Membrane-Scission Machinery. Trends Biochem Sci. 2017 Jan;42(1):42–56.

52. Henne WM, Buchkovich NJ, Emr SD. The ESCRT Pathway. Developmental Cell. 2011 Jul;21(1):77–91.

53. Kowal J, Tkach M, Théry C. Biogenesis and secretion of exosomes. Curr Opin Cell Biol. 2014 Aug;29:116–25.

54. Villarroya-Beltri C, Baixauli F, Mittelbrunn M, Fernández-Delgado I, Torralba D, Moreno-Gonzalo O, et al. ISGylation controls exosome secretion by promoting lysosomal degradation of MVB proteins. Nat Commun. 2016 24;7:13588

55. Fader CM, Sánchez D, Furlán M, Colombo MI. Induction of Autophagy Promotes Fusion of Multivesicular Bodies with Autophagic Vacuoles in K562 Cells. Traffic. 2007 Nov 12;9(2):230–50.

56. Whiteside TL. Tumor-Derived Exosomes and Their Role in Cancer Progression. Adv Clin Chem. 2016;74:103–41.

57. Baietti MF, Zhang Z, Mortier E, Melchior A, Degeest G, Geeraerts A, et al. Syndecan–syntenin–ALIX regulates the biogenesis of exosomes. Nat Cell Biol. 2012 Jul;14(7):677–85.

58. McCullough J, Fisher RD, Whitby FG, Sundquist WI, Hill CP. ALIX-CHMP4 interactions in the human ESCRT pathway. Proc Natl Acad Sci. 2008 Jun 3;105(22):7687–91.

59. Abels ER, Breakefield XO. Introduction to Extracellular Vesicles: Biogenesis, RNA Cargo Selection, Content, Release, and Uptake. Cell Mol Neurobiol. 2016 Apr;36(3):301–12.

60. Raiborg C, Stenmark H. The ESCRT machinery in endosomal sorting of ubiquitylated membrane proteins. Nature. 2009 Mar 26;458(7237):445–52.

61. Ostrowski M, Carmo NB, Krumeich S, Fanget I, Raposo G, Savina A, et al. Rab27a and Rab27b control different steps of the exosome secretion pathway. Nat Cell Biol. 2010 Jan;12(1):19–30.

62. Trajkovic K, Hsu C, Chiantia S, Rajendran L, Wenzel D, Wieland F, et al. Ceramide Triggers Budding of Exosome Vesicles into Multivesicular Endosomes. Science. 2008 Feb 29;319(5867):1244–7.

63. Kosaka N, Iguchi H, Yoshioka Y, Takeshita F, Matsuki Y, Ochiya T. Secretory Mechanisms and Intercellular Transfer of MicroRNAs in Living Cells. J Biol Chem. 2010 Jun;285(23):17442–52.

64. Mittelbrunn M, Gutiérrez-Vázquez C, Villarroya-Beltri C, González S, Sánchez-Cabo F, González MÁ, et al. Unidirectional transfer of microRNA-loaded exosomes from T cells to antigen-presenting cells. Nat Commun. 2011 Sep;2(1):282.

65. Phuyal S, Hessvik NP, Skotland T, Sandvig K, Llorente A. Regulation of exosome release by glycosphingolipids and flotillins. FEBS J. 2014 May;281(9):2214–27.

66. van Niel G, Charrin S, Simoes S, Romao M, Rochin L, Saftig P, et al. The Tetraspanin CD63 Regulates ESCRT-Independent and -Dependent Endosomal Sorting during Melanogenesis. Dev Cell. 2011 Oct;21(4):708–21.

67. Choi D-S, Lee J, Go G, Kim Y-K, Gho YS. Circulating extracellular vesicles in cancer diagnosis and monitoring: an appraisal of clinical potential. Mol Diagn Ther. 2013 Oct;17(5):265–71.

68. Mathivanan S, Simpson RJ. ExoCarta: A compendium of exosomal proteins and RNA. Proteomics. 2009 Nov;9(21):4997–5000.

69. Buzas EI, György B, Nagy G, Falus A, Gay S. Emerging role of extracellular vesicles in inflammatory diseases. Nat Rev Rheumatol. 2014 Jun;10(6):356–64.

70. Tetta C, Ghigo E, Silengo L, Deregibus MC, Camussi G. Extracellular vesicles as an emerging mechanism of cell-to-cell communication. Endocrine. 2013 Aug;44(1):11–9.

71. Bellingham SA, Guo BB, Coleman BM, Hill AF. Exosomes: vehicles for the transfer of toxic proteins associated with neurodegenerative diseases? Front Physiol. 2012;3:124.

72. Ciregia F, Urbani A, Palmisano G. Extracellular Vesicles in Brain Tumors and Neurodegenerative Diseases. Front Mol Neurosci. 2017;10:276.

73. Hannafon B, Ding W-Q. Intercellular Communication by Exosome-Derived microRNAs in Cancer. Int J Mol Sci. 2013 Jul 9;14(7):14240–69.

74. Eirin A, Riester SM, Zhu X-Y, Tang H, Evans JM, O'Brien D, et al. MicroRNA and mRNA cargo of extracellular vesicles from porcine adipose tissue-derived mesenchymal stem cells. Gene. 2014 Nov;551(1):55–64.

75. Asada H, Tomiyasu H, Uchikai T, Ishihara G, Goto-Koshino Y, Ohno K, et al. Comprehensive analysis of miRNA and protein profiles within exosomes derived from canine lymphoid tumour cell lines. Zheng Y, editor. PLoS ONE. 2019 Apr 29;14(4):e0208567.

76. Tsuno H, Suematsu N, Sato T, Arito M, Matsui T, Iizuka N, et al. Effects of methotrexate and salazosulfapyridine on protein profiles of exosomes derived from a human synovial sarcoma cell line of SW982. Proteomics - Clin Appl. 2016 Feb;10(2):164–71.

77. Rammal G, Fahs A, Kobeissy F, Mechref Y, Zhao J, Zhu R, et al. Proteomic Profiling of Rhabdomyosarcoma-Derived Exosomes Yield Insights into Their Functional Role in Paracrine Signaling. J Proteome Res. 2019 Oct 4;18(10):3567–79.

78. Zhang W, Ou X, Wu X. Proteomics profiling of plasma exosomes in epithelial ovarian cancer: A potential role in the coagulation cascade, diagnosis and prognosis. Int J Oncol. 2019 Mar 7.

79. Rontogianni S, Synadaki E, Li B, Liefaard MC, Lips EH, Wesseling J, et al. Proteomic profiling of extracellular vesicles allows for human breast cancer subtyping. Commun Biol. 2019 Dec;2(1).

80. Jia R, Li J, Rui C, Ji H, Ding H, Lu Y, et al. Comparative Proteomic Profile of the Human Umbilical Cord Blood Exosomes between Normal and Preeclampsia Pregnancies with High-Resolution Mass Spectrometry. Cell Physiol Biochem 2015;36(6):2299–306.

81. Menon R, Debnath C, Lai A, Guanzon D, Bhatnagar S, Kshetrapal P, et al. Protein Profile Changes in Circulating Placental Extracellular Vesicles in Term and Preterm Births: A Longitudinal Study. Endocrinol. 2020 Apr 1;161(4).

82. Smolarz M, Pietrowska M, Matysiak N, Mielańczyk Ł, Widłak P. Proteome Profiling of Exosomes Purified from a Small Amount of Human Serum: The Problem of Co-Purified Serum Components. Proteomes. 2019 Apr 28;7(2):18.

83. Gidlöf O, Evander M, Rezeli M, Marko-Varga G, Laurell T, Erlinge D. Proteomic profiling of extracellular vesicles reveals additional diagnostic biomarkers for myocardial infarction compared to plasma alone. Sci Rep. 2019 Dec;9(1).

84. Sun Y, Huo C, Qiao Z, Shang Z, Uzzaman A, Liu S, et al. Comparative Proteomic Analysis of Exosomes and Microvesicles in Human Saliva for Lung Cancer. J Proteome Res. 2018 Mar 2;17(3):1101–7.

85. Hu S, Xie Y, Ramachandran P, Ogorzalek Loo RR, Li Y, Loo JA, et al. Large-scale identification of proteins in human salivary proteome by liquid chromatography/mass spectrometry and two-dimensional gel electrophoresis-mass spectrometry. Proteomics. 2005 Apr;5(6):1714–28.

86. Muraoka S, Jedrychowski MP, Tatebe H, DeLeo AM, Ikezu S, Tokuda T, et al. Proteomic Profiling of Extracellular Vesicles Isolated From Cerebrospinal Fluid of Former National Football League Players at Risk for Chronic Traumatic Encephalopathy. Front Neurosci. 2019 Oct 9;13.

87. Street JM, Barran PE, Mackay CL, Weidt S, Balmforth C, Walsh TS, et al. Identification and proteomic profiling of exosomes in human cerebrospinal fluid. J Transl Med. 2012;10(1):5.

88. Wu C-X, Liu Z-F. Proteomic Profiling of Sweat Exosome Suggests its Involvement in Skin Immunity. J Invest Dermatol. 2018 Jan;138(1):89–97.

89. Lin J, Li J, Huang B, Liu J, Chen X, Chen X-M, et al. Exosomes: novel biomarkers for clinical diagnosis. Sci World J. 2015;2015:657086.

90. Rabinowits G, Gerçel-Taylor C, Day JM, Taylor DD, Kloecker GH. Exosomal microRNA: a diagnostic marker for lung cancer. Clin Lung Cancer. 2009 Jan;10(1):42–6.

91. Wu Y, Deng W, Klinke DJ. Exosomes: improved methods to characterize their morphology, RNA content, and surface protein biomarkers. Analyst. 2015 Oct 7;140(19):6631–42.

92. Hornick NI, Huan J, Doron B, Goloviznina NA, Lapidus J, Chang BH, et al. Serum Exosome MicroRNA as a Minimally-Invasive Early Biomarker of AML. Sci Rep. 2015 Sep;5(1).

93. Xiao Y, Zhong J, Zhong B, Huang J, Jiang L, Jiang Y, et al. Exosomes as potential sources of biomarkers in colorectal cancer. Cancer Lett. 2020 Apr;476:13–22.

94. Kim J-H, Kim E, Lee MY. Exosomes as diagnostic biomarkers in cancer. Mol Cell Toxicol. 2018 Apr;14(2):113–22.

95. Hon KW, Abu N, Ab Mutalib N-S, Jamal R. Exosomes As Potential Biomarkers and Targeted Therapy in Colorectal Cancer: A Mini-Review. Front Pharmacol. 2017 Aug 28;8.

96. Pluta R, Ułamek-Kozioł M, Januszewski S, Czuczwar SJ. Exosomes as possible spread factor and potential biomarkers in Alzheimer's disease: current concepts. Biomark Med. 2018 Sep;12(9):1025–33.

97. Mousavi S, Moallem R, Hassanian SM, Sadeghzade M, Mardani R, Ferns GA, et al. Tumor-derived exosomes: Potential biomarkers and therapeutic target in the treatment of colorectal cancer. J Cell Physiol. 2019 Aug;234(8):12422–32.

98. Morelli AE. Exosomes: From Cell Debris to Potential Biomarkers in Transplantation. Transplantation. 2017 Oct;101(10):2275–6.

99. Miranda KC, Bond DT, McKee M, Skog J, Păunescu TG, Da Silva N, et al. Nucleic acids within urinary exosomes/microvesicles are potential biomarkers for renal disease. Kidney Int. 2010 Jul;78(2):191–9.

100. Goto T, Fujiya M, Konishi H, Sasajima J, Fujibayashi S, Hayashi A, et al. An elevated expression of serum exosomal microRNA-191, − 21, −451a of pancreatic neoplasm is considered to be efficient diagnostic marker. BMC Cancer. 2018 Dec;18(1).

101. Chen I-H, Xue L, Hsu C-C, Paez JSP, Pan L, Andaluz H, et al. Phosphoproteins in extracellular vesicles as candidate markers for breast cancer. Proc Natl Acad Sci. 2017 Mar 21;114(12):3175–80.

102. Zhang Y, Liu Y, Liu H, Tang WH. Exosomes: biogenesis, biologic function and clinical potential. Cell Biosci. 2019 Dec;9(1).

103. van den Boorn JG, Daßler J, Coch C, Schlee M, Hartmann G. Exosomes as nucleic acid nanocarriers. Adv Drug Deliv Rev. 2013 Mar;65(3):331–5.

104. Perez-Hernandez D, Gutiérrez-Vázquez C, Jorge I, López-Martín S, Ursa A, Sánchez-Madrid F, et al. The Intracellular Interactome of Tetraspanin-enriched Microdomains Reveals Their Function as Sorting Machineries toward Exosomes. J Biol Chem. 2013 Apr 26;288(17):11649–61.

105. Nazarenko I, Rana S, Baumann A, McAlear J, Hellwig A, Trendelenburg M, et al. Cell Surface Tetraspanin Tspan8 Contributes to Molecular Pathways of Exosome-Induced Endothelial Cell Activation. Cancer Res. 2010 Feb 15;70(4):1668–78.

106. Abache T, Le Naour F, Planchon S, Harper F, Boucheix C, Rubinstein E. The transferrin receptor and the tetraspanin web molecules CD9, CD81, and CD9P-1 are differentially sorted into exosomes after TPA treatment of K562 cells. J Cell Biochem. 2007 Oct 15;102(3):650–64.

107. Rana S, Zöller M. The Functional Importance of Tetraspanins in Exosomes. In: Zhang H-G, editor. Emerging Concepts of Tumor Exosome–Mediated Cell-Cell Communication. New York, NY: Springer New York; 2013. p. 69–106.

108. Hemler ME. Tetraspanin Proteins Mediate Cellular Penetration, Invasion, and Fusion Events and Define a Novel Type of Membrane Microdomain. Ann Rev Cell Dev Biol. 2003 Nov;19(1):397–422.

109. Berditchevski F, Odintsova E. Tetraspanins as Regulators of Protein Trafficking. Traffic. 2007 Feb;8(2):89–96.

110. Marks MS, Ohno H, Kirchnausen T, Bonracino JS. Protein sorting by tyrosine-based signals: adapting to the Ys and wherefores. Trends Cell Biol. 1997 Mar;7(3):124–8.

111. Bari R, Guo Q, Xia B, Zhang YH, Giesert EE, Levy S, et al. Tetraspanins regulate the protrusive activities of cell membrane. Biochem Biophys Res Communic. 2011 Dec;415(4):619–26.

112. Cufaro MC, Pieragostino D, Lanuti P, Rossi C, Cicalini I, Federici L, et al. Extracellular Vesicles and Their Potential Use in Monitoring Cancer Progression and Therapy: The Contribution of Proteomics. J Oncol. 2019 Jun 9;2019:1–19.

113. Zaborowski MP, Balaj L, Breakefield XO, Lai CP. Extracellular Vesicles: Composition, Biological Relevance, and Methods of Study. BioScience. 2015 Aug 1;65(8):783–97.

114. Hough KP, Wilson LS, Trevor JL, Strenkowski JG, Maina N, Kim Y-I, et al. Unique Lipid Signatures of Extracellular Vesicles from the Airways of Asthmatics. Sci Rep. 2018 Dec;8(1).

115. Skotland T, Hessvik NP, Sandvig K, Llorente A. Exosomal lipid composition and the role of ether lipids and phosphoinositides in exosome biology. J Lipid Res. 2019 Jan;60(1):9–18.

116. Brzozowski JS, Jankowski H, Bond DR, McCague SB, Munro BR, Predebon MJ, et al. Lipidomic profiling of extracellular vesicles derived from prostate and prostate cancer cell lines. Lipids Health Disease. 2018 Dec ;17(1).

117. Mashouri L, Yousefi H, Aref AR, Ahadi A mohammad, Molaei F, Alahari SK. Exosomes: composition, biogenesis, and mechanisms in cancer metastasis and drug resistance. Mol Cancer. 2019 Dec;18(1).

118. Trivedi MS, Abreu M. Nucleic Acid Profiling in Tumor Exosomes. In: Diagnostic and Therapeutic Applications of Exosomes in Cancer. Elsevier; 2018. p. 93–117.

119. Gusachenko ON, Zenkova MA, Vlassov VV. Nucleic acids in exosomes: Disease markers and intercellular communication molecules. Biochem. 2013 Jan;78(1):1–7.

120. Skog J, Würdinger T, van Rijn S, Meijer DH, Gainche L, Curry WT, et al. Glioblastoma microvesicles transport RNA and proteins that promote tumour growth and provide diagnostic biomarkers. Nat Cell Biol. 2008 Dec;10(12):1470–6.

121. Valadi H, Ekström K, Bossios A, Sjöstrand M, Lee JJ, Lötvall JO. Exosome-mediated transfer of mRNAs and microRNAs is a novel mechanism of genetic exchange between cells. Nat Cell Biol. 2007 Jun;9(6):654–9.

122. Zomer A, Maynard C, Verweij FJ, Kamermans A, Schäfer R, Beerling E, et al. In Vivo Imaging Reveals Extracellular Vesicle-Mediated Phenocopying of Metastatic Behavior. Cell. 2015 May;161(5):1046–57.

123. Cui S, Cheng Z, Qin W, Jiang L. Exosomes as a liquid biopsy for lung cancer. Lung Cancer. 2018 Feb;116:46–54.

124. Bastos N, Ruivo CF, da Silva S, Melo SA. Exosomes in cancer: Use them or target them? Sem Cell Dev Biol. 2018 Jun;78:13–21.

125. Masaoutis C, Mihailidou C, Tsourouflis G, Theocharis S. Exosomes in lung cancer diagnosis and treatment. From the translating research into future clinical practice. Biochimie. 2018 Aug;151:27–36.

126. Vanni I, Alama A, Grossi F, Dal Bello MG, Coco S. Exosomes: a new horizon in lung cancer. Drug Discov Today. 2017 Jun;22(6):927–36.

127. Chen X, Liang H, Zhang J, Zen K, Zhang C-Y. microRNAs are ligands of Toll-like receptors. RNA. 2013 Jun 1;19(6):737–9.

128. Pegtel DM, Cosmopoulos K, Thorley-Lawson DA, van Eijndhoven MAJ, Hopmans ES, Lindenberg JL, et al. Functional delivery of viral miRNAs via exosomes. Proc Natl Acad Sci. 2010 Apr 6;107(14):6328–33.

129. Laganà A, Russo F, Veneziano D, Bella SD, Giugno R, Pulvirenti A, et al. Extracellular circulating viral microRNAs: current knowledge and perspectives. Front Genet. 2013;4.

130. Stern-Ginossar N, Elefant N, Zimmermann A, Wolf DG, Saleh N, Biton M, et al. Host Immune System Gene Targeting by a Viral miRNA. Science. 2007 Jul 20;317(5836):376–81.

131. Buck AH, Coakley G, Simbari F, McSorley HJ, Quintana JF, Le Bihan T, et al. Exosomes secreted by nematode parasites transfer small RNAs to mammalian cells and modulate innate immunity. Nat Communic. 2014 Dec;5(1).

132. Tkach M, Théry C. Communication by Extracellular Vesicles: Where We Are and Where We Need to Go. Cell. 2016 Mar;164(6):1226–32.

133. Zhang W, Dong R, Diao S, Du J, Fan Z, Wang F. Differential long noncoding RNA/mRNA expression profiling and functional network analysis during osteogenic differentiation of human bone marrow mesenchymal stem cells. Stem Cell Res Ther. 2017 Dec;8(1).

134. Wang K, Zhang S, Weber J, Baxter D, Galas DJ. Export of microRNAs and microRNA-protective protein by mammalian cells. Nucleic Acids Res. 2010 Nov;38(20):7248–59.

135. Boon RA, Vickers KC. Intercellular Transport of MicroRNAs. Arterioscler Thromb Vasc Biol. 2013 Feb;33(2):186–92.

136. Kahlert C, Melo SA, Protopopov A, Tang J, Seth S, Koch M, et al. Identification of Double-stranded Genomic DNA Spanning All Chromosomes with Mutated *KRAS* and *p53* DNA in the Serum Exosomes of Patients with Pancreatic Cancer. J Biol Chem. 2014 Feb 14;289(7):3869–75.

137. Thakur BK, Zhang H, Becker A, Matei I, Huang Y, Costa-Silva B, et al. Double-stranded DNA in exosomes: a novel biomarker in cancer detection. Cell Res. 2014 Jun;24(6):766–9.

138. Yokoi A, Villar-Prados A, Oliphint PA, Zhang J, Song X, De Hoff P, et al. Mechanisms of nuclear content loading to exosomes. Sci Adv 2019 Nov;5(11):eaax8849.

139. Verma M. Personalized Medicine and Cancer. J Personal Med. 2012 Jan 30;2(1):1–14.

140. Sharma A, Johnson A. Exosome DNA: Critical regulator of tumor immunity and a diagnostic biomarker. J Cell Physiol. 2020 Mar;235(3):1921–32.

141. Wang L, Li Y, Guan X, Zhao J, Shen L, Liu J. Exosomal double-stranded DNA as a biomarker for the diagnosis and preoperative assessment of pheochromocytoma and paraganglioma. Mol Cancer. 2018 Dec;17(1).

142. Qu X, Li Q, Yang J, Zhao H, Wang F, Zhang F, et al. Double-Stranded DNA in Exosomes of Malignant Pleural Effusions as a Novel DNA Source for EGFR Mutation Detection in Lung Adenocarcinoma. Front Oncol. 2019 Sep 25;9.

143. Vidal M, Sainte-Marie J, Philippot JR, Bienvenue A. Asymmetric distribution of phospholipids in the membrane of vesicles released during in vitro maturation of guinea pig reticulocytes: Evidence precluding a role for aminophospholipid translocase? J Cell Physiol. 1989 Sep;140(3):455–62.

144. Matsuo H. Role of LBPA and Alix in Multivesicular Liposome Formation and Endosome Organization. Sci. 2004 Jan 23;303(5657):531–4.

145. Record M, Carayon K, Poirot M, Silvente-Poirot S. Exosomes as new vesicular lipid transporters involved in cell–cell communication and various pathophysiologies. Biochim Biophys Acta (BBA) - Mol Cell Biol Lipids. 2014 Jan;1841(1):108–20.

146. Subra C, Laulagnier K, Perret B, Record M. Exosome lipidomics unravels lipid sorting at the level of multivesicular bodies. Biochimie. 2007 Feb;89(2):205–12.

147. Laulagnier K, Motta C, Hamdi S, Roy S, Fauvelle F, Pageaux J-F, et al. Mast cell- and dendritic cell-derived exosomes display a specific lipid composition and an unusual membrane organization. Biochem J. 2004 May 15;380(1):161–71.

148. Baig S, Lim JY, Fernandis AZ, Wenk MR, Kale A, Su LL, et al. Lipidomic analysis of human placental Syncytiotrophoblast microvesicles in adverse pregnancy outcomes. Placenta. 2013 May;34(5):436–42.

149. Han Y, Jia L, Zheng Y, Li W. Salivary Exosomes: Emerging Roles in Systemic Disease. Int J Biol Sci.. 2018;14(6):633–43.

150. McKelvey KJ, Powell KL, Ashton AW, Morris JM, McCracken SA. Exosomes: Mechanisms of Uptake. J Circ Biomark. 2015 Dec;4:7.

151. Harmati M, Gyukity-Sebestyen E, Dobra G, Janovak L, Dekany I, Saydam O, et al. Small extracellular vesicles convey the stress-induced adaptive responses of melanoma cells. Sci Rep. 2019 Dec;9(1).

152. Beninson LA, Brown PN, Loughridge AB, Saludes JP, Maslanik T, Hills AK, et al. Acute Stressor Exposure Modifies Plasma Exosome-Associated Heat Shock Protein 72 (Hsp72) and microRNA (miR-142-5p and miR-203). Abraham E, editor. PLoS ONE. 2014 Sep 26;9(9):e108748.

153. Sardar Sinha M, Ansell-Schultz A, Civitelli L, Hildesjö C, Larsson M, Lannfelt L, et al. Alzheimer's disease pathology propagation by exosomes containing toxic amyloid-beta oligomers. Acta Neuropathol. 2018 Jul;136(1):41–56.

154. Howitt J, Hill AF. Exosomes in the Pathology of Neurodegenerative Diseases. J Biol Chem. 2016 Dec 23;291(52):26589–97.

155. Kadota T, Yoshioka Y, Fujita Y, Kuwano K, Ochiya T. Extracellular vesicles in lung cancer—From bench to bedside. Sem Cell Dev Biol. 2017 Jul;67:39–47.

156. Sato Y, Goto Y, Narita N, Hoon DSB. Cancer Cells Expressing Toll-like Receptors and the Tumor Microenvironment. Cancer Microenviron. 2009 Sep;2 Suppl 1:205–14.

157. Shcheblyakov DV, Logunov DY, Tukhvatulin AI, Shmarov MM, Naroditsky BS, Gintsburg AL. Toll-Like Receptors (TLRs): The Role in Tumor Progression. Acta Naturae. 2010 Jul;2(3):21–9.

158. Pandey S, Singh S, Anang V, Bhatt AN, Natarajan K, Dwarakanath BS. Pattern Recognition Receptors in Cancer Progression and Metastasis. Cancer Growth Metastasis. 2015;8:25–34.

159. Oser MG, Niederst MJ, Sequist LV, Engelman JA. Transformation from non-small-cell lung cancer to small-cell lung cancer: molecular drivers and cells of origin. Lancet Oncol. 2015 Apr;16(4):e165–72.

160. Wang F, Shu L, Wang J, Pan X, Huang R, Lin Y, et al. Perspectives on the toxicology of cadmium-based quantum dots. Curr Drug Metab. 2013 Oct;14(8):847–56.

161. Maia J, Caja S, Strano Moraes MC, Couto N, Costa-Silva B. Exosome-Based Cell-Cell Communication in the Tumor Microenvironment. Front Cell Dev Biol. 2018;6:18.

162. Becker A, Thakur BK, Weiss JM, Kim HS, Peinado H, Lyden D. Extracellular Vesicles in Cancer: Cell-to-Cell Mediators of Metastasis. Cancer Cell. 2016 Dec;30(6):836–48.

163. Peinado H, Alečković M, Lavotshkin S, Matei I, Costa-Silva B, Moreno-Bueno G, et al. Melanoma exosomes educate bone marrow progenitor cells toward a pro-metastatic phenotype through MET. Nat Med. 2012 Jun;18(6):883–91.

164. Pucci F, Garris C, Lai CP, Newton A, Pfirschke C, Engblom C, et al. SCS macrophages suppress melanoma by restricting tumor-derived vesicle-B cell interactions. Sci. 2016 Apr 8;352(6282):242–6.

165. Thomou T, Mori MA, Dreyfuss JM, Konishi M, Sakaguchi M, Wolfrum C, et al. Adipose-derived circulating miRNAs regulate gene expression in other tissues. Nature. 2017 23;542(7642):450–5.

166. Whiteside TL. The potential of tumor-derived exosomes for noninvasive cancer monitoring. Expert Rev Mol Diagn. 2015;15(10):1293–310.

167. Dabitao D, Margolick JB, Lopez J, Bream JH. Multiplex measurement of proinflammatory cytokines in human serum: comparison of the Meso Scale Discovery electrochemiluminescence assay and the Cytometric Bead Array. J Immunol Methods. 2011 Sep 30;372(1–2):71–7.

168. Szczepanski MJ, Szajnik M, Welsh A, Whiteside TL, Boyiadzis M. Blast-derived microvesicles in sera from patients with acute myeloid leukemia suppress natural killer cell function via membrane-associated transforming growth factor-beta1. Haematologica. 2011 Sep;96(9):1302–9.

169. Wong C-H, Chen Y-C. Clinical significance of exosomes as potential biomarkers in cancer. World J Clin Cases. 2019 Jan 26;7(2):171–90.

170. Li W, Li C, Zhou T, Liu X, Liu X, Li X, et al. Role of exosomal proteins in cancer diagnosis. Mol Cancer. 2017 Dec;16(1).

171. Sandfeld-Paulsen B, Jakobsen KR, Bæk R, Folkersen BH, Rasmussen TR, Meldgaard P, et al. Exosomal Proteins as Diagnostic Biomarkers in Lung Cancer. J Thorac Oncol. 2016;11(10):1701–10.

172. Reclusa P, Taverna S, Pucci M, Durendez E, Calabuig S, Manca P, et al. Exosomes as diagnostic and predictive biomarkers in lung cancer. J Thorac Dis. 2017 Oct;9(Suppl 13):S1373–82.

173. Li Y, Zhang Y, Qiu F, Qiu Z. Proteomic identification of exosomal LRG1: a potential urinary biomarker for detecting NSCLC. Electrophoresis. 2011 Aug;32(15):1976–83.

174. Jakobsen KR, Paulsen BS, Bæk R, Varming K, Sorensen BS, Jørgensen MM. Exosomal proteins as potential diagnostic markers in advanced non-small cell lung carcinoma. J Extracell Vesicles. 2015;4:26659.

175. Yamashita T, Kamada H, Kanasaki S, Maeda Y, Nagano K, Abe Y, et al. Epidermal growth factor receptor localized to exosome membranes as a possible biomarker for lung cancer diagnosis. Pharmazie. 2013 Dec;68(12):969–73.

176. Huang T, Deng C-X. Current Progresses of Exosomes as Cancer Diagnostic and Prognostic Biomarkers. Int J Biol Sci. 2019;15(1):1–11.

177. Sigismund S, Avanzato D, Lanzetti L. Emerging functions of the EGFR in cancer. Mol Oncol. 2018;12(1):3–20.

178. Jurišić V, Obradovic J, Pavlović S, Djordjevic N. Epidermal Growth Factor Receptor Gene in Non-Small-Cell Lung Cancer: The Importance of Promoter Polymorphism Investigation. Anal Cell Pathol (Amst). 2018;2018:6192187.

179. Pancewicz-Wojtkiewicz J. Epidermal growth factor receptor and notch signaling in non-small-cell lung cancer. Cancer Med. 2016;5(12):3572–8.

180. Huang S-H, Li Y, Zhang J, Rong J, Ye S. Epidermal growth factor receptor-containing exosomes induce tumor-specific regulatory T cells. Cancer Invest. 2013 Jun;31(5):330–5.

181. Zhang H, Deng T, Liu R, Bai M, Zhou L, Wang X, et al. Exosome-delivered EGFR regulates liver microenvironment to promote gastric cancer liver metastasis. Nat Commun. 2017 10;8:15016.

182. Ogden A, Bhattarai S, Sahoo B, Mongan NP, Alsaleem M, Green AR, et al. Combined HER3-EGFR score in triple-negative breast cancer provides prognostic and predictive significance superior to individual biomarkers. Sci Rep. 2020 Dec;10(1).

183. Liu X, Feng C, Liu J, Liu J, Li C, Xu C, et al. The importance of EGFR as a biomarker in molecular apocrine breast cancer. Human Pathol. 2018 Jul;77:1–10.

184. Pogribny IP. MicroRNAs as biomarkers for clinical studies. Experimental Biology and Medicine. 2018 Feb;243(3):283–90.

185. Rolfo C, Chacartegui J, Giallombardo M, Alessandro R, Peeters M. 71P Exosomes isolated in plasma of non-small cell lung cancer patients contain microRNA related to the EGFR pathway: Proof of concept. J Thor Oncol. 2016 Apr;11(4):S85.

186. Zhang J, Li S, Li L, Li M, Guo C, Yao J, et al. Exosome and Exosomal MicroRNA: Trafficking, Sorting, and Function. Genomics Proteom Bioinform 2015 Feb;13(1):17–24.

187. Teng Y, Ren Y, Hu X, Mu J, Samykutty A, Zhuang X, et al. MVP-mediated exosomal sorting of miR-193a promotes colon cancer progression. Nat Communic. 2017 Apr;8(1).

188. Wei F, Ma C, Zhou T, Dong X, Luo Q, Geng L, et al. Exosomes derived from gemcitabine-resistant cells transfer malignant phenotypic traits via delivery of miRNA-222-3p. Mol Cancer. 2017 Dec;16(1).

189. Rodríguez-Martínez A, de Miguel-Pérez D, Ortega FG, García-Puche JL, Robles-Fernández I, Exposito J, et al. Exosomal miRNA profile as complementary tool in the diagnostic and prediction of treatment response in localized breast cancer under neoadjuvant chemotherapy. Breast Cancer Res. 2019 Dec;21(1):21.

190. Gu X, Wang C, Deng H, Qing C, Liu R, Liu S, et al. Exosomal piRNA profiling revealed unique circulating piRNA signatures of cholangiocarcinoma and gallbladder carcinoma. Acta Biochim Biophys Sinica. 2020 May 26;52(5):475–84.

191. McKiernan J, Donovan MJ, Margolis E, Partin A, Carter B, Brown G, et al. A Prospective Adaptive Utility Trial to Validate Performance of a Novel Urine Exosome Gene Expression Assay to Predict High-grade Prostate Cancer in Patients with Prostate-specific Antigen 2–10 ng/ml at Initial Biopsy. Eur Urol. 2018 Dec;74(6):731–8.

192. Castellanos-Rizaldos E, Grimm DG, Tadigotla V, Hurley J, Healy J, Neal PL, et al. Exosome-Based Detection of EGFR T790M in Plasma from Non-Small Cell Lung Cancer Patients. Clin Cancer Res. 2018 15;24(12):2944–50.

193. Bernard V, Kim DU, San Lucas FA, Castillo J, Allenson K, Mulu FC, et al. Circulating Nucleic Acids Are Associated With Outcomes of Patients With Pancreatic Cancer. Gastroenterology. 2019 Jan;156(1):108-118.e4.

194. Gao J, Qiu X, Li X, Fan H, Zhang F, Lv T, et al. Expression profiles and clinical value of plasma exosomal Tim-3 and Galectin-9 in non-small cell lung cancer. Biochem Biophys Res Communic. 2018 Apr;498(3):409–15.

195. Shin H, Oh S, Hong S, Kang M, Kang D, Ji Y, et al. Early-Stage Lung Cancer Diagnosis by Deep Learning-Based Spectroscopic Analysis of Circulating Exosomes. ACS Nano. 2020 May 26;14(5):5435–44.

196. Ning C-F, Wang L, Tian Y-F, Yin B-C, Ye B-C. Multiple and sensitive SERS detection of cancer-related exosomes based on gold–silver bimetallic nanotrepangs. Analyst. 2020;145(7):2795–804.

197. Zhang Y, Mi X, Tan X, Xiang R. Recent Progress on Liquid Biopsy Analysis using Surface-Enhanced Raman Spectroscopy. Theranostics. 2019;9(2):491–525.

198. Sung H, Ferlay J, Siegel RL, Laversanne M, Soerjomataram I, Jemal A, et al. Global Cancer Statistics 2020: GLOBOCAN Estimates of Incidence and Mortality Worldwide for 36 Cancers in 185 Countries. CA A Cancer J Clin. 2021 May;71(3):209–49.

199. World Health Organization. Global Health Estimates 2020:deaths By Cause, Age, Sex, by Country and by Region, 2000-201

200. Woodard GA, Jones KD, Jablons DM. Lung Cancer Staging and Prognosis. In: Reckamp KL, editor. Lung Cancer. Cham: Springer International Publishing; 2016. p. 47–75. (Cancer Treatment and Research; vol. 170).

201. López-Encuentra A, García-Luján R, José Rivas J, Rodríguez-Rodríguez J, Torres-Lanza J, Varela-Simo G. Comparison Between Clinical and Pathologic Staging in 2,994 Cases of Lung Cancer. Ann Thor Surg. 2005 Mar;79(3):974–9.

202. Goldstraw P, Crowley J, Chansky K, Giroux DJ, Groome PA, Rami-Porta R, et al. The IASLC Lung Cancer Staging Project: Proposals for the Revision of the TNM Stage Groupings in the Forthcoming (Seventh) Edition of the TNM Classification of Malignant Tumours. J Thor Oncol. 2007 Aug;2(8):706–14.

203. Shepherd FA, Crowley J, Van Houtte P, Postmus PE, Carney D, Chansky K, et al. The International Association for the Study of Lung Cancer Lung Cancer Staging Project: Proposals Regarding the Clinical Staging of Small Cell Lung Cancer in the Forthcoming (Seventh) Edition of the Tumor, Node, Metastasis Classification for Lung Cancer. J Thor Oncol. 2007 Dec;2(12):1067–77.

204. Bob T. Li, MD MPH. Types of lung cancer.

205. Blandin Knight S, Crosbie PA, Balata H, Chudziak J, Hussell T, Dive C. Progress and prospects of early detection in lung cancer. Open Biol. 2017;7(9).

206. Bernhardt EB, Jalal SI. Small Cell Lung Cancer. Lung Cancer. Cham: Springer International Publishing; 2016. p. 301–22. (Cancer Treatment and Research; vol. 170).

207. Yu T, Zhong D. [Clinical Development of Immunotherapy for Small Cell Lung Cancer]. Zhongguo Fei Ai Za Zhi. 2018 Dec 20;21(12):918–23.

208. Midthun DE. Early detection of lung cancer. F1000Res. 2016;5.

209. Sutedja G. New techniques for early detection of lung cancer. Eur Respir J. 2003 Jan 1;21(Supplement 39):57S – 66s.

210. Paleari L, Granone P, Grozio A, Cesario A, Russo P. Commentary: Early Diagnosis of Lung Cancer: Where Do We Stand? Oncol. 2007 Dec 1;12(12):1433–6.

211. Purandare N, Rangarajan V. Imaging of lung cancer: Implications on staging and management. Indian J Radiol Imaging. 2015;25(2):109.

212. Buccheri G. Lung cancer: clinical presentation and specialist referral time. Eur Respir J. 2004 Dec 1;24(6):898–904.

213. Schmidt GP, Baur-Melnyk A, Herzog P, Schmid R, Tiling R, Schmidt M, et al. High-Resolution Whole-Body Magnetic Resonance Image Tumor Staging With the Use of Parallel Imaging Versus Dual-Modality Positron Emission Tomography?Computed Tomography: Experience on a 32-Channel System. Investig Radiol. 2005 Dec;40(12):743–53.

214. Yung R. Tissue diagnosis of suspected lung cancer: selecting between bronchoscopy, transthoracic needle aspiration, and resectional biopsy. Respir Care Clinics. 2003 Mar;9(1):51–76.

215. Herth FJF, Eberhardt R, Vilmann P, Krasnik M, Ernst A. Real-time endobronchial ultrasound guided transbronchial needle aspiration for sampling mediastinal lymph nodes. Thorax. 2006 Sep 1;61(9):795–8.

216. Bradley SH, Hatton NLF, Aslam R, Bhartia B, Callister ME, Kennedy MP, et al. Estimating lung cancer risk from chest X-ray and symptoms: a prospective cohort study. Br J Gen Pract. 2021 Apr;71(705):e280–6.

217. Croswell JM. Cumulative Incidence of False-Positive Test Results in Lung Cancer Screening: A Randomized Trial. Ann Intern Med. 2010 Apr 20;152(8):505.

218. Hollings N, Shaw P. Diagnostic imaging of lung cancer. Eur Respir J 2002 Apr;19(4):722–42.

219. Haque N, Raza A, McGoey R, Boulmay B, Diethelm L, Kantrow S. Small cell lung cancer: time to diagnosis and treatment. South Med J. 2012 Aug;105(8):418–23.

220. Giroux Leprieur E, Herbretau G, Dumenil C, Julie C, Giraud V, Labrune S, et al. Circulating tumor DNA evaluated by Next-Generation Sequencing is predictive of tumor response and prolonged clinical benefit with nivolumab in advanced non-small cell lung cancer. OncoImmunology. 2018 May 4;7(5):e1424675.

221. Bettegowda C, Sausen M, Leary RJ, Kinde I, Wang Y, Agrawal N, et al. Detection of Circulating Tumor DNA in Early- and Late-Stage Human Malignancies. Sci Translat Med. 2014 Feb 19;6(224):224ra24-224ra24.

222. Abbosh C, Birkbak NJ, Wilson GA, Jamal-Hanjani M, Constantin T, Salari R, et al. Phylogenetic ctDNA analysis depicts early-stage lung cancer evolution. Nature. 2017 26;545(7655):446–51.

223. Merker JD, Oxnard GR, Compton C, Diehn M, Hurley P, Lazar AJ, et al. Circulating Tumor DNA Analysis in Patients With Cancer: Am J Clin Oncol Pathol Joint Rev. JCO. 2018 Jun 1;36(16):1631–41.

224. Navani N, Nankivell M, Lawrence DR, Lock S, Makker H, Baldwin DR, et al. Lung cancer diagnosis and staging with endobronchial ultrasound-guided transbronchial needle aspiration compared with conventional approaches: an open-label, pragmatic, randomised controlled trial. Lancet Respir Med 2015 Apr;3(4):282–9.

225. Medford A. Endobronchial ultrasound: what is it and when should it be used? Clin Med. 2010 Oct;10(5):458–63.

226. Paradis TJ, Dixon J, Tieu BH. The role of bronchoscopy in the diagnosis of airway disease. J Thorac Dis. 2016 Dec;8(12):3826–37.

227. Webb WR, Jensen BG, Sollitto R, de Geer G, McCowin M, Gamsu G, et al. Bronchogenic carcinoma: staging with MR compared with staging with CT and surgery. Radiology. 1985 Jul;156(1):117–24.

228. Hochhegger B, Marchiori E, Sedlaczek O, Irion K, Heussel CP, Ley S, et al. MRI in lung cancer: a pictorial essay. Brit J Radiol. 2011 Jul;84(1003):661–8.

229. Wang Y-XJ, Gong J-S, Suzuki K, Morcos SK. Evidence based imaging strategies for solitary pulmonary nodule. J Thorac Dis. 2014 Jul;6(7):872–87.

230. Wang Y-XJ, Lo GG, Yuan J, Larson PEZ, Zhang X. Magnetic resonance imaging for lung cancer screen. J Thorac Dis. 2014 Sep;6(9):1340–8.

231. Saccomanno G, Archer VE, Auerbach O, Saunders RP, Brennan LM. Development of carcinoma of the lung as reflected in exfoliated cells. Cancer. 1974 Jan;33(1):256–70.

232. Mehan MR, Ayers D, Thirstrup D, Xiong W, Ostroff RM, Brody EN, et al. Protein signature of lung cancer tissues. PLoS ONE. 2012;7(4):e35157.

233. Yu X, Li X, Song X, Dai D, Zhu L, Zhu Y, et al. Advantages and disadvantages of F-18 fluorodeoxyglucose positron emission tomography/computed tomography in carcinoma of unknown primary. Oncol Lett. 2016 Nov;12(5):3785–92.

234. Chang C-F, Rashtian A, Gould MK. The use and misuse of positron emission tomography in lung cancer evaluation. Clin Chest Med. 2011 Dec;32(4):749–62.

235. Yamashita H, Kubota K, Mimori A. Clinical value of whole-body PET/CT in patients with active rheumatic diseases. Arthrit Res Ther. 2014 Oct;16(4).

236. Griffeth LK. Use of Pet/Ct Scanning in Cancer Patients: Technical and Practical Considerations. Baylor University Medical Center Proceedings. 2005 Oct;18(4):321–30.

237. Wu N-Y, Cheng H-C, Ko JS, Cheng Y-C, Lin P-W, Lin W-C, et al. Magnetic resonance imaging for lung cancer detection: Experience in a population of more than 10,000 healthy individuals. BMC Cancer. 2011 Dec;11(1).

238. Hatabu H, Stock KW, Sher S, Edinburgh KJ, Levin DL, Garpestad E, et al. Magnetic resonance imaging of the thorax. Clinics in Chest Medicine. 1999 Dec;20(4):775–803.

239. Perlman EJ, Erozan YS, Howdon A. The Role of the Saccomano Technique in Sputum Cytopathologic Diagnosis of Lung Cancer. Am J Clin Pathol. 1989 Jan 1;91(1):57–60.

240. Rivera MP, Mehta AC. Initial Diagnosis of Lung Cancer. Chest. 2007 Sep;132(3):131S-148S.

241. Ammanagi AS, Dombale VD, Miskin AT, Dandagi GL, Sangolli SS. Sputum cytology in suspected cases of carcinoma of lung. Lung India. 2012 Jan;29(1):19–23.

242. Risse EKJ, Van't Hof MA, Laurini RN, Vooijs PG. Sputum cytology by the saccomanno method in diagnosing lung malignancy. Diagn Cytopatholog. 1985 Oct;1(4):286–91.

243. Lackey A, Donington J. Surgical Management of Lung Cancer. Sem Intervent Radiol. 2013 May 28;30(02):133–40.

244. Sihoe ADL, Hiranandani R, Wong H, Yeung ESL. Operating on a suspicious lung mass without a preoperative tissue diagnosis: pros and cons. Eur J Cardio-Thor Surg. 2013 Aug;44(2):231–7.

245. Schiffman JD, Fisher PG, Gibbs P. Early detection of cancer: past, present, and future. Am Soc Clin Oncol Educ Book. 2015;57–65.

246. Omura Y, Lu D, O'Young B, Jones M, Nihrane A, Duvvi H, et al. New non-invasive safe, quick, economical method of detecting various cancers was found using QRS complex or rising part of T-wave of recorded ECGs. Cancers can be screened along with their biochemical parameters & therapeutic effects of any cancer treatments can be evaluated using recorded ECGs of the same individual. Acupunct Electrother Res. 2015;40(1):1–15.

247. Whitney DH, Elashoff MR, Porta-Smith K, Gower AC, Vachani A, Ferguson JS, et al. Derivation of a bronchial genomic classifier for lung cancer in a prospective study of patients undergoing diagnostic bronchoscopy. BMC Med Genom. 2015 Dec;8(1).

248. Meng Y, Sun J, Qu N, Zhang G, Yu T, Piao H. Application of Radiomics for Personalized Treatment of Cancer Patients. Cancer Manag Res. 2019 Dec;Volume 11:10851–8.

249. Ghasemi M, Nabipour I, Omrani A, Alipour Z, Assadi M. Precision medicine and molecular imaging: new targeted approaches toward cancer therapeutic and diagnosis. Am J Nucl Med Mol Imaging. 2016;6(6):310–27.

250. Boyle P, Chapman CJ, Holdenrieder S, Murray A, Robertson C, Wood WC, et al. Clinical validation of an autoantibody test for lung cancer. Ann Oncol. 2011 Feb;22(2):383–9.

251. Jett JR, Peek LJ, Fredericks L, Jewell W, Pingleton WW, Robertson JFR. Audit of the autoantibody test, EarlyCDT®-Lung, in 1600 patients: An evaluation of its performance in routine clinical practice. Lung Cancer. 2014 Jan;83(1):51–5.

252. Ajona D, Pajares MJ, Corrales L, Perez-Gracia JL, Agorreta J, Lozano MD, et al. Investigation of Complement Activation Product C4d as a Diagnostic and Prognostic Biomarker for Lung Cancer. JNCI: J Natl Cancer Inst. 2013 Sep 18;105(18):1385–93.

253. Ajona D, Okrój M, Pajares MJ, Agorreta J, Lozano MD, Zulueta JJ, et al. Complement C4d-specific antibodies for the diagnosis of lung cancer. Oncotarget. 2018 Jan 19;9(5):6346–55.

254. Esteller M, Sanchez-Cespedes M, Rosell R, Sidransky D, Baylin SB, Herman JG. Detection of aberrant promoter hypermethylation of tumor suppressor genes in serum DNA from non-small cell lung cancer patients. Cancer Res. 1999 Jan 1;59(1):67–70.

255. Hulbert A, Jusue-Torres I, Stark A, Chen C, Rodgers K, Lee B, et al. Early Detection of Lung Cancer Using DNA Promoter Hypermethylation in Plasma and Sputum. Clinical Cancer Res. 2017 Apr 15;23(8):1998–2005.

256. Wielscher M, Vierlinger K, Kegler U, Ziesche R, Gsur A, Weinhäusel A. Diagnostic Performance of Plasma DNA Methylation Profiles in Lung Cancer, Pulmonary Fibrosis and COPD. EBioMedicine. 2015 Aug;2(8):929–36.

257. Ooki A, Maleki Z, Tsay J-CJ, Goparaju C, Brait M, Turaga N, et al. A Panel of Novel Detection and Prognostic Methylated DNA Markers in Primary Non-Small Cell Lung Cancer and Serum DNA. Clin Cancer Res. 2017 Nov 15;23(22):7141–52.

258. Sinha N, Tufail M, Eneje O, Abbas S, Yung B, Pannu K, et al. Endobronchial ultrasound guided transbronchial needle aspiration (EBUS-TBNA) reduces time for diagnosis of lung cancer if used as the initial diagnostic test of choice. Eur Respir Soc; 2016. p. PA2808.259. Dong Z, Li H, Jiang H, Wu C. Evaluation of cytology in lung cancer diagnosis based on EBUS-TBNA. J Cytol. 2017;34(2):73.

260. Murthi M, Donna E, Arias S, Villamizar NR, Nguyen DM, Holt GE, et al. Diagnostic Accuracy of Endobronchial Ultrasound-Guided Transbronchial Needle Aspiration (EBUS-TBNA) in Real Life. Front Med. 2020 Apr 7;7. 261. Claessens N, Maas K, Kummer A, Schramel F. Diagnostic yield, clinical impact and cost aspect of EBUS-TBNA in mediastinal staging in lung cancer. Eur Respir J. 2012 Sep 1;40(Suppl 56):P4403.

262. Lubas M, Damgaard CK, Tomecki R, Cysewski D, Jensen TH, Dziembowski A. Exonuclease hDIS3L2 specifies an exosome-independent 3′-5′ degradation pathway of human cytoplasmic mRNA. EMBO J. 2013 Jun 11;32(13):1855–68.

263. Lai J, Du B, Wang Y, Wu R, Yu Z. Next-generation sequencing of circulating tumor DNA for detection of gene mutations in lung cancer: implications for precision treatment. OncoTargets Ther. 2018 Dec;Volume 11:9111–6.

264. Aravanis AM, Lee M, Klausner RD. Next-Generation Sequencing of Circulating Tumor DNA for Early Cancer Detection. Cell. 2017 Feb;168(4):571–4.

265. Cohen JD, Javed AA, Thoburn C, Wong F, Tie J, Gibbs P, et al. Combined circulating tumor DNA and protein biomarker-based liquid biopsy for the earlier detection of pancreatic cancers. Proc Natl Acad Sci. 2017 Sep 19;114(38):10202–7.

266. Phallen J, Sausen M, Adleff V, Leal A, Hruban C, White J, et al. Direct detection of early-stage cancers using circulating tumor DNA. Sci Translat Med. 2017 Aug 16;9(403):eaan2415.

267. Wang Y, Springer S, Mulvey CL, Silliman N, Schaefer J, Sausen M, et al. Detection of somatic mutations and HPV in the saliva and plasma of patients with head and neck squamous cell carcinomas. Sci Translat Med. 2015 Jun 24;7(293):293ra104-293ra104.

268. Khan S, Ullah R, Javaid S, Shahzad S, Ali H, Bilal M, et al. Raman Spectroscopy Combined with Principal Component Analysis for Screening Nasopharyngeal Cancer in Human Blood Sera. Appl Spectr. 2017 Nov;71(11):2497–503.

269. Li Y, Huang W, Pan J, Ye Q, Lin S, Feng S, et al. Rapid detection of nasopharyngeal cancer using Raman spectroscopy and multivariate statistical analysis. Mol Clin Oncol. 2015 Mar;3(2):375–80.

270. Valdés R, Stefanov S, Chiussi S, López-Alvarez M, González P. Pilot research on the evaluation and detection of head and neck squamous cell carcinoma by Raman spectroscopy: Evaluation and detection of head and neck squamous cell carcinoma. J Raman Spectr. 2014 Jul;45(7):550–7.

271. Qian K, Wang Y, Hua L, Chen A, Zhang Y. New method of lung cancer detection by saliva test using surface-enhanced Raman spectroscopy: New detection method for lung cancer. Thor Cancer. 2018 Nov;9(11):1556–61.

272. McGregor HC, Short MA, McWilliams A, Shaipanich T, Ionescu DN, Zhao J, et al. Real-time endoscopic Raman spectroscopy for *in vivo* early lung cancer detection. J Biophotonics. 2017 Jan;10(1):98–110.

273. Clark DJ, Fondrie WE, Yang A, Mao L. Triple SILAC quantitative proteomic analysis reveals differential abundance of cell signaling proteins between normal and lung cancer-derived exosomes. J Proteom 2016 Feb;133:161–9.

274. Youssef O, Sarhadi VK, Armengol G, Piirilä P, Knuuttila A, Knuutila S. Exhaled breath condensate as a source of biomarkers for lung carcinomas. A focus on genetic and epigenetic markers-A mini-review: EBC Biomarkers in Lung Cancer. Genes Chromosomes Cancer. 2016 Dec;55(12):905–14.

275. Sinha A, Yadav AK, Chakraborty S, Kabra SK, Lodha R, Kumar M, et al. Exosome-enclosed microRNAs in exhaled breath hold potential for biomarker discovery in patients with pulmonary diseases. J Allergy Clin Immunol. 2013 Jul;132(1):219–22.

276. Sastre B, Cañas JA, Rodrigo-Muñoz JM, del Pozo V. Novel Modulators of Asthma and Allergy: Exosomes and MicroRNAs. Front Immunol. 2017 Jul 21;8.

277. Garbacki N, Di Valentin E, Huynh-Thu VA, Geurts P, Irrthum A, Crahay C, et al. MicroRNAs Profiling in Murine Models of Acute and Chronic Asthma: A Relationship with mRNAs Targets. Creighton C, editor. PLoS ONE. 2011 Jan 28;6(1):e16509.

278. Thomas PA, Berbis J, Falcoz P-E, Le Pimpec-Barthes F, Bernard A, Jougon J, et al. National perioperative outcomes of pulmonary lobectomy for cancer: the influence of nutritional status. Eur J Cardiothorac Surg. 2014 Apr;45(4):652–9; discussion 659.

279. Li S, Zhou K, Che G, Yang M, Su J, Shen C, et al. Enhanced recovery programs in lung cancer surgery: systematic review and meta-analysis of randomized controlled trials. Cancer Manag Res. 2017;9:657–70.

280. Li S, Zhou K, Wang M, Lin R, Fan J, Che G. Degree of pulmonary fissure completeness can predict postoperative cardiopulmonary complications and length of hospital stay in patients undergoing video-assisted thoracoscopic lobectomy for early-stage lung cancer. Interact Cardiovasc Thorac Surg. 2018 01;26(1):25–33.

281. Jackson AS, Sandrini A, Campbell C, Chow S, Thomas PS, Yates DH. Comparison of biomarkers in exhaled breath condensate and bronchoalveolar lavage. Am J Respir Crit Care Med. 2007 Feb 1;175(3):222–7.

282. Borrill ZL, Roy K, Singh D. Exhaled breath condensate biomarkers in COPD. Eur Respir J. 2008 Mar 19;32(2):472–86.

283. van Horck M, Alonso A, Wesseling G, de Winter—de Groot K, van Aalderen W, Hendriks H, et al. Biomarkers in Exhaled Breath Condensate Are Not Predictive for Pulmonary Exacerbations in Children with Cystic Fibrosis: Results of a One-Year Observational Study. Ryffel B, editor. PLoS ONE. 2016 Apr 6;11(4):e0152156.

284. Kačerová T, Novotný P, Boroň J, Kačer P. Molecular Diagnostics of Pulmonary Diseases Based on Analysis of Exhaled Breath Condensate. Biomarker - Indicator of Abnormal Physiological Process. InTech; 2018.

285. O'Reilly P, Bailey W. Clinical use of exhaled biomarkers in COPD. Int J Chron Obstruct Pulmon Dis. 2007;2(4):403–8.

286. Grob NM, Aytekin M, Dweik RA. Biomarkers in exhaled breath condensate: a review of collection, processing and analysis. J Breath Res. 2008 Sep;2(3):037004.

287. Limb SL, Hubbard WC, Wood RA, Adkinson N. Asthma Biomarkers in Exhaled Breath Condensate (EBC). J Allerg Clin Immunol. 2006 Feb;117(2):S194.

288. Murugan A, Prys-Picard C, Calhoun WJ. Biomarkers in asthma: Curr Opin Pulm Med. 2009 Jan;15(1):12–8.

289. Gessner C. Detection of p53 gene mutations in exhaled breath condensate of non-small cell lung cancer patients. Lung Cancer. 2004 Feb;43(2):215–22.

290. Zhang D, Takigawa N, Ochi N, Tanimoto Y, Noujima D, Chen YY, et al. Detection of the EGFR mutation in exhaled breath condensate from a heavy smoker with squamous cell carcinoma of the lung. Lung Cancer. 2011 Sep;73(3):379–80.

291. Kordiak J, Szemraj J, Hamara K, Bialasiewicz P, Nowak D. Complete surgical resection of lung tumor decreases exhalation of mutated KRAS oncogene. Respir Med. 2012 Sep;106(9):1293–300.

292. Carpagnano GE, Foschino-Barbaro MP, Spanevello A, Resta O, Carpagnano F, Mulé G, et al. 3p Microsatellite Signature in Exhaled Breath Condensate and Tumor Tissue of Patients with Lung Cancer. Am J Respir Critical Care Med. 2008 Feb;177(3):337–41.

293. Ahmadzai H, Huang S, Hettiarachchi R, Lin J-L, Thomas PS, Zhang Q. Exhaled breath condensate: a comprehensive update. Clin Chem Lab Med. 2013 Jan 1;51(7).

294. Chen J-L, Chen J-R, Huang F-F, Tao G-H, Zhou F, Tao Y-J. Analysis of p16 gene mutations and their expression using exhaled breath condensate in non-small-cell lung cancer. Oncol Lett. 2015 Sep;10(3):1477–80.

295. Youssef O, Knuuttila A, Piirilä P, Böhling T, Sarhadi V, Knuutila S. Presence of cancer-associated mutations in exhaled breath condensates of healthy individuals by next generation sequencing. Oncotarget. 2017 Mar 14;8(11):18166–76.

296. Youssef O, Knuuttila A, Piirilä P, Böhling T, Sarhadi V, Knuutila S. Hotspot Mutations Detectable by Next-generation Sequencing in Exhaled Breath Condensates from Patients with Lung Cancer. Anticancer Res. 2018 Oct;38(10):5627–34.

297. Conrad DH, Goyette J, Thomas PS. Proteomics as a Method for Early Detection of Cancer: A Review of Proteomics, Exhaled Breath Condensate, and Lung Cancer Screening. J Gen Int Med. 2008 Jan;23(S1):78–84.

298. Mazzone PJ. Analysis of Volatile Organic Compounds in the Exhaled Breath for the Diagnosis of Lung Cancer. J Thor Oncol. 2008 Jul;3(7):774–80.

299. López-Sánchez LM, Jurado-Gámez B, Feu-Collado N, Valverde A, Cañas A, Fernández-Rueda JL, et al. Exhaled breath condensate biomarkers for the early diagnosis of lung cancer using proteomics. Am J Physiol-Lung Cell Mol Physiol. 2017 Oct 1;313(4):L664–76.

300. Lim MY, Thomas PS. Biomarkers in Exhaled Breath Condensate and Serum of Chronic Obstructive Pulmonary Disease and Non-Small-Cell Lung Cancer. Int J Chronic Diseases. 2013;2013:1–15.

301. Szulejko JE, McCulloch M, Jackson J, McKee DL, Walker JC, Solouki T. Evidence for Cancer Biomarkers in Exhaled Breath. IEEE Sensors Journal. 2010 Jan;10(1):185–210.

302. Ma L, Muscat JE, Sinha R, Sun D, Xiu G. Proteomics of exhaled breath condensate in lung cancer and controls using data-independent acquisition (DIA): a pilot study. J Breath Res. 2021 Apr 1;15(2):026002.

303. Dent AG, Sutedja TG, Zimmerman PV. Exhaled breath analysis for lung cancer. J Thorac Dis. 2013 Oct;5 Suppl 5:S540-550.

304. Chen J-L, Han H-N, Lv X-D, Ma H, Wu J-N, Chen J-R. Clinical value of exhaled breath condensate let-7 in non-small cell lung cancer. Int J Clin Exp Pathol. 2020;13(2):163–71.

305. Carpagnano GE, Spanevello A, Curci C, Salerno F, Palladino GP, Resta O, et al. IL-2, TNF-α, and Leptin: Local Versus Systemic Concentrations in NSCLC Patients. oncol res. 2006 Aug 1;16(8):375–81.

306. Kolbasina NA, Gureev AP, Serzhantova OV, Mikhailov AA, Moshurov IP, Starkov AA, et al. Lung cancer increases H2O2 concentration in the exhaled breath condensate, extent of mtDNA damage, and mtDNA copy number in buccal mucosa. Heliyon. 2020 Jun;6(6):e04303.

307. Chan HP, Lewis C, Thomas PS. Oxidative Stress and Exhaled Breath Analysis: A Promising Tool for Detection of Lung Cancer. Cancers. 2010 Feb 8;2(1):32–42.

308. Crohns M, Saarelainen S, Laitinen J, Peltonen K, Alho H, Kellokumpu-Lehtinen P. Exhaled pentane as a possible marker for survival and lipid peroxidation during radiotherapy for lung cancer—a pilot study. Free Radical Res. 2009 Jan;43(10):965–74.

309. Khyshiktyev BS, Khyshiktueva NA, Ivanov VN, Darenskaia SD, Novikov SV. [Diagnostic value of investigating exhaled air condensate in lung cancer]. Vopr Onkol. 1994;40(4–6):161–4.

310. Carpagnano GE, Resta O, Foschino-Barbaro MP, Gramiccioni E, Carpagnano F. Interleukin-6 is increased in breath condensate of patients. JBM. 2002;17(2):141–5.

311. Stathopoulos D, Loukides S, Syrigos K. 8-Isoprostane in exhaled breath condensate of patients with non-small cell lung cancer: the effect of chemotherapy. Anticancer Res. 2014 Sep;34(9):5143–5.

312. Carpagnano GE, Foschino-Barbaro MP, Mulé G, Resta O, Tommasi S, Mangia A, et al. 3p Microsatellite Alterations in Exhaled Breath Condensate from Patients with Non–Small Cell Lung Cancer. Am J Respir Crit Care Med. 2005 Sep 15;172(6):738–44.

313. Carpagnano GE, Foschino-Barbaro MP, Resta O, Gramiccioni E, Carpagnano F. Endothelin-1 Is Increased in the Breath Condensate of Patients with Non-Small-Cell Lung Cancer. Oncology. 2004;66(3):180–4.

314. Guzman NA, Guzman DE. A Two-Dimensional Affinity Capture and Separation Mini-Platform for the Isolation, Enrichment, and Quantification of Biomarkers and Its Potential Use for Liquid Biopsy. Biomedicines. 2020 Jul 30;8(8):255.

315. Musante L, Tataruch-Weinert D, Kerjaschki D, Henry M, Meleady P, Holthofer H. Residual urinary extracellular vesicles in ultracentrifugation supernatants after hydrostatic filtration dialysis enrichment. J Extracell Vesicles. 2017 Dec 1;6(1):1267896.

316. Habibi R, He V, Ghavamian S, de Marco A, Lee T-H, Aguilar M-I, et al. Exosome trapping and enrichment using a sound wave activated nano-sieve (SWANS). Lab Chip. 2020;20(19):3633–43.

317. Haque S, Vaiselbuh SR. Exosomes molecular diagnostics: Direct conversion of exosomes into the cDNA for gene amplification by two-step polymerase chain reaction. J Biol Methods. 2018 Jul 25;5(3):96.

318. Chaput N, Théry C. Exosomes: immune properties and potential clinical implementations. Semin Immunopathol. 2011 Sep;33(5):419–40.

319. Huang Y, Li R, Ye S, Lin S, Yin G, Xie Q. Recent Advances in the Use of Exosomes in Sjögren's Syndrome. Front Immunol. 2020 Aug 6;11:1509.

320. Abramowicz A, Marczak L, Wojakowska A, Zapotoczny S, Whiteside TL, Widlak P, et al. Harmonization of exosome isolation from culture supernatants for optimized proteomics analysis. Ahmad A, editor. PLoS ONE. 2018 Oct 31;13(10):e0205496.

321. Pietrowska M, Funk S, Gawin M, Marczak Ł, Abramowicz A, Widłak P, et al. Isolation of Exosomes for the Purpose of Protein Cargo Analysis with the Use of Mass Spectrometry. Methods Mol Biol. 2017;1654:291–307.

322. Lötvall J, Hill AF, Hochberg F, Buzás EI, Di Vizio D, Gardiner C, et al. Minimal experimental requirements for definition of extracellular vesicles and their functions: a position statement from the International Society for Extracellular Vesicles. J Extracell Vesicles. 2014 Jan;3(1):26913.

323. Sódar BW, Kittel Á, Pálóczi K, Vukman KV, Osteikoetxea X, Szabó-Taylor K, et al. Low-density lipoprotein mimics blood plasma-derived exosomes and microvesicles during isolation and detection. Sci Rep. 2016 Jul;6(1):24316.

324. Théry C, Amigorena S, Raposo G, Clayton A. Isolation and Characterization of Exosomes from Cell Culture Supernatants and Biological Fluids. Curr Prot Cell Biol. 2006 Mar;30(1):3.22.1-3.22.29.

325. Yakimchuk K. Exosomes: isolation methods and specific markers. Materials and Methods. 2015 Aug 15;5.

326. Momen-Heravi F, Balaj L, Alian S, Mantel P-Y, Halleck AE, Trachtenberg AJ, et al. Current methods for the isolation of extracellular vesicles. Biol Chem. 2013 Oct 1;394(10):1253–62.

327. Lobb RJ, Becker M, Wen SW, Wong CSF, Wiegmans AP, Leimgruber A, et al. Optimized exosome isolation protocol for cell culture supernatant and human plasma. J Extracell Vesicles. 2015;4:27031.

328. Tjalsma H, Bolhuis A, Jongbloed JDH, Bron S, van Dijl JM. Signal Peptide-Dependent Protein Transport inBacillus subtilis: a Genome-Based Survey of the Secretome. Microbiol Mol Biol Rev. 2000 Sep 1;64(3):515–47.

329. Sjöqvist S, Imafuku A, Ghupta D, Andaloussi SEL. Isolation and Characterization of Extracellular Vesicles from Keratinocyte Cultures. Methods Mol Biol. 2019 Sep 21;

330. Livshits MA, Khomyakova E, Evtushenko EG, Lazarev VN, Kulemin NA, Semina SE, et al. Isolation of exosomes by differential centrifugation: Theoretical analysis of a commonly used protocol. Sci Rep. 2015 Dec;5(1).

331. Yu L-L, Zhu J, Liu J-X, Jiang F, Ni W-K, Qu L-S, et al. A Comparison of Traditional and Novel Methods for the Separation of Exosomes from Human Samples. BioMed Res Int. 2018 Jul 26;2018:1–9.

332. Gardiner C, Vizio DD, Sahoo S, Théry C, Witwer KW, Wauben M, et al. Techniques used for the isolation and characterization of extracellular vesicles: results of a worldwide survey. J Extracell Vesicles. 2016 Jan;5(1):32945.

333. Heinemann ML, Ilmer M, Silva LP, Hawke DH, Recio A, Vorontsova MA, et al. Benchtop isolation and characterization of functional exosomes by sequential filtration. J Chromatogr A. 2014 Dec 5;1371:125–35.

334. Baranyai T, Herczeg K, Onódi Z, Voszka I, Módos K, Marton N, et al. Isolation of Exosomes from Blood Plasma: Qualitative and Quantitative Comparison of Ultracentrifugation and Size Exclusion Chromatography Methods. PLoS ONE. 2015;10(12):e0145686.

335. Taylor DD, Shah S. Methods of isolating extracellular vesicles impact down-stream analyses of their cargoes. Methods. 2015 Oct;87:3–10.

336. Benedikter BJ, Bouwman FG, Vajen T, Heinzmann ACA, Grauls G, Mariman EC, et al. Ultrafiltration combined with size exclusion chromatography efficiently isolates extracellular vesicles from cell culture media for compositional and functional studies. Sci Rep. 2017 Nov 10;7(1):15297.

337. Stranska R, Gysbrechts L, Wouters J, Vermeersch P, Bloch K, Dierickx D, et al. Comparison of membrane affinity-based method with size-exclusion chromatography for isolation of exosome-like vesicles from human plasma. J Translat Med. 2018 Dec;16(1).

338. An M, Wu J, Zhu J, Lubman DM. Comparison of an Optimized Ultracentrifugation Method versus Size-Exclusion Chromatography for Isolation of Exosomes from Human Serum. J Proteome Res. 2018 Oct 5;17(10):3599–605.

339. Shelke GV, Lässer C, Gho YS, Lötvall J. Importance of exosome depletion protocols to eliminate functional and RNA-containing extracellular vesicles from fetal bovine serum. J Extracell Vesicles. 2014 Jan;3(1):24783.

340. Tang Y-T, Huang Y-Y, Zheng L, Qin S-H, Xu X-P, An T-X, et al. Comparison of isolation methods of exosomes and exosomal RNA from cell culture medium and serum.Int J Mol Med. 2017 Sep;40(3):834–44.

341. Guerreiro EM, Vestad B, Steffensen LA, Aass HCD, Saeed M, Øvstebø R, et al. Efficient extracellular vesicle isolation by combining cell media modifications, ultrafiltration, and size-exclusion chromatography. Ahmad A, editor. PLoS ONE. 2018 Sep 27;13(9):e0204276.

342. Davis CN, Phillips H, Tomes JJ, Swain MT, Wilkinson TJ, Brophy PM, et al. The importance of extracellular vesicle purification for downstream analysis: A comparison of differential centrifugation and size exclusion chromatography for helminth pathogens. Rinaldi G, editor. PLOS Neglected Tropical Diseases. 2019 Feb 27;13(2):e0007191.

343. Duong P, Chung A, Bouchareychas L, Raffai RL. Cushioned-Density Gradient Ultracentrifugation (C-DGUC) improves the isolation efficiency of extracellular vesicles. Hancock R, editor. PLoS ONE. 2019 Apr 11;14(4):e0215324.

344. Kamerkar S, LeBleu VS, Sugimoto H, Yang S, Ruivo CF, Melo SA, et al. Exosomes facilitate therapeutic targeting of oncogenic KRAS in pancreatic cancer. Nature. 2017 Jun;546(7659):498–503.

345. Onódi Z, Pelyhe C, Terézia Nagy C, Brenner GB, Almási L, Kittel Á, et al. Isolation of High-Purity Extracellular Vesicles by the Combination of Iodixanol Density Gradient Ultracentrifugation and Bind-Elute Chromatography From Blood Plasma. Front Physiol. 2018 Oct 23;9.

346. Chen B-Y, Sung CW-H, Chen C, Cheng C-M, Lin DP-C, Huang C-T, et al. Advances in exosomes technology. Clinica Chimica Acta. 2019 Jun;493:14–9.

347. Caradec J, Kharmate G, Hosseini-Beheshti E, Adomat H, Gleave M, Guns E. Reproducibility and efficiency of serum-derived exosome extraction methods. Clin Biochem. 2014 Sep;47(13–14):1286–92.

348. Zeringer E, Barta T, Li M, Vlassov AV. Strategies for Isolation of Exosomes. Cold Spring Harbor Protocols. 2015 Apr;2015(4):pdb.top074476.

349. Van Deun J, Mestdagh P, Sormunen R, Cocquyt V, Vermaelen K, Vandesompele J, et al. The impact of disparate isolation methods for extracellular vesicles on downstream RNA profiling. J Extracell Vesicles. 2014 Jan;3(1):24858.

350. Lane RE, Korbie D, Anderson W, Vaidyanathan R, Trau M. Analysis of exosome purification methods using a model liposome system and tunable-resistive pulse sensing. Sci Rep. 2015 Jul;5(1).

351. Karimi N, Cvjetkovic A, Jang SC, Crescitelli R, Hosseinpour Feizi MA, Nieuwland R, et al. Detailed analysis of the plasma extracellular vesicle proteome after separation from lipoproteins. Cell Mol Life Sci. 2018 Aug;75(15):2873–86.

352. Tauro BJ, Greening DW, Mathias RA, Ji H, Mathivanan S, Scott AM, et al. Comparison of ultracentrifugation, density gradient separation, and immunoaffinity capture methods for isolating human colon cancer cell line LIM1863-derived exosomes. Methods. 2012 Feb;56(2):293–304.

353. Sharma P, Ludwig S, Muller L, Hong CS, Kirkwood JM, Ferrone S, et al. Immunoaffinity-based isolation of melanoma cell-derived exosomes from plasma of patients with melanoma. J Extracell Vesicles. 2018 Dec;7(1):1435138.

354. Cai S, Luo B, Jiang P, Zhou X, Lan F, Yi Q, et al. Immuno-modified superparamagnetic nanoparticles *via* host–guest interactions for high-purity capture and mild release of exosomes. Nanoscale. 2018;10(29):14280–9.

355. Ayala-Mar S, Donoso-Quezada J, Gallo-Villanueva RC, Perez-Gonzalez VH, González-Valdez J. Recent advances and challenges in the recovery and purification of cellular exosomes. Electrophoresis. 2019;40(23–24):3036–49.

356. He F, Liu H, Guo X, Yin B-C, Ye B-C. Direct Exosome Quantification via Bivalent-Cholesterol-Labeled DNA Anchor for Signal Amplification. Anal Chem. 2017 Dec 5;89(23):12968–75.

357. Konoshenko MYu, Lekchnov EA, Vlassov AV, Laktionov PP. Isolation of Extracellular Vesicles: General Methodologies and Latest Trends. BioMed Res Int. 2018;2018:1–27.

358. Grant R, Ansa-Addo E, Stratton D, Antwi-Baffour S, Jorfi S, Kholia S, et al. A filtration-based protocol to isolate human Plasma Membrane-derived Vesicles and exosomes from blood plasma. Journal of Immunological Methods. 2011 Aug;371(1–2):143–51.

359. Campoy I, Lanau L, Altadill T, Sequeiros T, Cabrera S, Cubo-Abert M, et al. Exosome-like vesicles in uterine aspirates: a comparison of ultracentrifugation-based isolation protocols. J Translat Med. 2016 Dec;14(1).

360. Cheruvanky A, Zhou H, Pisitkun T, Kopp JB, Knepper MA, Yuen PST, et al. Rapid isolation of urinary exosomal biomarkers using a nanomembrane ultrafiltration concentrator. Am J Physiology-Renal Physiol. 2007 May;292(5):F1657–61.

361. Xu R, Greening DW, Zhu H-J, Takahashi N, Simpson RJ. Extracellular vesicle isolation and characterization: toward clinical application. J Clin Investig. 2016 Apr 1;126(4):1152–62.

362. Shu SL, Yang Y, Allen CL, Hurley E, Tung KH, Minderman H, et al. Purity and yield of melanoma exosomes are dependent on isolation method. J Extracell Vesicles. 2020 Jan 1;9(1):1692401.

363. Nordin JZ, Lee Y, Vader P, Mäger I, Johansson HJ, Heusermann W, et al. Ultrafiltration with size-exclusion liquid chromatography for high yield isolation of extracellular vesicles preserving intact biophysical and functional properties. Nanomed Nanotech Biol Med. 2015 May;11(4):879–83.

364. Mol EA, Goumans M-J, Doevendans PA, Sluijter JPG, Vader P. Higher functionality of extracellular vesicles isolated using size-exclusion chromatography compared to ultracentrifugation. Nanomedicine: Nanomed Nanotech Biol Med 2017 Aug;13(6):2061–5.

365. Salih M, Zietse R, Hoorn EJ. Urinary extracellular vesicles and the kidney: biomarkers and beyond. Am J Physiology-Renal Physiol. 2014 Jun 1;306(11):F1251–9.

366. Heath N, Grant L, De Oliveira TM, Rowlinson R, Osteikoetxea X, Dekker N, et al. Rapid isolation and enrichment of extracellular vesicle preparations using anion exchange chromatography. Sci Rep. 2018 Dec;8(1).

367. Busatto S, Vilanilam G, Ticer T, Lin W-L, Dickson D, Shapiro S, et al. Tangential Flow Filtration for Highly Efficient Concentration of Extracellular Vesicles from Large Volumes of Fluid. Cells. 2018 Dec 16;7(12):273.

368. García-Romero N, Madurga R, Rackov G, Palacín-Aliana I, Núñez-Torres R, Asensi-Puig A, et al. Polyethylene glycol improves current methods for circulating extracellular vesicle-derived DNA isolation. J Translat Med. 2019 Dec;17(1).

369. Ludwig A-K, De Miroschedji K, Doeppner TR, Börger V, Ruesing J, Rebmann V, et al. Precipitation with polyethylene glycol followed by washing and pelleting by ultracentrifugation enriches extracellular vesicles from tissue culture supernatants in small and large scales. J Extracell Vesicles. 2018 Dec;7(1):1528109.

370. Rider MA, Hurwitz SN, Meckes DG. ExtraPEG: A Polyethylene Glycol-Based Method for Enrichment of Extracellular Vesicles. Sci Rep. 2016 Apr 12;6:23978.

371. Gámez-Valero A, Monguió-Tortajada M, Carreras-Planella L, Franquesa M, Beyer K, Borràs FE. Size-Exclusion Chromatography-based isolation minimally alters Extracellular Vesicles' characteristics compared to precipitating agents. Sci Rep. 2016 Dec;6(1).

372. Bronson DL, Elliott AY, Ritzi D. Concentration of Rous sarcoma virus from tissue culture fluids with polyethylene glycol. Appl Microbiol. 1975 Sep;30(3):464–71.

373. Gallart-Palau X, Serra A, Wong ASW, Sandin S, Lai MKP, Chen CP, et al. Extracellular vesicles are rapidly purified from human plasma by PRotein Organic Solvent PRecipitation (PROSPR). Sci Rep. 2015 Sep 30;5:14664.

374. Deregibus MC, Figliolini F, D'antico S, Manzini PM, Pasquino C, De Lena M, et al. Charge-based precipitation of extracellular vesicles. Int K Mol Med. 2016 Nov;38(5):1359–66.

375. Klymiuk MC, Balz N, Elashry MI, Heimann M, Wenisch S, Arnhold S. Exosomes isolation and identification from equine mesenchymal stem cells. BMC Vet Res. 2019 Dec;15(1).

376. Brownlee Z, Lynn KD, Thorpe PE, Schroit AJ. A novel "salting-out" procedure for the isolation of tumor-derived exosomes. J Immunol Methods. 2014 May;407:120–6.

377. Kotmakçı M, Akbaba GE. Exosome Isolation: Is There an Optimal Method with Regard to Diagnosis or Treatment? Novel Implications of Exosomes in Diagnosis and Treatment of Cancer and Infectious Diseases. InTech; 2017.

378. Sáenz-Cuesta M. Methods for extracellular vesicles isolation in a hospital setting. Front Immunol. 2015;6.

379. Carnino JM, Lee H, Jin Y. Isolation and characterization of extracellular vesicles from Broncho-alveolar lavage fluid: a review and comparison of different methods. Respir Res. 2019 Dec;20(1).

380. Davies RT, Kim J, Jang SC, Choi E-J, Gho YS, Park J. Microfluidic filtration system to isolate extracellular vesicles from blood. Lab on a Chip. 2012;12(24):5202.

381. Oksvold MP, Neurauter A, Pedersen KW. Magnetic Bead-Based Isolation of Exosomes. RNA Interference. New York, NY: Springer New York; 2015. p. 465–81. (Methods in Molecular Biology; vol. 1218).

382. Pedersen KW, Kierulf B, Neurauter A. Specific and Generic Isolation of Extracellular Vesicles with Magnetic Beads. Extracellular Vesicles. New York, NY: Springer New York; 2017. p. 65–87. (Methods in Molecular Biology; vol. 1660).

383. Wu M, Ouyang Y, Wang Z, Zhang R, Huang P-H, Chen C, et al. Isolation of exosomes from whole blood by integrating acoustics and microfluidics. Proc Natl Acad Sci. 2017 Oct 3;114(40):10584–9.

384. Batrakova EV, Kim MS. Using exosomes, naturally-equipped nanocarriers, for drug delivery. J Controll Release. 2015 Dec;219:396–405.

385. Lee K, Shao H, Weissleder R, Lee H. Acoustic Purification of Extracellular Microvesicles. ACS Nano. 2015 Mar 24;9(3):2321–7.

386. Vaidyanathan R, Naghibosadat M, Rauf S, Korbie D, Carrascosa LG, Shiddiky MJA, et al. Detecting Exosomes Specifically: A Multiplexed Device Based on Alternating Current Electrohydrodynamic Induced *Nanoshearing*. Anal Chem. 2014 Nov 18;86(22):11125–32.

387. Cho S, Jo W, Heo Y, Kang JY, Kwak R, Park J. Isolation of extracellular vesicle from blood plasma using electrophoretic migration through porous membrane. Sensors and Actuators B: Chemical. 2016 Oct;233:289–97.

388. Kulasinghe A, Wu H, Punyadeera C, Warkiani M. The Use of Microfluidic Technology for Cancer Applications and Liquid Biopsy. Micromachines. 2018 Aug 10;9(8):397.

389. Jia Y, Ni Z, Sun H, Wang C. Microfluidic Approaches Toward the Isolation and Detection of Exosome Nanovesicles. IEEE Access. 2019;7:45080–98.

390. Ramirez MI, Amorim MG, Gadelha C, Milic I, Welsh JA, Freitas VM, et al. Technical challenges of working with extracellular vesicles. Nanoscale. 2018;10(3):881–906.

391. Paolini L, Zendrini A, Noto GD, Busatto S, Lottini E, Radeghieri A, et al. Residual matrix from different separation techniques impacts exosome biological activity. Sci Rep. 2016 Sep;6(1).

392. Babick F. Dynamic light scattering (DLS). Characterization of Nanoparticles. Elsevier; 2020. p. 137–72.

393. Wooff Y, Cioanca AV, Chu-Tan JA, Aggio-Bruce R, Schumann U, Natoli R. Small-Medium Extracellular Vesicles and Their miRNA Cargo in Retinal Health and Degeneration: Mediators of Homeostasis, and Vehicles for Targeted Gene Therapy. Front Cell Neurosci. 2020 Jun 25;14:160.

394. Stetefeld J, McKenna SA, Patel TR. Dynamic light scattering: a practical guide and applications in biomedical sciences. Biophys Rev. 2016 Dec;8(4):409–27.

395. Franke D, Harris DK, Xie L, Jensen KF, Bawendi MG. The Unexpected Influence of Precursor Conversion Rate in the Synthesis of III-V Quantum Dots. Angew Chem Int Ed Engl. 2015 Nov 23;54(48):14299–303.

396. Szatanek R, Baj-Krzyworzeka M, Zimoch J, Lekka M, Siedlar M, Baran J. The Methods of Choice for Extracellular Vesicles (EVs) Characterization. Int J Mol Sci. 2017 May 29;18(6):1153.

397. Hoo CM, Starostin N, West P, Mecartney ML. A comparison of atomic force microscopy (AFM) and dynamic light scattering (DLS) methods to characterize nanoparticle size distributions. J Nanoparticle Res. 2008 Dec;10(S1):89–96.

398. Bryant G, Abeynayake C, Thomas JC. Improved Particle Size Distribution Measurements Using Multiangle Dynamic Light Scattering. 2. Refinements and Applications. Langmuir. 1996 Jan;12(26):6224–8.

399. Gercel-Taylor C, Atay S, Tullis RH, Kesimer M, Taylor DD. Nanoparticle analysis of circulating cell-derived vesicles in ovarian cancer patients. Anal Biochem. 2012 Sep;428(1):44–53.

400. Lawrie AS, Albanyan A, Cardigan RA, Mackie IJ, Harrison P. Microparticle sizing by dynamic light scattering in fresh-frozen plasma. Vox Sanguinis. 2009 Apr;96(3):206–12.

401. Chiang C, Chen C. Toward characterizing extracellular vesicles at a single-particle level. J Biomed Sci. 2019 Dec;26(1).

402. Vestad B, Llorente A, Neurauter A, Phuyal S, Kierulf B, Kierulf P, et al. Size and concentration analyses of extracellular vesicles by nanoparticle tracking analysis: a variation study. J Extracell Vesicles. 2017 Dec;6(1):1344087.

403. Soo CY, Song Y, Zheng Y, Campbell EC, Riches AC, Gunn-Moore F, et al. Nanoparticle tracking analysis monitors microvesicle and exosome secretion from immune cells: Nanoparticle tracking analysis of microvesicles and exosomes. Immunology. 2012 Jun;136(2):192–7.

404. Gardiner C, Shaw M, Hole P, Smith J, Tannetta D, Redman CW, et al. Measurement of refractive index by nanoparticle tracking analysis reveals heterogeneity in extracellular vesicles. J Extracell Vesicles. 2014;3:25361.

405. van der Pol E, Coumans FAW, Sturk A, Nieuwland R, van Leeuwen TG. Refractive Index Determination of Nanoparticles in Suspension Using Nanoparticle Tracking Analysis. Nano Lett. 2014 Nov 12;14(11):6195–201.

406. Gardiner C, Ferreira YJ, Dragovic RA, Redman CWG, Sargent IL. Extracellular vesicle sizing and enumeration by nanoparticle tracking analysis. J Extracell Vesicles. 2013 Jan;2(1):19671.

407. Parsons MEM, McParland D, Szklanna PB, Guang MHZ, O'Connell K, O'Connor HD, et al. A Protocol for Improved Precision and Increased Confidence in Nanoparticle Tracking Analysis Concentration Measurements between 50 and 120 nm in Biological Fluids. Front Cardiovasc Med. 2017 Nov 3;4.

408. Maas SLN, Broekman MLD, de Vrij J. Tunable Resistive Pulse Sensing for the Characterization of Extracellular Vesicles. Exosomes and Microvesicles. New York, NY: Springer New York; 2017. p. 21–33. (Methods in Molecular Biology; vol. 1545).

409. Vogel R, Coumans FAW, Maltesen RG, Böing AN, Bonnington KE, Broekman ML, et al. A standardized method to determine the concentration of extracellular vesicles using tunable resistive pulse sensing. J Extracell Vesicles. 2016 Jan;5(1):31242.

410. Lerner N, Avissar S, Beit-Yannai E. Extracellular vesicles mediate signaling between the aqueous humor producing and draining cells in the ocular system. Katoh M, editor. PLoS ONE. 2017 Feb 27;12(2):e0171153.

411. Willmott GR, Platt M, Lee GU. Resistive pulse sensing of magnetic beads and supraparticle structures using tunable pores. Biomicrofluidics. 2012 Mar;6(1):014103.

412. Chen O, Zhao J, Chauhan VP, Cui J, Wong C, Harris DK, et al. Compact high-quality CdSe-CdS core-shell nanocrystals with narrow emission linewidths and suppressed blinking. Nat Mater. 2013 May;12(5):445–51.

413. Heijnen HF, Schiel AE, Fijnheer R, Geuze HJ, Sixma JJ. Activated platelets release two types of membrane vesicles: microvesicles by surface shedding and exosomes derived from exocytosis of multivesicular bodies and alpha-granules. Blood. 1999 Dec 1;94(11):3791–9.

414. Brisson AR, Tan S, Linares R, Gounou C, Arraud N. Extracellular vesicles from activated platelets: a semiquantitative cryo-electron microscopy and immuno-gold labeling study. Platelets. 2017 Apr 3;28(3):263–71.

415. Jung MK, Mun JY. Sample Preparation and Imaging of Exosomes by Transmission Electron Microscopy. J Visual Exp. 2018 Jan 4;(131).

416. Cizmar P, Yuana Y. Detection and Characterization of Extracellular Vesicles by Transmission and Cryo-Transmission Electron Microscopy. Extracellular Vesicles. New York, NY: Springer New York; 2017. p. 221–32.

417. Dobhal G, Datta A, Ayupova D, Teesdale-Spittle P, Goreham RV. Isolation, characterisation and detection of breath-derived extracellular vesicles. Sci Rep. 2020 Dec;10(1):17381.

418. Piffoux M, Ahmad N, Nelayah J, Wilhelm C, Silva A, Gazeau F, et al. Monitoring the dynamics of cell-derived extracellular vesicles at the nanoscale by liquid-cell transmission electron microscopy. Nanoscale. 2018;10(3):1234–44.

419. Yuana Y, Koning RI, Kuil ME, Rensen PCN, Koster AJ, Bertina RM, et al. Cryo-electron microscopy of extracellular vesicles in fresh plasma. J Extracell Vesicles. 2013 Jan;2(1):21494.

420. Choi H, Mun JY. Structural Analysis of Exosomes Using Different Types of Electron Microscopy. Appl Microsc. 2017 Sep 30;47(3):171–5.

421. Agarwal K, Saji M, Lazaroff SM, Palmer AF, Ringel MD, Paulaitis ME. Analysis of Exosome Release as a Cellular Response to MAPK Pathway Inhibition. Langmuir. 2015 May 19;31(19):5440–8.

422. Höög JL, Lötvall J. Diversity of extracellular vesicles in human ejaculates revealed by cryo-electron microscopy. J Extracell Vesicles. 2015 Jan 1;4(1):28680.

423. Issman L, Brenner B, Talmon Y, Aharon A. Cryogenic transmission electron microscopy nanostructural study of shed microparticles. PLoS ONE. 2013;8(12):e83680.

424. Chernyshev VS, Rachamadugu R, Tseng YH, Belnap DM, Jia Y, Branch KJ, et al. Size and shape characterization of hydrated and desiccated exosomes. Anal Bioanal Chem. 2015 May;407(12):3285–301.

425. Rikkert LG, Nieuwland R, Terstappen LWMM, Coumans FAW. Quality of extracellular vesicle images by transmission electron microscopy is operator and protocol dependent. J Extracell Vesicles. 2019 Dec 1;8(1):1555419.

426. Bidarimath M, Khalaj K, Kridli RT, Kan FWK, Koti M, Tayade C. Extracellular vesicle mediated intercellular communication at the porcine maternal-fetal interface: A new paradigm for conceptus-endometrial cross-talk. Sci Rep. 2017 Mar;7(1).

427. Arraud N, Linares R, Tan S, Gounou C, Pasquet J-M, Mornet S, et al. Extracellular vesicles from blood plasma: determination of their morphology, size, phenotype and concentration. J Thromb Haemost. 2014 May;12(5):614–27.

428. Hardij J, Cecchet F, Berquand A, Gheldof D, Chatelain C, Mullier F, et al. Characterisation of tissue factor-bearing extracellular vesicles with AFM: comparison of air-tapping-mode AFM and liquid Peak Force AFM. J Extracell Vesicles. 2013 Jan;2(1):21045.

429. Parisse P, Rago I, Ulloa Severino L, Perissinotto F, Ambrosetti E, Paoletti P, et al. Atomic force microscopy analysis of extracellular vesicles. Eur Biophys J. 2017 Dec;46(8):813–20.

430. Hoshino A, Costa-Silva B, Shen T-L, Rodrigues G, Hashimoto A, Tesic Mark M, et al. Tumour exosome integrins determine organotropic metastasis. Nature. 2015 Nov;527(7578):329–35.

431. Ohno S, Takanashi M, Sudo K, Ueda S, Ishikawa A, Matsuyama N, et al. Systemically Injected Exosomes Targeted to EGFR Deliver Antitumor MicroRNA to Breast Cancer Cells. Molecular Therapy. 2013 Jan;21(1):185–91.

432. Smyth T, Kullberg M, Malik N, Smith-Jones P, Graner MW, Anchordoquy TJ. Biodistribution and delivery efficiency of unmodified tumor-derived exosomes. J Controll Rel. 2015 Feb;199:145–55.

433. Roberts-Dalton HD, Cocks A, Falcon-Perez JM, Sayers EJ, Webber JP, Watson P, et al. Fluorescence labelling of extracellular vesicles using a novel thiol-based strategy for quantitative analysis of cellular delivery and intracellular traffic. Nanoscale. 2017;9(36):13693–706.

434. Thane KE, Davis AM, Hoffman AM. Improved methods for fluorescent labeling and detection of single extracellular vesicles using nanoparticle tracking analysis. Sci Rep. 2019 Dec;9(1).

435. Gramatikov BI. Modern technologies for retinal scanning and imaging: an introduction for the biomedical engineer. Biomed Eng Online. 2014 Apr 29;13:52.

436. Tumne A, Prasad VS, Chen Y, Stolz DB, Saha K, Ratner DM, et al. Noncytotoxic Suppression of Human Immunodeficiency Virus Type 1 Transcription by Exosomes Secreted from CD8 $^{+}$ T Cells. J Virol. 2009 May;83(9):4354–64.

437. Gangadaran P, Li XJ, Lee HW, Oh JM, Kalimuthu S, Rajendran RL, et al. A new bioluminescent reporter system to study the biodistribution of systematically injected tumor-derived bioluminescent extracellular vesicles in mice. Oncotarget. 2017 Dec 15;8(66):109894–914.

438. Ward M, Turner P, DeJohn M, Kaduchak G. Fundamentals of Acoustic Cytometry. Curr Prot Cytometry. 2009 Jul;49(1):1.22.1-1.22.12.

439. Panagopoulou MS, Wark AW, Birch DJS, Gregory CD. Phenotypic analysis of extracellular vesicles: a review on the applications of fluorescence. J Extracell Vesicles. 2020 Jan 1;9(1):1710020.

440. Lacroix R, Robert S, Poncelet P, Kasthuri RS, Key NS, Dignat-George F, et al. Standardization of platelet-derived microparticle enumeration by flow cytometry with calibrated beads: results of the International Society on Thrombosis and Haemostasis SSC Collaborative workshop: Standardization of platelet-derived microparticle enumeration by flow cytometry. J Thromb Haemost. 2010 Nov;8(11):2571–4.

441. Orozco AF, Lewis DE. Flow cytometric analysis of circulating microparticles in plasma. Cytometry Part A. 2010 Mar 16;77A(6):502–14.

442. Freyssinet J-M, Toti F. Membrane microparticle determination: at least seeing what's being size. J Thromb Haem. 2010 Feb;8(2):311–4.

443. Dragovic RA, Southcombe JH, Tannetta DS, Redman CWG, Sargent IL. Multicolor Flow Cytometry and Nanoparticle Tracking Analysis of Extracellular Vesicles in the Plasma of Normal Pregnant and Pre-eclamptic Women1. Biol Reprod. 2013 Dec 1;89(6).

444. Chandler WL, Yeung W, Tait JF. A new microparticle size calibration standard for use in measuring smaller microparticles using a new flow cytometer: Size calibration and microparticles. J Throm Haemost 2011 Jun;9(6):1216–24.

445. Pužar Dominkuš P, Stenovec M, Sitar S, Lasič E, Zorec R, Plemenitaš A, et al. PKH26 labeling of extracellular vesicles: Characterization and cellular internalization of contaminating PKH26 nanoparticles. Biochim Biophys Acta (BBA) - Biomembr. 2018 Jun;1860(6):1350–61.

446. Lai CP, Kim EY, Badr CE, Weissleder R, Mempel TR, Tannous BA, et al. Visualization and tracking of tumour extracellular vesicle delivery and RNA translation using multiplexed reporters. Nat Communic. 2015 Nov;6(1).

447. Erdbrügger U, Rudy CK, E. Etter M, Dryden KA, Yeager M, Klibanov AL, et al. Imaging flow cytometry elucidates limitations of microparticle analysis by conventional flow cytometry: Microparticle Detection by Imaging Flow Cytometry. Cytometry Part A. 2014 Sep;85(9):756–70.

448. Görgens A, Bremer M, Ferrer-Tur R, Murke F, Tertel T, Horn PA, et al. Optimisation of imaging flow cytometry for the analysis of single extracellular vesicles by using fluorescence-tagged vesicles as biological reference material. J Extracell Vesicles. 2019 Dec 1;8(1):1587567.

449. van der Pol E, Coumans FAW, Grootemaat AE, Gardiner C, Sargent IL, Harrison P, et al. Particle size distribution of exosomes and microvesicles determined by transmission electron microscopy, flow cytometry, nanoparticle tracking analysis, and resistive pulse sensing. J Throm Haemost. 2014 Jul;12(7):1182–92.

450. Varga Z, van der Pol E, Pálmai M, Garcia-Diez R, Gollwitzer C, Krumrey M, et al. Hollow organosilica beads as reference particles for optical detection of extracellular vesicles. J Throm Haemost. 2018 Aug;16(8):1646–55.

451. Lin H-Y, Yang KS, Curley C, Lee H, Welch MW, Wolpin BM, et al. Bead Enhancement of EV Analysis. Cancer Biol; 2018 Feb.

452. van der Vlist EJ, Nolte-'t Hoen ENM, Stoorvogel W, Arkesteijn GJA, Wauben MHM. Fluorescent labeling of nano-sized vesicles released by cells and subsequent quantitative and qualitative analysis by high-resolution flow cytometry. Nat Prot. 2012 Jul;7(7):1311–26.

453. Suárez H, Gámez-Valero A, Reyes R, López-Martín S, Rodríguez MJ, Carrascosa JL, et al. A bead-assisted flow cytometry method for the semi-quantitative analysis of Extracellular Vesicles. Sci Rep. 2017 Dec;7(1).

454. Popovic M, Mazzega E, Toffoletto B, de Marco A. Isolation of anti-extra-cellular vesicle single-domain antibodies by direct panning on vesicle-enriched fractions. Microb Cell Fact. 2018 Dec;17(1):6.

455. Coulter, Wallace H. Means for cou ting particles suspended in a fluid. US2656508, 1953.

456. Théry C, Ostrowski M, Segura E. Membrane vesicles as conveyors of immune responses. Nat Rev Immunol. 2009 Aug;9(8):581–93.

457. Jeong D-E, Lee Y, Lee S-JV. Western Blot Analysis of C. elegans Proteins. In: Huang LE, editor. Hypoxia. New York, NY: Springer New York; 2018. p. 213–25. (Methods in Molecular Biology; vol. 1742).

458. Grebe SK, Singh RJ. LC-MS/MS in the Clinical Laboratory - Where to From Here? Clin Biochem Rev. 2011 Feb;32(1):5–31.

459. Ma B. Challenges in Computational Analysis of Mass Spectrometry Data for Proteomics. J Comput Sci Technol. 2010 Jan;25(1):107–23.

460. Böttger F, Schaaij-Visser TB, de Reus I, Piersma SR, Pham TV, Nagel R, et al. Proteome analysis of non-small cell lung cancer cell line secretomes and patient sputum reveals biofluid biomarker candidates for cisplatin response prediction. J Proteom. 2019 Mar;196:106–19.

461. Liu J, Lu Y. Preparation of aptamer-linked gold nanoparticle purple aggregates for colorimetric sensing of analytes. Nat Prot. 2006 Jun;1(1):246–52.

462. Lim J, Choi M, Lee H, Kim Y-H, Han J-Y, Lee ES, et al. Direct isolation and characterization of circulating exosomes from biological samples using magnetic nanowires. J Nanobiotechnology. 2019 Jan 7;17(1):1.

463. Val S, Jeong S, Poley M, Krueger A, Nino G, Brown K, et al. Purification and characterization of microRNAs within middle ear fluid exosomes: implication in otitis media pathophysiology. Pediatric Res. 2017 Jun;81(6):911–8.

464. Kwist K, Bridges WC, Burg KJL. The effect of cell passage number on osteogenic and adipogenic characteristics of D1 cells. Cytotechnology. 2016 Aug;68(4):1661–7.

465. Callot G, Maurette M, Pottier L, Dubois A. Biogenic etching of microfractures in amorphous and crystalline silicates. Nature. 1987 Jul;328(6126):147–9.

466. Du X, He J. Spherical silica micro/nanomaterials with hierarchical structures: Synthesis and applications. Nanoscale. 2011;3(10):3984.

467. Kowal J, Arras G, Colombo M, Jouve M, Morath JP, Primdal-Bengtson B, et al. Proteomic comparison defines novel markers to characterize heterogeneous populations of extracellular vesicle subtypes. Proc Natl Acad Sci USA. 2016 Feb 23;113(8):E968-977.

468. Abramowicz A, Widlak P, Pietrowska M. Proteomic analysis of exosomal cargo: the challenge of high purity vesicle isolation. Mol Biosyst. 2016 26;12(5):1407–19.

469. Cvjetkovic A, Lötvall J, Lässer C. The influence of rotor type and centrifugation time on the yield and purity of extracellular vesicles. J Extracell Vesicles. 2014 Jan;3(1):23111.

470. Taylor DD, Zacharias W, Gercel-Taylor C. Exosome Isolation for Proteomic Analyses and RNA Profiling. Serum/Plasma Proteomics. Totowa, NJ: Humana Press; 2011. p. 235–46.

471. Ren K. Exosomes in perspective: a potential surrogate for stem cell therapy. Odontology. 2019 Jul;107(3):271–84.

472. Wen SW, Lima LG, Lobb RJ, Norris EL, Hastie ML, Krumeich S, et al. Breast Cancer-Derived Exosomes Reflect the Cell-of-Origin Phenotype. Proteomics. 2019 Apr;19(8):1800180.

473. Brlansky RH. Detection of Seedborne Plant Viruses Using Serologically Specific Electron Microscopy. Phytopathology. 1979;69(1):96.

474. O'Farrell PH. High resolution two-dimensional electrophoresis of proteins. J Biol Chem. 1975 May 25;250(10):4007–21.

475. Wilkins MR, Gasteiger E, Sanchez J-C, Bairoch A, Hochstrasser DF. Two-dimensional gel electrophoresis for proteome projects: The effects of protein hydrophobicity and copy number. Electrophoresis. 1998 Jun;19(8–9):1501–5.

476. Görg A, Postel W, Domscheit A, Günther S. Two-dimensional electrophoresis with immobilized pH gradients of leaf proteins from barley (Hordeum vulgare): Method, reproducibility and genetic aspects. Electrophoresis. 1988;9(11):681–92.

477. Edman P. A method for the determination of amino acid sequence in peptides. Arch Biochem. 1949 Jul;22(3):475.

478. Aebersold RH, Teplow DB, Hood LE, Kent SB. Electroblotting onto activated glass. High efficiency preparation of proteins from analytical sodium dodecyl sulfate-polyacrylamide gels for direct sequence analysis. J Biol Chem. 1986 Mar 25;261(9):4229–38.

479. Aebersold RH, Leavitt J, Saavedra RA, Hood LE, Kent SB. Internal amino acid sequence analysis of proteins separated by one- or two-dimensional gel electrophoresis after in situ protease digestion on nitrocellulose. Proc Natl Acad Sci. 1987 Oct 1;84(20):6970–4.

480. Aebersold RH, Pipes G, Hood LE, Kent SBH. N-terminal and internal sequence determination of microgram amounts of proteins separated by isoelectric focusing in immobilized pH gradients. Electrophoresis. 1988;9(9):520–30.

481. Swinbanks D. Australia backs innovation, shuns telescope. Nature. 1995 Dec;378(6558):653–653.

482. Yee A, Pardee K, Christendat D, Savchenko A, Edwards AM, Arrowsmith CH. Structural Proteomics: Toward High-Throughput Structural Biology as a Tool in Functional Genomics. Acc Chem Res. 2003 Mar;36(3):183–9.

483. Graves PR, Haystead TAJ. Molecular biologist's guide to proteomics. Microbiol Mol Biol Rev. 2002 Mar;66(1):39–63.

484. The UniProt Consortium. UniProt: a worldwide hub of protein knowledge. Nucleic Acids Research. 2019 Jan 8;47(D1):D506–15.

485. Yu L-R, Stewart NA, Veenstra TD. Proteomics. Essentials of Genomic and Personalized Medicine. Elsevier; 2010. p. 89–96.

486. Aebersold R, Mann M. Mass spectrometry-based proteomics. Nature. 2003 Mar;422(6928):198–207.

487. Jiang H, English AM. Quantitative Analysis of the Yeast Proteome by Incorporation of Isotopically Labeled Leucine. J Proteome Res. 2002 Aug;1(4):345–50.

488. Zhu H, Pan S, Gu S, Bradbury EM, Chen X. Amino acid residue specific stable isotope labeling for quantitative proteomics. Rapid Communic Mass Spectr. 2002 Nov 30;16(22):2115–23.

489. Ong S-E, Blagoev B, Kratchmarova I, Kristensen DB, Steen H, Pandey A, et al. Stable Isotope Labeling by Amino Acids in Cell Culture, SILAC, as a Simple and Accurate Approach to Expression Proteomics. Mol Cell Proteom. 2002 May;1(5):376–86.

490. Ong S-E, Mann M. A practical recipe for stable isotope labeling by amino acids in cell culture (SILAC). Nat Protoc. 2006 Dec;1(6):2650–60.

491. Gregorich ZR, Chang Y-H, Ge Y. Proteomics in heart failure: top-down or bottom-up? Pflugers Arch. 2014 Jun;466(6):1199–209.

492. Ong S-E, Mann M. Mass spectrometry–based proteomics turns quantitative. Nat Chem Biol. 2005 Oct;1(5):252–62.

493. Bantscheff M, Schirle M, Sweetman G, Rick J, Kuster B. Quantitative mass spectrometry in proteomics: a critical review. Anal Bioanal Chem. 2007 Sep 25;389(4):1017–31.

494. Wiese S, Reidegeld KA, Meyer HE, Warscheid B. Protein labeling by iTRAQ: A new tool for quantitative mass spectrometry in proteome research. Proteomics. 2007 Feb;7(3):340–50.

495. Bąchor R, Waliczek M, Stefanowicz P, Szewczuk Z. Trends in the Design of New Isobaric Labeling Reagents for Quantitative Proteomics. Molecules. 2019 Feb 15;24(4):701.

496. Wang Z, Yu K, Tan H, Wu Z, Cho J-H, Han X, et al. 27-Plex Tandem Mass Tag Mass Spectrometry for Profiling Brain Proteome in Alzheimer's Disease. Anal Chem. 2020 May 19;92(10):7162–70.

497. Jing C, Cornish VW. Chemical tags for labeling proteins inside living cells. Acc Chem Res. 2011 Sep 20;44(9):784–92.

498. Higgs RE, Knierman MD, Gelfanova V, Butler JP, Hale JE. Label-Free LC-MS Method for the Identification of Biomarkers. Clinical Proteomics Totowa, NJ: Humana Press; 2008. p. 209–30. (Methods in Molecular Biology; vol. 428).

499. Pan J, Chen H-Q, Sun Y-H, Zhang J-H, Luo X-Y. Comparative Proteomic Analysis of Non-small-cell Lung Cancer and Normal Controls Using Serum Label-Free Quantitative Shotgun Technology. Lung. 2008 Aug;186(4):255–61.

500. Lobb RJ, Hastie ML, Norris EL, van Amerongen R, Gorman JJ, Möller A. Oncogenic transformation of lung cells results in distinct exosome protein profile similar to the cell of origin. Proteomics. 2017 Dec;17(23–24):1600432.

501. Li P, Kaslan M, Lee SH, Yao J, Gao Z. Progress in Exosome Isolation Techniques. Theranostics. 2017;7(3):789–804.

502. Nilsson J, Skog J, Nordstrand A, Baranov V, Mincheva-Nilsson L, Breakefield XO, et al. Prostate cancer-derived urine exosomes: a novel approach to biomarkers for prostate cancer. Br J Cancer. 2009 May 19;100(10):1603–7.

503. Chen C-L, Lai Y-F, Tang P, Chien K-Y, Yu J-S, Tsai C-H, et al. Comparative and targeted proteomic analyses of urinary microparticles from bladder cancer and hernia patients. J Proteome Res. 2012 Dec 7;11(12):5611–29.

504. Mathivanan S, Lim JWE, Tauro BJ, Ji H, Moritz RL, Simpson RJ. Proteomics Analysis of A33 Immunoaffinity-purified Exosomes Released from the Human Colon Tumor Cell Line LIM1215 Reveals a Tissue-specific Protein Signature. Mol Cell Proteom. 2010 Feb;9(2):197–208.

505. Kalra H, Simpson RJ, Ji H, Aikawa E, Altevogt P, Askenase P, et al. Vesiclepedia: A Compendium for Extracellular Vesicles with Continuous Community Annotation. PLoS Biology. 2012 Dec 18;10(12):e1001450.

506. Choi D-S, Kim D-K, Kim Y-K, Gho YS. Proteomics of extracellular vesicles: Exosomes and ectosomes: Proteomics of extracellular vesicles. Mass Spectr Rev. 2015 Jul;34(4):474–90.

507. Gonzales PA, Pisitkun T, Hoffert JD, Tchapyjnikov D, Star RA, Kleta R, et al. Large-Scale Proteomics and Phosphoproteomics of Urinary Exosomes. J Am Society Nephrology. 2009 Feb;20(2):363–79.

508. Koller A, Patel P, Kim JK, Chen EI. Proteomics Analysis of Circulating Serum Exosomes. Methods Mol Biol. 2017;1619:213–25.

509. Yang C, Guo W -b., Zhang W -s., Bian J, Yang J -k., Zhou Q -z., et al. Comprehensive proteomics analysis of exosomes derived from human seminal plasma. Andrology. 2017 Sep;5(5):1007–15.

510. Welton JL, Khanna S, Giles PJ, Brennan P, Brewis IA, Staffurth J, et al. Proteomics Analysis of Bladder Cancer Exosomes. Mol Cell Proteom. 2010 Jun;9(6):1324–38.

511. Chemonges S, Gupta R, Mills PC, Kopp SR, Sadowski P. Characterisation of the circulating acellular proteome of healthy sheep using LC-MS/MS-based proteomics analysis of serum. Proteome Sci. 2016 Dec;15(1):11.

512. Yeung Y-G, Stanley ER. Rapid detergent removal from peptide samples with ethyl acetate for mass spectrometry analysis. Curr Protoc Protein Sci. 2010 Feb;Chapter 16:Unit 16.12.

513. Hulsen T, de Vlieg J, Alkema W. BioVenn – a web application for the comparison and visualization of biological lists using area-proportional Venn diagrams. BMC Genomics. 2008;9(1):488.

514. Szklarczyk D, Gable AL, Nastou KC, Lyon D, Kirsch R, Pyysalo S, et al. The STRING database in 2021: customizable protein–protein networks, and functional characterization of user-uploaded gene/measurement sets. Nucleic Acids Res. 2021 Jan 8;49(D1):D605–12.

515. Ge SX, Jung D, Yao R. ShinyGO: a graphical gene-set enrichment tool for animals and plants. Valencia A, editor. Bioinformatics. 2020 Apr 15;36(8):2628–9.

516. Raudvere U, Kolberg L, Kuzmin I, Arak T, Adler P, Peterson H, et al. g:Profiler: a web server for functional enrichment analysis and conversions of gene lists (2019 update). Nucleic Acids Res. 2019 Jul 2;47(W1):W191–8.

517. Haynes W. Benjamini–Hochberg Method. Encyclopedia of Systems Biology. New York, NY: Springer New York; 2013. p. 78–78.

518. Lim JWE, Mathias RA, Kapp EA, Layton MJ, Faux MC, Burgess AW, et al. Restoration of full-length APC protein in SW480 colon cancer cells induces exosome-mediated secretion of DKK-4: Proteomics and 2DE. Electrophoresis. 2012 Jul;33(12):1873–80.

519. Zhang T, Li J, He Y, Yang F, Hao Y, Jin W, et al. A small molecule targeting myoferlin exerts promising anti-tumor effects on breast cancer. Nat Commun. 2018 Dec;9(1):3726.

520. Dong Y, Kang H, Liu H, Wang J, Guo Q, Song C, et al. Myoferlin, a Membrane Protein with Emerging Oncogenic Roles. BioMed Res Int. 2019 Nov 19;2019:1–9.

521. Ke A-W, Shi G-M, Zhou J, Wu F-Z, Ding Z-B, Hu M-Y, et al. Role of overexpression of CD151 and/or c-Met in predicting prognosis of hepatocellular carcinoma. Hepatology. 2009 Feb;49(2):491–503.

522. Kim JH, Badawi M, Park J-K, Jiang J, Mo X, Roberts LR, et al. Anti-invasion and anti-migration effects of miR-199a-3p in hepatocellular carcinoma are due in part to targeting CD151. Int J Oncol. 2016 Nov;49(5):2037–45.

523. Rademaker G, Costanza B, Bellier J, Herfs M, Peiffer R, Agirman F, et al. Human colon cancer cells highly express myoferlin to maintain a fit mitochondrial network and escape p53-driven apoptosis. Oncogenesis. 2019 Mar;8(3):21.

524. Tokuhara T, Hasegawa H, Hattori N, Ishida H, Taki T, Tachibana S, et al. Clinical significance of CD151 gene expression in non-small cell lung cancer. Clin Cancer Res. 2001 Dec;7(12):4109–14.

525. Sun Z, Wang L, Eckloff BW, Deng B, Wang Y, Wampfler JA, et al. Conserved recurrent gene mutations correlate with pathway deregulation and clinical outcomes of lung adenocarcinoma in never-smokers. BMC Med Genomics. 2014 Dec;7(1):486.

526. Song DH, Ko GH, Lee JH, Lee JS, Lee G-W, Kim HC, et al. Myoferlin expression in non-small cell lung cancer: Prognostic role and correlation with VEGFR-2 expression. Oncology Lett. 2016 Feb;11(2):998–1006.

527. Lazar I, Clement E, Ducoux-Petit M, Denat L, Soldan V, Dauvillier S, et al. Proteome characterization of melanoma exosomes reveals a specific signature for metastatic cell lines. Pigment Cell Melanoma Res. 2015 Jul;28(4):464–75.

528. Wang W-S, Liu X-H, Liu L-X, Lou W-H, Jin D-Y, Yang P-Y, et al. iTRAQ-based quantitative proteomics reveals myoferlin as a novel prognostic predictor in pancreatic adenocarcinoma. J Proteomics. 2013 Oct;91:453–65.

529. Liang B, Peng P, Chen S, Li L, Zhang M, Cao D, et al. Characterization and proteomic analysis of ovarian cancer-derived exosomes. J Proteomics. 2013 Mar;80:171–82.

530. Griner EM, Dancik GM, Costello JC, Owens C, Guin S, Edwards MG, et al. RhoC Is an Unexpected Target of RhoGDI2 in Prevention of Lung Colonization of Bladder Cancer. Mol Cancer Res. 2015 Mar;13(3):483–92.

531. Nuzhat Z, Kinhal V, Sharma S, Rice GE, Joshi V, Salomon C. Tumour-derived exosomes as a signature of pancreatic cancer - liquid biopsies as indicators of tumour progression. Oncotarget. 2017 Mar 7;8(10):17279–91.

532. van Golen KL, Wu ZF, Qiao XT, Bao LW, Merajver SD. RhoC GTPase, a novel transforming oncogene for human mammary epithelial cells that partially recapitulates the inflammatory breast cancer phenotype. Cancer Res. 2000 Oct 15;60(20):5832–8.

533. Kleer CG, van Golen KL, Zhang Y, Wu Z-F, Rubin MA, Merajver SD. Characterization of RhoC Expression in Benign and Malignant Breast Disease. Am J Pathol. 2002 Feb;160(2):579–84.

534. Kleer CG, Zhang Y, Pan Q, Gallagher G, Wu M, Wu Z-F, et al. WISP3 and RhoC guanosine triphosphatase cooperate in the development of inflammatory breast cancer. Breast Cancer Res. 2004;6(1):R110.

535. Kleer CG, Griffith KA, Sabel MS, Gallagher G, van Golen KL, Wu Z-F, et al. RhoC-GTPase is a Novel Tissue Biomarker Associated with Biologically Aggressive Carcinomas of the Breast. Breast Cancer Res Treat. 2005 Sep;93(2):101–10.

536. Lo A-C, Kleer CG, Banerjee M, Omar S, Khaled H, Eissa S, et al. Molecular epidemiologic features of inflammatory breast cancer: a comparison between Egyptian and US patients. Breast Cancer Res Treat. 2008 Nov;112(1):141–7.

537. Kharaziha P, Chioureas D, Rutishauser D, Baltatzis G, Lennartsson L, Fonseca P, et al. Molecular profiling of prostate cancer derived exosomes may reveal a predictive signature for response to docetaxel. Oncotarget. 2015 Aug 28;6(25):21740–54.

538. Zhou W, Zhang C, Jiang H, Zhang Z, Xie L, He X. MiR-493 suppresses the proliferation and invasion of gastric cancer cells by targeting RhoC. Iran J Basic Med Sci. 2015 Oct;18(10):1027–33.

539. Faried A, Faried LS, Kimura H, Nakajima M, Sohda M, Miyazaki T, et al. RhoA and RhoC proteins promote both cell proliferation and cell invasion of human oesophageal squamous cell carcinoma cell lines in vitro and in vivo. Eur J Cancer. 2006 Jul;42(10):1455–65.

540. Wellberg EA, Johnson S, Finlay-Schultz J, Lewis AS, Terrell KL, Sartorius CA, et al. The glucose transporter GLUT1 is required for ErbB2-induced mammary tumorigenesis. Breast Cancer Res. 2016 Dec;18(1):131.

541. Wang W. Expression and significance of RhoC gene in hepatocellular carcinoma. WJG. 2003;9(9):1950.

542. Santasusagna S, Moreno I, Navarro A, Muñoz C, Martinez F, Hernández R, et al. miR-328 mediates a metabolic shift in colon cancer cells by targeting SLC2A1/GLUT1. Clin Transl Oncol. 2018 Sep;20(9):1161–7.

543. Lu X, Guo H, Chen X, Xiao J, Zou Y, Wang W, et al. Effect of RhoC on the epithelial-mesenchymal transition process induced by TGF-β1 in lung adenocarcinoma cells. Oncol Rep. 2016 Nov;36(6):3105–12.

544. Wudu M, Ren H, Hui L, Jiang J, Zhang S, Xu Y, et al. DRAM2 acts as an oncogene in non-small cell lung cancer and suppresses the expression of p53. J Exp Clin Cancer Res. 2019 Dec;38(1):72.

545. Ding X, Liu J, Liu T, Ma Z, Wen D, Zhu J. miR-148b inhibits glycolysis in gastric cancer through targeting SLC2A1. Cancer Med. 2017 Jun;6(6):1301–10.

546. Yan S, Wang Y, Chen M, Li G, Fan J. Deregulated SLC2A1 Promotes Tumor Cell Proliferation and Metastasis in Gastric Cancer. IJMS. 2015 Jul 16;16(7):16144–57.

547. Horiuchi A, Imai T, Wang C, Ohira S, Feng Y, Nikaido T, et al. Up-Regulation of Small GTPases, RhoA and RhoC, Is Associated with Tumor Progression in Ovarian Carcinoma. Lab Invest. 2003 Jun;83(6):861–70.

548. Chung J-H, Lee WW, Park SY, Choe G, Sung SW, Chung J-K, et al. FDG uptake and glucose transporter type 1 expression in lymph nodes of non-small cell lung cancer. Eur J Surg Oncol (EJSO). 2006 Nov;32(9):989–95.

549. Koh YW, Lee SJ, Park SY. Differential expression and prognostic significance of GLUT1 according to histologic type of non-small-cell lung cancer and its association with volume-dependent parameters. Lung Cancer. 2017 Feb;104:31–7.

550. Kang DY, Lee HW, Choi PJ, Lee KE, Roh MS. Sodium/iodide symporter expression in primary lung cancer and comparison with glucose transporter 1 expression. Pathol Int. 2009 Feb;59(2):73–9.

551. Mogi A, Koga K, Aoki M, Hamasaki M, Uesugi N, Iwasaki A, et al. Expression and role of GLUT-1, MCT-1, and MCT-4 in malignant pleural mesothelioma. Virchows Arch. 2013 Jan;462(1):83–93.

552. Do SK, Jeong JY, Lee SY, Choi JE, Hong MJ, Kang H-G, et al. Glucose Transporter 1 Gene Variants Predict the Prognosis of Patients with Early-Stage Non-small Cell Lung Cancer. Ann Surg Oncol. 2018 Oct;25(11):3396–403.

553. Kusama T, Mukai M, Endo H, Ishikawa O, Tatsuta M, Nakamura H, et al. Inactivation of Rho GTPases by p190 RhoGAP reduces human pancreatic cancer cell invasion and metastasis. Cancer Sci. 2006 Sep;97(9):848–53.

554. Tan X, He S, Han Y, Yu Y, Xiao J, Xu D, et al. Establishment and characterization of clear cell renal cell carcinoma cell lines with different metastatic potential from Chinese patients. Cancer Cell Int. 2013;13(1):20.

555. Maldonado MDM, Dharmawardhane S. Targeting Rac and Cdc42 GTPases in Cancer. Cancer Res. 2018 Jun 15;78(12):3101–11.

556. Chapman AM, Sun KY, Ruestow P, Cowan DM, Madl AK. Lung cancer mutation profile of EGFR, ALK, and KRAS: Meta-analysis and comparison of never and ever smokers. Lung Cancer. 2016 Dec;102:122–34.

557. Wu H-Z, Xiao J-Q, Xiao S-S, Cheng Y. KRAS: A Promising Therapeutic Target for Cancer Treatment. CTMC. 2019 Nov 15;19(23):2081–97.

558. Whelan S, Ophir E, Kotturi MF, Levy O, Ganguly S, Leung L, et al. PVRIG and PVRL2 Are Induced in Cancer and Inhibit CD8+ T-cell Function. Cancer Immunol Res. 2019 Feb;7(2):257–68.

559. Kanehisa M. KEGG: Kyoto Encyclopedia of Genes and Genomes. Nucleic Acids Res. 2000 Jan 1;28(1):27–30.

560. Pedersen AML, Sørensen CE, Proctor GB, Carpenter GH, Ekström J. Salivary secretion in health and disease. J Oral Rehabil. 2018 Sep;45(9):730–46.

561. Huang H-J, Liu C-W, Xu H-J, Bao Y-Y, Zhang C-X. Mucin-like protein, a saliva component involved in brown planthopper virulence and host adaptation. J Insect Physiol. 2017 Apr;98:223–30.

562. Inzitari R, Cabras T, Rossetti DV, Fanali C, Vitali A, Pellegrini M, et al. Detection in human saliva of different statherin and P-B fragments and derivatives. Proteomics. 2006 Dec;6(23):6370–9.

563. Phuyal S, Farhan H. Multifaceted Rho GTPase Signaling at the Endomembranes. Front Cell Dev Biol. 2019 Jul 16;7:127.

564. Cho ES, Cha YH, Kim HS, Kim NH, Yook JI. The Pentose Phosphate Pathway as a Potential Target for Cancer Therapy. Biomolecules Ther. 2018 Jan 1;26(1):29–38.

565. Yi H, Zheng X, Song J, Shen R, Su Y, Lin D. Exosomes mediated pentose phosphate pathway in ovarian cancer metastasis: a proteomics analysis. Int J Clin Exp Pathol. 2015;8(12):15719–28.

566. Ludwig N, Yerneni SS, Menshikova EV, Gillespie DG, Jackson EK, Whiteside TL. Simultaneous Inhibition of Glycolysis and Oxidative Phosphorylation Triggers a Multi-Fold Increase in Secretion of Exosomes: Possible Role of 2′,3′-cAMP. Sci Rep. 2020 Dec;10(1):6948.

567. Göran Ronquist K. Extracellular vesicles and energy metabolism. Clinica Chimica Acta. 2019 Jan;488:116–21.

568. Andreu Z, Yanez-Mo M. Tetraspanins in Extracellular Vesicle Formation and Function. Front Immunol. 2014 Sep 16;5.

569. Zhu J. Regulation of cortactin/dynamin interaction by actin polymerization during the fission of clathrin-coated pits. J Cell Sci. 2005 Jan 25;118(4):807–17.

570. Daugherty KM, Goode BL. Functional Surfaces on the p35/ARPC2 Subunit of Arp2/3 Complex Required for Cell Growth, Actin Nucleation, and Endocytosis. J Biol Chem. 2008 Jun;283(24):16950–9.

571. Sinha S, Hoshino D, Hong NH, Kirkbride KC, Grega-Larson NE, Seiki M, et al. Cortactin promotes exosome secretion by controlling branched actin dynamics. J Cell Biol. 2016 Jul 18;214(2):197–213.

572. Pisitkun T, Shen R-F, Knepper MA. Identification and proteomic profiling of exosomes in human urine. Proc Natl Acad Sci. 2004 Sep 7;101(36):13368–73.

573. The UniProt Consortium, Bateman A, Martin M-J, Orchard S, Magrane M, Agivetova R, et al. UniProt: the universal protein knowledgebase in 2021. Nucleic Acids Res. 2021 Jan 8;49(D1):D480–9.

574. American Cancer Society. Lung Cancer Survival Rates.

575. Ge Y, Guo S, Liu T, Zhao C, Li D, Liu Y, et al. Optimizing a production strategy for a nonspecific nuclease from Yersinia enterocolitica subsp. palearctica in genetically engineered Escherichia coli. FEMS Microbiology Lett. 2019 Dec 1;366(24):fnz208.

576. Peach M, Marsh N, Miskiewicz EI, MacPhee DJ. Solubilization of Proteins: The Importance of Lysis Buffer Choice. I Western Blotting. New York, NY: Springer New York; 2015. p. 49–60. (Methods in Molecular Biology; vol. 1312).

577. Peach M, Marsh N, MacPhee DJ. Protein Solubilization: Attend to the Choice of Lysis Buffer. Protein Electrophoresis. Totowa, NJ: Humana Press; 2012. p. 37–47. (Methods in Molecular Biology; vol. 869).

578. Subedi P, Schneider M, Atkinson MJ, Tapio S. Isolation of Proteins from Extracellular Vesicles (EVs) for Mass Spectrometry-Based Proteomic Analyses. Proteomic Profiling. New York, NY: Springer US; 2021. p. 207–12. (Methods in Molecular Biology; vol. 2261).

579. Görg A, Drews O, Weiss W. Extraction and Solubilization of Total Protein from Mammalian Tissue Samples. Cold Spring Harb Protoc. 2006 Jun;2006(1):pdb.prot4226.

580. Peuchen EH, Sun L, Dovichi NJ. Optimization and comparison of bottom-up proteomic sample preparation for early-stage Xenopus laevis embryos. Anal Bioanal Chem. 2016 Jul;408(17):4743–9.

581. Johnson KA, Lee JK, Chen AL, Tan M, Sütterlin C. Induction and inhibition of CPAF activity during analysis of Chlamydia-infected cells. Pathogens and Disease. 2015 Feb 1;73(1):1–8.

582. Lu X, Zhu H. Tube-gel digestion: a novel proteomic approach for high throughput analysis of membrane proteins. Mol Cell Proteomics. 2005 Dec;4(12):1948–58.

583. Balliau T, Blein-Nicolas M, Zivy M. Evaluation of Optimized Tube-Gel Methods of Sample Preparation for Large-Scale Plant Proteomics. Proteomes. 2018 Jan 30;6(1):6.

584. Muller L, Fornecker L, Van Dorsselaer A, Cianférani S, Carapito C. Benchmarking sample preparation/digestion protocols reveals tube-gel being a fast and repeatable method for quantitative proteomics. Proteomics. 2016 Dec;16(23):2953–61.

585. Muller L, Fornecker L, Chion M, Van Dorsselaer A, Cianférani S, Rabilloud T, et al. Extended investigation of tube-gel sample preparation: a versatile and simple choice for high throughput quantitative proteomics. Sci Rep. 2018 Dec;8(1):8260.

586. Griese M, Noss J, von Bredow C. Protein pattern of exhaled breath condensate and saliva. Proteomics. 2002 Jun;2(6):690–6.

587. Carter SR, Davis CS, Kovacs EJ. Exhaled breath condensate collection in the mechanically ventilated patient. Respir Med. 2012 May;106(5):601–13.

588. Effros RM, Peterson B, Casaburi R, Su J, Dunning M, Torday J, et al. Epithelial lining fluid solute concentrations in chronic obstructive lung disease patients and normal subjects. J Appl Physiol. 2005 Oct;99(4):1286–92.

589. Georganopoulou DG, Chang L, Nam J-M, Thaxton CS, Mufson EJ, Klein WL, et al. From The Cover: Nanoparticle-based detection in cerebral spinal fluid of a soluble pathogenic biomarker for Alzheimer's disease. Proc Natl Acad Sci. 2005 Feb 15;102(7):2273–6.

590. Hauswirth DW, Sundy JS, Mervin-Blake S, Fernandez CA, Patch KB, Alexander KM, et al. Normative values for exhaled breath condensate pH and its relationship to exhaled nitric oxide in healthy African Americans. J Allergy Clin Immunol. 2008 Jul;122(1):101–6.

591. Hoffmann HJ, Tabaksblat LM, Enghild JJ, Dahl R. Human skin keratins are the major proteins in exhaled breath condensate. Eur Respir J. 2008 Feb 1;31(2):380–4.

592. Kurova VS, Anaev EC, Kononikhin AS, Fedorchenko KYu, Popov IA, Kalupov TL, et al. Proteomics of exhaled breath: methodological nuances and pitfalls. Clin Chem Lab Med. 2009 Jan;47(6).

593. Li, Wang, Peng, Huyan, Cacalano. Exosomes: Versatile Nano Mediators of Immune Regulation. Cancers. 2019 Oct 14;11(10):1557.

594. Wang S, Chen G, Lin X, Xing X, Cai Z, Liu X, et al. Role of exosomes in hepatocellular carcinoma cell mobility alteration. Oncol Lett. 2017 Oct 23.

595. Ge M, Ke R, Cai T, Yang J, Mu X. Identification and proteomic analysis of osteoblast-derived exosomes. Biochem Biophys Res Communic. 2015 Nov;467(1):27–32.

596. Chen Y, Xie Y, Xu L, Zhan S, Xiao Y, Gao Y, et al. Protein content and functional characteristics of serum-purified exosomes from patients with colorectal cancer revealed by quantitative proteomics: Serum-purified exosomes from patients with CRC. Int J Cancer. 2017 Feb 15;140(4):900–13.

597. Rao A, Sharma N, Gajra A. Management of Lung Cancer in the Elderly. Lung Cancer. Cham: Springer International Publishing; 2016. p. 251–84. (Cancer Treatment and Research; vol. 170).

598. Shao C, Zhao M, Chen X, Sun H, Yang Y, Xiao X, et al. Comprehensive Analysis of Individual Variation in the Urinary Proteome Revealed Significant Gender Differences. Mol Cell Proteome. 2019 Jun;18(6):1110–22.

599. Jiang B, Hu L, Zhang X, Zhang H, Zhang F, Chen L, et al. Uncovering proteome variations of differently heat-treated sea cucumber (Apostichopus japonicus) by label-free mass spectrometry. Food Chem. 2021 May;344:128575.

600. Uhlen M, Fagerberg L, Hallstrom BM, Lindskog C, Oksvold P, Mardinoglu A, et al. Tissue-based map of the human proteome. Sci. 2015 Jan 23;347(6220):1260419–1260419.

601. Davis MD, Fowler SJ, Montpetit AJ. Exhaled breath testing – A tool for the clinician and researcher. Paediatric Respir Rev. 2019 Feb;29:37–41.

602. Fabri-Faja N, Calvo-Lozano O, Dey P, Terborg RA, Estevez M-C, Belushkin A, et al. Early sepsis diagnosis via protein and miRNA biomarkers using a novel point-of-care photonic biosensor. Analytica Chimica Acta. 2019 Oct;1077:232–42.

603. Wang T, Peng Q, Guo B, Zhang D, Zhao M, Que H, et al. An integrated electrochemical biosensor based on target-triggered strand displacement amplification and "four-way" DNA junction towards ultrasensitive detection of PIK3CA gene mutation. Biosens Bioelectron. 2020 Feb;150:111954.

604. Guilbault GG, Lubrano GJ. An enzyme electrode for the amperometric determination of glucose. Analytica Chimica Acta. 1973 May;64(3):439–55.

605. Heineman WR, Jensen WB. Leland C. Clark Jr. (1918–2005). Biosens Bioelectron. 2006 Feb;21(8):1403–4.

606. Guilbault GG, Montalvo JG. Urea-specific enzyme electrode. J Am Chem Soc. 1969 Apr;91(8):2164–5.

607. Bhalla N, Jolly P, Formisano N, Estrela P. Introduction to biosensors. Essays Biochem. 2016 Jun 30;60(1):1–8.

608. Yoo E-H, Lee S-Y. Glucose Biosensors: An Overview of Use in Clinical Practice. Sensors. 2010 May 4;10(5):4558–76.

609. Suzuki S, Takahashi F, Satoh I, Sonobe N. Ethanol and Lactic Acid Sensors Using Electrodes Coated with Dehydrogenase—Collagen Membranes. BCSJ. 1975 Nov;48(11):3246–9.

610. Cass AEG, Davis Graham, Francis GD, Hill HAO, Aston WJ, Higgins IJohn, et al. Ferrocene-mediated enzyme electrode for amperometric determination of glucose. Anal Chem. 1984 Apr;56(4):667–71.

611. Bo, Nylander C, Lunström I. Surface plasmon resonance for gas detection and biosensing. Sens Actuators. 1983 Jan;4:299–304.

612. Vigneshvar S, Sudhakumari CC, Senthilkumaran B, Prakash H. Recent Advances in Biosensor Technology for Potential Applications – An Overview. Front Bioeng Biotechnol. 2016 Feb 16;4.

613. Andryukov BG, Besednova NN, Romashko RV, Zaporozhets TS, Efimov TA. Label-Free Biosensors for Laboratory-Based Diagnostics of Infections: Current Achievements and New Trends. Biosensors. 2020 Feb 12;10(2):11.

614. Damborský P, Švitel J, Katrlík J. Optical biosensors. Essays Biochem. 2016 Jun 30;60(1):91–100.

615. Li B, Yu Q, Duan Y. Fluorescent labels in biosensors for pathogen detection. Critical Reviews in Biotechnology. 2015 Jan 2;35(1):82–93.

616. Liu L, He F, Yu Y, Wang Y. Application of FRET Biosensors in Mechanobiology and Mechanopharmacological Screening. Front Bioeng Biotechnol. 2020 Nov 9;8:595497.

617. EL Andaloussi S, Mäger I, Breakefield XO, Wood MJA. Extracellular vesicles: biology and emerging therapeutic opportunities. Nat Rev Drug Discov. 2013 May;12(5):347–57.

618. Bajar BT, Wang ES, Zhang S, Lin MZ, Chu J. A Guide to Fluorescent Protein FRET Pairs. Sensors (Basel). 2016 Sep 14;16(9).

619. Förster Th. Zwischenmolekulare Energiewanderung und Fluoreszenz. Ann Phys. 1948 Jan;437(1–2):55–75.

620. Miyawaki A. Development of Probes for Cellular Functions Using Fluorescent Proteins and Fluorescence Resonance Energy Transfer. Annu Rev Biochem. 2011 Jul 7;80(1):357–73.

621. Leavesley SJ, Britain AL, Cichon LK, Nikolaev VO, Rich TC. Assessing FRET using spectral techniques. Cytometry A. 2013 Oct;83(10):898–912.

622. Day RN. Measuring Förster Resonance Energy Transfer Using Fluorescence Lifetime Imaging Microscopy. Micros Today. 2015 May;23(3):44–51.

623. Datta R, Heaster TM, Sharick JT, Gillette AA, Skala MC. Fluorescence lifetime imaging microscopy: fundamentals and advances in instrumentation, analysis, and applications. J Biomed Opt. 2020 May 13;25(07):1.

624. Skruzny, Pohl, Abella. FRET Microscopy in Yeast. Biosensors. 2019 Oct 11;9(4):122.

625. Wojcik K, Solarczyk K, Kulakowski P. Measurements on MIMO-FRET Nano-Networks Based on Alexa Fluor Dyes. IEEE Trans Nanotechnology. 2015 May;14(3):531–9.

626. Yang C, Zhang J, Peng W-T, Sheng W, Liu D, Kuttipillai PS, et al. Impact of Stokes Shift on the Performance of Near-Infrared Harvesting Transparent Luminescent Solar Concentrators. Sci Rep. 2018 Dec;8(1):16359.

627. Lakowicz JR. Introduction to Fluorescence. Principles of Fluorescence Spectroscopy. Boston, MA: Springer US; 2006. p. 1–26.

628. Grecco HE, Verveer PJ. FRET in Cell Biology: Still Shining in the Age of Super-Resolution? ChemPhysChem. 2011 Feb 25;12(3):484–90.

629. Gert-Jan Kremers, David W Piston, Michael W Davidson. Basics of FRET microscopy. Nicon Microscopy

630. Piston DW, Kremers G-J. Fluorescent protein FRET: the good, the bad and the ugly. Trends Biochem Sci. 2007 Sep;32(9):407–14.

631. Loura L. FRET in membrane biophysics: an overview. Front Physio. 2011;2.

632. Teunissen AJP, Pérez-Medina C, Meijerink A, Mulder WJM. Investigating supramolecular systems using Förster resonance energy transfer. Chem Soc Rev. 2018;47(18):7027–44.

633. Qiu X, Hildebrandt N. A clinical role for Förster resonance energy transfer in molecular diagnostics of disease. Expert Rev Mol Diagnost. 2019 Sep 2;19(9):767–71.

634. Wong F, Coban O, Weitsman G, Ng T. Integrating imaging, exosome and protein network rewiring information to track early tumour evolution of resistance mechanisms. Converg Sci Phys Oncol. 2017 Feb 23;3(1):013004.

635. Tu C, Santo L, Mishima Y, Raje N, Smilansky Z, Zoldan J. Monitoring protein synthesis in single live cancer cells. Integr Biol. 2016;8(5):645–53.

636. Geißler D, Stufler S, Löhmannsröben H-G, Hildebrandt N. Six-Color Time-Resolved Förster Resonance Energy Transfer for Ultrasensitive Multiplexed Biosensing. J Am Chem Soc. 2013 Jan 23;135(3):1102–9.

637. Guo J, Mingoes C, Qiu X, Hildebrandt N. Simple, Amplified, and Multiplexed Detection of MicroRNAs Using Time-Gated FRET and Hybridization Chain Reaction. Anal Chem. 2019 Feb 19;91(4):3101–9.

638. Nobis M, Herrmann D, Warren SC, Kadir S, Leung W, Killen M, et al. A RhoA-FRET Biosensor Mouse for Intravital Imaging in Normal Tissue Homeostasis and Disease Contexts. Cell Reports. 2017 Oct;21(1):274–88.

639. Solomon M, Guo K, Sudlow GP, Berezin MY, Edwards WB, Achilefu S, et al. Detection of enzyme activity in orthotopic murine breast cancer by fluorescence lifetime imaging using a fluorescence resonance energy transfer–based molecular probe. J Biomed Opt. 2011;16(6):066019.

640. Nobis M, McGhee EJ, Morton JP, Schwarz JP, Karim SA, Quinn J, et al. Intravital FLIM-FRET Imaging Reveals Dasatinib-Induced Spatial Control of Src in Pancreatic Cancer. Cancer Res. 2013 Aug 1;73(15):4674–86.

641. Guala D, Bernhem K, Blal HA, Jans D, Lundberg E, Brismar H, et al. Experimental validation of predicted cancer genes using FRET. Methods Appl Fluoresc. 2018 Apr 25;6(3):035007.

642. Sato YT, Umezaki K, Sawada S, Mukai S, Sasaki Y, Harada N, et al. Engineering hybrid exosomes by membrane fusion with liposomes. Sci Rep. 2016 Apr;6(1):21933.

643. Zhu N, Li G, Zhou J, Zhang Y, Kang K, Ying B, et al. A light-up fluorescence resonance energy transfer magnetic aptamer-sensor for ultra-sensitive lung cancer exosome detection. J Mater Chem B. 2021;9(10):2483–93.

644. Lu S, Wang Y, Huang H, Pan Y, Chaney EJ, Boppart SA, et al. Quantitative FRET Imaging to Visualize the Invasiveness of Live Breast Cancer Cells. Yuan F, editor. PLoS ONE. 2013 Mar 13;8(3):e58569.

645. Kaufmann T, Herbert S, Hackl B, Besold JM, Schramek C, Gotzmann J, et al. Direct measurement of protein–protein interactions by FLIM-FRET at UV laser-induced DNA damage sites in living cells. Nucleic Acids Res. 2020 Dec 2;48(21):e122–e122.

646. Sun Y, Day RN, Periasamy A. Investigating protein-protein interactions in living cells using fluorescence lifetime imaging microscopy. Nat Protoc. 2011 Sep;6(9):1324–40.

647. Liu L, Wei G, Liu Z, He Z, Xiao S, Wang Q. Two-Photon Excitation Fluorescence Resonance Energy Transfer with Small Organic Molecule as Energy Donor for Bioassay. Bioconjug Chem. 2008 Feb;19(2):574–9.

648. Hayashi-Takanaka Y, Stasevich TJ, Kurumizaka H, Nozaki N, Kimura H. Evaluation of Chemical Fluorescent Dyes as a Protein Conjugation Partner for Live Cell Imaging. Cotterill S, editor. PLoS ONE. 2014 Sep 3;9(9):e106271.

649. Vira S, Mekhedov E, Humphrey G, Blank PS. Fluorescent-labeled antibodies: Balancing functionality and degree of labeling. Anal Biochem. 2010 Jul 15;402(2):146–50.

650. Chakraborty S, Hu S-Y, Wu S-H, Karmenyan A, Chiou A. The Interaction Affinity between Vascular Cell Adhesion Molecule-1 (VCAM-1) and Very Late Antigen-4 (VLA-4) Analyzed by Quantitative FRET. Koch K-W, editor. PLoS ONE. 2015 Mar 20;10(3):e0121399.

651. Berney C, Danuser G. FRET or No FRET: A Quantitative Comparison. Biophysical Journal. 2003 Jun;84(6):3992–4010.

652. Medina RA, Owen GI. Glucose transporters: expression, regulation and cancer. Biol Res. 2002;35(1).

653. Macheda ML, Rogers S, Best JD. Molecular and cellular regulation of glucose transporter (GLUT) proteins in cancer. J Cell Physiol. 2005 Mar;202(3):654–62.

654. Szablewski L. Expression of glucose transporters in cancers. Biochimica et Biophysica Acta (BBA) - Rev Cancer. 2013 Apr;1835(2):164–9.

655. Scafoglio C, Hirayama BA, Kepe V, Liu J, Ghezzi C, Satyamurthy N, et al. Functional expression of sodium-glucose transporters in cancer. Proc Natl Acad Sci. 2015 Jul 28;112(30):E4111–9.

656. Risha Y, Minic Z, Ghobadloo SM, Berezovski MV. The proteomic analysis of breast cell line exosomes reveals disease patterns and potential biomarkers. Sci Rep. 2020 Dec;10(1):13572.

657. Testa JE, Brooks PC, Lin JM, Quigley JP. Eukaryotic expression cloning with an antimetastatic monoclonal antibody identifies a tetraspanin (PETA-3/CD151) as an effector of human tumor cell migration and metastasis. Cancer Res. 1999 Aug 1;59(15):3812–20.

658. Wong AH, Tran T. CD151 in Respiratory Diseases. Front Cell Dev Biol. 2020 Feb 7;8:64.

659. Malla RR, Pandrangi S, Kumari S, Gavara MM, Badana AK. Exosomal tetraspanins as regulators of cancer progression and metastasis and novel diagnostic markers. Asia-Pacific J Clin Oncol. 2018 Dec;14(6):383–91.

660. Kwon MJ, Seo J, Kim YJ, Kwon MJ, Choi JY, Kim T-E, et al. Prognostic significance of CD151 overexpression in non-small cell lung cancer. Lung Cancer. 2013 Jul;81(1):109–16.

661. Zhu W, Zhou B, Zhao C, Ba Z, Xu H, Yan X, et al. Myoferlin, a multifunctional protein in normal cells, has novel and key roles in various cancers. J Cell Mol Med. 2019 Nov;23(11):7180–9.

662. Gu H, Peng Y, Chen Y. An Emerging Therapeutic Approach by Targeting Myoferlin (MYOF) for Malignant Tumors. CTMC. 2020 Aug 20;20(17):1509–15.

663. Han Y, Wu Y, Gao S, Xu Y, Guan Z, Qiu X, et al. [Expression and clinical significance of RhoC and RhoGDIa in non-small cell lung cancer.]. Zhongguo Fei Ai Za Zhi. 2008 Jun 20;11(3):391–7.

664. Ikoma T, Takahashi T, Nagano S, Li Y-M, Ohno Y, Ando K, et al. A Definitive Role of RhoC in Metastasis of Orthotopic Lung Cancer in Mice. Clin Cancer Res. 2004 Feb 1;10(3):1192–200.

665. Ruth MC, Xu Y, Maxwell IH, Ahn NG, Norris DA, Shellman YG. RhoC Promotes Human Melanoma Invasion in a PI3K/Akt-Dependent Pathway. J Investig Dermatol. 2006 Apr;126(4):862–8.

666. Lang S, Busch H, Boerries M, Brummer T, Timme S, Lassmann S, et al. Specific role of RhoC in tumor invasion and metastasis. Oncotarget. 2017 Oct 20;8(50):87364–78.

667. Chen M-J, Wu Y-S, Lin G-F, Hou J-Y, Li M, Liu T-C. Quantum-dot-based homogeneous time-resolved fluoroimmunoassay of alpha-fetoprotein. Anal Chim Acta. 2012 Sep;741:100–5.

668. Wegner KD, Jin Z, Lindén S, Jennings TL, Hildebrandt N. Quantum-Dot-Based Förster Resonance Energy Transfer Immunoassay for Sensitive Clinical Diagnostics of Low-Volume Serum Samples. ACS Nano. 2013 Aug 27;7(8):7411–9.

669. Wei Q, Lee M, Yu X, Lee EK, Seong GH, Choo J, et al. Development of an open sandwich fluoroimmunoassay based on fluorescence resonance energy transfer. Anal Biochem. 2006 Nov;358(1):31–7.

670. Hamd-Ghadareh S, Salimi A, Fathi F, Bahrami S. An amplified comparative fluorescence resonance energy transfer immunosensing of CA125 tumor marker and ovarian cancer cells using green and economic carbon dots for bio-applications in labeling, imaging and sensing. Biosens Bioelectron. 2017 Oct;96:308–16.

671. Tannenbaum C, Greaves L, Graham ID. Why sex and gender matter in implementation research. BMC Med Res Methodol. 2016 Dec;16(1):145, s12874-016-0247–7.

672. Campanella A, De Summa S, Tommasi S. Exhaled breath condensate biomarkers for lung cancer. J Breath Res. 2019 Aug 20;13(4):044002.

673. Li M-Y, Liu L-Z, Dong M. Progress on pivotal role and application of exosome in lung cancer carcinogenesis, diagnosis, therapy and prognosis. Mol Cancer. 2021 Dec;20(1):22.

674. Granville CA, Dennis PA. An Overview of Lung Cancer Genomics and Proteomics. Am J Respir Cell Mol Biol. 2005 Mar;32(3):169–76.

675. Mazzone PJ, Sears CR, Arenberg DA, Gaga M, Gould MK, Massion PP, et al. Evaluating Molecular Biomarkers for the Early Detection of Lung Cancer: When Is a Biomarker Ready for Clinical Use? An Official American Thoracic Society Policy Statement. Am J Respir Crit Care Med. 2017 Oct;196(7):e15–29.

APPENDIX

ETHICS APPROVAL

LIST OF FIGURES

LIST OF TABLES

ETHICS APPROVAL

***Document 2**. Health and Disability Ethics Committees approval*

Health and Disability Ethics Committees

Health and Disability Ethics Committees
Ministry of Health
133 Molesworth Street
PO Box 5013
Wellington
6011
0800 4 ETHICS
hdecs@moh.govt.nz

12 August 2020

Ms Déanna Ayupova
Victoria University of Wellington
Deanna.ayupova@vuw.ac.nz

Dear Ms Ayupova

Study title:	Determining the benchmark proteome of breath-derived exosomes from healthy volunteers

Thank you for contacting the Ethics team regarding whether your research proposal was in scope for HDEC review on 31 July 2020. The Secretariat has assessed the information provided in your proposal and supporting documents against the Standard Operating Procedures.

Your study will not require submission to HDEC as, on the basis of the information you have submitted, it does not appear to be within the scope of HDEC review. This scope is described in section three of the Standard Operating Procedures for Health and Disability Ethics Committees.

An observational study requires HDEC review only if the study involves more than minimal risk (that is, potential participants could reasonably be expected to regard the probability and magnitude of possible harms resulting from their participation in the study to be greater than those encountered in those aspects of their everyday life that relate to the study).

For the avoidance of doubt, an observational study always involves more than minimal risk if it involves one or more of the following:

- one or more participants who will not have given informed consent to participate, or
- one or more participants who are vulnerable (that is, who have restricted capability to make independent decisions about their participation in the study), or
- standard treatment being withheld from one or more participants, or
- the storage, preservation or use of identifiable human tissue without consent, or
- the disclosure of identifiable health information without authorisation.

If you consider that our advice on your project being out of scope is in incorrect please contact us as soon as possible giving reasons for this.

This letter does not constitute ethical approval or endorsement for the activity described in your application, but may be used as evidence that HDEC review is not required for it.

Please note, your locality may have additional ethical review policies, please check with your locality. If your study involves a DHB, you must contact the DHB's research office before you begin. If your study involves a university or polytechnic, you must contact its institutional ethics committee before you begin. We recommend you contact Auckland District Health Board's ethic committee(s) for guidance.

Please don't hesitate to contact us for further information.

Yours sincerely,

Courtney Parnell
Assistant Advisor
Health and Disability Ethics Committees
hdecs@moh.govt.nz

***Document 3**. VUW Ethics committee approval*

VICTORIA UNIVERSITY OF WELLINGTON
TE HERENGA WAKA

Phone 0-4-463 6028
Email judith.loveridge@vuw.ac.nz

TO	Deanna Ayupova
FROM	Associate Professor Judith Loveridge, Convenor, Human Ethics Committee
DATE	9 September 2020
PAGES	1
SUBJECT	**Ethics Approval** **Number:** 28700 **Title:** Determining disease biomarkers in breath-derived exosomes for new diagnostic tools

Thank you for your application for ethical approval, which has now been considered by the Human Ethics Committee.

Your application has been approved from the above date and this approval is valid for three years. If your data collection is not completed by this date you should apply to the Human Ethics Committee for an extension to this approval.

Best wishes with the research.

Kind regards,

J A Loveridge

Judith Loveridge

Convenor, Victoria University of Wellington Human Ethics Committee

LIST OF FIGURES

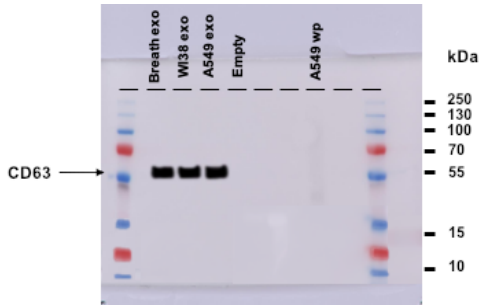

Figure S 1. Western blot analysis of general tetraspanin EV marker CD63 for all samples (breath- and cell-derived exosomes).

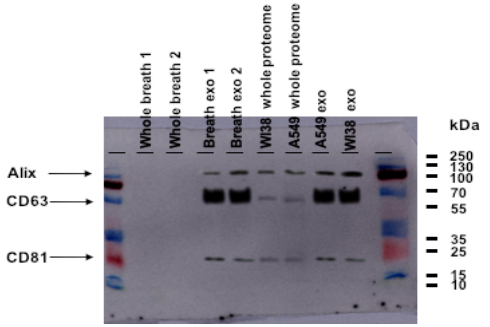

***Figure S 2. Western blot analysis of general tetraspanin EV markers Alix, CD63, and CD81.** 100 ng pure protein loaded for all exosome samples (10µl) and whole breath (10µL); for whole proteome 20 µg of lysate (20µL).*

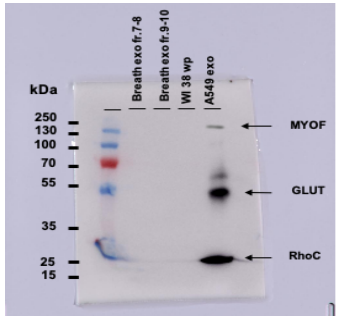

Figure S 3. Western blot analysis of MYOF, GLUT, and RhoC proposed biomarkers on all samples (breath- and cell-derived exosomes).

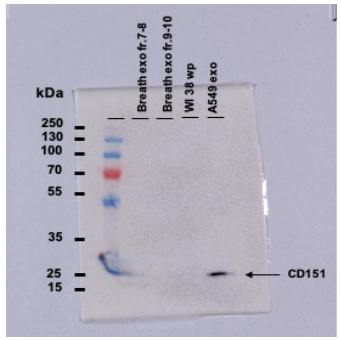

Figure S 4. Western blot analysis of CD151 proposed biomarker on all samples (breath- and cell-derived exosomes).

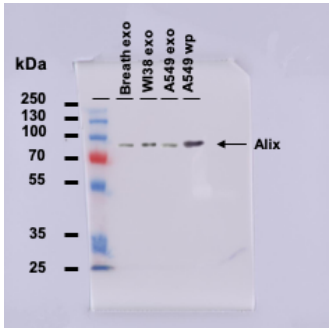

Figure S 5. Western blot analysis of general tetraspanin EV marker Alix on all samples (breath- and cell-derived exosomes).

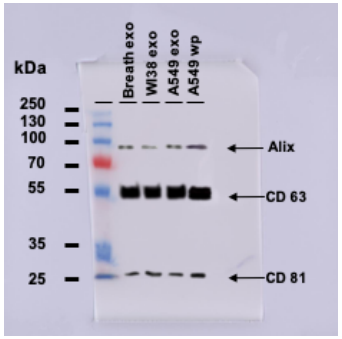

Figure S 6. Western blot analysis of general tetraspanin EV markers Alix, CD63, and CD81 on all samples (breath- and cell-derived exosomes).

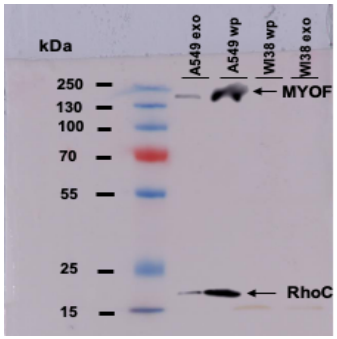

Figure S 7. Western blot analysis of proposed biomarkers MYOF and RhoC on cell (WI-38/A549)-derived exosomes and whole proteome of the same cell line.

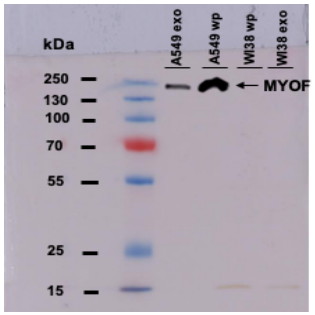

Figure S 8. Western blot analysis of proposed biomarker MYOF on cell (WI-38/A549) - derived exosomes and whole proteome of the same line.

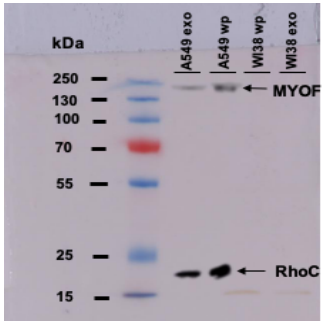

Figure S 9. Western blot analysis of proposed biomarkers MYOF and RhoC (2nd attempt) on cell (WI-38/A549)-derived exosomes.

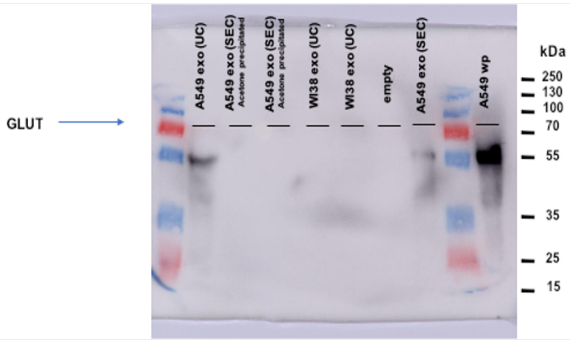

Figure S 10. Western blot analysis of proposed biomarker GLUT on cell (WI-38/A549) - derived exosomes.

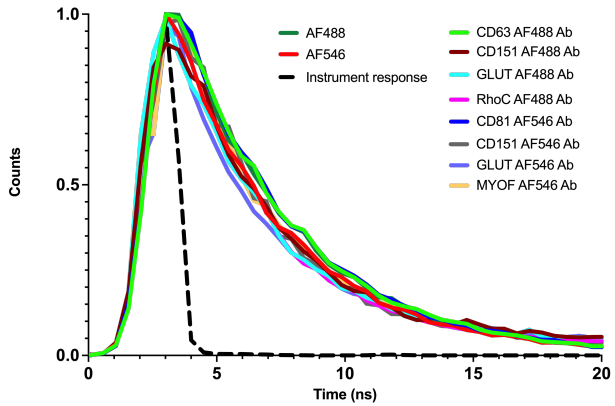

***Figure S 11. PL lifetimes of dyes and conjugated dyes**. PL lifetimes obtained by time-correlated single photon counting (TCSPC) (λ_{ex} = 380 nm; λ_{em} = 520 nm) of dyes and conjugated dyes with fluorescently labeled antibodies corresponding to the general tetraspanin EV markers (CD63 and CD81)and proposed biomarkers (CD151, GLUT, MYOF, and RhoC). The Y-axis represents normalized photon counts, and X-axis represents decay time (ns). The instrument response (IRF) is shown on each panel in black (dashed). The experiment was performed on three biological samples and run in duplicate. The error bars represent standard deviation. Some error bars are not visible as the data in the duplicates were close to identical. The figure was generated by using Prism GraphPad Software (version 9.1.1) for macOS, San Diego, California.*

LIST OF TABLES

Table S 1. Cell quantification data for A549 cell line. *The table showing the cell average resulted from counted per square of the hemocytometer ($\times 10^{-4}$),the number of those cells that were live or dead as revealed by trypan blue staining ($\times 10^{-4}$), viability during passaging, and total cell count over12 days.*

Day of the experiment	Cell average	Number of live cells per square	Number of dead cells per square	Viability, %	V of CCM, mL	Total cells
Day 1 (T25 flask 1)	71	69	2	n/a	4	4830000
(T25 flask 2)	63	60	3	n/a	4	4200000
(T25 flask 3)	62	60	2	n/a	4	4200000
Day 3 (T75 flask 1)	237	235	2	99	11	32900000
(T75 flask 2)	138	137	1	99	11	19180000
(T75 flask 3)	146	144	2	99	11	20160000
Day 6 (T75 flask 1)	118	116	2	98	11	16240000
(T75 flask 2)	119	117	2	98	11	16380000
(T75 flask 3)	126	125	1	99	11	17500000
(T75 flask 4)	120	118	2	98	11	16520000
(T75 flask 5)	275	270	5	98	11	37800000
(T75 flask 6)	136	133	3	98	11	18620000
(T75 flask 7)	161	158	3	98	11	22120000
(T75 flask 8)	168	165	3	98	11	23100000
Day 9 (T75 flask 1)	418	413	5	99	11	57820000
(T75 flask 2)	421	415	6	99	11	58100000
T75 flask 3-5 combined)	418	413	5	99	11	57820000
T75 flask 6-9 combined)	420	415	5	99	11	58100000
T75 flasks 10-11 combined	285	283	2	99	11	39620000
Day 12 (T75 flask 1)	114	122	2	98	11	17080000

Table S 2. *Raw list of proteins found at least once with a high quality peptide match identified in at least one sample of A549 cell-derived exosomes.*

Protein ID	Protein ID	Protein ID
D6RF35	P10643	P60033
O00299	P10809	P60174-1
O00468-5	P10909-1	P55263-1
O00560-1	P11021	P60660
O14950	P11047	P60709
O15230	P11142-1	P60842
O15427	P11166	P60900
O15484	P11413-1	P60953
O43707	P12109	P60981-1
O43795	P12110	P61224-1

O60218	P12111	P61247
O60701	P12236	P61254
O60814	P12259	P61353
O75083	P12814-1	P61604
O75367-1	P13473-1	P61981
O75369-1	P13639	P62241
O75955	P13645	P62258-1
O95084	P13647	P62266
O95445-1	P13929-1	P62424
O95497	P13987	P62701
P00338-1	P14618	P62736
P00352	P14625	P62753
P00390	P14923	P62805
P00488	P15121	P62820
P00505	P15151-1	P62826
P00533-1	P15311	P62854
P00558	P15531	P62873
P00734	P15559-1	P62879
P00747	P15880	P62906
P01008	P16070	P62910
P01023	P16401	P62937
P01024	P16402	P62987
P01031	P17812	P63104-1
P01116	P18124	P63267-1
P01857	P18206	P68104
P02042	P19338	P68363
P02452	P19823	P68366
P02461	P20742	P68371
P02649	P20774	P69905
P02656	P20908	P78527
P02675	P21333	P80723
P02679	P21399	P84103
P02748	P21796	P84243
P02749	P21926	P98160
P02751	P22314	P99999
P02753	P22626	Q00325-1
P02765	P22692	Q00610-1
P02768-1	P22695	Q00796
P02771	P23142	Q00839

P02774	P23284	Q01650
P02786	P23396-1	Q02241-1
P02787	P23526-1	Q02543
P02788	P23528	Q02878
P02794	P25705-1	Q04756
P04004	P26006	Q06033-1
P04075	P26038	Q06830
P04083	P26641	Q07020
P04114	P27105	Q07954
P04264	P27635	Q08380
P04406-1	P29401	Q08431
P04745	P29692	Q12805
P05023	P30041	Q12860
P05026	P30048	Q13011
P05106	P30101	Q13103
P05141	P31689-1	Q13200
P05156	P31939	Q13219
P05387	P33527	Q13418
P05388	P34931	Q13509
P05452	P35232	Q13885
P05543	P35268	Q14204
P05556-1	P35443	Q14254
P05783	P35527	Q14533
P05787	P35579-1	Q14764
P06396	P35580	Q14847
P06576	P35908	Q14974
P06733-1	P36578	Q15063-1
P06744	P36955	Q15084-1
P06748	P38646	Q15365
P06756	P39023	Q15493-1
P07195	P39060-1	Q15582
P07237	P40227-1	Q15758-1
P07355	P40926	Q16658
P07437	P42330	Q16777
P07602-1	P43652	Q16778
P07737	P46781	Q16853
P07814	P48509	Q16891
P07900	P49327	Q562R1
P07942	P49368-1	Q5QNW6-1

P07996	P49747	Q71U36
P08123	P50552	Q71UI9-1
P08134	P50914	Q7L7L0
P08195	P50990	Q8WUA8
P08238	P50991	Q8WUM4
P08697-1	P50995	Q8WWI5
P08729	P51570	Q969X5
P08754	P51884	Q9H4B7
P08758	P52209	Q9H8M2-1
P08865	P52895	Q9NQH7-1
P09525	P53396-1	Q9NZM1
P09651-1	P54652	Q9UGM3-1
P0C0L4-1	P55072	Q9Y490
P0DMV8	P55263-1	Q9Y4K0

Table S 3. *Raw list of proteins found at least once with a high quality peptide match identified in at least one sample of WI-38 cell-derived exosomes.*

Protein ID	**Protein ID**	**Protein ID**
A0A087X1T7	P0DMV8	P62753
A0A3B3IRI8	P10451-1	P62805
A6NMY6	P10643	P62826
A6NMZ7-1	P10909-1	P62873
B9A064-1	P11047	P62899
C9JCJ5	P11142-1	P62910
D6RF35	P11413-1	P62937
E9PFT6	P11717	P62987
G3V1N2	P11766	P63104-1
H7BZW2	P12109	P63267-1
O00468-5	P12110	P68366
O00560-1	P12111	P68371
O15031	P12259	P69905
O15230	P12814-1	P78509
O15484	P13639	P78524-1
O43505	P13645	P84243
O43707	P14550	P98160
O43765	P14618	Q00266
O43854-1	P14625	Q00610-1
O60218	P15531	Q01518-1
O75083	P15880	Q01955-1

O75369-1	P16070	Q02388-1
O75955	P16152	Q04721
O95466	P16402	Q04756
O95497	P17301	Q05639
P00338-1	P17405-1	Q06033-1
P00352	P18206	Q06210-1
P00558	P19320-1	Q06828
P00734	P19338	Q06830
P00738	P19823	Q07954
P00742	P19827-1	Q08431
P00747	P20742	Q12805
P00966	P20774	Q12841
P01008	P20908	Q13103
P01023	P21266	Q13162
P01024	P21333	Q13200
P01031	P21399	Q13219
P01033	P21810	Q13308-1
P01266-1	P21980	Q13332
P01344	P22105	Q13418
P01614	P22314	Q13509
P01857	P22626	Q13614-1
P01861	P22692	Q14112-1
P02100	P23142	Q14117
P02452	P23526-1	Q14204
P02458-1	P23528	Q14520-1
P02461	P23921	Q14624-1
P02545	P24043	Q14764
P02649	P24534	Q14974
P02656	P24821	Q15063-1
P02671-1	P25786-1	Q15274
P02675	P25789	Q15493-1
P02679	P26038	Q15582
P02748	P26447	Q16270-1
P02749	P27105	Q16610
P02751	P28827-1	Q16777
P02765	P30041	Q16778
P02768-1	P30050-1	Q16787-2
P02771	P30086	Q16819
P02787	P30101	Q16853

P02788	P30153	Q2TBE0
P02790	P31146	Q5JP53
P03956	P31939	Q5QNW6-1
P04004	P34096	Q6B0K9
P04040	P35052	Q6NVV1
P04075	P35080-1	Q6RFH5-1
P04083	P35443	Q71U36
P04114	P35527	Q7Z3S9-1
P04180	P35555	Q7Z4W1
P04264	P35556	Q86UX7
P04275	P35579-1	Q8N2S1
P04406-1	P35908	Q8ND82
P04792	P36578	Q8NG11-1
P05062	P36955	Q8WUM4
P05106	P37802	Q92520
P05121-1	P38606	Q92626
P05156	P43652	Q96F07
P05452	P46531	Q96KP4
P05556-1	P47914	Q96L12
P05783	P48740-1	Q96P31-1
P05787	P49189	Q99460
P06396	P49327	Q99715-1
P06727	P49368-1	Q99983
P06733-1	P49746	Q9BQ51-3
P06737-1	P49747	Q9BXJ4
P06744	P50990	Q9H0U4
P07195	P51148	Q9H2G4
P07358	P51884	Q9H8M2-1
P07437	P51991-1	Q9NR21-1
P07585	P52895	Q9NRN5-1
P07737	P54289	Q9NRY6
P07900	P55072	Q9NY65
P07942	P55263-1	Q9NZN3
P07996	P55287-1	Q9P2T1-1
P08123	P55290	Q9UBG0
P08238	P57721-1	Q9UBR2
P08253	P60174-1	Q9UGM3-1
P08670	P60660	Q9ULA0
P08697-1	P60709	Q9UM47

P08758	P60900	Q9UMY4-1
P09382	P61160-1	Q9UNP9-1
P09455-1	P61224-1	Q9Y240
P09486	P61353	Q9Y490
P09972	P61981	Q9Y4K0
P0C0L4-1	P62191	Q9Y696
P0DMV8	P62263	Q9Y6Z7
P10451-1	P62269	U3KQF2
P10643	P62491-1	

Table S 4. *Raw list of proteins found at least once with a high quality peptide match identified in at least one sample of whole proteome of A549 cells.*

Protein ID	**Protein ID**	**Protein ID**	**Protein ID**	**Protein ID**
A0A075B6Z8	P02748	P21796	P60174-1	Q16778
A0A087WT76	P02749	P21926	P60228	Q16819
A0A087WUL9	P02751	P21980	P60660	Q16853
A0A087WX80	P02753	P22033	P60709	Q16881-1
A0A087WYX9	P02765	P22105	P60763	Q16891
A0A0A0MRM9	P02768-1	P22234	P60842	Q2M389
A0A0D9SEM4	P02771	P22307-1	P60900	Q3SY69-1
A0A0J9YXZ5	P02774	P22314	P60903	Q4G163
A0A1W2PRJ5	P02786	P22626	P60953	Q4KMQ2-1
A0A2R8Y656	P02787	P22692	P60981-1	Q53GQ0
A0A2R8YG48	P02788	P22695	P61019-1	Q562R1
A0A3B3IRI8	P02790	P23141	P61026	Q58FF6
A0A3B3ISY1	P02794	P23142	P61106	Q5JWF2-1
A5A3E0	P03951	P23142-4	P61129	Q5M9N0-1
A6NLM8	P04004	P23229-1	P61158	Q5QNW6-1
A6NMY6	P04040	P23246-1	P61160-1	Q5SSJ5-1
B0QZK4	P04075	P23284	P61163	Q5T4S7-1
B1AK85	P04083	P23381	P61204	Q5T749
B4DLN1	P04114	P23396-1	P61221	Q5T7F0
B4DT28	P04179-4	P23526-1	P61224-1	Q5T8R3
B5MCV4	P04180	P23528	P61247	Q5TCZ1
B5ME19	P04259	P23634-1	P61254	Q5TG30
B7ZKQ9	P04264	P23921	P61313-1	Q5U649
B9A064-1	P04275	P24043	P61353	Q5VW38
C9J3L8	P04406-1	P24534	P61421	Q5W0H4
C9J5X1	P04745	P24752	P61604	Q658P3-1
C9J7B4	P04792	P25398	P61758	Q6DD88
C9JCJ5	P04843	P25445-1	P61769	Q6IAA8

D6RC77	P04899-1	P25705-1	P61970	Q6IQ42
D6RF35	P05023	P25786-1	P61978	Q6NVV1
D6RH06	P05026	P25788-1	P61981	Q6NZI2-1
E5RHG9	P05062	P26006	P62072	Q6P2Q9
E5RI99	P05067-1	P26038	P62081	Q6QEF8-1
E5RIE3	P05091	P26373-1	P62136-1	Q6ZMP0-1
E7EN89	P05106	P26447	P62140	Q6ZNJ1-1
E7EQS8	P05121-1	P26583	P62158	Q6ZS81-1
E7ESP4	P05141	P26599	P62191	Q71U36
E9PCY7	P05156	P26641	P62195-1	Q71UI9-1
E9PKY7	P05386	P26927	P62241	Q7L576-1
F5GY03	P05387	P27105	P62244	Q7L7L0
F5H608	P05388	P27348	P62249	Q7LBR1
F8WAV9	P05452	P27635	P62256	Q7Z3U7-1
G3V1N2	P05534	P27708	P62258-1	Q7Z4W1
G3V2M1	P05543	P27797	P62266	Q86UX7
G3V5G2	P05546	P27824	P62269	Q86VP6-1
H0Y2N6	P05556-1	P28074-1	P62277	Q86Y82
H0Y835	P05783	P28300	P62280	Q8IUE6
H0YAF8	P05787	P28331-1	P62316	Q8IUL8
H0YB56	P06132	P29144	P62318	Q8IV33
H0YCN1	P06396	P29317	P62333	Q8IZ83
H0YF61	P06576	P29401	P62424	Q8IZL8
H0YJU2	P06727	P29692	P62491-1	Q8IZP2
H3BMN1	P06733-1	P29966	P62701	Q8N0Y7
H3BN98	P06737-1	P30040-1	P62714	Q8N2S1
H3BPG0	P06744	P30041	P62736	Q8N474
H3BRJ0	P06748	P30043	P62753	Q8N7P7
H7C106	P06753-2	P30044-1	P62805	Q8NAF0
H7C1S9	P06756	P30048	P62820	Q8NBS9-1
I3L1A3	P07099	P30050-1	P62826	Q8NEM0
I3L1P5	P07195	P30086	P62829	Q8NFJ5
I3L397	P07225	P30101	P62854	Q8NG11-1
I3L425	P07237	P30153	P62857	Q8NI77
J3KND8	P07305	P30626	P62861	Q8TAA3-1
J3KRJ1	P07339	P30626-1	P62873	Q8TB61
J3KRX5	P07355	P30838	P62879	Q8TEX9-1
J3KRY3	P07357	P31040	P62888	Q8WTV0-1
J3KTD3	P07437	P31146	P62906	Q8WUA8
J3QS45	P07602-1	P31689-1	P62910	Q8WUM4
J3QSF4	P07711	P31930	P62913	Q8WWI5
K7EM90	P07737	P31939	P62917	Q8WWZ8-1

K7EME0	P07814	P31943	P62937	Q8WZ75-1
K7EMR1	P07858	P31946	P62987	Q92522
K7ER96	P07864	P31948	P63000-1	Q92539
M0QY96	P07900	P31949	P63010-1	Q92542-1
M0QYW9	P07910-1	P32119	P63104-1	Q92598
M0R3F1	P07942	P32856	P63220	Q92599-1
N0E644	P07947	P32969	P63244	Q92608-1
O00154	P07996	P33527	P63267-1	Q92614-1
O00159-1	P08123	P34096	P67870	Q92616
O00186	P08133-1	P34897-1	P67936	Q92734-1
O00231	P08134	P34931	P68032	Q92743
O00232-1	P08174-1	P34932	P68104	Q92859
O00264	P08195	P35052	P68363	Q92887
O00299	P08238	P35080-1	P68366	Q92930
O00338	P08263	P35222	P68371	Q92954-5
O00391	P08572	P35232	P68400	Q92973-1
O00468-5	P08582-1	P35241-1	P69905	Q93088
O00468-6	P08670	P35268	P78371-1	Q93099
O00469-1	P08697-1	P35443	P78417	Q969H8
O00483	P08708	P35527	P78527	Q969X5
O00487	P08729	P35555	P80723	Q96AG4
O00560-1	P08754	P35556	P82909	Q96AX1
O00567	P08758	P35579-1	P83731	Q96BM9
O00571	P08779	P35580	P84095	Q96CW1
O00764-1	P08865	P35590	P84098	Q96DG6
O14672	P08962	P35659-1	P84103	Q96EU6-2
O14744	P09211	P35908	P84243	Q96F07
O14786-1	P09382	P35998	P98088	Q96FJ2
O14828	P09429	P36268	P98160	Q96FN4
O14949	P09486	P36507	P99999	Q96FW1
O14950	P09493-1	P36542-1	Q00325-1	Q96HC4
O14980	P09496-1	P36578	Q00610-1	Q96HU8
O15027-1	P09525	P36871-1	Q00796	Q96IJ6
O15027-4	P09543-1	P36955	Q00839	Q96IY4
O15031	P09622	P36957	Q01433-1	Q96KG7-1
O15067	P09651-1	P37802	Q01469	Q96N64
O15127	P09936	P38117	Q01518-1	Q96N76
O15230	P09972	P38606	Q01650	Q96QK1
O15305	P0C0L4-1	P38646	Q01813	Q96QV6
O15400	P0CG39	P39023	Q01955-1	Q96S97
O15427	P0DMV8	P39060-1	Q02241-1	Q99497
O15484	P10114	P39656	Q02388-1	Q99536

O43143	P10301	P40227-1	Q02413	Q99623
O43242	P10451-1	P40429	Q02543	Q99714-1
O43252	P10606	P40925	Q02818	Q99732
O43324-1	P10620	P40926	Q02878	Q99816
O43396	P10643	P40939	Q02978	Q99829
O43491-1	P10768	P41250	Q04721	Q99832
O43505	P10809	P41252	Q04756	Q9BS26
O43570	P10909-1	P42224-1	Q04837	Q9BSJ8
O43633	P11021	P42330	Q05193-1	Q9BUJ2-1
O43657	P11047	P42704	Q05639	Q9BV38
O43707	P11142-1	P42766	Q06033-1	Q9BVK6
O43747-1	P11166	P43034	Q06210-1	Q9BX79-1
O43795	P11169	P43243	Q06828	Q9BXS4
O60218	P11171-1	P43490	Q06830	Q9BYT8
O60462-1	P11233	P43652	Q07020	Q9C0G0
O60488-1	P11279	P43686	Q07021	Q9H078-1
O60610-1	P11362	P45880	Q07954	Q9H0E2
O60701	P11387	P46459	Q07955-1	Q9H0H5
O60716-1	P11413-1	P46531	Q08209-1	Q9H1E3
O60812	P11586	P46776	Q08211	Q9H2G4
O60814	P11717	P46777	Q08257	Q9H2U2
O60832-1	P11766	P46778	Q08380	Q9H361
O60841	P11908	P46779	Q08431	Q9H3N1
O60884	P12004	P46781	Q08722	Q9H3Z4
O60888-1	P12109	P46782	Q08945	Q9H4B7
O75083	P12110	P46783	Q09666-1	Q9H4F8
O75131	P12111	P46821	Q0IIM8	Q9H4G4
O75144-1	P12236	P46940	Q12797	Q9H4M9
O75179-1	P12259	P47755	Q12805	Q9H583
O75340	P12268	P48047	Q12841	Q9H6X2
O75351	P12429	P48059	Q12860	Q9H832
O75352	P12814-1	P48506	Q12907	Q9H8M2-1
O75367-1	P12931	P48509	Q12913-1	Q9H9B4
O75369-1	P12955	P48556	Q12931	Q9HB63-1
O75382-1	P12956	P48740-1	Q12965	Q9HBH0
O75390	P13473-1	P48740-2	Q13011	Q9HBI1-1
O75400	P13489	P49023	Q13057	Q9HC10
O75531	P13497	P49189	Q13103	Q9HC38
O75695	P13639	P49207	Q13162	Q9HCK1
O75746	P13645	P49327	Q13200	Q9HD45
O75751	P13647	P49368-1	Q13219	Q9HDC9
O75807	P13667	P49411	Q13418	Q9NP58

O75874	P13693	P49588	Q13428-1	Q9NPA0
O75891-1	P13797	P49591	Q13509	Q9NPH3
O75897	P13804-1	P49720	Q13595-1	Q9NQC3
O75955	P13929-1	P49721	Q13614-1	Q9NQH7-1
O76003	P13987	P49747	Q13642-1	Q9NR30-1
O94907	P14314	P49755	Q13748-1	Q9NRN5-1
O94925-1	P14550	P49773	Q13813	Q9NRP0-1
O95084	P14618	P49888	Q13885	Q9NUM4
O95197	P14625	P50395-1	Q14019	Q9NV96
O95297-1	P14923	P50443	Q14112-1	Q9NY33
O95373	P14927	P50454	Q14117	Q9NYH9
O95445-1	P15121	P50552	Q14126	Q9NYL9
O95497	P15151-1	P50914	Q14152	Q9NYU2-1
O95573	P15291	P50990	Q14160	Q9NZI8
O95782	P15311	P50991	Q14204	Q9NZM1
O95819	P15531	P50995	Q14240-1	Q9NZN3
O95994	P15559-1	P51148	Q14254	Q9NZN4
O96005-1	P15586	P51149	Q14332	Q9P035
P00338-1	P15880	P51570	Q14344	Q9P0L0
P00352	P15924-1	P51587	Q14515	Q9P0W5-1
P00367	P16070	P51659-1	Q14520-1	Q9P2B2
P00390	P16152	P51665	Q14533	Q9P2J5
P00403	P16401	P51674	Q14624-1	Q9UBG0
P00439	P16402	P51884	Q14697-1	Q9UBR2
P00450	P16435	P51957-3	Q14764	Q9UGM3-1
P00488	P16615	P51991-1	Q14847	Q9UHD8-1
P00505	P17301	P52209	Q14914	Q9UHN6-1
P00533-1	P17405-1	P52272	Q14974	Q9UHV9
P00558	P17655-1	P52815	Q14978-1	Q9UJZ1
P00734	P17812	P52895	Q14997	Q9UL25
P00738	P17844	P52907	Q15019	Q9ULV4
P00740	P17987	P53396-1	Q15029	Q9UM00-1
P00742	P18065	P53634-1	Q15046	Q9UM47
P00747	P18077	P53985	Q15063-1	Q9UMS4
P00966	P18084	P53990-1	Q15084-1	Q9UMY4-1
P01008	P18085	P53999	Q15102	Q9UNN8
P01023	P18124	P54289	Q15149-1	Q9UNP9-1
P01024	P18206	P54577	Q15185	Q9UPY5
P01031	P18428	P54578	Q15286	Q9Y223-1
P01042	P18621	P54652	Q15293	Q9Y230
P01116	P18669	P54709	Q15323	Q9Y240
P01266-1	P18848	P54920	Q15365	Q9Y265

P01591	P19022	P55010	Q15366-1	Q9Y277
P01834	P19338	P55011	Q15404-1	Q9Y2A7-1
P01857	P19440	P55058	Q15493-1	Q9Y2G3
P02042	P19823	P55072	Q15582	Q9Y315
P02452	P19827-1	P55083	Q15758-1	Q9Y3B3-1
P02458-1	P20020	P55209	Q15836	Q9Y490
P02461	P20073-1	P55263-1	Q15907	Q9Y4K0
P02462	P20618	P55290	Q15942	Q9Y512
P02533	P20645	P55884	Q16181	Q9Y617-1
P02545	P20674	P56537-1	Q16394	Q9Y624
P02647	P20742	P56539	Q16555-1	Q9Y678
P02649	P20774	P57721-1	Q16563	Q9Y694-1
P02656	P20908	P58397	Q16610	Q9Y696
P02671-1	P21291	P59190-1	Q16658	Q9Y6C9
P02675	P21333	P59998	Q16719	Q9Y6M5
P02679	P21399	P60033	Q16777	

Table S 5*. Raw list of proteins found at least once with a high quality peptide match identified in at least one sample of WI-38 cells.*

Protein ID	**Protein ID**	**Protein ID**	**Protein ID**	**Protein ID**
A0A087WUV5	P09936	P53621-1	Q16775	Q99961
A0A087WWG1	P09960-1	P53634-1	Q16777	Q9BPX3
A0A087WYT5	P09972	P53677	Q16822	Q9BPX5
A0A087X295	P0C7P4	P53801	Q16850-1	Q9BPX7
A0A0A0MR09	P0C7V8	P53814-1	Q16851	Q9BQ39
A0A0A0MRF6	P0CG12	P53985	Q16881-1	Q9BQ51-1
A0A0A0MSK5	P0DJG4	P53992	Q16891	Q9BQ67
A0A0A0MT64	P0DMV8	P53999	Q1KMD3	Q9BQ70
A0A0A0MTQ5	P10109	P54105	Q27J81	Q9BQA1
A0A0C4DGA7	P10253	P54136-1	Q2M2I8-1	Q9BQB6-1
A0A0C4DH46	P10301	P54259	Q2TAA2	Q9BQE3
A0A0U1RQK7	P10319	P54289	Q32MZ4-2	Q9BQE5
A0A1W2PNV4	P10515	P54577	Q32MZ4-4	Q9BQG0
A0A1W2PQF8	P10599-1	P54578	Q32P28-1	Q9BQS8
A0A1W2PRK2	P10606	P54652	Q3KQU3	Q9BR61
A0A2R8Y4M1	P10619	P54687	Q3KQV9	Q9BR76
A0A2R8YE10	P10644	P54725-1	Q3LI59	Q9BRA2
A0A2R8YFE2	P10768	P54727	Q3LXA3	Q9BRF8-1
A0A2R8YH03	P10809	P54764	Q3MHD2	Q9BRJ2
A0A3B3ITJ4	P10909-1	P54819	Q3YEC7-1	Q9BRP1

A0A3B3ITX4	P11021	P54886	Q4G0F5	Q9BRP8
A0A3B3IU69	P11047	P54920	Q4J6C6	Q9BRR6-1
A0AVT1-1	P11142-1	P55010	Q4L180	Q9BRX2
A0FGR8-1	P11166	P55036-1	Q52LJ0	Q9BRZ2-1
A0MZ66	P11171-1	P55060-1	Q53EP0	Q9BS26
A1X283	P11177	P55072	Q53FA7-1	Q9BSC4-1
A2RRP1-1	P11216	P55084	Q53GQ0	Q9BSD7
A5YKK6	P11279	P55145	Q53GS9	Q9BSJ2-1
A6NDG6	P11362-16	P55209	Q53H82	Q9BSJ8
A6NEC2	P11387	P55263-1	Q53H96	Q9BT78
A6NHR9-1	P11388-1	P55265-1	Q53SF7-1	Q9BTC0-1
A6NKD9	P11413-1	P55268	Q53T59	Q9BTE1
A7XZE4	P11586	P55735-1	Q53TN4	Q9BTE3-1
A8CG34	P11717	P55769	Q562R1	Q9BTE6-1
B4DY09	P11766	P55809	Q567U6	Q9BTT0
B5MCF9	P11802	P55884	Q58FG1	Q9BTU6
B5ME19	P11940-1	P55957-1	Q5BKZ1	Q9BTV4
C9IZG4	P12004	P56181-2	Q5EBL4-1	Q9BTW9
C9JE98	P12081	P56182	Q5GLZ8-1	Q9BTY7
C9JM79	P12109	P56192	Q5H9L2	Q9BTZ2
C9JRD2	P12110	P56199	Q5H9R7-1	Q9BU23-1
C9JRJ5	P12111	P56211	Q5HYI8	Q9BUF5
D6R992	P12236	P56377	Q5JRA6-1	Q9BUH6
D6RBW3	P12268	P56385	Q5JRX3	Q9BUJ2-1
D6REX3	P12270	P56537-1	Q5JSH3	Q9BUL5-1
D6RHI9	P12277	P56539	Q5JTD0-1	Q9BUL8
E5RHC1	P12814-1	P56545	Q5JTJ3-1	Q9BUQ8
E5RHF2	P12955	P56945	Q5JVS0	Q9BUT1-1
E5RHL7	P12956	P57088	Q5JWF2-1	Q9BV20-1
E5RK69	P13010	P57740	Q5JXB2	Q9BV38
E7EQB8	P13073	P57764	Q5QJE6	Q9BV44
E7EVJ3	P13473-1	P57772	Q5RGS4	Q9BV81
E9PGT6	P13489	P58004	Q5SRE5	Q9BV86-1
E9PHY5	P13639	P58546	Q5SSJ5-1	Q9BVC6
E9PMS6	P13645	P59998	Q5SW79-1	Q9BVK6
E9PS63	P13647	P60033	Q5SXM8	Q9BVP2
F1T0I1	P13667	P60174-1	Q5T0W9	Q9BW27
F2Z2J1	P13674-1	P60228	Q5T1J5	Q9BW60
F5H479	P13693	P60468	Q5T1M5	Q9BWD1

F6TB26	P13797	P60660	Q5T200-1	Q9BWJ5
F8WAN1	P13798	P60709	Q5T447	Q9BX95
F8WCJ7	P13804-1	P60842	Q5T4B2-1	Q9BXB4
G3V1R5	P13861	P60866	Q5T4S7-1	Q9BXF6
G5E9Z2	P13987	P60891	Q5T4U5	Q9BXI6
G5EA48	P14174	P60900	Q5T653	Q9BXJ9
H0Y3N9	P14324	P60903	Q5T6F2	Q9BXP5
H0Y3T6	P14550	P60953	Q5T8D3-3	Q9BXS5-1
H0Y5B0	P14618	P60981-1	Q5T9L3	Q9BXX3
H0Y7B8	P14618-2	P60983	Q5TAH2	Q9BY43
H0YA82	P14625	P61006	Q5TAP6	Q9BY44-1
H0YB16	P14678-1	P61009	Q5TCZ1	Q9BY77
H0YBW4	P14854	P61011-1	Q5TFE4	Q9BYM8
H0YHW7	P14868	P61019-1	Q5TFQ8	Q9BYN0
H0YIV0	P15121	P61026	Q5VT25-1	Q9BYV8
H0YJV4	P15144	P61077-1	Q5VY43	Q9BZE4
H0YL43	P15151-1	P61081	Q5VYK3	Q9BZF9
H0YL68	P15153	P61158	Q5VYS8-1	Q9BZG1
H0YNJ0	P15170-3	P61160-1	Q5VZE5	Q9BZK3
H3BMM9	P15311	P61163	Q5VZL5	Q9BZL4
H3BND8	P15374	P61204	Q63HN8-4	Q9BZQ8
H3BUZ5	P15407	P61218	Q63HR2	Q9BZV1
H7BZJ3	P15531	P61221	Q63ZY3-1	Q9BZX2-1
H7BZT7	P15559-1	P61247	Q66K14-1	Q9BZZ5-4
H7C0S8	P15586	P61254	Q66K74	Q9C005
H7C2X7	P15880	P61289-1	Q68CQ4	Q9C0C2
H7C543	P16070	P61313-1	Q68CZ2-1	Q9C0C9
H7C5J7	P16104	P61353	Q68D10-1	Q9C0D5
I3L124	P16152	P61421	Q68EM7	Q9C0E8-1
I3L4I0	P16278	P61513	Q6AI12	Q9C0H2-1
J3KRH6	P16333-1	P61586	Q6DD88	Q9GZM8-1
J3QLH3	P16401	P61587	Q6DKJ4	Q9GZR2-1
J3QSF4	P16402	P61604	Q6EMK4	Q9GZR7
J3QTA6	P16435	P61758	Q6FI81-1	Q9GZS3
K7EIT2	P16615	P61764	Q6FIF0	Q9GZT3-1
K7ELL7	P16930	P61769	Q6GMV3	Q9GZT8-1
K7EM38	P16949-1	P61916	Q6IAN0	Q9GZT9-1
K7EMM8	P16989-1	P61923	Q6IBS0	Q9GZZ1-1
M0QZM1	P17050	P61927	Q6IQ22	Q9GZZ9-1

M0R0U0	P17096-1	P61956	Q6L8Q7-1	Q9H074
M0R1B0	P17096-2	P61970	Q6NUK1	Q9H098
O00115	P17174	P61978	Q6NUS6	Q9H0A0
O00116	P17252	P61981	Q6NVV1	Q9H0D6-1
O00139-2	P17301	P62081	Q6NXE6-1	Q9H0E3
O00148	P17302	P62136-1	Q6NYC8	Q9H0I9
O00151	P17405-1	P62140	Q6NZ67	Q9H0M0-1
O00154	P17480-1	P62158	Q6NZI2-1	Q9H0Q0
O00159-1	P17612	P62191	Q6NZY4	Q9H0U4
O00178	P17655-1	P62195-1	Q6P158-1	Q9H1B7
O00186	P17812	P62241	Q6P1J9	Q9H1E3
O00189	P17813	P62244	Q6P1N0	Q9H1E5
O00193	P17844	P62249	Q6P1X6	Q9H1I8-1
O00203-1	P17858-1	P62258-1	Q6P2E9-1	Q9H1Z4
O00214-1	P17900	P62263	Q6P2Q9	Q9H223
O00231	P17931	P62266	Q6P2S7	Q9H267
O00233-1	P17936	P62269	Q6P3W7	Q9H270
O00244	P17980	P62273-1	Q6P587-1	Q9H299
O00264	P17987	P62277	Q6P5R6	Q9H2D6
O00267	P18031	P62280	Q6P9B6	Q9H2G2-1
O00273-1	P18077	P62304	Q6PGP7	Q9H2J4
O00291	P18085	P62306	Q6PIU2	Q9H2K8
O00299	P18124	P62316	Q6PJG6-1	Q9H2M9
O00303	P18206	P62318	Q6PJT7-1	Q9H2P0
O00391	P18583-1	P62328	Q6PKG0-1	Q9H2U1
O00410	P18615	P62333	Q6QNY0	Q9H2V7
O00422	P18621	P62424	Q6RW13	Q9H2W6
O00425	P18669	P62491-1	Q6UB35-1	Q9H3F6-1
O00468-5	P18887	P62495	Q6UN15-1	Q9H3H3
O00469-1	P19338	P62633-1	Q6UUV7-1	Q9H3K6-1
O00487	P19367-1	P62701	Q6UVK1	Q9H3N1
O00488	P19388	P62750	Q6UW63	Q9H3P7
O00499	P19474	P62753	Q6UXH8-1	Q9H3S7
O00560-1	P19623	P62805	Q6VY07	Q9H3U1
O00562	P19784	P62820	Q6WCQ1	Q9H3U5
O00567	P19878	P62826	Q6XE24	Q9H3Z4
O00570	P20042	P62829	Q6XQN6-1	Q9H444
O00571	P20073-1	P62834	Q6XZF7	Q9H479
O00622	P20290-2	P62841	Q6Y7W6-1	Q9H4A3

O14497	P20340-1	P62847-1	Q6YN16	Q9H4A4
O14545	P20618	P62851	Q6YP21	Q9H4G4
O14558	P20674	P62854	Q6ZN50	Q9H4I3-1
O14562	P20700	P62857	Q6ZN55-1	Q9H4L4
O14579-1	P20810-6	P62861	Q6ZS17	Q9H4L5
O14617-1	P20908	P62873	Q6ZSJ8	Q9H4M9
O14618	P20933	P62879	Q6ZSR9	Q9H501
O14639-1	P20962	P62888	Q6ZUT6-1	Q9H583
O14647	P21266	P62899	Q6ZVK8	Q9H5N1
O14727	P21281	P62906	Q6ZVM7	Q9H5X1
O14744	P21283	P62910	Q6ZW31-1	Q9H6B4
O14757	P21291	P62913	Q709C8	Q9H6R4-1
O14776-1	P21333	P62917	Q70E73	Q9H6S3
O14777	P21399	P62937	Q70UQ0-4	Q9H6X2
O14818-1	P21589-1	P62942	Q71RC2	Q9H6Z4
O14828	P21675	P62979	Q71U36	Q9H7B2
O14879	P21796	P62993	Q71UI9-1	Q9H7C4-1
O14908-1	P21810	P63000-1	Q71UM5	Q9H7C9-1
O14936	P21912	P63010-1	Q7KZF4	Q9H7E9-1
O14950	P21926	P63104-1	Q7L014	Q9H7F0-1
O14964	P21964-1	P63165-1	Q7L1Q6-1	Q9H832
O14974	P21980	P63167	Q7L2J0-1	Q9H8Y8-1
O14976	P22061	P63172	Q7L576-1	Q9H910-1
O14979-1	P22087	P63173	Q7L7X3	Q9H939-1
O14981	P22102-1	P63208	Q7L8J4	Q9H944
O15027-4	P22234	P63218	Q7L9L4	Q9H992
O15031	P22307-1	P63220	Q7LBR1	Q9H9A6
O15042	P22314	P63241-1	Q7RTV0	Q9H9B1
O15056	P22392	P63244	Q7Z2W4	Q9H9B4
O15061-1	P22626	P63267-1	Q7Z392	Q9H9J2
O15066	P22681	P63272	Q7Z3E5-2	Q9H9Q2
O15067	P22695	P63279	Q7Z3Z0	Q9H9S5
O15085-1	P22830-1	P63313	Q7Z417	Q9HA38-1
O15126-1	P23193	P67809	Q7Z460-1	Q9HA65
O15127	P23219	P67870	Q7Z478	Q9HA77
O15143	P23229-1	P67936	Q7Z4G1-1	Q9HAB3
O15144	P23246-1	P67936-2	Q7Z4H3-1	Q9HAN9
O15145	P23258	P68036	Q7Z4H8	Q9HAU4
O15160	P23284	P68104	Q7Z4I7-1	Q9HAV4

O15173	P23381	P68366	Q7Z4V5	Q9HAV7
O15212	P23396-1	P68371	Q7Z4W1	Q9HB07
O15231-1	P23497	P68402-1	Q7Z6J0-1	Q9HB71
O15260-1	P23526-1	P69905	Q7Z6M1-1	Q9HBL0
O15270	P23528	P78318	Q7Z6Z7	Q9HC07
O15294	P23588	P78344-1	Q7Z739	Q9HC38
O15305	P23634-1	P78347	Q7Z7K6-1	Q9HCC0-1
O15347	P23743-1	P78356	Q7Z7M9	Q9HCD5
O15355	P23921	P78357	Q86SE5-1	Q9HCD6-1
O15357	P24534	P78362-1	Q86T03-1	Q9HCE1
O15371	P24593	P78371-1	Q86TB9	Q9HCN8
O15372	P24752	P78406	Q86TC9-1	Q9HCU0
O15427	P24844-1	P78417	Q86TS9-1	Q9HD15
O15446-1	P25054-1	P78527	Q86TX2	Q9HD20
O15460-1	P25205	P78537	Q86U42-1	Q9HD26-1
O15484	P25325	P78559-1	Q86UE4	Q9HD33-1
O15504	P25398	P78563-1	Q86UP2-1	Q9HD42-1
O15511-1	P25685	P80723	Q86UU1-2	Q9HD45
O15530-1	P25705-1	P82094	Q86V48-1	Q9HDC9
O15533-1	P25786-1	P82909	Q86V81	Q9NP77
O43143	P25787	P82979	Q86VM9	Q9NP79
O43175	P25788-1	P83731	Q86VP6-1	Q9NPD3
O43237	P25789	P83881	Q86VQ1	Q9NPE3
O43242	P26006	P84090	Q86VS8	Q9NPF4
O43251-1	P26038	P84095	Q86WN1-1	Q9NPJ6-1
O43252	P26368	P84098	Q86WV6	Q9NQ92
O43290	P26373-1	P84103	Q86X27-1	Q9NQA3
O43294-1	P26440	P84157-1	Q86X55	Q9NQC3
O43314-1	P26447	P84243	Q86X83	Q9NQG5
O43324-1	P26572	P85037-1	Q86XL3-1	Q9NQH7-1
O43353-1	P26583	P98082	Q86XP3-1	Q9NQR4
O43390-1	P26599	P98160	Q86XZ4	Q9NQT4
O43396	P26639-1	P98172	Q86Y56	Q9NQW6
O43399	P26640	P98175-1	Q86Y82	Q9NQW7-1
O43488	P26641	P98179	Q86YD1-1	Q9NQX3
O43516-1	P26885	P98194-1	Q86YP4	Q9NQX4
O43520	P27105	P99999	Q86YR5-1	Q9NR09
O43583	P27348	Q00325-1	Q86YV9	Q9NR12-1
O43615	P27361-1	Q00341-1	Q8IV08	Q9NR28-1

O43633	P27635	Q00587-1	Q8IVF2-1	Q9NR30-1
O43665	P27694	Q00610-1	Q8IVH8	Q9NR45
O43676	P27695	Q00653-1	Q8IVL5	Q9NR46
O43678	P27707	Q00688	Q8IVL6-1	Q9NR50-1
O43681	P27708	Q00765	Q8IVM0	Q9NR56-1
O43684	P27797	Q00796	Q8IWA5	Q9NRA2
O43707	P27816-1	Q00839	Q8IWE2	Q9NRL3
O43719	P27824	Q00872	Q8IWJ2	Q9NRV9
O43747-1	P28066-1	Q01082-1	Q8IWR0	Q9NRX2
O43765	P28070	Q01085	Q8IWZ3	Q9NRX4
O43795	P28072	Q01105	Q8IWZ6	Q9NRY5
O43813	P28074-1	Q01130	Q8IWZ8-1	Q9NRY6
O43815	P28290	Q01433-1	Q8IX01-1	Q9NS69
O43837-1	P28300	Q01469	Q8IX12	Q9NS86
O43852	P28331-1	Q01518-1	Q8IXB1-1	Q9NSD9
O43854-1	P28482	Q01650	Q8IXI2-1	Q9NSE4
O43896	P28799	Q01658	Q8IXJ6	Q9NSY0-3
O60218	P28838	Q01813	Q8IXL7	Q9NSY1
O60264	P29144	Q01955-1	Q8IXQ4	Q9NT62
O60271	P29218-1	Q01968-1	Q8IY63-1	Q9NTJ5
O60353-1	P29317	Q01970-1	Q8IY81	Q9NTK5-1
O60443	P29323	Q01995	Q8IY95	Q9NTZ6
O60488-1	P29353	Q02543	Q8IYD1	Q9NUL3
O60493-1	P29401	Q02790	Q8IYI6	Q9NUM4
O60502	P29466-1	Q02809	Q8IYL3	Q9NUP9
O60524	P29536-1	Q02818	Q8IYS2-1	Q9NUQ6
O60547-1	P29558-1	Q02878	Q8IZ07	Q9NUY8
O60551	P29590	Q02952-1	Q8IZ21-1	Q9NV70-1
O60565	P29692	Q03001-7	Q8IZ73	Q9NV92
O60568	P29692-3	Q03252	Q8IZD4	Q9NV96
O60610-1	P29966	Q03721-1	Q8IZL8	Q9NVA2-1
O60664-1	P29992	Q04206	Q8IZP0	Q9NVD7
O60678	P30040-1	Q04323-1	Q8IZP2	Q9NVE7
O60684	P30041	Q04446	Q8N0X7	Q9NVG8
O60701	P30042-1	Q04637	Q8N122	Q9NVJ2
O60716-1	P30043	Q04760-1	Q8N163-1	Q9NVM1
O60749	P30044-1	Q04828	Q8N1F7-1	Q9NVN3-1
O60762	P30048	Q04837	Q8N1F8	Q9NVU0
O60763-1	P30049	Q04917	Q8N1G4	Q9NVZ3

O60783	P30050-1	Q04941-1	Q8N2K0	Q9NW13-1
O60784	P30084	Q05519	Q8N335	Q9NW15-1
O60814	P30085-1	Q05682-4	Q8N392-1	Q9NW82
O60826	P30086	Q05682-6	Q8N3D4	Q9NWH9-1
O60828	P30101	Q06124	Q8N3F8	Q9NWK9
O60831	P30153	Q06210-1	Q8N3V7-2	Q9NWS0-1
O60832-1	P30419	Q06323-1	Q8N4C8-1	Q9NWV8
O60841	P30520	Q06830	Q8N4L2	Q9NWY4
O60869-1	P30530	Q07020	Q8N556-1	Q9NWZ3-1
O60884	P30533	Q07021	Q8N5N7	Q9NX05-1
O60907	P30566	Q07065	Q8N668	Q9NX14-1
O60925	P30622-1	Q07157	Q8N684-1	Q9NX24
O75083	P30626-1	Q07352	Q8N6H7	Q9NX40
O60925	P30520	Q07666	Q8N6M0	Q9NX46
O75083	P30530	Q07812	Q8N6T3-1	Q9NXG2
O75116	P30533	Q07817-1	Q8N6Y2-1	Q9NXV6
O75131	P30566	Q07866-1	Q8N766-1	Q9NXW2
O75153	P30622-1	Q07954	Q8N983	Q9NY33
O75157	P30626-1	Q07955-1	Q8N9I9-1	Q9NY93
O75165	P30837	Q07960	Q8N9N8	Q9NYB9
O75179-1	P30838	Q08170	Q8NAF0	Q9NYF8-1
O75312	P30876	Q08211	Q8NAX2	Q9NYJ8-1
O75347	P31040	Q08257	Q8NBF2-1	Q9NYK1
O75348	P31146	Q08345-1	Q8NBJ5	Q9NYL2-2
O75351	P31150	Q08378	Q8NBJ7-1	Q9NYL9
O75367-1	P31153	Q08379	Q8NBK3	Q9NYU2-1
O75368	P31350-1	Q08623	Q8NBS9-1	Q9NZ08-1
O75369-1	P31689-1	Q08722	Q8NC51-1	Q9NZ32
O75376-1	P31930	Q08752	Q8NCN4	Q9NZ52-3
O75379-1	P31937	Q08945	Q8NCW5	Q9NZ56
O75380	P31939	Q08AD1	Q8ND76	Q9NZB2-1
O75390	P31942	Q08AE8-1	Q8NDH3	Q9NZI8
O75396	P31943	Q08AM6	Q8NDI1	Q9NZL9
O75400	P31946	Q08J23	Q8NDV7	Q9NZM1
O75410-1	P31947-1	Q09328	Q8NE71-1	Q9NZM5
O75427	P31948	Q09666-1	Q8NE86	Q9NZN4
O75436-1	P31949	Q0IIM8	Q8NEU8-1	Q9NZT2-1
O75439	P32119	Q0ZGT2	Q8NEZ2	Q9NZU5
O75508	P32321	Q10471	Q8NF91	Q9NZZ3

O75531	P32322	Q10567	Q8NFD5	Q9P013
O75533-1	P32455	Q10713	Q8NFF5	Q9P0J7
O75534	P32969	Q12765	Q8NFH5	Q9P0K7-1
O75569-1	P33121	Q12769	Q8NFQ8	Q9P0M6
O75608	P33176	Q12792-2	Q8NFW8	Q9P0P0
O75643-1	P33240	Q12797	Q8NHH9	Q9P0V3-1
O75663	P33316-2	Q12841	Q8NHP8	Q9P1Q0
O75683	P33402	Q12846	Q8NHS3	Q9P246
O75694	P33897	Q12849	Q8NHV4	Q9P258
O75718	P33991	Q12873-1	Q8NI22	Q9P266
O75821	P33992	Q12874	Q8TAA9	Q9P270
O75822	P33993-1	Q12884-1	Q8TAD7	Q9P299
O75828	P34897-1	Q12888-1	Q8TAE8	Q9P2D3-1
O75832	P34932	Q12904-1	Q8TAQ2	Q9P2E9-1
O75844	P35052	Q12906-1	Q8TAT6-1	Q9P2E9-3
O75874	P35080-2	Q12907	Q8TB52	Q9P2J5
O75880	P35221	Q12929	Q8TB61	Q9P2N6
O75937	P35222	Q12931	Q8TBC4-1	Q9P2R3
O75940	P35232	Q12965	Q8TBX8-1	Q9P2R7
O75947-1	P35241-1	Q12972-1	Q8TC07-1	Q9P2T1-1
O75955	P35268	Q12974	Q8TC12	Q9P2X0-1
O75962-1	P35270	Q13017-1	Q8TCJ2	Q9P2X3
O76003	P35520-1	Q13033	Q8TCS8	Q9UBB4-1
O76021	P35527	Q13045-1	Q8TCT9-1	Q9UBB6
O76024	P35555	Q13049	Q8TD16	Q9UBB9-1
O76061	P35579-1	Q13057	Q8TD19	Q9UBC2-1
O76071	P35580	Q13098-7	Q8TD43-1	Q9UBE0-1
O76074	P35606	Q13123	Q8TD55	Q9UBG0
O76094	P35611-1	Q13131	Q8TDB4	Q9UBM7
O76095-1	P35613	Q13136	Q8TDD1	Q9UBN7-1
O94760-1	P35626	Q13151	Q8TDN6	Q9UBP4
O94776	P35637-1	Q13155	Q8TDZ2	Q9UBQ0
O94808	P35658-1	Q13162	Q8TEA8	Q9UBQ5
O94826	P35659-1	Q13177	Q8TED1	Q9UBQ7
O94842	P35813	Q13200	Q8TEX9-1	Q9UBR2
O94855	P35858-2	Q13217	Q8TF05	Q9UBS4
O94874-1	P35908	Q13243-1	Q8TF72	Q9UBS8-1
O94888	P35914	Q13247	Q8TF74	Q9UBT2
O94903	P35998	Q13263	Q8WTS6	Q9UBT6

O94905-1	P36021	Q13283	Q8WU79-1	Q9UBU9-1
O94919	P36507	Q13308-1	Q8WU90	Q9UDT6-1
O94925-3	P36542-1	Q13310	Q8WUA7	Q9UDY2
O94973	P36543	Q13330-1	Q8WUD1	Q9UDY4
O95140	P36551	Q13347	Q8WUH6	Q9UEE5
O95155	P36578	Q13356	Q8WUM4	Q9UER7-1
O95159	P36776	Q13363-1	Q8WUP2	Q9UEY8-1
O95168-1	P36871-1	Q13371	Q8WUQ7	Q9UG63
O95182	P36915-1	Q13409-7	Q8WUW1	Q9UGI8
O95183	P36957	Q13418	Q8WVM8	Q9UGR2-2
O95197	P37108	Q13422-2	Q8WVY7	Q9UGV2
O95208-1	P37268	Q13423	Q8WW01	Q9UH65
O95218-1	P37802	Q13425-1	Q8WW12	Q9UHB6
O95232-1	P37837	Q13428-1	Q8WWI1-3	Q9UHB9
O95249-1	P38117	Q13435	Q8WWM7-1	Q9UHD1
O95260	P38159-1	Q13438-7	Q8WWQ0	Q9UHD2
O95292	P38606	Q13439-1	Q8WWY3	Q9UHD8-1
O95297-1	P38646	Q13442	Q8WX93-1	Q9UHD9
O95302	P38919	Q13443	Q8WXF1	Q9UHJ6
O95336	P38936	Q13444	Q8WXI9	Q9UHN6-1
O95340	P39019	Q13492-1	Q8WYP3	Q9UHQ9
O95347-1	P39023	Q13501-1	Q8WZ82	Q9UHV9
O95352	P39656	Q13510	Q8WZA9	Q9UHX1-1
O95372	P39687	Q13523	Q92499	Q9UHY1
O95373	P40121	Q13557-10	Q92508	Q9UI10-1
O95394	P40123	Q13561-1	Q92520	Q9UI12-1
O95400	P40222	Q13563	Q92522	Q9UI42-1
O95425	P40227-1	Q13564-1	Q92538	Q9UIA9
O95433	P40261	Q13573	Q92567	Q9UID3-1
O95453	P40763	Q13586	Q92572	Q9UIG0
O95456	P40855-1	Q13596	Q92574-1	Q9UIJ7-1
O95479	P40925	Q13610	Q92597	Q9UJ70
O95487-1	P40926	Q13616	Q92598	Q9UJ99
O95571	P40939	Q13617-1	Q92614-1	Q9UJS0
O95573	P41091	Q13618	Q92616	Q9UJU6-1
O95633	P41208	Q13619-1	Q92621	Q9UJW0-1
O95671-1	P41214	Q13620-1	Q92626	Q9UJX4
O95674-1	P41227-1	Q13630	Q92686	Q9UJY1
O95696	P41236	Q13637	Q92692-1	Q9UJZ1

O95714	P41240	Q13641	Q92696	Q9UK41-1
O95721	P41250	Q13642	Q92734-1	Q9UK45
O95747	P41252	Q13685	Q92783	Q9UK76
O95757	P42166	Q13724-1	Q92785	Q9UKG1
O95782	P42224-1	Q13765-1	Q92820	Q9UKI2
O95785	P42285	Q13813	Q92839	Q9UKK3
O95793	P42345	Q13823	Q92841-1	Q9UKK9
O95801	P42356	Q13838-1	Q92859	Q9UKM9-1
O95810	P42574	Q13868	Q92871	Q9UKV3-1
O95816	P42677	Q13884	Q92879	Q9UKV8
O95817	P42696	Q13885	Q92888-1	Q9UKX7
O95819	P42704	Q13951	Q92890-1	Q9UKY7
O95825-1	P42765	Q13952-1	Q92896	Q9UL25
O95831-1	P42766	Q13976	Q92900	Q9UL46
O95861-1	P42768	Q14008	Q92917	Q9ULA0
O95865	P43034	Q14011	Q92930	Q9ULC4-1
O95881	P43121	Q14012	Q92945	Q9ULD0
O95980	P43243	Q14019	Q92973-1	Q9ULD4
O95989	P43246-1	Q14103	Q92974	Q9ULH1-1
O96005-1	P43304	Q14108-1	Q92979	Q9ULP9
O96019-1	P43487	Q14137	Q92995	Q9ULR0-1
P00167-1	P43490	Q14139	Q93008-1	Q9ULT8
P00338-1	P43686	Q14152	Q93050-1	Q9ULU4-13
P00352	P45880	Q14157-5	Q93052	Q9ULV4
P00367	P45954	Q14161-1	Q93062-1	Q9ULW0
P00374	P45973	Q14165	Q969E2-1	Q9UM54-6
P00387	P45974-1	Q14192	Q969G5	Q9UMR2-1
P00390	P46060	Q14195-1	Q969H8	Q9UMS4
P00441	P46063	Q14202	Q969M3	Q9UMX0-1
P00505	P46087	Q14203	Q969N2	Q9UMY1-1
P00533-1	P46108-1	Q14204	Q969T9	Q9UMY4-1
P00558	P46109	Q14232	Q969V3	Q9UN37
P00568	P46379-1	Q14240-1	Q969V6	Q9UN86
P00750-1	P46439	Q14247-1	Q969X5	Q9UNE7-1
P01023	P46459	Q14254	Q96A35	Q9UNF0
P01112	P46734-1	Q14257	Q96A49	Q9UNF1
P01116	P46776	Q14258	Q96A57	Q9UNH7-1
P01614	P46777	Q14315	Q96A65	Q9UNM6
P01834	P46778	Q14393-1	Q96AC1	Q9UNN5-1

P01857	P46779	Q14444-1	Q96AE4	Q9UNS2
P01859	P46781	Q14498-1	Q96AG3	Q9UNW1
P01892	P46782	Q14517	Q96AG4	Q9UNZ2
P02452	P46783	Q14533	Q96AY3	Q9UP83-1
P02461	P46821	Q14554	Q96B36	Q9UPN3
P02533	P46934	Q14644	Q96B54	Q9UPU5
P02545	P46937-1	Q14651	Q96B97-1	Q9UPY5
P02751	P46939	Q14669-1	Q96BJ3-1	Q9UPZ6
P02768-1	P46940	Q14677-1	Q96BY6-1	Q9UQ35
P02786	P46976-1	Q14678-1	Q96C01	Q9UQ80
P02787	P47756-2	Q14683	Q96C03-2	Q9UQ88-1
P02795	P47813	Q14684	Q96C19	Q9UQB8
P03956	P47897	Q14690	Q96C23	Q9UQE7
P04040	P47914	Q14692	Q96C57	Q9Y223-1
P04075	P48047	Q14694	Q96C86	Q9Y224
P04080	P48059-3	Q14696	Q96C90	Q9Y230
P04083	P48147	Q14697-1	Q96CG8	Q9Y240
P04114	P48163	Q14699	Q96CT7	Q9Y262
P04156-1	P48444	Q14764	Q96CV9	Q9Y263
P04179-4	P48449-1	Q14766-1	Q96CW1	Q9Y265
P04181-1	P48506	Q14767	Q96CX2	Q9Y266
P04259	P48509	Q14789	Q96D15	Q9Y277
P04264	P48556	Q147X3	Q96D46	Q9Y281-1
P04406-1	P48634-1	Q14839	Q96EC8-1	Q9Y285
P04632	P48637	Q14847	Q96EM0	Q9Y294
P04732-1	P48643	Q14914	Q96EP5	Q9Y295
P04792	P48681	Q14966-1	Q96F45	Q9Y2A7-1
P04843	P48723	Q14974	Q96FW1	Q9Y2B0
P04844-1	P48735	Q14978-1	Q96FZ7	Q9Y2B9
P04899-1	P48739	Q14980-1	Q96G03	Q9Y2D5
P05023	P49006	Q14C86-1	Q96G23	Q9Y2G9
P05026	P49023	Q15004-1	Q96G46	Q9Y2H5
P05067-1	P49137	Q15006	Q96GD0	Q9Y2H6
P05091	P49189	Q15007	Q96GK7	Q9Y2J2
P05114	P49207	Q15008	Q96GP6	Q9Y2K2
P05120	P49257	Q15018	Q96GS4	Q9Y2L1-1
P05121-1	P49321	Q15019	Q96GY0	Q9Y2Q3-1
P05141	P49327	Q15020	Q96HC4	Q9Y2Q9
P05198	P49368-1	Q15021	Q96HE7	Q9Y2S6

P05204	P49411	Q15029	Q96HY6-1	Q9Y2V2
P05362	P49419	Q15035	Q96I24-1	Q9Y2W1
P05386	P49458	Q15042-1	Q96I99-1	Q9Y2W2
P05387	P49585	Q15046	Q96II8-1	Q9Y2X3
P05388	P49588	Q15052	Q96IJ6	Q9Y2Y0
P05455	P49589-1	Q15056-1	Q96IZ0	Q9Y2Z0-1
P05556-1	P49591	Q15057	Q96J02	Q9Y305-1
P05783	P49720	Q15070-1	Q96J84-1	Q9Y314
P05787	P49721	Q15075	Q96JD6-1	Q9Y320
P05997	P49736	Q15084-1	Q96JH7	Q9Y333
P06132	P49748-1	Q15102	Q96JJ3	Q9Y371
P06396-2	P49750-1	Q15113	Q96JJ7-1	Q9Y376
P06454-1	P49756-1	Q15121	Q96JY6-1	Q9Y383
P06493	P49770	Q15126	Q96K17-1	Q9Y388
P06576	P49773	Q15149-1	Q96KG9	Q9Y399
P06703	P49790	Q15149-2	Q96KP4	Q9Y3A5
P06733-1	P49792	Q15149-4	Q96KR1	Q9Y3A6-1
P06737-1	P49810-1	Q15154-1	Q96L92	Q9Y3B2
P06744	P49821	Q15155	Q96L96	Q9Y3B4
P06748	P49841-1	Q15181	Q96LJ7	Q9Y3B8-1
P06753	P49903-1	Q15185	Q96M96-1	Q9Y3C1
P06753-2	P49915	Q15233	Q96ME1	Q9Y3D0
P06756	P50213-1	Q15257-1	Q96MW1	Q9Y3D6
P07195	P50281	Q15274	Q96MW5	Q9Y3E1
P07237	P50336	Q15276	Q96MX6	Q9Y3E5
P07305	P50395-1	Q15293	Q96N66-1	Q9Y3E7
P07339	P50402	Q15303	Q96N67	Q9Y3F4
P07355	P50416	Q15334	Q96P47	Q9Y3I0
P07384	P50454	Q15365	Q96PD2-1	Q9Y3L3-1
P07437	P50479-1	Q15366-1	Q96PE2	Q9Y3T9
P07585	P50552	Q15369-1	Q96PK6-1	Q9Y3U8
P07602-1	P50570-2	Q15393-1	Q96PK6-5	Q9Y3X0
P07686	P50579	Q15404-1	Q96PR1	Q9Y3Y2
P07711	P50613	Q15417	Q96PU5	Q9Y450-1
P07737	P50750	Q15424-1	Q96PU8	Q9Y490
P07741-1	P50897	Q15427	Q96QK1	Q9Y4B5
P07814	P50914	Q15434	Q96QZ7	Q9Y4E1
P07858	P50990	Q15435	Q96RE7	Q9Y4E8
P07900	P50991	Q15436	Q96RF0-2	Q9Y4F1

P07910-1	P50995	Q15459	Q96S44	Q9Y4I1-1
P07919	P51114-1	Q15477	Q96S52	Q9Y4K0
P07942	P51116	Q15532	Q96S59-1	Q9Y4K4
P07948-1	P51148	Q15555	Q96S66	Q9Y4L1
P07951-3	P51149	Q15572-1	Q96S82	Q9Y4P1-1
P07954	P51153	Q15599	Q96S97	Q9Y4W2
P07992-1	P51397	Q15629	Q96SB3	Q9Y4W6
P07996	P51452	Q15637	Q96SB4-3	Q9Y4X5
P08123	P51570	Q15642	Q96SL4	Q9Y520-7
P08133-1	P51572	Q15643	Q96SZ5	Q9Y570
P08134	P51610-1	Q15654-1	Q96T37-1	Q9Y5A9-1
P08195	P51659-1	Q15691	Q96T51	Q9Y5B9
P08237	P51665	Q15717	Q96T60	Q9Y5J1
P08238	P51812	Q15746-1	Q96T76-1	Q9Y5J9
P08240-1	P51858	Q15758-1	Q96TA1	Q9Y5K8
P08243-1	P51884	Q15785	Q96TC7	Q9Y5L0-1
P08572	P51911	Q15796-1	Q99417	Q9Y5M8
P08574	P51991-1	Q15811	Q99426	Q9Y5S1
P08579	P52209	Q15813	Q99436	Q9Y5S2
P08621-1	P52272	Q15819	Q99439	Q9Y5Y5
P08648	P52292	Q15836	Q99447-1	Q9Y5Z7
P08670	P52306-1	Q15843	Q99459	Q9Y608
P08708	P52565-1	Q15904	Q99460	Q9Y617-1
P08727	P52594-1	Q15942	Q99470	Q9Y657
P08729	P52597	Q16181	Q99471-1	Q9Y678
P08758	P52630-3	Q16204	Q99497	Q9Y680-2
P08865	P52701	Q16222-1	Q99536	Q9Y696
P09012	P52788-1	Q16270-1	Q99543-1	Q9Y6C9
P09067	P52789	Q16352	Q99567	Q9Y6D5
P09104	P52815	Q16512-1	Q99575	Q9Y6D9
P09110-1	P52895	Q16527	Q99614	Q9Y6E0
P09211	P52907	Q16531	Q99623	Q9Y6G9
P09326	P52926-1	Q16540	Q99653	Q9Y6I3
P09382	P52943	Q16543	Q99700-1	Q9Y6I9
P09417	P52948-1	Q16555-1	Q99707	Q9Y6K8
P09429	P53004	Q16576-1	Q99714-1	Q9Y6K9
P09493-10	P53041	Q16610	Q99715-1	Q9Y6M1
P09496-2	P53367	Q16626	Q99729-2	Q9Y6M5
P09497-2	P53396-1	Q16629	Q99733	Q9Y6N5

P09525	P53582	Q16630	Q99798	Q9Y6R0
P09543-1	P53597	Q16637	Q99805	Q9Y6W5
P09622	P53602	Q16643	Q99816	Q9Y6Y8
P09651-1	P53611	Q16658	Q99829	S4R3G0
P09661	P53618	Q16666-1	Q99832	S4R3N1
P09669	P53611	Q16698	Q99848	X6RLX0
P09874	P53618	Q16774-1	Q99879	

Table S 6. *GO analysis of A549 cell-derived exosomes. The analysis was performed by using g:Profiler software. *The list of proteins associated with each ontology is available on request deanna.shea@vuw.ac.nz*

Source	Term name	Term ID	Adjusted p-value	Negative_log10 of adjusted p-value	Term size	Query size	Intersection size	Effective domain size
GO:MF	cell adhesion molecule binding	GO:0050839	1.52174267071654E-44	43.81765878129500	548	301	74	18694
GO:MF	structural molecule activity	GO:0005198	4.89662747670285E-39	38.31010293477420	698	301	76	18694
GO:MF	protein-containing complex binding	GO:0044877	2.66719199052975E-26	25.57394572168300	1282	301	83	18694
GO:MF	cadherin binding	GO:0045296	6.81561988862626E-26	25.16649463844020	332	301	45	18694
GO:MF	RNA binding	GO:0003723	3.08387699142421E-25	24.51090295325760	1946	301	101	18694
GO:MF	enzyme binding	GO:0019899	2.95119789010994E-20	19.530001668269800	1866	301	91	18694
GO:MF	integrin binding	GO:0005178	2.94785924200929E-18	17.530493257542300	148	301	27	18694
GO:MF	structural constituent of ribosome	GO:0003735	1.28267787914999E-16	15.891882394967400	170	301	27	18694
GO:MF	extracellular matrix structural constituent	GO:0005201	1.65094410026637E-14	13.78226763137490	169	301	25	18694
GO:MF	unfolded protein binding	GO:0051082	3.36511836570182E-14	13.472999655164500	111	301	21	18694
GO:MF	signaling receptor binding	GO:0005102	3.25033508142E-12	11.488071864710300	1681	301	72	18694
GO:MF	protease binding	GO:0002020	3.88466141203877E-12	11.410646828418100	139	301	21	18694
GO:MF	organic cyclic compound binding	GO:0097159	1.30494497524665E-10	9.884407800548350	6387	301	164	18694
GO:MF	carbohydrate derivative binding	GO:0097367	4.88341806765885E-10	9.311276094330410	2286	301	82	18694
GO:MF	small molecule binding	GO:0036094	1.29102194836998E-09	8.889066374329290	2507	301	86	18694
GO:MF	heterocyclic compound binding	GO:1901363	5.53637302239327E-09	8.256774656248311	6302	301	158	18694
GO:MF	identical protein binding	GO:0042802	1.35300878176207E-08	7.868699384586090	2080	301	74	18694
GO:MF	protein binding	GO:0005515	1.90818816811895E-08	7.719378801358160	14752	301	279	18694
GO:MF	MHC class II protein complex binding	GO:0023026	2.30034479247615E-08	7.638207063874990	16	301	8	18694
GO:MF	peptidase regulator activity	GO:0061134	5.18364023076204E-08	7.285365148190080	225	301	21	18694

GO:MF	structural constituent of cytoskeleton	GO:0005200	5.721917470651 1E-08	7.2424584104768 10	104	301	15	18694
GO:MF	lipoprotein particle receptor binding	GO:0070325	7.701963771027 53E-08	7.1133985285696 70	26	301	9	18694
GO:MF	endopeptidase inhibitor activity	GO:0004866	3.447913443158 08E-07	6.4624436452924 10	179	301	18	18694
GO:MF	nucleoside-triphosphatase activity	GO:0017111	3.914263937615 36E-07	6.4073498933471 00	840	301	40	18694
GO:MF	peptidase inhibitor activity	GO:0030414	5.398648346759 84E-07	6.2677149603664 20	184	301	18	18694
GO:MF	nucleoside phosphate binding	GO:1901265	6.636826790470 22E-07	6.1780395165337 30	2173	301	72	18694
GO:MF	endopeptidase regulator activity	GO:0061135	7.646603782511 44E-07	6.1165314126915 40	188	301	18	18694
GO:MF	MHC protein complex binding	GO:0023023	0.000001175135 4211733100	5.9299120829416 80	24	301	8	18694
GO:MF	nucleotide binding	GO:0000166	0.000001598688 4330650600	5.7962361672638 50	2172	301	71	18694
GO:MF	ubiquitin protein ligase binding	GO:0031625	0.000001824870 741701890	5.7387678918396 50	300	301	22	18694
GO:MF	enzyme inhibitor activity	GO:0004857	0.000001963738 4123587700	5.7069163646323 00	386	301	25	18694
GO:MF	pyrophosphatase activity	GO:0016462	0.000002253355 4852308200	5.6471702893699 400	893	301	40	18694
GO:MF	hydrolase activity, acting on acid anhydrides	GO:0016817	0.000002555506 955266510	5.5925229326974 90	897	301	40	18694
GO:MF	hydrolase activity, acting on acid anhydrides, in phosphorus-containing anhydrides	GO:0016818	0.000002555506 955266510	5.5925229326974 90	897	301	40	18694
GO:MF	protein domain specific binding	GO:0019904	0.000002724960 500373840	5.5646397886512 00	718	301	35	18694
GO:MF	nucleic acid binding	GO:0003676	0.000003719128 3835295900	5.4295588296280 90	4353	301	114	18694
GO:MF	ubiquitin-like protein ligase binding	GO:0044389	0.000005305132 255959490	5.2753037847471	318	301	22	18694
GO:MF	anion binding	GO:0043168	0.000005586081 4193011400	5.2528927385785 30	2424	301	75	18694
GO:MF	collagen binding	GO:0005518	0.000006070143 3039277000	5.2168010559806 900	69	301	11	18694
GO:MF	lipid binding	GO:0008289	0.000006479860 513284850	5.1884343427347 60	779	301	36	18694
GO:MF	actin binding	GO:0003779	0.000007985520 782161870	5.0976967557379 00	445	301	26	18694
GO:MF	purine ribonucleoside triphosphate binding	GO:0035639	0.000008300102 038947060	5.0809165685059 40	1850	301	62	18694
GO:MF	low-density lipoprotein particle receptor binding	GO:0050750	0.000012175050 798285000	4.9145292180912 50	21	301	7	18694
GO:MF	kinase binding	GO:0019900	0.000012623682 777688400	4.8988139274450 50	763	301	35	18694
GO:MF	purine nucleotide binding	GO:0017076	0.000018300640 461246	4.7375337111483 80	1935	301	63	18694
GO:MF	double-stranded RNA binding	GO:0003725	0.000019837867 724024400	4.7025050098761 90	77	301	11	18694
GO:MF	actin filament binding	GO:0051015	0.000026994362 240371300	4.5687269285653 80	210	301	17	18694
GO:MF	disordered domain specific binding	GO:0097718	0.000032239423 09952750	4.4916127381738 20	35	301	8	18694

GO:MF	protein dimerization activity	GO:0046983	0.000036826815 7552572	4.4338358309606 10	1068	301	42	18694
GO:MF	cytoskeletal protein binding	GO:0008092	0.000043636249 78655650	4.3601525808836 40	995	301	40	18694
GO:MF	heparin binding	GO:0008201	0.000045841879 96487140	4.3387375803594 20	168	301	15	18694
GO:MF	chaperone binding	GO:0051087	0.000054666810 387509600	4.2622762648959 80	104	301	12	18694
GO:MF	misfolded protein binding	GO:0051787	0.000064275506 2322953	4.1919544941790 50	26	301	7	18694
GO:MF	protein folding chaperone	GO:0044183	0.000064275506 2322953	4.1919544941790 50	26	301	7	18694
GO:MF	purine ribonucleotide binding	GO:0032555	0.000077390581 52220150	4.1113118899867 10	1921	301	61	18694
GO:MF	ribonucleotide binding	GO:0032553	0.000105342420 89493600	3.9773967052567 7	1938	301	61	18694
GO:MF	extracellular matrix structural constituent conferring tensile strength	GO:0030020	0.000120351870 6376760	3.9195471550665 000	41	301	8	18694
GO:MF	sulfur compound binding	GO:1901681	0.000147038043 85375700	3.8325702836318 60	264	301	18	18694
GO:MF	glycosaminoglycan binding	GO:0005539	0.000154335077 3154370	3.8115353561583 50	237	301	17	18694
GO:MF	growth factor binding	GO:0019838	0.000164425585 76355200	3.7840306022987 20	137	301	13	18694
GO:MF	protein heterodimerization activity	GO:0046982	0.000187397671 98467700	3.7272358085949 200	358	301	21	18694
GO:MF	exogenous protein binding	GO:0140272	0.000207263882 2584040	3.6834763713383 20	77	301	10	18694
GO:MF	platelet-derived growth factor binding	GO:0048407	0.000216888143 28913100	3.6637641890870 10	11	301	5	18694
GO:MF	protein kinase binding	GO:0019901	0.000295636283 3311300	3.5292422662058 700	679	301	30	18694
GO:MF	oxidoreductase activity, acting on the CH-OH group of donors, NAD or NADP as acceptor	GO:0016616	0.000412460259 31831000	3.3846178895145 400	125	301	12	18694
GO:MF	antioxidant activity	GO:0016209	0.000655979008 8610940	3.1831100577000 30	87	301	10	18694
GO:MF	GTPase activity	GO:0003924	0.000781850703 1137840	3.1068761689402 100	327	301	19	18694
GO:MF	proteoglycan binding	GO:0043394	0.000864303094 2085160	3.0633339322211 700	37	301	7	18694
GO:MF	oxidoreductase activity, acting on CH-OH group of donors	GO:0016614	0.001096296591 188710	2.9600719362793 20	137	301	12	18694
GO:MF	ADP binding	GO:0043531	0.001256116573 3302300	2.9009700542256 00	39	301	7	18694
GO:MF	extracellular matrix binding	GO:0050840	0.001261388260 6225500	2.8991512151776 20	55	301	8	18694
GO:MF	enzyme regulator activity	GO:0030234	0.001464910640 2680000	2.8341888665195 30	1228	301	42	18694
GO:MF	virus receptor activity	GO:0001618	0.001734914274 696150	2.7607219796317 30	76	301	9	18694
GO:MF	serine-type endopeptidase inhibitor activity	GO:0004867	0.001965121096 914740	2.7066106818781 800	98	301	10	18694
GO:MF	retinal dehydrogenase activity	GO:0001758	0.002127782585 5984300	2.6720727498256 2	8	301	4	18694
GO:MF	fibronectin binding	GO:0001968	0.002249625451 4824200	2.6478897831752 800	28	301	6	18694

GO:MF	phospholipid binding	GO:0005543	0.002425686419587960	2.6151653432241600	455	301	22	18694
GO:MF	lipase inhibitor activity	GO:0055102	0.002683019884703400	2.5713760918267 40	17	301	5	18694
GO:MF	nucleoside binding	GO:0001882	0.003350413337832490	2.4749016110926100	395	301	20	18694
GO:MF	heat shock protein binding	GO:0031072	0.003493219945191660	2.4567740688210300	128	301	11	18694
GO:MF	oxidoreductase activity	GO:0016491	0.003827816558557590	2.4170488832032 20	771	301	30	18694
GO:MF	GTP binding	GO:0005525	0.007315819876 6506900	2.1357369958609700	382	301	19	18694
GO:MF	ATPase activity	GO:0016887	0.008315285370995490	2.0801228417034000	456	301	21	18694
GO:MF	MHC class I protein binding	GO:0042288	0.008368422728956100	2.0773563896364 70	21	301	5	18694
GO:MF	purine ribonucleoside binding	GO:0032550	0.008456241844553530	2.0728226049043 80	386	301	19	18694
GO:MF	purine nucleoside binding	GO:0001883	0.009413540588267930	2.0262470005109000	389	301	19	18694
GO:MF	ribonucleoside binding	GO:0032549	0.009413540588267930	2.0262470005109000	389	301	19	18694
GO:MF	intramolecular oxidoreductase activity	GO:0016860	0.010382340855381200	1.9837047172043100	53	301	7	18694
GO:MF	phospholipase inhibitor activity	GO:0004859	0.014297814108034400	1.8447303536805700	12	301	4	18694
GO:MF	alditol:NADP+ 1-oxidoreductase activity	GO:0004032	0.014297814108034400	1.8447303536805700	12	301	4	18694
GO:MF	guanyl nucleotide binding	GO:0019001	0.015291142463671	1.8155600654619500	403	301	19	18694
GO:MF	guanyl ribonucleotide binding	GO:0032561	0.015291142463671	1.8155600654619500	403	301	19	18694
GO:MF	MHC protein binding	GO:0042287	0.019485516852358300	1.7102880700791300	40	301	6	18694
GO:MF	C-X3-C chemokine binding	GO:0019960	0.019588891401190600	1.7079901414411500	5	301	3	18694
GO:MF	peptide disulfide oxidoreductase activity	GO:0015037	0.020390896101492400	1.6905636882296100	13	301	4	18694
GO:MF	adenyl nucleotide binding	GO:0030554	0.029715190353635700	1.5270214833337900	1580	301	46	18694
GO:MF	rRNA binding	GO:0019843	0.035977948560985500	1.4439636034708300	64	301	7	18694
GO:MF	tau protein binding	GO:0048156	0.038649890354305800	1.4128517337919000	45	301	6	18694
GO:MF	C3HC4-type RING finger domain binding	GO:0055131	0.038710026597 71820	1.4121765302765400	6	301	3	18694
GO:MF	hydrolase activity	GO:0016787	0.039110578770566800	1.4077057571748 50	2588	301	66	18694
GO:MF	ATP binding	GO:0005524	0.039222139295 79040	1.4064687222689800	1504	301	44	18694
GO:BP	establishment of localization	GO:0051234	9.762527764983 83E-29	28.010437717963600	5398	301	188	18092
GO:BP	biological process involved in symbiotic interaction	GO:0044403	2.351404444275 2E-28	27.628672665298600	996	301	78	18092
GO:BP	transport	GO:0006810	6.163438833998 53E-28	27.210176909601 90	5259	301	184	18092
GO:BP	establishment of localization in cell	GO:0051649	1.173972688485 62E-27	26.930342006476800	2840	301	131	18092

GO:BP	viral process	GO:0016032	8.655101248629 61E-27	26.062727847319 00	940	301	74	18092
GO:BP	localization	GO:0051179	5.218218002912 55E-26	25.282477781218 10	6935	301	211	18092
GO:BP	cellular localization	GO:0051641	3.328578905879 9E-25	24.477741143389500	3562	301	144	18092
GO:BP	platelet degranulation	GO:0002576	3.197477743748 68E-24	23.495192469773700	127	301	31	18092
GO:BP	regulated exocytosis	GO:0045055	8.415692153848 97E-24	23.074910159398 70	799	301	65	18092
GO:BP	biological process involved in interspecies interaction between organisms	GO:0044419	6.088408208870 72E-23	22.215496237164 40	2272	301	109	18092
GO:BP	exocytosis	GO:0006887	1.307104873822 94E-22	21.883689565980800	921	301	68	18092
GO:BP	SRP-dependent cotranslational protein targeting to membrane	GO:0006614	1.307369097706 77E-22	21.883601784670700	96	301	27	18092
GO:BP	cotranslational protein targeting to membrane	GO:0006613	5.970872864851 1E-22	21.223962175959600	101	301	27	18092
GO:BP	vesicle-mediated transport	GO:0016192	9.205291357999 25E-22	21.035962461025400	2193	301	105	18092
GO:BP	protein targeting to ER	GO:0045047	1.000968306499 6E-21	20.999579673300100	114	301	28	18092
GO:BP	establishment of protein localization to endoplasmic reticulum	GO:0072599	2.833969780405 59E-21	20.547604785095300	118	301	28	18092
GO:BP	export from cell	GO:0140352	5.223811674008 43E-21	20.282012488397100	1450	301	83	18092
GO:BP	establishment of protein localization to organelle	GO:0072594	6.043541589298 07E-20	19.218708484900300	589	301	52	18092
GO:BP	nuclear-transcribed mRNA catabolic process, nonsense-mediated decay	GO:0000184	1.854214678238 06E-19	18.731839985306500	123	301	27	18092
GO:BP	secretion by cell	GO:0032940	1.917682371657 53E-19	18.717223323995300	1396	301	79	18092
GO:BP	secretion	GO:0046903	1.087291023253 26E-18	17.963654197517400	1538	301	82	18092
GO:BP	wound healing	GO:0042060	1.110472477338 41E-18	17.954492200814900	553	301	49	18092
GO:BP	protein localization to endoplasmic reticulum	GO:0070972	1.815505999008 4E-18	17.741002311701800	147	301	28	18092
GO:BP	hemostasis	GO:0007599	1.009341663569 94E-17	16.995961799584 3	352	301	39	18092
GO:BP	coagulation	GO:0050817	1.371794276822 35E-17	16.862711013366 80	355	301	39	18092
GO:BP	cell activation	GO:0001775	2.498941804528 22E-17	16.602243857625700	1510	301	79	18092
GO:BP	regulation of biological quality	GO:0065008	2.581381504088 28E-17	16.588147806042 60	4194	301	143	18092
GO:BP	blood coagulation	GO:0007596	5.063908016954 8E-17	16.295514191634400	347	301	38	18092
GO:BP	protein localization to membrane	GO:0072657	6.326037223197 13E-17	16.198868256969 50	660	301	51	18092
GO:BP	protein targeting to membrane	GO:0006612	1.229758642370 73E-16	15.910180116668000	203	301	30	18092
GO:BP	establishment of protein localization to membrane	GO:0090150	2.518003061099 83E-16	15.598943746262300	342	301	37	18092

GO:BP	response to stress	GO:0006950	2.68847945249071E-16	15.570493278399800	4199	301	141	18092
GO:BP	response to organic substance	GO:0010033	3.52752845125135E-16	15.452529474761000	3459	301	125	18092
GO:BP	protein targeting	GO:0006605	6.34247970610802E-16	15.19774091370640	441	301	41	18092
GO:BP	response to chemical	GO:0042221	6.46592475459053E-16	15.189369353676900	4834	301	153	18092
GO:BP	establishment of protein localization	GO:0045184	6.71325957264613E-16	15.173066560205500	2044	301	91	18092
GO:BP	translational initiation	GO:0006413	9.05377578816878E-16	15.043170264774 10	200	301	29	18092
GO:BP	response to wounding	GO:0009611	1.46266070200202E-15	14.83485640684680	682	301	50	18092
GO:BP	organonitrogen compound metabolic process	GO:1901564	1.88705565488572E-15	14.724215291009800	6780	301	188	18092
GO:BP	protein localization to organelle	GO:0033365	2.18733718153638E-15	14.660084264610600	1014	301	61	18092
GO:BP	cellular component organization or biogenesis	GO:0071840	4.2155162512972E-15	14.375149232104400	6767	301	187	18092
GO:BP	cellular response to chemical stimulus	GO:0070887	5.99467737544883E-15	14.222234185014300	3438	301	122	18092
GO:BP	viral transcription	GO:0019083	6.52240432404303E-15	14.185592282767400	180	301	27	18092
GO:BP	regulation of body fluid levels	GO:0050878	4.00010894611813E-14	13.397928180158600	520	301	42	18092
GO:BP	protein transport	GO:0015031	5.12550842621296E-14	13.290263048175300	1946	301	85	18092
GO:BP	peptide transport	GO:0015833	5.78845670811894E-14	13.237437210450200	1989	301	86	18092
GO:BP	viral gene expression	GO:0019080	6.98298647602638E-14	13.155958799057800	197	301	27	18092
GO:BP	anion transport	GO:0006820	7.55093931149325E-14	13.121999020235200	2914	301	108	18092
GO:BP	tissue development	GO:0009888	8.57130438581572E-14	13.066953081874300	2161	301	90	18092
GO:BP	organic substance transport	GO:0071702	8.971843576426E-14	13.047118306922200	2790	301	105	18092
GO:BP	nitrogen compound transport	GO:0071705	1.64733118607545E-13	12.783219079746000	2347	301	94	18092
GO:BP	amide transport	GO:0042886	1.68834668914439E-13	12.772538369486100	2024	301	86	18092
GO:BP	neutrophil mediated immunity	GO:0002446	3.04903097945369E-13	12.515838162995 30	498	301	40	18092
GO:BP	intracellular transport	GO:0046907	3.75832771919222E-13	12.425005352912600	1777	301	79	18092
GO:BP	nuclear-transcribed mRNA catabolic process	GO:0000956	6.67401054362214E-13	12.175613111580900	215	301	27	18092
GO:BP	cellular component biogenesis	GO:0044085	7.11080921811625E-13	12.148080973255500	3276	301	114	18092
GO:BP	macromolecule localization	GO:0033036	8.46327930410237E-13	12.072461326355400	3238	301	113	18092
GO:BP	cellular protein localization	GO:0034613	1.78491943081505E-12	11.748381382656600	2024	301	84	18092
GO:BP	cellular macromolecule localization	GO:0070727	2.45335007938367E-12	11.610240475969500	2035	301	84	18092
GO:BP	cellular component organization	GO:0016043	2.96776546123658E-12	11.527570423782 30	6576	301	177	18092

GO:BP	neutrophil degranulation	GO:0043312	3.954496535148 2E-12	11.402908800643000	484	301	38	18092
GO:BP	mRNA catabolic process	GO:0006402	4.58733411229 75E-12	11.338439627462800	386	301	34	18092
GO:BP	ion transport	GO:0006811	4.79298095437454E-12	11.319394296738800	3689	301	121	18092
GO:BP	neutrophil activation involved in immune response	GO:0002283	4.83256620160 56E-12	11.315822187833 30	487	301	38	18092
GO:BP	protein localization	GO:0008104	6.65707096261301E-12	11.176716813559500	2789	301	101	18092
GO:BP	protein metabolic process	GO:0019538	8.36754687138452E-12	11.077401846233 20	5806	301	162	18092
GO:BP	biological adhesion	GO:0022610	1.02197809359327E-11	10.990558413333900	1501	301	69	18092
GO:BP	neutrophil activation	GO:0042119	1.13188650586 42E-11	10.946197088954500	500	301	38	18092
GO:BP	extracellular matrix organization	GO:0030198	1.22919314121463E-11	10.910379871732 40	399	301	34	18092
GO:BP	myeloid leukocyte mediated immunity	GO:0002444	1.27955499181083E-11	10.892941044574200	556	301	40	18092
GO:BP	extracellular structure organization	GO:0043062	1.32380193580341E-11	10.878176988176000	400	301	34	18092
GO:BP	negative regulation of biological process	GO:0048519	1.32436557638083E-11	10.877992116188000	5833	301	162	18092
GO:BP	protein folding	GO:0006457	1.66522065469376E-11	10.778528210946500	224	301	26	18092
GO:BP	granulocyte activation	GO:0036230	1.76921328631978E-11	10.752219807854500	507	301	38	18092
GO:BP	leukocyte mediated immunity	GO:0002443	1.79242215506228E-11	10.746559696670500	891	301	51	18092
GO:BP	immune effector process	GO:0002252	2.69546131981072E-11	10.569366895967900	1310	301	63	18092
GO:BP	cellular response to cytokine stimulus	GO:0071345	4.61823591001582E-11	10.335523886100300	1148	301	58	18092
GO:BP	intracellular protein transport	GO:0006886	7.21147808963951E-11	10.141975711649 00	1195	301	59	18092
GO:BP	RNA catabolic process	GO:0006401	7.86006151997274E-11	10.104574054764600	425	301	34	18092
GO:BP	cellular response to organic substance	GO:0071310	8.99373431118127E-11	10.046059946309100	2812	301	99	18092
GO:BP	cell adhesion	GO:0007155	9.31032842836118E-11	10.031034998706 20	1494	301	67	18092
GO:BP	immune system process	GO:0002376	1.10074759496862E-10	9.9583122547605 60	3322	301	110	18092
GO:BP	leukocyte degranulation	GO:0043299	1.23753197704315E-10	9.9074435703548 30	539	301	38	18092
GO:BP	cell activation involved in immune response	GO:0002263	1.94009610807263E-10	9.7121767555482 50	723	301	44	18092
GO:BP	cellular component assembly	GO:0022607	2.08704600068091E-10	9.6804679785235 70	3030	301	103	18092
GO:BP	myeloid cell activation involved in immune response	GO:0002275	2.20447093896815E-10	9.6566956220038 90	549	301	38	18092
GO:BP	response to cytokine	GO:0034097	3.82960041798312E-10	9.4168465381248 80	1242	301	59	18092
GO:BP	organic substance catabolic process	GO:1901575	4.40994881217495E-10	9.3555664515115 20	2271	301	85	18092
GO:BP	nucleobase-containing compound catabolic process	GO:0034655	5.70368554186 45E-10	9.2438444262132 80	566	301	38	18092

GO:BP	platelet activation	GO:0030168	6.24799395777945E-10	9.204259399121840	160	301	21	18092
GO:BP	leukocyte activation involved in immune response	GO:0002366	6.95713156564133E-10	9.157569783663800	719	301	43	18092
GO:BP	cellular protein metabolic process	GO:0044267	8.48821977839518E-10	9.071183384136340	5225	301	146	18092
GO:BP	myeloid leukocyte activation	GO:0002274	1.45242886301789E-09	8.837905129268340	673	301	41	18092
GO:BP	cell death	GO:0008219	1.51650391030501E-09	8.819156465523622	2322	301	85	18092
GO:BP	macromolecule catabolic process	GO:0009057	1.88439174968697E-09	8.724828805873660	1477	301	64	18092
GO:BP	anatomical structure morphogenesis	GO:0009653	2.07389130239957E-09	8.683214009762380	2865	301	97	18092
GO:BP	programmed cell death	GO:0012501	2.46803858221888E-09	8.607648055370660	2172	301	81	18092
GO:BP	negative regulation of apoptotic process	GO:0043066	2.54822471921721E-09	8.593762275703790	944	301	49	18092
GO:BP	regulation of protein stability	GO:0031647	2.93610588517346E-09	8.532228286454420	302	301	27	18092
GO:BP	response to stimulus	GO:0050896	3.12541168020832E-09	8.505092769146430	9469	301	217	18092
GO:BP	heterocycle catabolic process	GO:0046700	3.60394771356363E-09	8.443221518435345	601	301	38	18092
GO:BP	cellular nitrogen compound catabolic process	GO:0044270	4.63536037111624E-09	8.333916496448650	606	301	38	18092
GO:BP	platelet aggregation	GO:0070527	4.97347949639568E-09	8.303339668135560	64	301	14	18092
GO:BP	negative regulation of programmed cell death	GO:0043069	6.13845940477233E-09	8.211940611914070	967	301	49	18092
GO:BP	catabolic process	GO:0009056	7.62702653498037E-09	8.117644742666550	2746	301	93	18092
GO:BP	organic cyclic compound catabolic process	GO:1901361	9.01267425959035E-09	8.045146325130010	650	301	39	18092
GO:BP	aromatic compound catabolic process	GO:0019439	1.01829715839135E-08	7.992125468150980	622	301	38	18092
GO:BP	regulation of localization	GO:0032879	1.17328262952116E-08	7.930597359021180	2903	301	96	18092
GO:BP	negative regulation of coagulation	GO:0050819	1.37034734461996E-08	7.863169337418740	56	301	13	18092
GO:BP	regulation of proteolysis	GO:0030162	1.37981222458794E-08	7.860180011695870	754	301	42	18092
GO:BP	movement of cell or subcellular component	GO:0006928	1.58166848119322E-08	7.800884539723420	2337	301	83	18092
GO:BP	negative regulation of cell death	GO:0060548	1.74981528813 28E-08	7.757007793358580	1066	301	51	18092
GO:BP	protein stabilization	GO:0050821	2.04281306767167E-08	7.689771372669080	191	301	21	18092
GO:BP	monosaccharide biosynthetic process	GO:0046364	2.11044195792 28E-08	7.675626587456 73	100	301	16	18092
GO:BP	endocytosis	GO:0006897	2.22035373521085E-08	7.653577830498 87	701	301	40	18092
GO:BP	regulation of peptidase activity	GO:0052547	3.34282070879007E-08	7.475886916040170	469	301	32	18092
GO:BP	regulation of apoptotic process	GO:0042981	3.53077744021164E-08	7.452129656986390	1579	301	64	18092
GO:BP	leukocyte activation	GO:0045321	3.54478294147122E-08	7.450410352923060	1346	301	58	18092

GO:BP	homotypic cell-cell adhesion	GO:0034109	3.70995598088386E-08	7.430631243315590	88	301	15	18092
GO:BP	cellular macromolecule catabolic process	GO:0044265	4.00458149917374E-08	7.397442863374070	1237	301	55	18092
GO:BP	positive regulation of biological process	GO:0048518	4.20794812331428E-08	7.375929622917350	6466	301	164	18092
GO:BP	regulation of coagulation	GO:0050818	4.94520805417779E-08	7.305815432099040	75	301	14	18092
GO:BP	regulation of cell death	GO:0010941	5.12782695360723E-08	7.290066639175977	1754	301	68	18092
GO:BP	cell-substrate adhesion	GO:0031589	5.39785664695509E-08	7.267778653359170	368	301	28	18092
GO:BP	negative regulation of hemostasis	GO:1900047	5.94173854558786E-08	7.226086462378650	50	301	12	18092
GO:BP	negative regulation of peptidase activity	GO:0010466	6.72017672768 34E-08	7.172619305688960	271	301	24	18092
GO:BP	translation	GO:0006412	7.79034523010024E-08	7.108443296087980	763	301	41	18092
GO:BP	substrate adhesion-dependent cell spreading	GO:0034446	8.17741651673437E-08	7.087383880893800	109	301	16	18092
GO:BP	regulation of programmed cell death	GO:0043067	9.01863136446587E-08	7.044859364449110	1614	301	64	18092
GO:BP	viral life cycle	GO:0019058	9.74871788483229E-08	7.011052497343 1	351	301	27	18092
GO:BP	negative regulation of metabolic process	GO:0009892	1.08213616743775E-07	6.965718087615750	3539	301	107	18092
GO:BP	negative regulation of endopeptidase activity	GO:0010951	1.54435795384 52E-07	6.811252030838190	258	301	23	18092
GO:BP	cellular developmental process	GO:0048869	1.78778092339086E-07	6.747685701195430	4518	301	126	18092
GO:BP	regulation of hemostasis	GO:1900046	1.90252533030002E-07	6.720669552304410	68	301	13	18092
GO:BP	peptide biosynthetic process	GO:0043043	2.09980442657944E-07	6.677821153081640	788	301	41	18092
GO:BP	immune response	GO:0006955	2.18770109227652E-07	6.660012016361830	2326	301	80	18092
GO:BP	localization of cell	GO:0051674	2.29257871620462E-07	6.639675743803 4600	1856	301	69	18092
GO:BP	cell motility	GO:0048870	2.29257871620462E-07	6.639675743803 4600	1856	301	69	18092
GO:BP	negative regulation of macromolecule metabolic process	GO:0010605	2.45799913500426E-07	6.609418274282330 0	3297	301	101	18092
GO:BP	negative regulation of proteolysis	GO:0045861	2.52004822309792E-07	6.598591148573640	366	301	27	18092
GO:BP	peptide metabolic process	GO:0006518	3.63921668594518E-07	6.438992084917030	941	301	45	18092
GO:BP	supramolecular fiber organization	GO:0097435	4.20507513429904E-07	6.376226240027790 0	739	301	39	18092
GO:BP	NADH metabolic process	GO:0006734	4.26493531371854E-07	6.370087551391680	46	301	11	18092
GO:BP	apoptotic process	GO:0006915	5.15360391801051E-07	6.287888962353 3	2018	301	72	18092
GO:BP	response to inorganic substance	GO:0010035	5.67120641751966E-07	6.246324545209450	585	301	34	
GO:BP	cell differentiation	GO:0030154	5.76251280830 48E-07	6.239388096297320	4440	301	123	18092

GO:BP	anatomical structure development	GO:0048856	5.892954998428 28E-07	6.2296668753835 40	6210	301	156	18092
GO:BP	regulation of endopeptidase activity	GO:0052548	6.176028183869 51E-07	6.2092907307955 300	437	301	29	18092
GO:BP	positive regulation of cellular component organization	GO:0051130	7.200232868430 06E-07	6.1426534574800 20	1182	301	51	18092
GO:BP	positive regulation of transport	GO:0051050	8.390828339042 26E-07	6.0761951636864 70	930	301	44	18092
GO:BP	negative regulation of blood coagulation	GO:0030195	8.910505478395 39E-07	6.0500976584489 8	49	301	11	18092
GO:BP	negative regulation of protein metabolic process	GO:0051248	0.000001019233 2364856900	5.9917264227373 50	1156	301	50	18092
GO:BP	regulation of protein localization	GO:0032880	0.000001027018 893456050	5.9884215668718 20	936	301	44	18092
GO:BP	blood coagulation, fibrin clot formation	GO:0072378	0.000001080163 4609929200	5.9665105178135 20	28	301	9	18092
GO:BP	protein activation cascade	GO:0072376	0.000001080163 4609929200	5.9665105178135 20	28	301	9	18092
GO:BP	glycolytic process through glucose-6-phosphate	GO:0061620	0.000001080163 4609929200	5.9665105178135 20	28	301	9	18092
GO:BP	regulation of protein metabolic process	GO:0051246	0.000001091348 2121092900	5.9620366586972 70	2722	301	87	18092
GO:BP	locomotion	GO:0040011	0.000001161998 5723008700	5.9347944055448 60	2055	301	72	18092
GO:BP	cytoskeleton organization	GO:0007010	0.000001264949 734232240	5.8979267318631 00	1435	301	57	18092
GO:BP	cell migration	GO:0016477	0.000001451560 8110332900	5.8381647653142 30	1684	301	63	18092
GO:BP	anatomical structure homeostasis	GO:0060249	0.000001461329 392196080	5.8352518805137 50	483	301	30	18092
GO:BP	mRNA metabolic process	GO:0016071	0.000001541246 661676130	5.8121278510724 20	877	301	42	18092
GO:BP	glycolytic process through fructose-6-phosphate	GO:0061615	0.000001543519 0608075600	5.8114880030769 70	29	301	9	18092
GO:BP	regulation of blood coagulation	GO:0030193	0.000002280838 496737500	5.6419054654725 50	67	301	12	18092
GO:BP	negative regulation of catalytic activity	GO:0043086	0.000002429370 7537088300	5.6145062011262 50	855	301	41	18092
GO:BP	amide biosynthetic process	GO:0043604	0.000002584138 208561930	5.5876842624994 60	928	301	43	18092
GO:BP	membrane organization	GO:0061024	0.000002923483 2018855500	5.5340993972429 40	968	301	44	18092
GO:BP	developmental process	GO:0032502	0.000003577603 5135248000	5.4464077916136 80	6745	301	163	18092
GO:BP	cytoplasmic translation	GO:0002181	0.000003998460 767862170	5.3981071608408 10	103	301	14	18092
GO:BP	regulation of cellular protein metabolic process	GO:0032268	0.000004082611 301632350	5.3890619665359 70	2563	301	82	18092
GO:BP	positive regulation of cellular process	GO:0048522	0.000004362968 982190420	5.3602178745473 10	5863	301	147	18092
GO:BP	positive regulation of cellular protein localization	GO:1903829	0.000004490078 825679300	5.3477460346632 60	306	301	23	18092
GO:BP	receptor-mediated endocytosis	GO:0006898	0.000004568015 254149030	5.3402724545035 2	333	301	24	18092
GO:BP	response to external stimulus	GO:0009605	0.000004774034 740281340	5.3211144249904 30	2991	301	91	18092
GO:BP	post-translational protein modification	GO:0043687	0.000004995227 079037370	5.3014447643086 10	362	301	25	18092

GO:BP	plasminogen activation	GO:0031639	0.000005027880 699445840	5.2986150357169 900	23	301	8	18092
GO:BP	protein refolding	GO:0042026	0.000005027880 699445840	5.2986150357169 900	23	301	8	18092
GO:BP	cellular catabolic process	GO:0044248	0.000005315046 113539450	5.2744929631691 200	2350	301	77	18092
GO:BP	response to topologically incorrect protein	GO:0035966	0.000005335772 83722167	5.2728026681546 90	209	301	19	18092
GO:BP	organic substance metabolic process	GO:0071704	0.000005486392 3891106600	5.2607131346951 40	11403	301	237	18092
GO:BP	response to unfolded protein	GO:0006986	0.000005715082 057912700	5.2429775295656 70	187	301	18	18092
GO:BP	regulation of cellular protein localization	GO:1903827	0.000007140423 243376140	5.1462760449724 30	580	301	32	18092
GO:BP	regulation of biological process	GO:0050789	0.000008884983 906303410	5.0513433545114 6	12145	301	247	18092
GO:BP	organelle organization	GO:0006996	0.000009229851 920502390	5.0348052665390 50	4115	301	113	18092
GO:BP	regulation of complement activation	GO:0030449	0.000009617859 361245670	5.0169215777593 50	110	301	14	18092
GO:BP	regulation of catalytic activity	GO:0050790	0.000009902679 290792230	5.0042472858288 10	2428	301	78	18092
GO:BP	interleukin-12-mediated signaling pathway	GO:0035722	0.000010015551 238132200	4.9993251429165 00	47	301	10	18092
GO:BP	regulation of cellular component organization	GO:0051128	0.000010472206 742755900	4.9799617925123 30	2431	301	78	18092
GO:BP	fibrinolysis	GO:0042730	0.000010774418 479598400	4.9676061604170 50	25	301	8	18092
GO:BP	protein-containing complex assembly	GO:0065003	0.000011257726 682688300	4.9485492994350 30	1689	301	61	18092
GO:BP	response to abiotic stimulus	GO:0009628	0.000011606711 929473000	4.9352907943126 70	1282	301	51	18092
GO:BP	biological process involved in interaction with symbiont	GO:0051702	0.000014165981 710648700	4.8487533232442 10	95	301	13	18092
GO:BP	cellular response to interleukin-12	GO:0071349	0.000015434774 98503850	4.8114996974723 600	49	301	10	18092
GO:BP	cell morphogenesis involved in differentiation	GO:0000904	0.000015822553 297301300	4.8007234327566 00	769	301	37	18092
GO:BP	system development	GO:0048731	0.000016676171 476017000	4.7779036478042 50	5151	301	132	18092
GO:BP	cell morphogenesis	GO:0000902	0.000016752533 49999010	4.7759195049338 30	1063	301	45	18092
GO:BP	metabolic process	GO:0008152	0.000018834872 75839680	4.7250373093875 90	11998	301	244	18092
GO:BP	response to interleukin-12	GO:0070671	0.000019012065 294426500	4.7209707028477 00	50	301	10	18092
GO:BP	cellular amide metabolic process	GO:0043603	0.000019487188 246454700	4.7102508195351 10	1223	301	49	18092
GO:BP	proteolysis	GO:0006508	0.000021227589 905868700	4.6730993110623 70	1846	301	64	18092
GO:BP	glucose catabolic process to pyruvate	GO:0061718	0.000021484979 53864230	4.6678650555830 10	27	301	8	18092
GO:BP	NADH regeneration	GO:0006735	0.000021484979 53864230	4.6678650555830 10	27	301	8	18092
GO:BP	canonical glycolysis	GO:0061621	0.000021484979 53864230	4.6678650555830 10	27	301	8	18092
GO:BP	biological regulation	GO:0065007	0.000021800972 02024860	4.6615241424679 10	12801	301	255	18092

GO:BP	animal organ development	GO:0048513	0.000021973042953267500	4.658109795318840	3770	301	105	18092
GO:BP	monosaccharide metabolic process	GO:0005996	0.000025683785946311200	4.590340958235500	281	301	21	18092
GO:BP	NAD metabolic process	GO:0019674	0.000028432122045595300	4.546190725314840	52	301	10	18092
GO:BP	response to oxygen-containing compound	GO:1901700	0.000028499171506625600	4.545167765090810	1774	301	62	18092
GO:BP	regulation of hydrolase activity	GO:0051336	0.000029046048511983800	4.536912941627080	1318	301	51	18092
GO:BP	regulation of cell morphogenesis	GO:0022604	0.000032841495159036400	4.483577079185443	312	301	22	18092
GO:BP	negative regulation of cellular process	GO:0048523	0.000034799454214857200	4.458427567356140	5208	301	132	18092
GO:BP	primary metabolic process	GO:0044238	0.000041638376650560500	4.380506210608350	10575	301	222	18092
GO:BP	cell junction organization	GO:0034330	0.000045934537165292500	4.337860655201920	730	301	35	18092
GO:BP	positive regulation of establishment of protein localization	GO:1904951	0.000046049910501205500	4.336771209525120	346	301	23	18092
GO:BP	protein-containing complex subunit organization	GO:0043933	0.000048736099475721400	4.312149231900500	1974	301	66	18092
GO:BP	carbohydrate biosynthetic process	GO:0016051	0.000059905680987057700	4.222531990559920	217	301	18	18092
GO:BP	blood vessel development	GO:0001568	0.000061712955793165600	4.209623652193300	810	301	37	18092
GO:BP	negative regulation of hydrolase activity	GO:0051346	0.000071176915120195300	4.147660838688300	475	301	27	18092
GO:BP	hexose catabolic process	GO:0019320	0.000072114703930097200	4.141976175160810	57	301	10	18092
GO:BP	regulation of molecular function	GO:0065009	0.000077572681975996700	4.110291193121490	2969	301	87	18092
GO:BP	response to endogenous stimulus	GO:0009719	0.000086260346412278200	4.064188802106610	1698	301	59	18092
GO:BP	regulation of humoral immune response	GO:0002920	0.000093732855669443200	4.028108151536740	131	301	14	18092
GO:BP	regulation of establishment of protein localization	GO:0070201	0.000115080721623799000	3.938997423491380	618	301	31	18092
GO:BP	negative regulation of wound healing	GO:0061045	0.000117561283107918000	3.929735682520760	76	301	11	18092
GO:BP	hexose biosynthetic process	GO:0019319	0.000121731083619086000	3.914598511987010	94	301	12	18092
GO:BP	positive regulation of organelle organization	GO:0010638	0.000123783502756928000	3.907337232044870	620	301	31	18092
GO:BP	regulation of wound healing	GO:0061041	0.000125145830928457000	3.902583613773890	134	301	14	18092
GO:BP	homeostatic process	GO:0042592	0.000151222446320578000	3.820383740649320	2033	301	66	18092
GO:BP	multicellular organismal process	GO:0032501	0.000151256558965900000	3.820285783875920	8065	301	180	18092
GO:BP	multicellular organism development	GO:0007275	0.000167498242586594000	3.775989745277580	5718	301	139	18092
GO:BP	nitrogen compound metabolic process	GO:0006807	0.000168181346546044000	3.774222174657980	10057	301	212	18092
GO:BP	cell population proliferation	GO:0008283	0.000192689666419235000	3.715141575108110	2091	301	67	18092

GO:BP	vasculature development	GO:0001944	0.000193345341399463	3.713666287665858100	847	301	37	18092
GO:BP	monosaccharide catabolic process	GO:0046365	0.000195438174215988000	3.708990603196030	63	301	10	18092
GO:BP	anatomical structure formation involved in morphogenesis	GO:0048646	0.000196181186469055000	3.707342643258000000	1235	301	47	18092
GO:BP	cellular metabolic process	GO:0044237	0.000200873042239313000	3.697078342954460 0600	10855	301	224	18092
GO:BP	peptide cross-linking	GO:0018149	0.000202886535178068000	3.692746774513750 0	35	301	8	18092
GO:BP	epithelium development	GO:0060429	0.000213594293205848000	3.670410354931490	1361	301	50	18092
GO:BP	positive regulation of cellular protein metabolic process	GO:0032270	0.000233518557094497030	3.631678601506830	1490	301	53	18092
GO:BP	glucose catabolic process	GO:0006007	0.000257111435713980000	3.589878606527000	36	301	8	18092
GO:BP	actin filament-based process	GO:0030029	0.000293343558655817	3.532623443738590 0	824	301	36	18092
GO:BP	cell development	GO:0048468	0.000300312777018114000	3.522426190044050 0	2161	301	68	18092
GO:BP	humoral immune response	GO:0006959	0.000309046387026255	3.509976329256210	384	301	23	18092
GO:BP	cell-cell adhesion	GO:0098609	0.000313148072938573 0	3.504250256530830 0	901	301	38	18092
GO:BP	regulation of response to wounding	GO:1903034	0.000315426069396344 0	3.501102415867280	167	301	15	18092
GO:BP	organonitrogen compound biosynthetic process	GO:1901566	0.000341245320063513 00	3.466933295949810 0	1854	301	61	18092
GO:BP	negative regulation of cellular protein metabolic process	GO:0032269	0.000352980905279353 0	3.452248787405680	1099	301	43	18092
GO:BP	actin cytoskeleton organization	GO:0030036	0.000379819173446999 00	3.420423115659940 0	723	301	33	18092
GO:BP	regulation of developmental process	GO:0050793	0.000431902753994554 0	3.364614026698445	2648	301	78	18092
GO:BP	regulation of metabolic process	GO:0019222	0.000491690551938215 0	3.308308136799370 0	7174	301	163	18092
GO:BP	regulation of transport	GO:0051049	0.000500216683692632 0	3.300841827369980 0	1830	301	60	18092
GO:BP	regulation of cell-substrate adhesion	GO:0010810	0.000500465635531978 0	3.300625737987280 0	223	301	17	18092
GO:BP	'de novo' protein folding	GO:0006458	0.000500572568017895 0	3.300532953938520 0	39	301	8	18092
GO:BP	leukocyte migration	GO:0050900	0.000501652673758374 0	3.299596868665440 0	523	301	27	18092
GO:BP	establishment or maintenance of cell polarity	GO:0007163	0.000645038861761129 0	3.190414119566290	227	301	17	18092
GO:BP	negative regulation of fibrinolysis	GO:0051918	0.000691024043819737 0	3.160506841313830 0	10	301	5	18092
GO:BP	negative regulation of response to wounding	GO:1903035	0.000778688927287379 0	3.108636000791430 0	91	301	11	18092
GO:BP	positive regulation of protein localization to nucleus	GO:1900182	0.000778688927287379 0	3.108636000791430 0	91	301	11	18092
GO:BP	hexose metabolic process	GO:0019318	0.000822820252657261 0	3.084695027248290	258	301	18	18092
GO:BP	complement activation	GO:0006956	0.000839429273986342 0	3.076015889414440	180	301	15	18092
GO:BP	chaperone cofactor-dependent protein refolding	GO:0051085	0.000893344587289449 0	3.048980989608500 0	29	301	7	18092

GO:BP	circulatory system development	GO:0072359	0.000909475943 1581390	3.0412087841121 50	1219	301	45	18092
GO:BP	zymogen activation	GO:0031638	0.000921601433 5725130	3.0354568583651 500	57	301	9	18092
GO:BP	regulation of cell adhesion	GO:0030155	0.000929784482 1030280	3.0316177063711 100	752	301	33	18092
GO:BP	ribosomal large subunit biogenesis	GO:0042273	0.000934883133 4181520	3.0292426754203 300	74	301	10	18092
GO:BP	integrin-mediated signaling pathway	GO:0007229	0.000950893190 6390350	3.0218682625801 30	113	301	12	18092
GO:BP	diterpenoid metabolic process	GO:0016101	0.000950893190 6390350	3.0218682625801 30	113	301	12	18092
GO:BP	cell-matrix adhesion	GO:0007160	0.001118614644 457080	2.9513194993602 900	236	301	17	18092
GO:BP	chaperone-mediated protein folding	GO:0061077	0.001250282554 114570	2.9029918287313 00	59	301	9	18092
GO:BP	cell junction assembly	GO:0034329	0.001314412222 337920	2.8812684111758 300	449	301	24	18092
GO:BP	viral entry into host cell	GO:0046718	0.001374811088 2287500	2.8617569738165 00	139	301	13	18092
GO:BP	positive regulation of protein metabolic process	GO:0051247	0.001427136507 2787500	2.8455344841225 600	1578	301	53	18092
GO:BP	positive regulation of ion transport	GO:0043270	0.001564203928 6472000	2.8057066276746 90	696	301	31	18092
GO:BP	regulation of response to stress	GO:0080134	0.001614786347 8667500	2.7918849309679 400	1455	301	50	18092
GO:BP	substantia nigra development	GO:0021762	0.001918955040 462870	2.7169352003075 800	46	301	8	18092
GO:BP	regulation of multicellular organismal process	GO:0051239	0.001972292203 3409600	2.7050287420836 70	2894	301	81	18092
GO:BP	skin development	GO:0043588	0.002254307715 600970	2.6469868025462 900	430	301	23	18092
GO:BP	positive regulation of cell motility	GO:2000147	0.002262503291 8850100	2.6454107802348 200	600	301	28	18092
GO:BP	response to nitrogen compound	GO:1901698	0.002303533415 4749100	2.6376054834108 200	1178	301	43	18092
GO:BP	modulation by host of viral process	GO:0044788	0.002309594681 4788600	2.6364642292169 800	33	301	7	18092
GO:BP	terpenoid metabolic process	GO:0006721	0.002387248464 258790	2.6221023773732 600	123	301	12	18092
GO:BP	response to organic cyclic compound	GO:0014070	0.002403027150 8309800	2.6192413222508 400	978	301	38	18092
GO:BP	positive regulation of endocytosis	GO:0045807	0.002750076512 1624100	2.5606552231342 200	103	301	11	18092
GO:BP	response to drug	GO:0042493	0.002792863521 730270	2.5539502863568 70	403	301	22	18092
GO:BP	ribose phosphate metabolic process	GO:0019693	0.002858038568 1011900	2.5439319148730 70	436	301	23	18092
GO:BP	regulation of cellular localization	GO:0060341	0.002896952939 442360	2.5380585597864 00	868	301	35	18092
GO:BP	response to oxidative stress	GO:0006979	0.003432362312 0101800	2.4644068753100 20	474	301	24	18092
GO:BP	positive regulation of cellular component movement	GO:0051272	0.003442280017 501070	2.4631538042266 100	613	301	28	18092
GO:BP	blood vessel morphogenesis	GO:0048514	0.003490601994 1968300	2.4570996675359 10	723	301	31	18092
GO:BP	positive regulation of cell migration	GO:0030335	0.003503704362 6863600	2.4554725460743 400	578	301	27	18092

GO:BP	regulation of cellular component movement	GO:0051270	0.003530639847 7002700	2.4521465815402 10	1156	301	42	18092
GO:BP	'de novo' posttranslational protein folding	GO:0051084	0.003533291395 644010	2.4518205441950 300	35	301	7	18092
GO:BP	positive regulation of locomotion	GO:0040017	0.003667497424 8578900	2.4356301824254 800	615	301	28	18092
GO:BP	regulation of cell motility	GO:2000145	0.003677650670 4535100	2.4344295255328 300	1076	301	40	18092
GO:BP	entry into host	GO:0044409	0.003814249296 1878000	2.4185909252332 500	152	301	13	18092
GO:BP	positive regulation of cell population proliferation	GO:0008284	0.003818451085 5596200	2.4181127683473 900	997	301	38	18092
GO:BP	retinoid metabolic process	GO:0001523	0.004027894528 516400	2.3949219100854 100	107	301	11	18092
GO:BP	pyruvate metabolic process	GO:0006090	0.004419745982 052770	2.3546026903257 800	154	301	13	18092
GO:BP	small molecule biosynthetic process	GO:0044283	0.004962050448 123570	2.3043388246606 80	698	301	30	18092
GO:BP	cytokine-mediated signaling pathway	GO:0019221	0.005052199205 84263	2.2965195337515 90	812	301	33	18092
GO:BP	regulation of fibrinolysis	GO:0051917	0.005197053858 9106700	2.2842427824062 100	14	301	5	18092
GO:BP	reactive oxygen species metabolic process	GO:0072593	0.005440556048 468030	2.2643567112502 900	294	301	18	18092
GO:BP	regulation of protein transport	GO:0051223	0.005503728235 035130	2.2593430189837 600	592	301	27	18092
GO:BP	response to organonitrogen compound	GO:0010243	0.005535314095 618620	2.2568577304991 400	1094	301	40	18092
GO:BP	regulation of ion transport	GO:0043269	0.005865112176 41096	2.2317236771323 600	1391	301	47	18092
GO:BP	tube morphogenesis	GO:0035239	0.005872499117 696920	2.2311770398001 500	975	301	37	18092
GO:BP	apoptotic cell clearance	GO:0043277	0.005892326971 554410	2.2297131616933 20	53	301	8	18092
GO:BP	regulation of cell migration	GO:0030334	0.005980216404 711020	2.2232831000130 40	1016	301	38	18092
GO:BP	RNA-dependent DNA biosynthetic process	GO:0006278	0.006222962310 137120	2.2060028293464 10	71	301	9	18092
GO:BP	regulation of organelle organization	GO:0033043	0.006238986731 238450	2.2048859380042 00	1224	301	43	18092
GO:BP	small molecule metabolic process	GO:0044281	0.006347776501 236580	2.1973783727156 20	1929	301	59	18092
GO:BP	negative regulation of molecular function	GO:0044092	0.006505517735 9738200	2.1867181347781 800	1226	301	43	18092
GO:BP	purine nucleoside triphosphate metabolic process	GO:0009144	0.006519836661 940410	2.1857632842844 200	91	301	10	18092
GO:BP	gluconeogenesis	GO:0006094	0.006519836661 940410	2.1857632842844 200	91	301	10	18092
GO:BP	regulation of anatomical structure morphogenesis	GO:0022603	0.006762765784 803870	2.1698756532561 10	1062	301	39	18092
GO:BP	cellular detoxification	GO:1990748	0.006918964303 175410	2.1599589100344 5	113	301	11	18092
GO:BP	positive regulation of protein transport	GO:0051222	0.007031447559 37996	2.1529552578628 400	330	301	19	18092
GO:BP	positive regulation of molecular function	GO:0044093	0.007043075689 336240	2.1522376443800 10	1844	301	57	18092
GO:BP	ribonucleoside triphosphate metabolic process	GO:0009199	0.007208658328 898660	2.1421455583841 10	92	301	10	18092

GO:BP	organelle assembly	GO:0070925	0.007228238311906370	2.1409675373729	904	301	35	18092
GO:BP	carbohydrate derivative metabolic process	GO:1901135	0.007321082488038410	2.135424699839910	1148	301	41	18092
GO:BP	nucleoside triphosphate metabolic process	GO:0009141	0.007546050439269590	2.1222802962164900	114	301	11	18092
GO:BP	positive regulation by host of viral process	GO:0044794	0.007689603628961480	2.1140960459191600	15	301	5	18092
GO:BP	regulation of protein localization to chromosome, telomeric region	GO:1904814	0.007689603628961480	2.1140960459191600	15	301	5	18092
GO:BP	carboxylic acid metabolic process	GO:0019752	0.007704197718 2379600	2.1132725801361400	1027	301	38	18092
GO:BP	regulation of anion transport	GO:0044070	0.007971770140840450	2.0984452323001 80	908	301	35	18092
GO:BP	carbohydrate metabolic process	GO:0005975	0.008132232244989790	2.0897902270240100	641	301	28	18092
GO:BP	positive regulation of NF-kappaB transcription factor activity	GO:0051092	0.008336095250882390	2.0790373316289700	163	301	13	18092
GO:BP	glucose metabolic process	GO:0006006	0.008380425411 9814	2.0767339349035300	216	301	15	18092
GO:BP	spindle organization	GO:0007051	0.008400303457491010	2.0757050249460500	189	301	14	18092
GO:BP	positive regulation of response to wounding	GO:1903036	0.008841186423 6824	2.0534894518777 60	74	301	9	18092
GO:BP	regulation of substrate adhesion-dependent cell spreading	GO:1900024	0.009043988559876810	2.0436399956837 70	56	301	8	18092
GO:BP	collagen fibril organization	GO:0030199	0.009043988559876810	2.0436399956837 70	56	301	8	18092
GO:BP	regulation of transforming growth factor beta production	GO:0071634	0.009122524315658750	2.0398849703702 90	40	301	7	18092
GO:BP	regulation of locomotion	GO:0040012	0.009380783319553040	2.0277608953996500	1118	301	40	18092
GO:BP	biological process involved in interaction with host	GO:0051701	0.009384390265544670	2.0275939396555100	218	301	15	18092
GO:BP	ribosome biogenesis	GO:0042254	0.010450542647043700	1.9808611581177100	308	301	18	18092
GO:BP	establishment of protein localization to chromosome	GO:0070199	0.010593519529 0166	1.9749597284580700	27	301	6	18092
GO:BP	regulation of cell morphogenesis involved in differentiation	GO:0010769	0.010635715728557100	1.9732332790096 00	96	301	10	18092
GO:BP	protein targeting to lysosome involved in chaperone-mediated autophagy	GO:0061740	0.010857302265331800	1.9642780713239900	3	301	3	18092
GO:BP	hexitol metabolic process	GO:0006059	0.010857302265331800	1.9642780713239900	3	301	3	18092
GO:BP	positive regulation of anion transport	GO:1903793	0.010953999021 52080	1.9604273022011100	507	301	24	18092
GO:BP	chaperone-mediated autophagy	GO:0061684	0.011032879674 9622	1.9573111182289400	16	301	5	18092
GO:BP	regulation of macromolecule metabolic process	GO:0060255	0.011652552980645200	1.9335789137848 20	6626	301	148	18092
GO:BP	isoprenoid metabolic process	GO:0006720	0.011731479928536400	1.9306471980928800	143	301	12	18092
GO:BP	cellular response to toxic substance	GO:0097237	0.012461947829696200	1.9044140711941200	120	301	11	18092
GO:BP	DNA biosynthetic process	GO:0071897	0.012826194237847000	1.8919021874823700	196	301	14	18092

GO:BP	transforming growth factor beta production	GO:0071604	0.012830311479064400	1.8917628002114400	42	301	7	18092
GO:BP	tube development	GO:0035295	0.013762388616073500	1.8613061829063200	1178	301	41	18092
GO:BP	regulation of peptide transport	GO:0090087	0.014155243223342800	1.8490826639429500	623	301	27	18092
GO:BP	regulation of vesicle-mediated transport	GO:0060627	0.014934894370 01000	1.8257978446824800	552	301	25	18092
GO:BP	positive regulation of wound healing	GO:0090303	0.015378285449114000	1.8130920820571300	60	301	8	18092
GO:BP	cellular oxidant detoxification	GO:0098869	0.015394196067769600	1.8126429863611700	100	301	10	18092
GO:BP	ATP metabolic process	GO:0046034	0.015568959022630300	1.8077404244158 9	317	301	18	18092
GO:BP	epithelial cell differentiation	GO:0030855	0.015619991936533400	1.8063191946533400	817	301	32	18092
GO:BP	cellular response to stress	GO:0033554	0.015741866920 49090	1.8029437633881900	2126	301	62	18092
GO:BP	oxoacid metabolic process	GO:0043436	0.016032430029339800	1.7950006468068200	1060	301	38	18092
GO:BP	ribose phosphate biosynthetic process	GO:0046390	0.016194325791654500	1.7906371279908900	200	301	14	18092
GO:BP	positive regulation of intracellular transport	GO:0032388	0.016201066158933700	1.7904564044878600	228	301	15	18092
GO:BP	movement in host environment	GO:0052126	0.018189420914737400	1.7401811270793100	175	301	13	18092
GO:BP	positive regulation of response to stimulus	GO:0048584	0.018318738611010100	1.7371044342237400	2374	301	67	18092
GO:BP	modulation of process of other organism involved in symbiotic interaction	GO:0051817	0.018397089686 96650	1.7352508744284600	102	301	10	18092
GO:BP	heterotypic cell-cell adhesion	GO:0034113	0.019744972905316400	1.7045434578798100	62	301	8	18092
GO:BP	endodermal cell differentiation	GO:0035987	0.020679808420677000	1.6844534888966700	45	301	7	18092
GO:BP	telomere maintenance via telomere lengthening	GO:0010833	0.020870226398161400	1.6804728397252100	82	301	9	18092
GO:BP	daunorubicin metabolic process	GO:0044597	0.021096514025541700	1.6757893013158 40	9	301	4	18092
GO:BP	polyketide metabolic process	GO:0030638	0.021096514025541700	1.6757893013158 40	9	301	4	18092
GO:BP	doxorubicin metabolic process	GO:0044598	0.021096514025541700	1.6757893013158 40	9	301	4	18092
GO:BP	activation of immune response	GO:0002253	0.022967743573 78900	1.6388816692188900	566	301	25	18092
GO:BP	ribonucleotide metabolic process	GO:0009259	0.022999400808967200	1.6382834782758400	425	301	21	18092
GO:BP	formation of primary germ layer	GO:0001704	0.023228740653978500	1.6339743348340 1	128	301	11	18092
GO:BP	phosphorylation	GO:0016310	0.024896577259556800	1.6038603548906900	2157	301	62	18092
GO:BP	modulation by host of symbiont process	GO:0051851	0.025114650101464600	1.6000728680742800	64	301	8	18092
GO:BP	purine ribonucleoside triphosphate metabolic process	GO:0009205	0.028072665222346600	1.5517163534357300	85	301	9	18092
GO:BP	cellular response to endogenous stimulus	GO:0071495	0.029589098367 67530	1.5288682683611 40	1434	301	46	18092

GO:BP	neural nucleus development	GO:0048857	0.031665506500 72090	1.4994135608907 600	66	301	8	18092
GO:BP	organic acid metabolic process	GO:0006082	0.032761700974 13050	1.4846335579341 700	1094	301	38	18092
GO:BP	tissue homeostasis	GO:0001894	0.032925803302 3096	1.4824636206029 400	272	301	16	18092
GO:BP	negative regulation of gene expression	GO:0010629	0.034039855833 487100	1.4680122879192 200	2516	301	69	18092
GO:BP	positive regulation of intracellular signal transduction	GO:1902533	0.034097268335 683200	1.4672804126280 100	1054	301	37	18092
GO:BP	positive regulation of establishment of protein localization to telomere	GO:1904851	0.034700174013 35630	1.4596683473171 700	10	301	4	18092
GO:BP	aminoglycoside antibiotic metabolic process	GO:0030647	0.034700174013 35630	1.4596683473171 700	10	301	4	18092
GO:BP	detoxification	GO:0098754	0.035927070629 23230	1.4445781922421 700	134	301	11	18092
GO:BP	growth	GO:0040007	0.036832032445 724400	1.4337743154755 600	1016	301	36	18092
GO:BP	regulation of endocytosis	GO:0030100	0.036881183629 95760	1.4331951495568 400	215	301	14	18092
GO:BP	nucleoside triphosphate biosynthetic process	GO:0009142	0.037296303106 882300	1.4283342142999 200	88	301	9	18092
GO:BP	positive regulation of cell adhesion	GO:0045785	0.037444043461 91790	1.4266172593361 700	439	301	21	18092
GO:BP	positive regulation of supramolecular fiber organization	GO:1902905	0.038856483704 470800	1.4105365031917 300	216	301	14	18092
GO:BP	generation of precursor metabolites and energy	GO:0006091	0.039969880524 94100	1.3982671498994 200	548	301	24	18092
GO:BP	cellular response to chemical stress	GO:0062197	0.040313132455 99260	1.3945534545014 500	373	301	19	18092
GO:BP	nucleoside diphosphate phosphorylation	GO:0006165	0.041324524491 3301	1.3837921350216 00	136	301	11	18092
GO:BP	cornification	GO:0070268	0.042233908469 042800	1.3743387256318 600	112	301	10	18092
GO:BP	establishment or maintenance of bipolar cell polarity	GO:0061245	0.042395013733 70410	1.3726852197110 400	50	301	7	18092
GO:BP	establishment or maintenance of apical/basal cell polarity	GO:0035088	0.042395013733 70410	1.3726852197110 400	50	301	7	18092
GO:BP	actin filament fragmentation	GO:0030043	0.042892616202 39600	1.3676174634925 100	4	301	3	18092
GO:BP	protein targeting to vacuole involved in autophagy	GO:0071211	0.042892616202 39600	1.3676174634925 100	4	301	3	18092
GO:BP	pentose biosynthetic process	GO:0019322	0.042892616202 39600	1.3676174634925 100	4	301	3	18092
GO:BP	telomere maintenance via telomerase	GO:0007004	0.044152078971 82920	1.3550488421490 100	69	301	8	18092
GO:BP	nucleotide phosphorylation	GO:0046939	0.044277313889 7279	1.3538187337340 00	137	301	11	18092
GO:BP	regulation of DNA biosynthetic process	GO:2000278	0.045662543824 95220	1.3404398979626 00	113	301	10	18092
GO:BP	purine ribonucleotide metabolic process	GO:0009150	0.046821421780 099900	1.3295554026454 500	411	301	20	18092
GO:BP	response to heat	GO:0009408	0.047415130503 99180	1.3240830497639 100	164	301	12	18092
GO:BP	chaperone-mediated protein complex assembly	GO:0051131	0.048003181358 48880	1.3187299792774 900	21	301	5	18092

GO:CC	extracellular exosome	GO:0070062	9.061888786088 37E-169	168.04278127209 300	2180	301	241	18963
GO:CC	extracellular vesicle	GO:1903561	3.877792795954 88E-166	165.41141540051 200	2266	301	242	18963
GO:CC	extracellular organelle	GO:0043230	4.825636291821 06E-166	165.31644541396 60	2268	301	242	18963
GO:CC	extracellular space	GO:0005615	1.674776814187 02E-140	139.77604306016 500	3598	301	259	18963
GO:CC	extracellular region	GO:0005576	8.333898306417 05E-120	119.07915180328 300	4602	301	264	18963
GO:CC	vesicle	GO:0031982	4.862720984549 59E-116	115.31312064886 600	4071	301	251	18963
GO:CC	focal adhesion	GO:0005925	2.957487277617 53E-50	49.529077114924	418	301	71	18963
GO:CC	cell-substrate junction	GO:0030055	1.168006731872 46E-49	48.932554654135 70	426	301	71	18963
GO:CC	blood microparticle	GO:0072562	5.062282102091 94E-41	40.295653656892 500	141	301	43	18963
GO:CC	anchoring junction	GO:0070161	1.981572397464 15E-39	38.702990055934 000	843	301	82	18963
GO:CC	collagen-containing extracellular matrix	GO:0062023	9.778502935973 61E-32	31.009727629508 200	424	301	55	18963
GO:CC	membrane-bounded organelle	GO:0043227	1.861923356889 64E-30	29.730038200027 600	12836	301	287	18963
GO:CC	melanosome	GO:0042470	4.865536060626 4E-30	29.312869304348	105	301	32	18963
GO:CC	pigment granule	GO:0048770	4.865536060626 4E-30	29.312869304348	105	301	32	18963
GO:CC	vesicle lumen	GO:0031983	5.846556035771 65E-30	29.233099883507 50	326	301	48	18963
GO:CC	secretory granule lumen	GO:0034774	3.823557826800 9E-28	27.417532337233 700	320	301	46	18963
GO:CC	cytoplasmic vesicle lumen	GO:0060205	6.705731301117 32E-28	27.173553852753 300	324	301	46	18963
GO:CC	cytoplasm	GO:0005737	1.593879055433 44E-26	25.797544636233 90	11888	301	273	18963
GO:CC	extracellular matrix	GO:0031012	3.195563587246 45E-26	25.495452536176 600	564	301	56	18963
GO:CC	secretory granule	GO:0030141	9.010046295868 11E-26	25.045272977501 700	855	301	67	18963
GO:CC	organelle	GO:0043226	9.525745465113 4E-26	25.021101027335 600	13974	301	292	18963
GO:CC	cell junction	GO:0030054	2.485601150198 17E-25	24.604568558785 70	2131	301	105	18963
GO:CC	cytosolic ribosome	GO:0022626	9.043660244170 22E-24	23.043655761768 300	109	301	28	18963
GO:CC	cytoplasmic vesicle	GO:0031410	1.386442546546 75E-23	22.858098122649 20	2437	301	110	18963
GO:CC	intracellular vesicle	GO:0097708	1.592691899975 23E-23	22.797868228644 500	2441	301	110	18963
GO:CC	cytosol	GO:0005829	2.829697713830 71E-23	22.548259956075 400	5231	301	169	18963
GO:CC	protein-containing complex	GO:0032991	2.936171609726 51E-23	22.532218564907 500	5556	301	175	18963
GO:CC	secretory vesicle	GO:0099503	6.618203448773 04E-22	21.179259886417 40	1028	301	68	18963
GO:CC	endoplasmic reticulum lumen	GO:0005788	1.514556892720 87E-18	17.819714408213 80	307	301	36	18963

GO:CC	endomembrane system	GO:0012505	6.93424071102465E-18	17.159001086582800	4633	301	147	18963
GO:CC	ribosomal subunit	GO:0044391	8.72637206274192E-18	17.059166274119000	191	301	29	18963
GO:CC	intracellular non-membrane-bounded organelle	GO:0043232	2.04007497290785E-17	16.690353871926100	4326	301	140	18963
GO:CC	non-membrane-bounded organelle	GO:0043228	2.37894836076647E-17	16.623614984981500	4333	301	140	18963
GO:CC	organelle lumen	GO:0043233	3.83208440211151E-16	15.4165649341009	5468	301	159	18963
GO:CC	membrane-enclosed lumen	GO:0031974	3.83208440211151E-16	15.4165649341009	5468	301	159	18963
GO:CC	ribosome	GO:0005840	9.86359567562569E-16	15.005964738464600	245	301	30	18963
GO:CC	cytosolic large ribosomal subunit	GO:0022625	3.84935696332014E-15	14.414611813506100	57	301	17	18963
GO:CC	supramolecular fiber	GO:0099512	1.62457992944172E-13	12.789258916475600	1006	301	55	18963
GO:CC	ficolin-1-rich granule lumen	GO:1904813	1.65825988288339E-13	12.780347405717030	124	301	21	18963
GO:CC	supramolecular polymer	GO:0099081	2.28255863680739E-13	12.641578057029200	1014	301	55	18963
GO:CC	supramolecular complex	GO:0099080	2.73450914760089E-13	12.563120619465800	1337	301	64	18963
GO:CC	intracellular anatomical structure	GO:0005622	2.85578715699596E-12	11.544274163838000	14764	301	283	18963
GO:CC	ribonucleoprotein complex	GO:1990904	5.06173465827972E-12	11.295700624777400	693	301	43	18963
GO:CC	endoplasmic reticulum	GO:0005783	1.27071051771519E-11	10.8959533753926600	1975	301	77	18963
GO:CC	platelet alpha granule	GO:0031091	1.60886448626575E-11	10.793480534736000	90	301	17	18963
GO:CC	cell surface	GO:0009986	2.37546468568491E-11	10.624251421538700	922	301	49	18963
GO:CC	platelet alpha granule lumen	GO:0031093	2.78677546733554E-11	10.554898021320090	66	301	15	18963
GO:CC	ficolin-1-rich granule	GO:0101002	5.74488947907488E-11	10.240718321908600	184	301	22	18963
GO:CC	polysome	GO:0005844	1.36683464731598E-10	9.8642840209857 8	73	301	15	18963
GO:CC	large ribosomal subunit	GO:0015934	1.59947932915 7E-10	9.79602136814071 0	119	301	18	18963
GO:CC	intracellular organelle	GO:0043229	3.07504556622669E-10	9.5121484444368 00	12431	301	252	18963
GO:CC	cytoskeleton	GO:0005856	5.68036180106376E-10	9.24562400175352	2302	301	81	18963
GO:CC	lysosome	GO:0005764	9.42822694738676E-10	9.0255699720947 30	709	301	40	18963
GO:CC	lytic vacuole	GO:0000323	9.42822694738676E-10	9.0255699720947 30	709	301	40	18963
GO:CC	cytosolic small ribosomal subunit	GO:0022627	1.94701012789079E-09	8.7106317893758 90	47	301	12	18963
GO:CC	membrane raft	GO:0045121	9.09916701735264E-09	8.0409983633190 6	336	301	26	18963
GO:CC	membrane microdomain	GO:0098857	9.72079886857477E-09	8.0122980426913 00	337	301	26	18963
GO:CC	vacuole	GO:0005773	1.32127910210311E-08	7.8790054339372 30	807	301	41	18963

GO:CC	vacuolar lumen	GO:0005775	1.32161909822115E-08	7.8788936941519 20	174	301	19	18963
GO:CC	intracellular organelle lumen	GO:0070013	1.42436308588723E-08	7.8463792901250 10	5304	301	137	18963
GO:CC	cell cortex	GO:0005938	1.57865810838566E-08	7.8017119154120 80	318	301	25	18963
GO:CC	basement membrane	GO:0005604	2.50314039111143E-08	7.6015147918719 40	103	301	15	18963
GO:CC	basolateral plasma membrane	GO:0016323	2.51378808033022E-08	7.5996713373988 70	249	301	22	18963
GO:CC	membrane	GO:0016020	3.36639495981 65E-08	7.4728349320897 70	9813	301	210	18963
GO:CC	small ribosomal subunit	GO:0015935	5.82442959750316E-08	7.2347465998790 300	76	301	13	18963
GO:CC	actin cytoskeleton	GO:0015629	5.88278919315969E-08	7.2304167140616 20	513	301	31	18963
GO:CC	cortical cytoskeleton	GO:0030863	9.62422566855998E-08	7.0166342022246 00	113	301	15	18963
GO:CC	intracellular membrane-bounded organelle	GO:0043231	1.59649879842 08E-07	6.7968314039891 80	11250	301	229	18963
GO:CC	synapse	GO:0045202	1.68796964220161E-07	6.7726353683400 30	1382	301	54	18963
GO:CC	cell-cell junction	GO:0005911	1.84949799184343E-07	6.7329461358986 20	506	301	30	18963
GO:CC	filopodium	GO:0030175	4.59355176771522E-07	6.3378513849148 60	107	301	14	18963
GO:CC	side of membrane	GO:0098552	6.20492627128086E-07	6.2072633745465 80	632	301	33	18963
GO:CC	polysomal ribosome	GO:0042788	6.25637773260445E-07	6.2036770383635 800	34	301	9	18963
GO:CC	actin-based cell projection	GO:0098858	8.56145049817307E-07	6.0674526500440 60	222	301	19	18963
GO:CC	cell periphery	GO:0071944	9.34891190711589E-07	6.0292389324680 00	5786	301	140	18963
GO:CC	primary lysosome	GO:0005766	9.67841959930073E-07	6.0141955533670 30	154	301	16	18963
GO:CC	azurophil granule	GO:0042582	9.67841959930073E-07	6.0141955533670 30	154	301	16	18963
GO:CC	perinuclear region of cytoplasm	GO:0048471	0.000002518964555025500	5.5987779606829 20	740	301	35	18963
GO:CC	cell leading edge	GO:0031252	0.000007477760135245090	5.1262284698598 20	429	301	25	18963
GO:CC	polymeric cytoskeletal fiber	GO:0099513	0.000008038282962766630	5.0948367098875 60	775	301	35	18963
GO:CC	lamellipodium	GO:0030027	0.000008810290388779000	5.0550097769266 70	204	301	17	18963
GO:CC	endocytic vesicle	GO:0030139	0.000009458758703590170	5.0241658534029 20	313	301	21	18963
GO:CC	fibrinogen complex	GO:0005577	0.000015624875562723000	4.8061834327127 20	8	301	5	18963
GO:CC	COP9 signalosome	GO:0008180	0.000017726018 01416640	4.7513888136772 4	35	301	8	18963
GO:CC	cortical actin cytoskeleton	GO:0030864	0.000023388734931279800	4.6309932680250 80	83	301	11	18963
GO:CC	plasma membrane region	GO:0098590	0.000026481801967689900	4.5770524664378 50	1255	301	46	18963
GO:CC	endoplasmic reticulum chaperone complex	GO:0034663	0.000068496259 71768730	4.1643331427896 00	10	301	5	18963

GO:CC	plasma membrane	GO:0005886	0.000088221876 57875230	4.0544237085262 20	5663	301	131	18963
GO:CC	sarcolemma	GO:0042383	0.000093472859 72318110	4.0293144702342 30	138	301	13	18963
GO:CC	endocytic vesicle lumen	GO:0071682	0.000145563161 80314600	3.8369485195962 100	20	301	6	18963
GO:CC	platelet dense granule	GO:0042827	0.000201079360 57866900	3.6966325044743 80	21	301	6	18963
GO:CC	banded collagen fibril	GO:0098643	0.000209718607 65504900	3.6783630342776 800	12	301	5	18963
GO:CC	fibrillar collagen trimer	GO:0005583	0.000209718607 65504900	3.6783630342776 800	12	301	5	18963
GO:CC	cell trailing edge	GO:0031254	0.000336369000 51163100	3.4731840352495 300	13	301	5	18963
GO:CC	uropod	GO:0001931	0.000336369000 51163100	3.4731840352495 300	13	301	5	18963
GO:CC	brush border	GO:0005903	0.000385802708 34376300	3.4136347279243 2	109	301	11	18963
GO:CC	rough endoplasmic reticulum	GO:0005791	0.000437669880 80435400	3.3588533392688 700	89	301	10	18963
GO:CC	chaperone complex	GO:0101031	0.000479137856 96042400	3.3195395139268 900	24	301	6	18963
GO:CC	nucleosome	GO:0000786	0.000505884420 2074210	3.2959486954128 100	112	301	11	18963
GO:CC	platelet dense granule lumen	GO:0031089	0.000516450932 89807	3.2869709337452 70	14	301	5	18963
GO:CC	azurophil granule lumen	GO:0035578	0.000537929165 1843650	3.2692749087107 90	91	301	10	18963
GO:CC	cell body	GO:0044297	0.000571334876 1225490	3.2431092643951 300	614	301	27	18963
GO:CC	microvillus	GO:0005902	0.000595161303 0924640	3.2253653140209 000	92	301	10	18963
GO:CC	DNA packaging complex	GO:0044815	0.000921231437 9512540	3.0356312497180 3	119	301	11	18963
GO:CC	cell-cell contact zone	GO:0044291	0.000947980188 8673940	3.0232007385643 30	76	301	9	18963
GO:CC	lysosomal membrane	GO:0005765	0.000971726850 6814700	3.0124557967127 000	381	301	20	18963
GO:CC	lytic vacuole membrane	GO:0098852	0.000971726850 6814700	3.0124557967127 000	381	301	20	18963
GO:CC	invadopodium	GO:0071437	0.001097763086 3992200	2.9594913769818 6	16	301	5	18963
GO:CC	laminin-10 complex	GO:0043259	0.001178602168 2850600	2.9286327642646 5	3	301	3	18963
GO:CC	external side of plasma membrane	GO:0009897	0.001179173233 1832700	2.9284223877047 80	420	301	21	18963
GO:CC	zona pellucida receptor complex	GO:0002199	0.001232965326 1724500	2.9090491365946 30	8	301	4	18963
GO:CC	high-density lipoprotein particle	GO:0034364	0.001581699295 3487100	2.8008760788559 90	29	301	6	18963
GO:CC	ruffle	GO:0001726	0.001876834244 8043500	2.7265740809990 7	180	301	13	18963
GO:CC	protein-DNA complex	GO:0032993	0.002333406681 772340	2.6320095628532 7	212	301	14	18963
GO:CC	chaperonin-containing T-complex	GO:0005832	0.003606966466 051200	2.4428578952964 50	10	301	4	18963
GO:CC	cell projection membrane	GO:0031253	0.003699645764 3953400	2.4318398569960 500	348	301	18	18963

GO:CC	cluster of actin-based cell projections	GO:0098862	0.003976024952 519730	2.4005508987446 400	165	301	12	18963
GO:CC	basal plasma membrane	GO:0009925	0.004485048633 638730	2.3482328433208 000	51	301	7	18963
GO:CC	very-low-density lipoprotein particle	GO:0034361	0.004791328881 252390	2.3195440177432 000	21	301	5	18963
GO:CC	complex of collagen trimers	GO:0098644	0.004791328881 252390	2.3195440177432 000	21	301	5	18963
GO:CC	triglyceride-rich plasma lipoprotein particle	GO:0034385	0.004791328881 252390	2.3195440177432 000	21	301	5	18963
GO:CC	intercalated disc	GO:0014704	0.005811734907 732240	2.2356942035162 60	53	301	7	18963
GO:CC	collagen trimer	GO:0005581	0.006009765056 8621600	2.2211425057847 40	95	301	9	18963
GO:CC	plasma membrane protein complex	GO:0098797	0.006044920440 5499800	2.2186094106770 700	699	301	27	18963
GO:CC	lamellipodium membrane	GO:0031258	0.006120305145 676950	2.2132269242956 20	22	301	5	18963
GO:CC	ruffle membrane	GO:0032587	0.006540381951 4946900	2.1843968885896 800	96	301	9	18963
GO:CC	lysosomal lumen	GO:0043202	0.007110277949 8640900	2.1481134218113 300	97	301	9	18963
GO:CC	vacuolar membrane	GO:0005774	0.007490172760 91822	2.1255081651779 400	438	301	20	18963
GO:CC	plasma lipoprotein particle	GO:0034358	0.008152538621 143190	2.0887071351273 90	38	301	6	18963
GO:CC	lipoprotein particle	GO:1990777	0.008152538621 143190	2.0887071351273 90	38	301	6	18963
GO:CC	leading edge membrane	GO:0031256	0.008483638691 772990	2.0714178358545 1	178	301	12	18963
GO:CC	cytoplasmic ribonucleoprotein granule	GO:0036464	0.008566489408 807540	2.0671971177198 700	238	301	14	18963
GO:CC	intermediate-density lipoprotein particle	GO:0034363	0.011509896187 438800	1.9389285934358 70	5	301	3	18963
GO:CC	midbody	GO:0030496	0.011755087719 423400	1.9297741257122 100	184	301	12	18963
GO:CC	protein-lipid complex	GO:0032994	0.012758196726 801500	1.8942107054693 300	41	301	6	18963
GO:CC	actomyosin	GO:0042641	0.012875502853 468700	1.8902358005607 800	81	301	8	18963
GO:CC	ribonucleoprotein granule	GO:0035770	0.014047314347 916400	1.8524066989168 700	249	301	14	18963
GO:CC	chylomicron	GO:0042627	0.016350442847 800200	1.7864704800831 200	14	301	4	18963
GO:CC	microvillus membrane	GO:0031528	0.017580773153 836900	1.7549620297706 800	27	301	5	18963
GO:CC	cell projection	GO:0042995	0.019905887126 672000	1.7010184628609 300	2352	301	61	18963
GO:CC	membrane protein complex	GO:0098796	0.020182207018 775800	1.6950313433683 900	1326	301	40	18963
GO:CC	nucleus	GO:0005634	0.020797309378 51130	1.6819928476165 700	7565	301	153	18963
GO:CC	plasma membrane bounded cell projection	GO:0120025	0.021088749653 39870	1.6759491687065 400	2255	301	59	18963
GO:CC	apical part of cell	GO:0045177	0.027479787614 233800	1.5609866281744 500	443	301	19	18963
GO:CC	glutamatergic synapse	GO:0098978	0.031083704017 908100	1.5074672350870 200	373	301	17	18963

GO:CC	basal part of cell	GO:0045178	0.032762226916378500	1.4846265860134200	69	301	7	18963
GO:CC	adherens junction	GO:0005912	0.034193225141802600	1.4660599341484100	175	301	11	18963
GO:CC	contractile actin filament bundle	GO:0097517	0.039308173408 39750	1.4055171367213700	71	301	7	18963
GO:CC	stress fiber	GO:0001725	0.039308173408 39750	1.4055171367213700	71	301	7	18963
GO:CC	membrane attack complex	GO:0005579	0.039342257486 36760	1.4051407235792800	7	301	3	18963
GO:CC	contractile fiber	GO:0043292	0.041218847329429100	1.3849041572794600	242	301	13	18963
GO:CC	microtubule cytoskeleton	GO:0015630	0.045342873913 3215	1.3434909569677 30	1283	301	38	18963
GO:CC	filopodium membrane	GO:0031527	0.047537190080 77930	1.3229664929586600	18	301	4	18963
KEGG	Coronavirus disease - COVID-19	KEGG:05171	1.317376100476 46E-15	14.880290219690 10	231	237	37	7987
KEGG	Ribosome	KEGG:03010	4.607017727499 16E-12	11.336580116607700	154	237	27	7987
KEGG	Focal adhesion	KEGG:04510	1.234021792792 3E-11	10.908677170606000	200	237	30	7987
KEGG	ECM-receptor interaction	KEGG:04512	6.853878733915 4E-10	9.1640635838363 10	88	237	19	7987
KEGG	Complement and coagulation cascades	KEGG:04610	3.551108694129 17E-09	8.4496360343900 00	85	237	18	7987
KEGG	Phagosome	KEGG:04145	0.000006647513762126080	5.1773407548900 8	148	237	19	7987
KEGG	Prion disease	KEGG:05020	0.000012452610364241100	4.9047396005396 80	273	237	26	7987
KEGG	Pathogenic Escherichia coli infection	KEGG:05130	0.000031079191 89699530	4.5075302819959 1	196	237	21	7987
KEGG	Legionellosis	KEGG:05134	0.000071133920 90934830	4.1479232522839 7	57	237	11	7987
KEGG	Regulation of actin cytoskeleton	KEGG:04810	0.000168891072 28294900	3.7723933069756 30	217	237	21	7987
KEGG	PI3K-Akt signaling pathway	KEGG:04151	0.000174238473 18112600	3.7588559432122500	353	237	28	7987
KEGG	Systemic lupus erythematosus	KEGG:05322	0.000182834016259361	3.7379430006186800	133	237	16	7987
KEGG	Carbon metabolism	KEGG:01200	0.000192267657 39324700	3.7160937651477900	118	237	15	7987
KEGG	Proteoglycans in cancer	KEGG:05205	0.000266367905 20887900	3.5745181046908600	205	237	20	7987
KEGG	Salmonella infection	KEGG:05132	0.000432636961 29060900	3.3638763804150700	249	237	22	7987
KEGG	Parkinson disease	KEGG:05012	0.001484059319 6142000	2.8285487394436200	249	237	21	7987
KEGG	Platelet activation	KEGG:04611	0.001723293612740790	2.7636407216641900	124	237	14	7987
KEGG	Glycolysis / Gluconeogenesis	KEGG:00010	0.002538304522675390	2.5954562764162600	67	237	10	7987
KEGG	Central carbon metabolism in cancer	KEGG:05230	0.003755708824 2674600	2.4253080854463300	70	237	10	7987
KEGG	Amoebiasis	KEGG:05146	0.004190930706738070	2.3776895197746200	101	237	12	7987
KEGG	Protein digestion and absorption	KEGG:04974	0.005101480990176960	2.2923037273349600	103	237	12	7987

KEGG	Gap junction	KEGG:04540	0.005483845566 2239	2.2609147841307300	88	237	11	7987
KEGG	Biosynthesis of amino acids	KEGG:01230	0.006891624708 36129	2.1616783806038 00	75	237	10	7987
KEGG	HIF-1 signaling pathway	KEGG:04066	0.008933495535899970	2.0489785752759300	109	237	12	7987
KEGG	Tight junction	KEGG:04530	0.013664862468169600	1.8643947349640500	168	237	15	7987
KEGG	Leukocyte transendothelial migration	KEGG:04670	0.013813343875 65930	1.8597011765293800	114	237	12	7987
KEGG	Amyotrophic lateral sclerosis	KEGG:05014	0.018930164546598100	1.7228456110035000	363	237	24	7987
KEGG	Estrogen signaling pathway	KEGG:04915	0.020990232265536700	1.6779827557442 90	137	237	13	7987
KEGG	Pentose phosphate pathway	KEGG:00030	0.021604702371727900	1.6654517121903600	30	237	6	7987

Table S 7. *GO analysis of WI-38 cell-derived exosome. The analysis was performed by using g:Profiler software.*
**The list of proteins associated with each ontology is available on request deanna.shea@vuw.ac.nz*

Source	Term name	Term ID	Adjusted p-value	Negative_log10 of adjusted p-value	Term size	Query size	Intersection size	Effective domain size
GO:MF	structural molecule activity	GO:0005198	2.412352006127 33E-42	41.617559320427 20	698	307	80	18694
GO:MF	extracellular matrix structural constituent	GO:0005201	5.207081651559 05E-42	41.283405612156 60	169	307	47	18694
GO:MF	cell adhesion molecule binding	GO:0050839	1.650866912378 07E-34	33.782287936761 20	548	307	65	18694
GO:MF	integrin binding	GO:0005178	7.140091192197 45E-23	22.146296241443000	148	307	31	18694
GO:MF	signaling receptor binding	GO:0005102	4.993562548682 65E-19	18.301589505840 2	1681	307	85	18694
GO:MF	protein-containing complex binding	GO:0044877	4.267379641734 46E-18	17.369838718993000	1282	307	72	18694
GO:MF	cadherin binding	GO:0045296	2.572955902416 32E-12	11.589567657047100	332	307	31	18694
GO:MF	collagen binding	GO:0005518	8.034958622142 69E-12	11.095016355393700	69	307	16	18694
GO:MF	glycosaminoglycan binding	GO:0005539	9.987825402491 43E-12	11.000529058170600	237	307	26	18694
GO:MF	peptidase regulator activity	GO:0061134	2.404839431816 91E-11	10.618913915632700	225	307	25	18694
GO:MF	identical protein binding	GO:0042802	2.707320471408 26E-11	10.567460332804 90	2080	307	81	18694
GO:MF	endopeptidase inhibitor activity	GO:0004866	1.046071122823 9E-10	9.9804387865969 70	179	307	22	18694
GO:MF	peptidase inhibitor activity	GO:0030414	1.850535470635 77E-10	9.7327025860329 40	184	307	22	18694
GO:MF	endopeptidase regulator activity	GO:0061135	2.882199598735 53E-10	9.5402759466213 3	188	307	22	18694
GO:MF	protease binding	GO:0002020	6.906767771084 67E-10	9.1607251461991 50	139	307	19	18694
GO:MF	extracellular matrix structural constituent conferring tensile strength	GO:0030020	7.781708302130 49E-10	9.1089250527856 1	41	307	12	18694
GO:MF	extracellular matrix binding	GO:0050840	1.862494465400 74E-09	8.7299050091297 30	55	307	13	18694

GO:MF	calcium ion binding	GO:0005509	1.942531072236 6E-09	8.7116320256066 00	722	307	41	18694
GO:MF	heparin binding	GO:0008201	2.423870911406 36E-09	8.6154905132007 70	168	307	20	18694
GO:MF	proteoglycan binding	GO:0043394	5.563997265902 67E-09	8.2546130920882 70	37	307	11	18694
GO:MF	sulfur compound binding	GO:1901681	6.127828276297 29E-09	8.2126934136922 70	264	307	24	18694
GO:MF	enzyme inhibitor activity	GO:0004857	2.552930348800 16E-08	7.5929610338226 10	386	307	28	18694
GO:MF	growth factor binding	GO:0019838	5.121814720333 09E-08	7.2905761360183 800	137	307	17	18694
GO:MF	lipoprotein particle receptor binding	GO:0070325	9.175352771122 54E-08	7.0373772291351 00	26	307	9	18694
GO:MF	carbohydrate derivative binding	GO:0097367	1.797100443940 44E-07	6.7454276485282 10	2286	307	77	18694
GO:MF	enzyme binding	GO:0019899	2.547870113993 48E-07	6.5938227153530 50	1866	307	67	18694
GO:MF	protein binding	GO:0005515	7.384154820285 39E-07	6.1316992062277 10	14752	307	281	18694
GO:MF	antioxidant activity	GO:0016209	8.206025433856 66E-07	6.0858671413093 40	87	307	13	18694
GO:MF	RNA binding	GO:0003723	0.000003591225 170743800	5.4447573636442 70	1946	307	66	18694
GO:MF	serine-type endopeptidase inhibitor activity	GO:0004867	0.000003666739 981099860	5.4357198859972 2	98	307	13	18694
GO:MF	platelet-derived growth factor binding	GO:0048407	0.000003910390 433680990	5.4077798782236	11	307	6	18694
GO:MF	structural constituent of cytoskeleton	GO:0005200	0.000007643345 15548826	5.1167165282549 600	104	307	13	18694
GO:MF	enzyme regulator activity	GO:0030234	0.000062807503 61194520	4.2019884680049 8	1228	307	46	18694
GO:MF	peroxidase activity	GO:0004601	0.000088185976 74907810	4.0546004704770 10	53	307	9	18694
GO:MF	oxidoreductase activity, acting on peroxide as acceptor	GO:0016684	0.000169011587 26184100	3.7720835195794 00	57	307	9	18694
GO:MF	low-density lipoprotein particle receptor binding	GO:0050750	0.000399814695 5721960	3.3981412470147 500	21	307	6	18694
GO:MF	oxidoreductase activity, acting on the CH-OH group of donors, NAD or NADP as acceptor	GO:0016616	0.000507591368 3053100	3.2944857717807 300	125	307	12	18694
GO:MF	extracellular matrix structural constituent conferring compression resistance	GO:0030021	0.000542184163 2269750	3.2658531719705 50	22	307	6	18694
GO:MF	disordered domain specific binding	GO:0097718	0.000661938276 1019850	3.1791825054214 50	35	307	7	18694
GO:MF	unfolded protein binding	GO:0051082	0.001047552736 1853700	2.9798241044401 40	111	307	11	18694
GO:MF	oxidoreductase activity, acting on CH-OH group of donors	GO:0016614	0.001344381412 9681800	2.8714775005920 00	137	307	12	18694
GO:MF	oxidoreductase activity	GO:0016491	0.002075069434 6489600	2.6829673666240 000	771	307	31	18694
GO:MF	fructose-bisphosphate aldolase activity	GO:0004332	0.002129390951 4240100	2.6717445957440 00	3	307	3	18694
GO:MF	actin binding	GO:0003779	0.002337243398 6905500	2.6312960581666 50	445	307	22	18694
GO:MF	laminin binding	GO:0043236	0.002519529095 4222200	2.5986806220637 80	28	307	6	18694

GO:MF	heparan sulfate proteoglycan binding	GO:0043395	0.002953662036 5049400	2.5296391989624 000	17	307	5	18694
GO:MF	haptoglobin binding	GO:0031720	0.006725776412 8521200	2.1722575741725 20	10	307	4	18694
GO:MF	small molecule binding	GO:0036094	0.007935423020 672960	2.1004299169687 200	2507	307	68	18694
GO:MF	endopeptidase activity	GO:0004175	0.010125395297 548900	1.9945880128349 700	453	307	21	18694
GO:MF	ion binding	GO:0043167	0.010160992932 480400	1.9930638507108 800	6055	307	134	18694
GO:MF	nucleoside binding	GO:0001882	0.015245897377 406000	1.8168470078623 400	395	307	19	18694
GO:MF	molecular carrier activity	GO:0140104	0.016998441197 23440	1.7695909027675 500	56	307	7	18694
GO:MF	lipid binding	GO:0008289	0.017830884676 69860	1.7488271088337 90	779	307	29	18694
GO:MF	cytoskeletal protein binding	GO:0008092	0.021321313957 612000	1.6711860347788 300	995	307	34	18694
GO:MF	actin filament binding	GO:0051015	0.022478870520 99580	1.6482255142249 600	210	307	13	18694
GO:MF	protein folding chaperone	GO:0044183	0.027810851163 434700	1.5557857191572 000	26	307	5	18694
GO:MF	carbohydrate binding	GO:0030246	0.029116869680 908000	1.5358553173186 000	278	307	15	18694
GO:MF	GTP binding	GO:0005525	0.032080134210 225500	1.4937638234727 10	382	307	18	18694
GO:MF	serine-type peptidase activity	GO:0008236	0.032723013046 16100	1.4851467145032 900	188	307	12	18694
GO:MF	purine ribonucleoside binding	GO:0032550	0.036637249887 5066	1.4360771333531 400	386	307	18	18694
GO:MF	purine nucleoside binding	GO:0001883	0.040421483285 96840	1.3933877538812 900	389	307	18	18694
GO:MF	ribonucleoside binding	GO:0032549	0.040421483285 96840	1.3933877538812 900	389	307	18	18694
GO:MF	oxygen carrier activity	GO:0005344	0.040966121014 79300	1.3875751564184 60	15	307	4	18694
GO:MF	serine hydrolase activity	GO:0017171	0.042092426322 854600	1.3757960396058 300	193	307	12	18694
GO:BP	regulated exocytosis	GO:0045055	4.240491780238 8E-36	35.372583774289 60	799	308	80	18092
GO:BP	exocytosis	GO:0006887	3.316460460850 37E-34	33.479325176033 90	921	308	83	18092
GO:BP	platelet degranulation	GO:0002576	3.771013705213 35E-32	31.423541889209 900	127	308	37	18092
GO:BP	vesicle-mediated transport	GO:0016192	8.035578411145 92E-32	31.094982856706 800	2193	308	122	18092
GO:BP	extracellular matrix organization	GO:0030198	1.060096340200 88E-31	30.974654664814 10	399	308	56	18092
GO:BP	extracellular structure organization	GO:0043062	1.215455797190 74E-31	30.915260830638 200	400	308	56	18092
GO:BP	secretion by cell	GO:0032940	1.679046494880 24E-25	24.774937277542 50	1396	308	89	18092
GO:BP	export from cell	GO:0140352	2.71541613508E -24	23.566163605736 200	1450	308	89	18092
GO:BP	secretion	GO:0046903	8.680603294288 94E-24	23.061450090690 40	1538	308	91	18092
GO:BP	wound healing	GO:0042060	2.594845695434 11E-23	22.585888462714 900	553	308	55	18092

GO:BP	response to wounding	GO:0009611	6.87481238246714E-23	22.162739149478900	682	308	60	18092
GO:BP	hemostasis	GO:0007599	4.46499483275367E-22	21.35017903937520	352	308	44	18092
GO:BP	organonitrogen compound metabolic process	GO:1901564	1.57656474610212E-21	20.80228818901540	6780	308	204	18092
GO:BP	blood coagulation	GO:0007596	2.35060638521064E-21	20.628820088460200	347	308	43	18092
GO:BP	coagulation	GO:0050817	5.93785293283332E-21	20.22637056309730	355	308	43	18092
GO:BP	biological adhesion	GO:0022610	2.82318342615176E-19	18.549260904220020	1501	308	83	18092
GO:BP	response to organic substance	GO:0010033	1.20549174621156E-18	17.918835758813700	3459	308	132	18092
GO:BP	response to stress	GO:0006950	1.60803696733808E-18	17.793703971429400	4199	308	148	18092
GO:BP	cell activation	GO:0001775	1.76214655049065E-18	17.753957975933800	1510	308	82	18092
GO:BP	transport	GO:0006810	3.35108053896138E-18	17.474815134323400	5259	308	169	18092
GO:BP	cell adhesion	GO:0007155	3.74795629441431E-18	17.426205482140000	1494	308	81	18092
GO:BP	response to chemical	GO:0042221	6.03236687309989E-18	17.219512253657200	4834	308	160	18092
GO:BP	cellular response to chemical stimulus	GO:0070887	7.26194253711667E-18	17.138947191929900	3438	308	130	18092
GO:BP	establishment of localization	GO:0051234	2.22369347160813E-17	16.652925078944300	5398	308	170	18092
GO:BP	establishment of localization in cell	GO:0051649	2.55923567432783E-17	16.591889719057200	2840	308	115	18092
GO:BP	tissue development	GO:0009888	2.66705462861026E-17	16.5739680886742	2161	308	98	18092
GO:BP	regulation of body fluid levels	GO:0050878	6.91746700590329E-17	16.160052903627300	520	308	46	18092
GO:BP	localization	GO:0051179	1.06238976217698E-16	15.973716123077200	6935	308	197	18092
GO:BP	regulation of biological quality	GO:0065008	3.80466012813366E-16	15.419684132866800	4194	308	143	18092
GO:BP	protein metabolic process	GO:0019538	4.55290764865874E-16	15.341711158847200	5806	308	175	18092
GO:BP	neutrophil mediated immunity	GO:0002446	5.23114609604894E-16	15.281403150777000	498	308	44	18092
GO:BP	immune effector process	GO:0002252	5.53760443590741E-16	15.256678070157500	1310	308	72	18092
GO:BP	leukocyte mediated immunity	GO:0002443	1.49927525877086E-15	14.824118625730200	891	308	58	18092
GO:BP	anatomical structure morphogenesis	GO:0009653	1.73570681146886E-15	14.760523632221000	2865	308	112	18092
GO:BP	biological process involved in interspecies interaction between organisms	GO:0044419	3.16187427999093E-15	14.500055402143100	2272	308	97	18092
GO:BP	neutrophil degranulation	GO:0043312	7.23476507661098E-15	14.14057556649210	484	308	42	18092
GO:BP	neutrophil activation involved in immune response	GO:0002283	9.07633368301885E-15	14.042089546058400	487	308	42	18092
GO:BP	immune system process	GO:0002376	9.74876319667199E-15	14.011050478756000	3322	308	121	18092

GO:BP	neutrophil activation	GO:0042119	2.37706771524744E-14	13.623958446400000	500	308	42	18092
GO:BP	myeloid leukocyte mediated immunity	GO:0002444	3.49818301461119E-14	13.456157473257400	556	308	44	18092
GO:BP	granulocyte activation	GO:0036230	3.94055360898811E-14	13.404442759788900	507	308	42	18092
GO:BP	anatomical structure development	GO:0048856	4.66546019624892E-14	13.331105511438600	6210	308	178	18092
GO:BP	cell-substrate adhesion	GO:0031589	4.94515113142333E-14	13.305820431156700	368	308	36	18092
GO:BP	immune response	GO:0006955	5.09919660834969E-14	13.292498242734400	2326	308	96	18092
GO:BP	leukocyte degranulation	GO:0043299	6.30497683482675E-14	13.200316504733300	539	308	43	18092
GO:BP	cellular localization	GO:0051641	1.17503449314734E-13	12.929949384487000	3562	308	124	18092
GO:BP	post-translational protein modification	GO:0043687	2.05564983101809E-13	12.6870508631245	362	308	35	18092
GO:BP	cellular response to organic substance	GO:0071310	3.46522571226074E-13	12.460268471760200	2812	308	106	18092
GO:BP	myeloid cell activation involved in immune response	GO:0002275	6.86262513804755E-13	12.163509723231400	549	308	42	18092
GO:BP	response to stimulus	GO:0050896	1.00184771381128E-12	11.999198288526400	9469	308	230	18092
GO:BP	cell activation involved in immune response	GO:0002263	1.12992479848898E-12	11.946950459780400	723	308	48	18092
GO:BP	leukocyte activation involved in immune response	GO:0002366	4.29010137668438E-12	11.367532445154600	719	308	47	18092
GO:BP	endocytosis	GO:0006897	7.70523377771777E-12	11.113214180199000	701	308	46	18092
GO:BP	myeloid leukocyte activation	GO:0002274	8.05637767540083E-12	11.093860182660 80	673	308	45	18092
GO:BP	platelet activation	GO:0030168	1.01353513364454E-11	10.994161192127900	160	308	23	18092
GO:BP	developmental process	GO:0032502	1.07210397007709E-11	10.969763095761 50	6745	308	182	18092
GO:BP	negative regulation of proteolysis	GO:0045861	1.27679238054448E-11	10.893879717704900	366	308	33	18092
GO:BP	proteolysis	GO:0006508	1.34323007449773E-11	10.871849593044700	1846	308	79	18092
GO:BP	regulation of proteolysis	GO:0030162	2.57232185087965E-11	10.589674693089900	754	308	47	18092
GO:BP	multicellular organism development	GO:0007275	2.88039434091 51E-11	10.540548051004800	5718	308	162	18092
GO:BP	cellular component organization or biogenesis	GO:0071840	3.77265704034079E-11	10.423352673266 40	6767	308	181	18092
GO:BP	cellular protein metabolic process	GO:0044267	4.73896388963482E-11	10.324316600562500	5225	308	152	18092
GO:BP	negative regulation of peptidase activity	GO:0010466	5.50709952632301E-11	10.259077074718600	271	308	28	18092
GO:BP	cellular component organization	GO:0016043	6.22176511440754E-11	10.206086388508900	6576	308	177	18092
GO:BP	plasminogen activation	GO:0031639	8.21249967496809E-11	10.085524634620500	23	308	11	18092
GO:BP	response to external stimulus	GO:0009605	1.87280166237281E-10	9.7275082138143 10	2991	308	104	18092
GO:BP	platelet aggregation	GO:0070527	3.91773459981E-10	9.4069649878772 80	64	308	15	18092

GO:BP	regulation of developmental process	GO:0050793	5.941879338939 29E-10	9.2260761716109 30	2648	308	95	18092
GO:BP	multicellular organismal process	GO:0032501	8.362075169876 25E-10	9.0776859327296 70	8065	308	200	18092
GO:BP	negative regulation of endopeptidase activity	GO:0010951	8.729417704462 48E-10	9.0590147249282 30	258	308	26	18092
GO:BP	protein activation cascade	GO:0072376	1.209126906879 46E-09	8.9175281143046 50	28	308	11	18092
GO:BP	blood coagulation, fibrin clot formation	GO:0072378	1.209126906879 46E-09	8.9175281143046 50	28	308	11	18092
GO:BP	zymogen activation	GO:0031638	1.274865472857 27E-09	8.8945356407031 20	57	308	14	18092
GO:BP	system development	GO:0048731	2.539320282195 16E-09	8.5952825184970 70	5151	308	146	18092
GO:BP	animal organ development	GO:0048513	2.870821770919 9E-09	8.5419937689485 20	3770	308	118	18092
GO:BP	regulation of anatomical structure morphogenesis	GO:0022603	3.285778890038 94E-09	8.4833616649018 30	1062	308	53	18092
GO:BP	cell morphogenesis	GO:0000902	3.407806112642 22E-09	8.4675251224161 8	1063	308	53	18092
GO:BP	biological process involved in symbiotic interaction	GO:0044403	3.573872865062 78E-09	8.4468609009025 00	996	308	51	18092
GO:BP	negative regulation of hemostasis	GO:1900047	3.953634302597 27E-09	8.4030035038915 9	50	308	13	18092
GO:BP	homotypic cell-cell adhesion	GO:0034109	4.049665034314 27E-09	8.3925808977150 00	88	308	16	18092
GO:BP	cell surface receptor signaling pathway	GO:0007166	5.370591261850 73E-09	8.2699778991004 90	3242	308	106	18092
GO:BP	cell differentiation	GO:0030154	5.670344406757 34E-09	8.2463905620221 30	4440	308	131	18092
GO:BP	cellular developmental process	GO:0048869	9.152132645521 6E-09	8.0384776941016 80	4518	308	132	18092
GO:BP	anatomical structure formation involved in morphogenesis	GO:0048646	9.836316725938 83E-09	8.0071674955786 10	1235	308	57	18092
GO:BP	positive regulation of biological process	GO:0048518	9.995409007002 78E-09	8.0001994300751 20	6466	308	169	18092
GO:BP	fibrinolysis	GO:0042730	1.152509845189 66E-08	7.9383553560092 20	25	308	10	18092
GO:BP	response to cytokine	GO:0034097	1.234779793439 5E-08	7.9084104861461 50	1242	308	57	18092
GO:BP	catabolic process	GO:0009056	1.337760056784 56E-08	7.8736217754764 00	2746	308	94	18092
GO:BP	regulation of peptidase activity	GO:0052547	1.346633722451 32E-08	7.8707505141134 70	469	308	33	18092
GO:BP	supramolecular fiber organization	GO:0097435	1.627958615422 45E-08	7.7883566395709 70	739	308	42	18092
GO:BP	regulation of hemostasis	GO:1900046	1.725880188293 8E-08	7.7629893565750 00	68	308	14	18092
GO:BP	negative regulation of coagulation	GO:0050819	1.921519100908 87E-08	7.7163552940629 70	56	308	13	18092
GO:BP	collagen fibril organization	GO:0030199	1.921519100908 87E-08	7.7163552940629 70	56	308	13	18092
GO:BP	cellular response to cytokine stimulus	GO:0071345	1.949749264382 93E-08	7.7100212348407 500	1148	308	54	18092
GO:BP	cellular detoxification	GO:1990748	1.978067811422 18E-08	7.7037588241535 700	113	308	17	18092
GO:BP	cell migration	GO:0016477	2.591685195342 77E-08	7.5864177521180 10	1684	308	68	18092

GO:BP	leukocyte activation	GO:0045321	3.195987176705 03E-08	7.4953949718791 40	1346	308	59	18092
GO:BP	cell-matrix adhesion	GO:0007160	4.202970641700 38E-08	7.3764436435877 20	236	308	23	18092
GO:BP	humoral immune response	GO:0006959	5.152138807576 94E-08	7.2880124448422 2	384	308	29	18092
GO:BP	receptor-mediated endocytosis	GO:0006898	5.196595121491 41E-08	7.2842811187268 50	333	308	27	18092
GO:BP	cellular response to toxic substance	GO:0097237	5.334878128279 33E-08	7.2728754972930 00	120	308	17	18092
GO:BP	cell morphogenesis involved in differentiation	GO:0000904	5.794484145692 53E-08	7.2369852210724 60	769	308	42	18092
GO:BP	movement of cell or subcellular component	GO:0006928	6.059890991510 49E-08	7.2175351880798 00	2337	308	83	18092
GO:BP	negative regulation of blood coagulation	GO:0030195	6.288945647458 24E-08	7.2014221586680 10	49	308	12	18092
GO:BP	viral process	GO:0016032	6.959593882166 18E-08	7.1574161023262 50	940	308	47	18092
GO:BP	regulation of coagulation	GO:0050818	7.055626324420 45E-08	7.1514644280944 3	75	308	14	18092
GO:BP	regulation of cellular component organization	GO:0051128	7.185951260449 8E-08	7.1435157327742 20	2431	308	85	18092
GO:BP	blood vessel development	GO:0001568	8.138747979359 24E-08	7.0894423994691 30	810	308	43	18092
GO:BP	cell motility	GO:0048870	9.818887774385 36E-08	7.0079377037409 100	1856	308	71	18092
GO:BP	localization of cell	GO:0051674	9.818887774385 36E-08	7.0079377037409 100	1856	308	71	18092
GO:BP	hydrogen peroxide catabolic process	GO:0042744	9.824227725616 65E-08	7.0077015791393 50	30	308	10	18092
GO:BP	negative regulation of catalytic activity	GO:0043086	1.285406226288 64E-07	6.8909596007720 90	855	308	44	18092
GO:BP	positive regulation of response to stimulus	GO:0048584	1.356581707622 5E-07	6.8675540433318 60	2374	308	83	18092
GO:BP	negative regulation of biological process	GO:0048519	1.386122316881 45E-07	6.8581984441810 900	5833	308	154	18092
GO:BP	nitrogen compound metabolic process	GO:0006807	1.546447204775 71E-07	6.8106649020856 1	10057	308	226	18092
GO:BP	regulation of blood coagulation	GO:0030193	2.181354009977 61E-07	6.6612738474412 00	67	308	13	18092
GO:BP	locomotion	GO:0040011	2.187900964755 7E-07	6.6599723402149 90	2055	308	75	18092
GO:BP	response to oxygen-containing compound	GO:1901700	2.620021757064 23E-07	6.5816951022170 10	1774	308	68	18092
GO:BP	detoxification	GO:0098754	3.199230554410 08E-07	6.4949544611037 4	134	308	17	18092
GO:BP	vasculature development	GO:0001944	3.357807598660 34E-07	6.4739441924249 000	847	308	43	18092
GO:BP	defense response	GO:0006952	3.889226566679 71E-07	6.4101367563144 40	1831	308	69	18092
GO:BP	negative regulation of hydrolase activity	GO:0051346	4.087276424006 06E-07	6.3885659897998 10	475	308	31	18092
GO:BP	positive regulation of cellular process	GO:0048522	4.516301958968 47E-07	6.3452170289415 60	5863	308	153	18092
GO:BP	peptide cross-linking	GO:0018149	5.567084936296 02E-07	6.2543721526676 80	35	308	10	18092
GO:BP	organic substance catabolic process	GO:1901575	5.998975129184 04E-07	6.2219229385760 50	2271	308	79	18092

GO:BP	tube morphogenesis	GO:0035239	7.913983113753 77E-07	6.1016048807330 40	975	308	46	18092
GO:BP	glucose catabolic process to pyruvate	GO:0061718	9.570253282440 6E-07	6.0190765682095 00	27	308	9	18092
GO:BP	NADH regeneration	GO:0006735	9.570253282440 6E-07	6.0190765682095 00	27	308	9	18092
GO:BP	canonical glycolysis	GO:0061621	9.570253282440 6E-07	6.0190765682095 00	27	308	9	18092
GO:BP	negative regulation of response to wounding	GO:1903035	0.000001052853 4070578400	5.9776320931429	91	308	14	18092
GO:BP	regulation of endopeptidase activity	GO:0052548	0.000001117154 0806624800	5.9518869237808 7	437	308	29	18092
GO:BP	regulation of response to wounding	GO:1903034	0.000001377792 8589330900	5.8608160705157 90	167	308	18	18092
GO:BP	glycolytic process through glucose-6-phosphate	GO:0061620	0.000001389405 0311605000	5.8571711328394 60	28	308	9	18092
GO:BP	regulation of complement activation	GO:0030449	0.000001428646 0810573800	5.8450753457933 20	110	308	15	18092
GO:BP	blood vessel morphogenesis	GO:0048514	0.000001693865 8427961400	5.7711209895428 40	723	308	38	18092
GO:BP	metabolic process	GO:0008152	0.000001957805 3463505900	5.7082304898608 700	11998	308	252	18092
GO:BP	glycolytic process through fructose-6-phosphate	GO:0061615	0.000001984717 010303260	5.7023014081075 1	29	308	9	18092
GO:BP	regulation of humoral immune response	GO:0002920	0.000002004438 8441270800	5.6980071896321 20	131	308	16	18092
GO:BP	regulation of cell motility	GO:2000145	0.000002011081 1528435200	5.6965704040322 9	1076	308	48	18092
GO:BP	NAD metabolic process	GO:0019674	0.000002364574 1387389700	5.6262470645876 70	52	308	11	18092
GO:BP	negative regulation of protein metabolic process	GO:0051248	0.000002423629 4618727900	5.6155337768179 40	1156	308	50	18092
GO:BP	biological regulation	GO:0065007	0.000002511812 6872568800	5.6000127502548 50	12801	308	263	18092
GO:BP	regulation of cell migration	GO:0030334	0.000002980627 116899660	5.5256923517775 20	1016	308	46	18092
GO:BP	negative regulation of cellular process	GO:0048523	0.000003163825 694600310	5.4997874512042 20	5208	308	138	18092
GO:BP	regulation of multicellular organismal process	GO:0051239	0.000003299344 125456800	5.4815723846690 50	2894	308	91	18092
GO:BP	regulation of protein metabolic process	GO:0051246	0.000004008874 781808800	5.3969775088327 40	2722	308	87	18092
GO:BP	complement activation	GO:0006956	0.000004671883 733368570	5.3305079738119 20	180	308	18	18092
GO:BP	response to other organism	GO:0051707	0.000004777472 800596470	5.3208017768181 10	1610	308	61	18092
GO:BP	response to external biotic stimulus	GO:0043207	0.000005011441 357313400	5.3000373472864 70	1612	308	61	18092
GO:BP	regulation of cell adhesion	GO:0030155	0.000005063740 94923932	5.2955285200510 50	752	308	38	18092
GO:BP	organic substance metabolic process	GO:0071704	0.000005637368 491616890	5.2489235762060 10	11403	308	242	18092
GO:BP	regulation of catalytic activity	GO:0050790	0.000005874255 3736053200	5.2310471771634 40	2428	308	80	18092
GO:BP	regulation of locomotion	GO:0040012	0.000007030088 418871180	5.1530392127346 10	1118	308	48	18092
GO:BP	regulation of cellular component movement	GO:0051270	0.000007135246 38667975	5.1465910256988 90	1156	308	49	18092

GO:BP	regulation of localization	GO:0032879	0.000008712599 033224100	5.0598522723845 20	2903	308	90	18092
GO:BP	cellular response to stimulus	GO:0051716	0.000009841847 82922226	5.0069233541403 80	7840	308	184	18092
GO:BP	NADH metabolic process	GO:0006734	0.000010474558 85195100	4.9798642587862 80	46	308	10	18092
GO:BP	regulation of cell morphogenesis	GO:0022604	0.000010637918 656135100	4.9731433348771 40	312	308	23	18092
GO:BP	response to biotic stimulus	GO:0009607	0.000010873278 237626100	4.9636394986121 80	1645	308	61	18092
GO:BP	negative regulation of fibrinolysis	GO:0051918	0.000011497224 769855400	4.9394069781325 90	10	308	6	18092
GO:BP	regulation of response to stimulus	GO:0048583	0.000011539694 497634300	4.9378056885587 90	4324	308	119	18092
GO:BP	negative regulation of cellular protein metabolic process	GO:0032269	0.000011930174 358916100	4.9233532090906 20	1099	308	47	18092
GO:BP	substrate adhesion-dependent cell spreading	GO:0034446	0.000012006121 056999200	4.9205972819928 30	109	308	14	18092
GO:BP	tube development	GO:0035295	0.000013195553 18057840	4.8795723986810 00	1178	308	49	18092
GO:BP	negative regulation of wound healing	GO:0061045	0.000014030232 446191100	4.8529351337284 50	76	308	12	18092
GO:BP	response to endogenous stimulus	GO:0009719	0.000014239081 874793300	4.8465180127754 10	1698	308	62	18092
GO:BP	defense response to other organism	GO:0098542	0.000015437404 924300900	4.8114257041155 20	1222	308	50	18092
GO:BP	cellular component assembly	GO:0022607	0.000015539012 029463100	4.8085765971047 5	3030	308	92	18092
GO:BP	innate immune response	GO:0045087	0.000016503385 106302500	4.7824269659555 70	999	308	44	18092
GO:BP	glucose catabolic process	GO:0006007	0.000016802314 709174900	4.7746308851684 60	36	308	9	18092
GO:BP	cellular catabolic process	GO:0044248	0.000016803711 903093000	4.7745947729784 60	2350	308	77	18092
GO:BP	cellular component biogenesis	GO:0044085	0.000018295260 52074870	4.7376614018692 00	3276	308	97	18092
GO:BP	cell-cell adhesion	GO:0098609	0.000023009320 101728200	4.6380962140315 00	901	308	41	18092
GO:BP	regulation of wound healing	GO:0061041	0.000023016735 639481700	4.6379562703799 00	134	308	15	18092
GO:BP	cytoskeleton organization	GO:0007010	0.000023706761 336458400	4.6251277724569 10	1435	308	55	18092
GO:BP	response to oxygen levels	GO:0070482	0.000023833367 35690140	4.6228145929366 00	410	308	26	18092
GO:BP	regulation of cell-substrate adhesion	GO:0010810	0.000023915889 732861700	4.6213134576151 60	223	308	19	18092
GO:BP	protein folding	GO:0006457	0.000025734918 702478100	4.5894771993633 30	224	308	19	18092
GO:BP	cell junction organization	GO:0034330	0.000026350499 329238900	4.5792111507027 30	730	308	36	18092
GO:BP	cell development	GO:0048468	0.000030683182 74934020	4.5130995932633 700	2161	308	72	18092
GO:BP	regulation of cellular protein metabolic process	GO:0032268	0.000030983816 143731900	4.5088650930940 00	2563	308	81	18092
GO:BP	primary metabolic process	GO:0044238	0.000033599701 862043900	4.4736645761888 40	10575	308	227	18092
GO:BP	cellular oxidant detoxification	GO:0098869	0.000036980971 737919200	4.4320216812008 70	100	308	13	18092

GO:BP	monosaccharide biosynthetic process	GO:0046364	0.000036980971737919200	4.432021681200870	100	308	13	18092
GO:BP	circulatory system development	GO:0072359	0.000039560727676403 10	4.402735728628450	1219	308	49	18092
GO:BP	cytokine-mediated signaling pathway	GO:0019221	0.000040549601910021 80	4.392013405056510	812	308	38	18092
GO:BP	carbohydrate derivative metabolic process	GO:1901135	0.000046434654815712000	4.333157778546850	1148	308	47	18092
GO:BP	positive regulation of signal transduction	GO:0009967	0.000046560905942446 00	4.331978578143870 0	1627	308	59	18092
GO:BP	regulation of plasminogen activation	GO:0010755	0.000049151712495752900	4.308461346305920	12	308	6	18092
GO:BP	cell death	GO:0008219	0.000052317616339273 00	4.281352051271770 0	2322	308	75	18092
GO:BP	regulation of biological process	GO:0050789	0.000055000888114907 20	4.259630297773220	12145	308	250	18092
GO:BP	ossification	GO:0001503	0.000057252012772896 40	4.242209240502550	428	308	26	18092
GO:BP	regulation of vesicle-mediated transport	GO:0060627	0.000057430319828971 70	4.240858765129750 0	552	308	30	18092
GO:BP	response to hypoxia	GO:0001666	0.000061883034333646 90	4.208428399529060	371	308	24	18092
GO:BP	positive regulation of cell communication	GO:0010647	0.000061974560445360 20	4.207786544783320	1808	308	63	18092
GO:BP	macromolecule catabolic process	GO:0009057	0.000063983401562122 7	4.193932675155470	1477	308	55	18092
GO:BP	regulation of hydrolase activity	GO:0051336	0.000066515590952312 9	4.177076546111310	1318	308	51	18092
GO:BP	positive regulation of signaling	GO:0023056	0.000068725618032296 60	4.162881345965260	1813	308	63	18092
GO:BP	hydrogen peroxide metabolic process	GO:0042743	0.000078715603528198 50	4.103939170379156	308	10	18092	
GO:BP	angiogenesis	GO:0001525	0.000083446836127456	4.078590124873720	627	308	32	18092
GO:BP	negative regulation of apoptotic process	GO:0043066	0.000084830355953731 10	4.071448710666420	944	308	41	18092
GO:BP	cellular metabolic process	GO:0044237	0.000086588151566757 30	4.062541531322390	10855	308	230	18092
GO:BP	programmed cell death	GO:0012501	0.000087182811214609 50	4.059569131242760	2172	308	71	18092
GO:BP	ameboidal-type cell migration	GO:0001667	0.000088481443690455 40	4.053147799899200	499	308	28	18092
GO:BP	hexose catabolic process	GO:0019320	0.000094038811578 12	4.026692867938480	57	308	10	18092
GO:BP	regulation of apoptotic process	GO:0042981	0.000100166993325632 00	3.999275362081850 0	1579	308	57	18092
GO:BP	activation of immune response	GO:0002253	0.000100322816676462 00	3.998600283033770	566	308	30	18092
GO:BP	response to growth factor	GO:0070848	0.000106008234311385 00	3.974660399102180 0	771	308	36	18092
GO:BP	regulation of cell death	GO:0010941	0.000117168267181251 00	3.931189992875300 0	1754	308	61	18092
GO:BP	response to decreased oxygen levels	GO:0036293	0.000124950922381551 00	3.903260533585240 0	385	308	24	18092
GO:BP	negative regulation of molecular function	GO:0044092	0.000127803913731163 00	3.893455846601540 0	1226	308	48	18092
GO:BP	response to toxic substance	GO:0009636	0.000142000805027824 00	3.847709193517290 0	249	308	19	18092

GO:BP	regulation of fibrinolysis	GO:0051917	0.000155210641989763 0	3.809078504733880 0	14	308	6	18092
GO:BP	negative regulation of programmed cell death	GO:0043069	0.000164202038363881 0	3.784621455957800 0	967	308	41	18092
GO:BP	establishment or maintenance of cell polarity	GO:0007163	0.000178417291783900 00	3.748563057112800 0	227	308	18	18092
GO:BP	epithelium development	GO:0060429	0.000185491943267962 00	3.731674948961350	1361	308	51	18092
GO:BP	regulation of programmed cell death	GO:0043067	0.000212475720907344 00	3.672690688570740	1614	308	57	18092
GO:BP	regulation of signaling	GO:0023051	0.000222756709589809 00	3.652169205836790 0	3636	308	101	18092
GO:BP	mucopolysaccharide metabolic process	GO:1903510	0.000224334782241489 00	3.649103385514480	116	308	13	18092
GO:BP	glycosaminoglycan metabolic process	GO:0030203	0.000233288727772412 00	3.632106245280440	159	308	15	18092
GO:BP	response to nutrient	GO:0007584	0.000251559452501471 0	3.599359359148800	183	308	16	18092
GO:BP	regulation of signal transduction	GO:0009966	0.000253021636286899 0	3.596842340016900 0	3207	308	92	18092
GO:BP	negative regulation of multicellular organismal process	GO:0051241	0.000253512001586292 0	3.596001475781050 0	1175	308	46	18092
GO:BP	monosaccharide catabolic process	GO:0046365	0.000254315152168525 00	3.594627763665660	63	308	10	18092
GO:BP	regulation of molecular function	GO:0065009	0.000255198539348404 0	3.593121815666960	2969	308	87	18092
GO:BP	regulation of immune system process	GO:0002682	0.000267521994286129 0	3.572640506710300 0	1625	308	57	18092
GO:BP	regulation of cell communication	GO:0010646	0.000268176469102099 0	3.571579331583010 0	3600	308	100	18092
GO:BP	protein localization to membrane	GO:0072657	0.000271282274454716	3.566578582051150 0	660	308	32	18092
GO:BP	negative regulation of cell death	GO:0060548	0.000307376994068443 0	3.512328640814880 0	1066	308	43	18092
GO:BP	regulation of multicellular organismal development	GO:2000026	0.000358134020065283 0	3.445954422286450 0	1472	308	53	18092
GO:BP	positive regulation of cell motility	GO:2000147	0.000359273062255604 00	3.444575344310290 0	600	308	30	18092
GO:BP	reactive oxygen species metabolic process	GO:0072593	0.000417575923176147 00	3.379264550075690 0	294	308	20	18092
GO:BP	cellular response to growth factor stimulus	GO:0071363	0.000417763145011119 00	3.379069876046230	743	308	34	18092
GO:BP	glucose metabolic process	GO:0006006	0.000461249458800587 00	3.336064130404820 0	216	308	17	18092
GO:BP	regulation of cell differentiation	GO:0045595	0.000469878358214881 00	3.328014557369690 0	1695	308	58	18092
GO:BP	positive regulation of transport	GO:0051050	0.000472521728171166 0	3.325578216344400	930	308	39	18092
GO:BP	tissue migration	GO:0090130	0.000513736065401873 0	3.289259944777470 0	385	308	23	18092
GO:BP	mRNA catabolic process	GO:0006402	0.000537973346158386 0	3.269239240882100	386	308	23	18092
GO:BP	positive regulation of cell migration	GO:0030335	0.000545985728109114 0	3.262818709464620	578	308	29	18092
GO:BP	positive regulation of cellular component movement	GO:0051272	0.000569241834195379 0	3.244703190645760	613	308	30	18092
GO:BP	positive regulation of locomotion	GO:0040017	0.000610226827450488 0	3.214508703351100	615	308	30	18092

GO:BP	negative regulation of response to stimulus	GO:0048585	0.000620635679 1527630	3.2071632612788 30	1752	308	59	18092
GO:BP	organic cyclic compound catabolic process	GO:1901361	0.000623084357 3265060	3.2054531516694 200	650	308	31	18092
GO:BP	phagocytosis	GO:0006909	0.000645856110 2947350	3.1898642273076 80	390	308	23	18092
GO:BP	cell projection organization	GO:0030030	0.000661080706 1770030	3.1797455176584 800	1627	308	56	18092
GO:BP	apoptotic process	GO:0006915	0.000668839392 4189630	3.1746781563131 00	2018	308	65	18092
GO:BP	plasma membrane bounded cell projection organization	GO:0120036	0.000679040113 5991510	3.1681045694600 20	1586	308	55	18092
GO:BP	tissue morphogenesis	GO:0048729	0.000690131380 3996310	3.1610682246957 900	688	308	32	18092
GO:BP	response to inorganic substance	GO:0010035	0.000701547555 9318280	3.1539428840386 90	585	308	29	18092
GO:BP	aminoglycan metabolic process	GO:0006022	0.000707030751 7860530	3.1505616964710 700	173	308	15	18092
GO:BP	negative regulation of cell-substrate adhesion	GO:0010812	0.000710587501 0124340	3.1483824358687 40	70	308	10	18092
GO:BP	positive regulation of cellular component organization	GO:0051130	0.000784077827 4913620	3.1056408271465 70	1182	308	45	18092
GO:BP	positive regulation of immune system process	GO:0002684	0.000912825503 2668870	3.0396122347452 400	1070	308	42	18092
GO:BP	negative regulation of macromolecule metabolic process	GO:0010605	0.000924729142 6706020	3.0339854554440 000	3297	308	92	18092
GO:BP	inflammatory response	GO:0006954	0.001000467049 240110	2.9997972104449 10	808	308	35	18092
GO:BP	regulation of immune response	GO:0050776	0.001050515844 2788000	2.9785973930143 70	998	308	40	18092
GO:BP	protein processing	GO:0016485	0.001127312292 3165200	2.9479557573858 900	230	308	17	18092
GO:BP	nucleobase-containing compound catabolic process	GO:0034655	0.001185650419 1098800	2.9260433408461 700	566	308	28	18092
GO:BP	hexose metabolic process	GO:0019318	0.001210151573 6736100	2.9171602301072 10	258	308	18	18092
GO:BP	positive regulation of response to wounding	GO:1903036	0.001211814985 445960	2.9165636812698 80	74	308	10	18092
GO:BP	heterocycle catabolic process	GO:0046700	0.001224194941 7538700	2.9121494192927 400	601	308	29	18092
GO:BP	integrin-mediated signaling pathway	GO:0007229	0.001275141478 425060	2.8944416270805 5	113	308	12	18092
GO:BP	membrane organization	GO:0061024	0.001306359500 6949300	2.8839372919099 000	968	308	39	18092
GO:BP	signal transduction	GO:0007165	0.001346331783 2321700	2.8708479015750 000	6353	308	150	18092
GO:BP	epithelial cell migration	GO:0010631	0.001353933273 1535600	2.8684027387640 900	376	308	22	18092
GO:BP	protein targeting to ER	GO:0045047	0.001403730605 9690800	2.8527162309290 900	114	308	12	18092
GO:BP	cellular nitrogen compound catabolic process	GO:0044270	0.001450304042 9534800	2.8385409423615 30	606	308	29	18092
GO:BP	small molecule metabolic process	GO:0044281	0.001461230130 361330	2.8352813812762 000	1929	308	62	18092
GO:BP	response to topologically incorrect protein	GO:0035966	0.001543598316 0299400	2.8114657038887 40	209	308	16	18092

GO:BP	collagen metabolic process	GO:0032963	0.001543709283 6131800	2.8114344840588 100	115	308	12	18092
GO:BP	epithelium migration	GO:0090132	0.001547885996 8417500	2.8102610286439 300	379	308	22	18092
GO:BP	response to organonitrogen compound	GO:0010243	0.001640240759 8110600	2.7850924001333 000	1094	308	42	18092
GO:BP	negative regulation of metabolic process	GO:0009892	0.001717950627 8526200	2.7649893215055 200	3539	308	96	18092
GO:BP	macromolecule metabolic process	GO:0043170	0.001746125166 1453400	2.7579246283177 900	9885	308	210	18092
GO:BP	SRP-dependent cotranslational protein targeting to membrane	GO:0006614	0.001775632870 7855000	2.7506468238468 200	96	308	11	18092
GO:BP	response to nitrogen compound	GO:1901698	0.001813930229 3792800	2.7413794215638 6	1178	308	44	18092
GO:BP	positive regulation of wound healing	GO:0090303	0.001843902788 6167200	2.7342619788790 300	60	308	9	18092
GO:BP	glycosaminoglycan catabolic process	GO:0006027	0.001843902788 6167200	2.7342619788790 300	60	308	9	18092
GO:BP	response to unfolded protein	GO:0006986	0.001924972953 7864600	2.7155753680275 900	187	308	15	18092
GO:BP	endodermal cell differentiation	GO:0035987	0.002008065773 599890	2.6972220661068 70	45	308	8	18092
GO:BP	establishment of protein localization to endoplasmic reticulum	GO:0072599	0.002040933098 394610	2.6901712311850 800	118	308	12	18092
GO:BP	protein-containing complex assembly	GO:0065003	0.002201896017 5580300	2.6572031940232 30	1689	308	56	18092
GO:BP	anatomical structure homeostasis	GO:0060249	0.002208732779 28182	2.6558568235144 00	483	308	25	18092
GO:BP	cellular response to endogenous stimulus	GO:0071495	0.002230088548 4911400	2.6516778923968 60	1434	308	50	18092
GO:BP	regulation of endocytosis	GO:0030100	0.002252675376 114990	2.6473013881783 70	215	308	16	18092
GO:BP	signaling	GO:0023052	0.002636365220 297690	2.5789944263341 100	6864	308	158	18092
GO:BP	protein maturation	GO:0051604	0.002796814131 3040300	2.5533363947050 700	302	308	19	18092
GO:BP	endoderm development	GO:0007492	0.002852519790 0937000	2.5447713338690 200	81	308	10	18092
GO:BP	RNA catabolic process	GO:0006401	0.002881043212 0688400	2.5404502277930 600	425	308	23	18092
GO:BP	cotranslational protein targeting to membrane	GO:0006613	0.002967720373 5265000	2.5275770218416 200	101	308	11	18092
GO:BP	response to abiotic stimulus	GO:0009628	0.002996458831 8924600	2.5233916846635 6	1282	308	46	18092
GO:BP	negative regulation of plasminogen activation	GO:0010757	0.003007355073 212300	2.5218152924738 200	6	308	4	18092
GO:BP	skeletal system development	GO:0001501	0.003035338390 9354	2.5177928851080 800	525	308	26	18092
GO:BP	cell communication	GO:0007154	0.003161606005 224460	2.5000922521831 300	6882	308	158	18092
GO:BP	nuclear-transcribed mRNA catabolic process, nonsense-mediated decay	GO:0000184	0.003189891220 992520	2.4962241266381 800	123	308	12	18092
GO:BP	homeostatic process	GO:0042592	0.004052683674 001510	2.3922572931240 700	2033	308	63	18092
GO:BP	positive regulation of intracellular signal transduction	GO:1902533	0.004157374787 721800	2.3811808220411 900	1054	308	40	18092

GO:BP	monosaccharide metabolic process	GO:0005996	0.004163504570153030	2.3805409542935100	281	308	18	18092
GO:BP	aminoglycan catabolic process	GO:0006026	0.004221896674194840 0	2.3744923997294800	66	308	9	18092
GO:BP	actin filament-based process	GO:0030029	0.004418499119452950	2.3547252272195 10	824	308	34	18092
GO:BP	positive regulation of blood coagulation	GO:0030194	0.004584470819 51217	2.3387107872413400	23	308	6	18092
GO:BP	positive regulation of hemostasis	GO:1900048	0.004584470819 51217	2.3387107872413400	23	308	6	18092
GO:BP	morphogenesis of a polarized epithelium	GO:0001738	0.004796799433027550	2.3190484401645 80	151	308	13	18092
GO:BP	formation of primary germ layer	GO:0001704	0.004878245867274270	2.3117363147009300	128	308	12	18092
GO:BP	positive regulation of immune response	GO:0050778	0.004897308853018050	2.3100425059610 00	753	308	32	18092
GO:BP	regulation of G2/M transition of mitotic cell cycle	GO:0010389	0.005090269109946160	2.2932592569804 90	202	308	15	18092
GO:BP	retinoid metabolic process	GO:0001523	0.005285100720745520	2.2769467317156500	107	308	11	18092
GO:BP	carboxylic acid metabolic process	GO:0019752	0.005597950977998560	2.2519709090277600	1027	308	39	18092
GO:BP	actin cytoskeleton organization	GO:0030036	0.005956701846501090	2.2249941372958 00	723	308	31	18092
GO:BP	positive regulation of coagulation	GO:0050820	0.006025529154928420	2.2200048078444800	24	308	6	18092
GO:BP	triglyceride-rich lipoprotein particle remodeling	GO:0034370	0.006108358417488380	2.2140754879596 60	14	308	5	18092
GO:BP	humoral immune response mediated by circulating immunoglobulin	GO:0002455	0.006431521709203480	2.1916862600893900	155	308	13	18092
GO:BP	enzyme linked receptor protein signaling pathway	GO:0007167	0.006706443434 8284200	2.1735077340965 60	1115	308	41	18092
GO:BP	viral life cycle	GO:0019058	0.006728169413235880	2.1721030816710 30	351	308	20	18092
GO:BP	apoptotic cell clearance	GO:0043277	0.007336883443483930	2.1344883802374600	53	308	8	18092
GO:BP	sulfur compound catabolic process	GO:0044273	0.007336883443483930	2.1344883802374600	53	308	8	18092
GO:BP	aromatic compound catabolic process	GO:0019439	0.007508636574581980	2.1244389154448 20	622	308	28	18092
GO:BP	establishment of protein localization to organelle	GO:0072594	0.008122198258 48554	2.0903264138221 70	589	308	27	18092
GO:BP	gluconeogenesis	GO:0006094	0.008400849623179330	2.0756767891763 30	91	308	10	18092
GO:BP	endoderm formation	GO:0001706	0.008486707517197090	2.0712607649325900	54	308	8	18092
GO:BP	positive regulation by host of viral process	GO:0044794	0.009035042832509050	2.0440697842344000	15	308	5	18092
GO:BP	diterpenoid metabolic process	GO:0016101	0.009059329775105290	2.0429039309920900	113	308	11	18092
GO:BP	leukocyte migration	GO:0050900	0.009180964282718370	2.0371117021680 10	523	308	25	18092
GO:BP	axonogenesis	GO:0007409	0.009229712350347430	2.0348118338173700	489	308	24	18092
GO:BP	cell population proliferation	GO:0008283	0.010322604325246300	1.9862107192403900	2091	308	63	18092

GO:BP	hexose biosynthetic process	GO:0019319	0.011298676232041100	1.9469724360561300	94	308	10	18092
GO:BP	oxoacid metabolic process	GO:0043436	0.011896038048677300	1.9245976554222000	1060	308	39	18092
GO:BP	carbohydrate biosynthetic process	GO:0016051	0.012313727183072100	1.9096104726544700	217	308	15	18092
GO:BP	developmental growth involved in morphogenesis	GO:0060560	0.012370443592 68920	1.9076147266923800	245	308	16	18092
GO:BP	biological process involved in interaction with symbiont	GO:0051702	0.012440158956051900	1.9051740703449500	95	308	10	18092
GO:BP	acute inflammatory response	GO:0002526	0.012729497004 03810	1.8951887568087600	117	308	11	18092
GO:BP	positive regulation of heterotypic cell-cell adhesion	GO:0034116	0.012959081575304600	1.8874257763135000	16	308	5	18092
GO:BP	complement activation, alternative pathway	GO:0006957	0.012959081575304600	1.8874257763135000	16	308	5	18092
GO:BP	axon development	GO:0061564	0.013209381050731000	1.8791175315565300	534	308	25	18092
GO:BP	regulation of cell morphogenesis involved in differentiation	GO:0010769	0.013680220128 75730	1.8639069143165 30	96	308	10	18092
GO:BP	regulation of cell cycle G2/M phase transition	GO:1902749	0.013769635310490200	1.8610775619027800	219	308	15	18092
GO:BP	complement activation, classical pathway	GO:0006958	0.014475911655081000	1.8393540760078800	142	308	12	18092
GO:BP	morphogenesis of an epithelium	GO:0002009	0.016365063780 25140	1.7860822977585 30	576	308	26	18092
GO:BP	cell growth	GO:0016049	0.016467010298 65660	1.7833852428859000	506	308	24	18092
GO:BP	establishment of protein localization to membrane	GO:0090150	0.017249493479549100	1.7632236531858 70	342	308	19	18092
GO:BP	response to vitamin	GO:0033273	0.018064312383618000	1.7431785651606 70	99	308	10	18092
GO:BP	terpenoid metabolic process	GO:0006721	0.020657249573878100	1.6849275034555600	123	308	11	18092
GO:BP	protein localization to endoplasmic reticulum	GO:0070972	0.020673739946093000	1.6845809509959800	147	308	12	18092
GO:BP	plasma membrane bounded cell projection morphogenesis	GO:0120039	0.020974452002 53790	1.6783093771206100	694	308	29	18092
GO:BP	negative regulation of response to external stimulus	GO:0032102	0.022213485989145200	1.6533832817464000	413	308	21	18092
GO:BP	negative regulation of cellular component movement	GO:0051271	0.022894545621969600	1.6402679713033300	381	308	20	18092
GO:BP	cell projection morphogenesis	GO:0048858	0.023384877996033200	1.6310648915578200	698	308	29	18092
GO:BP	cellular component morphogenesis	GO:0032989	0.023894068554 36900	1.6217098946088600	813	308	32	18092
GO:BP	chylomicron remodeling	GO:0034371	0.024258017719751500	1.6151446910435300	9	308	4	18092
GO:BP	heterotypic cell-cell adhesion	GO:0034113	0.024509853590406000	1.6106592829979700	62	308	8	18092
GO:BP	blood coagulation, intrinsic pathway	GO:0007597	0.024717884641193300	1.6069886989540400	18	308	5	18092
GO:BP	high-density lipoprotein particle remodeling	GO:0034375	0.024717884641193300	1.6069886989540400	18	308	5	18092
GO:BP	organic acid metabolic process	GO:0006082	0.024812003725967000	1.6053381622899700	1094	308	39	18092
GO:BP	positive regulation of endocytosis	GO:0045807	0.025764299921 09340	1.5889816538835500	103	308	10	18092

GO:BP	protein targeting to membrane	GO:0006612	0.026172734786400400	1.5821508956027900	203	308	14	18092
GO:BP	extracellular matrix disassembly	GO:0022617	0.026343977656476100	1.5793186506408700	82	308	9	18092
GO:BP	growth	GO:0040007	0.026782127878126900	1.5721549206393100	1016	308	37	18092
GO:BP	response to organic cyclic compound	GO:0014070	0.028221859992061 9	1.5494143669931000	978	308	36	18092
GO:BP	protein-containing complex subunit organization	GO:0043933	0.028654926465956100	1.5428007016878400	1974	308	59	18092
GO:BP	regulation of response to external stimulus	GO:0032101	0.028749151011 38610	1.5413749758965900	1060	308	38	18092
GO:BP	endothelial cell migration	GO:0043542	0.030104082756663800	1.5213746008032 30	293	308	17	18092
GO:BP	animal organ morphogenesis	GO:0009887	0.031855506621 27800	1.4968154836261 80	1106	308	39	18092
GO:BP	regulation of response to stress	GO:0080134	0.038031085788 35740	1.4198612752941600	1455	308	47	18092
GO:BP	cell part morphogenesis	GO:0032990	0.038683299653 24820	1.4124764880513300	717	308	29	18092
GO:BP	glycosaminoglycan biosynthetic process	GO:0006024	0.039241071244031000	1.4062591453027600	108	308	10	18092
GO:BP	neuron projection development	GO:0031175	0.039415353392 69590	1.4043345752584000	1034	308	37	18092
GO:BP	neuron projection morphogenesis	GO:0048812	0.039497662924 01160	1.4034286008098200	680	308	28	18092
GO:BP	bone trabecula formation	GO:0060346	0.039887860829 20470	1.3991592541134100	10	308	4	18092
GO:BP	regulation of intracellular signal transduction	GO:1902531	0.043322860168 34470	1.3632828790475200	1864	308	56	18092
GO:BP	modulation by host of viral process	GO:0044788	0.043582871082 32300	1.3606841633936000	33	308	6	18092
GO:BP	plasma lipoprotein particle remodeling	GO:0034369	0.043582871082 32300	1.3606841633936000	33	308	6	18092
GO:BP	protein-lipid complex remodeling	GO:0034368	0.043582871082 32300	1.3606841633936000	33	308	6	18092
GO:BP	regulation of protein processing	GO:0070613	0.043924289618008900	1.3572952535657 00	67	308	8	18092
GO:BP	negative regulation of signal transduction	GO:0009968	0.044448693797 45640	1.3521409970085500	1377	308	45	18092
GO:BP	tissue homeostasis	GO:0001894	0.045902773390 9766	1.3381610741139300	272	308	16	18092
GO:BP	cellular response to oxygen-containing compound	GO:1901701	0.046604555311 604600	1.3315716315931700	1251	308	42	18092
GO:BP	regulation of receptor-mediated endocytosis	GO:0048259	0.049938933236 62680	1.3015607390049900	111	308	10	18092
GO:CC	extracellular exosome	GO:0070062	7.677610029782 28E-139	138.11477395085 60	2180	308	223	18963
GO:CC	extracellular vesicle	GO:1903561	9.416473618674 87E-138	137.02611170598400	2266	308	225	18963
GO:CC	extracellular organelle	GO:0043230	1.149086414652 7E-137	136.93964730987 10	2268	308	225	18963
GO:CC	extracellular space	GO:0005615	6.701719866510 58E-130	129.17381372973400	3598	308	255	18963
GO:CC	extracellular region	GO:0005576	1.786238614591 79E-122	121.74806052636700	4602	308	270	18963
GO:CC	vesicle	GO:0031982	1.795079519710 53E-98	97.745916307973 40	4071	308	240	18963

GO:CC	collagen-containing extracellular matrix	GO:0062023	5.144066050655 23E-64	63.288693463635 40	424	308	83	18963
GO:CC	extracellular matrix	GO:0031012	5.818054722958 06E-57	56.235222198220 100	564	308	86	18963
GO:CC	blood microparticle	GO:0072562	4.091195817991 E-45	44.388149733252 10	141	308	46	18963
GO:CC	vesicle lumen	GO:0031983	1.249225603205 03E-44	43.903359123371 800	326	308	61	18963
GO:CC	secretory granule lumen	GO:0034774	6.723026936890 22E-44	43.172435148671	320	308	60	18963
GO:CC	cytoplasmic vesicle lumen	GO:0060205	1.453175557724 77E-43	42.837681915539 90	324	308	60	18963
GO:CC	secretory granule	GO:0030141	7.641382578812 3E-32	31.116828056080 70	855	308	75	18963
GO:CC	endoplasmic reticulum lumen	GO:0005788	1.314560075406 18E-29	28.881219561842 700	307	308	47	18963
GO:CC	cell-substrate junction	GO:0030055	4.919365583742 43E-29	28.308090901550 80	426	308	53	18963
GO:CC	secretory vesicle	GO:0099503	6.283557782626 17E-29	28.201794386859 800	1028	308	78	18963
GO:CC	focal adhesion	GO:0005925	1.946378646224 71E-28	27.710772668708 20	418	308	52	18963
GO:CC	cytoplasmic vesicle	GO:0031410	4.781349656298 14E-25	24.320449495532 800	2437	308	114	18963
GO:CC	intracellular vesicle	GO:0097708	5.526367613173 84E-25	24.257560229252 50	2441	308	114	18963
GO:CC	endomembrane system	GO:0012505	3.280515357635 49E-23	22.484057924765 200	4633	308	160	18963
GO:CC	anchoring junction	GO:0070161	2.469791727890 52E-22	21.607339668295 600	843	308	63	18963
GO:CC	membrane-bounded organelle	GO:0043227	1.165817182271 5E-20	19.933369548166 800	12836	308	281	18963
GO:CC	platelet alpha granule lumen	GO:0031093	1.847378586893 26E-19	18.733444094624 6	66	308	21	18963
GO:CC	cytoplasm	GO:0005737	3.272866013785 69E-18	17.485071773691 300	11888	308	266	18963
GO:CC	platelet alpha granule	GO:0031091	1.199170418407 11E-17	16.921119093369 40	90	308	22	18963
GO:CC	ficolin-1-rich granule lumen	GO:1904813	8.378078052462 84E-17	16.076855597950 000	124	308	24	18963
GO:CC	cell junction	GO:0030054	3.826589643954 09E-15	14.417188108175 700	2131	308	89	18963
GO:CC	organelle	GO:0043226	2.277604161078 28E-14	13.642521752424 300	13974	308	284	18963
GO:CC	basement membrane	GO:0005604	8.075554398845 75E-14	13.092827653009 90	103	308	20	18963
GO:CC	cytosol	GO:0005829	2.094790777964 35E-13	12.678859346689 600	5231	308	151	18963
GO:CC	vacuolar lumen	GO:0005775	2.821050074050 45E-13	12.549589204985 800	174	308	24	18963
GO:CC	ficolin-1-rich granule	GO:0101002	1.024981524796 22E-12	11.989283962658 30	184	308	24	18963
GO:CC	melanosome	GO:0042470	1.800377156889 74E-12	11.744636506008 90	105	308	19	18963
GO:CC	pigment granule	GO:0048770	1.800377156889 74E-12	11.744636506008 90	105	308	19	18963
GO:CC	collagen trimer	GO:0005581	4.060689117657 64E-12	11.391400258393 200	95	308	18	18963

GO:CC	membrane-enclosed lumen	GO:0031974	5.04715969784618E-12	11.296952953479900	5468	308	152	18963
GO:CC	organelle lumen	GO:0043233	5.04715969784618E-12	11.296952953479900	5468	308	152	18963
GO:CC	endoplasmic reticulum	GO:0005783	5.10342451826872E-12	11.292138304238200	1975	308	79	18963
GO:CC	cell surface	GO:0009986	1.48212807139055E-11	10.829114267142 80	922	308	50	18963
GO:CC	lysosome	GO:0005764	2.54281271468446E-11	10.594685625657 7	709	308	43	18963
GO:CC	lytic vacuole	GO:0000323	2.54281271468446E-11	10.594685625657 7	709	308	43	18963
GO:CC	supramolecular polymer	GO:0099081	1.46505459893972E-10	9.8341461899335 00	1014	308	51	18963
GO:CC	supramolecular fiber	GO:0099512	3.99876567317605E-10	9.3980740446857 60	1006	308	50	18963
GO:CC	vacuole	GO:0005773	4.94569075112773E-10	9.3057730431056 70	807	308	44	18963
GO:CC	protein-containing complex	GO:0032991	6.55190655057267E-10	9.1836323055181 00	5556	308	148	18963
GO:CC	supramolecular complex	GO:0099080	1.38807156132421E-09	8.8575881434726	1337	308	58	18963
GO:CC	endocytic vesicle lumen	GO:0071682	3.00998758377284E-09	8.5214352958712 90	20	308	9	18963
GO:CC	endocytic vesicle	GO:0030139	1.04614563205989E-07	6.9804078539032 300	313	308	24	18963
GO:CC	fibrinogen complex	GO:0005577	1.42691667948052E-07	6.8456013854686	8	308	6	18963
GO:CC	complex of collagen trimers	GO:0098644	2.24312708031262E-07	6.6491461215507 20	21	308	8	18963
GO:CC	platelet dense granule lumen	GO:0031089	2.59689277155119E-07	6.5855459824789 20	14	308	7	18963
GO:CC	perinuclear region of cytoplasm	GO:0048471	0.000001349743 9682645700	5.8697486046274 30	740	308	36	18963
GO:CC	lysosomal lumen	GO:0043202	0.000001749294 8836575400	5.7571369740831 20	97	308	13	18963
GO:CC	cell cortex	GO:0005938	0.000003858851 371228060	5.4135419485337 00	318	308	22	18963
GO:CC	fibrillar collagen trimer	GO:0005583	0.000004457060 2573208100	5.3509514944206 60	12	308	6	18963
GO:CC	banded collagen fibril	GO:0098643	0.000004457060 2573208100	5.3509514944206 60	12	308	6	18963
GO:CC	platelet dense granule	GO:0042827	0.000007979099 220573580	5.0980461344156 20	21	308	7	18963
GO:CC	azurophil granule	GO:0042582	0.000009944418 39640148	5.0024206116968 8	154	308	15	18963
GO:CC	primary lysosome	GO:0005766	0.000009944418 39640148	5.0024206116968 8	154	308	15	18963
GO:CC	synapse	GO:0045202	0.000021378588 88217740	4.6700209642773 30	1382	308	50	18963
GO:CC	cytosolic ribosome	GO:0022626	0.000062632838 16021780	4.2031979081231 600	109	308	12	18963
GO:CC	cell-cell junction	GO:0005911	0.000075344313 23337430	4.1229495213794 40	506	308	26	18963
GO:CC	azurophil granule lumen	GO:0035578	0.000077571618 83308630	4.1102971452202 4	91	308	11	18963
GO:CC	intracellular anatomical structure	GO:0005622	0.000081102442 9712922	4.0909660637546 60	14764	308	274	18963

GO:CC	cortical cytoskeleton	GO:0030863	0.000093222697 97083950	4.0304783322456 10	113	308	12	18963
GO:CC	high-density lipoprotein particle	GO:0034364	0.000095793292 09517390	4.0186649012351 00	29	308	7	18963
GO:CC	haptoglobin-hemoglobin complex	GO:0031838	0.000139721796 70235400	3.8547358383442 90	11	308	5	18963
GO:CC	chylomicron	GO:0042627	0.000581646366 7419890	3.2353409803856 900	14	308	5	18963
GO:CC	plasma lipoprotein particle	GO:0034358	0.000683341924 716555	3.1653619334197 100	38	308	7	18963
GO:CC	lipoprotein particle	GO:1990777	0.000683341924 716555	3.1653619334197 100	38	308	7	18963
GO:CC	membrane attack complex	GO:0005579	0.000688221946 7886950	3.1622714822276 600	7	308	4	18963
GO:CC	sarcolemma	GO:0042383	0.000800443235 5496520	3.0966694611983 50	138	308	12	18963
GO:CC	intracellular organelle lumen	GO:0070013	0.001002081324 5658900	2.9990970315855 300	5304	308	123	18963
GO:CC	actin cytoskeleton	GO:0015629	0.001135937521 5645400	2.9446455548802 400	513	308	24	18963
GO:CC	protein-lipid complex	GO:0032994	0.001167572584 8777400	2.9327161109914 000	41	308	7	18963
GO:CC	collagen beaded filament	GO:0098647	0.001270608119 1421600	2.8959883738651 000	3	308	3	18963
GO:CC	collagen type VI trimer	GO:0005589	0.001270608119 1421600	2.8959883738651 000	3	308	3	18963
GO:CC	laminin-10 complex	GO:0043259	0.001270608119 1421600	2.8959883738651 000	3	308	3	18963
GO:CC	Golgi lumen	GO:0005796	0.001437727107 045800	2.8423235389539 10	99	308	10	18963
GO:CC	cell projection	GO:0042995	0.001565430452 7051900	2.8053662219961 50	2352	308	66	18963
GO:CC	intracellular non-membrane-bounded organelle	GO:0043232	0.001947670762 8574700	2.7104844550338 00	4326	308	104	18963
GO:CC	non-membrane-bounded organelle	GO:0043228	0.002098378762 088650	2.6781161179354 20	4333	308	104	18963
GO:CC	podosome	GO:0002102	0.002238247611 7435100	2.6500918702360 00	30	308	6	18963
GO:CC	cell periphery	GO:0071944	0.002381677486 3688900	2.6231170486355 20	5786	308	130	18963
GO:CC	cortical actin cytoskeleton	GO:0030864	0.002402563135 00242	2.6193251910380 200	83	308	9	18963
GO:CC	cytoskeleton	GO:0005856	0.003052102064 2134700	2.5154009473935 800	2302	308	64	18963
GO:CC	proteasome complex	GO:0000502	0.003357098929 4374000	2.4740358604571 70	66	308	8	18963
GO:CC	glutamatergic synapse	GO:0098978	0.003667894489 1447400	2.4355831657613 60	373	308	19	18963
GO:CC	triglyceride-rich plasma lipoprotein particle	GO:0034385	0.005384514080 635100	2.2688534830105 100	21	308	5	18963
GO:CC	very-low-density lipoprotein particle	GO:0034361	0.005384514080 635100	2.2688534830105 100	21	308	5	18963
GO:CC	external side of plasma membrane	GO:0009897	0.005759980368 777480	2.2395789967410 500	420	308	20	18963
GO:CC	plasma membrane bounded cell projection	GO:0120025	0.006127708882 20211	2.2127018755321 800	2255	308	62	18963
GO:CC	endopeptidase complex	GO:1905369	0.006430538531 0176400	2.1917526551853 10	72	308	8	18963

GO:CC	ribonucleoprotein complex	GO:1990904	0.007862004323767770	2.1044667216723800	693	308	27	18963
GO:CC	lamellipodium	GO:0030027	0.009175311632713730	2.0373791763326000	204	308	13	18963
GO:CC	cytosolic large ribosomal subunit	GO:0022625	0.010996018085288300	1.9587645545384200	57	308	7	18963
GO:CC	side of membrane	GO:0098552	0.012329032089182800	1.9090710170642000	632	308	25	18963
GO:CC	intermediate-density lipoprotein particle	GO:0034363	0.012401453117334000	1.9065274242034600	5	308	3	18963
GO:CC	hemoglobin complex	GO:0005833	0.013014208507106100	1.8855822394985700	13	308	4	18963
GO:CC	ribosomal subunit	GO:0044391	0.021192676492 42720	1.6738141913548900	191	308	12	18963
GO:CC	cell leading edge	GO:0031252	0.024569257259 66830	1.6096079722502100	429	308	19	18963
GO:CC	plasma membrane	GO:0005886	0.027593136851 04550	1.5591989251220800	5663	308	123	18963
GO:CC	cytosolic small ribosomal subunit	GO:0022627	0.032101006573 04560	1.4934813494560100	47	308	6	18963
GO:CC	microvillus	GO:0005902	0.037786483428605900	1.4226635235001500	92	308	8	18963
GO:CC	adherens junction	GO:0005912	0.042085202183 35800	1.3758705820699800	175	308	11	18963
KEGG	ECM-receptor interaction	KEGG:04512	5.095553980262 86E-21	20.292808593307700	88	218	28	7987
KEGG	Focal adhesion	KEGG:04510	3.657712750637 19E-17	16.436790403756 20	200	218	35	7987
KEGG	Complement and coagulation cascades	KEGG:04610	3.867591358592 86E-14	13.412559418788500	85	218	22	7987
KEGG	PI3K-Akt signaling pathway	KEGG:04151	1.880103221876 95E-09	8.7258183063422 00	353	218	35	7987
KEGG	Human papillomavirus infection	KEGG:05165	6.589188751555 77E-09	8.1811680516291 2	331	218	33	7987
KEGG	Amoebiasis	KEGG:05146	1.490842646867 75E-07	6.8265681923641 20	101	218	17	7987
KEGG	Glycolysis / Gluconeogenesis	KEGG:00010	2.332572189791 12E-07	6.6321649065770 50	67	218	14	7987
KEGG	Phagosome	KEGG:04145	2.81159108956E -07	6.5510478417108 90	148	218	20	7987
KEGG	Coronavirus disease - COVID-19	KEGG:05171	0.000001481598 6323689400	5.8292694315496 30	231	218	24	7987
KEGG	Proteoglycans in cancer	KEGG:05205	0.000070586972 93243770	4.1512754420868 50	205	218	20	7987
KEGG	Platelet activation	KEGG:04611	0.000125596238 9938840	3.9010233654448 30	124	218	15	7987
KEGG	Carbon metabolism	KEGG:01200	0.000362764229 97977000	3.4403755426931800	118	218	14	7987
KEGG	Protein digestion and absorption	KEGG:04974	0.000406995798 91927700	3.3904100736140700	103	218	13	7987
KEGG	Biosynthesis of amino acids	KEGG:01230	0.000524160951 4256820	3.2805353359495500	75	218	11	7987
KEGG	HIF-1 signaling pathway	KEGG:04066	0.003918467746074300	2.4068837236720200	109	218	12	7987
KEGG	Salmonella infection	KEGG:05132	0.004769796699479230	2.3215001312693100	249	218	19	7987
KEGG	Prion disease	KEGG:05020	0.005350386815183960	2.2716148187961300	273	218	20	7987

KEGG	Systemic lupus erythematosus	KEGG:05322	0.006592866409 1156700	2.1809257242520 10	133	218	13	7987
KEGG	Regulation of actin cytoskeleton	KEGG:04810	0.008732623040 141890	2.0588552865631 20	217	218	17	7987
KEGG	Pentose phosphate pathway	KEGG:00030	0.013506770983 822200	1.8694484638218 9	30	218	6	7987
KEGG	Staphylococcus aureus infection	KEGG:05150	0.017734671924 015100	1.7511768411874 00	91	218	10	7987
KEGG	Malaria	KEGG:05144	0.033865409705 90260	1.4702436659032 900	49	218	7	7987
KEGG	Cholesterol metabolism	KEGG:04979	0.038478904782 172900	1.4147772977004 400	50	218	7	7987

Table S 8. *List of proteins candidate biomarkers identified in A549 cell-derived exosomal proteome found at least twice with their Sum of PEP score.*

A549 exo proteins	Description	# of replicates	Sum of PEP score
O00468-5	Isoform 5 of Agrin	2	23.128
O00560-1	Syntenin-1	2	21.5605
O43795	Unconventional myosin-Ib	2	35.1345
P02786	Transferrin receptor protein 1	2	19.842
P05023	Sodium/potassium-transporting ATPase subunit alpha-1	2	27.0535
P06576	ATP synthase subunit beta, mitochondrial	2	36.7945
P07355	Annexin A2	2	67.3405
P08195	4F2 cell-surface antigen heavy chain	2	86.061
P10809	60 kDa heat shock protein, mitochondrial	2	59.013
P16401	Histone H1.5	2	23.368
P25705-1	ATP synthase subunit alpha, mitochondrial	2	26.285
P26006	Integrin alpha-3	2	29.465
P29401	Transketolase	2	19.679
P40926	Malate dehydrogenase, mitochondrial	2	36.5445
P54652	Heat shock-related 70 kDa protein 2	2	25.768
P62701	40S ribosomal protein S4, X isoform	2	15.7245
P68104	Elongation factor 1-alpha 1	2	25.314
Q00610-1	Clathrin heavy chain 1	2	85.869
Q07020	60S ribosomal protein L18	2	19.4515
Q13885	Tubulin beta-2A chain	2	43.28
Q7L7L0	Histone H2A type 3	2	21.9595
Q9NZM1	Tubulin beta-1 chain	2	48.0405

Table S 9. *Protein concentration of the exosome samples (E- breath-derived exosomes from a single individual, WHB – whole breath sample from a single individual, S- breath-derived exosomes collected from volunteers) in the vial.*

Sample name	Peptide quant (ng/µL)	V total (µL)	Total protein (ng)	Conc (mg/mL)
E1	87.8	20	1756	0.0878
E2	99.7	20	1994	0.0997
E3	108	18	1944	0.108
E4	98.6	20	1972	0.0986
WHB1	36.94	45	1662.3	0.03694
WHB2	36.551	45	1644.795	0.036551
WHB3	21.53	45	968.85	0.02153
WHB4	21.815	45	981.675	0.021815
S1	21.873	45	984.285	0.021873
S2	18.37	45	826.65	0.01837
S3	13.799	20	275.98	0.013799

Table S 10. *List of proteins found at least once with a high quality peptide match identified in breath-derived exosomes collected from volunteers.*

Protein ID	Protein ID	Protein ID	Protein ID	Protein ID	Protein ID
A0A075B6H7	O95498	P06870	P22392	P60660	Q5JTV8
A0A075B6H9	O95716	P07195	P22735	P60842	Q5QNW6
A0A075B6I6	P00338	P07237	P22894	P60900	Q5SSG8
A0A075B6I9	P00450	P07339	P23246	P60953	Q5SZK8
A0A075B6J9	P00491	P07355	P23280	P61019	Q5T749
A0A075B6K4	P00558	P07358	P23284	P61020	Q5T750
A0A075B6S5	P00734	P07360	P23381	P61026	Q5TEC6
A0A075B7B8	P00736	P07437	P23526	P61106	Q5VT79
A0A075B7D0	P00738	P07476	P23528	P61158	Q5VVJ2
A0A087WSY6	P00739	P07602	P24158	P61160	Q5VZK9
A0A087WUI2	P00747	P07737	P24534	P61224	Q68DW7
A0A087X0Q4	P00751	P07858	P25311	P61247	Q6A163
A0A0A0MQZ1	P01008	P07864	P25705	P61313	Q6F5E8
A0A0A0MRZ8	P01009	P07900	P26038	P61626	Q6MZM9
A0A0A0MS15	P01011	P07996	P26447	P61769	Q6P4A8
A0A0A0MT36	P01023	P08123	P26583	P61978	Q6P5S2
A0A0B4J1U3	P01024	P08133	P26641	P61981	Q6PCB0
A0A0B4J1U7	P01033	P08174	P27105	P62081	Q6UWP8
A0A0B4J1V0	P01034	P08238	P27348	P62158	Q6XQN6
A0A0B4J1X5	P01036	P08246	P27482	P62241	Q6YP21
A0A0B4J1Y9	P01037	P08294	P27487	P62269	Q6ZSL4
A0A0C4DGG8	P01040	P08311	P27797	P62328	Q70J99

A0A0C4DH25	P01042	P08493	P27918	P62491	Q71U36
A0A0C4DH29	P01591	P08571	P28062	P62701	Q75VX8
A0A0C4DH31	P01602	P08575	P28066	P62714	Q7RTR2
A0A0C4DH35	P01614	P08582	P28325	P62753	Q7Z569
A0A0C4DH38	P01619	P08603	P28676	P62805	Q7Z794
A0A0C4DH55	P01624	P08637	P28799	P62820	Q7Z7M9
A0A0C4DH68	P01699	P08670	P29350	P62826	Q86UX7
A0A0C4DH72	P01700	P08758	P29373	P62857	Q86V81
A0A0G2JMB2	P01701	P08779	P29401	P62873	Q86VR7
A0A0G2JPR0	P01703	P08865	P29508	P62937	Q86VZ4
A0A0G2JRQ6	P01706	P09211	P30040	P62987	Q86X29
A0A0J9YY99	P01709	P09228	P30041	P63104	Q86XI8
A0A140TA29	P01714	P09237	P30044	P63241	Q86Y34
A0A1X7SBS1	P01718	P09382	P30086	P67775	Q86Y46
A0A2Q2TTZ9	P01721	P09429	P30153	P68104	Q86YZ3
A0A2R8Y5S7	P01762	P09493	P30273	P68133	Q8IWL2
A0A2R8YEA7	P01763	P09958	P30501	P68366	Q8IZ83
A0A3B3IRN5	P01766	P09972	P30520	P68371	Q8IZP0
A0M8Q6	P01768	P0CG39	P30626	P68871	Q8N0Y7
A8K2U0	P01782	P0DJI8	P30740	P69905	Q8N1N4
A8MTF8	P01833	P0DJI9	P30838	P78371	Q8N4F0
A8MUU1	P01834	P0DMV8	P31025	P80188	Q8NBB4
A8MVU1	P01857	P0DOX7	P31146	P80511	Q8NBJ4
B3EWG6	P01859	P0DOY2	P31150	P80723	Q8NEL9
B4DEH5	P01860	P0DOY3	P31151	P80748	Q8TAA3
B9A064	P01861	P0DP01	P31943	P81605	Q8TAX7
C9IZR8	P01871	P0DP04	P31944	P84243	Q8TCU6
C9J7B7	P01876	P10153	P31946	P98160	Q8TDL5
C9J8J7	P02042	P10599	P31947	Q00610	Q8TEA7
C9JX95	P02452	P10606	P31949	Q01469	Q8TF09
D3DSM0	P02533	P10809	P31997	Q01518	Q8WUM4
D6RF35	P02538	P10909	P32119	Q01546	Q92743
E9PDK7	P02545	P11021	P32320	Q01968	Q92817
E9PKU7	P02647	P11142	P32926	Q02413	Q92876
E9PLE9	P02649	P11215	P33241	Q02487	Q92882
E9PLZ3	P02652	P11413	P34096	Q02543	Q92888
F5GXS2	P02654	P12109	P34931	Q02809	Q92896
G3V1R1	P02656	P12236	P35268	Q02818	Q96AE4
G3V1R6	P02671	P12273	P35527	Q03591	Q96BQ1

G5EA09	P02675	P12429	P35579	Q04446	Q96C03
H0Y4V9	P02679	P12724	P35754	Q04609	Q96DA0
H0Y8Z5	P02748	P12814	P35858	Q04695	Q96DR5
H0YAL9	P02749	P13639	P35908	Q04917	Q96DR8
H0YER0	P02751	P13645	P36578	Q05315	Q96GQ7
H0YF32	P02760	P13646	P36952	Q05639	Q96HE7
H0YGX7	P02763	P13647	P37802	Q06830	Q96P63
H0YJW5	P02765	P13667	P37837	Q07020	Q96QB1
H3BSZ8	P02766	P13716	P38606	Q07065	Q96QR1
H7BZJ3	P02768	P13796	P39019	Q07654	Q99439
H7C169	P02787	P13797	P39060	Q07955	Q99497
J3QLF6	P02788	P13804	P39687	Q07960	Q99519
J3QS37	P02790	P13929	P40121	Q08188	Q99536
K7ELH5	P02794	P13987	P40197	Q08380	Q99715
K7EPJ3	P02808	P14174	P40227	Q08431	Q99829
K7EQX2	P02810	P14314	P40394	Q08554	Q99935
M0QY96	P02812	P14317	P40926	Q08AI8	Q9BRA2
M0R251	P02814	P14618	P41218	Q09666	Q9BRK5
O00160	P03973	P14625	P41240	Q0VD83	Q9BVC6
O00299	P04004	P14780	P42167	Q11201	Q9BW30
O00391	P04040	P14854	P43490	Q12931	Q9BXJ4
O00592	P04066	P14923	P46783	Q13043	Q9GZM7
O00602	P04075	P15104	P46940	Q13126	Q9GZZ8
O00748	P04080	P15153	P47755	Q13162	Q9H0E2
O14647	P04083	P15311	P47929	Q13217	Q9H173
O14727	P04114	P15328	P48382	Q13231	Q9H1E1
O14745	P04196	P15515	P48643	Q13421	Q9H299
O14773	P04217	P15516	P49189	Q13438	Q9H2K2
O14950	P04259	P15814	P49368	Q13561	Q9H4G4
O14983	P04264	P15924	P49458	Q13748	Q9H4M9
O15131	P04350	P15941	P49788	Q13813	Q9H7E2
O15143	P04406	P16070	P49913	Q13835	Q9HC84
O15144	P04430	P16401	P50395	Q14005	Q9HCY8
O15145	P04432	P16402	P50552	Q14103	Q9HD89
O15511	P04632	P16870	P50570	Q14118	Q9NQ38
O43240	P04745	P17213	P50990	Q14134	Q9NYL9
O43296	P04792	P17858	P50991	Q14254	Q9NZT1
O43399	P04839	P17931	P50995	Q14508	Q9UBC9
O43490	P04899	P17980	P51148	Q14515	Q9UBG3

O43504	P05089	P17987	P51149	Q14520	Q9UBQ0
O43866	P05090	P18124	P51858	Q14624	Q9UBR2
O60234	P05109	P18510	P51888	Q14764	Q9UBX7
O60343	P05155	P18669	P51991	Q14847	Q9UEF7
O60437	P05164	P19013	P51993	Q14CN2	Q9UGM3
O60565	P05166	P19823	P52209	Q15080	Q9UJJ9
O60664	P05204	P19878	P52565	Q15084	Q9UJU6
O60701	P05387	P19957	P52790	Q15149	Q9UKG1
O60812	P06310	P19971	P52907	Q15365	Q9UKR0
O60814	P06312	P20061	P53634	Q15517	Q9UKR3
O75015	P06331	P20160	P54108	Q15691	Q9UL52
O75083	P06396	P20618	P55000	Q15847	Q9UQ07
O75367	P06576	P20742	P55058	Q15904	Q9Y272
O75531	P06702	P20810	P55072	Q15942	Q9Y2J8
O75594	P06703	P20930	P55268	Q16610	Q9Y490
O75874	P06727	P21281	P55786	Q16629	Q9Y4L1
O75888	P06731	P21333	P58107	Q16777	Q9Y653
O75955	P06733	P21926	P59665	Q16851	Q9Y6R7
O94985	P06737	P22061	P59998	Q2I0M4	S4R3R4
O95171	P06744	P22079	P60022	Q32P51	S4R460
O95274	P06748	P22307	P60033	Q562R1	
O95445	P06753	P22314	P60174	Q5D862	

Table S 11. *Raw list of proteins found at least twice with a high quality peptide match identified as core breath proteome (297).*

Protein ID	**Protein ID**	**Protein ID**	**Protein ID**	**Protein ID**	**Protein ID**
A0A075B6H7	P01699	P06576	P14780	P35579	Q08188
A0A075B6I9	P01700	P06702	P14923	P35908	Q08380
A0A0A0MRZ8	P01701	P06703	P15153	P37837	Q09666
A0A0A0MS15	P01714	P06733	P15311	P38606	Q11201
A0A0B4J1V0	P01721	P06737	P15515	P40121	Q13043
A0A0B4J1X5	P01833	P06744	P15516	P41218	Q13162
A0A0B4J1Y9	P01834	P06753	P15924	P47929	Q13231
A0A0C4DH25	P01859	P06870	P16401	P49913	Q13438
A0A0C4DH31	P01860	P07195	P16402	P50990	Q13835
A0A0G2JMB2	P01861	P07237	P16870	P51149	Q14103
A0A2Q2TTZ9	P01871	P07339	P18669	P52209	Q14508
A0A2R8YEA7	P01876	P07355	P19013	P52790	Q14515
A0M8Q6	P02533	P07437	P19823	P53634	Q14764
A8K2U0	P02538	P07737	P19971	P54108	Q15904

B4DEH5	P02647	P07900	P20061	P55000	Q16610
B9A064	P02671	P07996	P20160	P59665	Q16777
G3V1R1	P02675	P08133	P21333	P59998	Q2I0M4
H7BZJ3	P02679	P08238	P21926	P60022	Q32P51
O00160	P02749	P08246	P22079	P60660	Q562R1
O00299	P02751	P08493	P22314	P60842	Q5QNW6
O00391	P02760	P08571	P23280	P61158	Q5T749
O14773	P02768	P08670	P23381	P61160	Q6MZM9
O14950	P02787	P08779	P23528	P61224	Q6P5S2
O15143	P02788	P09211	P24158	P61626	Q6UWP8
O15144	P02790	P09228	P25311	P61769	Q71U36
O15145	P02808	P09958	P25705	P61978	Q8N1N4
O15511	P02810	P0DJI8	P27482	P62328	Q8N4F0
O43240	P02812	P0DJI9	P27487	P62805	Q8TAX7
O43490	P02814	P0DMV8	P28062	P62826	Q8TDL5
O75083	P03973	P0DOY3	P28066	P62937	Q8WUM4
O75594	P04004	P0DUB6	P28325	P62987	Q92743
O75874	P04040	P10153	P28676	P63104	Q92817
O75955	P04075	P10606	P28799	P68104	Q92882
O95716	P04080	P10809	P29401	P68133	Q96DA0
P00338	P04083	P10909	P30040	P68366	Q96DR5
P00491	P04196	P11021	P30041	P68371	Q96QR1
P00558	P04259	P11142	P30153	P68871	Q99536
P00734	P04264	P11413	P30740	P69905	Q9BRK5
P00747	P04406	P12273	P31025	P78371	Q9HC84
P01008	P04792	P12429	P31146	P80188	Q9HD89
P01009	P04839	P12724	P31151	P80748	Q9NZT1
P01023	P04899	P13639	P31944	P81605	Q9UBG3
P01024	P05089	P13645	P31946	Q01518	Q9UBX7
P01034	P05090	P13646	P31947	Q02413	Q9UGM3
P01036	P05109	P13647	P31949	Q02818	Q9Y490
P01037	P05164	P13716	P32320	Q04695	Q9Y6R7
P01040	P05204	P13796	P32926	Q05315	S4R460
P01591	P06310	P13987	P33241	Q06830	
P01614	P06331	P14174	P34096	Q07065	
P01619	P06396	P14618	P35527	Q07654	

***Table S 12**. Subset of core breath proteome found at least twice with a high quality peptide match consisting of 184 proteins.*

Protein ID	**Protein ID**	**Protein ID**	**Protein ID**	**Protein ID**	**Protein ID**
A0A075B6H7	P01036	P05204	P15515	P37837	Q14508
A0A075B6I9	P01037	P06310	P15516	P38606	Q14515
A0A0A0MRZ8	P01040	P06331	P16401	P40121	Q15904
A0A0A0MS15	P01591	P06576	P16402	P47929	Q16777
A0A0B4J1V0	P01614	P06703	P16870	P52209	Q2I0M4
A0A0B4J1X5	P01619	P06733	P19013	P55000	Q32P51
A0A0B4J1Y9	P01699	P06753	P19823	P59998	Q562R1
A0A0C4DH25	P01700	P06870	P19971	P60022	Q5QNW6
A0A0C4DH31	P01701	P07195	P22079	P60660	Q5T749
A0A0G2JMB2	P01714	P07237	P22314	P60842	Q6MZM9
A0A2Q2TTZ9	P01721	P07737	P23280	P61158	Q6P5S2
A0A2R8YEA7	P01834	P08133	P23381	P61978	Q6UWP8
A0M8Q6	P01859	P08493	P23528	P62805	Q71U36
A8K2U0	P01860	P08670	P25311	P62826	Q8N1N4
B9A064	P01861	P08779	P25705	P62987	Q8N4F0
G3V1R1	P01871	P09228	P27482	P63104	Q8TAX7
H7BZJ3	P01876	P09958	P27487	P68133	Q8TDL5
O00160	P02533	P0DJI8	P28062	P69905	Q8WUM4
O00299	P02538	P0DJI9	P28325	P80748	Q92743
O14773	P02760	P0DOY3	P29401	P81605	Q92817
O14950	P02790	P0DUB6	P30040	Q02818	Q96DA0
O15143	P02808	P10606	P30153	Q04695	Q96DR5
O15144	P02810	P10809	P31025	Q05315	Q96QR1
O15145	P02812	P11021	P31944	Q06830	Q9HC84
O43240	P02814	P11413	P31946	Q07654	Q9UBG3
O43490	P04004	P12273	P31947	Q08188	Q9UBX7
O75955	P04083	P13645	P32926	Q09666	Q9UGM3
P00338	P04259	P13646	P33241	Q11201	Q9Y6R7
P00558	P04406	P13647	P34096	Q13043	S4R460
P00734	P04792	P13796	P35527	Q13438	
P01008	P05090	P15311	P35908	Q14103	

Table S 13. *GO analysis of breath exosomal proteome (297 proteins). The analysis was performed by using g:Profiler software.*
**The list of proteins associated with each ontology is available on request deanna.shea@vuw.ac.nz*

Source	Term name	Term ID	Adjusted p-value	Negative log10 of adjusted p-value	Term	Query size	Intersection size	Effective domain size
GO:MF	structural constituent of cytoskeleton	GO:0005200	3.56E-19	18.4491073		286	24	18679
GO:MF	cell adhesion molecule binding	GO:0050839	6.6NE-18	17.1775235	544	286	45	18679
GO:MF	antigen binding	GO:0003823	1.39E-16	15.858446	163	286	26	18679
GO:MF	cadherin binding	GO:0045296	6.00E-15	14.2220133	333	286	33	18679
GO:MF	endopeptidase inhibitor activity	GO:0004866	1.22E-13	12.9120381	175	286	24	18679
GO:MF	peptidase inhibitor activity	GO:0030414	2.68E-13	12.5712631	181	286	24	18679
GO:MF	peptidase regulator activity	GO:0061134	3.43E-13	12.4648782	222	286	26	18679
GO:MF	endopeptidase regulator activity	GO:0061135	5.71E-13	12.243628	187	286	24	18679
GO:MF	structural molecule activity	GO:0005198	5.97E-13	12.2240176	701	286	44	18679
GO:MF	enzyme inhibitor activity	GO:0004857	2.94E-11	10.5315229	391	286	31	18679
GO:MF	signaling receptor binding	GO:0005102	2.14E-10	9.66993416	1551	286	63	18679
GO:MF	immunoglobulin receptor binding	GO:0034987	2.73E-10	9.56398203	77	286	15	18679
GO:MF	protein-containing complex binding	GO:0044877	6.19E-10	9.20827271	1304	286	56	18679
GO:MF	actin filament binding	GO:0051015	6.46E-09	8.1900157	213	286	21	18679
GO:MF	identical protein binding	GO:0042802	3.72E-08	7.42940097	2063	286	70	18679
GO:MF	protease binding	GO:0002020	7.52E-08	7.12404684	131	286	16	18679
GO:MF	cysteine-type endopeptidase inhibitor activity	GO:0004869	1.36E-07	6.86685915	52	286	11	18679
GO:MF	actin binding	GO:0003779	1.47E-07	6.83252306	449	286	28	18679
GO:MF	calcium-dependent protein binding	GO:0048306	1.73E-07	6.76310209	83	286	13	18679
GO:MF	cytoskeletal protein binding	GO:0008092	1.1828E-06	5.92710429	1001	286	42	18679
GO:MF	enzyme binding	GO:0019899	3.2008E-06	5.49474041	2048	286	65	18679
GO:MF	serine-type endopeptidase inhibitor activity	GO:0004867	1.456E-05	4.83682839	98	286	12	18679
GO:MF	serine-type endopeptidase activity	GO:0004252	1.978E-05	4.70377325	167	286	15	18679
GO:MF	antioxidant activity	GO:0016209	3.92E-05	4.40670865	87	286	11	18679
GO:MF	peroxidase activity	GO:0004601	4.3954E-05	4.3570064	53	286	9	18679
GO:MF	glycosaminoglycan binding	GO:0005539	7.252E-05	4.13954296	238	286	17	18679
GO:MF	serine-type peptidase activity	GO:0008236	7.6602E-05	4.11575833	185	286	15	18679
GO:MF	oxidoreductase activity, acting on peroxide as acceptor	GO:0016684	8.4577E-05	4.07274748	57	286	9	18679
GO:MF	serine hydrolase activity	GO:0017171	0.00010124	3.99466335	189	286	15	18679
GO:MF	carbohydrate derivative binding	GO:0097367	0.00018875	3.72412397	2282	286	65	18679
GO:MF	lipopolysaccharide binding	GO:0001530	0.00019499	3.70999876	32	286	7	18679
GO:MF	chaperone binding	GO:0051087	0.00030091	3.52156904	106	286	11	18679
GO:MF	calcium ion binding	GO:0005509	0.00033891	3.46991324	723	286	30	18679
GO:MF	protein folding chaperone	GO:0044183	0.00045889	3.33828738	36	286	7	18679
GO:MF	unfolded protein binding	GO:0051082	0.00057247	3.24224983	113	286	11	18679
GO:MF	S100 protein binding	GO:0044548	0.00063723	3.19570144	14	286	5	18679
GO:MF	endopeptidase activity	GO:0004175	0.00064796	3.18845381	444	286	22	18679
GO:MF	lipid binding	GO:0008289	0.00135763	2.86721831	774	286	30	18679

GO:MF	sulfur compound binding	GO:1901681	0.00146993	2.83270313	264	286	16	18679
GO:MF	small molecule binding	GO:0036094	0.0026774	2.57228599	2516	286	66	18679
GO:MF	molecular function regulator	GO:0098772	0.00338698	2.47018793	1115	286	37	18679
GO:MF	enzyme regulator activity	GO:0030234	0.00478119	2.32046362	911	286	32	18679
GO:MF	heparin binding	GO:0008201	0.00489319	2.31040779	168	286	12	18679
GO:MF	disordered domain specific binding	GO:0097718	0.00502854	2.29855818	34	286	6	18679
GO:MF	binding	GO:0005488	0.00650883	2.18649739	17070	286	279	18679
GO:MF	peptidase activity	GO:0008233	0.00988025	2.00523228	647	286	25	18679
GO:MF	phospholipase A2 inhibitor activity	GO:0019834	0.01522927	1.81732102	5	286	3	18679
GO:MF	protein binding	GO:0005515	0.017468	1.75775669	14767	286	252	18679
GO:MF	protein dimerization activity	GO:0046983	0.02077981	1.68235835	1073	286	34	18679
GO:MF	protein homodimerization activity	GO:0042803	0.02176566	1.66222821	679	286	25	18679
GO:MF	structural constituent of skin epidermis	GO:0030280	0.02820419	1.54968642	15	286	4	18679
GO:MF	intermediate filament binding	GO:0019215	0.02820419	1.54968642	15	286	4	18679
GO:MF	lipase inhibitor activity	GO:0055102	0.04800195	1.31874111	17	286	4	18679
GO:MF	MHC class II protein complex binding	GO:0023026	0.04800195	1.31874111	17	286	4	18679
GO:MF	structural constituent of cytoskeleton	GO:0005200	3.56E-19	18.4491073	104	286	24	18679
GO:MF	cell adhesion molecule binding	GO:0050839	6.64E-18	17.1775235	544	286	45	18679
GO:MF	antigen binding	GO:0003823	1.39E-16	15.858446	163	286	26	18679
GO:MF	cadherin binding	GO:0045296	6.00E-15	14.2220133	333	286	33	18679
GO:MF	endopeptidase inhibitor activity	GO:0004866	1.22E-13	12.9120381	175	286	24	18679
GO:MF	peptidase inhibitor activity	GO:0030414	2.68E-13	12.5712631	181	286	24	18679
GO:MF	peptidase regulator activity	GO:0061134	3.43E-13	12.4648782	222	286	26	18679
GO:MF	endopeptidase regulator activity	GO:0061135	5.71E-13	12.243628	187	286	24	18679
GO:MF	structural molecule activity	GO:0005198	5.97E-13	12.2240176	701	286	44	18679
GO:MF	enzyme inhibitor activity	GO:0004857	2.94E-11	10.5315229	391	286	31	18679
GO:MF	signaling receptor binding	GO:0005102	2.14E-10	9.66993416	1551	286	63	18679
GO:MF	immunoglobulin receptor binding	GO:0034987	2.73E-10	9.56398203	77	286	15	18679
GO:MF	protein-containing complex binding	GO:0044877	6.19E-10	9.20827271	1304	286	56	18679
GO:MF	actin filament binding	GO:0051015	6.46E-09	8.1900157	213	286	21	18679
GO:MF	identical protein binding	GO:0042802	3.72E-08	7.42940097	2063	286	70	18679
GO:MF	protease binding	GO:0002020	7.52E-08	7.12404684	131	286	16	18679
GO:MF	cysteine-type endopeptidase inhibitor activity	GO:0004869	1.36E-07	6.86685915	52	286	11	18679
GO:MF	actin binding	GO:0003779	1.47E-07	6.83252306	449	286	28	18679
GO:MF	calcium-dependent protein binding	GO:0048306	1.73E-07	6.76310209	83	286	13	18679
GO:MF	cytoskeletal protein binding	GO:0008092	1.1828E-06	5.92710429	1001	286	42	18679
GO:MF	enzyme binding	GO:0019899	3.2008E-06	5.49474041	2048	286	65	18679
GO:MF	serine-type endopeptidase inhibitor activity	GO:0004867	1.456E-05	4.83682839	98	286	12	18679
GO:MF	serine-type endopeptidase activity	GO:0004252	1.978E-05	4.70377325	167	286	15	18679
GO:MF	antioxidant activity	GO:0016209	3.92E-05	4.40670865	87	286	11	18679
GO:MF	peroxidase activity	GO:0004601	4.3954E-05	4.3570064	53	286	9	18679
GO:MF	glycosaminoglycan binding	GO:0005539	7.252E-05	4.13954296	238	286	17	18679

GO:MF	serine-type peptidase activity	GO:0008236	7.6602E-05	4.11575833	185	286	15	18679
GO:MF	oxidoreductase activity, acting on peroxide as acceptor	GO:0016684	8.4577E-05	4.07274748	57	286	9	18679
GO:MF	serine hydrolase activity	GO:0017171	0.00010124	3.99466335	189	286	15	18679
GO:MF	carbohydrate derivative binding	GO:0097367	0.00018875	3.72412397	2282	286	65	18679
GO:MF	lipopolysaccharide binding	GO:0001530	0.00019499	3.70999876	32	286	7	18679
GO:MF	chaperone binding	GO:0051087	0.00030091	3.52156904	106	286	11	18679
GO:MF	calcium ion binding	GO:0005509	0.00033891	3.46991324	723	286	30	18679
GO:MF	protein folding chaperone	GO:0044183	0.00045889	3.33828738	36	286	7	18679
GO:MF	unfolded protein binding	GO:0051082	0.00057247	3.24224983	113	286	11	18679
GO:MF	S100 protein binding	GO:0044548	0.00063723	3.19570144	14	286	5	18679
GO:MF	endopeptidase activity	GO:0004175	0.00064796	3.18845381	444	286	22	18679
GO:MF	lipid binding	GO:0008289	0.00135763	2.86721831	774	286	30	18679
GO:MF	sulfur compound binding	GO:1901681	0.00146993	2.83270313	264	286	16	18679
GO:MF	small molecule binding	GO:0036094	0.0026774	2.57228599	2516	286	66	18679
GO:MF	molecular function regulator	GO:0098772	0.00338698	2.47018793	1115	286	37	18679
GO:MF	enzyme regulator activity	GO:0030234	0.00478119	2.32046362	911	286	32	18679
GO:MF	heparin binding	GO:0008201	0.00489319	2.31040779	168	286	12	18679
GO:MF	disordered domain specific binding	GO:0097718	0.00502854	2.29855818	34	286	6	18679
GO:MF	binding	GO:0005488	0.00650883	2.18649739	17070	286	279	18679
GO:MF	peptidase activity	GO:0008233	0.00988025	2.00523228	647	286	25	18679
GO:MF	phospholipase A2 inhibitor activity	GO:0019834	0.01522927	1.81732102	5	286	3	18679
GO:MF	protein binding	GO:0005515	0.017468	1.75775669	14767	286	252	18679
GO:MF	protein dimerization activity	GO:0046983	0.02077981	1.68235835	1073	286	34	18679
GO:MF	protein homodimerization activity	GO:0042803	0.02176566	1.66222821	679	286	25	18679
GO:MF	structural constituent of skin epidermis	GO:0030280	0.02820419	1.54968642	15	286	4	18679
GO:MF	intermediate filament binding	GO:0019215	0.02820419	1.54968642	15	286	4	18679
GO:MF	lipase inhibitor activity	GO:0055102	0.04800195	1.31874111	17	286	4	18679
GO:MF	MHC class II protein complex binding	GO:0023026	0.04800195	1.31874111	17	286	4	18679
GO:BP	immune effector process	GO:0002252	2.50E-78	77.6024241	1135	288	132	18123
GO:BP	leukocyte mediated immunity	GO:0002443	1.56E-77	76.8074492	888	288	120	18123
GO:BP	regulated exocytosis	GO:0045055	5.05E-75	74.2966595	790	288	113	18123
GO:BP	exocytosis	GO:0006887	8.87E-72	71.0520087	906	288	116	18123
GO:BP	immune response	GO:0006955	2.26E-68	67.6464266	2544	288	170	18123
GO:BP	vesicle-mediated transport	GO:0016192	1.89E-66	65.7242567	2193	288	158	18123
GO:BP	neutrophil mediated immunity	GO:0002446	1.44E-65	64.840947	500	288	89	18123
GO:BP	neutrophil degranulation	GO:0043312	2.23E-64	63.6522074	483	288	87	18123
GO:BP	neutrophil activation involved in immune response	GO:0002283	5.64E-64	63.2484677	488	288	87	18123
GO:BP	neutrophil activation	GO:0042119	7.19E-63	62.1433144	502	288	87	18123
GO:BP	leukocyte degranulation	GO:0043299	1.19E-62	61.9233427	538	288	89	18123
GO:BP	myeloid leukocyte mediated immunity	GO:0002444	1.96E-62	61.7074614	558	288	90	18123
GO:BP	granulocyte activation	GO:0036230	2.49E-62	61.6041998	509	288	87	18123
GO:BP	cell activation	GO:0001775	1.08E-60	59.9681373	1507	288	130	18123
GO:BP	myeloid cell activation involved in immune response	GO:0002275	2.06E-60	59.686503	552	288	88	18123

GO:BP	immune system process	GO:0002376	1.53E-59	58.8156547	3438	288	183	18123
GO:BP	secretion by cell	GO:0032940	2.45E-57	56.6101168	1351	288	121	18123
GO:BP	myeloid leukocyte activation	GO:0002274	2.49E-56	55.6037848	671	288	91	18123
GO:BP	leukocyte activation involved in immune response	GO:0002366	1.21E-55	54.9159717	723	288	93	18123
GO:BP	cell activation involved in immune response	GO:0002263	2.01E-55	54.6970091	727	288	93	18123
GO:BP	export from cell	GO:0140352	3.88E-55	54.4107173	1413	288	121	18123
GO:BP	secretion	GO:0046903	2.17E-54	53.6632118	1492	288	123	18123
GO:BP	leukocyte activation	GO:0045321	5.97E-50	49.224289	1341	288	113	18123
GO:BP	humoral immune response	GO:0006959	8.06E-45	44.0934814	383	288	65	18123
GO:BP	transport	GO:0006810	1.18E-37	36.9299465	5214	288	192	18123
GO:BP	establishment of localization	GO:0051234	3.98E-37	36.4006131	5364	288	194	18123
GO:BP	establishment of localization in cell	GO:0051649	1.71E-32	31.7672174	2778	288	133	18123
GO:BP	antimicrobial humoral response	GO:0019730	1.95E-32	31.7096374	144	288	38	18123
GO:BP	defense response	GO:0006952	2.39E-31	30.6214787	1956	288	110	18123
GO:BP	biological process involved in interspecies interaction between organisms	GO:0044419	2.16E-29	28.6647252	1768	288	102	18123
GO:BP	response to external stimulus	GO:0009605	3.74E-29	28.4275491	3114	288	136	18123
GO:BP	response to stress	GO:0006950	1.50E-28	27.8227604	4321	288	161	18123
GO:BP	response to other organism	GO:0051707	2.10E-26	25.6773767	1600	288	93	18123
GO:BP	response to external biotic stimulus	GO:0043207	2.21E-26	25.6564687	1601	288	93	18123
GO:BP	response to biotic stimulus	GO:0009607	2.62E-26	25.5818974	1639	288	94	18123
GO:BP	localization	GO:0051179	4.11E-26	25.3866372	6938	288	204	18123
GO:BP	cellular localization	GO:0051641	5.81E-26	25.2357235	3519	288	140	18123
GO:BP	phagocytosis	GO:0006909	1.52E-25	24.8191105	388	288	48	18123
GO:BP	defense response to other organism	GO:0098542	2.48E-25	24.605158	1222	288	80	18123
GO:BP	defense response to bacterium	GO:0042742	1.58E-24	23.8012777	349	288	45	18123
GO:BP	peptide cross-linking	GO:0018149	2.57E-20	19.5899207	96	288	25	18123
GO:BP	complement activation	GO:0006956	4.71E-20	19.3269671	178	288	31	18123
GO:BP	response to stimulus	GO:0050896	8.55E-20	19.0680445	9487	288	231	18123
GO:BP	response to bacterium	GO:0009617	1.37E-18	17.8630065	743	288	55	18123
GO:BP	endocytosis	GO:0006897	3.08E-18	17.5111988	700	288	53	18123
GO:BP	positive regulation of immune response	GO:0050778	3.31E-18	17.4805084	757	288	55	18123
GO:BP	positive regulation of immune system process	GO:0002684	9.20E-18	17.0362858	1079	288	65	18123
GO:BP	activation of immune response	GO:0002253	1.86E-17	16.7300364	566	288	47	18123
GO:BP	innate immune response	GO:0045087	2.47E-17	16.6068267	1003	288	62	18123
GO:BP	humoral immune response mediated by circulating immunoglobulin	GO:0002455	2.59E-17	16.5863754	153	288	27	18123
GO:BP	complement activation, classical pathway	GO:0006958	3.57E-17	16.447622	140	288	26	18123
GO:BP	Fc-gamma receptor signaling pathway involved in phagocytosis	GO:0038096	2.15E-16	15.6667281	135	288	25	18123
GO:BP	immune response-regulating cell surface receptor signaling pathway involved in phagocytosis	GO:0002433	2.15E-16	15.6667281	135	288	25	18123
GO:BP	receptor-mediated endocytosis	GO:0006898	2.31E-16	15.6367546	335	288	36	18123
GO:BP	Fc-gamma receptor signaling pathway	GO:0038094	3.14E-16	15.5032741	137	288	25	18123

GO:BP	regulation of immune system process	GO:0002682	3.68E-16	15.4346711	1734	288	81	18123
GO:BP	Fc receptor mediated stimulatory signaling pathway	GO:0002431	6.54E-16	15.1847034	141	288	25	18123
GO:BP	platelet degranulation	GO:0002576	7.30E-16	15.1368364	127	288	24	18123
GO:BP	regulation of immune response	GO:0050776	1.75E-15	14.7569082	1159	288	64	18123
GO:BP	phagocytosis, recognition	GO:0006910	2.27E-15	14.6440186	133	288	24	18123
GO:BP	lymphocyte mediated immunity	GO:0002449	2.51E-15	14.6007503	360	288	36	18123
GO:BP	cornification	GO:0070268	9.78E-15	14.0094718	112	288	22	18123
GO:BP	immune response-activating cell surface receptor signaling pathway	GO:0002429	1.21E-14	13.9186618	475	288	40	18123
GO:BP	immune response-activating signal transduction	GO:0002757	1.21E-14	13.9186618	475	288	40	18123
GO:BP	immune response-regulating cell surface receptor signaling pathway	GO:0002768	2.35E-14	13.6292597	510	288	41	18123
GO:BP	immune response-regulating signaling pathway	GO:0002764	2.89E-14	13.5383815	513	288	41	18123
GO:BP	retina homeostasis	GO:0001895	3.44E-14	13.4636898	79	288	19	18123
GO:BP	immunoglobulin mediated immune response	GO:0016064	4.56E-14	13.3413924	221	288	28	18123
GO:BP	B cell mediated immunity	GO:0019724	6.53E-14	13.1849054	224	288	28	18123
GO:BP	negative regulation of peptidase activity	GO:0010466	7.45E-14	13.1280982	265	288	30	18123
GO:BP	regulation of complement activation	GO:0030449	1.07E-13	12.9708018	110	288	21	18123
GO:BP	antibacterial humoral response	GO:0019731	1.17E-13	12.9304088	61	288	17	18123
GO:BP	leukocyte migration	GO:0050900	1.54E-13	12.8114101	511	288	40	18123
GO:BP	negative regulation of endopeptidase activity	GO:0010951	1.66E-13	12.7807013	252	288	29	18123
GO:BP	regulation of response to external stimulus	GO:0032101	1.94E-13	12.7129891	1238	288	63	18123
GO:BP	cell killing	GO:0001906	2.14E-13	12.6692194	196	288	26	18123
GO:BP	regulation of peptidase activity	GO:0052547	2.77E-13	12.557545	467	288	38	18123
GO:BP	Fc receptor signaling pathway	GO:0038093	3.26E-13	12.4863695	238	288	28	18123
GO:BP	regulation of response to stress	GO:0080134	3.44E-13	12.4635056	1626	288	73	18123
GO:BP	positive regulation of response to stimulus	GO:0048584	3.77E-13	12.4240307	2368	288	91	18123
GO:BP	regulation of humoral immune response	GO:0002920	5.44E-13	12.2645441	134	288	22	18123
GO:BP	negative regulation of proteolysis	GO:0045861	7.42E-13	12.129755	356	288	33	18123
GO:BP	cell recognition	GO:0008037	1.18E-12	11.9282087	271	288	29	18123
GO:BP	adaptive immune response based on somatic recombination of immune receptors built from immunoglobulin superfamily domains	GO:0002460	1.68E-12	11.7746189	366	288	33	18123
GO:BP	programmed cell death	GO:0012501	4.28E-12	11.3688604	2158	288	84	18123
GO:BP	negative regulation of response to external stimulus	GO:0032102	7.28E-12	11.1376621	601	288	41	18123
GO:BP	regulation of endopeptidase activity	GO:0052548	7.98E-12	11.098218	437	288	35	18123
GO:BP	killing of cells of other organism	GO:0031640	8.54E-12	11.0685313	77	288	17	18123
GO:BP	regulation of proteolysis	GO:0030162	9.00E-12	11.0459398	756	288	46	18123
GO:BP	cell death	GO:0008219	2.16E-11	10.6648525	2306	288	86	18123
GO:BP	membrane organization	GO:0061024	3.21E-11	10.4935133	1016	288	53	18123
GO:BP	locomotion	GO:0040011	5.25E-11	10.2800628	2039	288	79	18123
GO:BP	regulation of biological quality	GO:0065008	5.97E-11	10.2237029	4116	288	123	18123

GO:BP	cell motility	GO:0048870	6.91E-11	10.1603288	1840	288	74	18123
GO:BP	localization of cell	GO:0051674	6.91E-11	10.1603288	1840	288	74	18123
GO:BP	proteolysis	GO:0006508	9.40E-11	10.0267583	1851	288	74	18123
GO:BP	hemostasis	GO:0007599	2.12E-10	9.67405228	355	288	30	18123
GO:BP	biological process involved in symbiotic interaction	GO:0044403	2.24E-10	9.64989467	331	288	29	18123
GO:BP	movement of cell or subcellular component	GO:0006928	2.63E-10	9.58000022	2319	288	84	18123
GO:BP	opsonization	GO:0008228	4.75E-10	9.32345989	69	288	15	18123
GO:BP	keratinization	GO:0031424	4.76E-10	9.32273516	225	288	24	18123
GO:BP	adaptive immune response	GO:0002250	5.37E-10	9.26986814	715	288	42	18123
GO:BP	regulation of immune effector process	GO:0002697	5.62E-10	9.25012504	421	288	32	18123
GO:BP	biological process involved in interaction with symbiont	GO:0051702	7.02E-10	9.15337235	99	288	17	18123
GO:BP	negative regulation of hydrolase activity	GO:0051346	9.13E-10	9.03960435	456	288	33	18123
GO:BP	blood coagulation	GO:0007596	9.97E-10	9.00121333	351	288	29	18123
GO:BP	supramolecular fiber organization	GO:0097435	1.10E-09	8.96026071	863	288	46	18123
GO:BP	cell surface receptor signaling pathway	GO:0007166	1.25E-09	8.90392992	3226	288	102	18123
GO:BP	keratinocyte differentiation	GO:0030216	1.41E-09	8.84929668	306	288	27	18123
GO:BP	coagulation	GO:0050817	1.64E-09	8.78497833	358	288	29	18123
GO:BP	wound healing	GO:0042060	1.87E-09	8.72731318	555	288	36	18123
GO:BP	response to wounding	GO:0009611	2.05E-09	8.68879389	680	288	40	18123
GO:BP	phagocytosis, engulfment	GO:0006911	3.20E-09	8.49482689	125	288	18	18123
GO:BP	defense response to fungus	GO:0050832	3.73E-09	8.42820974	42	288	12	18123
GO:BP	tissue homeostasis	GO:0001894	4.29E-09	8.36721603	272	288	25	18123
GO:BP	cell migration	GO:0016477	4.34E-09	8.36256424	1660	288	66	18123
GO:BP	antimicrobial humoral immune response mediated by antimicrobial peptide	GO:0061844	5.75E-09	8.24026335	81	288	15	18123
GO:BP	negative regulation of blood coagulation	GO:0030195	6.29E-09	8.20161699	55	288	13	18123
GO:BP	negative regulation of hemostasis	GO:1900047	8.07E-09	8.09305825	56	288	13	18123
GO:BP	fibrinolysis	GO:0042730	9.33E-09	8.03032445	26	288	10	18123
GO:BP	regulation of blood coagulation	GO:0030193	1.04E-08	7.9826602	70	288	14	18123
GO:BP	plasma membrane invagination	GO:0099024	1.08E-08	7.96770377	134	288	18	18123
GO:BP	regulation of hemostasis	GO:1900046	1.56E-08	7.80571485	72	288	14	18123
GO:BP	homotypic cell-cell adhesion	GO:0034109	1.71E-08	7.7678501	87	288	15	18123
GO:BP	positive regulation of biological process	GO:0048518	2.15E-08	7.66680788	6474	288	159	18123
GO:BP	organonitrogen compound metabolic process	GO:1901564	2.58E-08	7.58776195	6904	288	166	18123
GO:BP	negative regulation of coagulation	GO:0050819	2.61E-08	7.58298592	61	288	13	18123
GO:BP	anatomical structure homeostasis	GO:0060249	2.63E-08	7.57940677	486	288	32	18123
GO:BP	membrane invagination	GO:0010324	2.93E-08	7.53333831	142	288	18	18123
GO:BP	regulation of body fluid levels	GO:0050878	3.13E-08	7.50472809	519	288	33	18123
GO:BP	killing by host of symbiont cells	GO:0051873	3.37E-08	7.47216481	29	288	10	18123
GO:BP	regulation of coagulation	GO:0050818	4.10E-08	7.38771455	77	288	14	18123
GO:BP	regulation of defense response	GO:0031347	4.49E-08	7.34799289	889	288	44	18123
GO:BP	inflammatory response	GO:0006954	4.72E-08	7.3259117	962	288	46	18123

GO:BP	platelet aggregation	GO:0070527	5.01E-08	7.30028873	64	288	13	18123
GO:BP	protein metabolic process	GO:0019538	6.41E-08	7.19286818	5912	288	148	18123
GO:BP	killing of cells in other organism involved in symbiotic interaction	GO:0051883	7.26E-08	7.13911902	31	288	10	18123
GO:BP	epidermal cell differentiation	GO:0009913	1.19E-07	6.92453132	370	288	27	18123
GO:BP	response to fungus	GO:0009620	1.55E-07	6.81097891	56	288	12	18123
GO:BP	platelet activation	GO:0030168	3.02E-07	6.51970596	163	288	18	18123
GO:BP	regulation of response to stimulus	GO:0048583	3.24E-07	6.48936053	4416	288	119	18123
GO:BP	negative regulation of catalytic activity	GO:0043086	3.79E-07	6.42150824	841	288	41	18123
GO:BP	negative regulation of immune system process	GO:0002683	6.20E-07	6.20729825	614	288	34	18123
GO:BP	multicellular organismal process	GO:0032501	1.1311E-06	5.94650686	8000	288	179	18123
GO:BP	negative regulation of defense response	GO:0031348	1.2147E-06	5.91552871	440	288	28	18123
GO:BP	regulation of inflammatory response	GO:0050727	1.2456E-06	5.90461926	565	288	32	18123
GO:BP	negative regulation of wound healing	GO:0061045	1.5404E-06	5.81235425	83	288	13	18123
GO:BP	response to chemical	GO:0042221	2.5387E-06	5.59539256	4829	288	124	18123
GO:BP	skin development	GO:0043588	2.7553E-06	5.55983692	426	288	27	18123
GO:BP	negative regulation of response to stimulus	GO:0048585	3.5193E-06	5.45354175	1938	288	66	18123
GO:BP	negative regulation of immune response	GO:0050777	3.7643E-06	5.42431642	373	288	25	18123
GO:BP	cytoskeleton organization	GO:0007010	4.678E-06	5.32993969	1473	288	55	18123
GO:BP	cellular response to cytokine stimulus	GO:0071345	4.9139E-06	5.30857303	1148	288	47	18123
GO:BP	glucose catabolic process to pyruvate	GO:0061718	5.443E-06	5.26415965	24	288	8	18123
GO:BP	NADH regeneration	GO:0006735	5.443E-06	5.26415965	24	288	8	18123
GO:BP	canonical glycolysis	GO:0061621	5.443E-06	5.26415965	24	288	8	18123
GO:BP	regulation of response to wounding	GO:1903034	5.6385E-06	5.24883869	172	288	17	18123
GO:BP	regulation of localization	GO:0032879	5.9658E-06	5.22433385	2906	288	86	18123
GO:BP	epidermis development	GO:0008544	7.7423E-06	5.1111281	478	288	28	18123
GO:BP	negative regulation of inflammatory response	GO:0050728	8.5418E-06	5.06844923	359	288	24	18123
GO:BP	inflammatory response to antigenic stimulus	GO:0002437	9.4411E-06	5.02497775	251	288	20	18123
GO:BP	biological adhesion	GO:0022610	1.1053E-05	4.95650677	1509	288	55	18123
GO:BP	glycolytic process through glucose-6-phosphate	GO:0061620	1.1247E-05	4.9489588	26	288	8	18123
GO:BP	cellular protein metabolic process	GO:0044267	1.213E-05	4.91615488	5280	288	130	18123
GO:BP	response to oxidative stress	GO:0006979	1.2536E-05	4.90185358	457	288	27	18123
GO:BP	protein folding	GO:0006457	1.2939E-05	4.88810859	230	288	19	18123
GO:BP	regulation of protein metabolic process	GO:0051246	1.3662E-05	4.86449507	2759	288	82	18123
GO:BP	regulation of wound healing	GO:0061041	1.3673E-05	4.86415129	138	288	15	18123
GO:BP	negative regulation of biological process	GO:0048519	1.3965E-05	4.85495218	5861	288	140	18123
GO:BP	negative regulation of response to wounding	GO:1903035	1.4361E-05	4.84281669	99	288	13	18123
GO:BP	glycolytic process through fructose-6-phosphate	GO:0061615	1.5764E-05	4.80234299	27	288	8	18123
GO:BP	response to cytokine	GO:0034097	2.064E-05	4.68529864	1242	288	48	18123
GO:BP	blood coagulation, fibrin clot formation	GO:0072378	2.1767E-05	4.66220849	28	288	8	18123
GO:BP	protein activation cascade	GO:0072376	2.1767E-05	4.66220849	28	288	8	18123
GO:BP	cellular component organization	GO:0016043	2.1888E-05	4.6598009	6661	288	153	18123

GO:BP	regulation of multicellular organismal process	GO:0051239	2.2835E-05	4.64139565	2888	288	84	18123
GO:BP	negative regulation of protein metabolic process	GO:0051248	3.0219E-05	4.51972279	1216	288	47	18123
GO:BP	defense response to Gram-negative bacterium	GO:0050829	3.6158E-05	4.44179494	88	288	12	18123
GO:BP	regulation of inflammatory response to antigenic stimulus	GO:0002861	3.8421E-05	4.41543145	220	288	18	18123
GO:BP	response to inorganic substance	GO:0010035	4.0687E-05	4.39054214	583	288	30	18123
GO:BP	positive regulation of cellular component organization	GO:0051130	4.3066E-05	4.36586201	1189	288	46	18123
GO:BP	regulation of cellular protein metabolic process	GO:0032268	4.8778E-05	4.3117751	2591	288	77	18123
GO:BP	epithelial cell differentiation	GO:0030855	5.6427E-05	4.24851395	807	288	36	18123
GO:BP	regulation of cell activation	GO:0050865	5.7599E-05	4.23958379	662	288	32	18123
GO:BP	response to organic substance	GO:0010033	6.1088E-05	4.21404553	3457	288	94	18123
GO:BP	actin filament-based process	GO:0030029	6.2008E-05	4.2075508	810	288	36	18123
GO:BP	cell adhesion	GO:0007155	6.657E-05	4.17671946	1502	288	53	18123
GO:BP	multicellular organismal homeostasis	GO:0048871	8.1511E-05	4.08878377	533	288	28	18123
GO:BP	B cell receptor signaling pathway	GO:0050853	8.1582E-05	4.08840479	135	288	14	18123
GO:BP	negative regulation of inflammatory response to antigenic stimulus	GO:0002862	8.5682E-05	4.06710831	206	288	17	18123
GO:BP	cell-cell adhesion	GO:0098609	8.9323E-05	4.04903442	898	288	38	18123
GO:BP	glucose catabolic process	GO:0006007	9.0753E-05	4.04214029	33	288	8	18123
GO:BP	negative regulation of cellular protein metabolic process	GO:0032269	0.00010147	3.99365808	1141	288	44	18123
GO:BP	cellular response to chemical stimulus	GO:0070887	0.00010521	3.97796099	3443	288	93	18123
GO:BP	negative regulation of molecular function	GO:0044092	0.00011364	3.94447939	1228	288	46	18123
GO:BP	regulation of catalytic activity	GO:0050790	0.00012203	3.9135443	2452	288	73	18123
GO:BP	respiratory burst	GO:0045730	0.00014966	3.82490698	35	288	8	18123
GO:BP	pentose biosynthetic process	GO:0019322	0.00015619	3.80635128	4	288	4	18123
GO:BP	plasminogen activation	GO:0031639	0.00016335	3.7868718	24	288	7	18123
GO:BP	intermediate filament organization	GO:0045109	0.00016335	3.7868718	24	288	7	18123
GO:BP	NAD metabolic process	GO:0019674	0.00016792	3.77490567	49	288	9	18123
GO:BP	Fc-epsilon receptor signaling pathway	GO:0038095	0.00018229	3.7392477	167	288	15	18123
GO:BP	amyloid fibril formation	GO:1990000	0.0001952	3.70952689	102	288	12	18123
GO:BP	regulation of hydrolase activity	GO:0051336	0.00020144	3.69584372	1252	288	46	18123
GO:BP	intermediate filament cytoskeleton organization	GO:0045104	0.00020195	3.69475786	50	288	9	18123
GO:BP	signal transduction	GO:0007165	0.00021291	3.67179963	6447	288	146	18123
GO:BP	protein stabilization	GO:0050821	0.00023647	3.62621927	195	288	16	18123
GO:BP	intermediate filament-based process	GO:0045103	0.00024184	3.61647467	51	288	9	18123
GO:BP	cellular component organization or biogenesis	GO:0071840	0.00025093	3.60044527	6880	288	153	18123
GO:BP	modulation of process of other organism	GO:0035821	0.00028488	3.5453316	149	288	14	18123
GO:BP	glucose 6-phosphate metabolic process	GO:0051156	0.00030212	3.51981757	26	288	7	18123
GO:BP	actin cytoskeleton organization	GO:0030036	0.00030806	3.51136134	712	288	32	18123
GO:BP	positive regulation of B cell activation	GO:0050871	0.00033663	3.47284151	151	288	14	18123
GO:BP	mucosal immune response	GO:0002385	0.00037022	3.43153671	39	288	8	18123
GO:BP	regulation of biological process	GO:0050789	0.00037878	3.42161678	12122	288	232	18123

GO:BP	detection of chemical stimulus involved in sensory perception of bitter taste	GO:0001580	0.00045645	3.34061041	40	288	8	18123
GO:BP	actin nucleation	GO:0045010	0.00047811	3.32047475	55	288	9	18123
GO:BP	positive regulation of gene expression	GO:0010628	0.00049025	3.30958618	1206	288	44	18123
GO:BP	actin filament organization	GO:0007015	0.00050761	3.29446592	445	288	24	18123
GO:BP	innate immune response in mucosa	GO:0002227	0.00052921	3.27637378	28	288	7	18123
GO:BP	negative regulation of fibrinolysis	GO:0051918	0.00057783	3.23819827	10	288	5	18123
GO:BP	NADPH regeneration	GO:0006740	0.00060433	3.21872742	18	288	6	18123
GO:BP	zymogen activation	GO:0031638	0.00076803	3.11462035	58	288	9	18123
GO:BP	NADH metabolic process	GO:0006734	0.00082582	3.08311583	43	288	8	18123
GO:BP	organ or tissue specific immune response	GO:0002251	0.00082582	3.08311583	43	288	8	18123
GO:BP	regulation of protein stability	GO:0031647	0.00098731	3.00554685	302	288	19	18123
GO:BP	sensory perception of bitter taste	GO:0050913	0.00099553	3.001946	44	288	8	18123
GO:BP	regulation of apoptotic signaling pathway	GO:2001233	0.00105445	2.97697483	365	288	21	18123
GO:BP	positive regulation of transport	GO:0051050	0.00111565	2.95247202	951	288	37	18123
GO:BP	hydrogen peroxide catabolic process	GO:0042744	0.00112826	2.94758955	31	288	7	18123
GO:BP	cellular oxidant detoxification	GO:0098869	0.00123124	2.90965828	99	288	11	18123
GO:BP	regulation of programmed cell death	GO:0043067	0.00131897	2.87976543	1603	288	52	18123
GO:BP	detection of chemical stimulus involved in sensory perception of taste	GO:0050912	0.00142587	2.84591914	46	288	8	18123
GO:BP	regulation of transport	GO:0051049	0.00148793	2.82741805	1839	288	57	18123
GO:BP	regulation of B cell activation	GO:0050864	0.00156999	2.80410279	197	288	15	18123
GO:BP	regulation of cell morphogenesis	GO:0022604	0.00162028	2.79041049	312	288	19	18123
GO:BP	regulation of anatomical structure morphogenesis	GO:0022603	0.00162118	2.79016965	1048	288	39	18123
GO:BP	homeostatic process	GO:0042592	0.00163013	2.78777741	1985	288	60	18123
GO:BP	regulation of leukocyte activation	GO:0002694	0.00164373	2.78417027	617	288	28	18123
GO:BP	regulation of cytokine production	GO:0001817	0.00169109	2.77183405	847	288	34	18123
GO:BP	interleukin-12-mediated signaling pathway	GO:0035722	0.00169487	2.77086368	47	288	8	18123
GO:BP	cellular response to stimulus	GO:0051716	0.00185323	2.73207082	7873	288	166	18123
GO:BP	extracellular matrix disassembly	GO:0022617	0.00192208	2.71622794	83	288	10	18123
GO:BP	biological regulation	GO:0065007	0.00196686	2.70622669	12802	288	239	18123
GO:BP	regulation of molecular function	GO:0065009	0.00201045	2.6967061	3191	288	84	18123
GO:BP	cytokine production	GO:0001816	0.00203737	2.69093083	854	288	34	18123
GO:BP	regulation of cellular component organization	GO:0051128	0.00221247	2.65512338	2439	288	69	18123
GO:BP	positive regulation of response to external stimulus	GO:0032103	0.00222278	2.65310297	518	288	25	18123
GO:BP	regulation of cellular process	GO:0050794	0.00223691	2.65035127	11517	288	221	18123
GO:BP	induction of bacterial agglutination	GO:0043152	0.00228445	2.64121774	6	288	4	18123
GO:BP	cellular response to interleukin-12	GO:0071349	0.0023647	2.62622324	49	288	8	18123
GO:BP	positive regulation of organelle organization	GO:0010638	0.00248161	2.60526657	630	288	28	18123
GO:BP	regulation of lymphocyte activation	GO:0051249	0.00264694	2.57725581	523	288	25	18123
GO:BP	sensory perception of taste	GO:0050909	0.00272159	2.5651775	67	288	9	18123
GO:BP	response to interleukin-12	GO:0070671	0.00277666	2.55647774	50	288	8	18123

GO:BP	reactive oxygen species metabolic process	GO:0072593	0.00279685	2.55333142	234	288	16	18123
GO:BP	regulation of cell death	GO:0010941	0.00303181	2.51829753	1740	288	54	18123
GO:BP	chaperone-mediated protein complex assembly	GO:0051131	0.00307345	2.51237392	23	288	6	18123
GO:BP	protein refolding	GO:0042026	0.00307345	2.51237392	23	288	6	18123
GO:BP	regulation of fibrinolysis	GO:0051917	0.00435667	2.36084566	14	288	5	18123
GO:BP	cellular detoxification	GO:1990748	0.00466545	2.33110664	113	288	11	18123
GO:BP	positive regulation of supramolecular fiber organization	GO:1902905	0.00472997	2.32514118	215	288	15	18123
GO:BP	hexose catabolic process	GO:0019320	0.00509309	2.29301827	54	288	8	18123
GO:BP	regulation of vesicle-mediated transport	GO:0060627	0.00537217	2.26985005	544	288	25	18123
GO:BP	Arp2/3 complex-mediated actin nucleation	GO:0034314	0.0059192	2.22773718	39	288	7	18123
GO:BP	cell communication	GO:0007154	0.00634816	2.19735247	6961	288	149	18123
GO:BP	positive regulation of response to wounding	GO:1903036	0.00638403	2.19490477	74	288	9	18123
GO:BP	lymphocyte activation	GO:0046649	0.00669968	2.17394584	780	288	31	18123
GO:BP	hydrogen peroxide metabolic process	GO:0042743	0.00676476	2.16974749	56	288	8	18123
GO:BP	cellular response to organic substance	GO:0071310	0.00693718	2.15881718	2821	288	75	18123
GO:BP	response to metal ion	GO:0010038	0.00697248	2.15661258	377	288	20	18123
GO:BP	positive regulation of protein polymerization	GO:0032273	0.00715303	2.14550971	142	288	12	18123
GO:BP	regulation of cell-substrate adhesion	GO:0010810	0.00743906	2.12848194	223	288	15	18123
GO:BP	tissue migration	GO:0090130	0.00786055	2.10454724	380	288	20	18123
GO:BP	response to reactive oxygen species	GO:0000302	0.00786065	2.1045418	224	288	15	18123
GO:BP	positive regulation of leukocyte activation	GO:0002696	0.00792838	2.10081542	414	288	21	18123
GO:BP	negative regulation of programmed cell death	GO:0043069	0.00844185	2.07356259	952	288	35	18123
GO:BP	positive regulation of cellular process	GO:0048522	0.00851111	2.07001364	5863	288	130	18123
GO:BP	signaling	GO:0023052	0.00891812	2.04972647	6937	288	148	18123
GO:BP	cellular response to toxic substance	GO:0097237	0.00915809	2.03819504	121	288	11	18123
GO:BP	regulation of respiratory burst	GO:0060263	0.00926038	2.03337097	16	288	5	18123
GO:BP	pentose-phosphate shunt	GO:0006098	0.00926038	2.03337097	16	288	5	18123
GO:BP	apoptotic process	GO:0006915	0.00948456	2.02298278	1998	288	58	18123
GO:BP	monosaccharide biosynthetic process	GO:0046364	0.00984647	2.00671945	99	288	10	18123
GO:BP	positive regulation of substrate adhesion-dependent cell spreading	GO:1900026	0.00996774	2.00140336	42	288	7	18123
GO:BP	negative regulation of multicellular organismal process	GO:0051241	0.01026828	1.9885025	1174	288	40	18123
GO:BP	external encapsulating structure organization	GO:0045229	0.01067889	1.97147394	422	288	21	18123
GO:BP	monosaccharide catabolic process	GO:0046365	0.01153315	1.93805206	60	288	8	18123
GO:BP	cell redox homeostasis	GO:0045454	0.01174533	1.93013462	43	288	7	18123
GO:BP	positive regulation of cell activation	GO:0050867	0.01235657	1.90810218	426	288	21	18123
GO:BP	positive regulation of cell-substrate adhesion	GO:0010811	0.01257533	1.90048077	125	288	11	18123
GO:BP	negative regulation of cellular process	GO:0048523	0.01268534	1.89669779	5153	288	117	18123
GO:BP	negative regulation of apoptotic process	GO:0043066	0.01270119	1.89615561	928	288	34	18123
GO:BP	apoptotic signaling pathway	GO:0097190	0.01274108	1.89479359	609	288	26	18123

GO:BP	anatomical structure morphogenesis	GO:0009653	0.01274496	1.89466146	2816	288	74	18123
GO:BP	positive regulation of actin filament polymerization	GO:0030838	0.01291088	1.88904409	102	288	10	18123
GO:BP	cell junction organization	GO:0034330	0.013376	1.87367362	727	288	29	18123
GO:BP	positive regulation of protein-containing complex assembly	GO:0031334	0.01402912	1.85296945	265	288	16	18123
GO:BP	post-translational protein modification	GO:0043687	0.01448382	1.83911678	362	288	19	18123
GO:BP	anatomical structure development	GO:0048856	0.01601036	1.79559892	6164	288	134	18123
GO:BP	regulation of apoptotic process	GO:0042981	0.01672779	1.77656138	1560	288	48	18123
GO:BP	positive regulation of lymphocyte activation	GO:0051251	0.01694871	1.77086323	366	288	19	18123
GO:BP	angiogenesis	GO:0001525	0.01802467	1.74413274	621	288	26	18123
GO:BP	epithelium development	GO:0060429	0.01880272	1.72577925	1338	288	43	18123
GO:BP	tissue development	GO:0009888	0.01915473	1.71772385	2093	288	59	18123
GO:BP	regulation of actin filament-based process	GO:0032970	0.01959768	1.70779538	404	288	20	18123
GO:BP	cytokine-mediated signaling pathway	GO:0019221	0.02029365	1.69263978	824	288	31	18123
GO:BP	epithelial cell migration	GO:0010631	0.02055889	1.68700029	371	288	19	18123
GO:BP	protein polymerization	GO:0051258	0.02254642	1.6469224	307	288	17	18123
GO:BP	epithelium migration	GO:0090132	0.02304407	1.63744085	374	288	19	18123
GO:BP	protein-containing complex assembly	GO:0065003	0.02465889	1.60802656	1724	288	51	18123
GO:BP	cell chemotaxis	GO:0060326	0.02560235	1.59172022	310	288	17	18123
GO:BP	regulation of establishment of protein localization	GO:0070201	0.02561607	1.59148748	595	288	25	18123
GO:BP	ephrin receptor signaling pathway	GO:0048013	0.02718343	1.56569571	88	288	9	18123
GO:BP	regulation of cell adhesion	GO:0030155	0.02813063	1.55082056	756	288	29	18123
GO:BP	response to cadmium ion	GO:0046686	0.02985421	1.52499448	68	288	8	18123
GO:BP	establishment or maintenance of cell polarity	GO:0007163	0.03001834	1.52261329	220	288	14	18123
GO:BP	myeloid leukocyte migration	GO:0097529	0.03001834	1.52261329	220	288	14	18123
GO:BP	regulation of actin polymerization or depolymerization	GO:0008064	0.03010199	1.52140479	191	288	13	18123
GO:BP	neutrophil-mediated killing of symbiont cell	GO:0070943	0.03041074	1.51697298	10	288	4	18123
GO:BP	actin polymerization or depolymerization	GO:0008154	0.0315984	1.50033491	221	288	14	18123
GO:BP	regulation of actin filament length	GO:0030832	0.0318358	1.49708422	192	288	13	18123
GO:BP	leukocyte mediated cytotoxicity	GO:0001909	0.03228312	1.49102446	113	288	10	18123
GO:BP	extracellular matrix organization	GO:0030198	0.03338679	1.47642539	419	288	20	18123
GO:BP	extracellular structure organization	GO:0043062	0.03456012	1.46142479	420	288	20	18123
GO:BP	response to toxic substance	GO:0009636	0.03585527	1.44544698	254	288	15	18123
GO:BP	regulation of protein-containing complex assembly	GO:0043254	0.03713534	1.43021263	458	288	21	18123
GO:BP	acute inflammatory response	GO:0002526	0.03769252	1.42374485	115	288	10	18123
GO:BP	regulation of intrinsic apoptotic signaling pathway	GO:2001242	0.03790212	1.42133646	167	288	12	18123
GO:BP	system development	GO:0048731	0.03847193	1.41485605	5095	288	114	18123
GO:BP	ameboidal-type cell migration	GO:0001667	0.03878637	1.41132081	496	288	22	18123
GO:BP	response to ethanol	GO:0045471	0.03985333	1.39953535	141	288	11	18123
GO:BP	antigen receptor-mediated signaling pathway	GO:0050851	0.0402315	1.39543375	321	288	17	18123
GO:BP	detoxification	GO:0098754	0.0455075	1.34191703	143	288	11	18123

GO:BP	positive regulation of receptor-mediated endocytosis	GO:0048260	0.04905683	1.30930056	53	288	7	18123
GO:BP	NADP metabolic process	GO:0006739	0.04985034	1.3023319	36	288	6	18123
GO:BP	immune effector process	GO:0002252	2.50E-78	77.6024241	1135	288	132	18123
GO:BP	leukocyte mediated immunity	GO:0002443	1.56E-77	76.8074492	888	288	120	18123
GO:BP	regulated exocytosis	GO:0045055	5.05E-75	74.2966595	790	288	113	18123
GO:BP	exocytosis	GO:0006887	8.87E-72	71.0520087	906	288	116	18123
GO:BP	immune response	GO:0006955	2.26E-68	67.6464266	2544	288	170	18123
GO:BP	vesicle-mediated transport	GO:0016192	1.89E-66	65.7242567	2193	288	158	18123
GO:BP	neutrophil mediated immunity	GO:0002446	1.44E-65	64.840947	500	288	89	18123
GO:BP	neutrophil degranulation	GO:0043312	2.23E-64	63.6522074	483	288	87	18123
GO:BP	neutrophil activation involved in immune response	GO:0002283	5.64E-64	63.2484677	488	288	87	18123
GO:BP	neutrophil activation	GO:0042119	7.19E-63	62.1433144	502	288	87	18123
GO:BP	leukocyte degranulation	GO:0043299	1.19E-62	61.9233427	538	288	89	18123
GO:BP	myeloid leukocyte mediated immunity	GO:0002444	1.96E-62	61.7074614	558	288	90	18123
GO:BP	granulocyte activation	GO:0036230	2.49E-62	61.6041998	509	288	87	18123
GO:BP	cell activation	GO:0001775	1.08E-60	59.9681373	1507	288	130	18123
GO:BP	myeloid cell activation involved in immune response	GO:0002275	2.06E-60	59.686503	552	288	88	18123
GO:BP	immune system process	GO:0002376	1.53E-59	58.8156547	3438	288	183	18123
GO:BP	secretion by cell	GO:0032940	2.45E-57	56.6101168	1351	288	121	18123
GO:BP	myeloid leukocyte activation	GO:0002274	2.49E-56	55.6037848	671	288	91	18123
GO:BP	leukocyte activation involved in immune response	GO:0002366	1.21E-55	54.9159717	723	288	93	18123
GO:BP	cell activation involved in immune response	GO:0002263	2.01E-55	54.6970091	727	288	93	18123
GO:BP	export from cell	GO:0140352	3.88E-55	54.4107173	1413	288	121	18123
GO:BP	secretion	GO:0046903	2.17E-54	53.6632118	1492	288	123	18123
GO:BP	leukocyte activation	GO:0045321	5.97E-50	49.224289	1341	288	113	18123
GO:BP	humoral immune response	GO:0006959	8.06E-45	44.0934814	383	288	65	18123
GO:BP	transport	GO:0006810	1.18E-37	36.9299465	5214	288	192	18123
GO:BP	establishment of localization	GO:0051234	3.98E-37	36.4006131	5364	288	194	18123
GO:BP	establishment of localization in cell	GO:0051649	1.71E-32	31.7672174	2778	288	133	18123
GO:BP	antimicrobial humoral response	GO:0019730	1.95E-32	31.7096374	144	288	38	18123
GO:BP	defense response	GO:0006952	2.39E-31	30.6214787	1956	288	110	18123
GO:BP	biological process involved in interspecies interaction between organisms	GO:0044419	2.16E-29	28.6647252	1768	288	102	18123
GO:BP	response to external stimulus	GO:0009605	3.74E-29	28.4275491	3114	288	136	18123
GO:BP	response to stress	GO:0006950	1.50E-28	27.8227604	4321	288	161	18123
GO:BP	response to other organism	GO:0051707	2.10E-26	25.6773767	1600	288	93	18123
GO:BP	response to external biotic stimulus	GO:0043207	2.21E-26	25.6564687	1601	288	93	18123
GO:BP	response to biotic stimulus	GO:0009607	2.62E-26	25.5818974	1639	288	94	18123
GO:BP	localization	GO:0051179	4.11E-26	25.3866372	6938	288	204	18123
GO:BP	cellular localization	GO:0051641	5.81E-26	25.2357235	3519	288	140	18123
GO:BP	phagocytosis	GO:0006909	1.52E-25	24.8191105	388	288	48	18123
GO:BP	defense response to other organism	GO:0098542	2.48E-25	24.605158	1222	288	80	18123
GO:BP	defense response to bacterium	GO:0042742	1.58E-24	23.8012777	349	288	45	18123

GO:BP	peptide cross-linking	GO:0018149	2.57E-20	19.5899207	96	288	25	18123
GO:BP	complement activation	GO:0006956	4.71E-20	19.3269671	178	288	31	18123
GO:BP	response to stimulus	GO:0050896	8.55E-20	19.0680445	9487	288	231	18123
GO:BP	response to bacterium	GO:0009617	1.37E-18	17.8630065	743	288	55	18123
GO:BP	endocytosis	GO:0006897	3.08E-18	17.5111988	700	288	53	18123
GO:BP	positive regulation of immune response	GO:0050778	3.31E-18	17.4805084	757	288	55	18123
GO:BP	positive regulation of immune system process	GO:0002684	9.20E-18	17.0362858	1079	288	65	18123
GO:BP	activation of immune response	GO:0002253	1.86E-17	16.7300364	566	288	47	18123
GO:BP	innate immune response	GO:0045087	2.47E-17	16.6068267	1003	288	62	18123
GO:BP	humoral immune response mediated by circulating immunoglobulin	GO:0002455	2.59E-17	16.5863754	153	288	27	18123
GO:BP	complement activation, classical pathway	GO:0006958	3.57E-17	16.447622	140	288	26	18123
GO:BP	Fc-gamma receptor signaling pathway involved in phagocytosis	GO:0038096	2.15E-16	15.6667281	135	288	25	18123
GO:BP	immune response-regulating cell surface receptor signaling pathway involved in phagocytosis	GO:0002433	2.15E-16	15.6667281	135	288	25	18123
GO:BP	receptor-mediated endocytosis	GO:0006898	2.31E-16	15.6367546	335	288	36	18123
GO:BP	Fc-gamma receptor signaling pathway	GO:0038094	3.14E-16	15.5032741	137	288	25	18123
GO:BP	regulation of immune system process	GO:0002682	3.68E-16	15.4346711	1734	288	81	18123
GO:BP	Fc receptor mediated stimulatory signaling pathway	GO:0002431	6.54E-16	15.1847034	141	288	25	18123
GO:BP	platelet degranulation	GO:0002576	7.30E-16	15.1368364	127	288	24	18123
GO:BP	regulation of immune response	GO:0050776	1.75E-15	14.7569082	1159	288	64	18123
GO:BP	phagocytosis, recognition	GO:0006910	2.27E-15	14.6440186	133	288	24	18123
GO:BP	lymphocyte mediated immunity	GO:0002449	2.51E-15	14.6007503	360	288	36	18123
GO:BP	cornification	GO:0070268	9.78E-15	14.0094718	112	288	22	18123
GO:BP	immune response-activating cell surface receptor signaling pathway	GO:0002429	1.21E-14	13.9186618	475	288	40	18123
GO:BP	immune response-activating signal transduction	GO:0002757	1.21E-14	13.9186618	475	288	40	18123
GO:BP	immune response-regulating cell surface receptor signaling pathway	GO:0002768	2.35E-14	13.6292597	510	288	41	18123
GO:BP	immune response-regulating signaling pathway	GO:0002764	2.89E-14	13.5383815	513	288	41	18123
GO:BP	retina homeostasis	GO:0001895	3.44E-14	13.4636898	79	288	19	18123
GO:BP	immunoglobulin mediated immune response	GO:0016064	4.56E-14	13.3413924	221	288	28	18123
GO:BP	B cell mediated immunity	GO:0019724	6.53E-14	13.1849054	224	288	28	18123
GO:BP	negative regulation of peptidase activity	GO:0010466	7.45E-14	13.1280982	265	288	30	18123
GO:BP	regulation of complement activation	GO:0030449	1.07E-13	12.9708018	110	288	21	18123
GO:BP	antibacterial humoral response	GO:0019731	1.17E-13	12.9304088	61	288	17	18123
GO:BP	leukocyte migration	GO:0050900	1.54E-13	12.8114101	511	288	40	18123
GO:BP	negative regulation of endopeptidase activity	GO:0010951	1.66E-13	12.7807013	252	288	29	18123
GO:BP	regulation of response to external stimulus	GO:0032101	1.94E-13	12.7129891	1238	288	63	18123
GO:BP	cell killing	GO:0001906	2.14E-13	12.6692194	196	288	26	18123
GO:BP	regulation of peptidase activity	GO:0052547	2.77E-13	12.557545	467	288	38	18123
GO:BP	Fc receptor signaling pathway	GO:0038093	3.26E-13	12.4863695	238	288	28	18123

GO:BP	regulation of response to stress	GO:0080134	3.44E-13	12.4635056	1626	288	73	18123
GO:BP	positive regulation of response to stimulus	GO:0048584	3.77E-13	12.4240307	2368	288	91	18123
GO:BP	regulation of humoral immune response	GO:0002920	5.44E-13	12.2645441	134	288	22	18123
GO:BP	negative regulation of proteolysis	GO:0045861	7.42E-13	12.129755	356	288	33	18123
GO:BP	cell recognition	GO:0008037	1.18E-12	11.9282087	271	288	29	18123
GO:BP	adaptive immune response based on somatic recombination of immune receptors built from immunoglobulin superfamily domains	GO:0002460	1.68E-12	11.7746189	366	288	33	18123
GO:BP	programmed cell death	GO:0012501	4.28E-12	11.3688604	2158	288	84	18123
GO:BP	negative regulation of response to external stimulus	GO:0032102	7.28E-12	11.1376621	601	288	41	18123
GO:BP	regulation of endopeptidase activity	GO:0052548	7.98E-12	11.098218	437	288	35	18123
GO:BP	killing of cells of other organism	GO:0031640	8.54E-12	11.0685313	77	288	17	18123
GO:BP	regulation of proteolysis	GO:0030162	9.00E-12	11.0459398	756	288	46	18123
GO:BP	cell death	GO:0008219	2.16E-11	10.6648525	2306	288	86	18123
GO:BP	membrane organization	GO:0061024	3.21E-11	10.4935133	1016	288	53	18123
GO:BP	locomotion	GO:0040011	5.25E-11	10.2800628	2039	288	79	18123
GO:BP	regulation of biological quality	GO:0065008	5.97E-11	10.2237029	4116	288	123	18123
GO:BP	cell motility	GO:0048870	6.91E-11	10.1603288	1840	288	74	18123
GO:BP	localization of cell	GO:0051674	6.91E-11	10.1603288	1840	288	74	18123
GO:BP	proteolysis	GO:0006508	9.40E-11	10.0267583	1851	288	74	18123
GO:BP	hemostasis	GO:0007599	2.12E-10	9.67405228	355	288	30	18123
GO:BP	biological process involved in symbiotic interaction	GO:0044403	2.24E-10	9.64989467	331	288	29	18123
GO:BP	movement of cell or subcellular component	GO:0006928	2.63E-10	9.58000022	2319	288	84	18123
GO:BP	opsonization	GO:0008228	4.75E-10	9.32345989	69	288	15	18123
GO:BP	keratinization	GO:0031424	4.76E-10	9.32273516	225	288	24	18123
GO:BP	adaptive immune response	GO:0002250	5.37E-10	9.26986814	715	288	42	18123
GO:BP	regulation of immune effector process	GO:0002697	5.62E-10	9.25012504	421	288	32	18123
GO:BP	biological process involved in interaction with symbiont	GO:0051702	7.02E-10	9.15337235	99	288	17	18123
GO:BP	negative regulation of hydrolase activity	GO:0051346	9.13E-10	9.03960435	456	288	33	18123
GO:BP	blood coagulation	GO:0007596	9.97E-10	9.00121333	351	288	29	18123
GO:BP	supramolecular fiber organization	GO:0097435	1.10E-09	8.96026071	863	288	46	18123
GO:BP	cell surface receptor signaling pathway	GO:0007166	1.25E-09	8.90392992	3226	288	102	18123
GO:BP	keratinocyte differentiation	GO:0030216	1.41E-09	8.84929668	306	288	27	18123
GO:BP	coagulation	GO:0050817	1.64E-09	8.78497833	358	288	29	18123
GO:BP	wound healing	GO:0042060	1.87E-09	8.72731318	555	288	36	18123
GO:BP	response to wounding	GO:0009611	2.05E-09	8.68879389	680	288	40	18123
GO:BP	phagocytosis, engulfment	GO:0006911	3.20E-09	8.49482689	125	288	18	18123
GO:BP	defense response to fungus	GO:0050832	3.73E-09	8.42820974	42	288	12	18123
GO:BP	tissue homeostasis	GO:0001894	4.29E-09	8.36721603	272	288	25	18123
GO:BP	cell migration	GO:0016477	4.34E-09	8.36256424	1660	288	66	18123
GO:BP	antimicrobial humoral immune response mediated by antimicrobial peptide	GO:0061844	5.75E-09	8.24026335	81	288	15	18123

GO:BP	negative regulation of blood coagulation	GO:0030195	6.29E-09	8.20161699	55	288	13	18123
GO:BP	negative regulation of hemostasis	GO:1900047	8.07E-09	8.09305825	56	288	13	18123
GO:BP	fibrinolysis	GO:0042730	9.33E-09	8.03032445	26	288	10	18123
GO:BP	regulation of blood coagulation	GO:0030193	1.04E-08	7.9826602	70	288	14	18123
GO:BP	plasma membrane invagination	GO:0099024	1.08E-08	7.96770377	134	288	18	18123
GO:BP	regulation of hemostasis	GO:1900046	1.56E-08	7.80571485	72	288	14	18123
GO:BP	homotypic cell-cell adhesion	GO:0034109	1.71E-08	7.7678501	87	288	15	18123
GO:BP	positive regulation of biological process	GO:0048518	2.15E-08	7.66680788	6474	288	159	18123
GO:BP	organonitrogen compound metabolic process	GO:1901564	2.58E-08	7.58776195	6904	288	166	18123
GO:BP	negative regulation of coagulation	GO:0050819	2.61E-08	7.58298592	61	288	13	18123
GO:BP	anatomical structure homeostasis	GO:0060249	2.63E-08	7.57940677	486	288	32	18123
GO:BP	membrane invagination	GO:0010324	2.93E-08	7.53333831	142	288	18	18123
GO:BP	regulation of body fluid levels	GO:0050878	3.13E-08	7.50472809	519	288	33	18123
GO:BP	killing by host of symbiont cells	GO:0051873	3.37E-08	7.47216481	29	288	10	18123
GO:BP	regulation of coagulation	GO:0050818	4.10E-08	7.38771455	77	288	14	18123
GO:BP	regulation of defense response	GO:0031347	4.49E-08	7.34799289	889	288	44	18123
GO:BP	inflammatory response	GO:0006954	4.72E-08	7.3259117	962	288	46	18123
GO:BP	platelet aggregation	GO:0070527	5.01E-08	7.30028873	64	288	13	18123
GO:BP	protein metabolic process	GO:0019538	6.41E-08	7.19286818	5912	288	148	18123
GO:BP	killing of cells in other organism involved in symbiotic interaction	GO:0051883	7.26E-08	7.13911902	31	288	10	18123
GO:BP	epidermal cell differentiation	GO:0009913	1.19E-07	6.92453132	370	288	27	18123
GO:BP	response to fungus	GO:0009620	1.55E-07	6.81097891	56	288	12	18123
GO:BP	platelet activation	GO:0030168	3.02E-07	6.51970596	163	288	18	18123
GO:BP	regulation of response to stimulus	GO:0048583	3.24E-07	6.48936053	4416	288	119	18123
GO:BP	negative regulation of catalytic activity	GO:0043086	3.79E-07	6.42150824	841	288	41	18123
GO:BP	negative regulation of immune system process	GO:0002683	6.20E-07	6.20729825	614	288	34	18123
GO:BP	multicellular organismal process	GO:0032501	1.1311E-06	5.94650686	8000	288	179	18123
GO:BP	negative regulation of defense response	GO:0031348	1.2147E-06	5.91552871	440	288	28	18123
GO:BP	regulation of inflammatory response	GO:0050727	1.2456E-06	5.90461926	565	288	32	18123
GO:BP	negative regulation of wound healing	GO:0061045	1.5404E-06	5.81235425	83	288	13	18123
GO:BP	response to chemical	GO:0042221	2.5387E-06	5.59539256	4829	288	124	18123
GO:BP	skin development	GO:0043588	2.7553E-06	5.55983692	426	288	27	18123
GO:BP	negative regulation of response to stimulus	GO:0048585	3.5193E-06	5.45354175	1938	288	66	18123
GO:BP	negative regulation of immune response	GO:0050777	3.7643E-06	5.42431642	373	288	25	18123
GO:BP	cytoskeleton organization	GO:0007010	4.678E-06	5.32993969	1473	288	55	18123
GO:BP	cellular response to cytokine stimulus	GO:0071345	4.9139E-06	5.30857303	1148	288	47	18123
GO:BP	glucose catabolic process to pyruvate	GO:0061718	5.443E-06	5.26415965	24	288	8	18123
GO:BP	NADH regeneration	GO:0006735	5.443E-06	5.26415965	24	288	8	18123
GO:BP	canonical glycolysis	GO:0061621	5.443E-06	5.26415965	24	288	8	18123
GO:BP	regulation of response to wounding	GO:1903034	5.6385E-06	5.24883869	172	288	17	18123
GO:BP	regulation of localization	GO:0032879	5.9658E-06	5.22433385	2906	288	86	18123

GO:BP	epidermis development	GO:0008544	7.7423E-06	5.1111281	478	288	28	18123
GO:BP	negative regulation of inflammatory response	GO:0050728	8.5418E-06	5.06844923	359	288	24	18123
GO:BP	inflammatory response to antigenic stimulus	GO:0002437	9.4411E-06	5.02497775	251	288	20	18123
GO:BP	biological adhesion	GO:0022610	1.1053E-05	4.95650677	1509	288	55	18123
GO:BP	glycolytic process through glucose-6-phosphate	GO:0061620	1.1247E-05	4.9489588	26	288	8	18123
GO:BP	cellular protein metabolic process	GO:0044267	1.213E-05	4.91615488	5280	288	130	18123
GO:BP	response to oxidative stress	GO:0006979	1.2536E-05	4.90185358	457	288	27	18123
GO:BP	protein folding	GO:0006457	1.2939E-05	4.88810859	230	288	19	18123
GO:BP	regulation of protein metabolic process	GO:0051246	1.3662E-05	4.86449507	2759	288	82	18123
GO:BP	regulation of wound healing	GO:0061041	1.3673E-05	4.86415129	138	288	15	18123
GO:BP	negative regulation of biological process	GO:0048519	1.3965E-05	4.85495218	5861	288	140	18123
GO:BP	negative regulation of response to wounding	GO:1903035	1.4361E-05	4.84281669	99	288	13	18123
GO:BP	glycolytic process through fructose-6-phosphate	GO:0061615	1.5764E-05	4.80234299	27	288	8	18123
GO:BP	response to cytokine	GO:0034097	2.064E-05	4.68529864	1242	288	48	18123
GO:BP	blood coagulation, fibrin clot formation	GO:0072378	2.1767E-05	4.66220849	28	288	8	18123
GO:BP	protein activation cascade	GO:0072376	2.1767E-05	4.66220849	28	288	8	18123
GO:BP	cellular component organization	GO:0016043	2.1888E-05	4.6598009	6661	288	153	18123
GO:BP	regulation of multicellular organismal process	GO:0051239	2.2835E-05	4.64139565	2888	288	84	18123
GO:BP	negative regulation of protein metabolic process	GO:0051248	3.0219E-05	4.51972279	1216	288	47	18123
GO:BP	defense response to Gram-negative bacterium	GO:0050829	3.6158E-05	4.44179494	88	288	12	18123
GO:BP	regulation of inflammatory response to antigenic stimulus	GO:0002861	3.8421E-05	4.41543145	220	288	18	18123
GO:BP	response to inorganic substance	GO:0010035	4.0687E-05	4.39054214	583	288	30	18123
GO:BP	positive regulation of cellular component organization	GO:0051130	4.3066E-05	4.36586201	1189	288	46	18123
GO:BP	regulation of cellular protein metabolic process	GO:0032268	4.8778E-05	4.3117751	2591	288	77	18123
GO:BP	epithelial cell differentiation	GO:0030855	5.6427E-05	4.24851395	807	288	36	18123
GO:BP	regulation of cell activation	GO:0050865	5.7599E-05	4.23958379	662	288	32	18123
GO:BP	response to organic substance	GO:0010033	6.1088E-05	4.21404553	3457	288	94	18123
GO:BP	actin filament-based process	GO:0030029	6.2008E-05	4.2075508	810	288	36	18123
GO:BP	cell adhesion	GO:0007155	6.657E-05	4.17671946	1502	288	53	18123
GO:BP	multicellular organismal homeostasis	GO:0048871	8.1511E-05	4.08878377	533	288	28	18123
GO:BP	B cell receptor signaling pathway	GO:0050853	8.1582E-05	4.08840479	135	288	14	18123
GO:BP	negative regulation of inflammatory response to antigenic stimulus	GO:0002862	8.5682E-05	4.06710831	206	288	17	18123
GO:BP	cell-cell adhesion	GO:0098609	8.9323E-05	4.04903442	898	288	38	18123
GO:BP	glucose catabolic process	GO:0006007	9.0753E-05	4.04214029	33	288	8	18123
GO:BP	negative regulation of cellular protein metabolic process	GO:0032269	0.00010147	3.99365808	1141	288	44	18123
GO:BP	cellular response to chemical stimulus	GO:0070887	0.00010521	3.97796099	3443	288	93	18123
GO:BP	negative regulation of molecular function	GO:0044092	0.00011364	3.94447939	1228	288	46	18123
GO:BP	regulation of catalytic activity	GO:0050790	0.00012203	3.9135443	2452	288	73	18123
GO:BP	respiratory burst	GO:0045730	0.00014966	3.82490698	35	288	8	18123
GO:BP	pentose biosynthetic process	GO:0019322	0.00015619	3.80635128	4	288	4	18123
GO:BP	plasminogen activation	GO:0031639	0.00016335	3.7868718	24	288	7	18123

GO:BP	intermediate filament organization	GO:0045109	0.00016335	3.7868718	24	288	7	18123
GO:BP	NAD metabolic process	GO:0019674	0.00016792	3.77490567	49	288	9	18123
GO:BP	Fc-epsilon receptor signaling pathway	GO:0038095	0.00018229	3.7392477	167	288	15	18123
GO:BP	amyloid fibril formation	GO:1990000	0.0001952	3.70952689	102	288	12	18123
GO:BP	regulation of hydrolase activity	GO:0051336	0.00020144	3.69584372	1252	288	46	18123
GO:BP	intermediate filament cytoskeleton organization	GO:0045104	0.00020195	3.69475786	50	288	9	18123
GO:BP	signal transduction	GO:0007165	0.00021291	3.67179963	6447	288	146	18123
GO:BP	protein stabilization	GO:0050821	0.00023647	3.62621927	195	288	16	18123
GO:BP	intermediate filament-based process	GO:0045103	0.00024184	3.61647467	51	288	9	18123
GO:BP	cellular component organization or biogenesis	GO:0071840	0.00025093	3.60044527	6880	288	153	18123
GO:BP	modulation of process of other organism	GO:0035821	0.00028488	3.5453316	149	288	14	18123
GO:BP	glucose 6-phosphate metabolic process	GO:0051156	0.00030212	3.51981757	26	288	7	18123
GO:BP	actin cytoskeleton organization	GO:0030036	0.00030806	3.51136134	712	288	32	18123
GO:BP	positive regulation of B cell activation	GO:0050871	0.00033663	3.47284151	151	288	14	18123
GO:BP	mucosal immune response	GO:0002385	0.00037022	3.43153671	39	288	8	18123
GO:BP	regulation of biological process	GO:0050789	0.00037878	3.42161678	12122	288	232	18123
GO:BP	detection of chemical stimulus involved in sensory perception of bitter taste	GO:0001580	0.00045645	3.34061041	40	288	8	18123
GO:BP	actin nucleation	GO:0045010	0.00047811	3.32047475	55	288	9	18123
GO:BP	positive regulation of gene expression	GO:0010628	0.00049025	3.30958618	1206	288	44	18123
GO:BP	actin filament organization	GO:0007015	0.00050761	3.29446592	445	288	24	18123
GO:BP	innate immune response in mucosa	GO:0002227	0.00052921	3.27637378	28	288	7	18123
GO:BP	negative regulation of fibrinolysis	GO:0051918	0.00057783	3.23819827	10	288	5	18123
GO:BP	NADPH regeneration	GO:0006740	0.00060433	3.21872742	18	288	6	18123
GO:BP	zymogen activation	GO:0031638	0.00076803	3.11462035	58	288	9	18123
GO:BP	NADH metabolic process	GO:0006734	0.00082582	3.08311583	43	288	8	18123
GO:BP	organ or tissue specific immune response	GO:0002251	0.00082582	3.08311583	43	288	8	18123
GO:BP	regulation of protein stability	GO:0031647	0.00098731	3.00554685	302	288	19	18123
GO:BP	sensory perception of bitter taste	GO:0050913	0.00099553	3.001946	44	288	8	18123
GO:BP	regulation of apoptotic signaling pathway	GO:2001233	0.00105445	2.97697483	365	288	21	18123
GO:BP	positive regulation of transport	GO:0051050	0.00111565	2.95247202	951	288	37	18123
GO:BP	hydrogen peroxide catabolic process	GO:0042744	0.00112826	2.94758955	31	288	7	18123
GO:BP	cellular oxidant detoxification	GO:0098869	0.00123124	2.90965828	99	288	11	18123
GO:BP	regulation of programmed cell death	GO:0043067	0.00131897	2.87976543	1603	288	52	18123
GO:BP	detection of chemical stimulus involved in sensory perception of taste	GO:0050912	0.00142587	2.84591914	46	288	8	18123
GO:BP	regulation of transport	GO:0051049	0.00148793	2.82741805	1839	288	57	18123
GO:BP	regulation of B cell activation	GO:0050864	0.00156999	2.80410279	197	288	15	18123
GO:BP	regulation of cell morphogenesis	GO:0022604	0.00162028	2.79041049	312	288	19	18123
GO:BP	regulation of anatomical structure morphogenesis	GO:0022603	0.00162118	2.79016965	1048	288	39	18123
GO:BP	homeostatic process	GO:0042592	0.00163013	2.78777741	1985	288	60	18123
GO:BP	regulation of leukocyte activation	GO:0002694	0.00164373	2.78417027	617	288	28	18123

GO:BP	regulation of cytokine production	GO:0001817	0.00169109	2.77183405	847	288	34	18123
GO:BP	interleukin-12-mediated signaling pathway	GO:0035722	0.00169487	2.77086368	47	288	8	18123
GO:BP	cellular response to stimulus	GO:0051716	0.00185323	2.73207082	7873	288	166	18123
GO:BP	extracellular matrix disassembly	GO:0022617	0.00192208	2.71622794	83	288	10	18123
GO:BP	biological regulation	GO:0065007	0.00196686	2.70622669	12802	288	239	18123
GO:BP	regulation of molecular function	GO:0065009	0.00201045	2.6967061	3191	288	84	18123
GO:BP	cytokine production	GO:0001816	0.00203737	2.69093083	854	288	34	18123
GO:BP	regulation of cellular component organization	GO:0051128	0.00221247	2.65512338	2439	288	69	18123
GO:BP	positive regulation of response to external stimulus	GO:0032103	0.00222278	2.65310297	518	288	25	18123
GO:BP	regulation of cellular process	GO:0050794	0.00223691	2.65035127	11517	288	221	18123
GO:BP	induction of bacterial agglutination	GO:0043152	0.00228445	2.64121774	6	288	4	18123
GO:BP	cellular response to interleukin-12	GO:0071349	0.0023647	2.62622324	49	288	8	18123
GO:BP	positive regulation of organelle organization	GO:0010638	0.00248161	2.60526657	630	288	28	18123
GO:BP	regulation of lymphocyte activation	GO:0051249	0.00264694	2.57725581	523	288	25	18123
GO:BP	sensory perception of taste	GO:0050909	0.00272159	2.5651775	67	288	9	18123
GO:BP	response to interleukin-12	GO:0070671	0.00277666	2.55647774	50	288	8	18123
GO:BP	reactive oxygen species metabolic process	GO:0072593	0.00279685	2.55333142	234	288	16	18123
GO:BP	regulation of cell death	GO:0010941	0.00303181	2.51829753	1740	288	54	18123
GO:BP	chaperone-mediated protein complex assembly	GO:0051131	0.00307345	2.51237392	23	288	6	18123
GO:BP	protein refolding	GO:0042026	0.00307345	2.51237392	23	288	6	18123
GO:BP	regulation of fibrinolysis	GO:0051917	0.00435667	2.36084566	14	288	5	18123
GO:BP	cellular detoxification	GO:1990748	0.00466545	2.33110664	113	288	11	18123
GO:BP	positive regulation of supramolecular fiber organization	GO:1902905	0.00472997	2.32514118	215	288	15	18123
GO:BP	hexose catabolic process	GO:0019320	0.00509309	2.29301827	54	288	8	18123
GO:BP	regulation of vesicle-mediated transport	GO:0060627	0.00537217	2.26985005	544	288	25	18123
GO:BP	Arp2/3 complex-mediated actin nucleation	GO:0034314	0.0059192	2.22773718	39	288	7	18123
GO:BP	cell communication	GO:0007154	0.00634816	2.19735247	6961	288	149	18123
GO:BP	positive regulation of response to wounding	GO:1903036	0.00638403	2.19490477	74	288	9	18123
GO:BP	lymphocyte activation	GO:0046649	0.00669968	2.17394584	780	288	31	18123
GO:BP	hydrogen peroxide metabolic process	GO:0042743	0.00676476	2.16974749	56	288	8	18123
GO:BP	cellular response to organic substance	GO:0071310	0.00693718	2.15881718	2821	288	75	18123
GO:BP	response to metal ion	GO:0010038	0.00697248	2.15661258	377	288	20	18123
GO:BP	positive regulation of protein polymerization	GO:0032273	0.00715303	2.14550971	142	288	12	18123
GO:BP	regulation of cell-substrate adhesion	GO:0010810	0.00743906	2.12848194	223	288	15	18123
GO:BP	tissue migration	GO:0090130	0.00786055	2.10454724	380	288	20	18123
GO:BP	response to reactive oxygen species	GO:0000302	0.00786065	2.1045418	224	288	15	18123
GO:BP	positive regulation of leukocyte activation	GO:0002696	0.00792838	2.10081542	414	288	21	18123
GO:BP	negative regulation of programmed cell death	GO:0043069	0.00844185	2.07356259	952	288	35	18123
GO:BP	positive regulation of cellular process	GO:0048522	0.00851111	2.07001364	5863	288	130	18123
GO:BP	signaling	GO:0023052	0.00891812	2.04972647	6937	288	148	18123

GO:BP	cellular response to toxic substance	GO:0097237	0.00915809	2.03819504	121	288	11	18123
GO:BP	regulation of respiratory burst	GO:0060263	0.00926038	2.03337097	16	288	5	18123
GO:BP	pentose-phosphate shunt	GO:0006098	0.00926038	2.03337097	16	288	5	18123
GO:BP	apoptotic process	GO:0006915	0.00948456	2.02298278	1998	288	58	18123
GO:BP	monosaccharide biosynthetic process	GO:0046364	0.00984647	2.00671945	99	288	10	18123
GO:BP	positive regulation of substrate adhesion-dependent cell spreading	GO:1900026	0.00996774	2.00140336	42	288	7	18123
GO:BP	negative regulation of multicellular organismal process	GO:0051241	0.01026828	1.9885025	1174	288	40	18123
GO:BP	external encapsulating structure organization	GO:0045229	0.01067889	1.97147394	422	288	21	18123
GO:BP	monosaccharide catabolic process	GO:0046365	0.01153315	1.93805206	60	288	8	18123
GO:BP	cell redox homeostasis	GO:0045454	0.01174533	1.93013462	43	288	7	18123
GO:BP	positive regulation of cell activation	GO:0050867	0.01235657	1.90810218	426	288	21	18123
GO:BP	positive regulation of cell-substrate adhesion	GO:0010811	0.01257533	1.90048077	125	288	11	18123
GO:BP	negative regulation of cellular process	GO:0048523	0.01268534	1.89669779	5153	288	117	18123
GO:BP	negative regulation of apoptotic process	GO:0043066	0.01270119	1.89615561	928	288	34	18123
GO:BP	apoptotic signaling pathway	GO:0097190	0.01274108	1.89479359	609	288	26	18123
GO:BP	anatomical structure morphogenesis	GO:0009653	0.01274496	1.89466146	2816	288	74	18123
GO:BP	positive regulation of actin filament polymerization	GO:0030838	0.01291088	1.88904409	102	288	10	18123
GO:BP	cell junction organization	GO:0034330	0.013376	1.87367362	727	288	29	18123
GO:BP	positive regulation of protein-containing complex assembly	GO:0031334	0.01402912	1.85296945	265	288	16	18123
GO:BP	post-translational protein modification	GO:0043687	0.01448382	1.83911678	362	288	19	18123
GO:BP	anatomical structure development	GO:0048856	0.01601036	1.79559892	6164	288	134	18123
GO:BP	regulation of apoptotic process	GO:0042981	0.01672779	1.77656138	1560	288	48	18123
GO:BP	positive regulation of lymphocyte activation	GO:0051251	0.01694871	1.77086323	366	288	19	18123
GO:BP	angiogenesis	GO:0001525	0.01802467	1.74413274	621	288	26	18123
GO:BP	epithelium development	GO:0060429	0.01880272	1.72577925	1338	288	43	18123
GO:BP	tissue development	GO:0009888	0.01915473	1.71772385	2093	288	59	18123
GO:BP	regulation of actin filament-based process	GO:0032970	0.01959768	1.70779538	404	288	20	18123
GO:BP	cytokine-mediated signaling pathway	GO:0019221	0.02029365	1.69263978	824	288	31	18123
GO:BP	epithelial cell migration	GO:0010631	0.02055889	1.68700029	371	288	19	18123
GO:BP	protein polymerization	GO:0051258	0.02254642	1.6469224	307	288	17	18123
GO:BP	epithelium migration	GO:0090132	0.02304407	1.63744085	374	288	19	18123
GO:BP	protein-containing complex assembly	GO:0065003	0.02465889	1.60802656	1724	288	51	18123
GO:BP	cell chemotaxis	GO:0060326	0.02560235	1.59172022	310	288	17	18123
GO:BP	regulation of establishment of protein localization	GO:0070201	0.02561607	1.59148748	595	288	25	18123
GO:BP	ephrin receptor signaling pathway	GO:0048013	0.02718343	1.56569571	88	288	9	18123
GO:BP	regulation of cell adhesion	GO:0030155	0.02813063	1.55082056	756	288	29	18123
GO:BP	response to cadmium ion	GO:0046686	0.02985421	1.52499448	68	288	8	18123
GO:BP	establishment or maintenance of cell polarity	GO:0007163	0.03001834	1.52261329	220	288	14	18123
GO:BP	myeloid leukocyte migration	GO:0097529	0.03001834	1.52261329	220	288	14	18123

GO:BP	regulation of actin polymerization or depolymerization	GO:0008064	0.03010199	1.52140479	191	288	13	18123
GO:BP	neutrophil-mediated killing of symbiont cell	GO:0070943	0.03041074	1.51697298	10	288	4	18123
GO:BP	actin polymerization or depolymerization	GO:0008154	0.0315984	1.50033491	221	288	14	18123
GO:BP	regulation of actin filament length	GO:0030832	0.0318358	1.49708422	192	288	13	18123
GO:BP	leukocyte mediated cytotoxicity	GO:0001909	0.03228312	1.49102446	113	288	10	18123
GO:BP	extracellular matrix organization	GO:0030198	0.03338679	1.47642539	419	288	20	18123
GO:BP	extracellular structure organization	GO:0043062	0.03456012	1.46142479	420	288	20	18123
GO:BP	response to toxic substance	GO:0009636	0.03585527	1.44544698	254	288	15	18123
GO:BP	regulation of protein-containing complex assembly	GO:0043254	0.03713534	1.43021263	458	288	21	18123
GO:BP	acute inflammatory response	GO:0002526	0.03769252	1.42374485	115	288	10	18123
GO:BP	regulation of intrinsic apoptotic signaling pathway	GO:2001242	0.03790212	1.42133646	167	288	12	18123
GO:BP	system development	GO:0048731	0.03847193	1.41485605	5095	288	114	18123
GO:BP	ameboidal-type cell migration	GO:0001667	0.03878637	1.41132081	496	288	22	18123
GO:BP	response to ethanol	GO:0045471	0.03985333	1.39953535	141	288	11	18123
GO:BP	antigen receptor-mediated signaling pathway	GO:0050851	0.0402315	1.39543375	321	288	17	18123
GO:BP	detoxification	GO:0098754	0.0455075	1.34191703	143	288	11	18123
GO:BP	positive regulation of receptor-mediated endocytosis	GO:0048260	0.04905683	1.30930056	53	288	7	18123
GO:BP	NADP metabolic process	GO:0006739	0.04985034	1.3023319	36	288	6	18123
GO:CC	extracellular exosome	GO:0070062	3.43E-166	165.464669	2178	291	235	18964
GO:CC	extracellular vesicle	GO:1903561	3.48E-162	161.458778	2263	291	235	18964
GO:CC	extracellular membrane-bounded organelle	GO:0065010	4.30E-162	161.366514	2265	291	235	18964
GO:CC	extracellular organelle	GO:0043230	4.30E-162	161.366514	2265	291	235	18964
GO:CC	extracellular space	GO:0005615	8.67E-157	156.061801	3595	291	264	18964
GO:CC	extracellular region	GO:0005576	2.51E-145	144.600098	4564	291	274	18964
GO:CC	vesicle	GO:0031982	2.30E-126	125.638439	4058	291	253	18964
GO:CC	secretory granule lumen	GO:0034774	8.91E-79	78.0501465	320	291	84	18964
GO:CC	cytoplasmic vesicle lumen	GO:0060205	2.85E-78	77.5451298	324	291	84	18964
GO:CC	vesicle lumen	GO:0031983	5.06E-78	77.2954413	326	291	84	18964
GO:CC	secretory granule	GO:0030141	2.80E-72	71.5534479	857	291	112	18964
GO:CC	secretory vesicle	GO:0099503	1.22E-63	62.9139476	1027	291	112	18964
GO:CC	cytoplasmic vesicle	GO:0031410	1.80E-49	48.7437679	2433	291	143	18964
GO:CC	intracellular vesicle	GO:0097708	2.33E-49	48.6317521	2438	291	143	18964
GO:CC	blood microparticle	GO:0072562	5.23E-42	41.2811424	139	291	43	18964
GO:CC	ficolin-1-rich granule lumen	GO:1904813	3.16E-38	37.4999676	124	291	39	18964
GO:CC	ficolin-1-rich granule	GO:0101002	7.98E-35	34.0978114	184	291	42	18964
GO:CC	azurophil granule lumen	GO:0035578	2.90E-22	21.5371026	91	291	25	18964
GO:CC	endomembrane system	GO:0012505	3.76E-22	21.4242576	4651	291	152	18964
GO:CC	primary lysosome	GO:0005766	5.82E-21	20.2350713	154	291	29	18964
GO:CC	azurophil granule	GO:0042582	5.82E-21	20.2350713	154	291	29	18964
GO:CC	collagen-containing extracellular matrix	GO:0062023	1.04E-20	19.9839159	421	291	43	18964
GO:CC	immunoglobulin complex	GO:0019814	4.53E-20	19.3439023	165	291	29	18964
GO:CC	vacuolar lumen	GO:0005775	2.16E-19	18.6655233	174	291	29	18964

GO:CC	extracellular matrix	GO:0031012	2.70E-18	17.5682762	562	291	46	18964
GO:CC	external encapsulating structure	GO:0030312	2.90E-18	17.5369303	563	291	46	18964
GO:CC	focal adhesion	GO:0005925	5.10E-18	17.2928492	420	291	40	18964
GO:CC	cell-substrate junction	GO:0030055	9.29E-18	17.0318551	427	291	40	18964
GO:CC	tertiary granule lumen	GO:1904724	3.23E-17	16.4910719	55	291	18	18964
GO:CC	membrane-bounded organelle	GO:0043227	1.46E-16	15.8358633	13201	291	265	18964
GO:CC	anchoring junction	GO:0070161	6.35E-15	14.1974039	838	291	51	18964
GO:CC	lysosome	GO:0005764	1.06E-14	13.9753658	723	291	47	18964
GO:CC	lytic vacuole	GO:0000323	1.06E-14	13.9753658	723	291	47	18964
GO:CC	melanosome	GO:0042470	8.17E-14	13.0879763	109	291	20	18964
GO:CC	pigment granule	GO:0048770	8.17E-14	13.0879763	109	291	20	18964
GO:CC	cell surface	GO:0009986	1.00E-13	12.9984142	896	291	51	18964
GO:CC	tertiary granule	GO:0070820	1.89E-13	12.722488	163	291	23	18964
GO:CC	specific granule lumen	GO:0035580	1.94E-13	12.7124678	61	291	16	18964
GO:CC	vacuole	GO:0005773	2.62E-13	12.5816446	818	291	48	18964
GO:CC	cell periphery	GO:0071944	3.47E-12	11.4599687	6178	291	158	18964
GO:CC	immunoglobulin complex, circulating	GO:0042571	6.74E-12	11.1711964	75	291	16	18964
GO:CC	organelle	GO:0043226	8.46E-12	11.0726524	14027	291	266	18964
GO:CC	side of membrane	GO:0098552	2.16E-11	10.6653458	622	291	39	18964
GO:CC	specific granule	GO:0042581	1.28E-10	9.89430479	158	291	20	18964
GO:CC	actin cytoskeleton	GO:0015629	2.59E-10	9.58694898	517	291	34	18964
GO:CC	platelet alpha granule lumen	GO:0031093	3.16E-10	9.50022942	66	291	14	18964
GO:CC	endoplasmic reticulum lumen	GO:0005788	8.18E-10	9.08740858	313	291	26	18964
GO:CC	platelet alpha granule	GO:0031091	1.99E-09	8.70096483	90	291	15	18964
GO:CC	membrane-enclosed lumen	GO:0031974	3.02E-09	8.52057389	5579	291	140	18964
GO:CC	intracellular organelle lumen	GO:0070013	3.02E-09	8.52057389	5579	291	140	18964
GO:CC	organelle lumen	GO:0043233	3.02E-09	8.52057389	5579	291	140	18964
GO:CC	cytoskeleton	GO:0005856	3.83E-09	8.41664118	2339	291	78	18964
GO:CC	endocytic vesicle lumen	GO:0071682	4.95E-09	8.30565005	22	291	9	18964
GO:CC	external side of plasma membrane	GO:0009897	1.18E-08	7.9282247	409	291	28	18964
GO:CC	cornified envelope	GO:0001533	1.28E-08	7.89327475	44	291	11	18964
GO:CC	Arp2/3 protein complex	GO:0005885	1.66E-08	7.78030014	11	291	7	18964
GO:CC	cytosol	GO:0005829	1.82E-08	7.74080428	5361	291	134	18964
GO:CC	polymeric cytoskeletal fiber	GO:0099513	5.10E-08	7.29270151	766	291	38	18964
GO:CC	supramolecular fiber	GO:0099512	6.89E-08	7.1620648	997	291	44	18964
GO:CC	supramolecular polymer	GO:0099081	8.86E-08	7.05250542	1005	291	44	18964
GO:CC	endocytic vesicle	GO:0030139	1.24E-07	6.9065204	335	291	24	18964
GO:CC	intermediate filament cytoskeleton	GO:0045111	1.83E-07	6.73692411	260	291	21	18964
GO:CC	IgA immunoglobulin complex, circulating	GO:0071746	2.34E-07	6.63150015	5	291	5	18964
GO:CC	IgA immunoglobulin complex	GO:0071745	2.34E-07	6.63150015	5	291	5	18964
GO:CC	secretory IgA immunoglobulin complex	GO:0071751	2.34E-07	6.63150015	5	291	5	18964
GO:CC	polymeric IgA immunoglobulin complex	GO:0071749	2.34E-07	6.63150015	5	291	5	18964
GO:CC	intermediate filament	GO:0005882	3.71E-07	6.43017726	219	291	19	18964

GO:CC	cytoplasm	GO:0005737	1.3253E-06	5.87769294	11951	291	229	18964
GO:CC	phagocytic vesicle	GO:0045335	8.7887E-06	5.05607765	139	291	14	18964
GO:CC	fibrinogen complex	GO:0005577	1.2595E-05	4.89978918	8	291	5	18964
GO:CC	cortical cytoskeleton	GO:0030863	1.2708E-05	4.89592901	121	291	13	18964
GO:CC	cell leading edge	GO:0031252	1.3645E-05	4.86503857	426	291	24	18964
GO:CC	monomeric IgA immunoglobulin complex	GO:0071748	1.5433E-05	4.81154372	4	291	4	18964
GO:CC	supramolecular complex	GO:0099080	1.667E-05	4.7780559	1325	291	47	18964
GO:CC	desmosome	GO:0030057	2.009E-05	4.69702735	25	291	7	18964
GO:CC	plasma membrane	GO:0005886	6.7254E-05	4.17227899	5680	291	128	18964
GO:CC	cell junction	GO:0030054	8.8728E-05	4.05194049	2107	291	62	18964
GO:CC	lamellipodium	GO:0030027	0.00016992	3.7697552	203	291	15	18964
GO:CC	protein-containing complex	GO:0032991	0.00018814	3.72551029	5541	291	124	18964
GO:CC	cell cortex	GO:0005938	0.00021369	3.67020642	326	291	19	18964
GO:CC	cortical actin cytoskeleton	GO:0030864	0.00041917	3.37761358	92	291	10	18964
GO:CC	actin filament	GO:0005884	0.00058385	3.23370147	118	291	11	18964
GO:CC	keratin filament	GO:0045095	0.0007509	3.12441547	98	291	10	18964
GO:CC	IgM immunoglobulin complex, circulating	GO:0071754	0.00101607	2.99307497	3	291	3	18964
GO:CC	IgM immunoglobulin complex	GO:0071753	0.00101607	2.99307497	3	291	3	18964
GO:CC	secretory dimeric IgA immunoglobulin complex	GO:0071752	0.00101607	2.99307497	3	291	3	18964
GO:CC	dimeric IgA immunoglobulin complex	GO:0071750	0.00101607	2.99307497	3	291	3	18964
GO:CC	pentameric IgM immunoglobulin complex	GO:0071756	0.00101607	2.99307497	3	291	3	18964
GO:CC	podosome	GO:0002102	0.0015341	2.81414641	30	291	6	18964
GO:CC	cell-cell junction	GO:0005911	0.0025887	2.58691768	496	291	22	18964
GO:CC	lysosomal membrane	GO:0005765	0.00349065	2.45709422	395	291	19	18964
GO:CC	lytic vacuole membrane	GO:0098852	0.00349065	2.45709422	395	291	19	18964
GO:CC	COP9 signalosome	GO:0008180	0.00393191	2.40539635	35	291	6	18964
GO:CC	membrane microdomain	GO:0098857	0.00593442	2.22662149	339	291	17	18964
GO:CC	membrane raft	GO:0045121	0.00593442	2.22662149	339	291	17	18964
GO:CC	vacuolar membrane	GO:0005774	0.00646691	2.18930291	450	291	20	18964
GO:CC	phagocytic vesicle lumen	GO:0097013	0.00993064	2.00302292	5	291	3	18964
GO:CC	high-density lipoprotein particle	GO:0034364	0.02050173	1.6882094	29	291	5	18964
GO:CC	ruffle	GO:0001726	0.03111583	1.50701855	180	291	11	18964
GO:CC	proton-transporting two-sector ATPase complex, catalytic domain	GO:0033178	0.03136481	1.50355731	17	291	4	18964
GO:CC	phagocytic vesicle membrane	GO:0030670	0.04309801	1.36554275	75	291	7	18964
GO:CC	extracellular exosome	GO:0070062	3.43E-166	165.464669	2178	291	235	18964
GO:CC	extracellular vesicle	GO:1903561	3.48E-162	161.458778	2263	291	235	18964
GO:CC	extracellular membrane-bounded organelle	GO:0065010	4.30E-162	161.366514	2265	291	235	18964
GO:CC	extracellular organelle	GO:0043230	4.30E-162	161.366514	2265	291	235	18964
GO:CC	extracellular space	GO:0005615	8.67E-157	156.061801	3595	291	264	18964
GO:CC	extracellular region	GO:0005576	2.51E-145	144.600098	4564	291	274	18964
GO:CC	vesicle	GO:0031982	2.30E-126	125.638439	4058	291	253	18964
GO:CC	secretory granule lumen	GO:0034774	8.91E-79	78.0501465	320	291	84	18964
GO:CC	cytoplasmic vesicle lumen	GO:0060205	2.85E-78	77.5451298	324	291	84	18964

GO:CC	vesicle lumen	GO:0031983	5.06E-78	77.2954413	326	291	84	18964
GO:CC	secretory granule	GO:0030141	2.80E-72	71.5534479	857	291	112	18964
GO:CC	secretory vesicle	GO:0099503	1.22E-63	62.9139476	1027	291	112	18964
GO:CC	cytoplasmic vesicle	GO:0031410	1.80E-49	48.7437679	2433	291	143	18964
GO:CC	intracellular vesicle	GO:0097708	2.33E-49	48.6317521	2438	291	143	18964
GO:CC	blood microparticle	GO:0072562	5.23E-42	41.2811424	139	291	43	18964
GO:CC	ficolin-1-rich granule lumen	GO:1904813	3.16E-38	37.4999676	124	291	39	18964
GO:CC	ficolin-1-rich granule	GO:0101002	7.98E-35	34.0978114	184	291	42	18964
GO:CC	azurophil granule lumen	GO:0035578	2.90E-22	21.5371026	91	291	25	18964
GO:CC	endomembrane system	GO:0012505	3.76E-22	21.4242576	4651	291	152	18964
GO:CC	primary lysosome	GO:0005766	5.82E-21	20.2350713	154	291	29	18964
GO:CC	azurophil granule	GO:0042582	5.82E-21	20.2350713	154	291	29	18964
GO:CC	collagen-containing extracellular matrix	GO:0062023	1.04E-20	19.9839159	421	291	43	18964
GO:CC	immunoglobulin complex	GO:0019814	4.53E-20	19.3439023	165	291	29	18964
GO:CC	vacuolar lumen	GO:0005775	2.16E-19	18.6655233	174	291	29	18964
GO:CC	extracellular matrix	GO:0031012	2.70E-18	17.5682762	562	291	46	18964
GO:CC	external encapsulating structure	GO:0030312	2.90E-18	17.5369303	563	291	46	18964
GO:CC	focal adhesion	GO:0005925	5.10E-18	17.2928492	420	291	40	18964
GO:CC	cell-substrate junction	GO:0030055	9.29E-18	17.0318551	427	291	40	18964
GO:CC	tertiary granule lumen	GO:1904724	3.23E-17	16.4910719	55	291	18	18964
GO:CC	membrane-bounded organelle	GO:0043227	1.46E-16	15.8358633	13201	291	265	18964
GO:CC	anchoring junction	GO:0070161	6.35E-15	14.1974039	838	291	51	18964
GO:CC	lysosome	GO:0005764	1.06E-14	13.9753658	723	291	47	18964
GO:CC	lytic vacuole	GO:0000323	1.06E-14	13.9753658	723	291	47	18964
GO:CC	melanosome	GO:0042470	8.17E-14	13.0879763	109	291	20	18964
GO:CC	pigment granule	GO:0048770	8.17E-14	13.0879763	109	291	20	18964
GO:CC	cell surface	GO:0009986	1.00E-13	12.9984142	896	291	51	18964
GO:CC	tertiary granule	GO:0070820	1.89E-13	12.722488	163	291	23	18964
GO:CC	specific granule lumen	GO:0035580	1.94E-13	12.7124678	61	291	16	18964
GO:CC	vacuole	GO:0005773	2.62E-13	12.5816446	818	291	48	18964
GO:CC	cell periphery	GO:0071944	3.47E-12	11.4599687	6178	291	158	18964
GO:CC	immunoglobulin complex, circulating	GO:0042571	6.74E-12	11.1711964	75	291	16	18964
GO:CC	organelle	GO:0043226	8.46E-12	11.0726524	14027	291	266	18964
GO:CC	side of membrane	GO:0098552	2.16E-11	10.6653458	622	291	39	18964
GO:CC	specific granule	GO:0042581	1.28E-10	9.89430479	158	291	20	18964
GO:CC	actin cytoskeleton	GO:0015629	2.59E-10	9.58694898	517	291	34	18964
GO:CC	platelet alpha granule lumen	GO:0031093	3.16E-10	9.50022942	66	291	14	18964
GO:CC	endoplasmic reticulum lumen	GO:0005788	8.18E-10	9.08740858	313	291	26	18964
GO:CC	platelet alpha granule	GO:0031091	1.99E-09	8.70096483	90	291	15	18964
GO:CC	membrane-enclosed lumen	GO:0031974	3.02E-09	8.52057389	5579	291	140	18964
GO:CC	intracellular organelle lumen	GO:0070013	3.02E-09	8.52057389	5579	291	140	18964
GO:CC	organelle lumen	GO:0043233	3.02E-09	8.52057389	5579	291	140	18964
GO:CC	cytoskeleton	GO:0005856	3.83E-09	8.41664118	2339	291	78	18964
GO:CC	endocytic vesicle lumen	GO:0071682	4.95E-09	8.30565005	22	291	9	18964

GO:CC	external side of plasma membrane	GO:0009897	1.18E-08	7.9282247	409	291	28	18964
GO:CC	cornified envelope	GO:0001533	1.28E-08	7.89327475	44	291	11	18964
GO:CC	Arp2/3 protein complex	GO:0005885	1.66E-08	7.78030014	11	291	7	18964
GO:CC	cytosol	GO:0005829	1.82E-08	7.74080428	5361	291	134	18964
GO:CC	polymeric cytoskeletal fiber	GO:0099513	5.10E-08	7.29270151	766	291	38	18964
GO:CC	supramolecular fiber	GO:0099512	6.89E-08	7.1620648	997	291	44	18964
GO:CC	supramolecular polymer	GO:0099081	8.86E-08	7.05250542	1005	291	44	18964
GO:CC	endocytic vesicle	GO:0030139	1.24E-07	6.9065204	335	291	24	18964
GO:CC	intermediate filament cytoskeleton	GO:0045111	1.83E-07	6.73692411	260	291	21	18964
GO:CC	IgA immunoglobulin complex, circulating	GO:0071746	2.34E-07	6.63150015	5	291	5	18964
GO:CC	IgA immunoglobulin complex	GO:0071745	2.34E-07	6.63150015	5	291	5	18964
GO:CC	secretory IgA immunoglobulin complex	GO:0071751	2.34E-07	6.63150015	5	291	5	18964
GO:CC	polymeric IgA immunoglobulin complex	GO:0071749	2.34E-07	6.63150015	5	291	5	18964
GO:CC	intermediate filament	GO:0005882	3.71E-07	6.43017726	219	291	19	18964
GO:CC	cytoplasm	GO:0005737	1.3253E-06	5.87769294	11951	291	229	18964
GO:CC	phagocytic vesicle	GO:0045335	8.7887E-06	5.05607765	139	291	14	18964
GO:CC	fibrinogen complex	GO:0005577	1.2595E-05	4.89978918	8	291	5	18964
GO:CC	cortical cytoskeleton	GO:0030863	1.2708E-05	4.89592901	121	291	13	18964
GO:CC	cell leading edge	GO:0031252	1.3645E-05	4.86503857	426	291	24	18964
GO:CC	monomeric IgA immunoglobulin complex	GO:0071748	1.5433E-05	4.81154372	4	291	4	18964
GO:CC	supramolecular complex	GO:0099080	1.667E-05	4.7780559	1325	291	47	18964
GO:CC	desmosome	GO:0030057	2.009E-05	4.69702735	25	291	7	18964
GO:CC	plasma membrane	GO:0005886	6.7254E-05	4.17227899	5680	291	128	18964
GO:CC	cell junction	GO:0030054	8.8728E-05	4.05194049	2107	291	62	18964
GO:CC	lamellipodium	GO:0030027	0.00016992	3.7697552	203	291	15	18964
GO:CC	protein-containing complex	GO:0032991	0.00018814	3.72551029	5541	291	124	18964
GO:CC	cell cortex	GO:0005938	0.00021369	3.67020642	326	291	19	18964
GO:CC	cortical actin cytoskeleton	GO:0030864	0.00041917	3.37761358	92	291	10	18964
GO:CC	actin filament	GO:0005884	0.00058385	3.23370147	118	291	11	18964
GO:CC	keratin filament	GO:0045095	0.0007509	3.12441547	98	291	10	18964
GO:CC	IgM immunoglobulin complex, circulating	GO:0071754	0.00101607	2.99307497	3	291	3	18964
GO:CC	IgM immunoglobulin complex	GO:0071753	0.00101607	2.99307497	3	291	3	18964
GO:CC	secretory dimeric IgA immunoglobulin complex	GO:0071752	0.00101607	2.99307497	3	291	3	18964
GO:CC	dimeric IgA immunoglobulin complex	GO:0071750	0.00101607	2.99307497	3	291	3	18964
GO:CC	pentameric IgM immunoglobulin complex	GO:0071756	0.00101607	2.99307497	3	291	3	18964
GO:CC	podosome	GO:0002102	0.0015341	2.81414641	30	291	6	18964
GO:CC	cell-cell junction	GO:0005911	0.0025887	2.58691768	496	291	22	18964
GO:CC	lysosomal membrane	GO:0005765	0.00349065	2.45709422	395	291	19	18964
GO:CC	lytic vacuole membrane	GO:0098852	0.00349065	2.45709422	395	291	19	18964
GO:CC	COP9 signalosome	GO:0008180	0.00393191	2.40539635	35	291	6	18964
GO:CC	membrane microdomain	GO:0098857	0.00593442	2.22662149	339	291	17	18964
GO:CC	membrane raft	GO:0045121	0.00593442	2.22662149	339	291	17	18964
GO:CC	vacuolar membrane	GO:0005774	0.00646691	2.18930291	450	291	20	18964

GO:CC	phagocytic vesicle lumen	GO:0097013	0.00993064	2.00302292	5	291	3	18964
GO:CC	high-density lipoprotein particle	GO:0034364	0.02050173	1.6882094	29	291	5	18964
GO:CC	ruffle	GO:0001726	0.03111583	1.50701855	180	291	11	18964
GO:CC	proton-transporting two-sector ATPase complex, catalytic domain	GO:0033178	0.03136481	1.50355731	17	291	4	18964
GO:CC	phagocytic vesicle membrane	GO:0030670	0.04309801	1.36554275	75	291	7	18964
KEGG	Salivary secretion	KEGG:04970	4.88E-12	11.3116881	91	175	19	8000
KEGG	Salmonella infection	KEGG:05132	1.9526E-06	5.70939441	249	175	22	8000
KEGG	Staphylococcus aureus infection	KEGG:05150	4.0995E-06	5.38727309	87	175	13	8000
KEGG	Carbon metabolism	KEGG:01200	1.9318E-05	4.71403767	116	175	14	8000
KEGG	Estrogen signaling pathway	KEGG:04915	2.5575E-05	4.59219099	137	175	15	8000
KEGG	Complement and coagulation cascades	KEGG:04610	2.6347E-05	4.57926592	85	175	12	8000
KEGG	Regulation of actin cytoskeleton	KEGG:04810	9.8597E-05	4.00613481	216	175	18	8000
KEGG	Pathogenic Escherichia coli infection	KEGG:05130	0.00011486	3.93984487	196	175	17	8000
KEGG	Glycolysis / Gluconeogenesis	KEGG:00010	0.0001596	3.79696132	67	175	10	8000
KEGG	Phagosome	KEGG:04145	0.00035236	3.45301673	147	175	14	8000
KEGG	Tight junction	KEGG:04530	0.0003785	3.42193447	169	175	15	8000
KEGG	Biosynthesis of amino acids	KEGG:01230	0.00045868	3.33848606	75	175	10	8000
KEGG	Pentose phosphate pathway	KEGG:00030	0.0037617	2.42461576	30	175	6	8000
KEGG	Bacterial invasion of epithelial cells	KEGG:05100	0.00408906	2.38837694	77	175	9	8000
KEGG	Fc gamma R-mediated phagocytosis	KEGG:04666	0.0042006	2.37668861	96	175	10	8000
KEGG	Biosynthesis of amino acids	KEGG:01230	0.00045868	3.33848606	75	175	10	8000
KEGG	Pentose phosphate pathway	KEGG:00030	0.0037617	2.42461576	30	175	6	8000
KEGG	Bacterial invasion of epithelial cells	KEGG:05100	0.00408906	2.38837694	77	175	9	8000
KEGG	Fc gamma R-mediated phagocytosis	KEGG:04666	0.0042006	2.37668861	96	175	10	8000
KEGG	Neutrophil extracellular trap formation	KEGG:04613	0.00618118	2.2089288	189	175	14	8000
KEGG	Shigellosis	KEGG:05131	0.02990563	1.52424697	246	175	15	8000

Table S 14*.GO analysis of breath exosomal proteome with proteins associated with "regulated exocytosis" removed (184 proteins). The analysis was performed by using g:Profiler software.*
**The list of proteins associated with each ontology is available on request deanna.shea@vuw.ac.nz*

Source	Term name	Term ID	Adjusted p-value	Negative log10 of adjusted p-value	Term size	Query size	Intersection size	Effective domain size
GO:MF	antigen binding	GO:0003823	5.7463610345 7402E-23	22.24060709146 6700	163	182	27	18694
GO:MF	immunoglobulin receptor binding	GO:0034987	2.7552817540 6458E-14	13.55983398375 2700	80	182	16	18694
GO:MF	structural constituent of cytoskeleton	GO:0005200	1.0301079689 2422E-13	12.98711725310 980	104	182	17	18694
GO:MF	structural molecule activity	GO:0005198	9.9793182410 6046E-08	7.000899127476 060	698	182	28	18694
GO:MF	endopeptidase inhibitor activity	GO:0004866	1.2760220960 1989E-07	6.894141805163 110	179	182	15	18694
GO:MF	peptidase inhibitor activity	GO:0030414	1.8807210072 174E-07	6.725675624445 660	184	182	15	18694
GO:MF	endopeptidase regulator activity	GO:0061135	2.5429137994 1407E-07	6.594668361441 800	188	182	15	18694

GO:MF	enzyme inhibitor activity	GO:0004857	6.6780889566 5373E-07	6.175347800147 400	386	182	20	18694
GO:MF	peptidase regulator activity	GO:0061134	0.0000030336 76668828510	5.518030708462 410	225	182	15	18694
GO:MF	cadherin binding	GO:0045296	0.0000147587 57541583500	4.830950201831 8300	332	182	17	18694
GO:MF	cell adhesion molecule binding	GO:0050839	0.0000490991 6024458210	4.308925935662 430	548	182	21	18694
GO:MF	cysteine-type endopeptidase inhibitor activity	GO:0004869	0.0005318295 303777910	3.274227551690 3100	55	182	7	18694
GO:MF	actin filament binding	GO:0051015	0.0005553348 196708230	3.255445095270 790	210	182	12	18694
GO:MF	actin binding	GO:0003779	0.0040473431 263316500	2.392829975357 500	445	182	16	18694
GO:MF	protein-containing complex binding	GO:0044877	0.0093700411 59286080	2.028258501405 5400	1282	182	29	18694
GO:MF	enzyme regulator activity	GO:0030234	0.0115557489 795888	1.937201900711 8400	1228	182	28	18694
GO:MF	signaling receptor binding	GO:0005102	0.0167239437 02746500	1.776661303070 1800	1681	182	34	18694
GO:MF	proton-transporting ATP synthase activity, rotational mechanism	GO:0046933	0.0291756370 29161600	1.534979652669 7600	22	182	4	18694
GO:MF	protease binding	GO:0002020	0.0346488681 12971900	1.460310948074 3800	139	182	8	18694
GO:BP	humoral immune response	GO:0006959	1.5756103388 3263E-30	29.80255117810 2000	384	183	44	18092
GO:BP	humoral immune response mediated by circulating immunoglobulin	GO:0002455	6.5459348347 4649E-24	23.18402832243 9400	155	183	28	18092
GO:BP	complement activation, classical pathway	GO:0006958	1.3535656363 6743E-23	22.86852067981 1400	142	183	27	18092
GO:BP	complement activation	GO:0006956	2.3360536997 9412E-23	22.63151717814 5200	180	183	29	18092
GO:BP	immunoglobulin mediated immune response	GO:0016064	2.2102243287 455E-20	19.65556364496 100	227	183	29	18092
GO:BP	B cell mediated immunity	GO:0019724	3.2357736141 811E-20	19.49002187072 8200	230	183	29	18092
GO:BP	phagocytosis	GO:0006909	7.0101502517 4999E-19	18.15427267350 170	390	183	34	18092
GO:BP	activation of immune response	GO:0002253	2.1343487065 6997E-18	17.67073462475 8200	566	183	39	18092
GO:BP	immune response-activating cell surface receptor signaling pathway	GO:0002429	4.7459765265 2044E-18	17.32367441412 2900	477	183	36	18092
GO:BP	immune response-activating signal transduction	GO:0002757	4.7459765265 2044E-18	17.32367441412 2900	477	183	36	18092
GO:BP	immune response-regulating cell surface receptor signaling pathway involved in phagocytosis	GO:0002433	3.2352984419 0179E-17	16.49008565141 17	135	183	22	18092
GO:BP	Fc-gamma receptor signaling pathway involved in phagocytosis	GO:0038096	3.2352984419 0179E-17	16.49008565141 17	135	183	22	18092
GO:BP	immune response-regulating cell surface receptor signaling pathway	GO:0002768	4.7084313763 5417E-17	16.32712375487 9600	511	183	36	18092
GO:BP	immune response-regulating signaling pathway	GO:0002764	5.7157380178 557E-17	16.24292768541 070	514	183	36	18092

GO:BP	Fc-gamma receptor signaling pathway	GO:0038094	6.2790074625 4861E-17	16.2021090007 8590	139	183	22	18092
GO:BP	Fc receptor mediated stimulatory signaling pathway	GO:0002431	8.6764746065 3706E-17	16.0616566999 3090	141	183	22	18092
GO:BP	lymphocyte mediated immunity	GO:0002449	1.2626219785 1614E-16	15.8987266551 5980	365	183	31	18092
GO:BP	positive regulation of immune response	GO:0050778	1.3540484041 4269E-16	15.8683658103 36000	753	183	42	18092
GO:BP	adaptive immune response based on somatic recombination of immune receptors built from immunoglobulin superfamily domains	GO:0002460	1.8806887962 7614E-16	15.7256830626 32300	370	183	31	18092
GO:BP	regulation of complement activation	GO:0030449	4.7529057496 2451E-15	14.3230407977 02700	110	183	19	18092
GO:BP	regulation of humoral immune response	GO:0002920	7.4393349799 9882E-15	14.1284658853 44600	131	183	20	18092
GO:BP	endocytosis	GO:0006897	2.7704813253 8607E-14	13.5574447728 85100	701	183	38	18092
GO:BP	defense response to bacterium	GO:0042742	7.0537082041 7298E-14	13.1515825100 6950	356	183	28	18092
GO:BP	immune response	GO:0006955	1.0853082403 6957E-13	12.9644468995 29800	2326	183	68	18092
GO:BP	regulation of immune response	GO:0050776	1.1493495305 0126E-13	12.9395478772 44100	998	183	44	18092
GO:BP	Fc receptor signaling pathway	GO:0038093	8.0030288127 2537E-13	12.0967456195 44200	240	183	23	18092
GO:BP	antimicrobial humoral response	GO:0019730	8.8777430682 4499E-13	12.0516974280 93900	144	183	19	18092
GO:BP	positive regulation of immune system process	GO:0002684	1.4843042141 8775E-12	11.8284770795 13200	1070	183	44	18092
GO:BP	cornification	GO:0070268	3.0321187673 3889E-12	11.5182537914 99800	112	183	17	18092
GO:BP	adaptive immune response	GO:0002250	6.8918735724 3622E-12	11.1616626980 40200	698	183	35	18092
GO:BP	receptor-mediated endocytosis	GO:0006898	1.1872272198 6454E-11	10.9254661547 69400	333	183	25	18092
GO:BP	immune system process	GO:0002376	1.3941071515 7804E-11	10.8557038449 24800	3322	183	79	18092
GO:BP	phagocytosis, recognition	GO:0006910	1.8110554759 326E-10	9.742068246250 050	100	183	15	18092
GO:BP	regulation of immune system process	GO:0002682	2.3761889831 1763E-10	9.624119021998 380	1625	183	51	18092
GO:BP	immune effector process	GO:0002252	4.3920093903 6124E-10	9.357336740011 130	1310	183	45	18092
GO:BP	keratinization	GO:0031424	3.0913581053 2801E-09	8.509850683011 890	224	183	19	18092
GO:BP	defense response to other organism	GO:0098542	3.3399841279 376E-09	8.476255597010 44	1222	183	42	18092
GO:BP	biological process involved in interspecies interaction between organisms	GO:0044419	5.4778639180 662E-09	8.261388760758 040	2272	183	59	18092
GO:BP	response to biotic stimulus	GO:0009607	5.8345955027 5456E-09	8.233989247075 490	1645	183	49	18092
GO:BP	phagocytosis, engulfment	GO:0006911	6.5834131107 792E-09	8.181548891968 13	127	183	15	18092
GO:BP	response to other organism	GO:0051707	1.0137046165 8696E-08	7.994088575648 410	1610	183	48	18092

GO:BP	response to external biotic stimulus	GO:0043207	1.0598505049 2916E-08	7.974755388945 650	1612	183	48	18092
GO:BP	keratinocyte differentiation	GO:0030216	1.1635581833 432E-08	7.934211895081 930	306	183	21	18092
GO:BP	plasma membrane invagination	GO:0099024	1.8025299116 6474E-08	7.744117519749 640	136	183	15	18092
GO:BP	B cell receptor signaling pathway	GO:0050853	1.8025299116 6474E-08	7.744117519749 640	136	183	15	18092
GO:BP	membrane invagination	GO:0010324	4.1476192770 3297E-08	7.382201115704 480	144	183	15	18092
GO:BP	retina homeostasis	GO:0001895	5.1512173105 3986E-08	7.288090128477 490	79	183	12	18092
GO:BP	positive regulation of B cell activation	GO:0050871	9.0655481281 6144E-08	7.042605932126 750	152	183	15	18092
GO:BP	regulation of immune effector process	GO:0002697	9.6975856104 1552E-08	7.013336377753 490	458	183	24	18092
GO:BP	leukocyte mediated immunity	GO:0002443	1.8555984657 4222E-07	6.731515995239 270	891	183	33	18092
GO:BP	immunoglobulin production	GO:0002377	3.0024669123 0236E-07	6.522521769897 970	194	183	16	18092
GO:BP	epidermal cell differentiation	GO:0009913	3.6898015705 7271E-07	6.432996988616 6800	368	183	21	18092
GO:BP	response to bacterium	GO:0009617	4.6797532250 3965E-07	6.329777047744 090	771	183	30	18092
GO:BP	defense response	GO:0006952	9.0030016933 28E-07	6.045612668171 280	1831	183	48	18092
GO:BP	negative regulation of endopeptidase activity	GO:0010951	0.0000025671 412593196900	5.590550233215 910	258	183	17	18092
GO:BP	Fc-epsilon receptor signaling pathway	GO:0038095	0.0000036168 079934303300	5.441674546147 7100	167	183	14	18092
GO:BP	regulation of B cell activation	GO:0050864	0.0000037877 01235057710	5.421624284442 510	198	183	15	18092
GO:BP	negative regulation of peptidase activity	GO:0010466	0.0000054250 532595050200	5.265595993848 910	271	183	17	18092
GO:BP	skin development	GO:0043588	0.0000061633 919782197600	5.210180211213 910	430	183	21	18092
GO:BP	cell recognition	GO:0008037	0.0000064397 44622325650	5.191131354893 900	239	183	16	18092
GO:BP	response to stress	GO:0006950	0.0000092050 17800183040	5.035975367343 15	4199	183	78	18092
GO:BP	innate immune response	GO:0045087	0.0000134717 48275181000	4.870576040728 7200	999	183	32	18092
GO:BP	pentose biosynthetic process	GO:0019322	0.0000230260 05437108200	4.637781397124 400	4	183	4	18092
GO:BP	membrane organization	GO:0061024	0.0000242954 2096709870	4.614475571509 220	968	183	31	18092
GO:BP	production of molecular mediator of immune response	GO:0002440	0.0000288816 97935607100	4.539377278471 210	303	183	17	18092
GO:BP	leukocyte migration	GO:0050900	0.0000383326 7449917820	4.416430878639 880	523	183	22	18092
GO:BP	epidermis development	GO:0008544	0.0000506094 07716544800	4.295768745223 150	485	183	21	18092
GO:BP	positive regulation of lymphocyte activation	GO:0051251	0.0000808140 6289598590	4.092513058696 940	366	183	18	18092

GO:BP	negative regulation of proteolysis	GO:0045861	0.0000808140 6289598590	4.092513058696 940	366	183	18	18092
GO:BP	antigen receptor-mediated signaling pathway	GO:0050851	0.0000809166 1540707030	4.091962291259 290	325	183	17	18092
GO:BP	vesicle-mediated transport	GO:0016192	0.0001111979 5762856700	3.953903189361 780	2193	183	49	18092
GO:BP	epithelial cell differentiation	GO:0030855	0.0001291644 0276893800	3.888857159801 780	817	183	27	18092
GO:BP	B cell activation	GO:0042113	0.0001370020 9101154300	3.863272804319 1800	337	183	17	18092
GO:BP	positive regulation of response to stimulus	GO:0048584	0.0001920876 509448580	3.716500554445 410	2374	183	51	18092
GO:BP	regulation of endopeptidase activity	GO:0052548	0.0002319863 7025293100	3.634537530185 930	437	183	19	18092
GO:BP	tissue homeostasis	GO:0001894	0.0002693516 549762930	3.569680351675 990	272	183	15	18092
GO:BP	detection of chemical stimulus involved in sensory perception of bitter taste	GO:0001580	0.0003086800 9535022000	3.510491374269 990	40	183	7	18092
GO:BP	cell surface receptor signaling pathway	GO:0007166	0.0003341092 7643926400	3.476111466144 400	3242	183	62	18092
GO:BP	antibacterial humoral response	GO:0019731	0.0004532613 331682490	3.343651328168 140	62	183	8	18092
GO:BP	positive regulation of leukocyte activation	GO:0002696	0.0005312732 605973440	3.274682041924 360	415	183	18	18092
GO:BP	sensory perception of bitter taste	GO:0050913	0.0006132007 111825400	3.212397350128 050	44	183	7	18092
GO:BP	response to external stimulus	GO:0009605	0.0006465111 82270932	3.189423959017 8300	2991	183	58	18092
GO:BP	regulation of peptidase activity	GO:0052547	0.0006899666 047802230	3.161171929133 2600	469	183	19	18092
GO:BP	establishment of localization	GO:0051234	0.0007120255 126063500	3.147504444866 4400	5398	183	87	18092
GO:BP	positive regulation of cell activation	GO:0050867	0.0008074031 993702880	3.092909534011 5200	427	183	18	18092
GO:BP	sensory perception of taste	GO:0050909	0.0008375359 656655340	3.076996534315 3500	67	183	8	18092
GO:BP	detection of chemical stimulus involved in sensory perception of taste	GO:0050912	0.0008420199 833329030	3.074677601435 95	46	183	7	18092
GO:BP	regulation of lymphocyte activation	GO:0051249	0.0008529041 382336410	3.069099778417 1000	524	183	20	18092
GO:BP	response to stimulus	GO:0050896	0.0008541684 26837562	3.068456485711 4	9469	183	129	18092
GO:BP	cell motility	GO:0048870	0.0009571955 186523500	3.018999343310 9100	1856	183	42	18092
GO:BP	localization of cell	GO:0051674	0.0009571955 186523500	3.018999343310 9100	1856	183	42	18092
GO:BP	transport	GO:0006810	0.0009894328 477033220	3.004613675799 720	5259	183	85	18092
GO:BP	killing of cells of other organism	GO:0031640	0.0010553713 724943600	2.976594690466 22	69	183	8	18092
GO:BP	intermediate filament cytoskeleton organization	GO:0045104	0.0017453551 253858200	2.758116194318 5700	51	183	7	18092
GO:BP	intermediate filament-based process	GO:0045103	0.0019997503 80685540	2.699024211864 320	52	183	7	18092
GO:BP	cytoskeleton organization	GO:0007010	0.0020012024 27849250	2.698708978904 3100	1435	183	35	18092

GO:BP	movement of cell or subcellular component	GO:0006928	0.0020068757 45422200	2.697479515777 5900	2337	183	48	18092
GO:BP	locomotion	GO:0040011	0.0021755007 012690000	2.662440772377 150	2055	183	44	18092
GO:BP	peptide cross-linking	GO:0018149	0.0028523063 192504900	2.544803835897 1300	35	183	6	18092
GO:BP	negative regulation of hydrolase activity	GO:0051346	0.0037425186 21231980	2.426836030108 9800	475	183	18	18092
GO:BP	anatomical structure homeostasis	GO:0060249	0.0047382032 80567640	2.324386310912 7500	483	183	18	18092
GO:BP	regulation of cell activation	GO:0050865	0.0091625445 29118860	2.037983901714 6800	666	183	21	18092
GO:BP	lymphocyte activation	GO:0046649	0.0100411904 66760300	1.998214794910 5600	783	183	23	18092
GO:BP	intermediate filament organization	GO:0045109	0.0102712683 39334600	1.988375924585 4600	25	183	5	18092
GO:BP	regulation of response to stimulus	GO:0048583	0.0106988069 43073700	1.970664649130 5100	4324	183	71	18092
GO:BP	regulation of leukocyte activation	GO:0002694	0.0115419087 6680960	1.937722362901 0100	621	183	20	18092
GO:BP	proteolysis	GO:0006508	0.0146145876 4402970	1.835213433912 3600	1846	183	39	18092
GO:BP	positive regulation of biological process	GO:0048518	0.0226356866 1864640	1.645206327315 550	6466	183	94	18092
GO:BP	cell migration	GO:0016477	0.0277745409 13944800	1.556353110791 7100	1684	183	36	18092
GO:BP	pentose metabolic process	GO:0019321	0.0288028219 05524200	1.540564960922 69	15	183	4	18092
GO:BP	epithelium development	GO:0060429	0.0369356145 2509410	1.432554670904 880	1361	183	31	18092
GO:BP	pentose-phosphate shunt	GO:0006098	0.0381006946 8467650	1.419067105821 2000	16	183	4	18092
GO:BP	tissue development	GO:0009888	0.0464635608 64673600	1.332887509890 5400	2161	183	42	18092
GO:CC	extracellular space	GO:0005615	2.0497506352 7921E-94	93.68829897031 470	3598	188	167	18963
GO:CC	extracellular exosome	GO:0070062	2.9385790556 6614E-94	93.53186262110 490	2180	188	144	18963
GO:CC	extracellular vesicle	GO:1903561	7.4420323209 2277E-92	91.12830844815 920	2266	188	144	18963
GO:CC	extracellular organelle	GO:0043230	8.4412766487 4414E-92	91.07359186622 080	2268	188	144	18963
GO:CC	extracellular region	GO:0005576	3.0579953528 3917E-87	86.51456317890 990	4602	188	174	18963
GO:CC	vesicle	GO:0031982	8.2511192250 1632E-60	59.08348713747 67	4071	188	147	18963
GO:CC	immunoglobulin complex	GO:0019814	8.4702320398 3511E-27	26.07210469212 030	167	188	30	18963
GO:CC	blood microparticle	GO:0072562	3.5485845023 7704E-26	25.44994484846 5500	141	188	28	18963
GO:CC	immunoglobulin complex, circulating	GO:0042571	4.0356986501 2468E-16	15.39408127045 150	77	188	17	18963
GO:CC	pigment granule	GO:0048770	7.5739444234 9401E-10	9.120677885993 440	105	188	14	18963
GO:CC	melanosome	GO:0042470	7.5739444234 9401E-10	9.120677885993 440	105	188	14	18963
GO:CC	focal adhesion	GO:0005925	9.8158643106 4653E-09	8.008071453698 410	418	188	23	18963

GO:CC	cell-substrate junction	GO:0030055	1.4351244399115E-08	7.843110439540610	426	188	23	18963
GO:CC	cell surface	GO:0009986	1.7874444835 2665E-07	6.747767438126860	922	188	32	18963
GO:CC	side of membrane	GO:0098552	0.0000012994 16724860960	5.886251547707570	632	188	25	18963
GO:CC	intermediate filament	GO:0005882	0.0000017161 08976514010 0	5.765455137002490	219	188	15	18963
GO:CC	external side of plasma membrane	GO:0009897	0.0000024806 91301362250 0	5.605427276218 01	420	188	20	18963
GO:CC	actin cytoskeleton	GO:0015629	0.0000028472 15984554060	5.545579586824900	513	188	22	18963
GO:CC	monomeric IgA immunoglobulin complex	GO:0071748	0.0000031194 07522932680 0	5.505927884813340	4	188	4	18963
GO:CC	intermediate filament cytoskeleton	GO:0045111	0.0000132404 2858428850	4.878097956831440	255	188	15	18963
GO:CC	IgA immunoglobulin complex, circulating	GO:0071746	0.0000154759 40302733600	4.810342954205 6000	5	188	4	18963
GO:CC	IgA immunoglobulin complex	GO:0071745	0.0000154759 40302733600	4.810342954205 6000	5	188	4	18963
GO:CC	secretory IgA immunoglobulin complex	GO:0071751	0.0000154759 40302733600	4.810342954205 6000	5	188	4	18963
GO:CC	polymeric IgA immunoglobulin complex	GO:0071749	0.0000154759 40302733600	4.810342954205 6000	5	188	4	18963
GO:CC	membrane-bounded organelle	GO:0043227	0.0000323140 72837106000	4.490608300440 8400	12836	188	159	18963
GO:CC	Arp2/3 protein complex	GO:0005885	0.0000365267 0245045130	4.437389533159 410	13	188	5	18963
GO:CC	polymeric cytoskeletal fiber	GO:0099513	0.0000689749 9880173190	4.161308298393 560	775	188	25	18963
GO:CC	anchoring junction	GO:0070161	0.0000916230 2605982310	4.037995368755 3000	843	188	26	18963
GO:CC	cytoskeleton	GO:0005856	0.0001118182 8440805500	3.951487175266 6700	2302	188	48	18963
GO:CC	keratin filament	GO:0045095	0.0001717807 517291480	3.765025501076 0300	97	188	9	18963
GO:CC	supramolecular fiber	GO:0099512	0.0002421224 981236110	3.615964853858 6800	1006	188	28	18963
GO:CC	supramolecular polymer	GO:0099081	0.0002832205 753390020	3.547875199317 000	1014	188	28	18963
GO:CC	IgM immunoglobulin complex, circulating	GO:0071754	0.0003196971 16944885	3.495261280214 310	3	188	3	18963
GO:CC	secretory dimeric IgA immunoglobulin complex	GO:0071752	0.0003196971 16944885	3.495261280214 310	3	188	3	18963
GO:CC	dimeric IgA immunoglobulin complex	GO:0071750	0.0003196971 16944885	3.495261280214 310	3	188	3	18963
GO:CC	pentameric IgM immunoglobulin complex	GO:0071756	0.0003196971 16944885	3.495261280214 310	3	188	3	18963
GO:CC	IgM immunoglobulin complex	GO:0071753	0.0003196971 16944885	3.495261280214 310	3	188	3	18963
GO:CC	protein-containing complex	GO:0032991	0.0008334698 709956400	3.079110094812 3900	5556	188	85	18963
GO:CC	cornified envelope	GO:0001533	0.0015081372 253341500	2.821559140234 1600	44	188	6	18963

GO:CC	endoplasmic reticulum lumen	GO:0005788	0.0041568279 20143590	2.381237953573 870	307	188	13	18963
GO:CC	proton-transporting two-sector ATPase complex, catalytic domain	GO:0033178	0.0085603304 63079390	2.067509469490 880	18	188	4	18963
GO:CC	actin filament	GO:0005884	0.0098495743 67682090	2.006582536381 6700	122	188	8	18963
GO:CC	lamellipodium	GO:0030027	0.0125771122 46363400	1.900419063138 4100	204	188	10	18963
GO:CC	endocytic vesicle lumen	GO:0071682	0.0133450730 9781710	1.874679043016 100	20	188	4	18963
GO:CC	cell periphery	GO:0071944	0.0170789729 7529270	1.767538248668 8900	5786	188	83	18963
GO:CC	supramolecular complex	GO:0099080	0.0182428982 89635100	1.738906163200 4200	1337	188	29	18963
GO:CC	collagen-containing extracellular matrix	GO:0062023	0.0296235241 6542730	1.528363276856 1600	424	188	14	18963
GO:CC	cell leading edge	GO:0031252	0.0335225041 4778920	1.474663546815 4500	429	188	14	18963
GO:CC	organelle	GO:0043226	0.0391685757 6300100	1.407062219861 7600	13974	188	160	18963
KEGG	Salivary secretion	KEGG:04970	1.0683987225 4917E-12	11.97126663992 260	93	98	16	7987
KEGG	Tight junction	KEGG:04530	0.0004794556 567297980	3.319251553098 300	168	98	11	7987
KEGG	Staphylococcus aureus infection	KEGG:05150	0.0011481623 496322400	2.939996698554 4900	91	98	8	7987
KEGG	Pathogenic Escherichia coli infection	KEGG:05130	0.0020672069 404387200	2.684616045582 66	196	98	11	7987
KEGG	Regulation of actin cytoskeleton	KEGG:04810	0.0052675256 33485350	2.278393342297 1500	217	98	11	7987
KEGG	Salmonella infection	KEGG:05132	0.0178952753 41643600	1.747261615047 8500	249	98	11	7987
KEGG	Bacterial invasion of epithelial cells	KEGG:05100	0.0278434844 28300300	1.555276416572 55	77	98	6	7987
KEGG	Pentose phosphate pathway	KEGG:00030	0.0370535592 274054	1.431170068964 5500	30	98	4	7987
KEGG	Carbon metabolism	KEGG:01200	0.0475077632 5858160	1.323235416377 740	118	98	7	7987
HPA	spleen; cells in red pulp[High]	HPA:0530713	0.0050472998 94272230	2.296940890123 0200	771	126	23	10596
HPA	salivary gland; glandular cells[High]	HPA:0420053	0.0458993433 5880240	1.338193527484 280	1386	126	31	10596
HPA	tonsil; non-germinal center cells[High]	HPA:0600443	0.0468033773 0768620	1.329722807328 210	1260	126	29	10596